

**NASA Technical Memorandum 102643**  
**AVSCOM Technical Memorandum 90-B-008**

**INFLOW MEASUREMENTS MADE WITH A LASER VELOCIMETER ON A  
HELICOPTER MODEL IN FORWARD FLIGHT**

**Volume IX: RECTANGULAR PLANFORM BLADES AT AN ADVANCE RATIO  
OF 0.23, 0.75 CHORD ABOVE THE TIP PATH PLANE**

Susan L. Althoff, Joe W. Elliott, and Danny R. Hoad  
Aerostructures Directorate  
USAARTA - AVSCOM  
Langley Research Center  
Hampton, Virginia

Richard H. Sailey  
Lockheed Engineering & Sciences Company  
Hampton, Virginia

May 1990

**LIBRARY COPY**

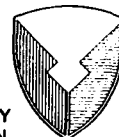
MAY 24 1990

LANGLEY RESEARCH CENTER  
LIBRARY NASA  
HAMPTON, VIRGINIA



National Aeronautics and  
Space Administration

**Langley Research Center**  
Hampton, Virginia 23665-5225



**US ARMY  
AVIATION  
SYSTEMS COMMAND**  
AVIATION R&T ACTIVITY



Inflow Measurements Made With a Laser Velocimeter  
on a Helicopter Model in Forward Flight  
Volume IX: Rectangular Planform Blades  
at an Advance Ratio of 0.23, 0.75 Chord  
Above the Tip Path Plane

Susan L. Althoff, Joe W. Elliott, and Danny R. Hoad  
Aerostructures Directorate  
USAARTA - AVSCOM  
Langley Research Center  
Hampton, Virginia

Richard H. Sailey  
Lockheed Engineering & Sciences Company  
Hampton, Virginia

## SUMMARY

An experimental investigation was conducted in the 14- by 22-Foot Subsonic Tunnel at the NASA Langley Research Center to measure the inflow into a scale model helicopter rotor in forward flight ( $\mu = 0.23$ ). The measurements were made with a two-component Laser Velocimeter (LV) 0.75 chord above the plane formed by the path of the rotor tips (tip-path-plane). A conditional sampling technique was employed to determine the position of the rotor at the time that each velocity measurement was made so that the azimuthal fluctuations in velocity could be determined. Measurements were made at a total of 180 separate locations in order to clearly define the inflow character. The mean and standard deviation of the induced inflow ratios and the azimuthally dependent induced inflow ratios are included on 5.25 flexible disk in the pocket on the inside of the rear cover of this report. These data are presented herein without analysis.

## INTRODUCTION

One of the problems confronting the helicopter industry is the lack of detailed information about the velocity fluctuations around and through rotating blades. This information is needed for two reasons: to ensure a more complete understanding of the flow field environment associated with a thrusting rotor and to provide data for the validation of rapidly emerging computational codes. One explanation for the lack of available data is the absence, until recent years, of a suitable device for making

such measurements. Making measurements of the velocity around a system of rotating blades requires an accurate, nonintrusive measurement capability that presents a minimum risk to the systems involved. The Laser Velocimeter (LV), which uses high energy light beams to measure velocities, is ideally suited to this task.

The Laser Velocimeter has been successfully used to measure specific areas and localized phenomena within the rotor disk (references 1 thru 3). In addition, the hotwire anemometer and pressure probe, both having directional measuring limitations, have been employed in similar programs (references 4 and 5). This comprehensive investigation has been conducted to measure the flow into a representative rotor system as a function of azimuth using a two-component (streamwise and vertical direction) LV system.

#### NOTATION

A	rotor disc area, $(\pi R^2)$ , ft <sup>2</sup>
A <sub>0</sub>	Constant term in Fourier series of blade feathering (collective) at $r/R = 0.75$ , deg
A <sub>1</sub>	Coefficient of cosine term in Fourier series of blade feathering, deg
b	Number of blades
B <sub>1</sub>	Coefficient of sine term in Fourier series of blade feathering, deg
C <sub>Q</sub>	Rotor torque coefficient, $Q/(\rho A (12R) V_{tip}^2)$ , nondimensional
C <sub>D</sub>	Rotor drag coefficient, $D/(\rho A V_{tip}^2)$ , nondimensional
C <sub>T</sub>	Rotor thrust coefficient, $T/(\rho A V_{tip}^2)$ , nondimensional
D	Rotor drag, lbf (positive to the rear)
q	Dynamic pressure, lb/ft <sup>2</sup>
Q	Rotor torque, in-lbf
r	Local radius of the rotor system, ft
R	Rotor radius, ft
T	Thrust produced by the rotor, lbf
U	Freestream component of velocity, ft/sec, (positive downstream)

- $u_i$  Induced component of velocity parallel to the tip path plane, ft/sec, (positive downstream)
- $V$  Vertical component of velocity, ft/sec, (positive up)
- $v_i$  Induced component of velocity normal to the tip path plane, ft/sec, (positive up)
- $V_{tip}$  Rotor blade hover-tip velocity, ft/sec, ( $\Omega R$ )
- $V_\infty$  Tunnel freestream velocity, ft/sec, (positive downstream)

## SYMBOLS

- $\alpha$  Angle between rotor disk and freestream velocity (positive nose up), deg
- $\lambda$  Inflow Ratio normal to tip path plane (positive up),  $(V_\infty \sin \alpha + v_i)/V_{tip}$
- $\lambda_i$  Induced Inflow Ratio normal to tip path plane (positive up),  $v_i/V_{tip}$
- $\mu_\infty$  Rotor advance ratio,  $V_\infty \cos \alpha/V_{tip}$
- $\mu$  Inflow Ratio parallel to tip path plane (positive downstream),  $(V_\infty \cos \alpha + u_i)/V_{tip}$
- $\mu_i$  Induced Inflow Ratio parallel to tip path plane (positive downstream),  $u_i/V_{tip}$
- $\Omega$  Rotor rotational speed, radians/sec
- $\psi$  Rotor azimuth measured from downstream position, positive counterclockwise, as viewed from above, deg
- $\rho$  Air density, slug/ft<sup>3</sup>
- $\theta$  Blade pitch angle at a specific azimuth (positive nose up),  
deg,  $\theta = A_0 - A_1 \cos \psi - B_1 \sin \psi$
- $\overline{xx}$  Mean value

## EXPERIMENTAL APPARATUS

The experimental apparatus used in this investigation included the NASA Langley Research Center 14- by 22-Foot Subsonic Tunnel, the 2-Meter Rotor Test System (2MRTS), and a two-component laser velocimeter system.

The 14- by 22-Foot Subsonic Tunnel is an atmospheric, closed-circuit wind tunnel of conventional design with enhancements for the testing of powered and high-lift configurations (reference 6). The tunnel is pictured in figure 1 and shown schematically in figure 2. When the tunnel is operated in the open configuration, the walls and ceiling of the test section are lifted out of the flow, leaving only a solid floor and a flow collector. In this configuration, the tunnel can be driven to about 170 knots. This investigation was conducted with the tunnel in the open configuration to allow complete optical access to the rotor flow field.

The 2MRTS is a general purpose rotorcraft model testing system which was mounted on a strut in the forward part of the test section (see figure 3). The system consists of a 29-horsepower electric drive motor and 90 degree speed-reducing transmission, a blade pitch remote control system, and two six-component strain gage balances used for measuring forces and moments on the rotor system and the generic fuselage shell (ROBIN). The four-bladed rotor hub is fully articulated with viscous dampers for lead-lag motion and coincident flap and lag hinges. A more detailed description of the 2MRTS and the ROBIN fuselage can be found in reference 7. The characteristics of the rotor blades used during this investigation can be found in table 1. No attempt was made to dynamically scale the rotor blades; rather, they were very rigid to minimize blade aeroelastic response uncertainties.

The LV system used in this investigation was designed to measure the instantaneous components of velocity in the longitudinal (freestream) and vertical directions. The LV system is described in reference 8. The system is comprised of four subsystems: optics, traverse, data acquisition, and seeding. The optics subsystem, which is shown in figure 4, operates in backscatter mode and at high power (3 watts in all lines) in order to accommodate the long focal lengths needed to scan the wide test section. The transmitting and receiving optics packages are augmented by a zoom lens system consisting of a 3-inch clear aperture negative lens and a 12-inch clear aperture positive lens. Bragg cells in each of the optical paths provide a directional measurement capability. The velocity measurements are made at a point in space where the four beams cross, called the sample volume. The length of the sample volume (transverse to the flow direction) increases as the sample volume is moved away from the optics assembly. The sample volume length, over the 10- to 20 foot focal length of the system, is less than 1 cm and has a nearly constant diameter of 0.2 mm.

The traverse subsystem provides five degrees of freedom in positioning the sample volume and is controlled by the same computer that is used for data acquisition. Translation of the sample volume in the horizontal and vertical direction is accomplished by displacing the entire optics platform. Translation along the lateral axes is accomplished by displacing the negative lens located in the zoom lens assembly, thus refocusing the sample volume along the axis of optical transmission. The other two degrees of freedom, pan and tilt, are implemented by rotating the final mirror about its vertical and horizontal axes in order to change the direction of optical transmission. The total range of the traversing system is 7 feet vertically, 6 feet streamwise, 16.5 feet laterally, and  $10^\circ$  in both pan and tilt. Measurements can be made outside of this envelope by re-positioning the optics platform, which is mounted on wheels to facilitate such relocations. For this study the traversing system was positioned to the left of the test section when looking downstream as shown in figure 3.

The data acquisition subsystem is shown schematically in figure 5 and interfaces with the optical signal processing equipment to receive two channels of raw LV data and up to five channels of auxiliary data. In this investigation, two of the auxiliary channels were used for the acquisition of data relative to blade position (one each for the U and V components). The system converts the raw LV data to engineering units and determines the statistical characteristics of the acquired data so that the test results can be evaluated during the acquisition process. The raw data and 64 parameters from the tunnel static data acquisition system are written to magnetic tape for later analysis. The final function performed by the data system is to control the five degree-of-freedom scan system.

The seeding subsystem, shown schematically in figure 6 and in the photo in figure 7, is a solid particle, liquid dispensing system (reference 9). Polystyrene latex microspheres are suspended in a mixture containing, by volume, 50 percent distilled water and 50 percent ethyl alcohol. The advantages of the polystyrene particles are their low density, high reflectivity, and precise particle size. The particles used in this investigation were 1.7 microns in diameter with a standard deviation of 0.0239 microns. The particle mixture is pumped to an array of nozzles where compressed air is used to atomize the mixture. These nozzles are mounted on a frame in the settling chamber of the tunnel; the position of the frame is remotely controlled by the laser operator during the data acquisition process. The low vapor pressure of water/alcohol mixture allows it to evaporate as it travels the 85 feet from the settling

chamber to the test section. This process provides isolated single particles in the flow field whose velocities are measured as they pass through the sample volume. The local fluid velocity is inferred from the seed particle velocity.

## ERROR ANALYSIS

The overall LV system error is obtained by summing the the error of all of the components that contribute to an error in the velocity measurement. The error sources are summarized the table below, and are defined in references 10 and 11. The resulting total bias error of 0.81 to 1.82 percent is obtained by adding the percents contributed by each error source. The total random error of 1.12 percent is obtained by taking the square root of the sum of the squared percents of the random sources. Taking the square root of the sum of the squares of the random and bias errors gives a total system error of 1.38 to 2.14 percent.

Error Source	Bias Error (percent)	Random Error (percent)
Cross beam angle measurement	±0.81	N/A
Diverging fringes	A	A
Time jitter	N/A	N/A
Clock synchronization	0.51	± 0.51
Quantization	A	± .99
Velocity bias	B	B
Bragg Bias	B	B
Velocity Gradient	B	B
Particle Lag	<u>± 0.50</u>	<u>B</u>

Total error	-0.81 to 1.82	1.12
-------------	---------------	------

Total system error	1.38 to 2.14 percent velocity
--------------------	-------------------------------

A	Not measured
---	--------------

B	Negligible
---	------------

N/A	Not Applicable
-----	----------------



## TEST PROCEDURES

In all cases measurements were made at azimuthal increments of  $30^\circ$  from  $\psi = 0$ , at 1.95 inches (approximately 0.75 chord) above the plane formed by the tips of the blades. Measurements were made from a radial location of  $r/R = 0.2$  to  $r/R = 1.10$ , with the majority of the measurement locations concentrated toward the outboard portion of the disk. Figure 8 shows the measurement locations superimposed on the rotor disk. During the test, the rotor tip path plane was maintained at  $-3^\circ$  relative to the freestream by zeroing the blade flapping relative to the shaft and setting the shaft angle to  $-3^\circ$ . The operating tip speed for the test was held at 624 feet/sec (2113 rpm), the nominal tunnel speed was 144 ft/sec ( $\mu = 0.23$ ), and the nominal rotor thrust coefficient was 0.0065. Table 2 lists the nominal test conditions and selected test parameters. The LV data acquisition process consisted of placing the sample volume at the measurement location and acquiring data for a period of one minute or until 4096 velocity measurements were made in either the longitudinal or the vertical component. During this process, conditional sampling techniques were employed to permanently associate each measured velocity with the location of the rotor blades at the time when the measurement was made. At the conclusion of the process, the measurement location was changed and the acquisition process was repeated.

## DATA REDUCTION

Independent velocity measurements in the freestream and vertical direction were made at each measurement location. At the same instant in time that a velocity measurement was made, the location of the blades was recorded for that velocity component. The maximum time required to acquire this data was one minute (2113 rotor revolutions for this test) and the minimum approximately 10 seconds. These data, collected over many revolutions, were sorted into 128 equally spaced azimuth segments ( $2.81^\circ$  wide) that are representative of blade position. Careful measurements indicated that the lead-lag motion was well within this azimuth resolution ( $2.81^\circ$ ); therefore, no corrections to blade position were made due to lead-lag. The velocity value assigned to each interval at a measurement location is the arithmetic mean of all the measurements that were taken in the respective 2.81 degree wide azimuthal range. The results of this sorting process provide the azimuthally dependent velocity data. The "mean velocity" value refers to the velocity calculated from the arithmetic mean of all the measurements made at a single measurement location.

## EXPERIMENTAL RESULTS

Table 3 lists the measurement locations, the mean and standard deviation of the two components of induced inflow ratio, and the number of measurements in each of the measured components (U and V). In figure 9 the mean longitudinal induced component of velocity,  $\mu_i$ , with a band of  $\pm$  one standard deviation is plotted vs. blade radius for each radial scan. The standard deviation represents the fluctuation in velocity at a given measurement location; it is not an indication of the error in the mean measurements. The size of the symbols used for plotting the mean velocity values is an approximation of the calculated error in the measurements. Figure 10 presents in the same format the mean normal induced component of velocity,  $\lambda_i$ . The same data without the  $\pm$  one standard deviation is presented in a contour plot format in figures 11 and 12 in order to show more clearly the interactions over the whole disk (viewed from above). Azimuth dependent data are presented in figures 13-192. The format of each of these figures shows the induced velocity vs azimuth at the top of the figure, the number of measurements that were used to determine the induced inflow velocity ratio for each azimuth segment in the center, and an order ratio analysis of the azimuthal variation at the bottom of the figure. The figure numbers for the azimuthal and radial measurement locations follow:

Azimuth	0	30	60	90	120	150	180	210	240	270	300	330
r/R												
0.20	13	28	43	58	73	88	103	118	133	148	163	178
0.40	14	29	44	59	74	89	104	119	134	149	164	179
0.50	15	30	45	60	75	90	105	120	135	150	165	180
0.60	16	31	46	61	76	91	106	121	136	151	166	181
0.70	17	32	47	62	77	92	107	122	137	152	167	182
0.74	18	33	48	63	78	93	108	123	138	153	168	183
0.78	19	34	49	64	79	94	109	124	139	154	169	184
0.82	20	35	50	65	80	95	110	125	140	155	170	185
0.86	21	36	51	66	81	96	111	126	141	156	171	186
0.90	22	37	52	67	82	97	112	127	142	157	172	187
0.94	23	38	53	68	83	98	113	128	143	158	173	188
0.98	24	39	54	69	84	99	114	129	144	159	174	189
1.02	25	40	55	70	85	100	115	130	145	160	175	190
1.04	26	41	56	71	86	101	116	131	146	161	176	191
1.10	27	42	57	72	87	102	117	132	147	162	177	192

The mean and standard deviation of the induced inflow velocities (table 3) and the azimuthally dependent induced inflow velocities (figures 13 through 192) are included on a 5.25 flexible disk in the pocket on the inside of the rear cover of this report. The details of the data format and the file structure are located in the file "README.DOC". The disk format is 360 kbyte double-sided, written using the Microsoft Corporation MS-DOS operating system.

## CONCLUDING REMARKS

The laser velocimeter provides an effective system for making measurements in the dynamic environment associated with rotor blades. It has been used on numerous occasions to measure the localized flow phenomena encountered in such flows. This investigation demonstrates the use of a matured LV system to map the flow into a representative rotor in forward flight by making velocity measurements at 177 locations above the rotor disk. These measurements provide both the mean and azimuthally-dependent velocity values, and they provide a detailed look at the nature of this flow. The mean and standard deviation of the induced inflow velocities and the azimuthally dependent induced inflow velocities are included on a 5.25 flexible disk in the pocket on the inside of the rear cover of this report.

## REFERENCES

1. Landgrebe, A. J.; and Johnson, B. V.: Measurement of Model Helicopter Rotor Flow Velocities with a Laser Doppler Velocimeter. American Helicopter Society Journal, Vol 19, July 1974, p. 39-43.
2. Biggers, J. C.; and Orloff, K. L.: Laser Velocimeter Measurements of the Helicopter Rotor-Induced Flowfield. American Helicopter Society, Annual National V/STOL Forum, 30th, Washington, D.C. May 7-9, 1974.
3. Owen F. K.; and Taubert M. E.: Measurement and Prediction of Model-Rotor Flowfields. AIAA, 18th Fluid Dynamics, Plasmadynamics and Laser Conference, Cincinnati, Ohio, July 16-18, 1985.
4. Tangler, J. L.; Wohlfeld, R. M.; and Miley, S. J.: An Experimental Investigation of Vortex Stability, Tip Shapes, Compressibility and Noise for Hovering Models. NASA CR-2305, September 1973.
5. Junker, B.: Investigations of Blade-vortices in the Rotor Downwash. Twelfth European Rotorcraft Forum, Garmish-Partenkirchen, Federal Republic of Germany, September 22-25, 1986.
6. Applin, Z. T.: Flow Improvements in the Circuit of the Langley 4- by 7-Meter Tunnel. NASA TM 85662, December 1983.
7. Phelps, A. E. III; and Berry, J. D.: Description of the U.S. Army 2-Meter Rotor Test System. NASA TM 87762, AVSCOM TM 86-B-4, January 1987.
8. Sellers, W. L.; and Elliott, J. W.: Applications of a Laser Velocimeter in the Langley 4- by 7-Meter Tunnel. Proceedings of the Workshop on Flow Visualization and Laser Velocimetry for Wind Tunnels, NASA CP 2243, March 1982, pp. 283-293.
9. Elliott, J. W.; and Nichols, C. E.: Seeding Systems for Use with a Laser Velocimeter in Large Scale Wind Tunnels. Proceedings of the Workshop on Wind Tunnel Seeding Systems for Laser Velocimeters, NASA CP 2393, March 1985, pp. 93-103.
10. Young, W. H.; Meyers, J. F.; and Hepner, T. E.: Laser Velocimeter Systems Analysis to a Flow Survey above a Stalled Wing. NASA TN D-8408, August 1977.
11. Dring, R. P.: Sizing Criteria for Laser Anemometry Particles. Journal of Fluids Engineering, Vol. 104, March 1982, p. 15-17.

**TABLE 1 - 2MRTS ROTOR AND BLADE CHARACTERSTICS**

Hub Type	Fully Articulated
Number of blades	4
Airfoil section	NACA 0012
Hinge offset, in, $r/R$	2.00, .06
Root cutout, in, $r/R$	8.25, .24
Pitch-flap coupling angle, deg	0.0
Twist linear, deg	-8.0
Radius, R, in	33.88
Airfoil chord, C, in	2.6
Rotor solidity, $bc/\pi R$	0.0977
Blade stiffness	
Flapwise lb-in <sup>2</sup>	11500
Torsional lb-in <sup>2</sup>	25500
Blade weight, grams	259.3
Lead/lag damping in-lb/deg/sec	182.4

**TABLE 2 - NOMINAL ROTOR CONTROL AND PERFORMANCE PARAMETERS**

$C_T$	0.0065
$C_Q$	0.00034
$C_D$	0.00003
$\alpha$ , deg	-3.01
Coning, deg	0.5
$A_0$ , deg	6.8
$A_1$ , deg	-1.9
$B_1$ , deg	3.3
$\mu_\infty$	0.23
$V_\infty$ , ft/sec	143.8
$V_{tip}$ , ft/sec	624.8
Lag angle (mean), degrees	0.90

TABLE 3 - INFLOW VELOCITY SUMMARY

$\Psi$	r/R	$\mu_i$			$\lambda_i$		
		Mean	Standard deviation	# of Measurements	Mean	Standard deviation	# of Measurements
0	0.20	0.0171	0.0156	2259	-0.0183	0.0160	2863
0	0.40	0.0184	0.0112	2270	-0.0220	0.0106	2731
0	0.50	0.0186	0.0102	2270	-0.0247	0.0099	2628
0	0.60	0.0163	0.0107	1988	-0.0255	0.0089	2665
0	0.70	0.0146	0.0089	2053	-0.0275	0.0079	2628
0	0.74	0.0138	0.0087	2140	-0.0291	0.0071	2593
0	0.78	0.0112	0.0088	2238	-0.0313	0.0073	2715
0	0.82	0.0100	0.0085	2068	-0.0319	0.0073	2805
0	0.86	0.0096	0.0085	2165	-0.0319	0.0072	2864
0	0.90	0.0071	0.0090	2269	-0.0340	0.0069	2944
0	0.94	0.0059	0.0100	2031	-0.0349	0.0069	2952
0	0.98	0.0043	0.0105	1992	-0.0348	0.0063	2937
0	1.02	-0.0008	0.0089	2642	-0.0349	0.0055	2918
0	1.04	-0.0020	0.0089	2615	-0.0349	0.0054	2904
0	1.10	-0.0029	0.0084	2313	-0.0340	0.0047	2861
30	0.20	0.0121	0.0163	2295	0.0048	0.0223	2677
30	0.40	0.0157	0.0084	2497	-0.0156	0.0107	2797
30	0.50	0.0139	0.0070	2577	-0.0247	0.0070	2733
30	0.60	0.0107	0.0065	2625	-0.0298	0.0069	2780
30	0.70	0.0087	0.0076	2100	-0.0338	0.0066	2853
30	0.74	0.0075	0.0075	2385	-0.0352	0.0062	2938
30	0.78	0.0057	0.0073	2378	-0.0355	0.0059	2910
30	0.82	0.0056	0.0074	2379	-0.0353	0.0054	2874
30	0.86	0.0051	0.0073	2228	-0.0353	0.0054	2874
30	0.90	0.0056	0.0087	1763	-0.0342	0.0067	2799
30	0.94	0.0014	0.0077	2620	-0.0343	0.0060	2370
30	0.98	0.0017	0.0076	2681	-0.0338	0.0049	2433
30	1.02	0.0004	0.0077	2571	-0.0327	0.0044	2288
30	1.04	-0.0015	0.0080	2088	-0.0329	0.0042	2698
30	1.10	-0.0046	0.0074	2039	-0.0317	0.0041	2744
60	0.20	0.0135	0.0091	2507	0.0001	0.0102	2743
60	0.40	0.0141	0.0074	2600	-0.0252	0.0067	2974
60	0.50	0.0131	0.0069	2603	-0.0261	0.0073	2878
60	0.60	0.0110	0.0067	2658	-0.0274	0.0080	3039
60	0.70	-0.0031	0.0057	2471	0.0244	0.0038	2708
60	0.74	-0.0027	0.0056	2473	0.0240	0.0037	2745
60	0.78	-0.0039	0.0056	2488	0.0236	0.0036	2768
60	0.82	-0.0042	0.0056	2544	0.0231	0.0035	2804
60	0.86	-0.0040	0.0054	2528	0.0228	0.0034	2762
60	0.90	-0.0042	0.0055	2581	0.0225	0.0033	2771
60	0.94	-0.0036	0.0055	2544	0.0220	0.0034	2783
60	0.98	-0.0042	0.0055	2573	0.0217	0.0033	2783
60	1.02	-0.0043	0.0054	2590	0.0214	0.0033	2748
60	1.04	-0.0034	0.0055	2597	0.0212	0.0034	2789
60	1.10	-0.0039	0.0053	2612	0.0203	0.0033	2801

TABLE 3 - CONTINUED

$\Psi$	$r/R$	$\mu_i$			$\lambda_i$		
		Mean	Standard deviation	# of Measurements	Mean	Standard deviation	# of Measurements
90	0.20	0.0065	0.0082	2391	-0.0038	0.0070	2616
90	0.40	0.0128	0.0071	2560	-0.0213	0.0073	2983
90	0.50	0.0136	0.0076	2625	-0.0193	0.0084	3012
90	0.60	0.0116	0.0078	2732	-0.0162	0.0095	3059
90	0.70	-0.0032	0.0055	2561	0.0170	0.0037	2929
90	0.74	-0.0026	0.0055	2542	0.0168	0.0034	2871
90	0.78	-0.0028	0.0055	2600	0.0163	0.0035	2886
90	0.82	-0.0022	0.0055	2521	0.0160	0.0034	2916
90	0.86	-0.0031	0.0054	2575	0.0156	0.0033	2917
90	0.90	-0.0031	0.0056	2598	0.0152	0.0034	2921
90	0.94	-0.0033	0.0054	2579	0.0151	0.0032	2909
90	0.98	-0.0029	0.0055	2542	0.0147	0.0031	2886
90	1.02	-0.0027	0.0057	2561	0.0145	0.0032	2926
90	1.04	-0.0031	0.0055	2577	0.0142	0.0031	2940
90	1.10	-0.0030	0.0056	2595	0.0136	0.0032	2851
120	0.20	0.0035	0.0081	2330	-0.0014	0.0065	2618
120	0.40	0.0125	0.0070	2471	-0.0124	0.0099	2902
120	0.50	0.0132	0.0085	2553	-0.0102	0.0098	3013
120	0.60	0.0129	0.0078	2709	-0.0062	0.0121	3193
120	0.70	-0.0045	0.0049	2741	0.0109	0.0031	3099
120	0.74	-0.0041	0.0051	2766	0.0104	0.0029	3067
120	0.78	-0.0042	0.0051	2672	0.0098	0.0031	3090
120	0.82	-0.0044	0.0058	2463	0.0087	0.0035	2745
120	0.86	-0.0045	0.0056	2512	0.0084	0.0038	2916
120	0.90	-0.0046	0.0056	2448	0.0082	0.0034	2838
120	0.94	-0.0056	0.0058	2507	0.0079	0.0034	2861
120	0.98	-0.0043	0.0056	2508	0.0074	0.0033	2825
120	1.02	-0.0059	0.0057	2531	0.0073	0.0032	2852
120	1.04	-0.0053	0.0055	2535	0.0069	0.0034	2802
120	1.10	-0.0050	0.0057	2531	0.0066	0.0036	2811
150	0.20	-0.0025	0.0079	2513	0.0021	0.0072	2662
150	0.40	0.0100	0.0087	2624	-0.0026	0.0086	2772
150	0.50	0.0095	0.0065	2635	-0.0007	0.0112	2841
150	0.60	0.0100	0.0074	2582	0.0026	0.0101	2849
150	0.70	0.0099	0.0086	2629	0.0079	0.0078	2812
150	0.74	0.0071	0.0065	2623	0.0093	0.0103	2875
150	0.78	0.0038	0.0061	2491	0.0097	0.0078	2608
150	0.82	0.0021	0.0065	2473	0.0113	0.0090	2701
150	0.86	0.0002	0.0062	2444	0.0117	0.0064	2633
150	0.90	-0.0013	0.0063	2460	0.0121	0.0064	2648
150	0.94	-0.0029	0.0058	2456	0.0120	0.0053	2643
150	0.98	-0.0045	0.0053	2496	0.0113	0.0044	2715
150	1.02	-0.0058	0.0049	2480	0.0106	0.0039	2764
150	1.04	-0.0068	0.0048	2554	0.0100	0.0038	2821
150	1.10	-0.0071	0.0044	2559	0.0080	0.0033	2847

TABLE 3 - CONTINUED

$\Psi$	r/R	$\mu_i$			$\lambda_i$		
		Mean	Standard deviation	# of Measurements	Mean	Standard deviation	# of Measurements
180	0.20	-0.0010	0.0077	2758	0.0022	0.0049	2621
180	0.40	0.0069	0.0079	2454	0.0010	0.0103	2635
180	0.50	0.0082	0.0078	2448	0.0034	0.0097	2623
180	0.60	0.0099	0.0086	2459	0.0076	0.0068	2582
180	0.70	0.0046	0.0084	2418	0.0117	0.0136	2623
180	0.74	0.0043	0.0091	2490	0.0120	0.0125	2630
180	0.78	0.0029	0.0087	2454	0.0125	0.0110	2654
180	0.82	0.0004	0.0084	2488	0.0124	0.0097	2635
180	0.86	-0.0004	0.0083	2488	0.0127	0.0084	2573
180	0.90	-0.0011	0.0078	2496	0.0139	0.0084	2690
180	0.94	-0.0047	0.0059	2371	0.0115	0.0053	2535
180	0.98	-0.0048	0.0053	2466	0.0132	0.0050	2786
180	1.02	-0.0067	0.0046	2549	0.0116	0.0041	2700
180	1.04	-0.0069	0.0044	2519	0.0108	0.0039	2790
180	1.10	-0.0073	0.0042	2500	0.0085	0.0035	2789
210	0.20	-0.0018	0.0082	2912	0.0027	0.0057	2720
210	0.40	0.0042	0.0097	2746	-0.0022	0.0095	2708
210	0.50	0.0075	0.0073	2576	-0.0025	0.0096	2614
210	0.60	0.0096	0.0096	2419	0.0023	0.0081	2522
210	0.70	0.0082	0.0122	2500	0.0058	0.0169	2681
210	0.74	0.0068	0.0133	2478	0.0074	0.0159	2719
210	0.78	0.0046	0.0130	2472	0.0080	0.0153	2686
210	0.82	0.0029	0.0120	2465	0.0093	0.0137	2714
210	0.86	0.0018	0.0105	2487	0.0097	0.0114	2640
210	0.90	-0.0001	0.0097	2460	0.0110	0.0094	2614
210	0.94	-0.0016	0.0083	2435	0.0114	0.0073	2615
210	0.98	-0.0031	0.0064	2447	0.0113	0.0053	2616
210	1.02	-0.0057	0.0052	2395	0.0102	0.0046	2612
210	1.04	-0.0063	0.0048	2459	0.0092	0.0044	2649
210	1.10	-0.0069	0.0044	2390	0.0069	0.0035	2618
240	0.20	0.0004	0.0081	2837	0.0015	0.0064	2718
240	0.40	0.0035	0.0086	2838	-0.0060	0.0076	2674
240	0.50	0.0060	0.0086	2919	-0.0068	0.0076	2784
240	0.60	0.0058	0.0080	2644	-0.0042	0.0058	2618
240	0.70	0.0099	0.0129	2762	-0.0015	0.0150	2759
240	0.74	0.0112	0.0152	2800	0.0024	0.0180	2646
240	0.78	0.0101	0.0145	2721	0.0038	0.0174	2603
240	0.82	0.0086	0.0125	2712	0.0051	0.0148	2638
240	0.86	0.0066	0.0122	2710	0.0069	0.0139	2575
240	0.90	0.0042	0.0106	2641	0.0095	0.0116	2520
240	0.94	0.0031	0.0090	2554	0.0119	0.0077	2445
240	0.98	0.0012	0.0065	2427	0.0122	0.0049	2442
240	1.02	-0.0020	0.0062	2369	0.0110	0.0047	2429
240	1.04	-0.0011	0.0060	2422	0.0102	0.0043	2446
240	1.10	-0.0013	0.0059	2509	0.0081	0.0039	2464



TABLE 3 - CONCLUDED

$\Psi$	$r/R$	$\mu_i$			$\lambda_i$		
		Mean	Standard deviation	# of Measurements	Mean	Standard deviation	# of Measurements
270	0.20	0.0027	0.0082	2763	-0.0071	0.0059	2736
270	0.40	0.0035	0.0087	2955	-0.0150	0.0057	2828
270	0.50	0.0018	0.0094	2980	-0.0178	0.0064	2879
270	0.60	0.0039	0.0090	2999	-0.0205	0.0067	2847
270	0.70	0.0059	0.0091	2989	-0.0224	0.0067	2899
270	0.74	0.0066	0.0093	3059	-0.0231	0.0065	2982
270	0.78	0.0071	0.0091	2947	-0.0222	0.0063	2870
270	0.82	0.0092	0.0084	2682	-0.0182	0.0073	2803
270	0.86	0.0099	0.0098	2607	-0.0136	0.0121	2828
270	0.90	0.0118	0.0082	2416	-0.0050	0.0157	2689
270	0.94	0.0099	0.0071	2208	0.0012	0.0133	2554
270	0.98	0.0063	0.0062	2000	0.0095	0.0063	2343
270	1.02	0.0009	0.0072	2039	0.0112	0.0039	2197
270	1.04	-0.0005	0.0074	2167	0.0103	0.0043	2374
270	1.10	-0.0019	0.0075	2525	0.0058	0.0031	2539
300	0.20	0.0085	0.0094	2349	0.0008	0.0059	2616
300	0.40	0.0076	0.0081	2288	-0.0039	0.0050	2797
300	0.50	0.0065	0.0082	2333	-0.0077	0.0055	2886
300	0.60	0.0081	0.0089	1988	-0.0121	0.0067	2855
300	0.70	0.0076	0.0097	2090	-0.0182	0.0080	2913
300	0.74	0.0084	0.0097	2015	-0.0193	0.0085	2873
300	0.78	0.0079	0.0100	1864	-0.0216	0.0084	2908
300	0.82	0.0065	0.0088	1780	-0.0232	0.0088	2950
300	0.86	0.0073	0.0094	1708	-0.0237	0.0083	2767
300	0.90	0.0069	0.0087	1543	-0.0245	0.0079	2781
300	0.94	0.0058	0.0086	1620	-0.0254	0.0072	2750
300	0.98	0.0035	0.0092	1331	-0.0231	0.0065	2677
300	1.02	0.0041	0.0086	1317	-0.0184	0.0068	2530
300	1.04	0.0041	0.0081	1281	-0.0127	0.0073	2372
300	1.10	0.0056	0.0086	1623	0.0173	0.0093	1927
330	0.20	0.0144	0.0088	2217	-0.0009	0.0060	2613
330	0.40	0.0100	0.0102	2243	-0.0032	0.0066	2555
330	0.50	0.0122	0.0100	2097	-0.0040	0.0064	2519
330	0.60	0.0108	0.0096	2120	-0.0079	0.0072	2514
330	0.70	0.0110	0.0087	2213	-0.0116	0.0066	2462
330	0.74	0.0103	0.0087	2154	-0.0140	0.0068	2513
330	0.78	0.0083	0.0086	2172	-0.0167	0.0074	2475
330	0.82	0.0086	0.0085	2057	-0.0178	0.0066	2424
330	0.86	0.0084	0.0088	2098	-0.0213	0.0072	2459
330	0.90	0.0055	0.0091	2049	-0.0230	0.0078	2379
330	0.94	0.0038	0.0096	2088	-0.0244	0.0084	2372
330	0.98	0.0061	0.0086	2011	-0.0239	0.0070	2398
330	1.02	0.0036	0.0092	1826	-0.0248	0.0100	2450
330	1.04	0.0019	0.0097	1841	-0.0249	0.0099	2459
330	1.10	-0.0016	0.0094	1886	-0.0238	0.0106	2571

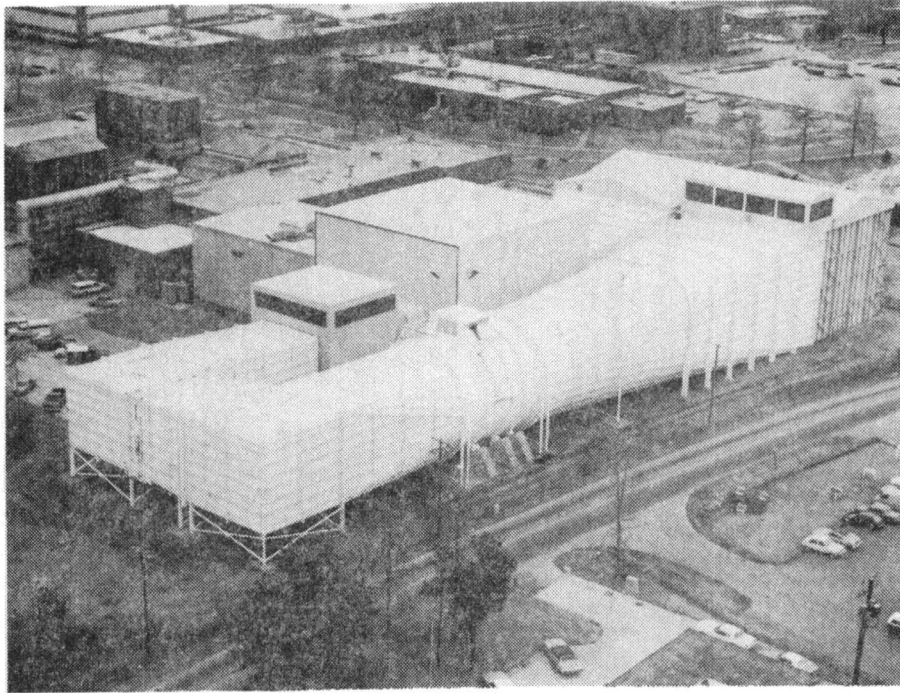


Figure 1. Aerial view of 14- by 22-Foot Subsonic Tunnel.

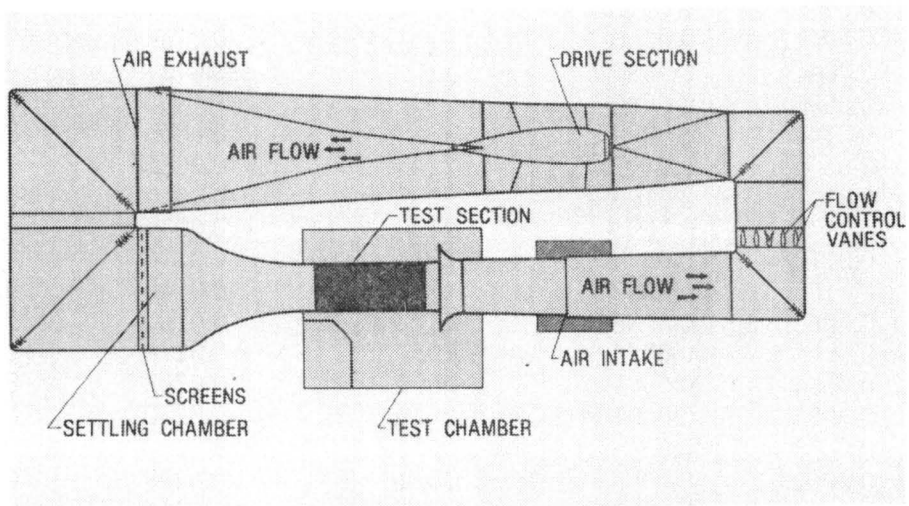


Figure 2. Schematic of 14- by 22-Foot Subsonic Tunnel.

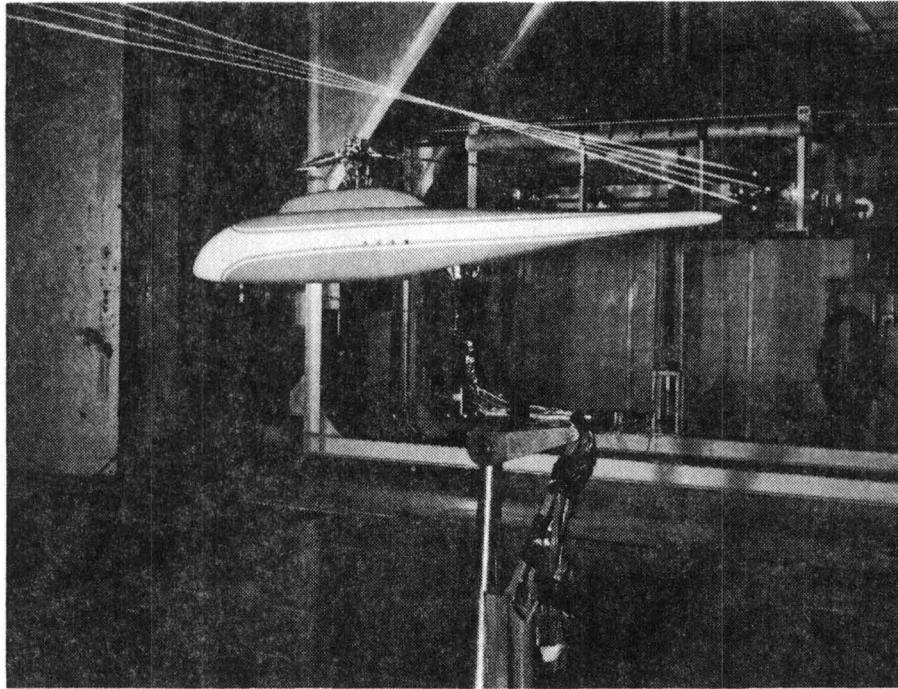


Figure 3. 2MRTS mounted in forward bay of the test section.

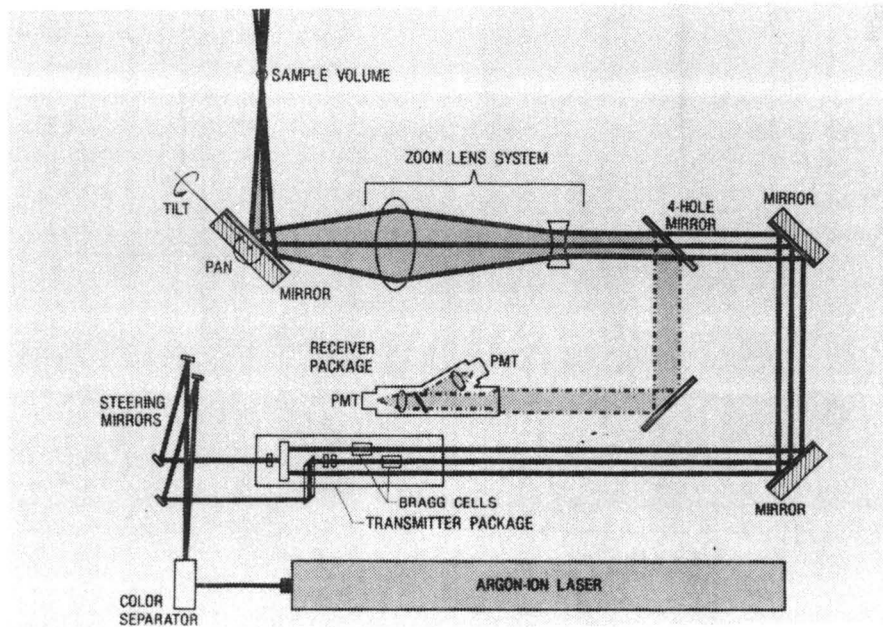


Figure 4. Schematic of laser velocimeter optics subsystem.

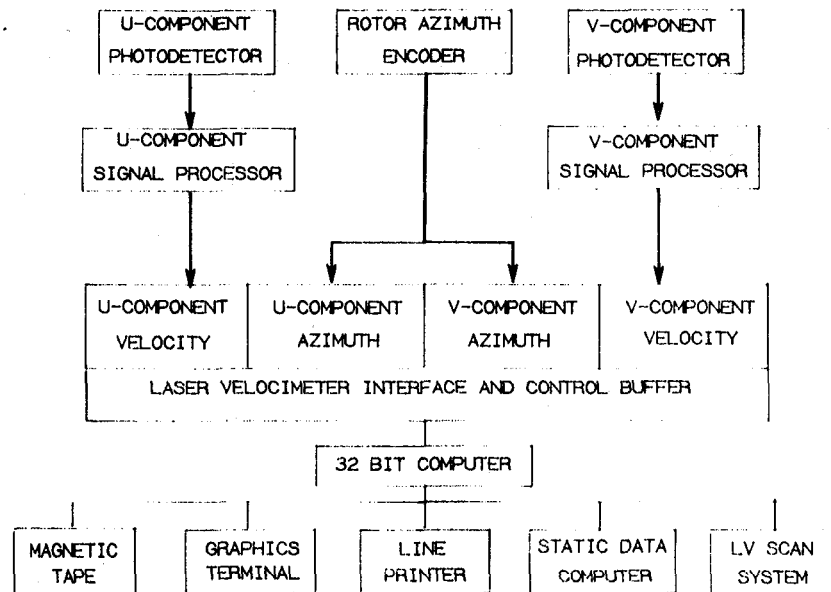


Figure 5. Schematic of data acquisition subsystem.

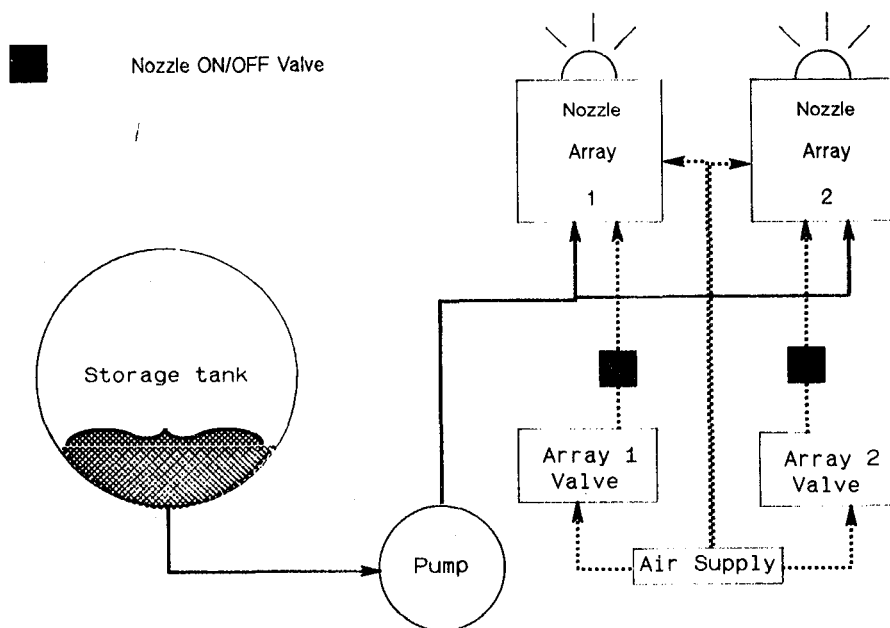


Figure 6. Schematic of seeding subsystem.

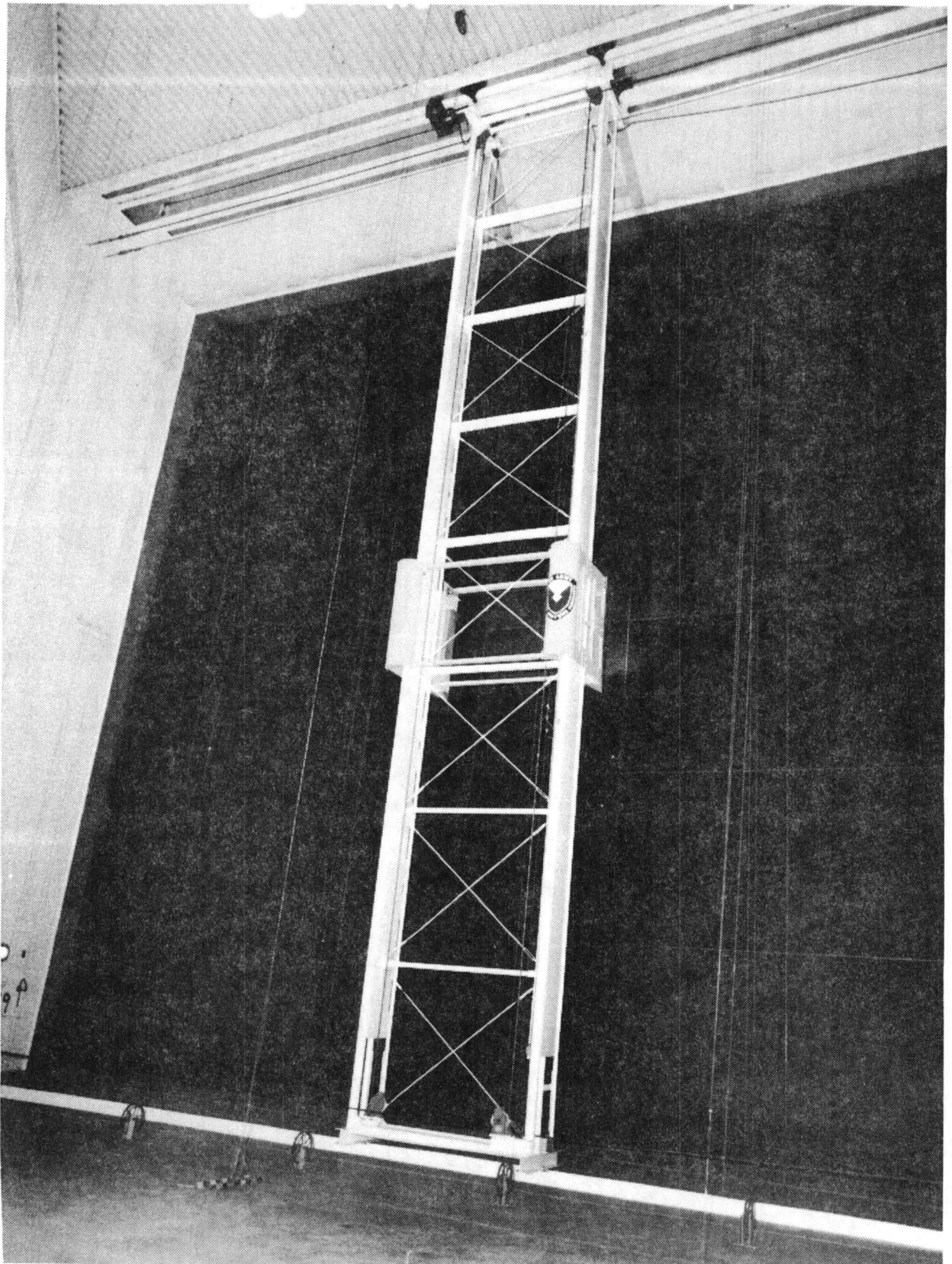


Figure 7. Photograph of remote control positioner for seeding system.

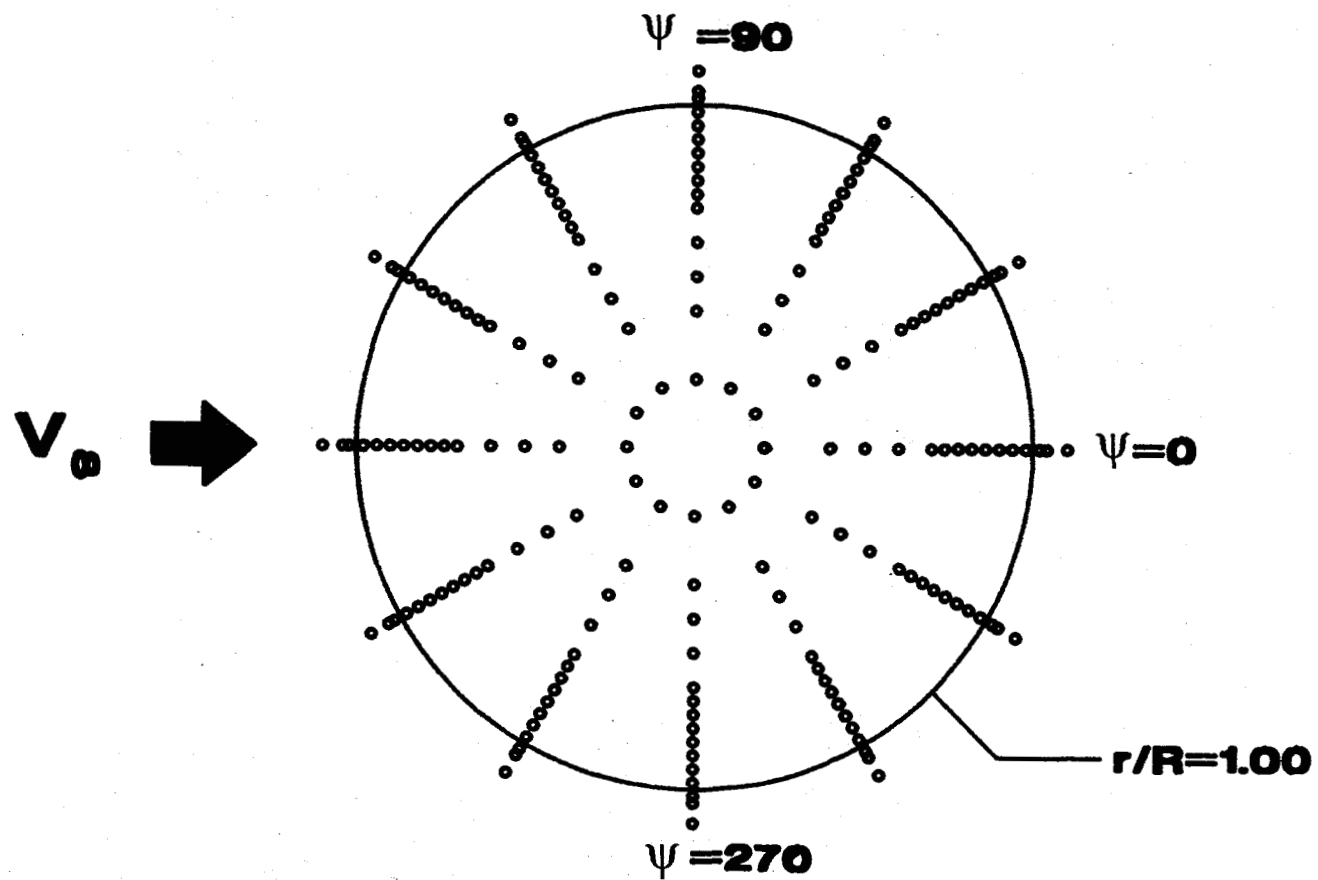
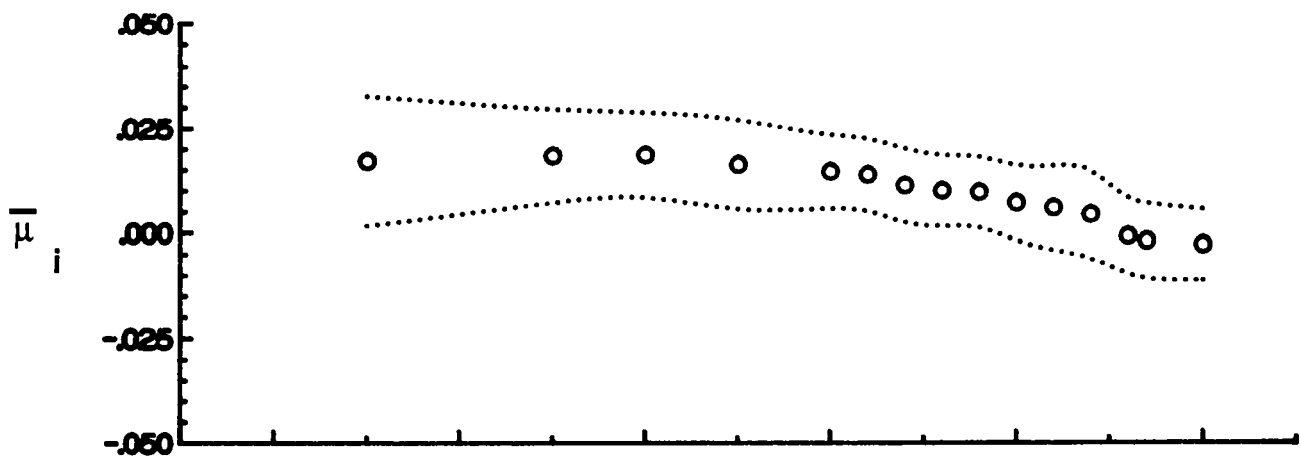
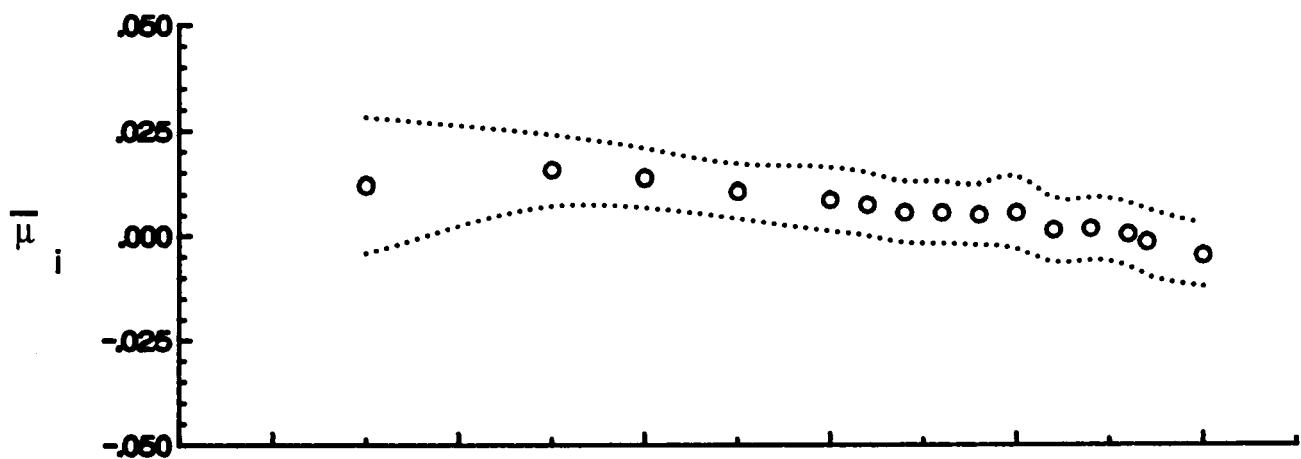


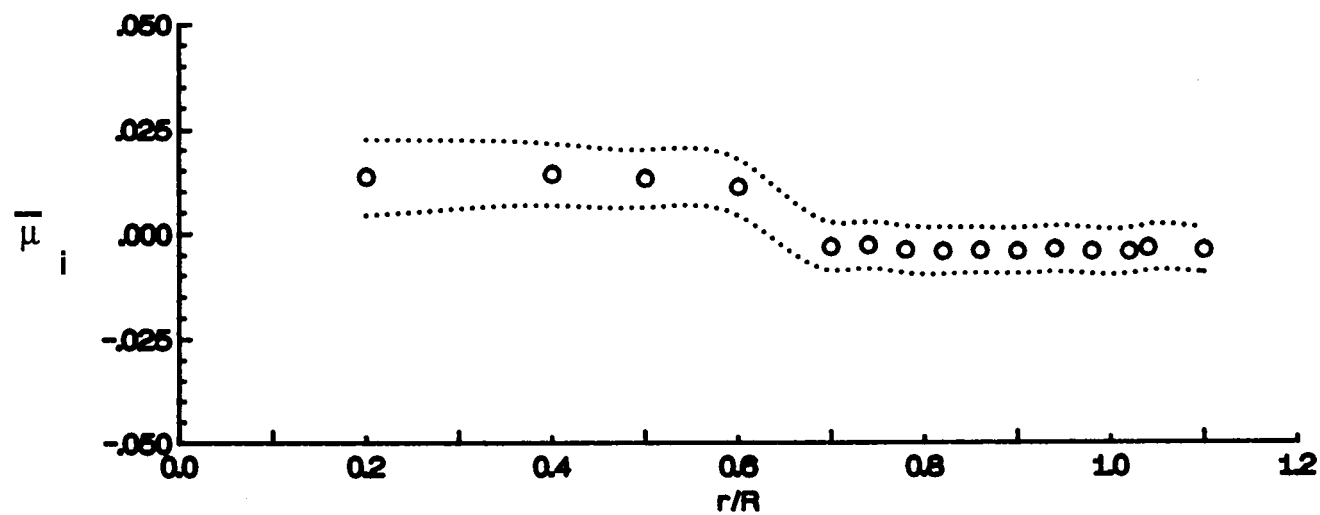
Figure 8. Locations of velocity measurements, 1.95 inches above rotor tip path plane.



(a) rotor azimuth = 0 degrees



(b) rotor azimuth = 30 degrees



(c) rotor azimuth = 60 degrees

Figure 9.- Radial distribution of mean induced inflow ratio ( $\mu_i$ ).

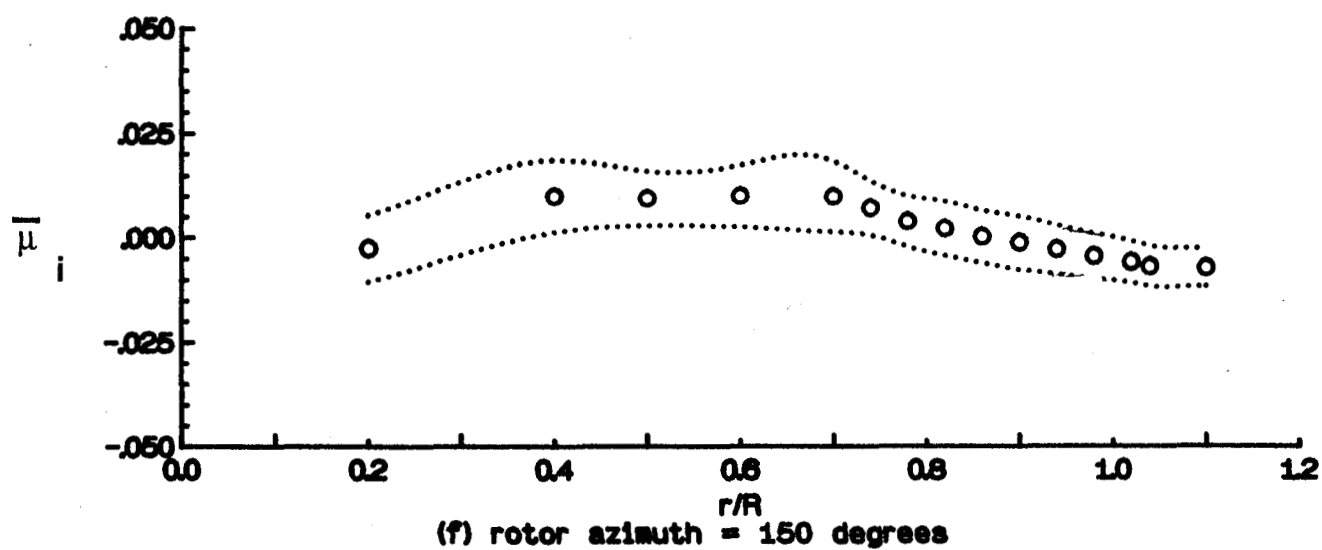
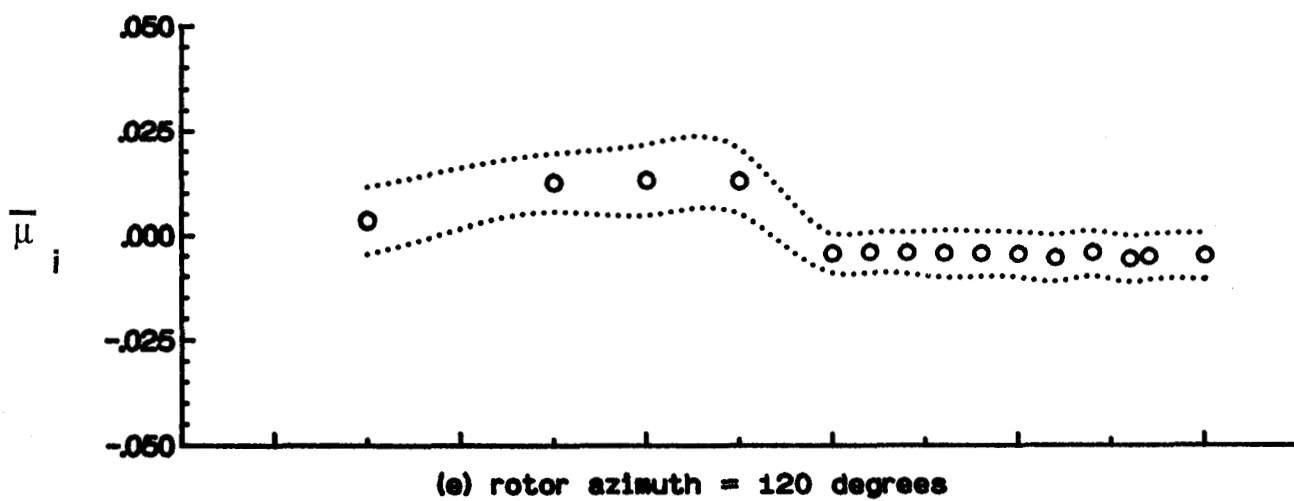
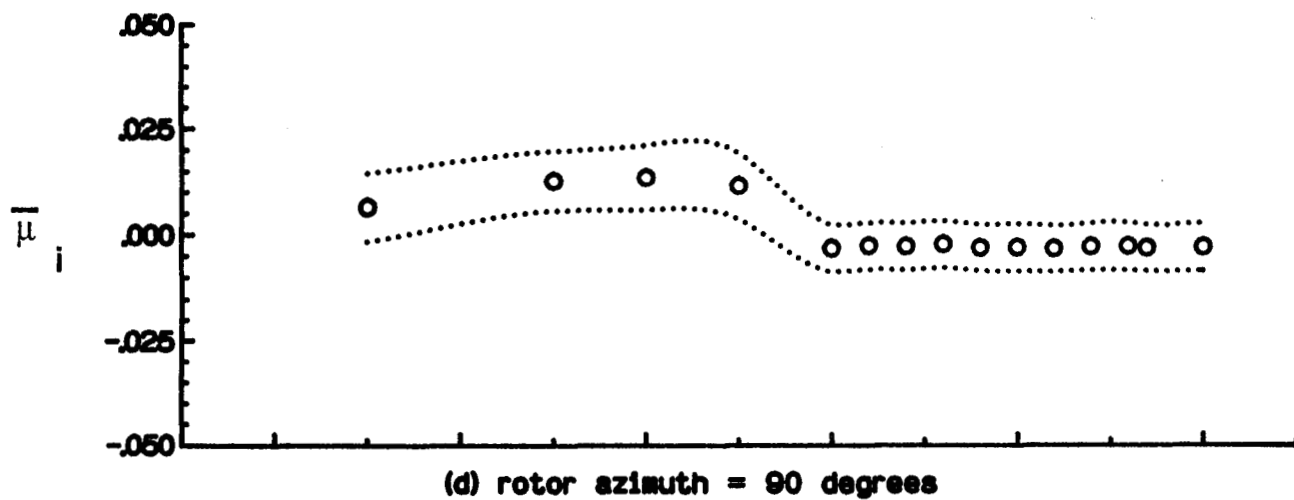


Figure 9.- Continued.



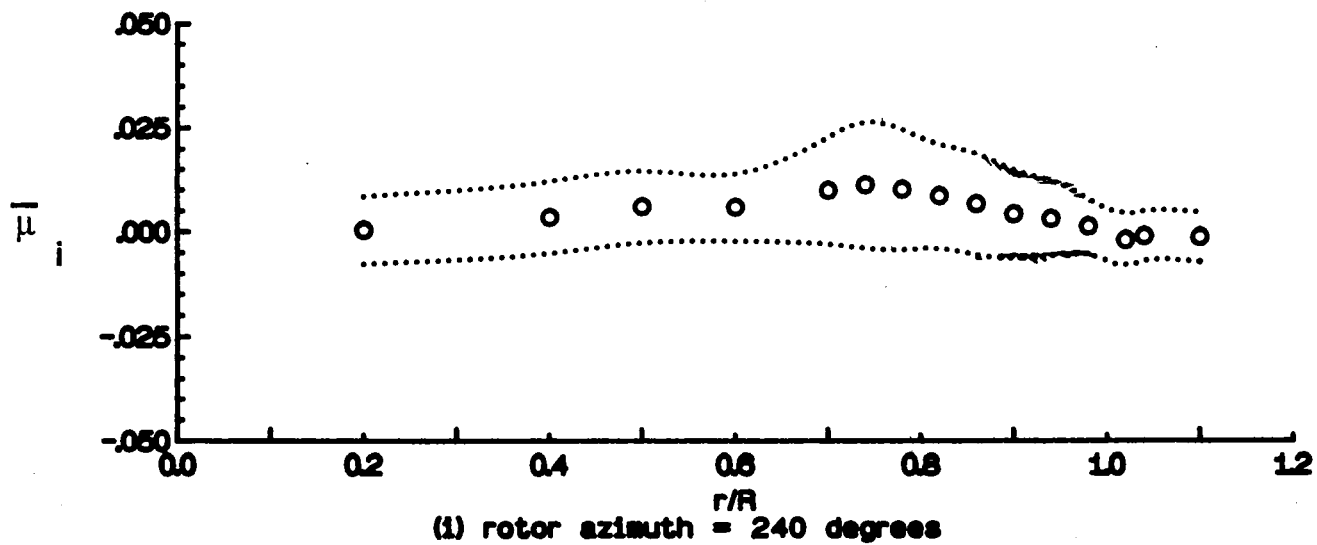
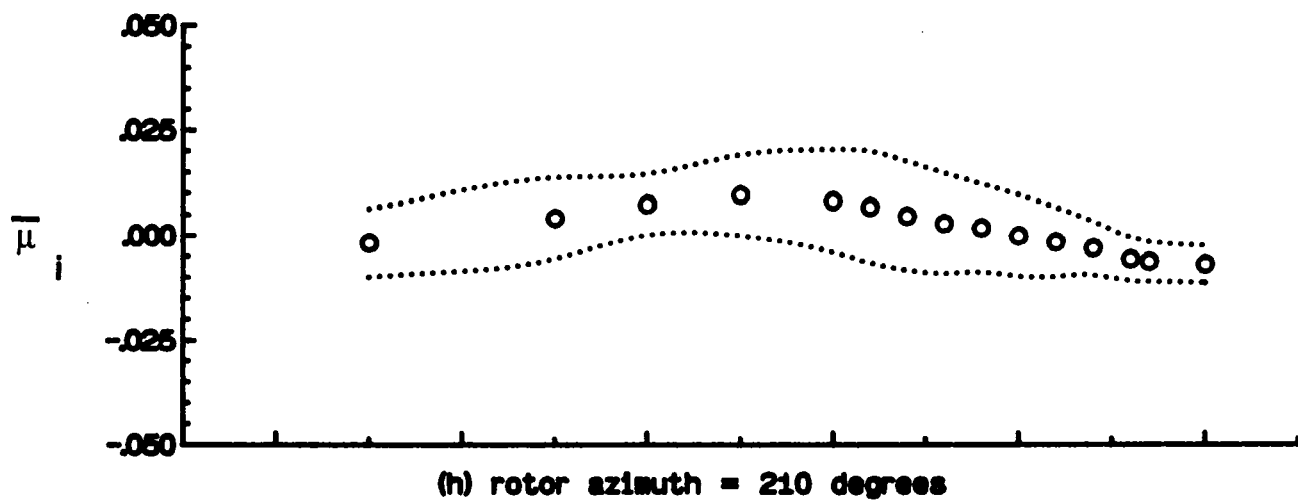
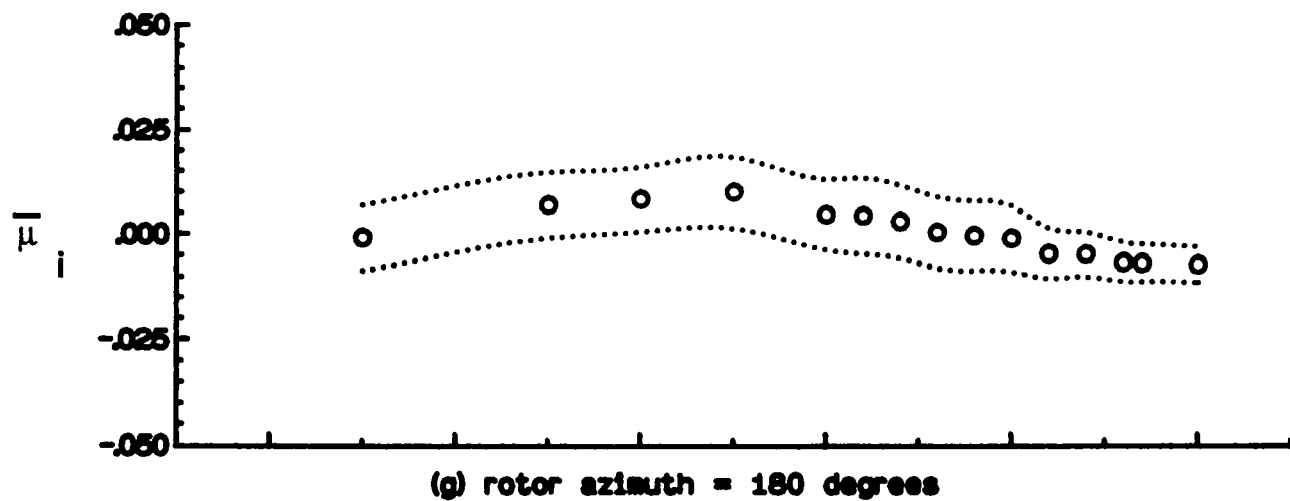


Figure 9.- Continued.

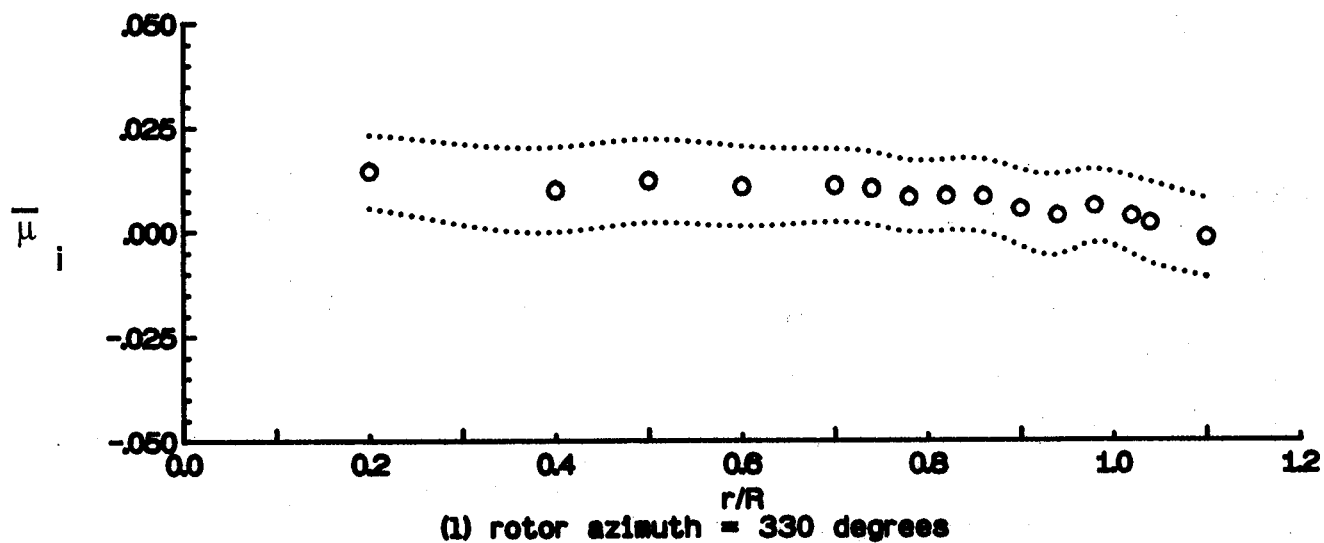
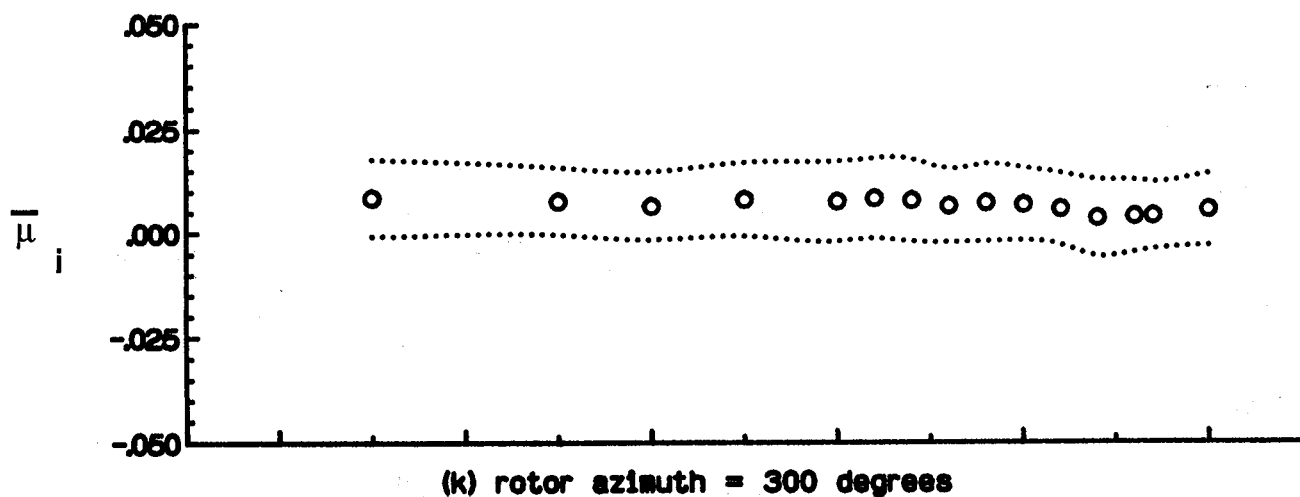
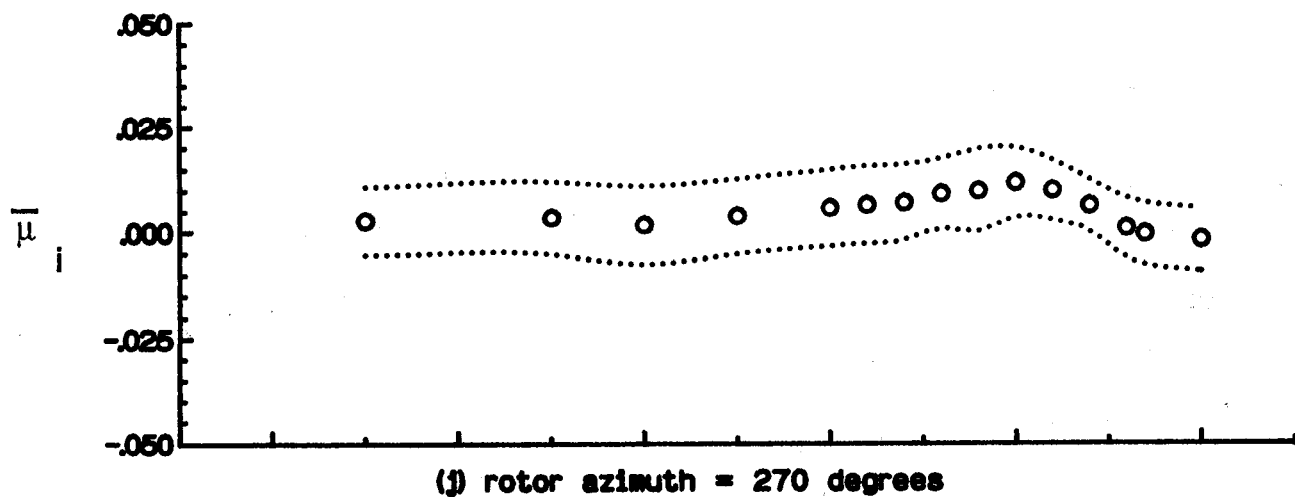


Figure 9.- Concluded.

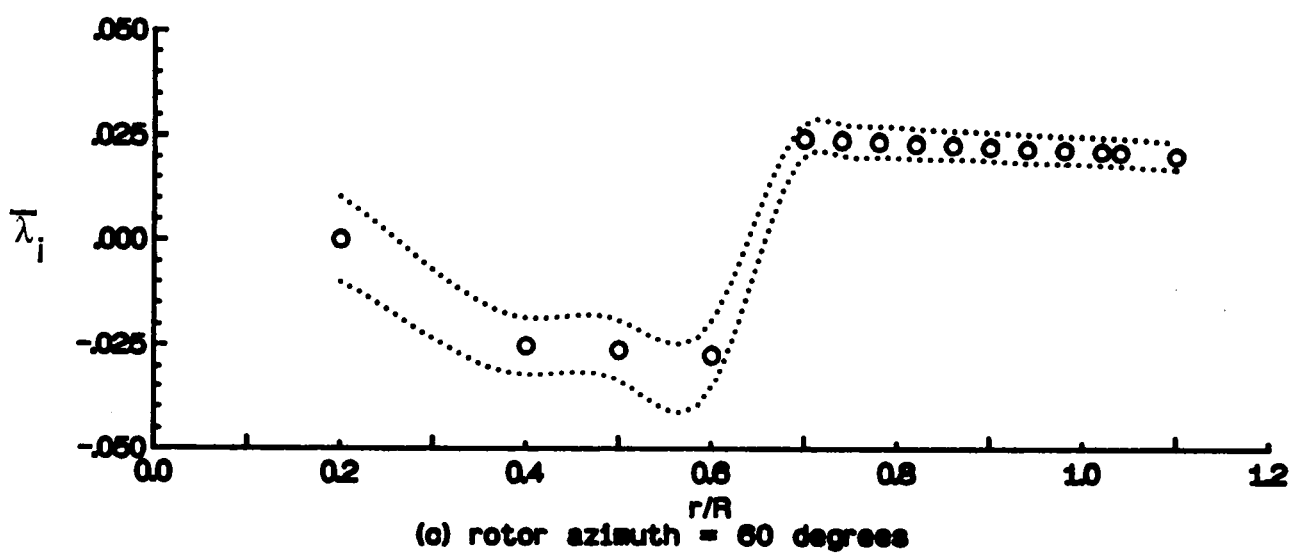
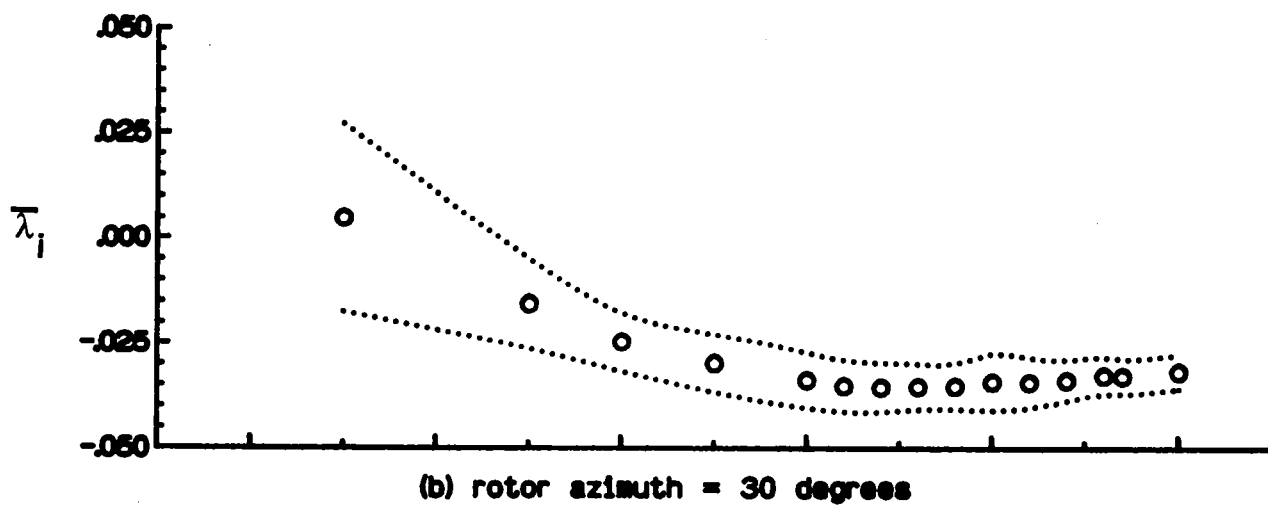
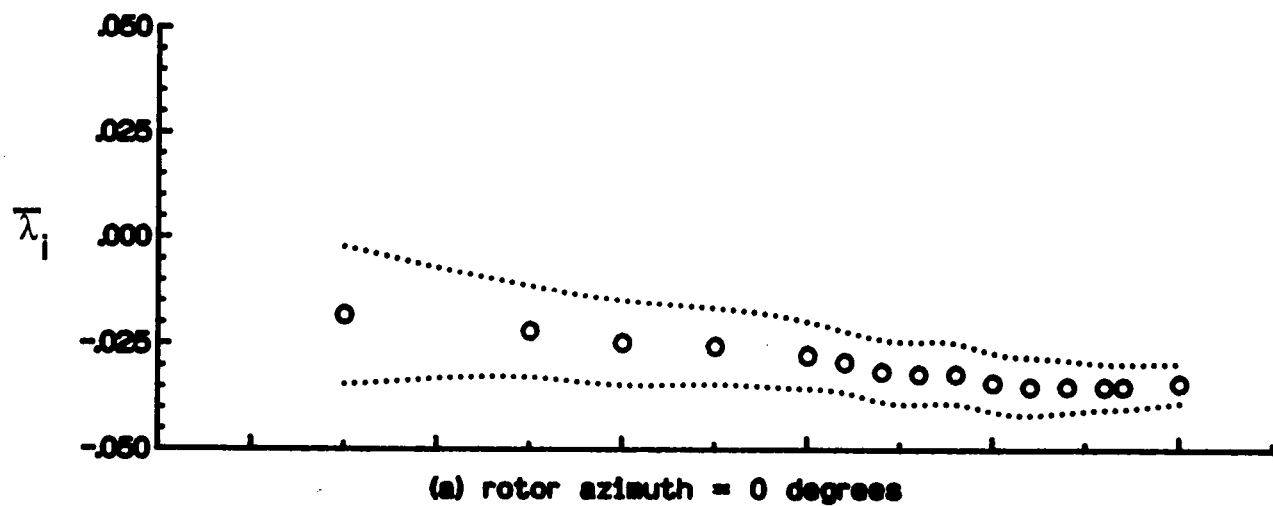


Figure 10.- Radial distribution of mean induced inflow ratio ( $\lambda_i$ ).

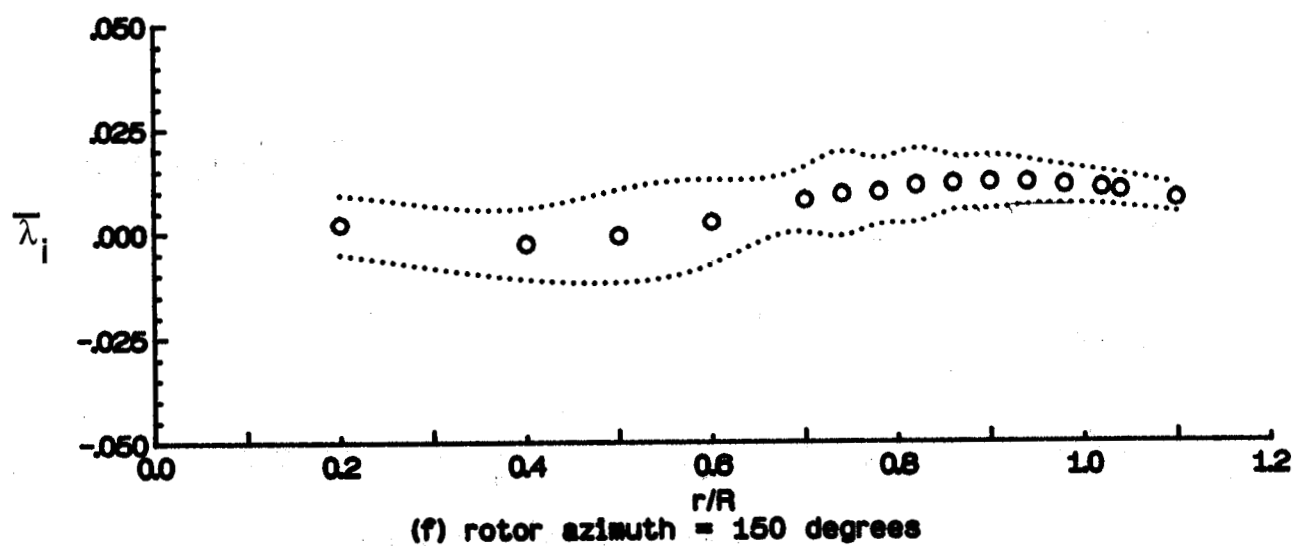
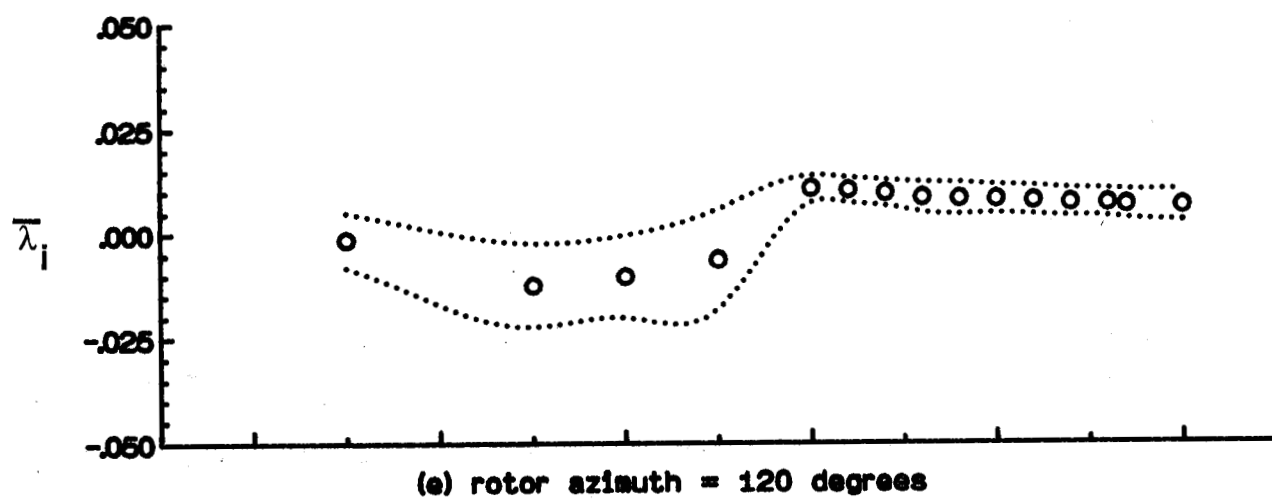
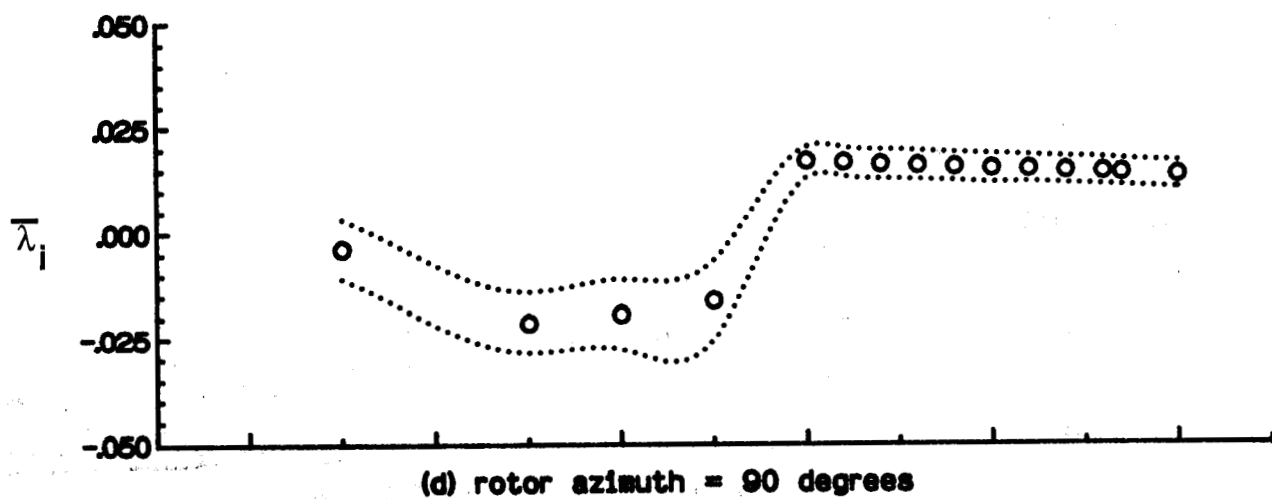


Figure 10.- Continued.

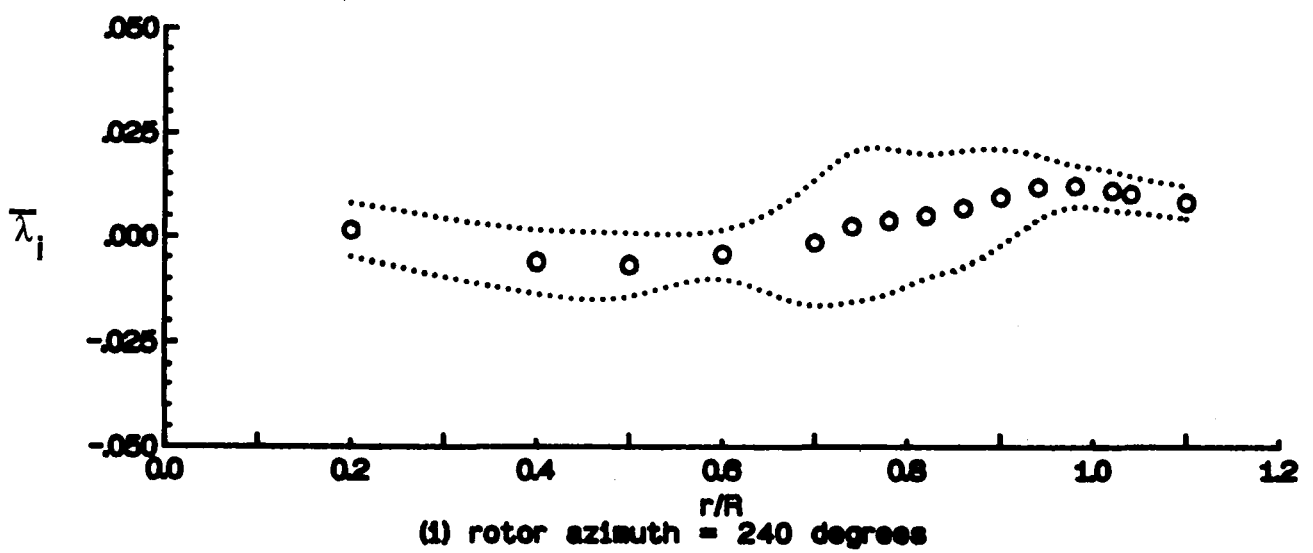
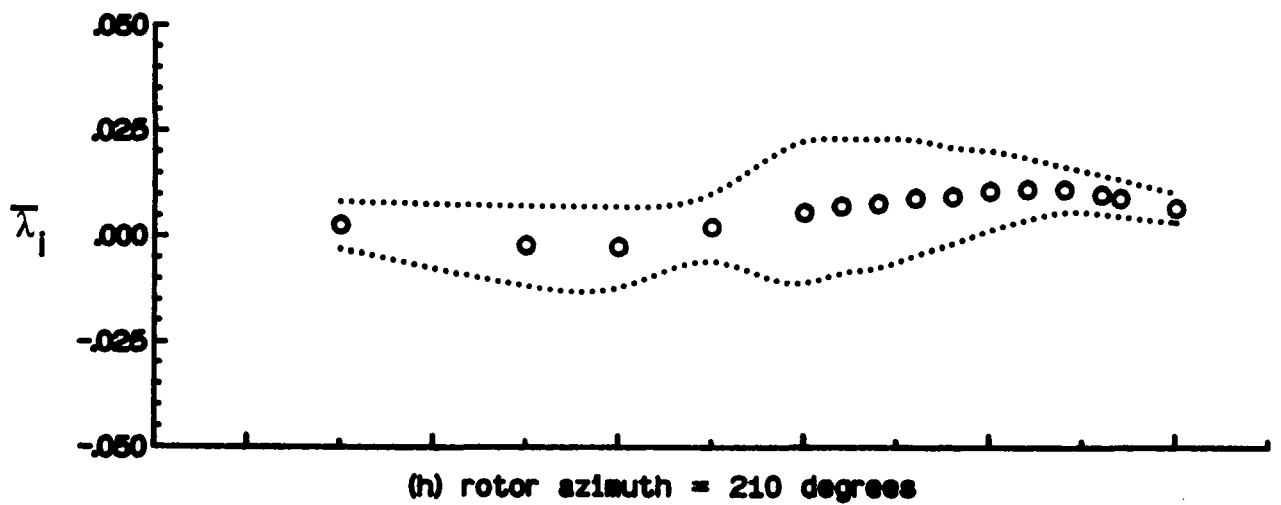
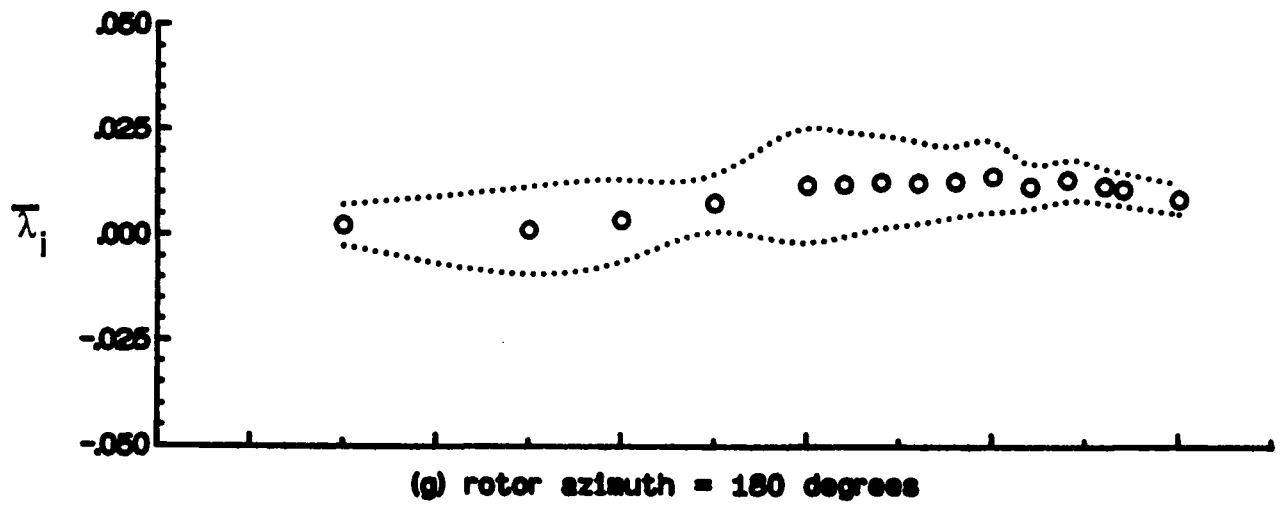


Figure 10.- Continued.

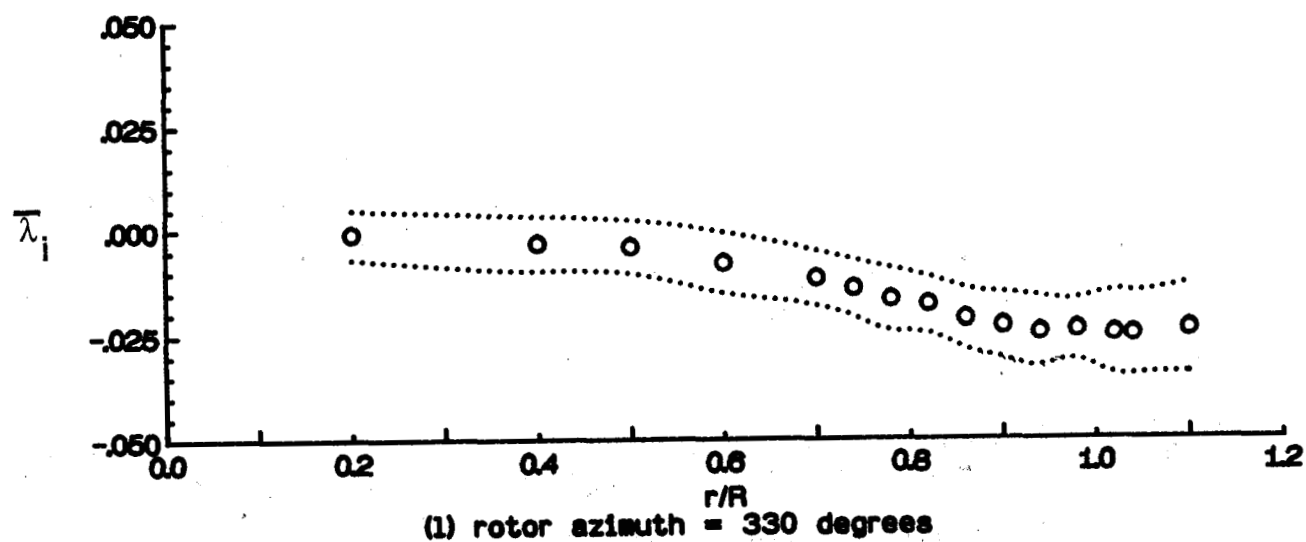
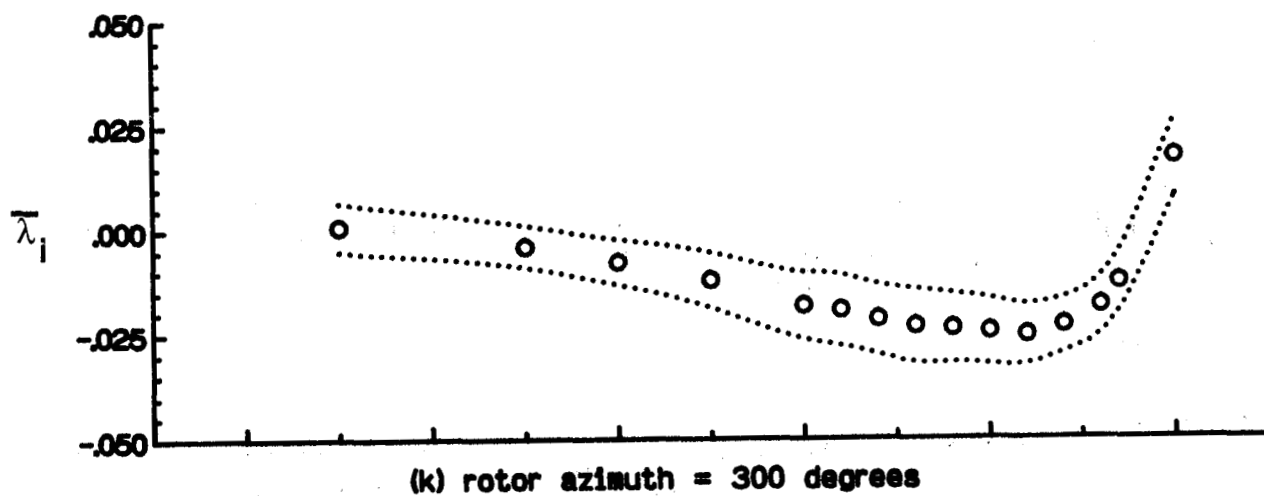
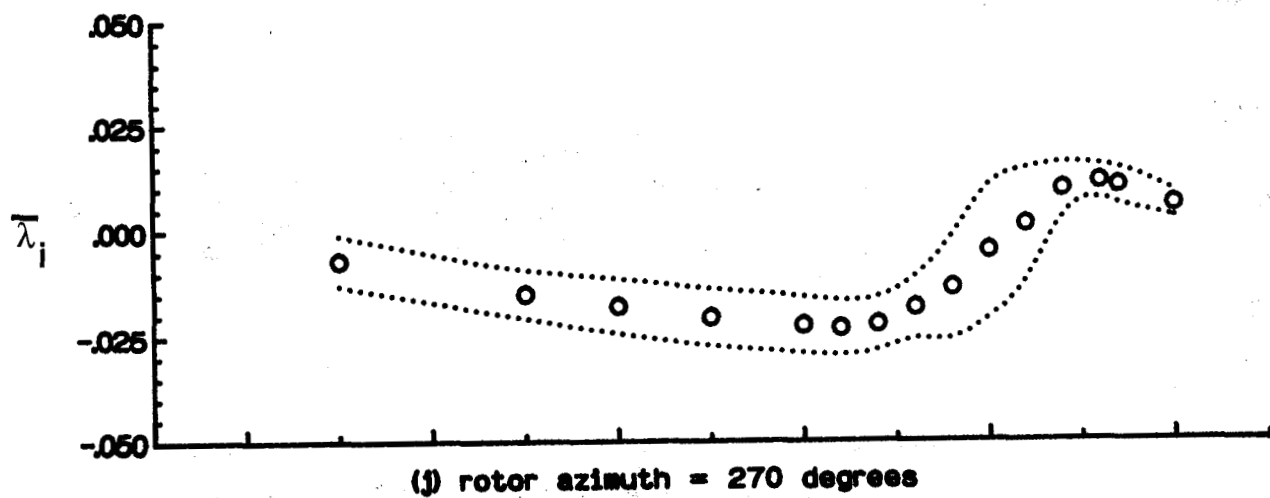
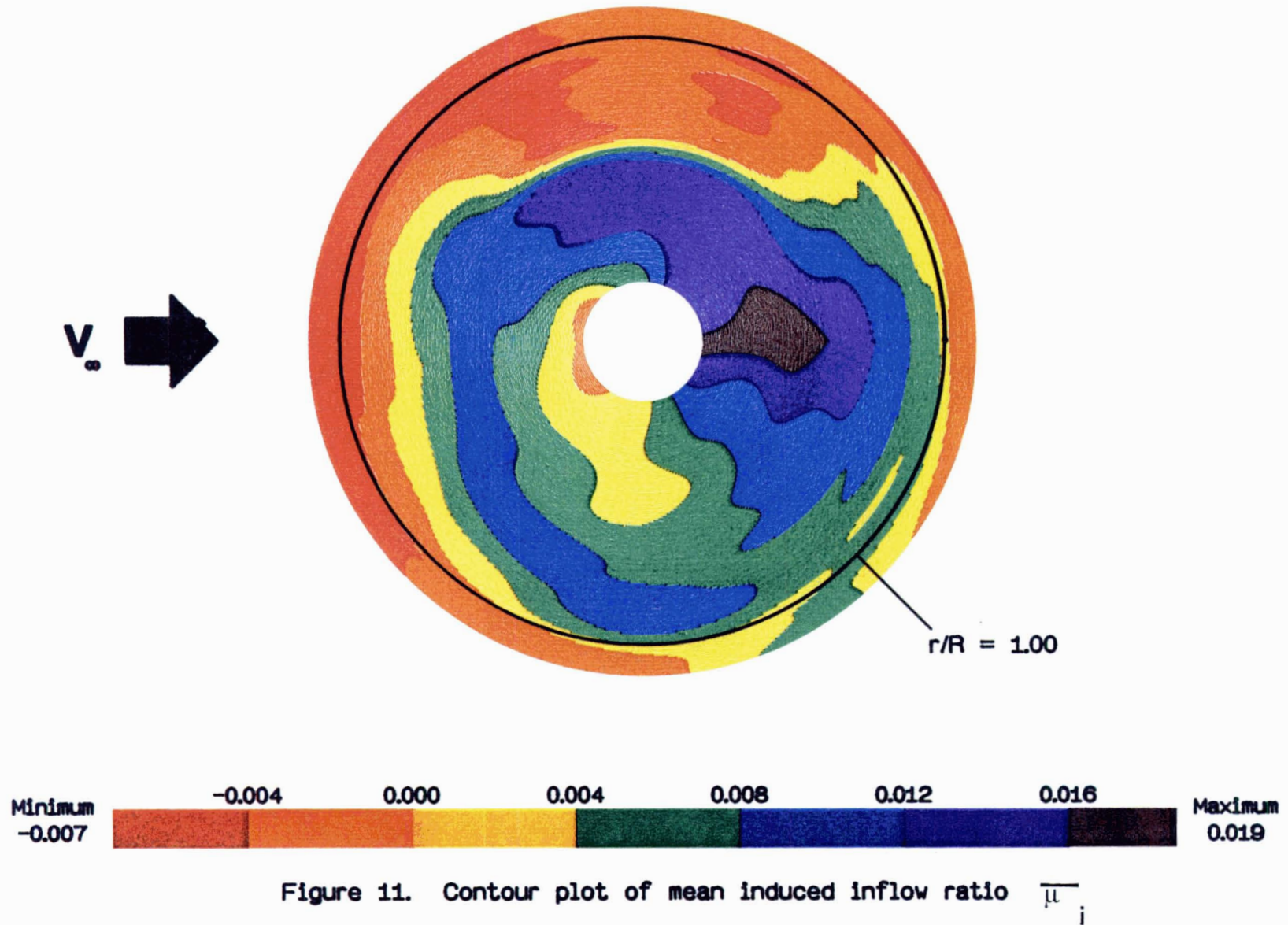


Figure 10.- Concluded.

This page intentionally left blank.





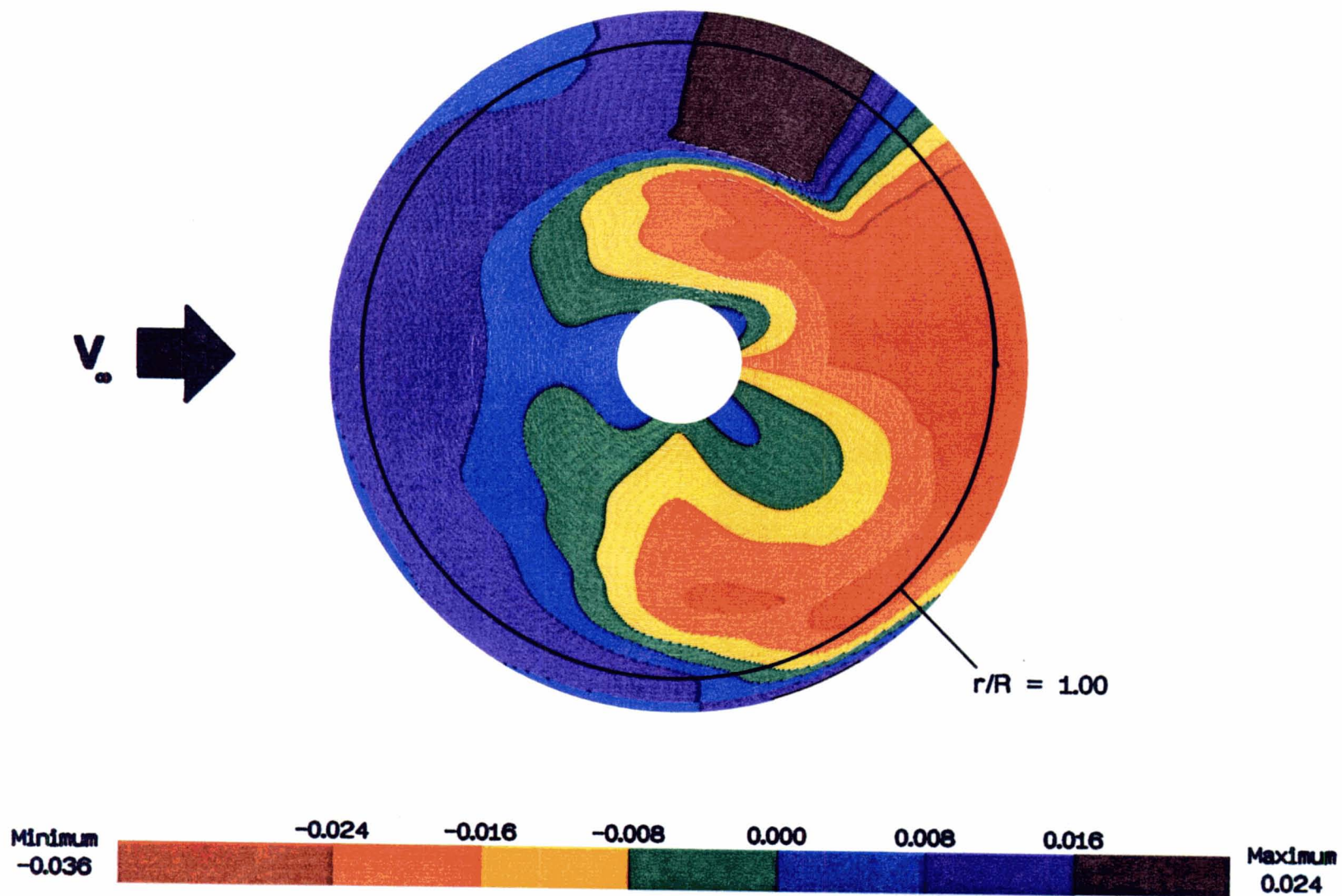


Figure 12. Contour plot of mean induced inflow ratio  $\bar{\lambda}_i$

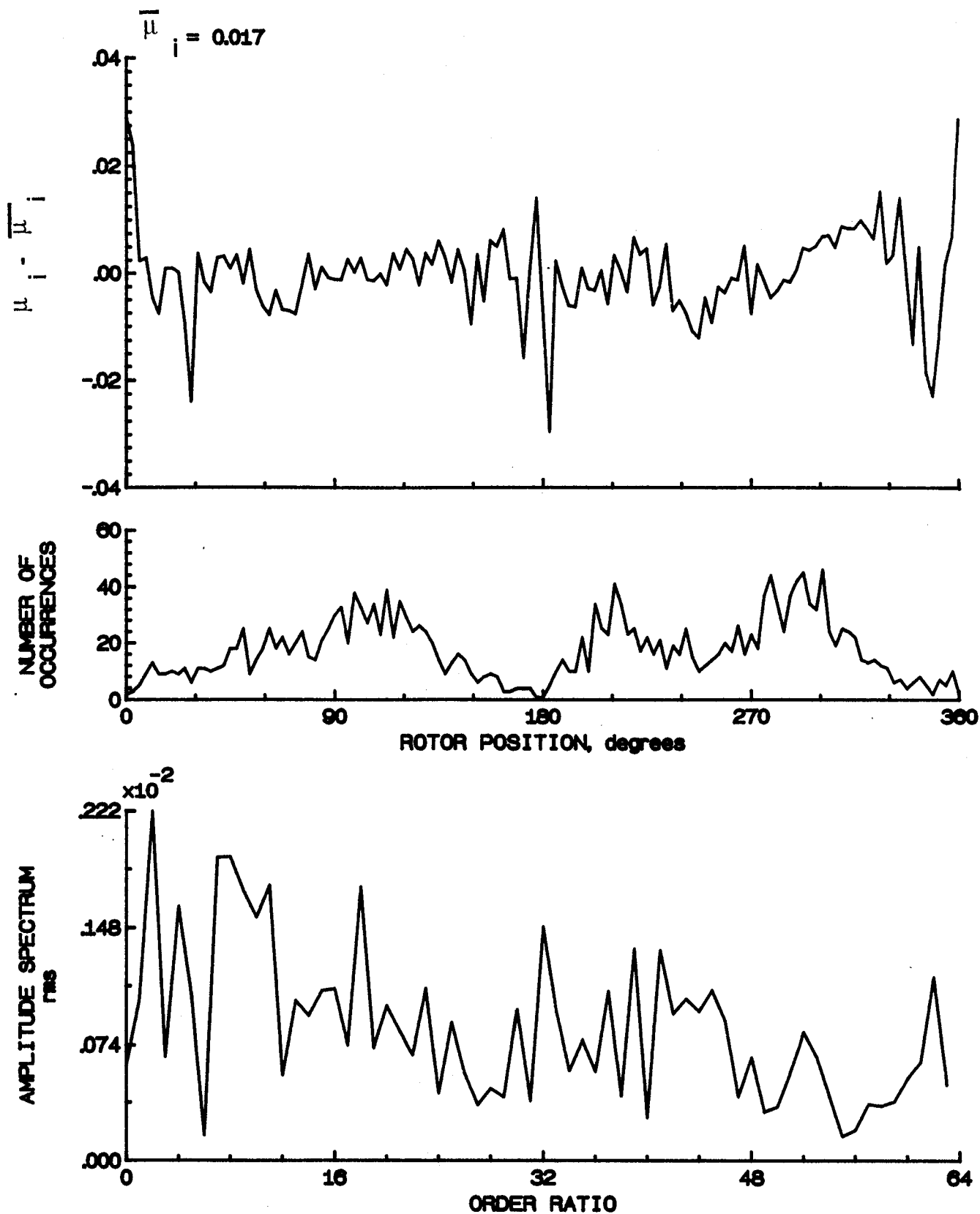


Figure 13.- Induced inflow velocity measured at 0 degrees and r/R of 0.20.

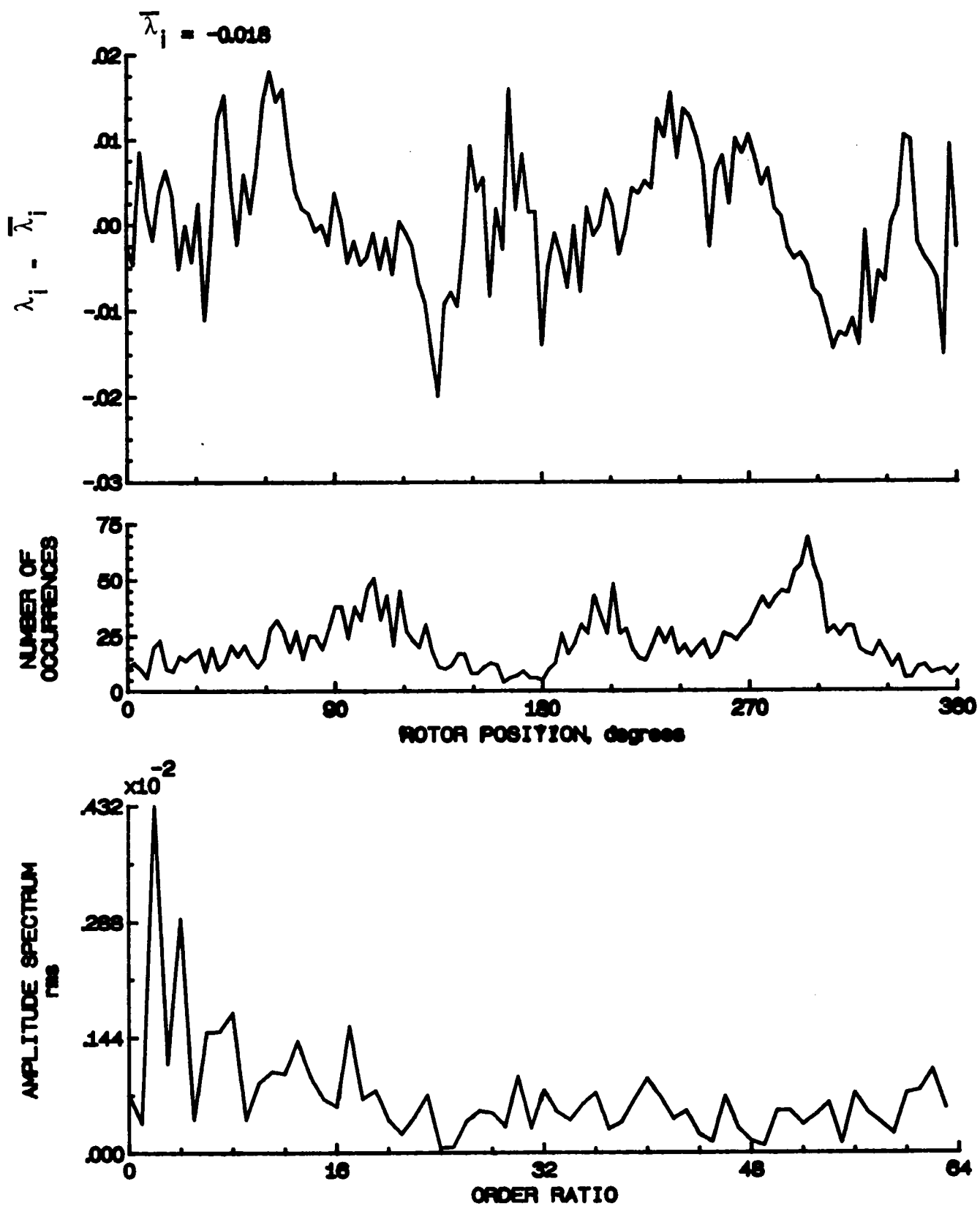


Figure 13.- Concluded.

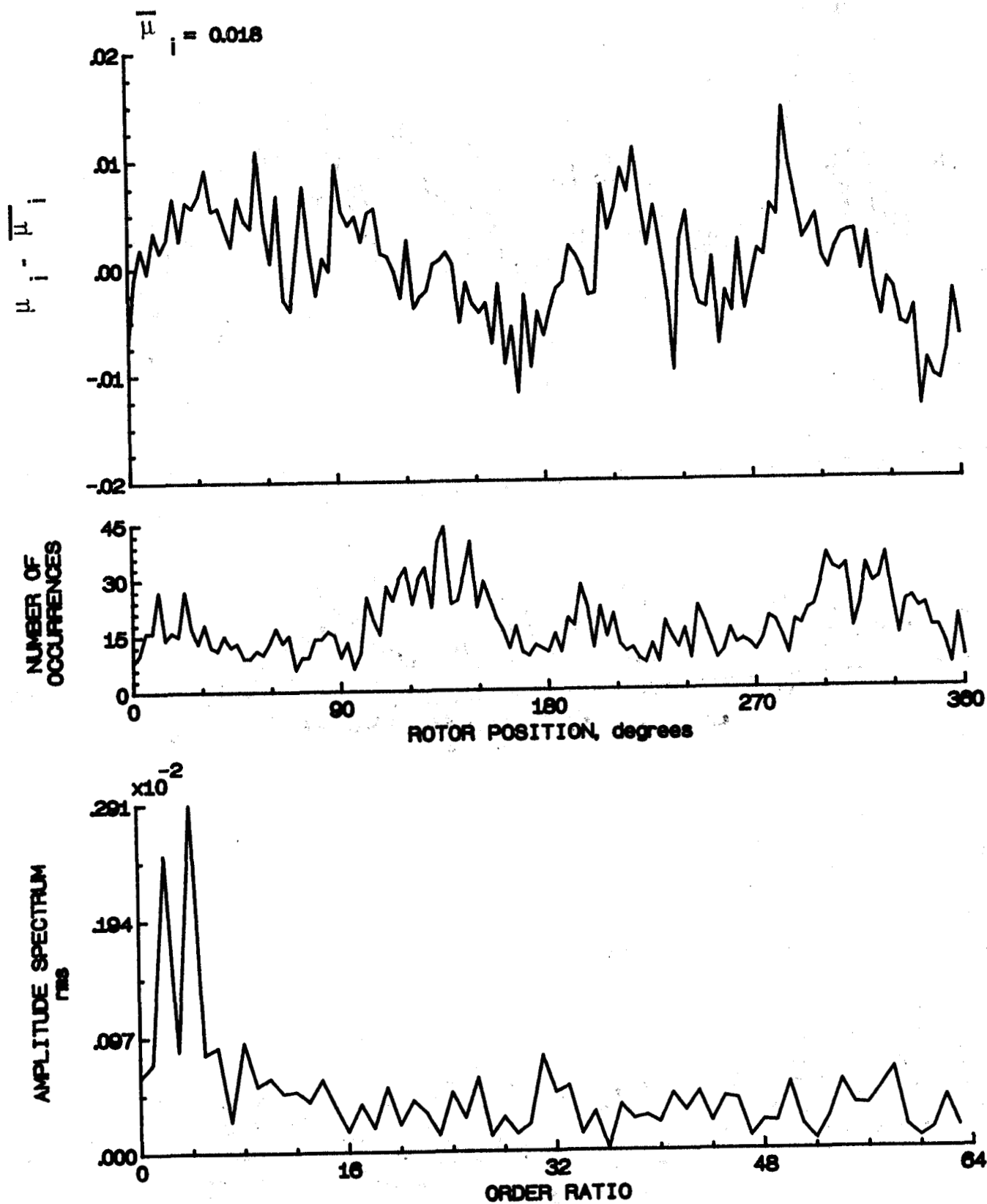


Figure 14.- Induced inflow velocity measured at 0 degrees and r/R of 0.40.

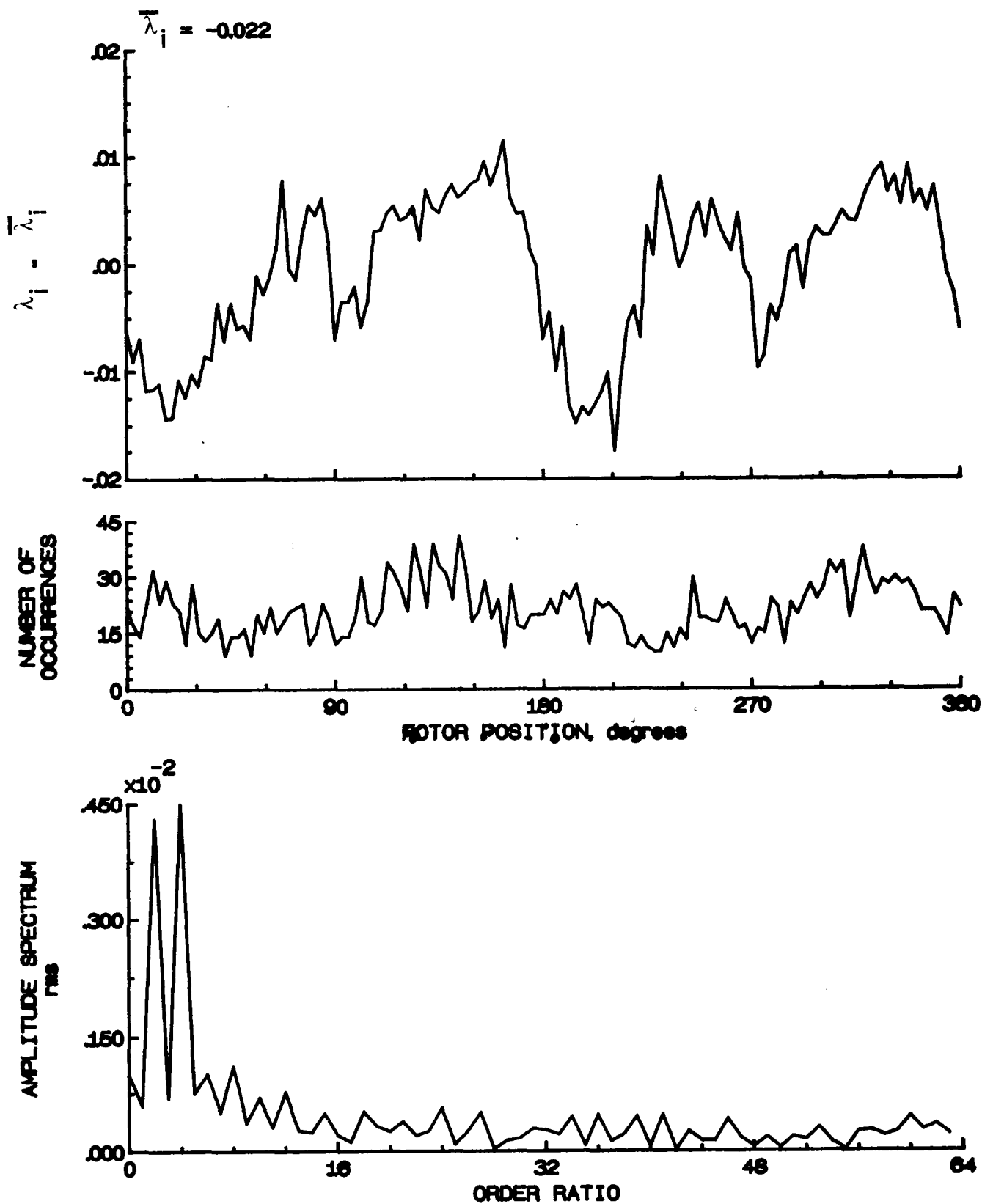


Figure 14.- Concluded.

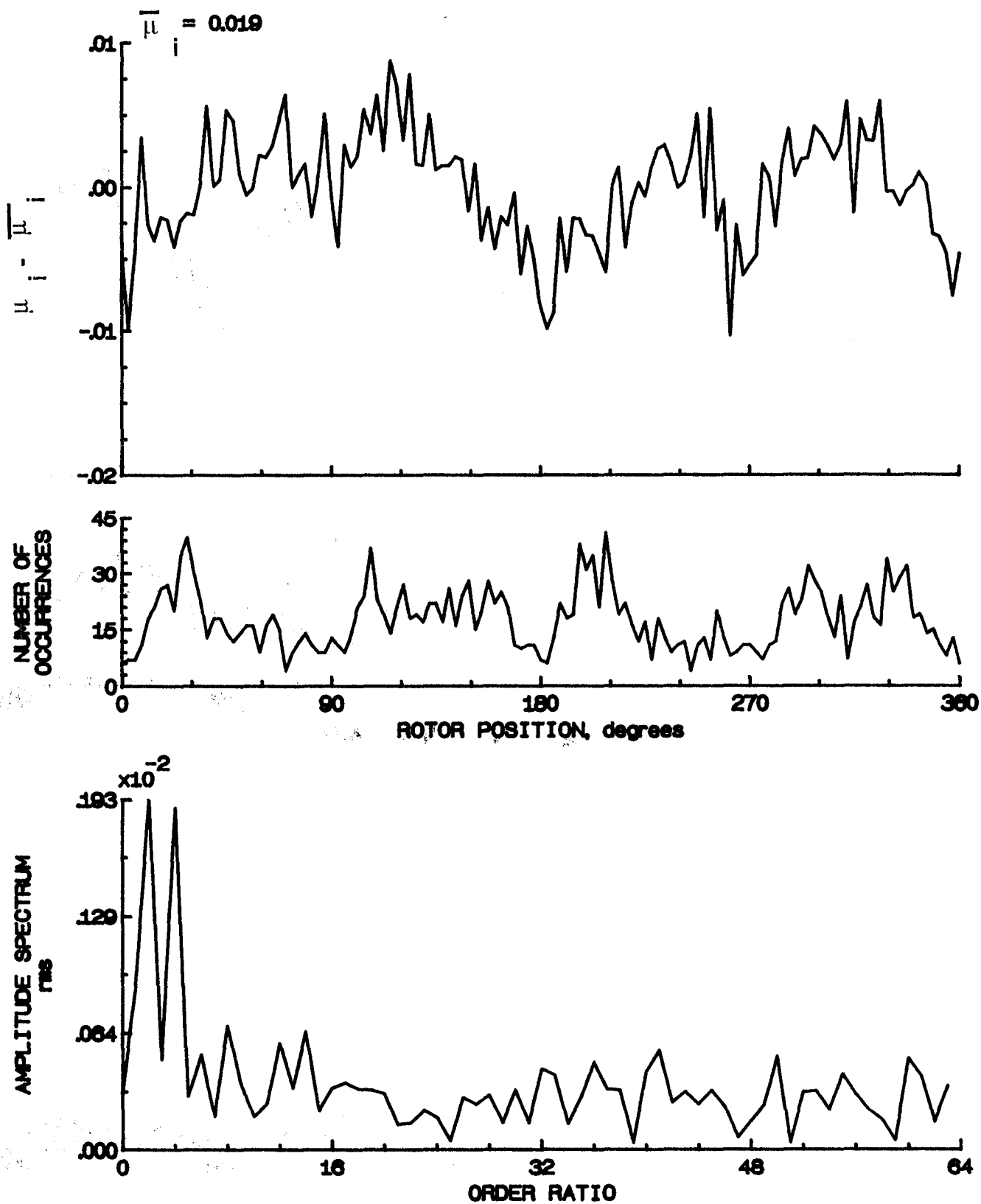


Figure 15.- Induced inflow velocity measured at 0 degrees and  $r/R$  of 0.50.

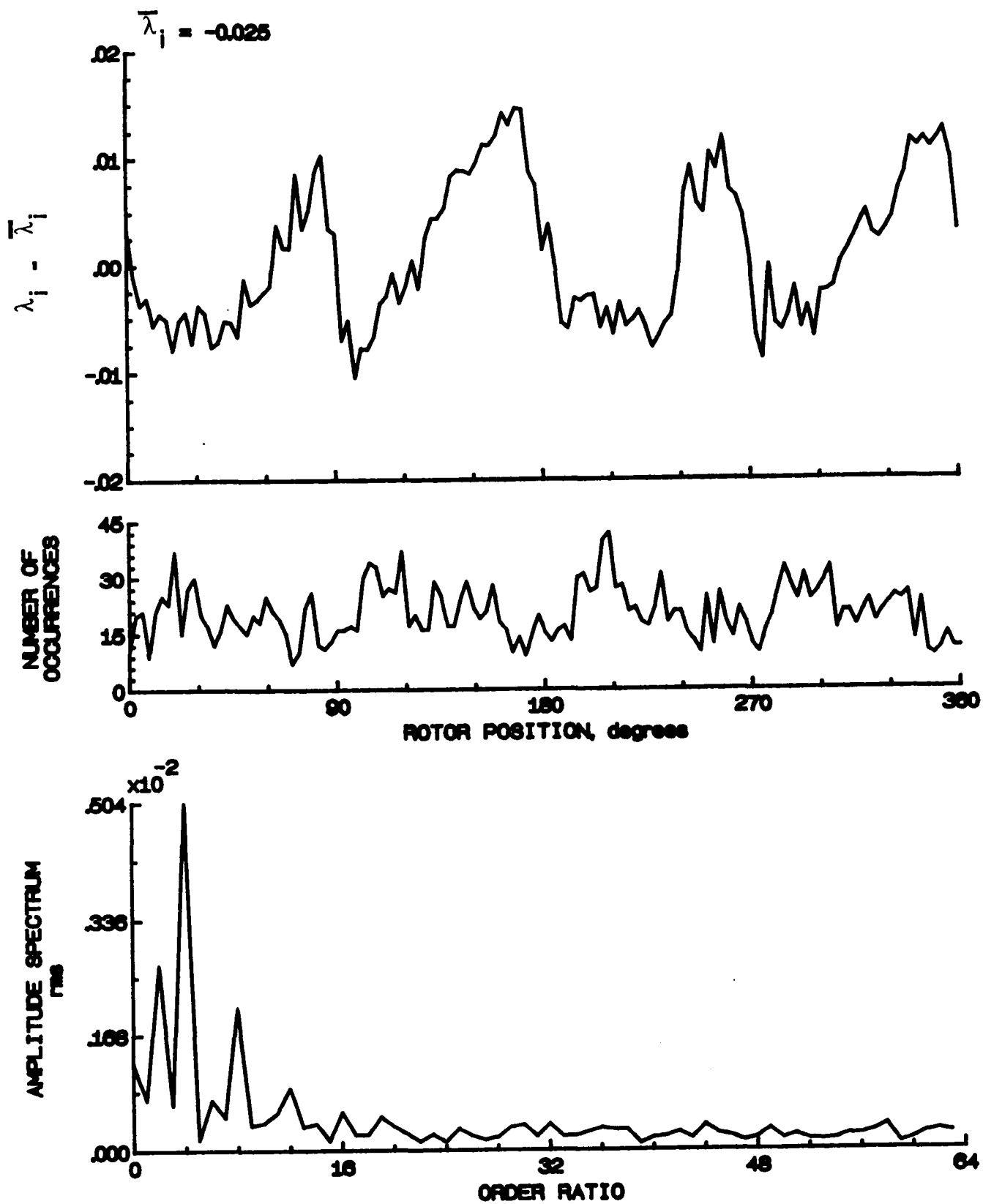


Figure 15.- Concluded.

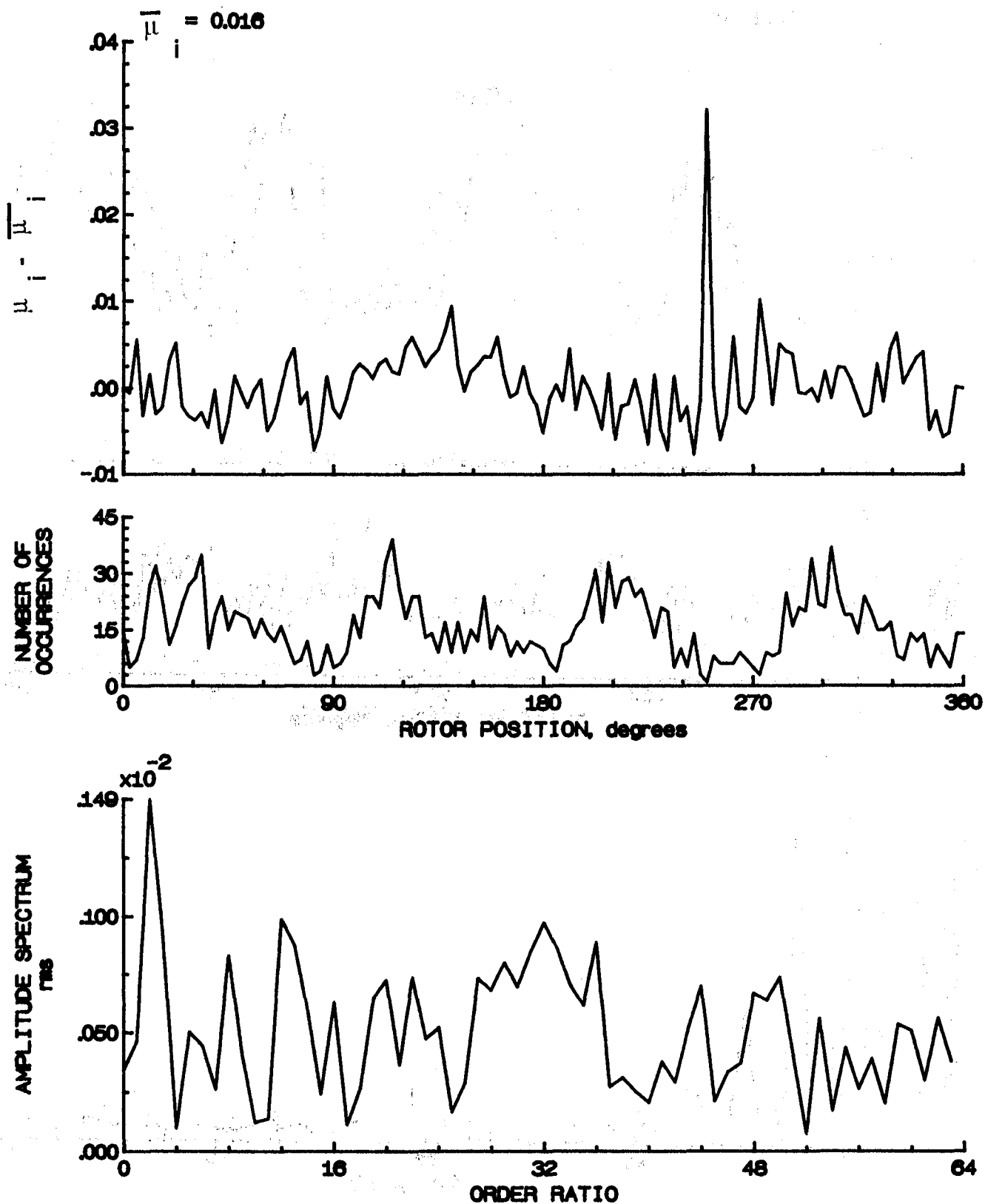


Figure 16.- Induced inflow velocity measured at 0 degrees and  $r/R$  of 0.60.



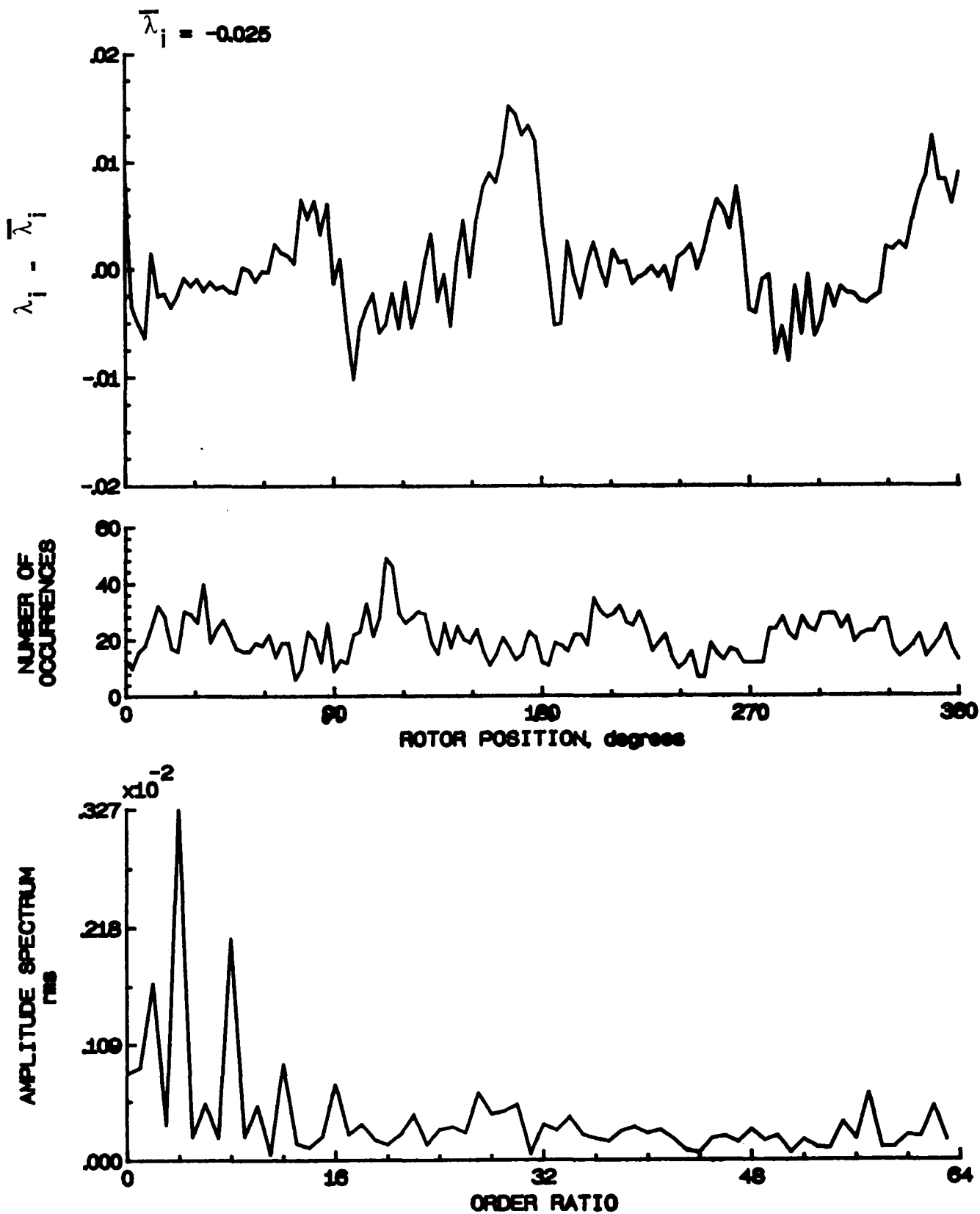


Figure 16.- Concluded.

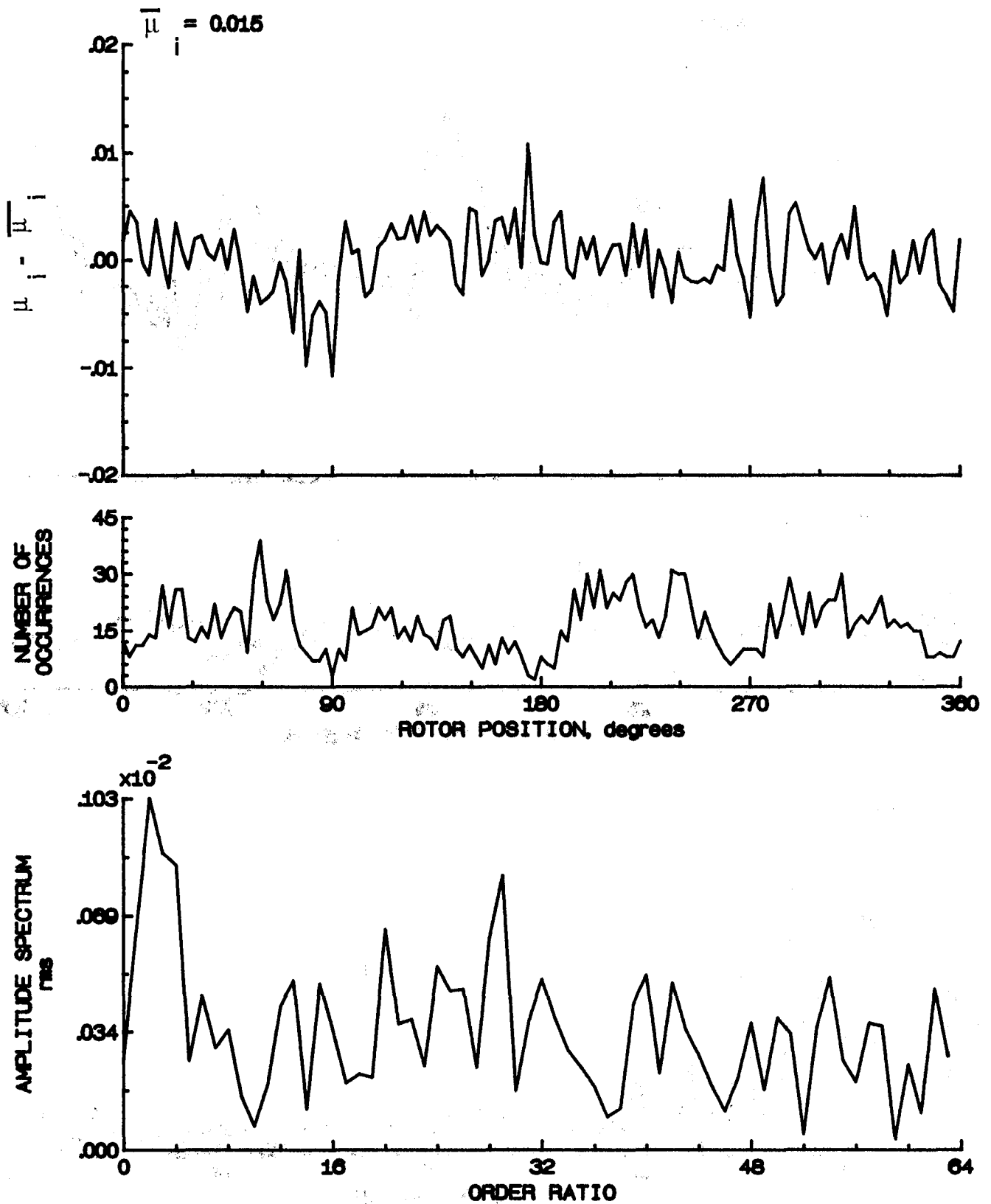


Figure 17.- Induced inflow velocity measured at 0 degrees and  $r/R$  of 0.70.

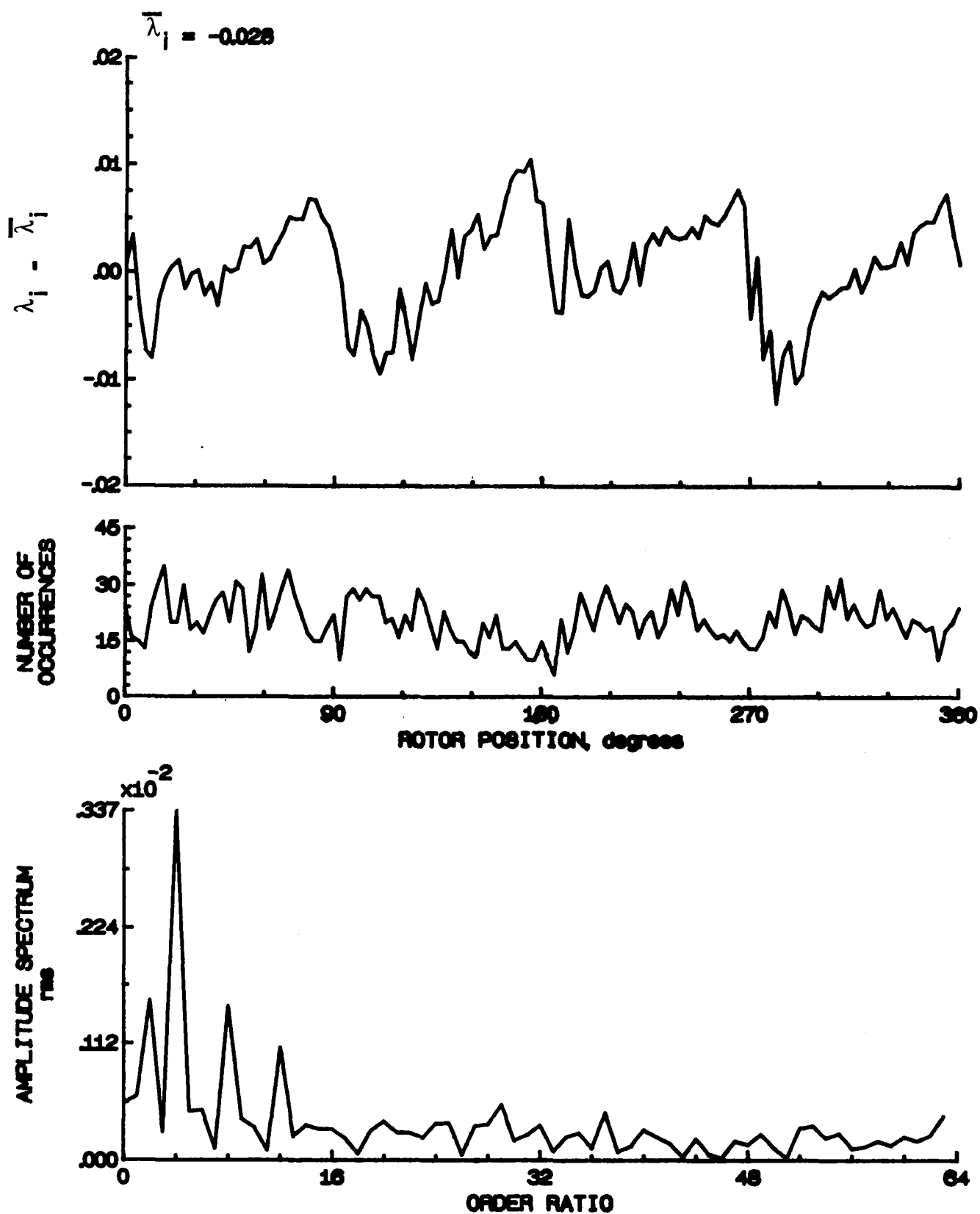


Figure 17.- Concluded.

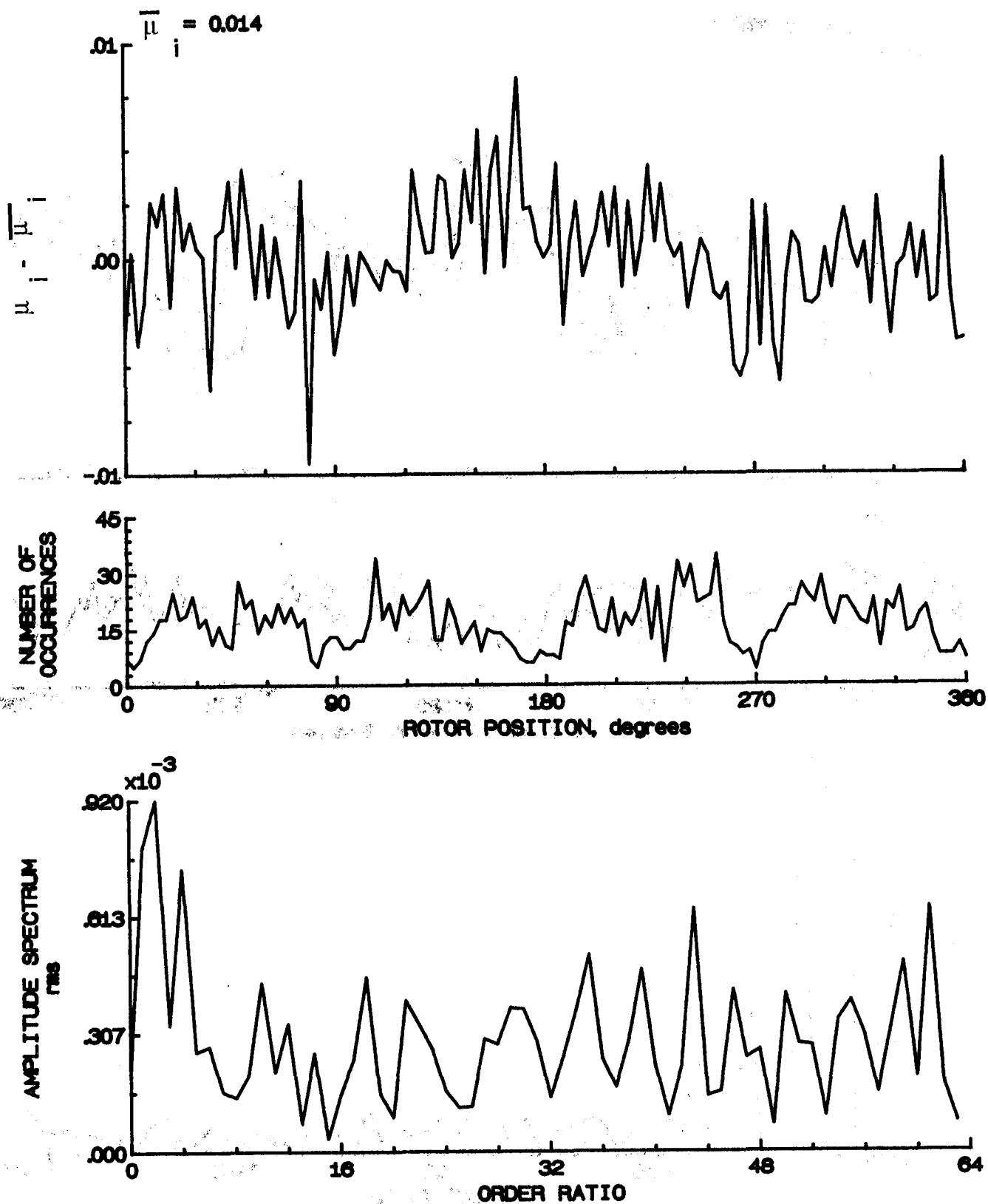


Figure 18.- Induced inflow velocity measured at 0 degrees and  $r/R$  of 0.74.

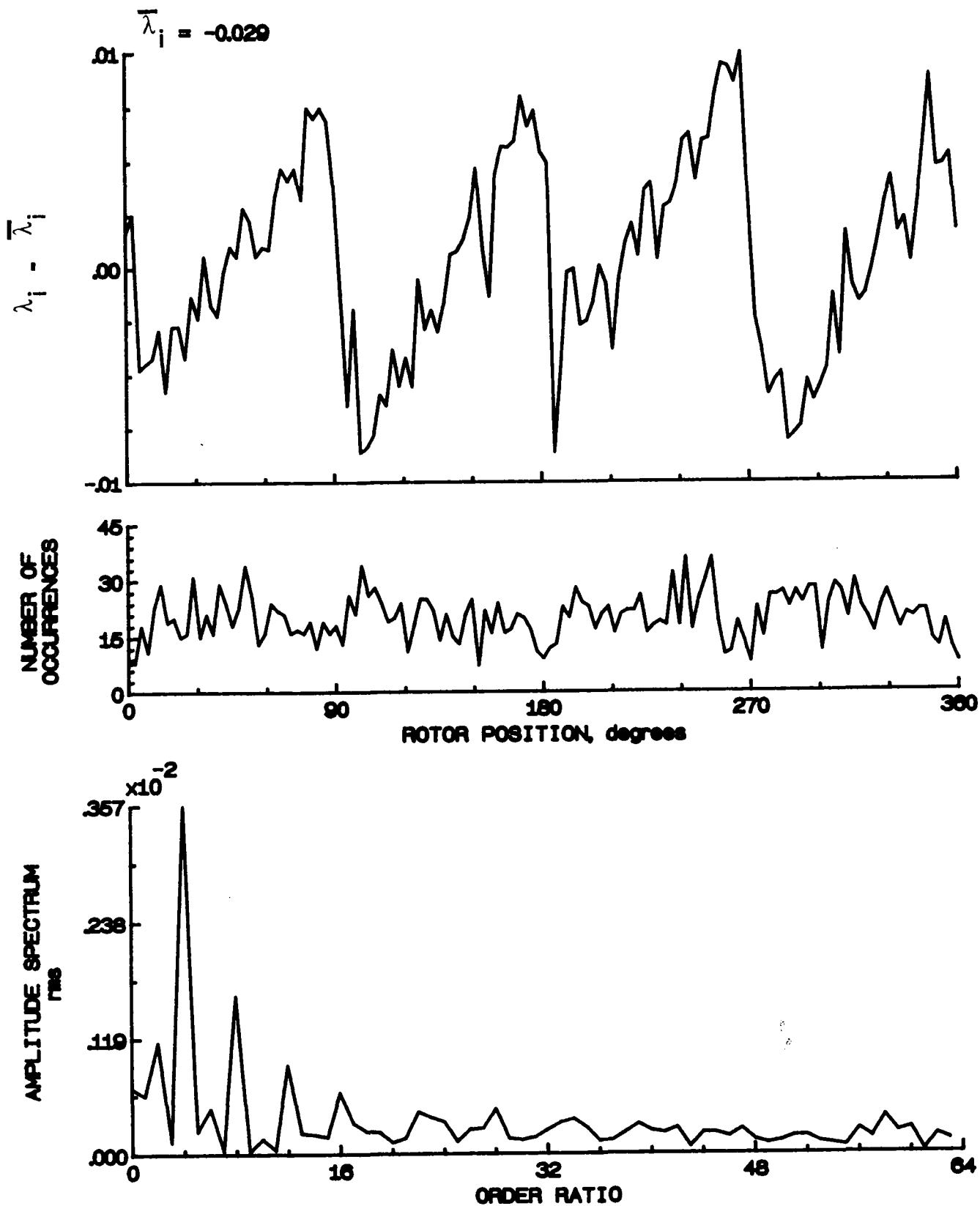


Figure 18.- Concluded.

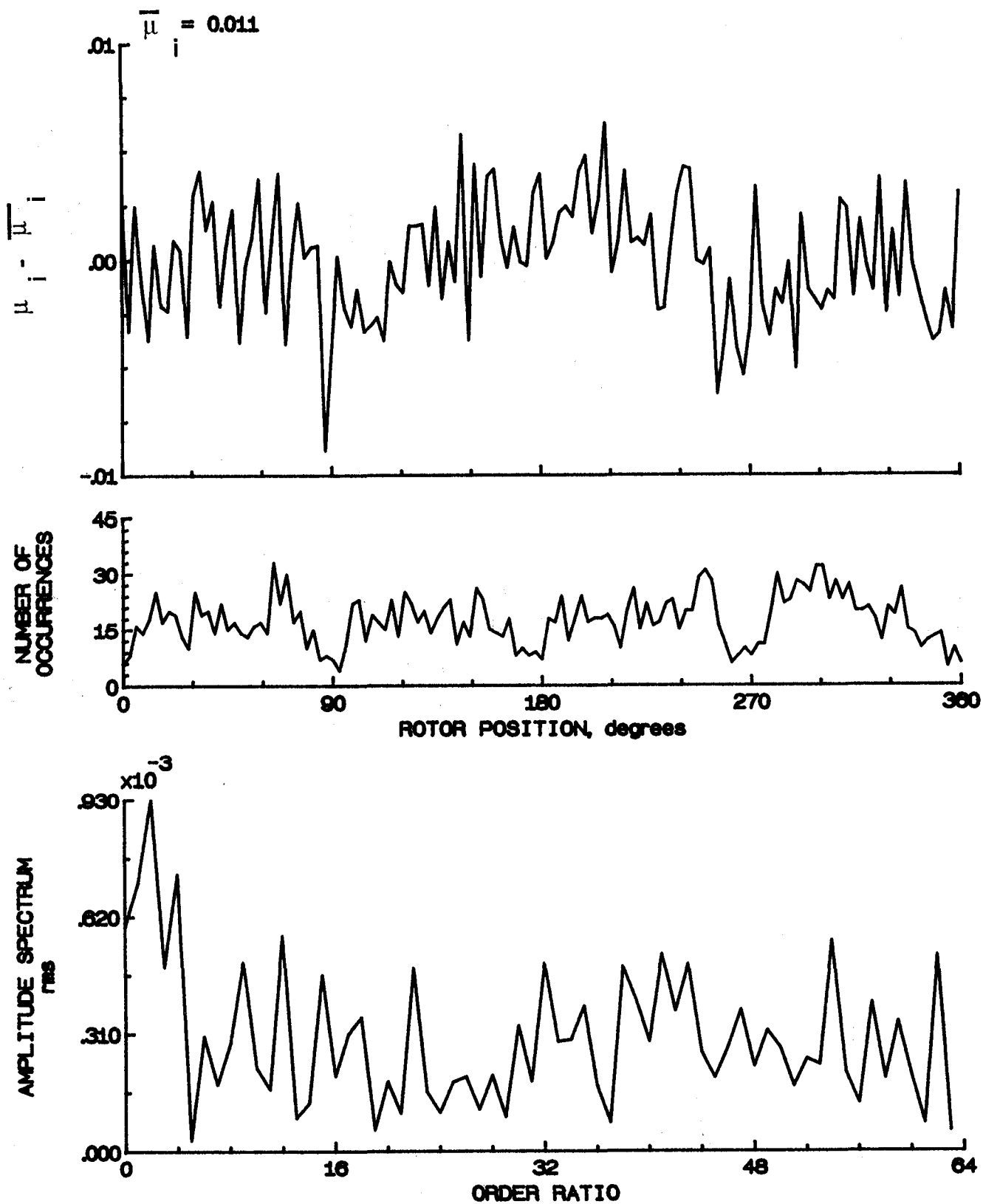


Figure 19.- Induced inflow velocity measured at 0 degrees and r/R of 0.78.

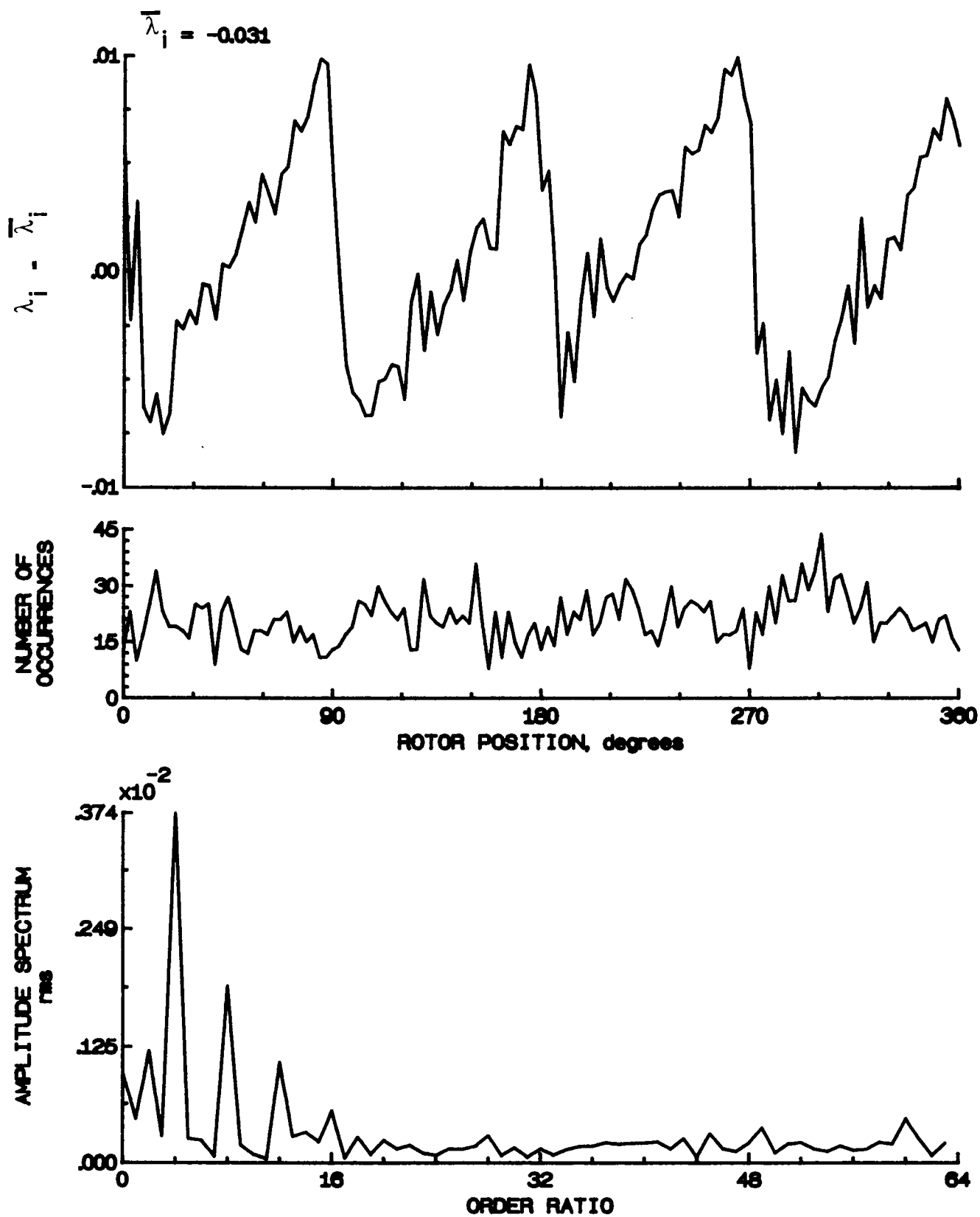


Figure 19.- Concluded.

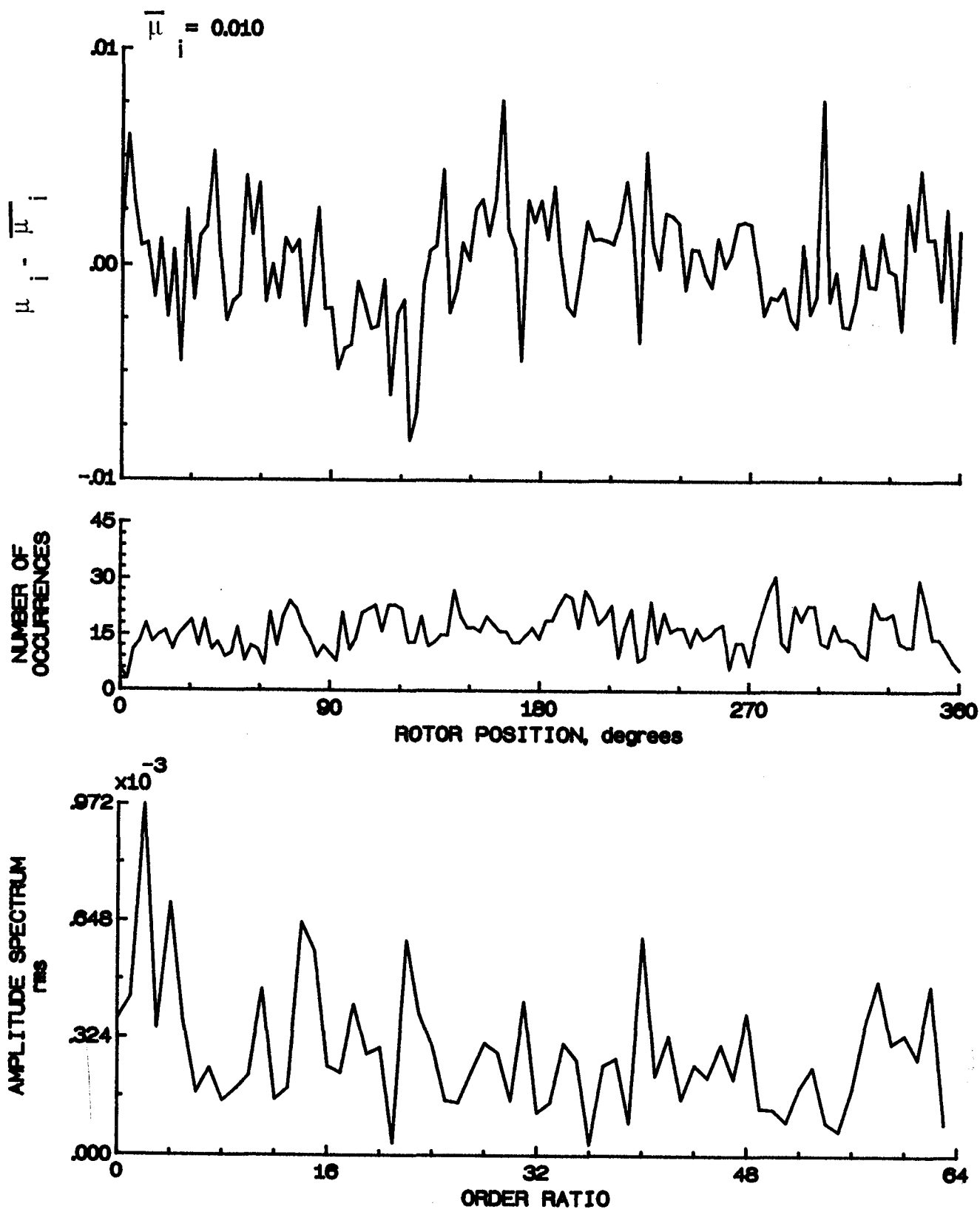


Figure 20.- Induced inflow velocity measured at 0 degrees and r/R of 0.82.



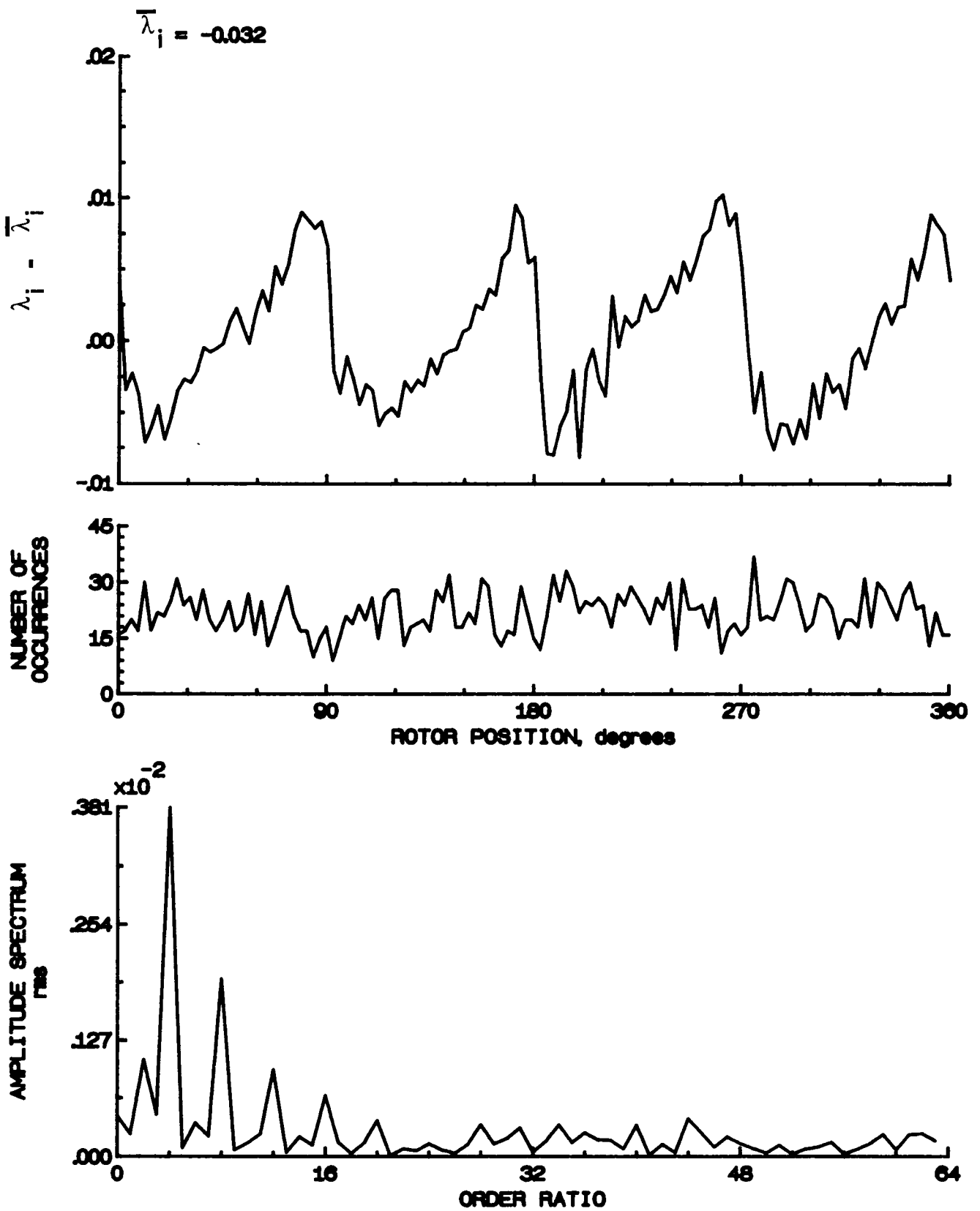


Figure 20.- Concluded.

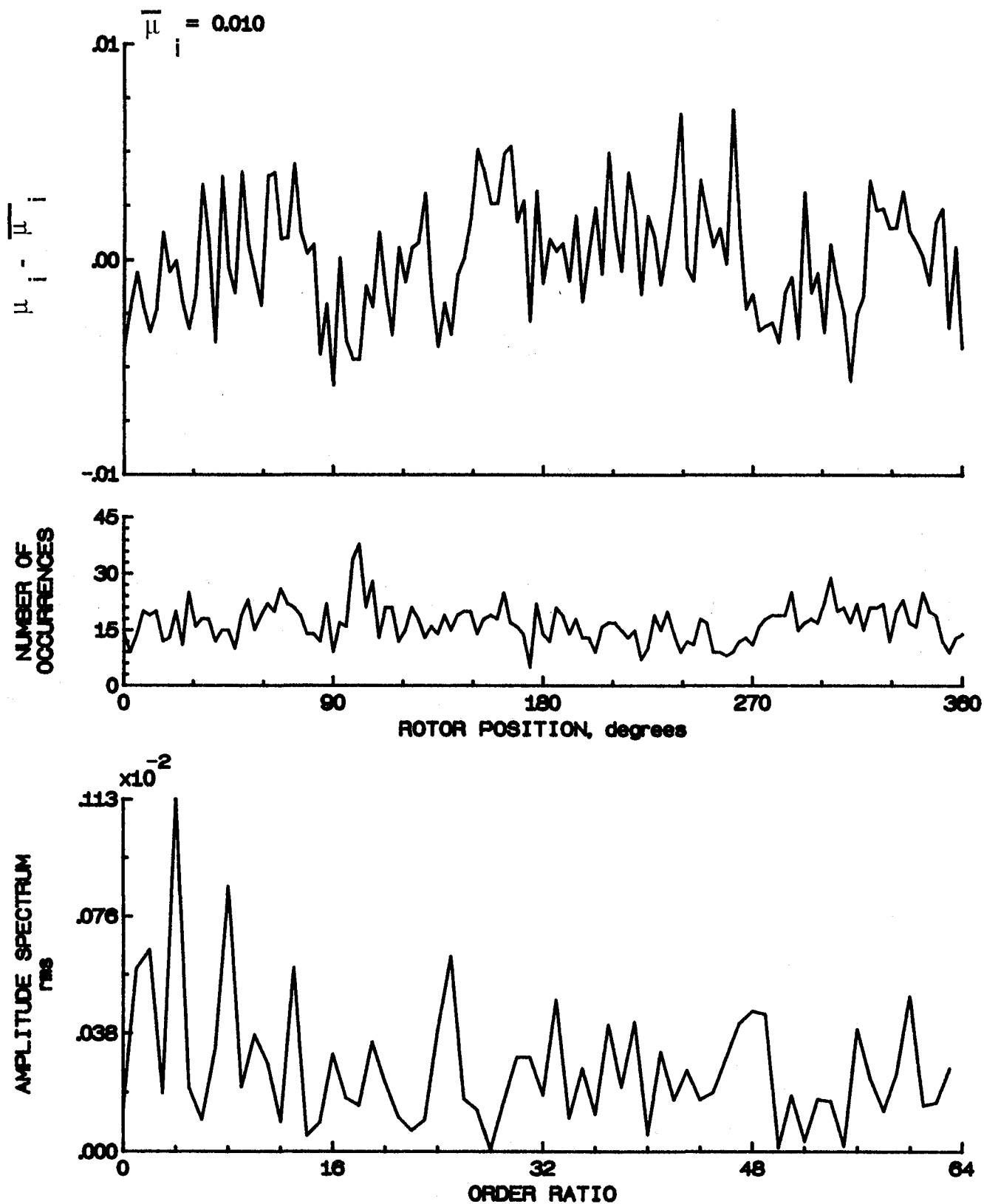


Figure 21.- Induced inflow velocity measured at 0 degrees and r/R of 0.86.

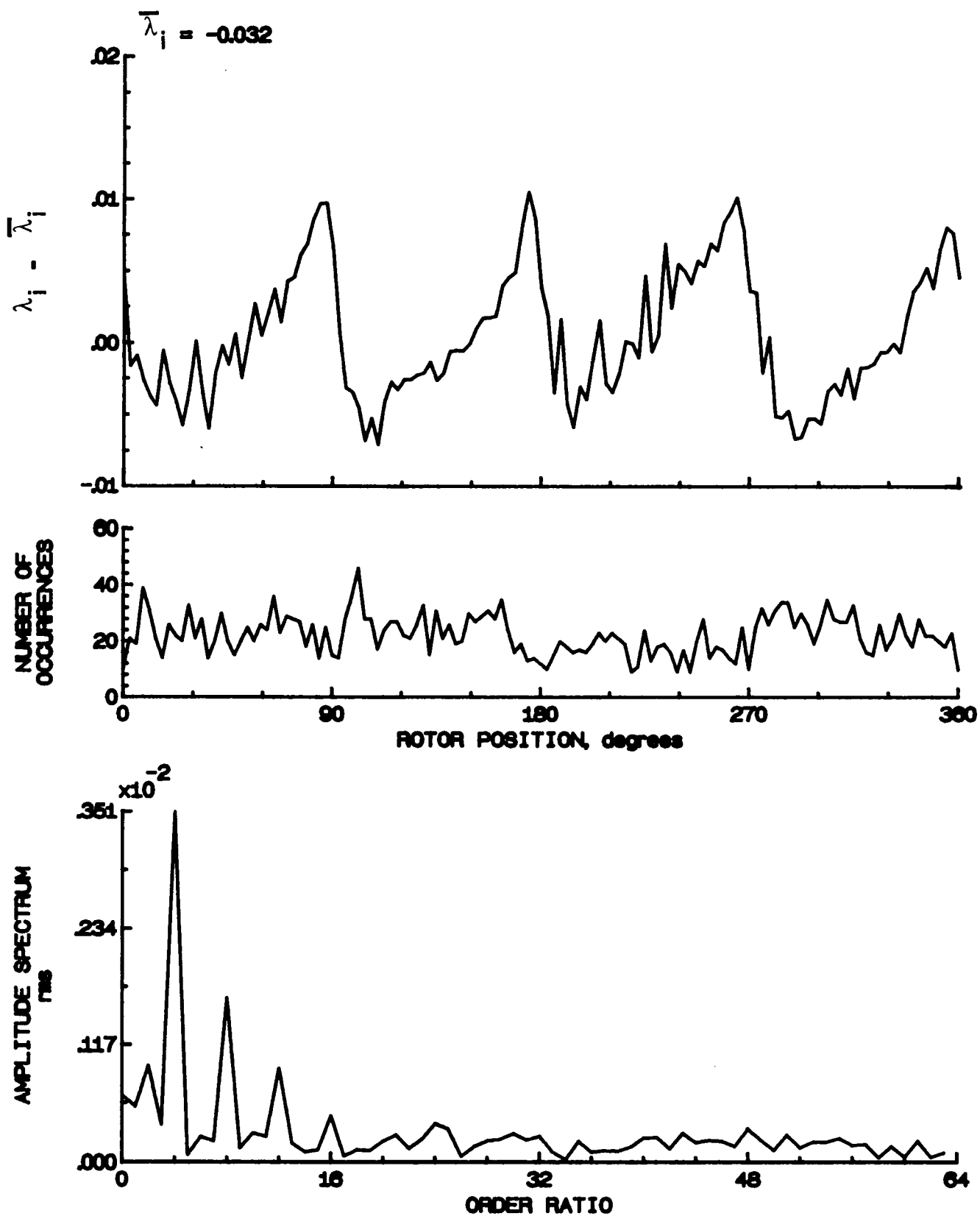


Figure 21- Concluded.

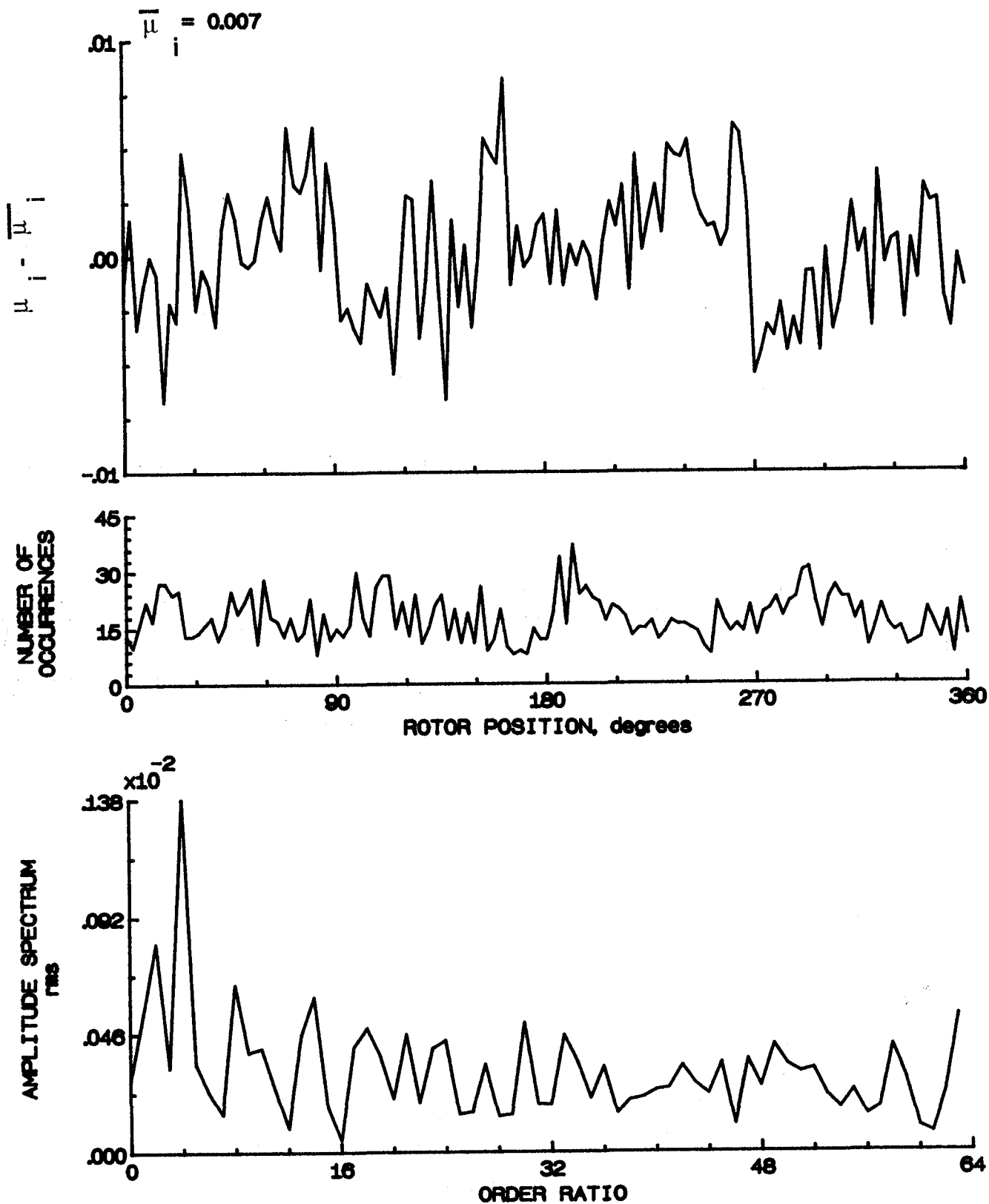


Figure 22.- Induced inflow velocity measured at 0 degrees and r/R of 0.90.

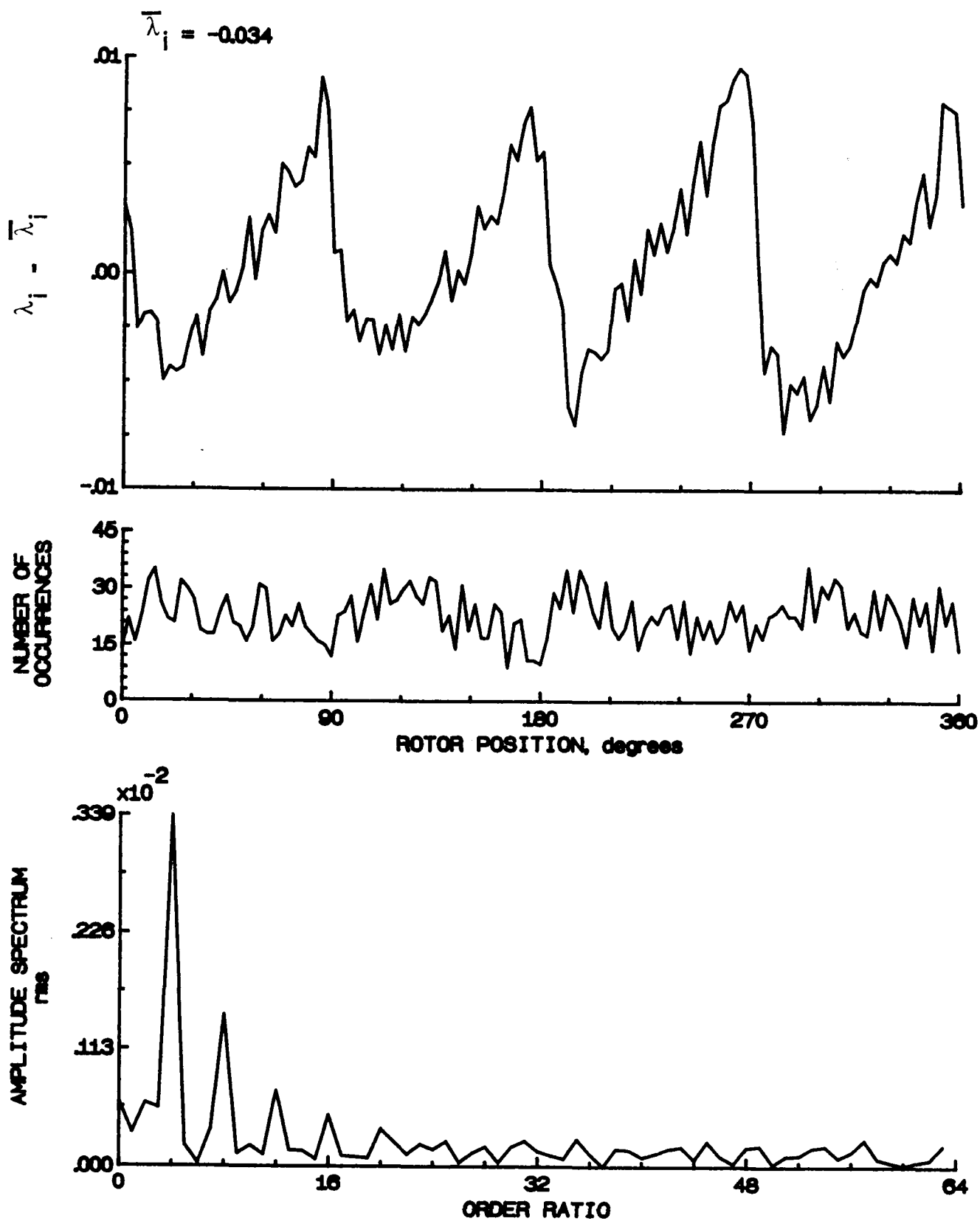


Figure 22.- Concluded.

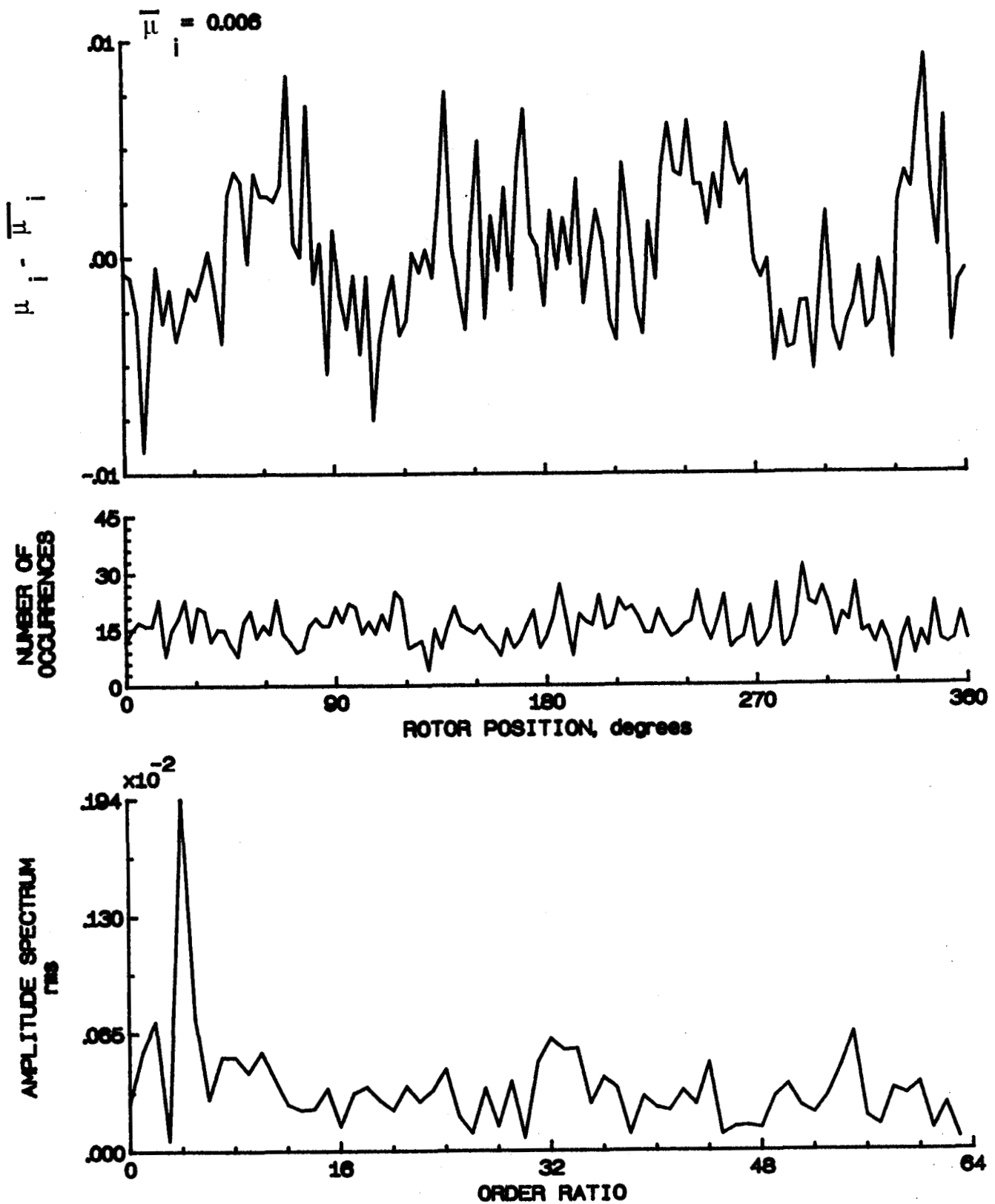


Figure 23.- Induced inflow velocity measured at 0 degrees and r/R of 0.94.

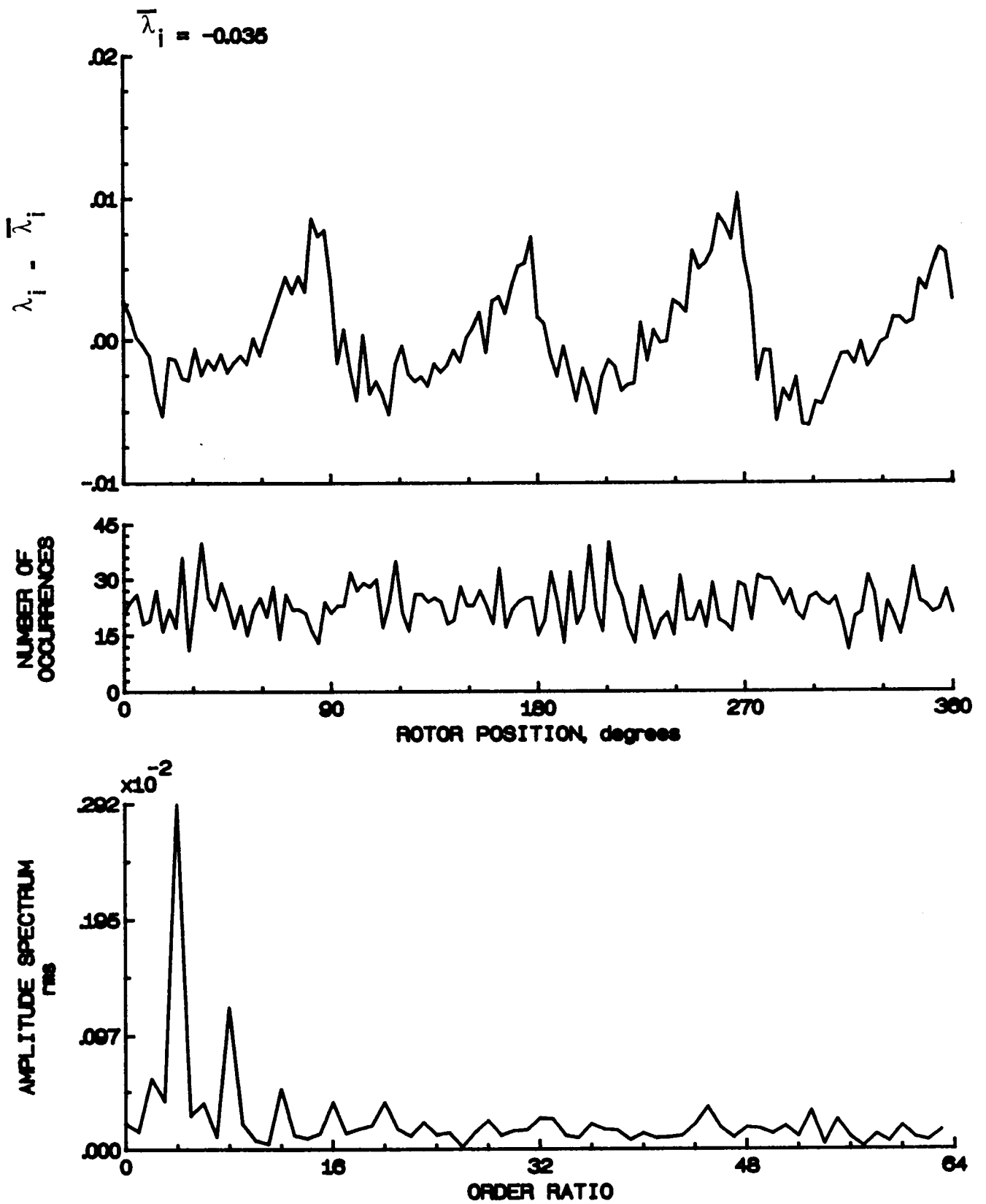


Figure 23.- Concluded.

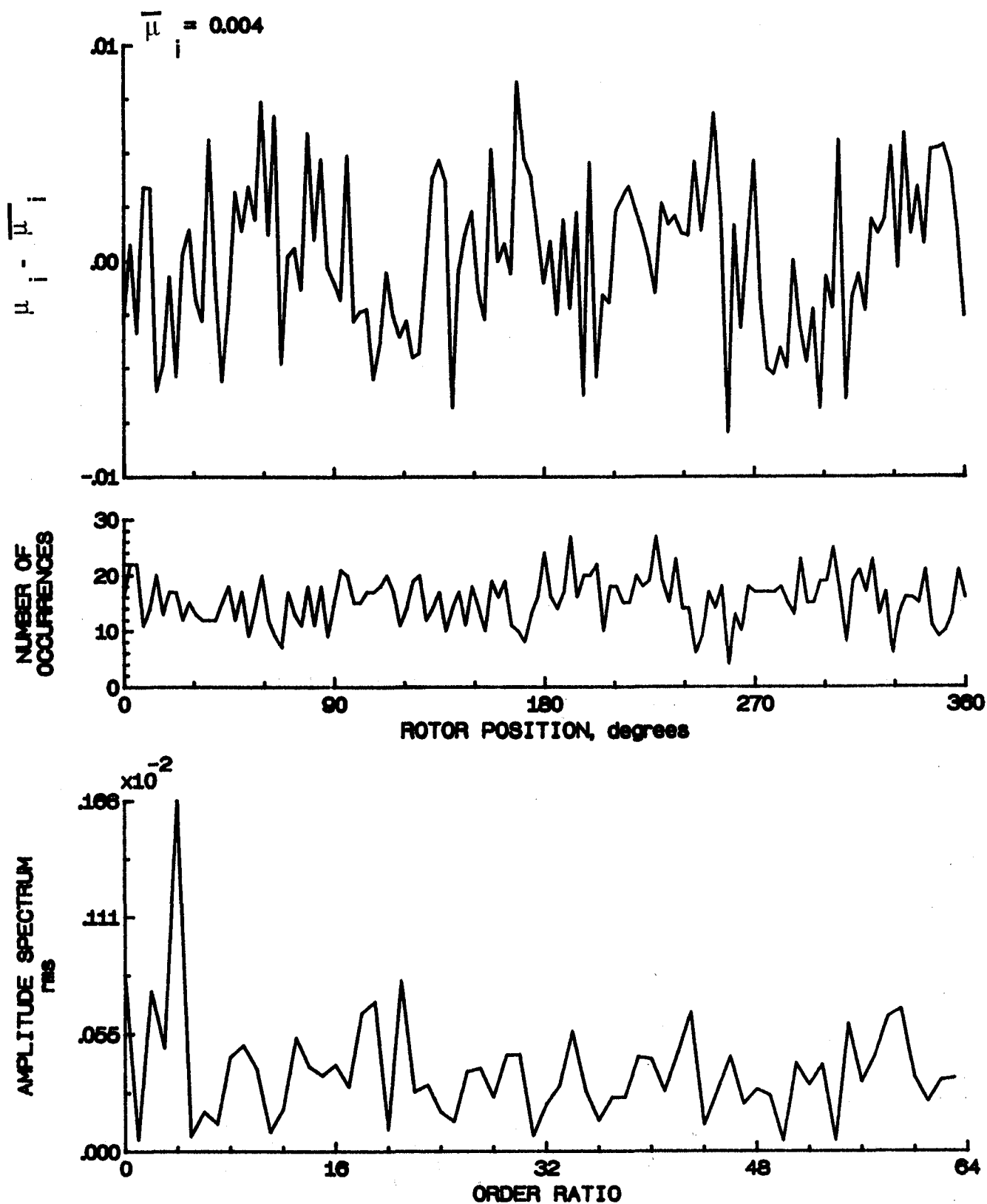


Figure 24.- Induced inflow velocity measured at 0 degrees and  $r/R$  of 0.98.



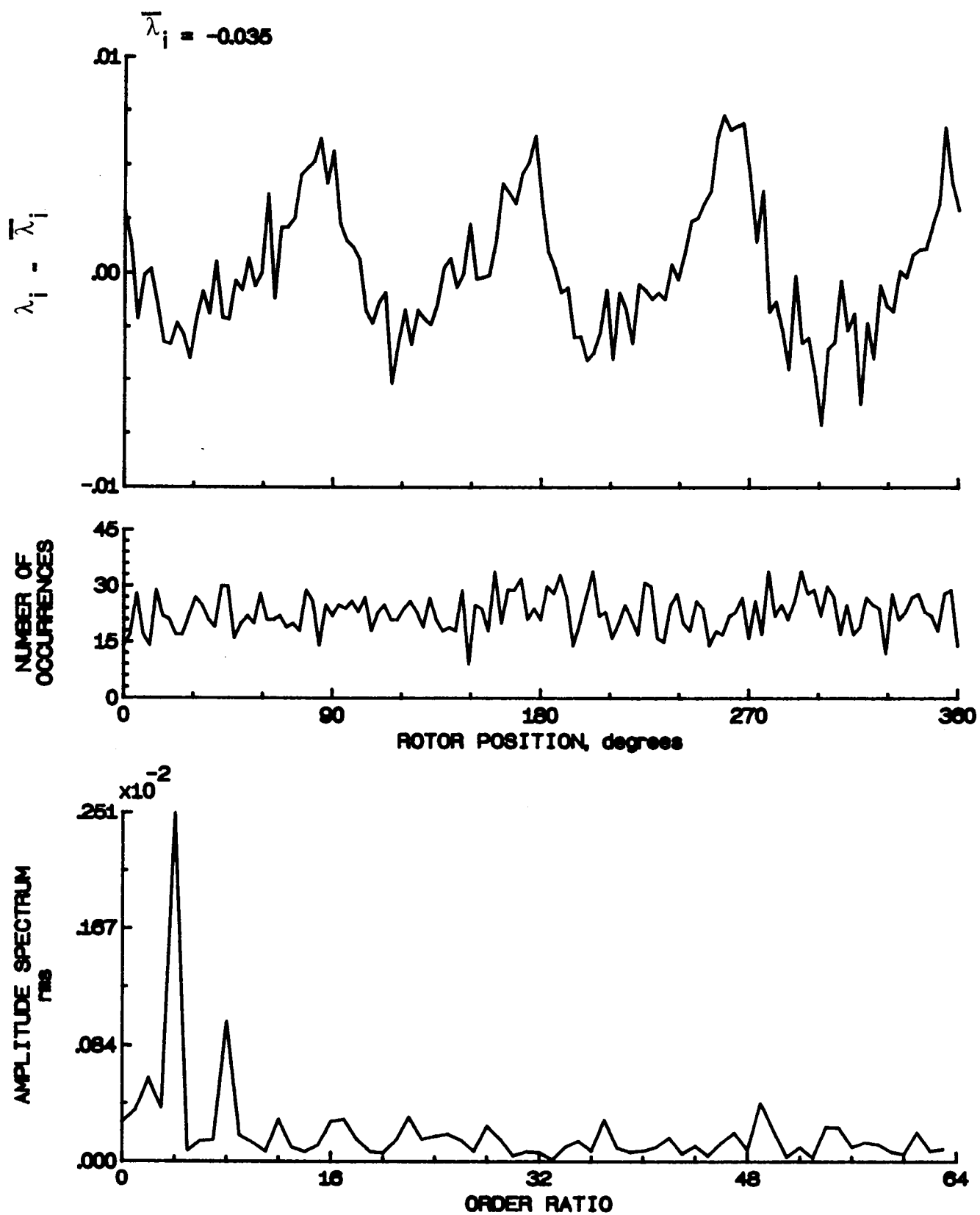


Figure 24.- Concluded.

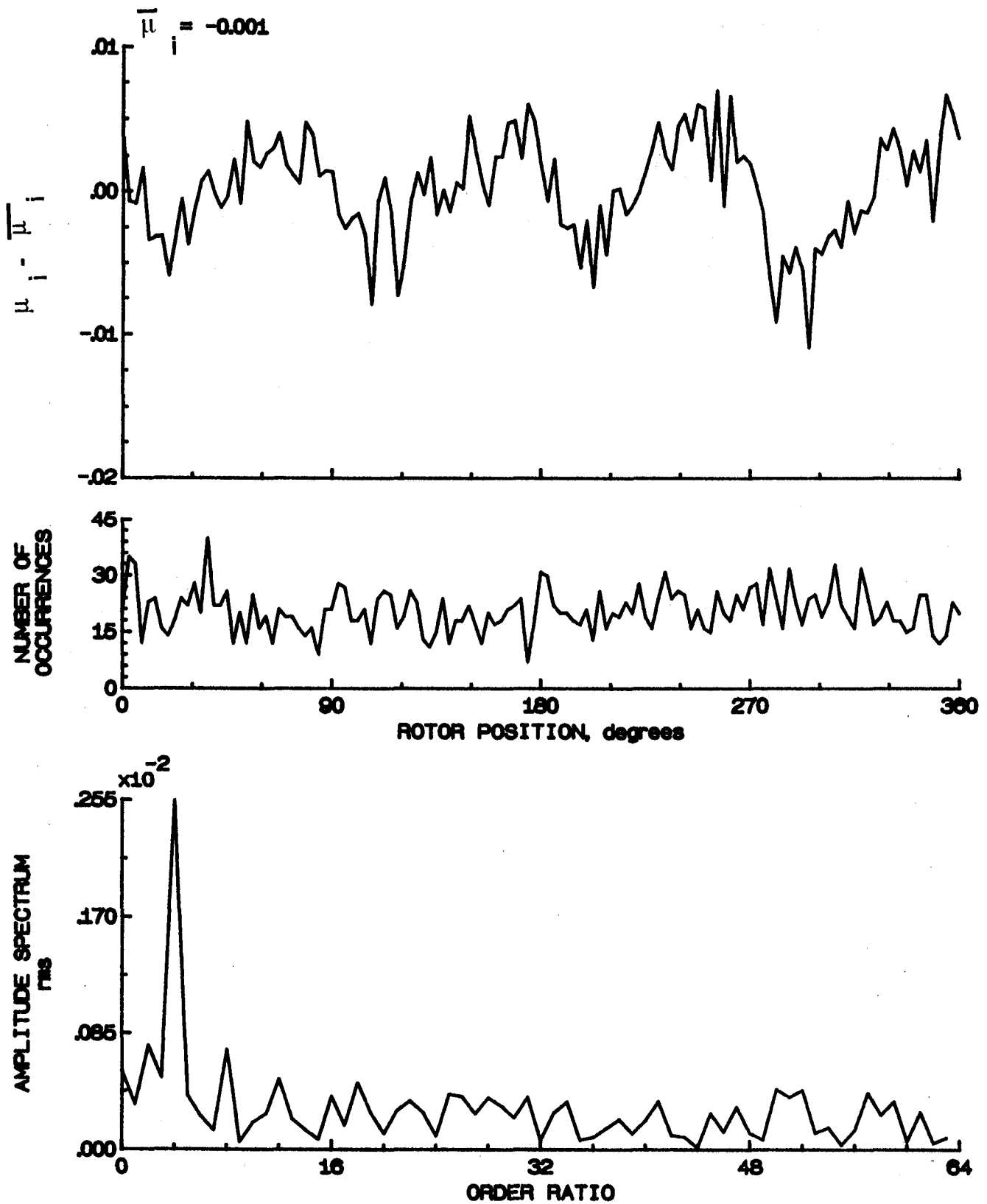


Figure 25.- Induced inflow velocity measured at 0 degrees and r/R of 1.02.

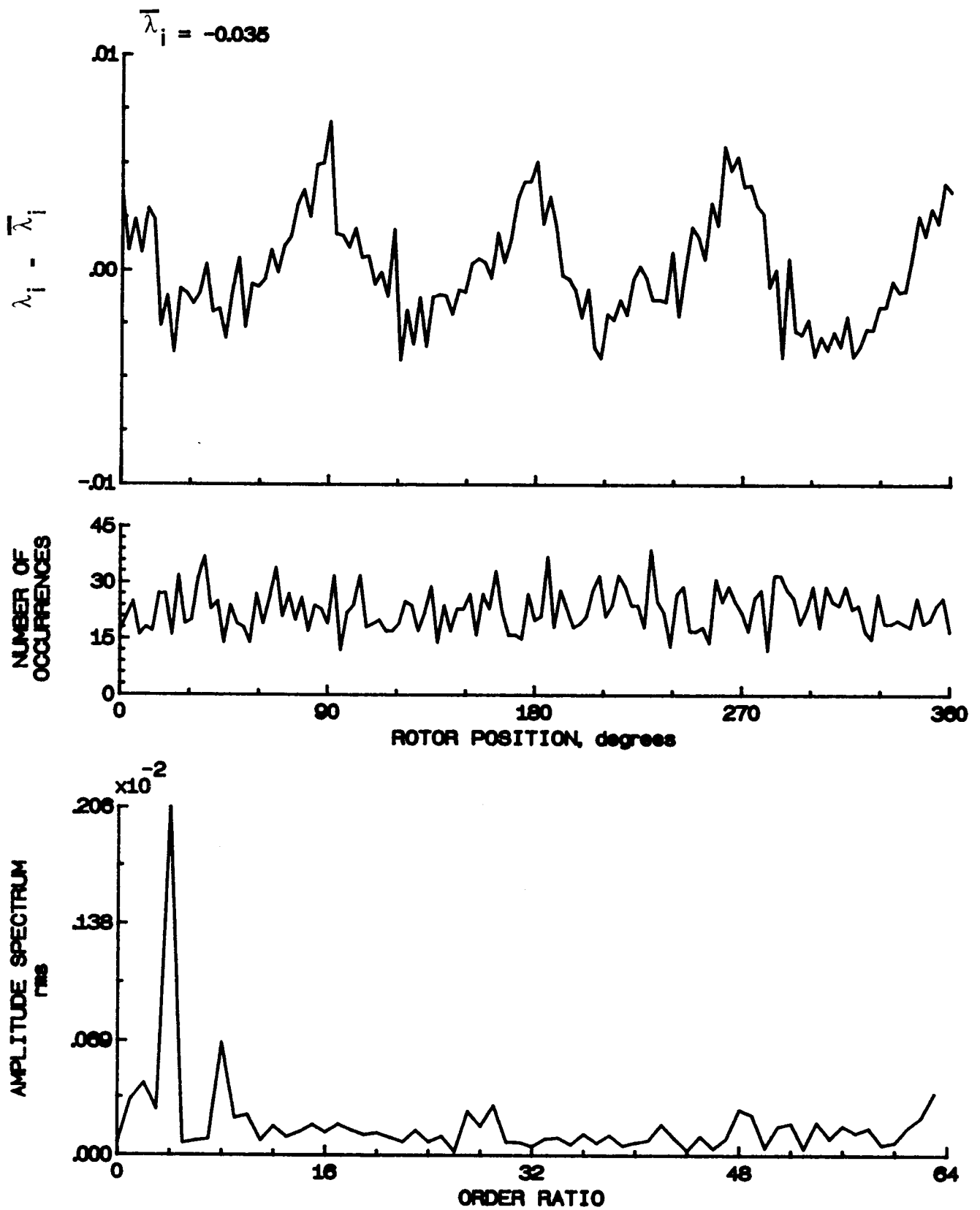


Figure 25.- Concluded.

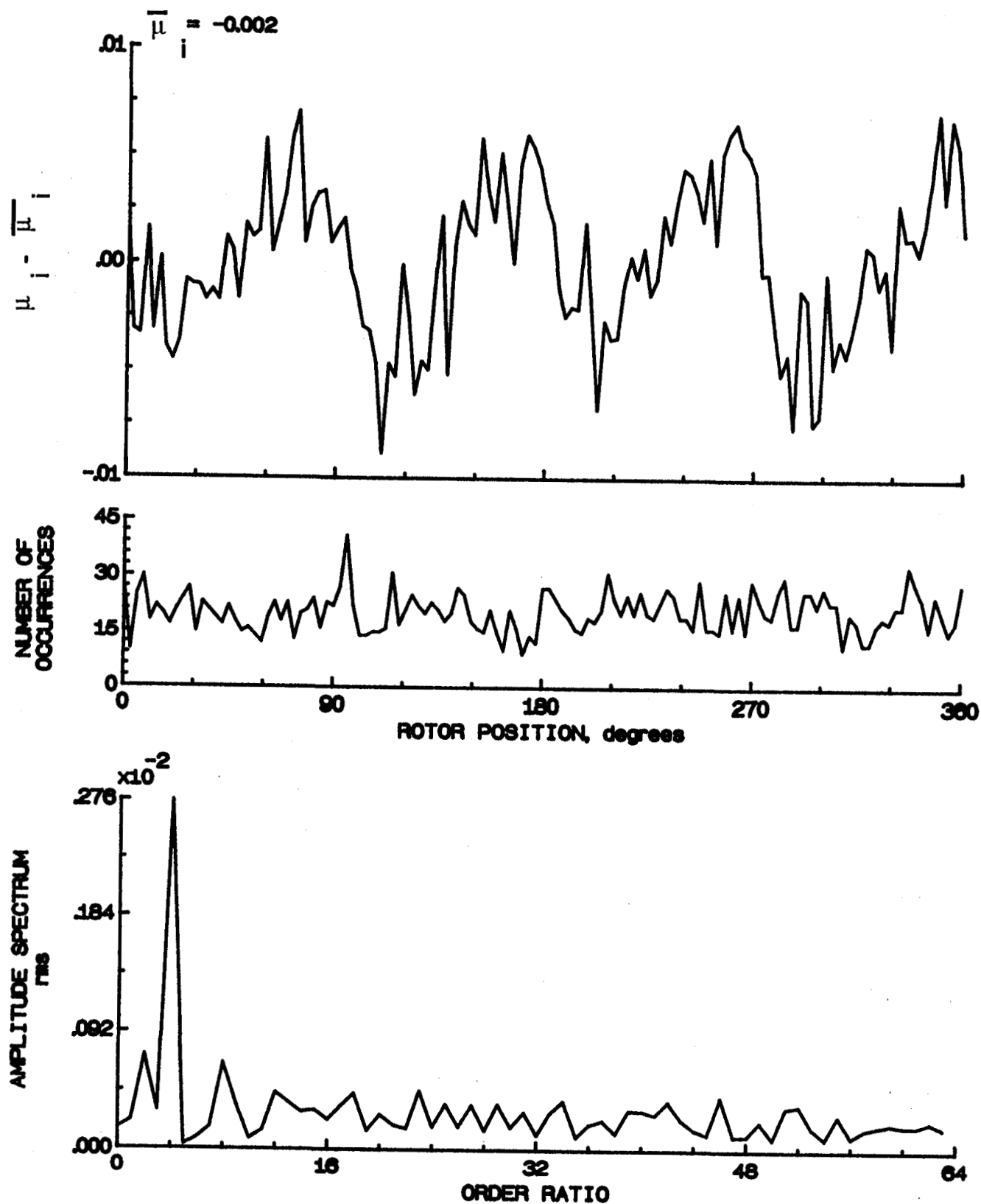


Figure 26.- Induced inflow velocity measured at 0 degrees and r/R of 1.04.

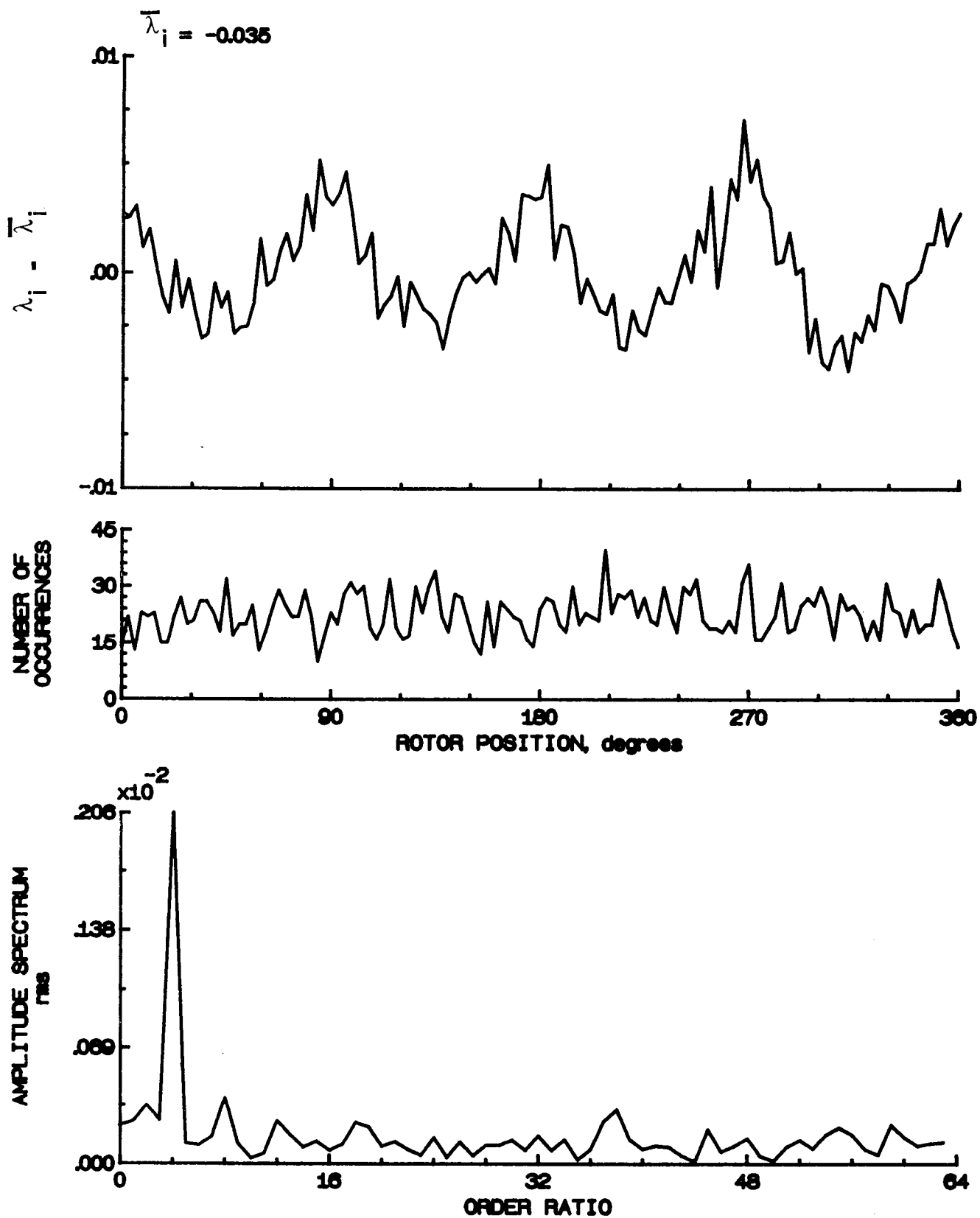


Figure 26.- Concluded.

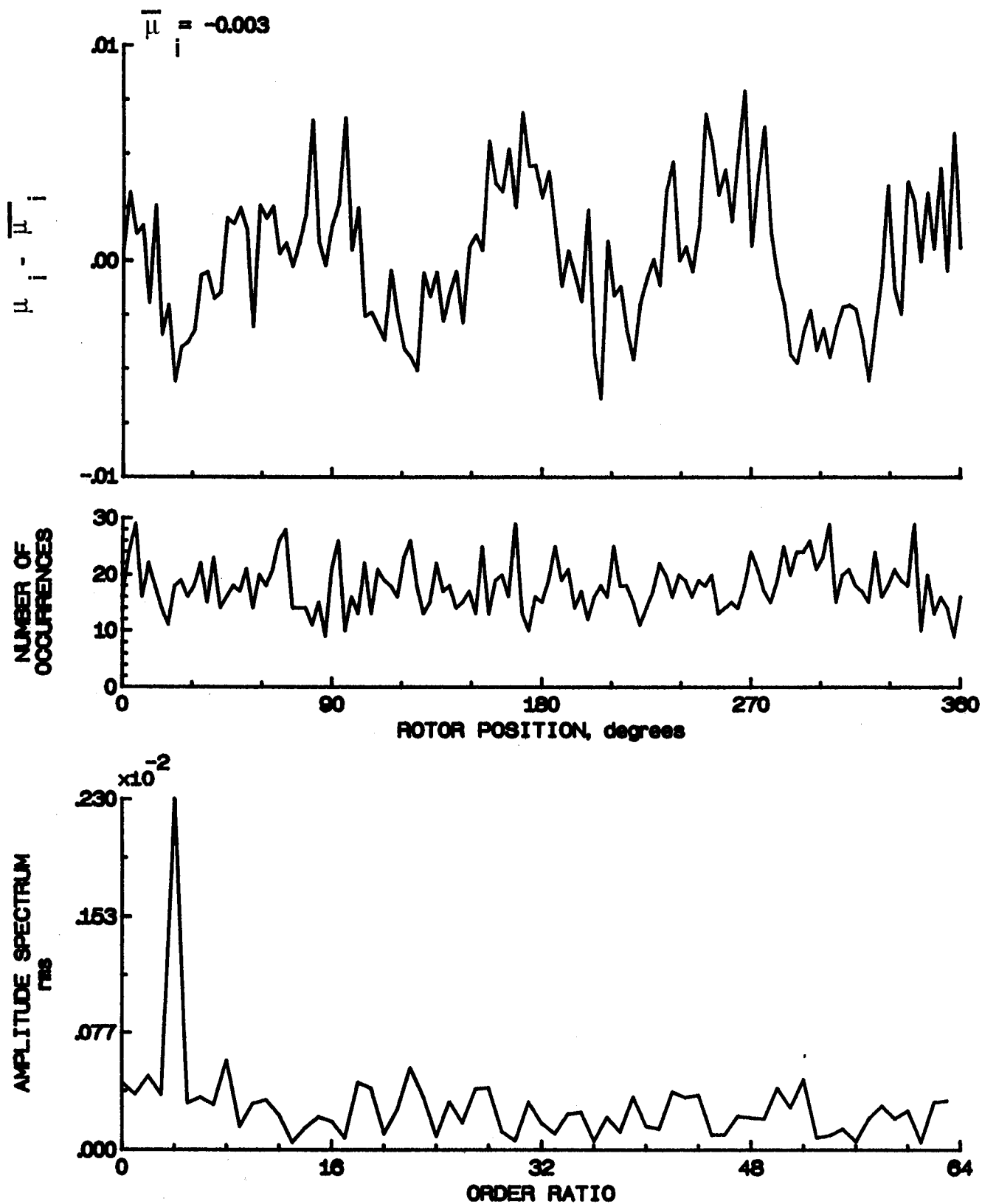


Figure 27.- Induced inflow velocity measured at 0 degrees and r/R of 1.10.

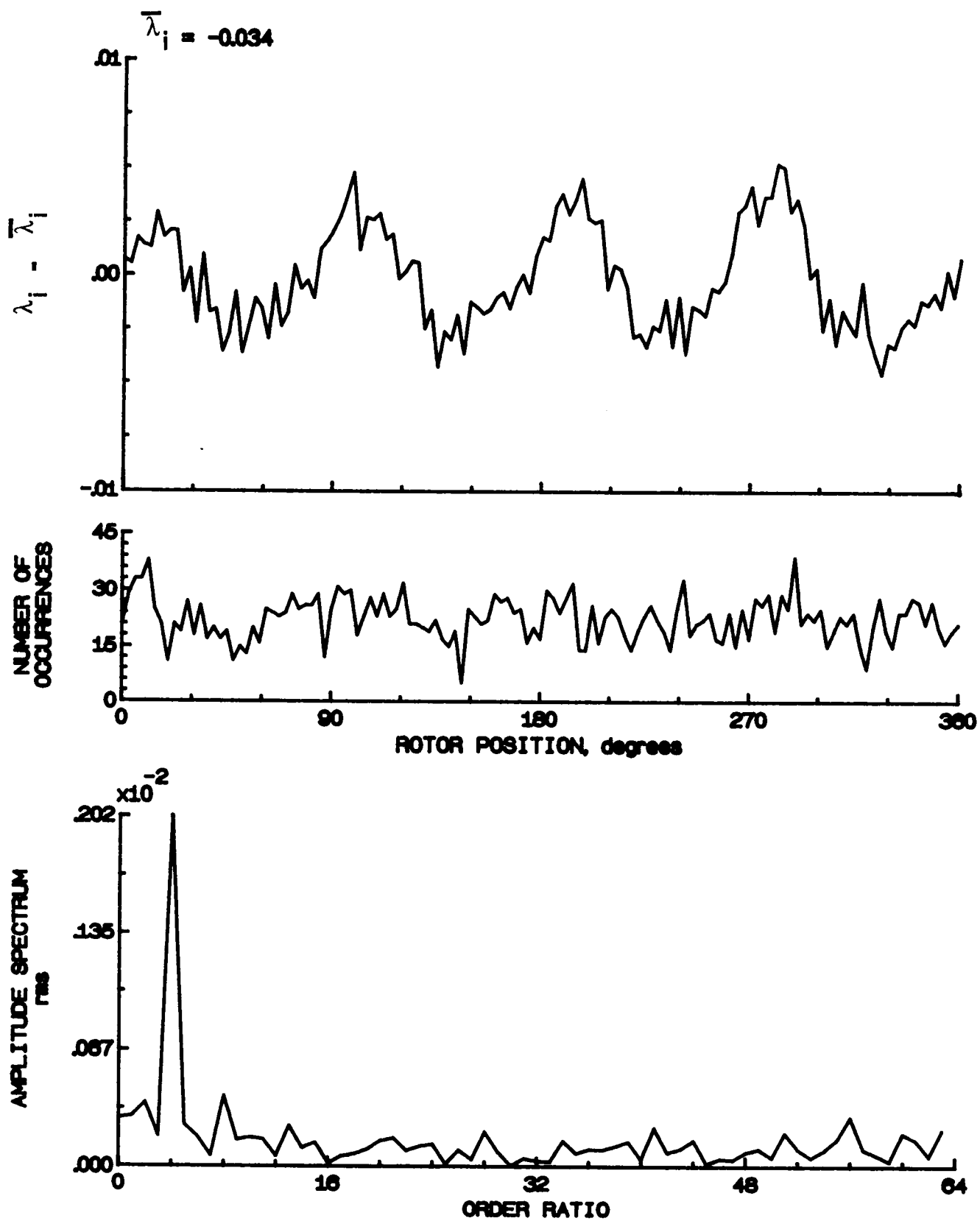


Figure 27.- Concluded.

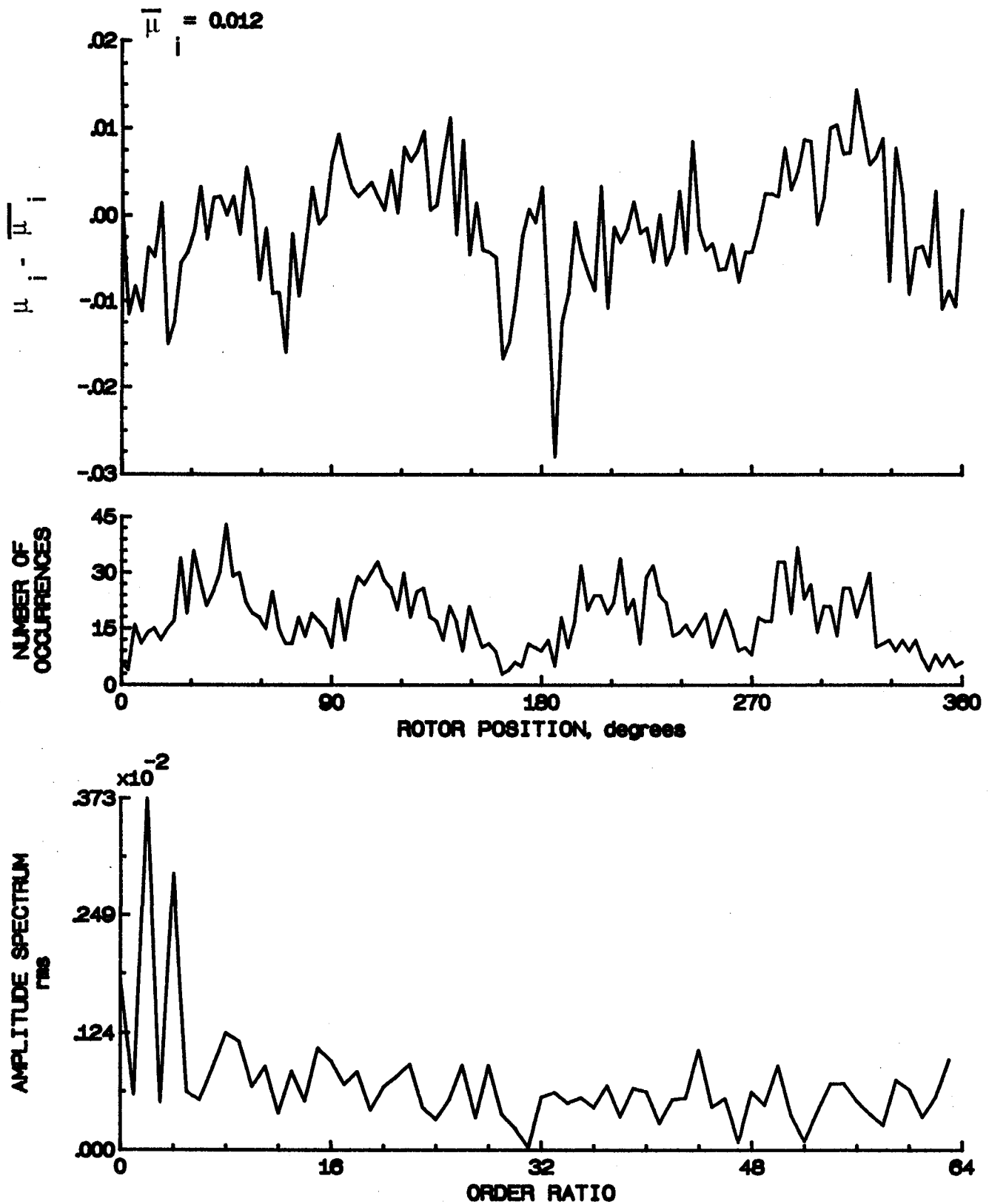


Figure 28.- Induced inflow velocity measured at 30 degrees and r/R of 0.20.



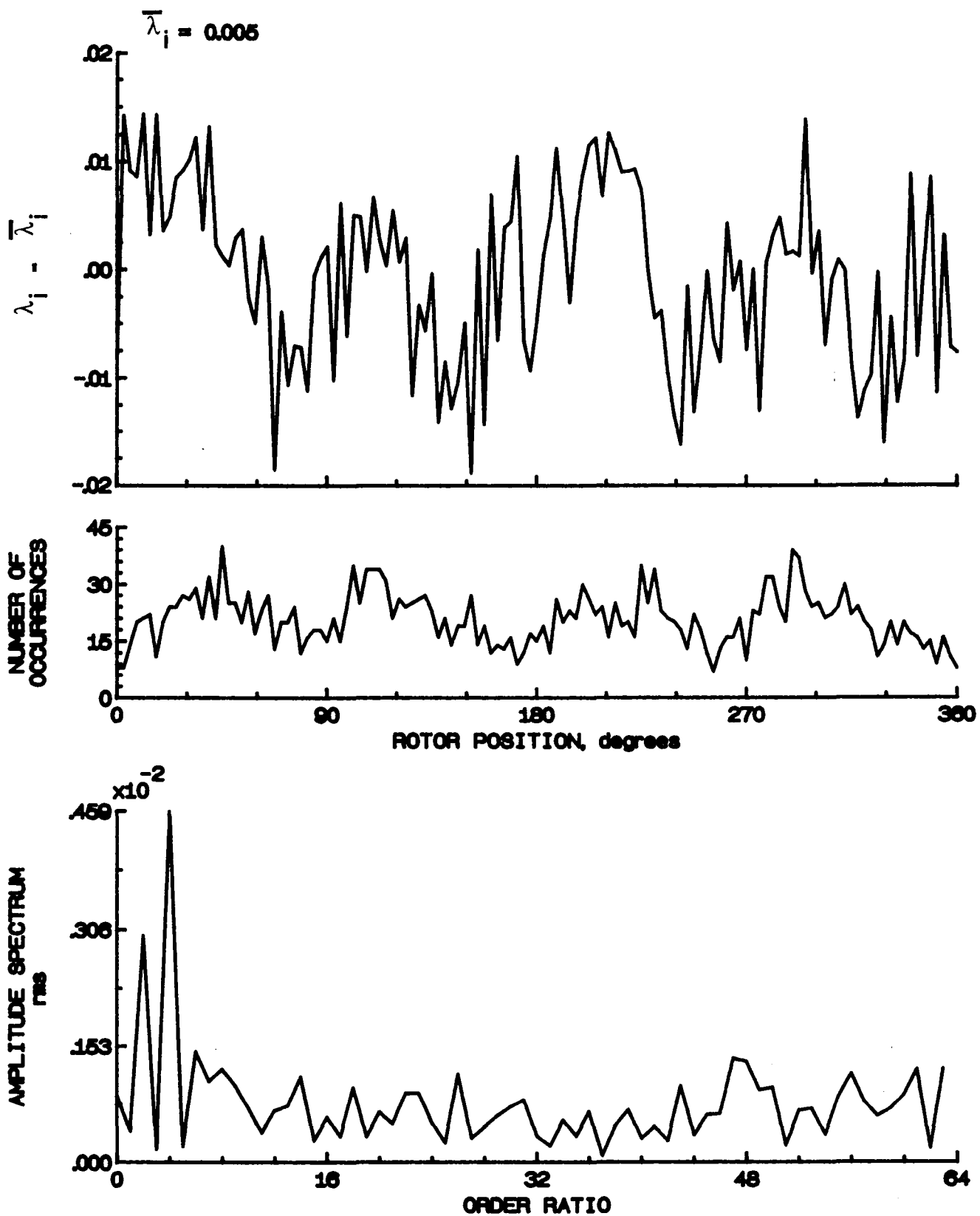


Figure 28.- Concluded.

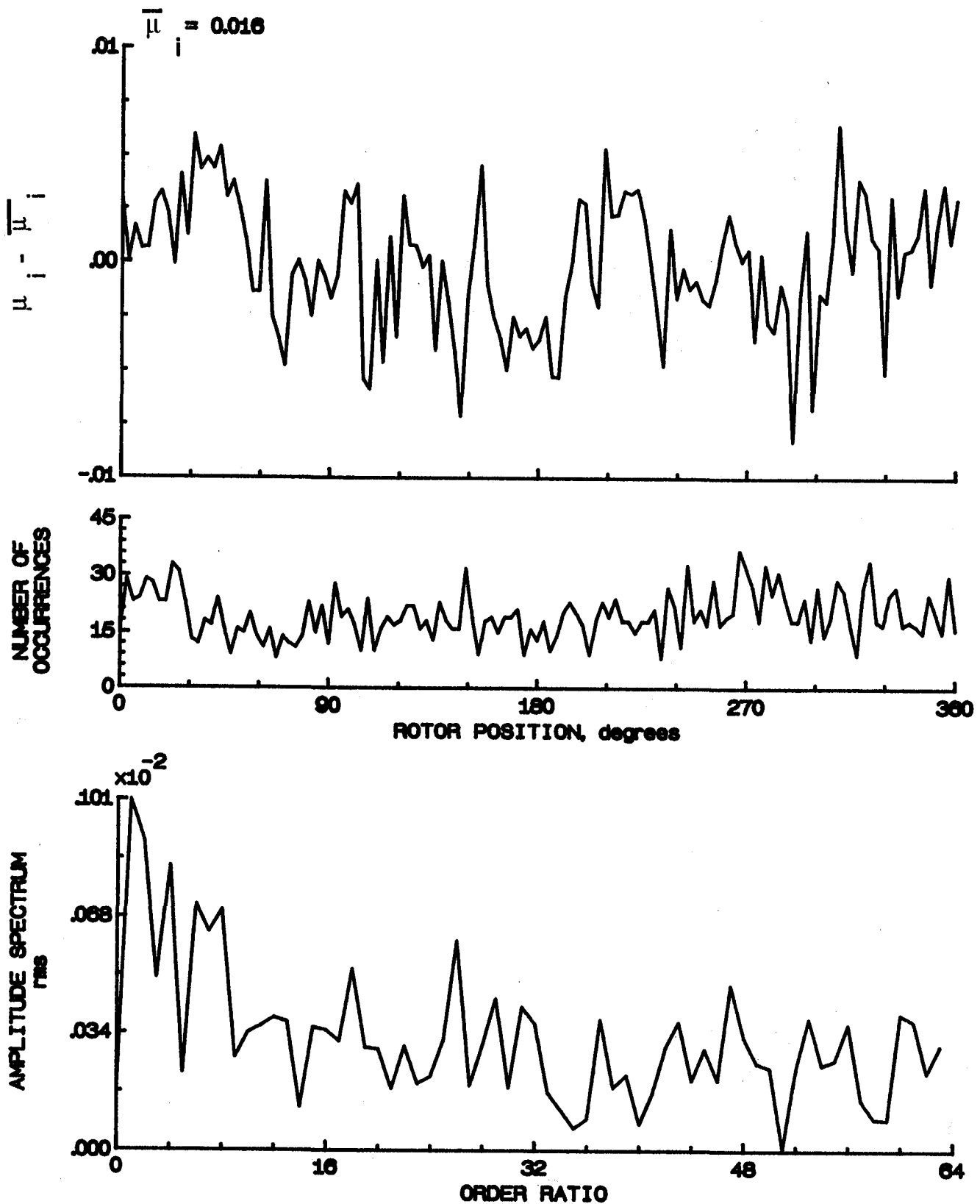


Figure 29.- Induced inflow velocity measured at 30 degrees and r/R of 0.40.

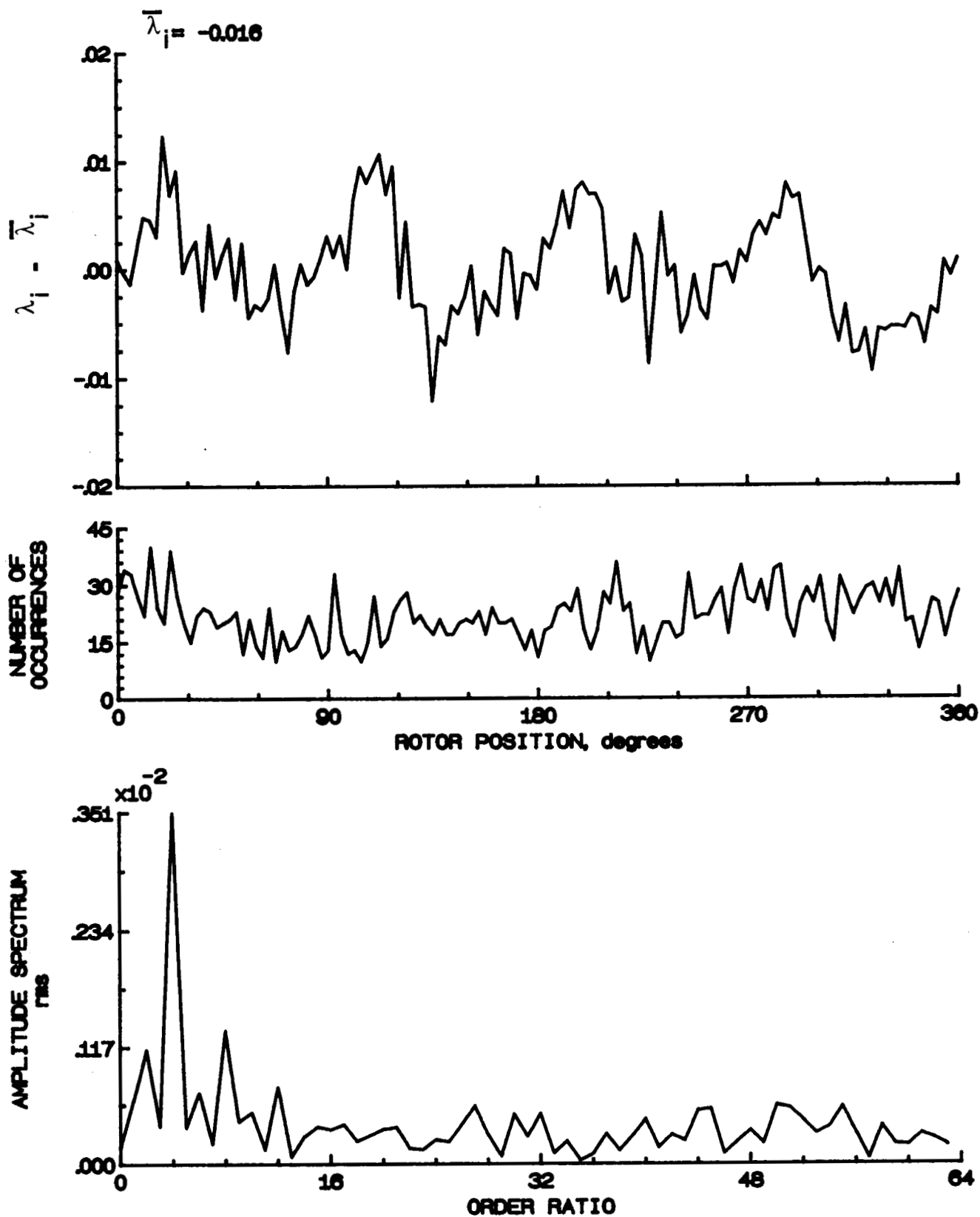


Figure 29.- Concluded.

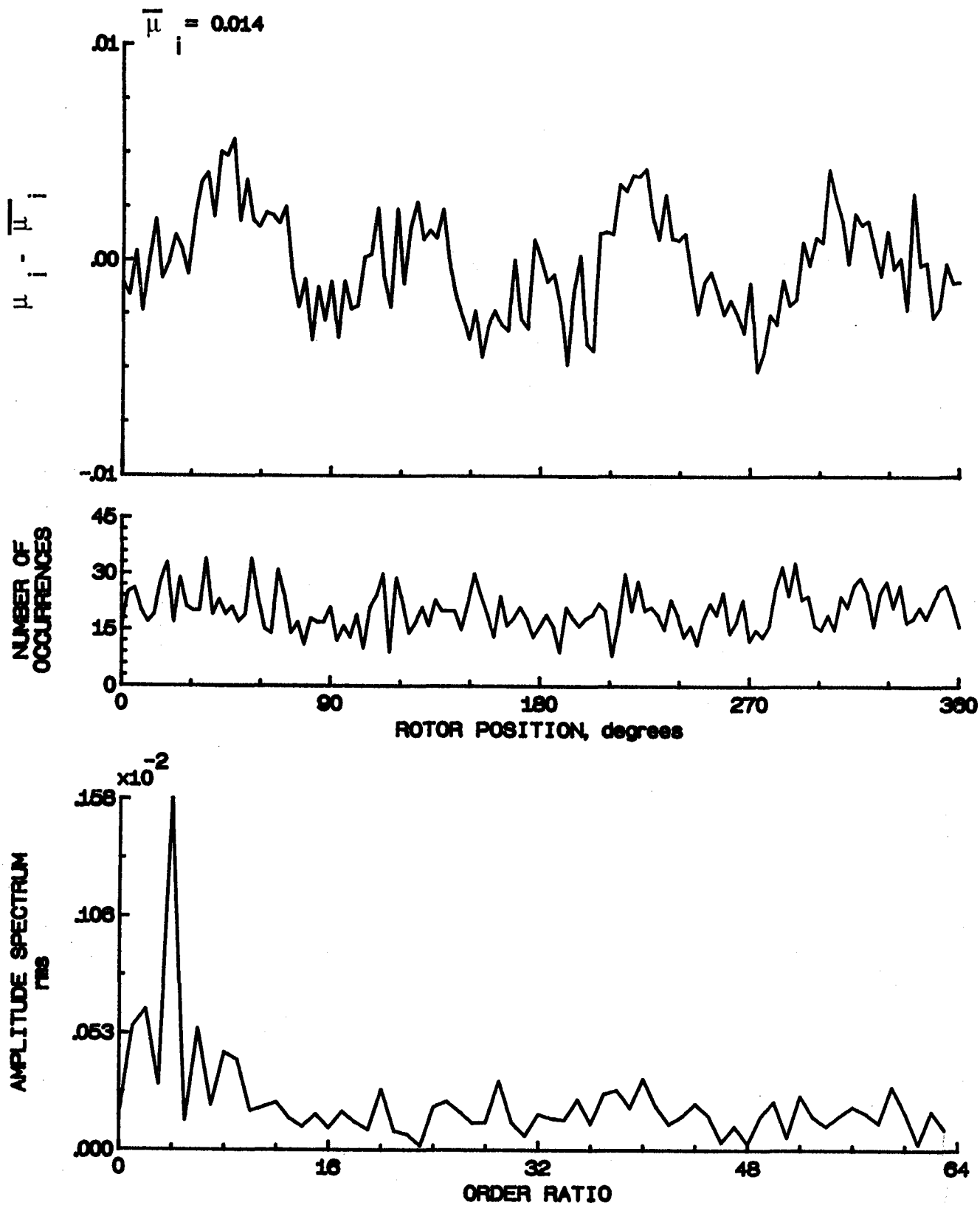


Figure 30.- Induced inflow velocity measured at 30 degrees and  $r/R$  of 0.50.

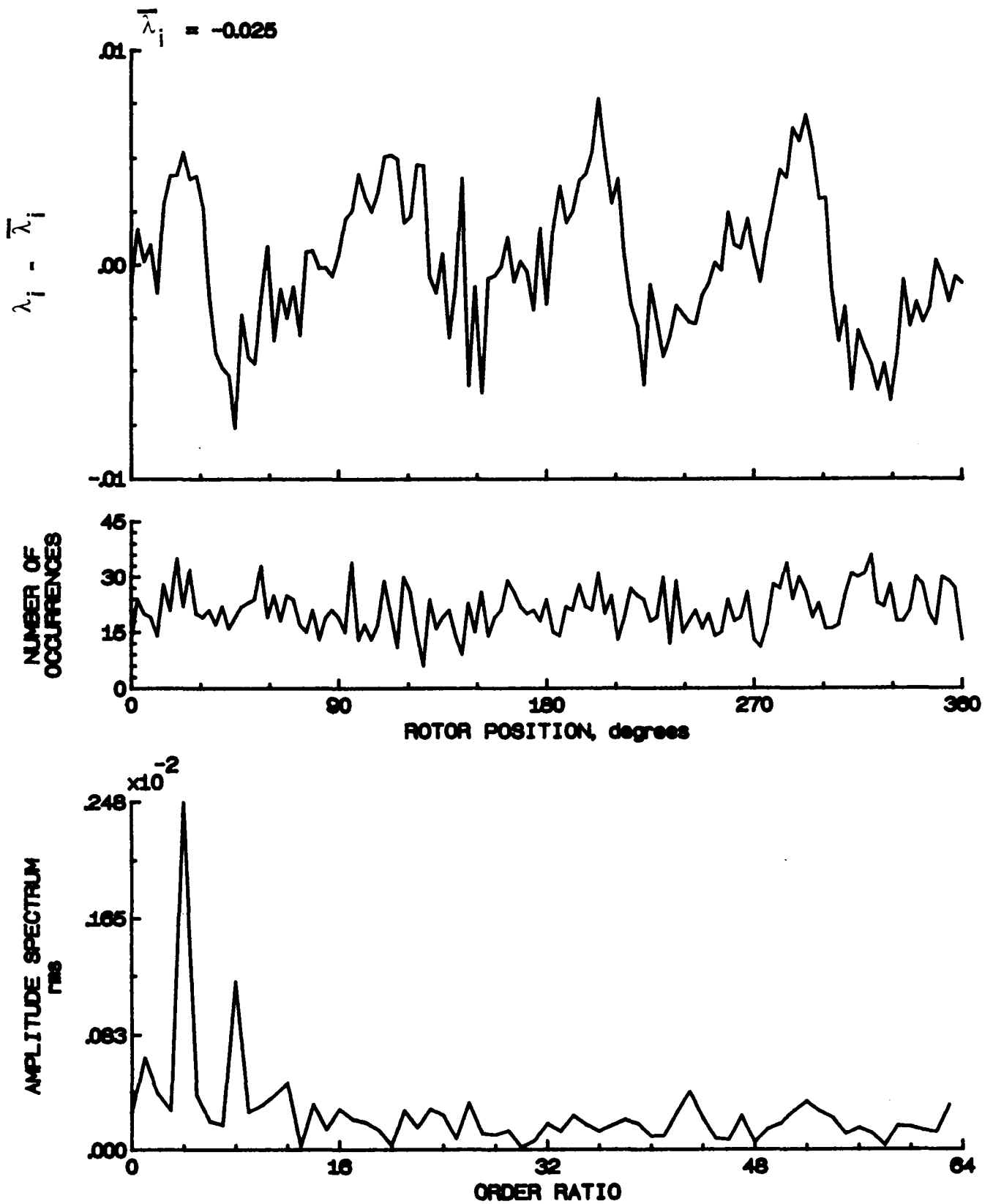


Figure 30.- Concluded.

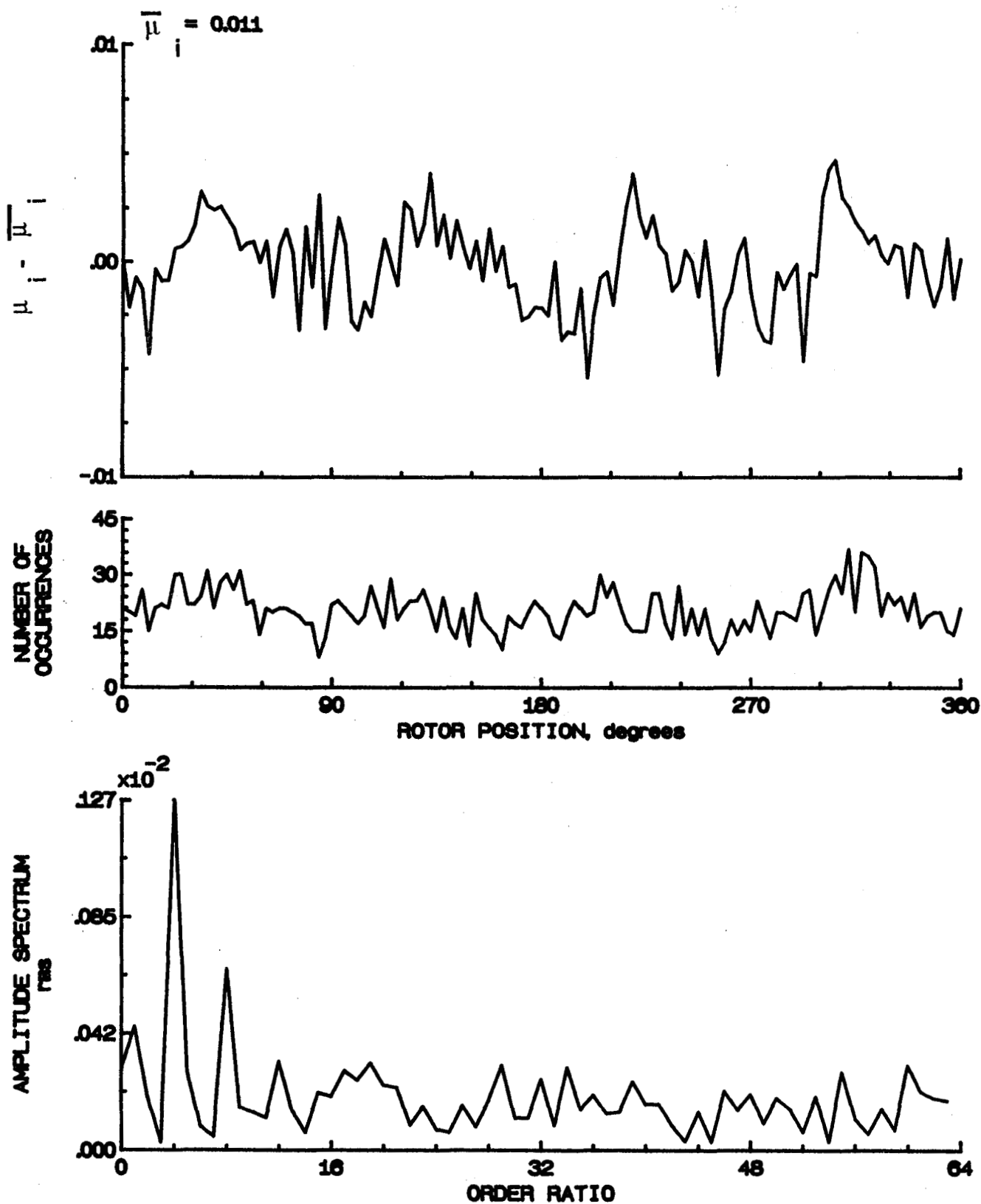


Figure 31.- Induced inflow velocity measured at 30 degrees and r/R of 0.60.

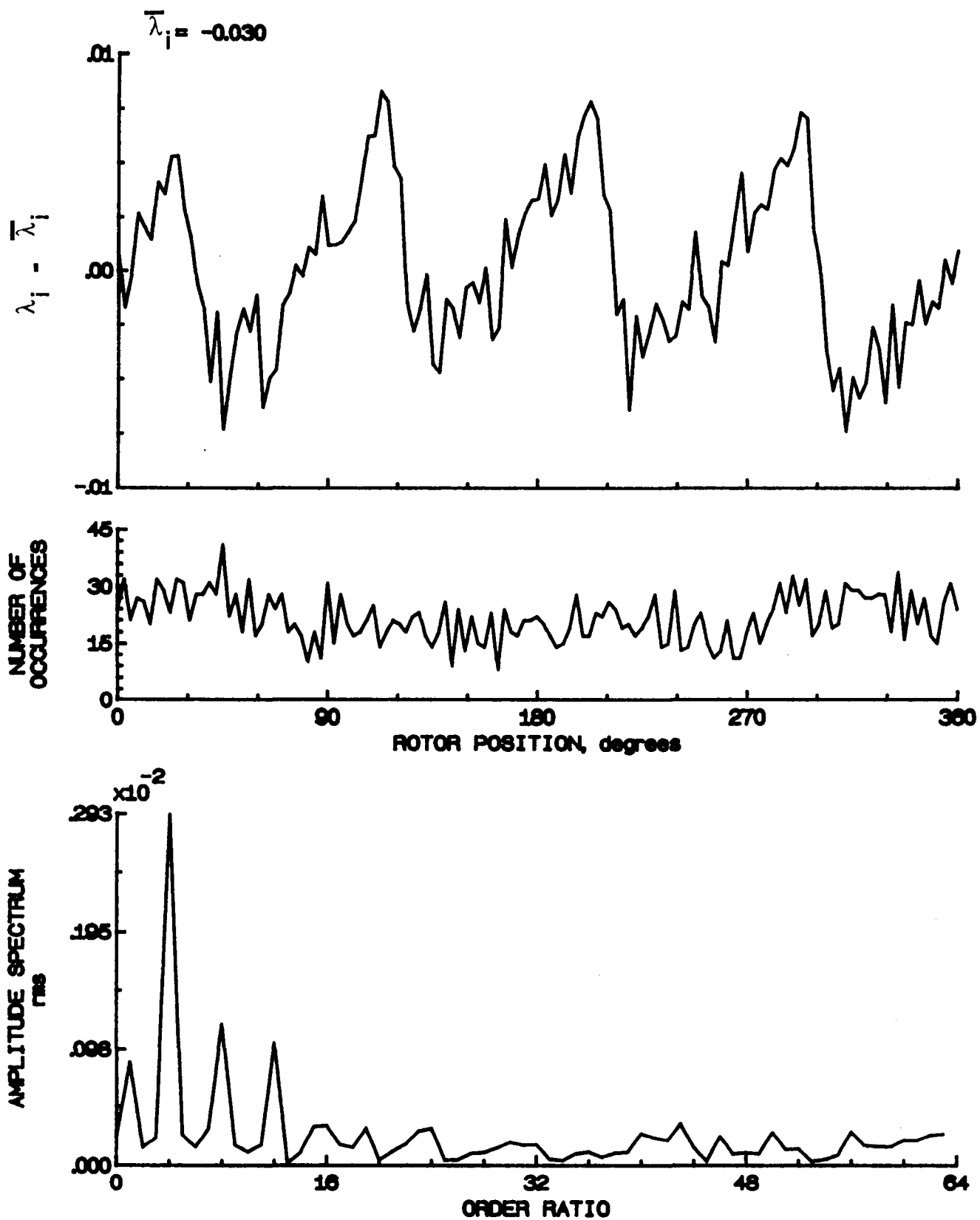


Figure 31.- Concluded.

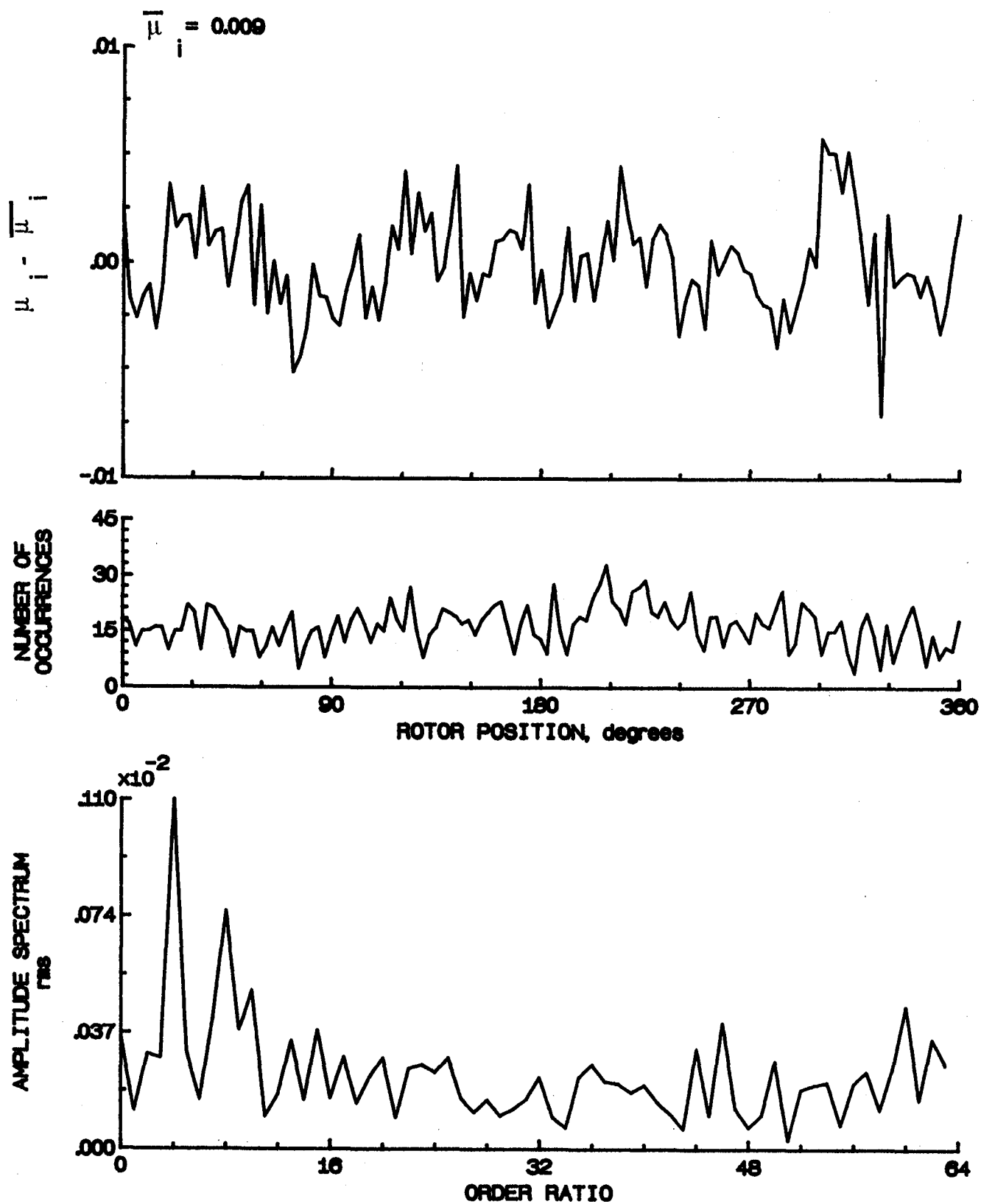


Figure 32.- Induced inflow velocity measured at 30 degrees and r/R of 0.70.



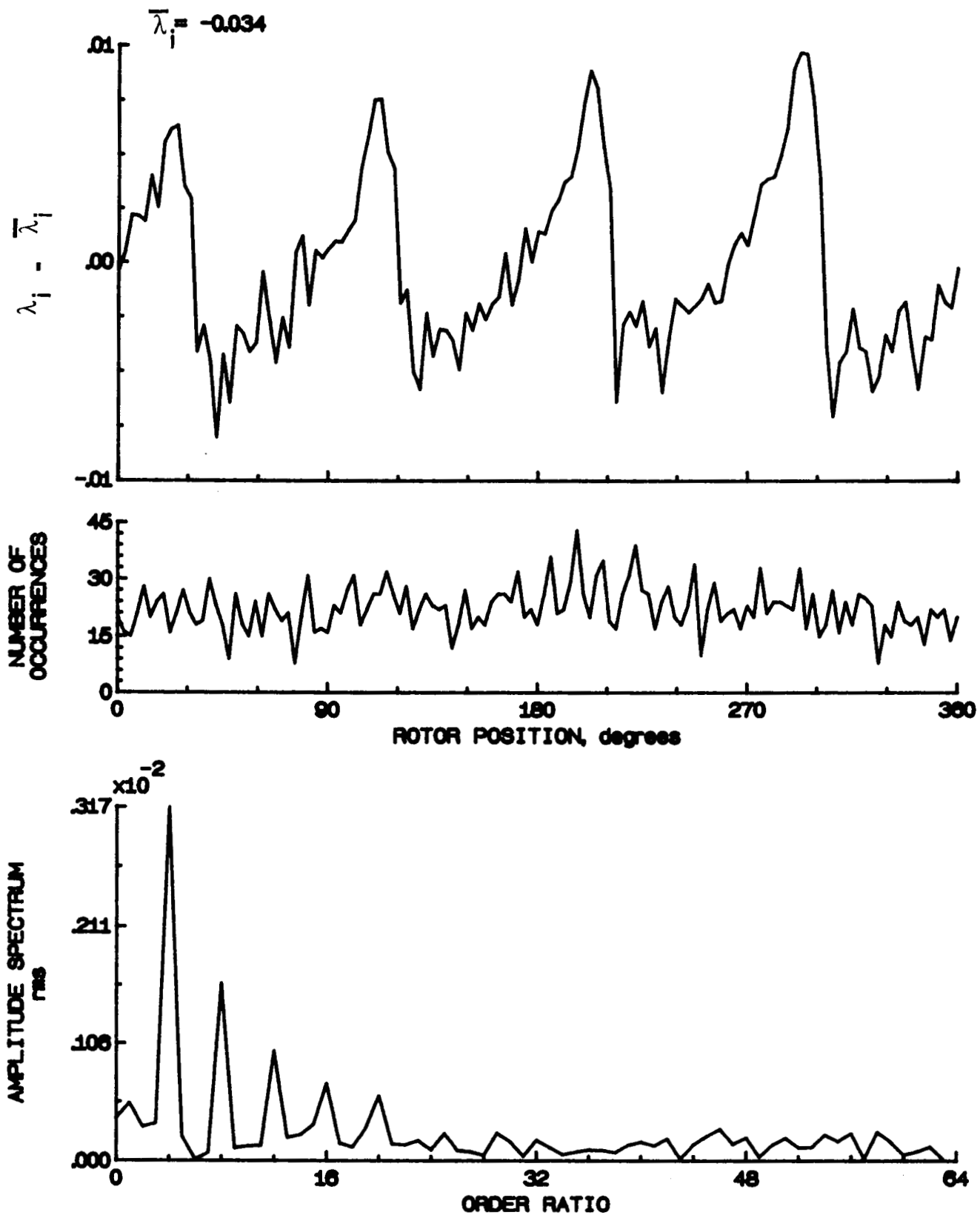


Figure 32.- Concluded.

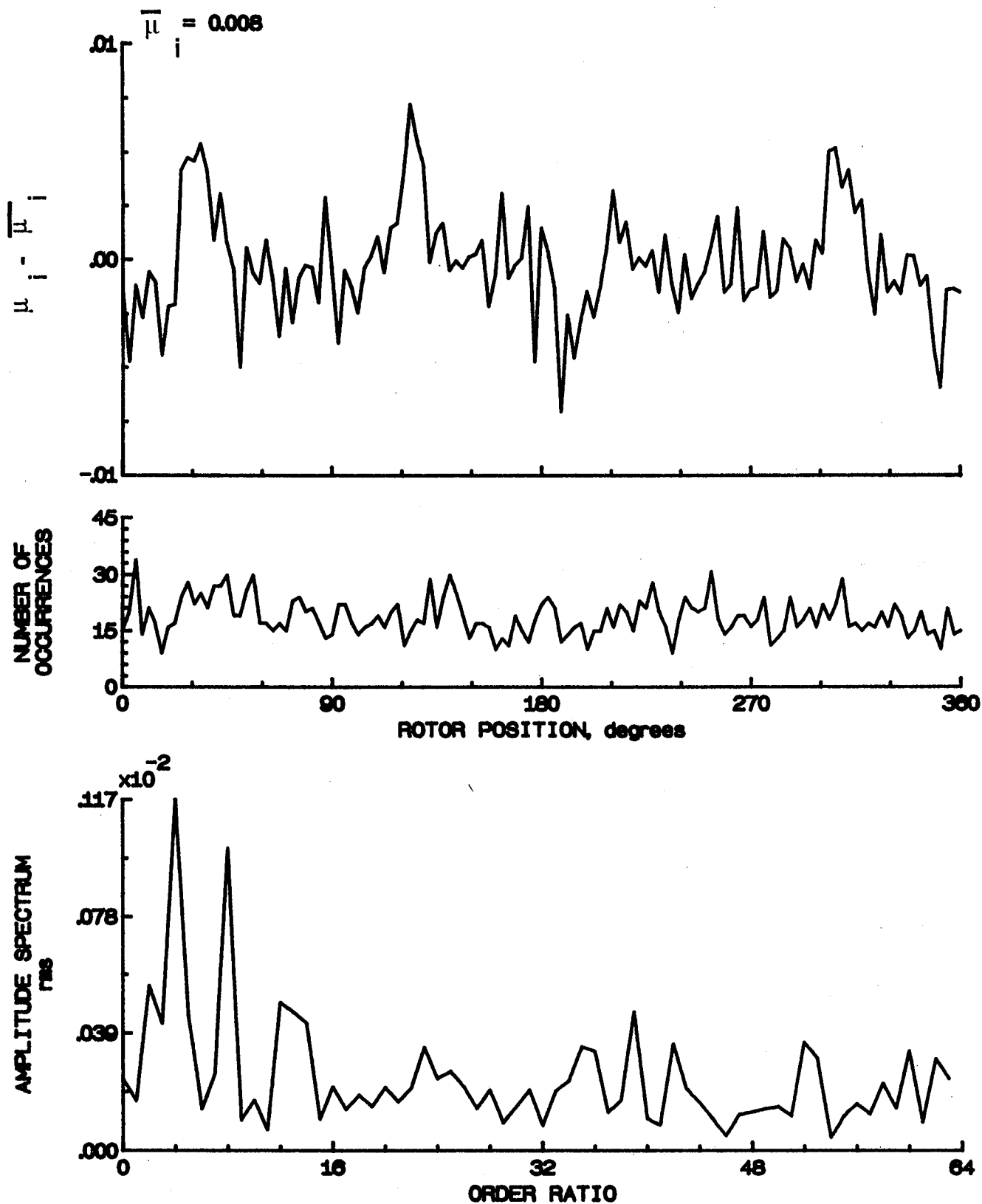


Figure 33.- Induced inflow velocity measured at 30 degrees and  $r/R$  of 0.74.

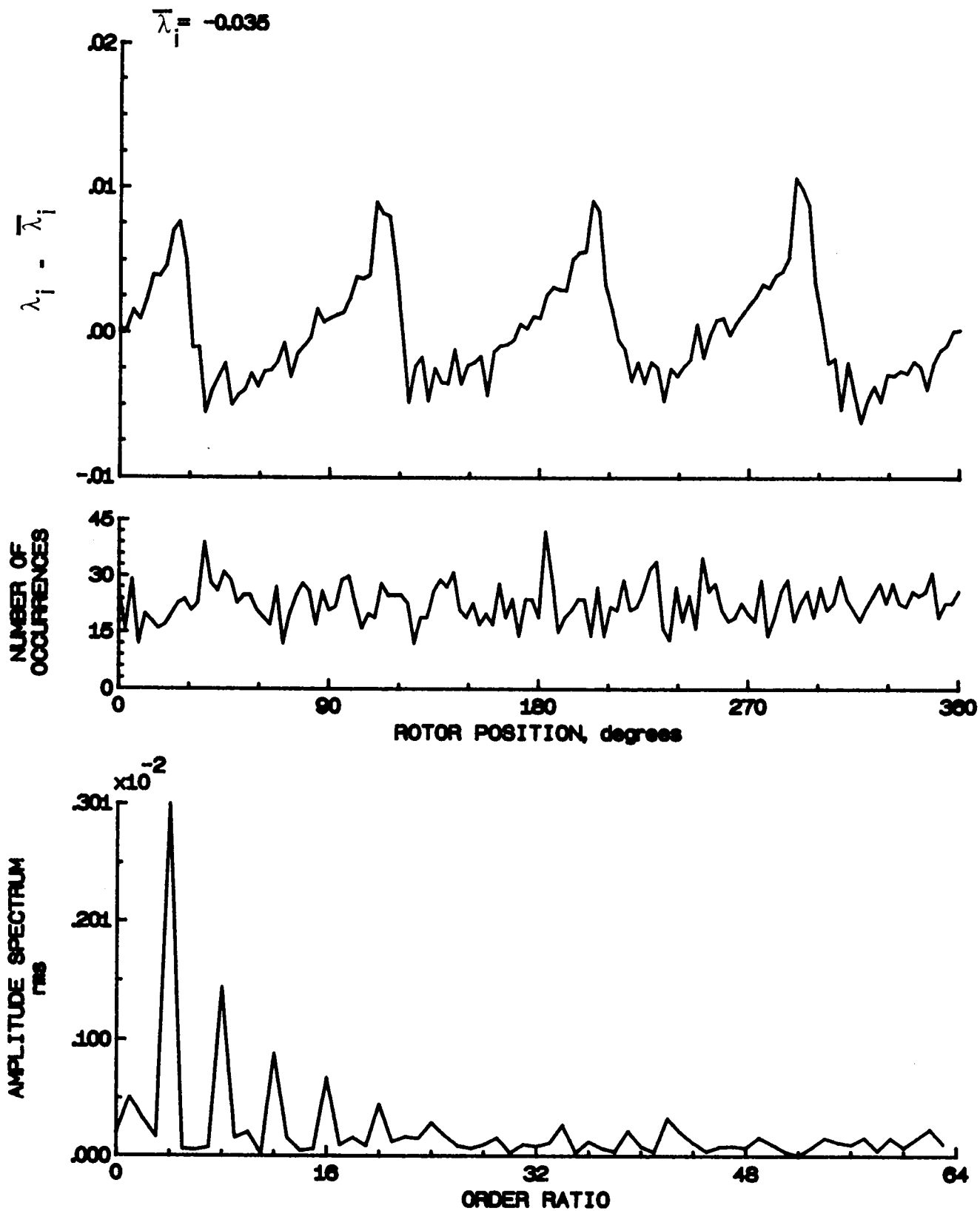


Figure 33.- Concluded.

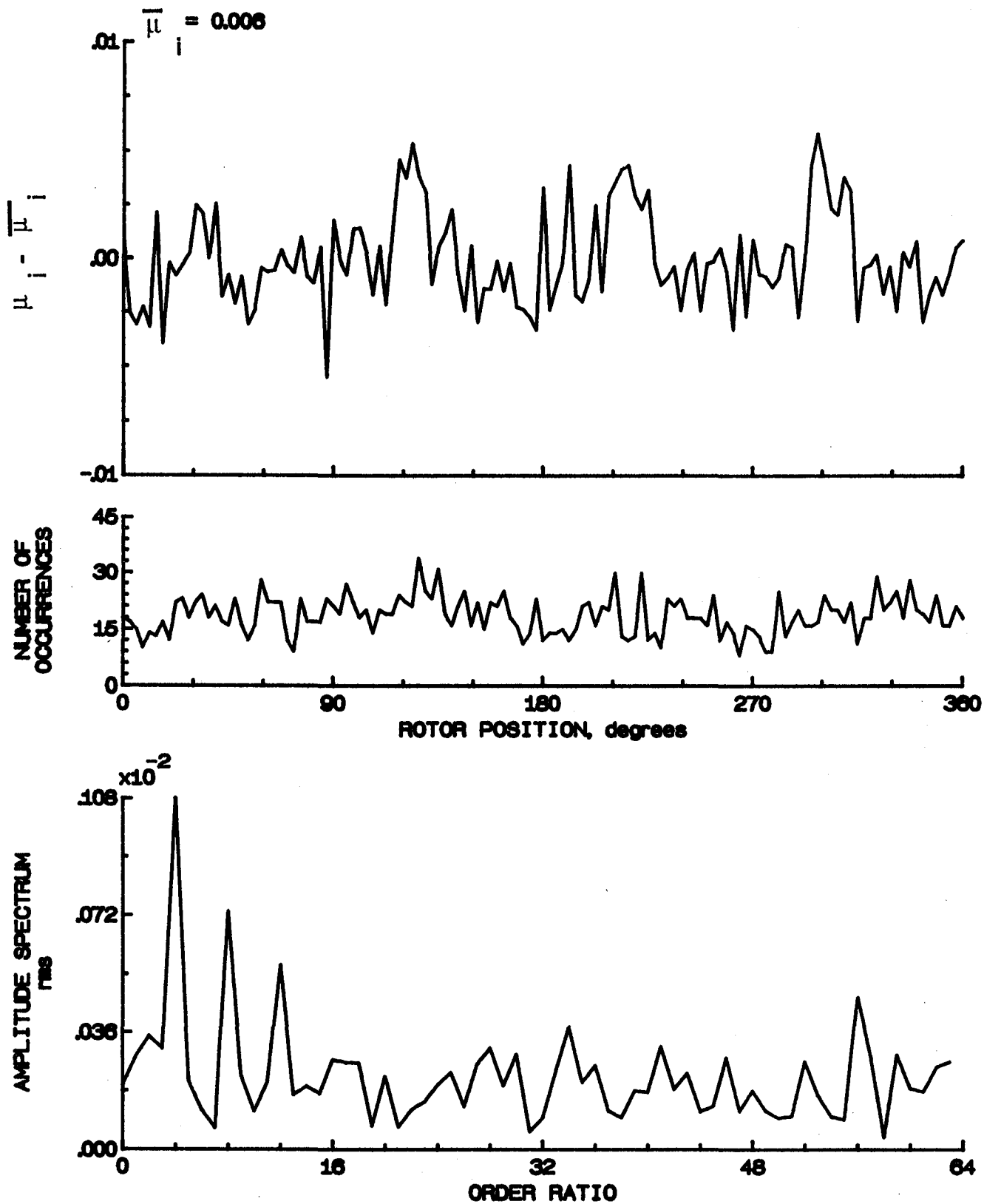


Figure 34.- Induced inflow velocity measured at 30 degrees and  $r/R$  of 0.78.

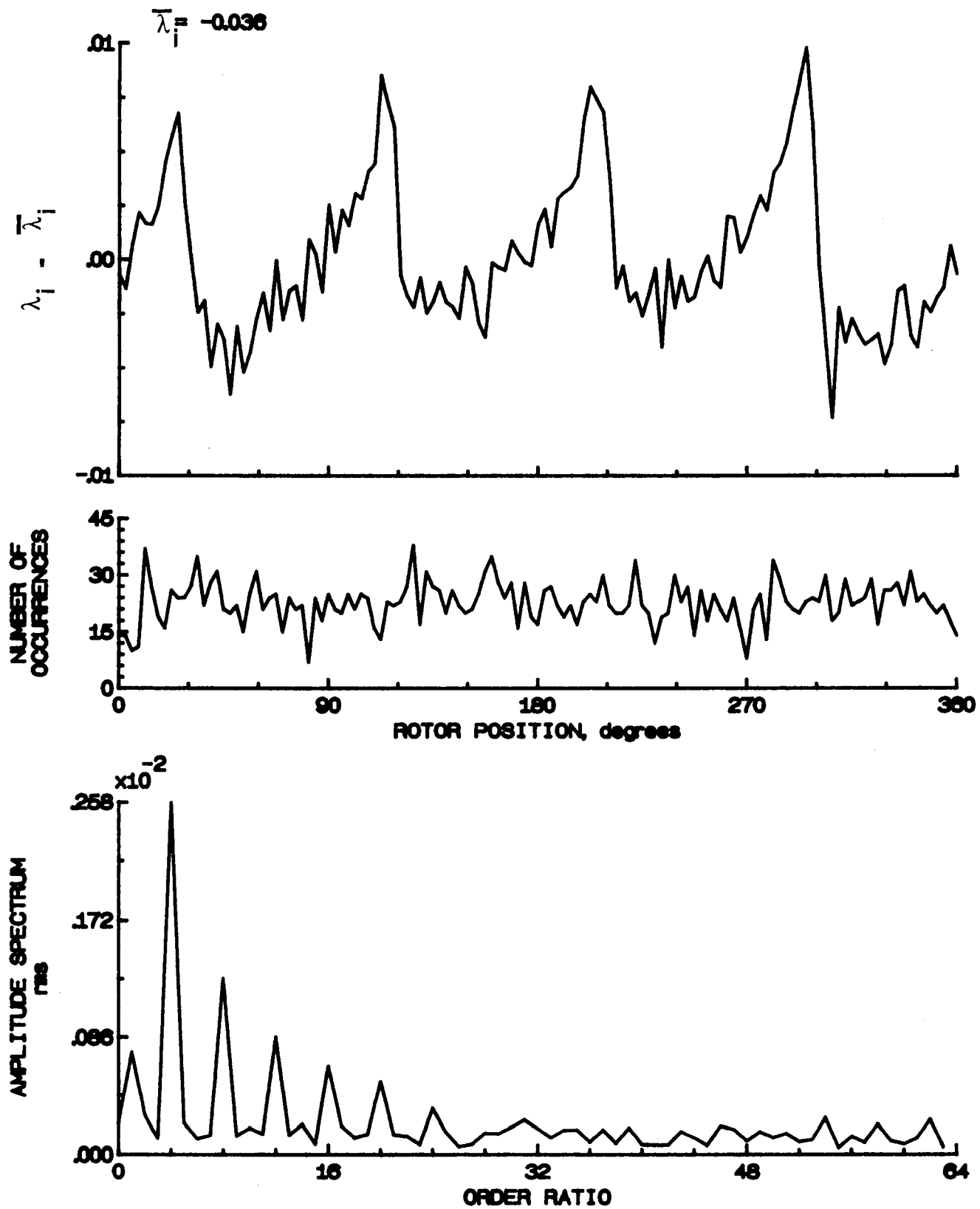


Figure 34.- Concluded.

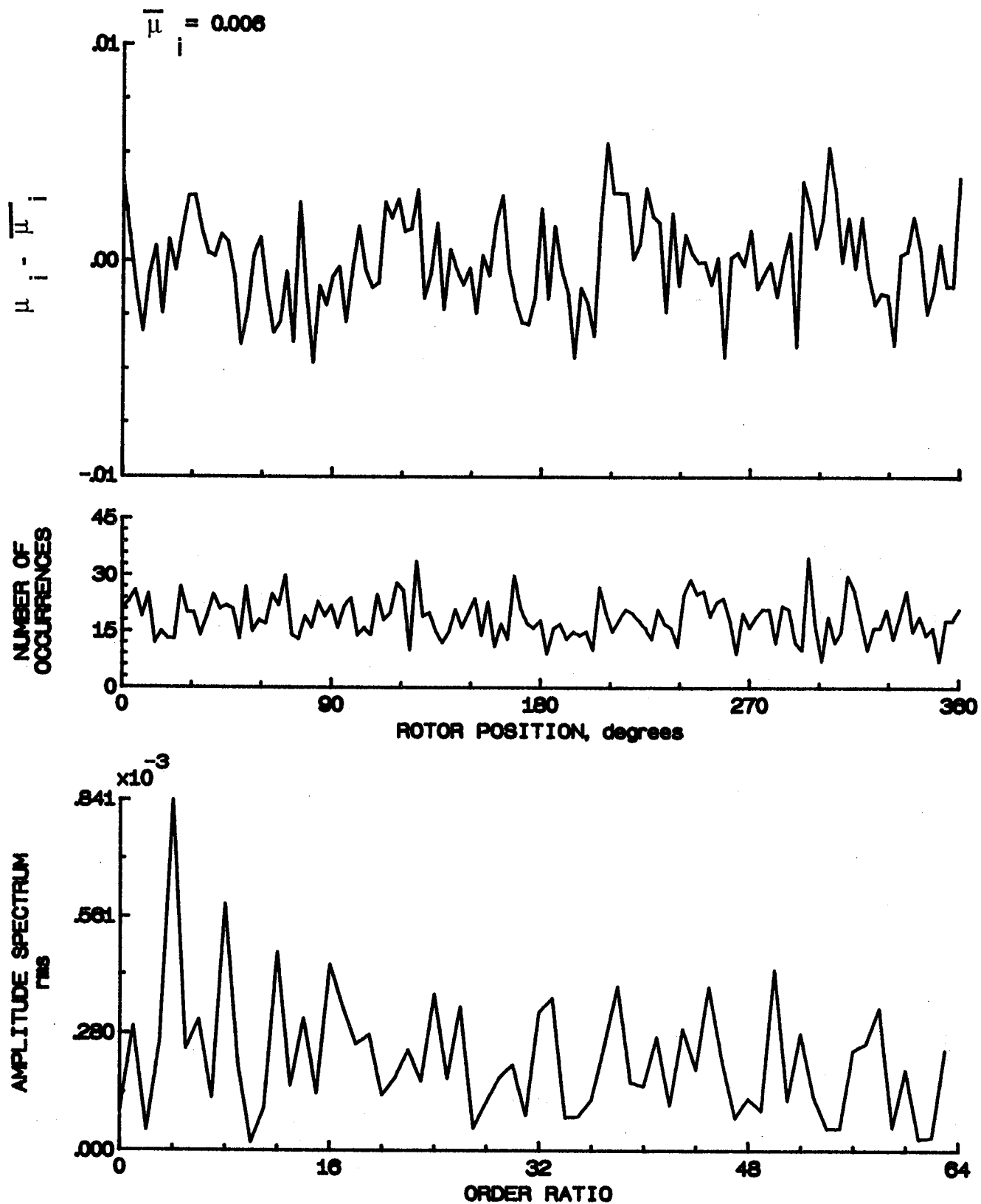


Figure 35.- Induced inflow velocity measured at 30 degrees and  $r/R$  of 0.82.

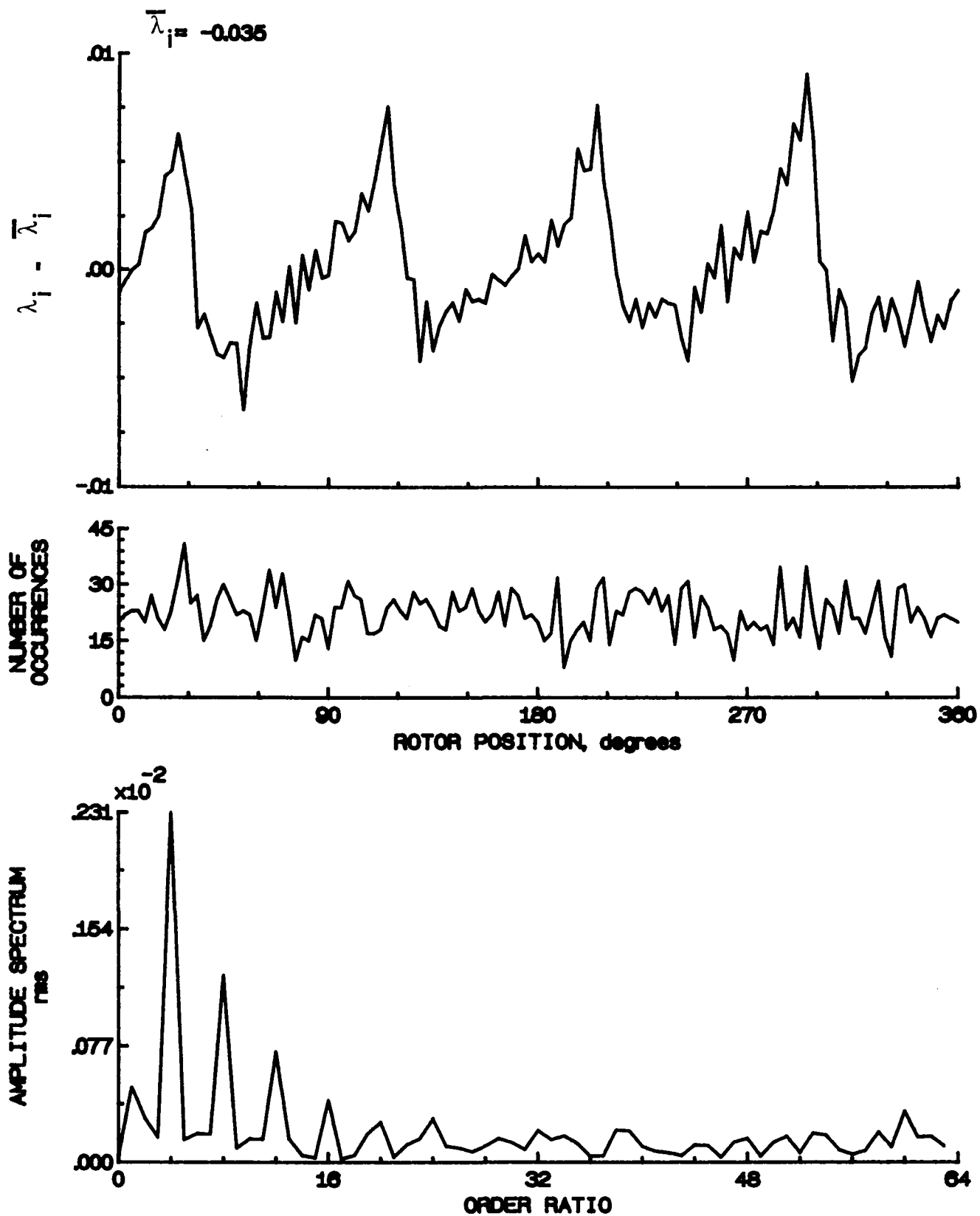


Figure 35.- Concluded.

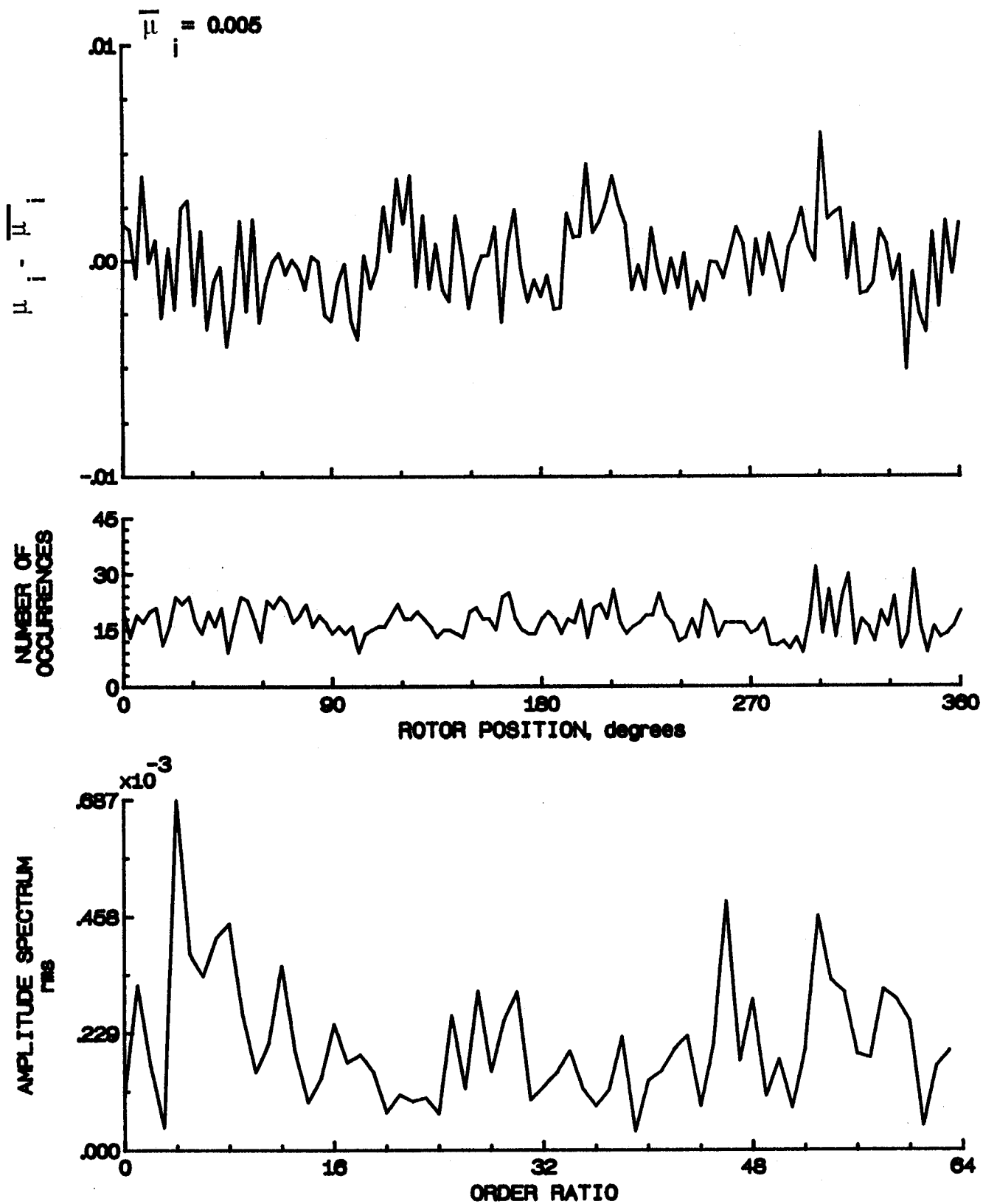


Figure 36.- Induced inflow velocity measured at 30 degrees and  $r/R$  of 0.86.



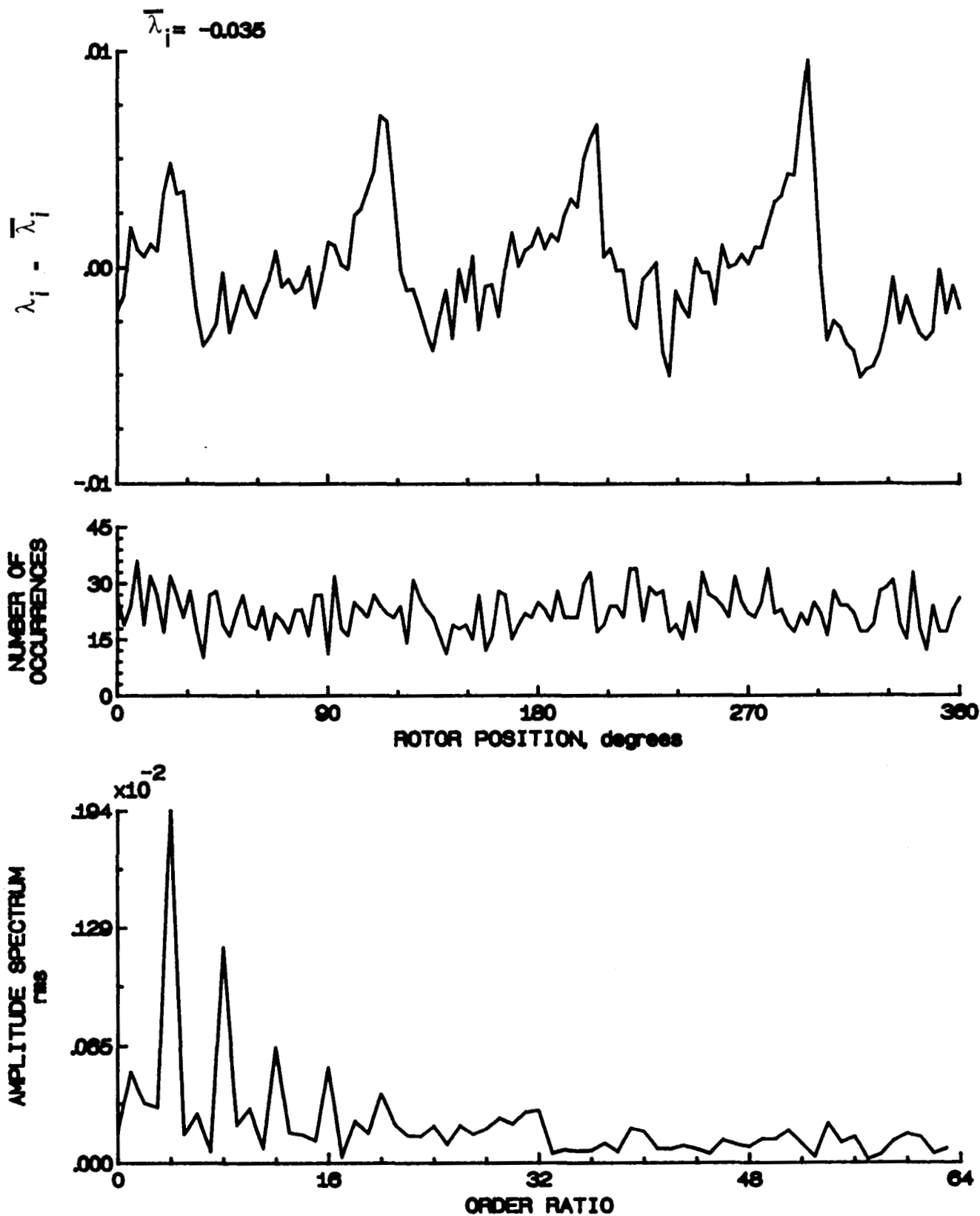


Figure 36.- Concluded.

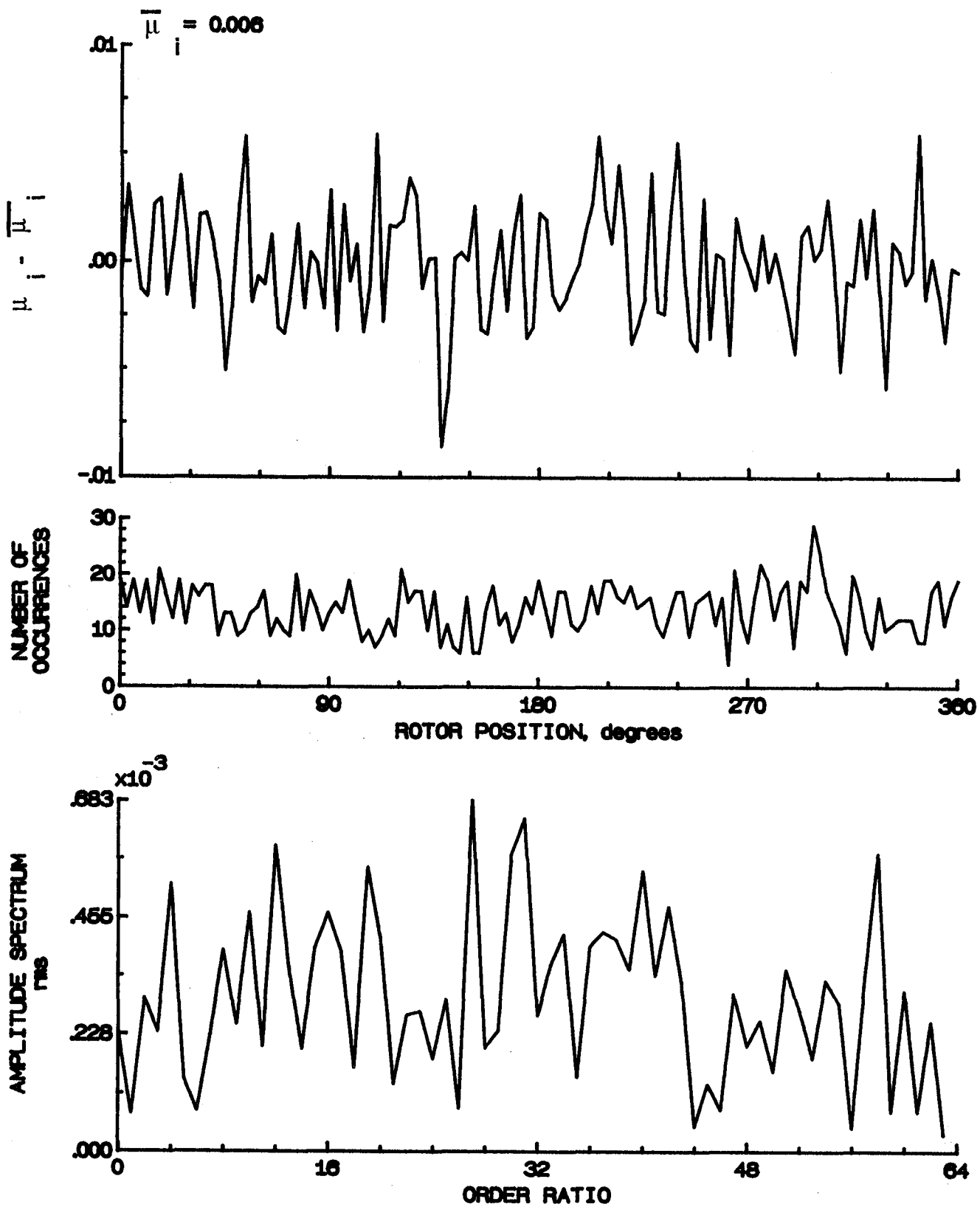


Figure 37.- Induced inflow velocity measured at 30 degrees and r/R of 0.90.

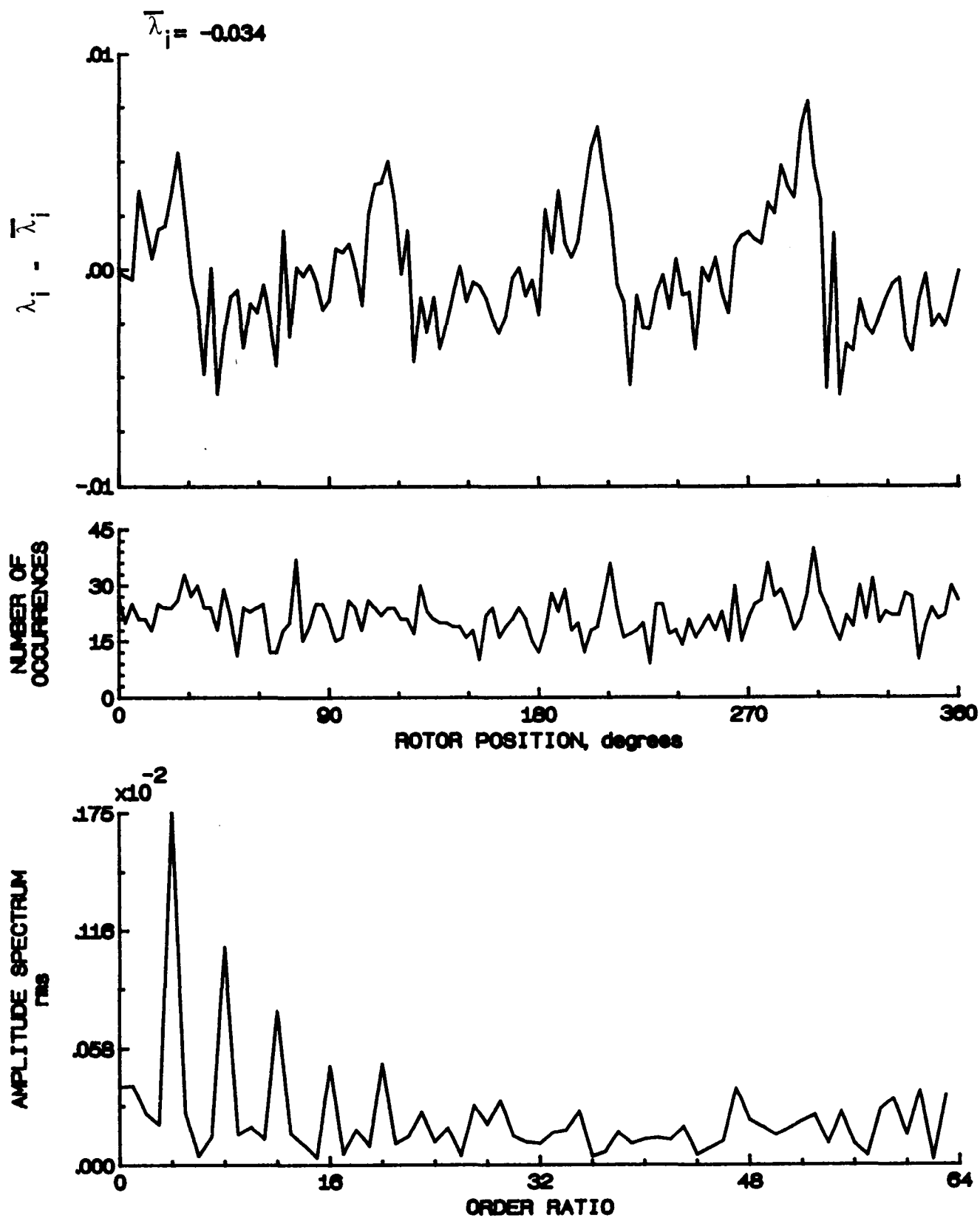


Figure 37.- Concluded.

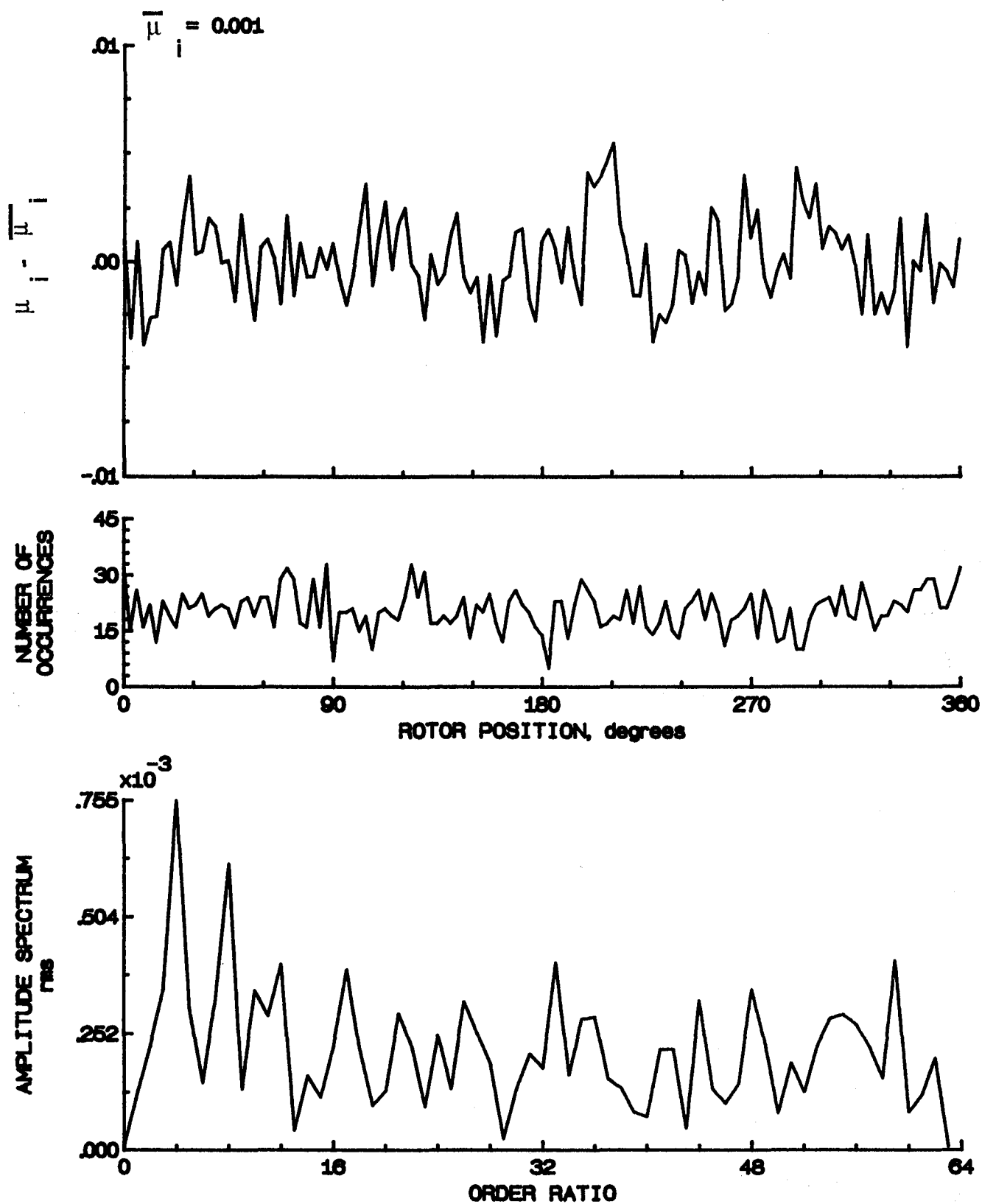


Figure 38.- Induced inflow velocity measured at 30 degrees and  $r/R$  of 0.94.

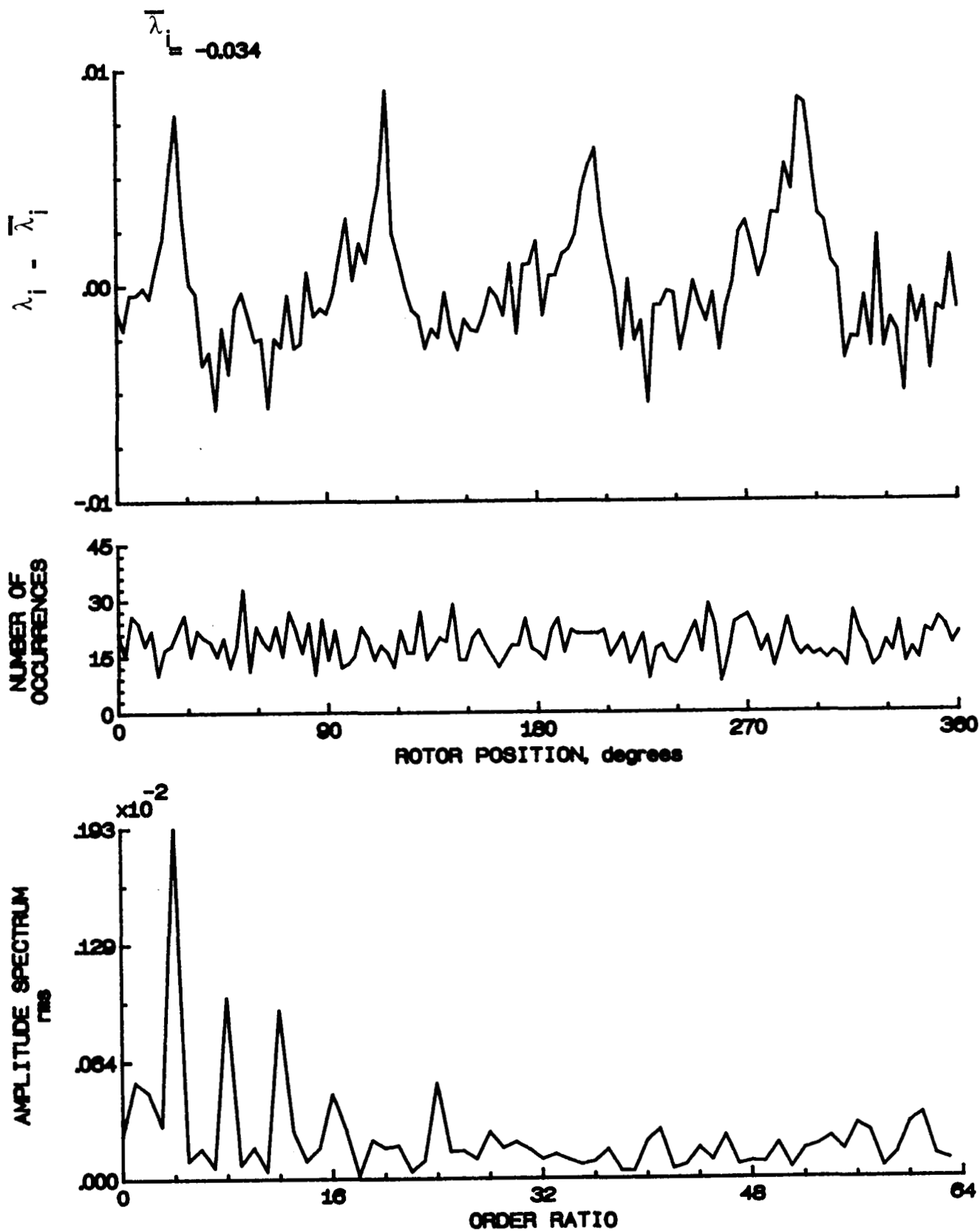


Figure 38.- Concluded.

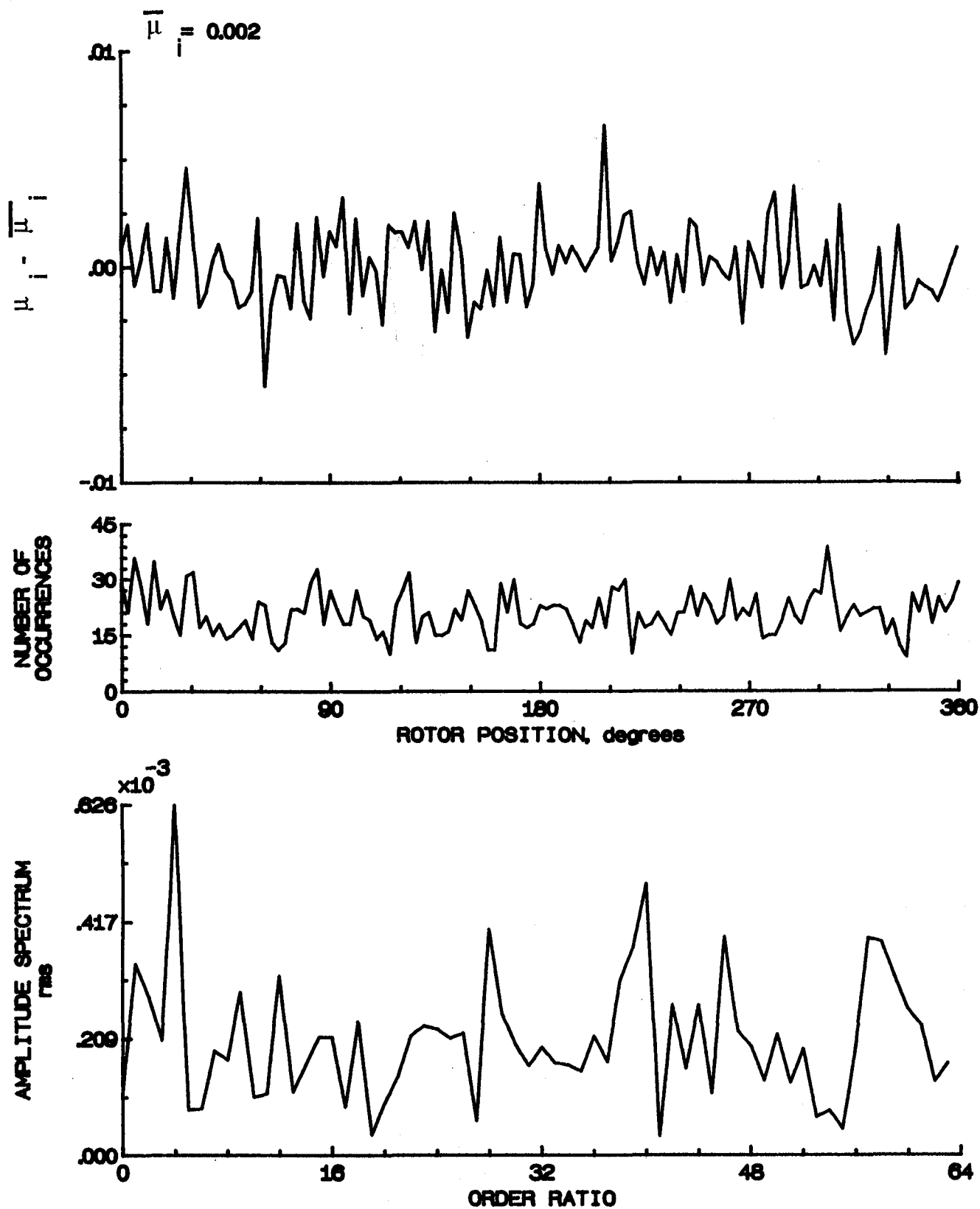


Figure 39.- Induced inflow velocity measured at 30 degrees and  $r/R$  of 0.98.

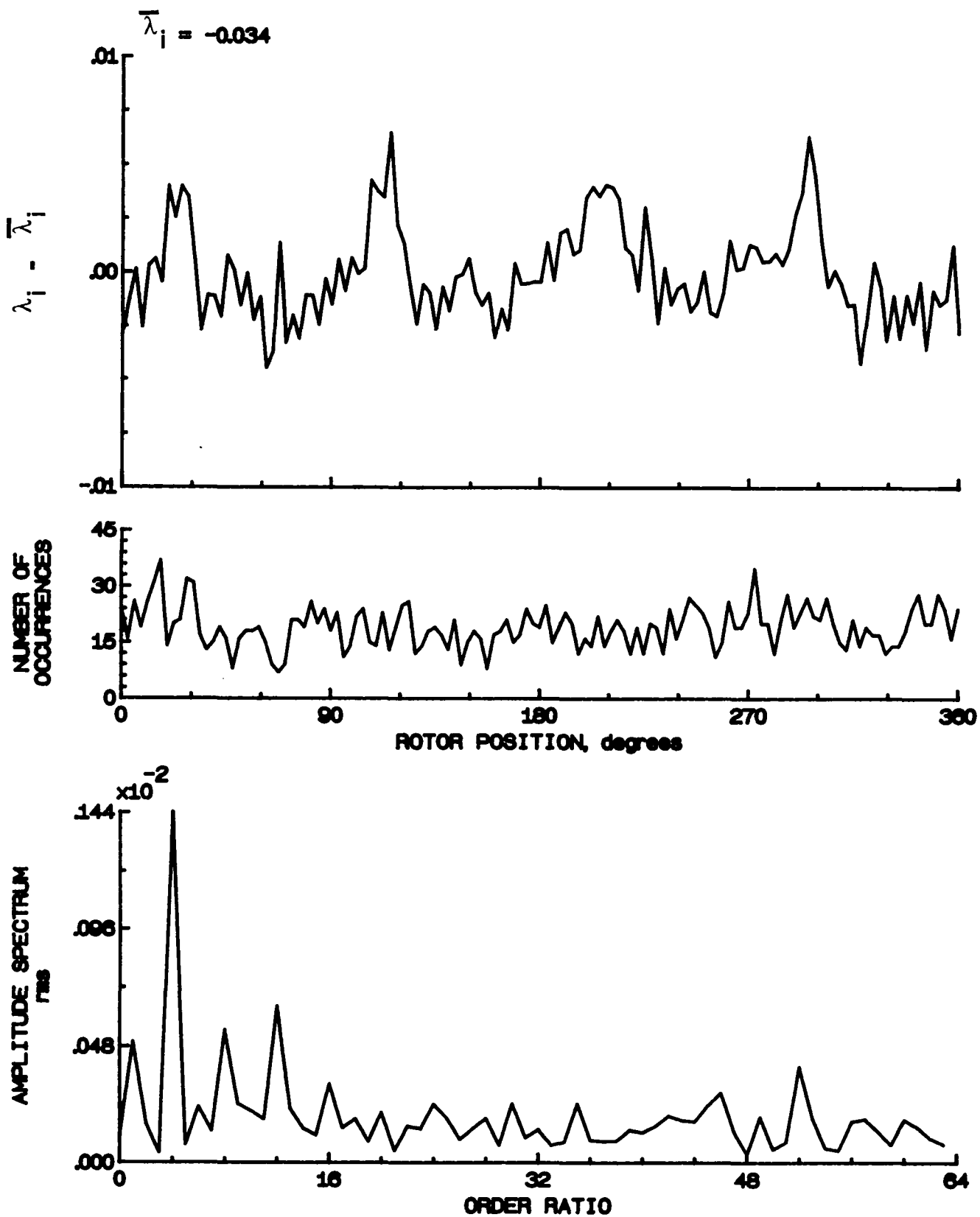


Figure 39.- Concluded.

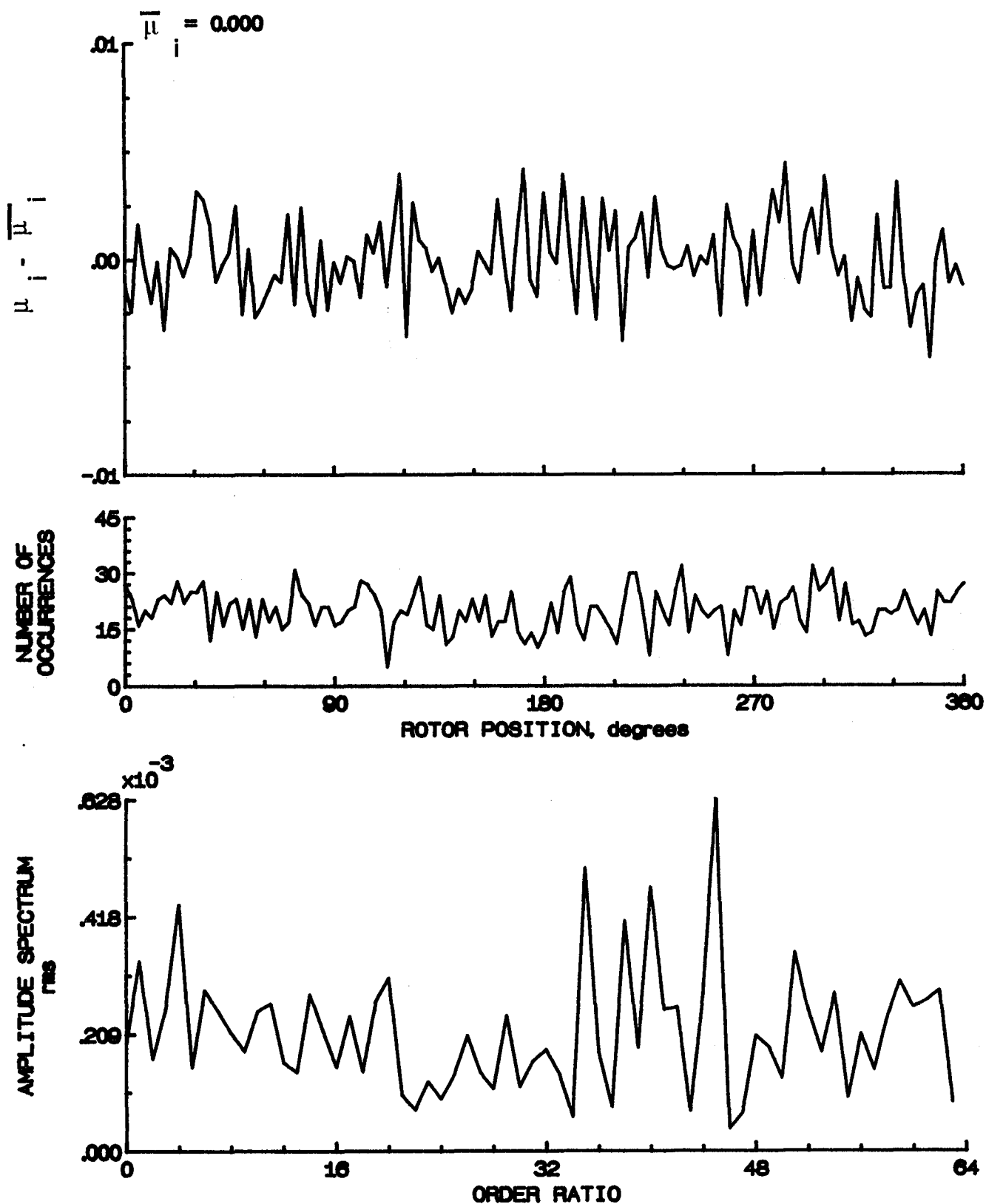


Figure 40.- Induced inflow velocity measured at 30 degrees and  $r/R$  of 1.02.



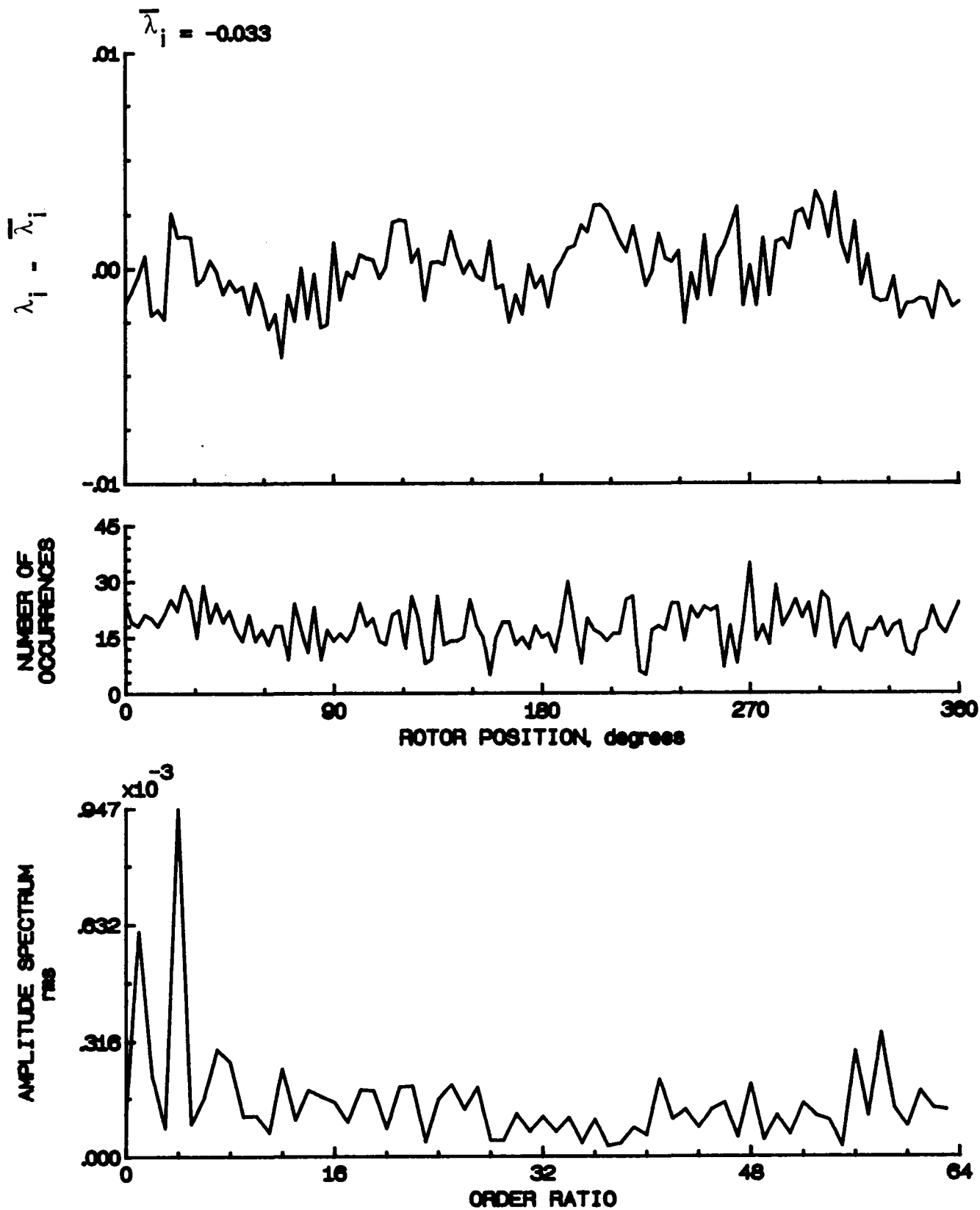


Figure 40.- Concluded.

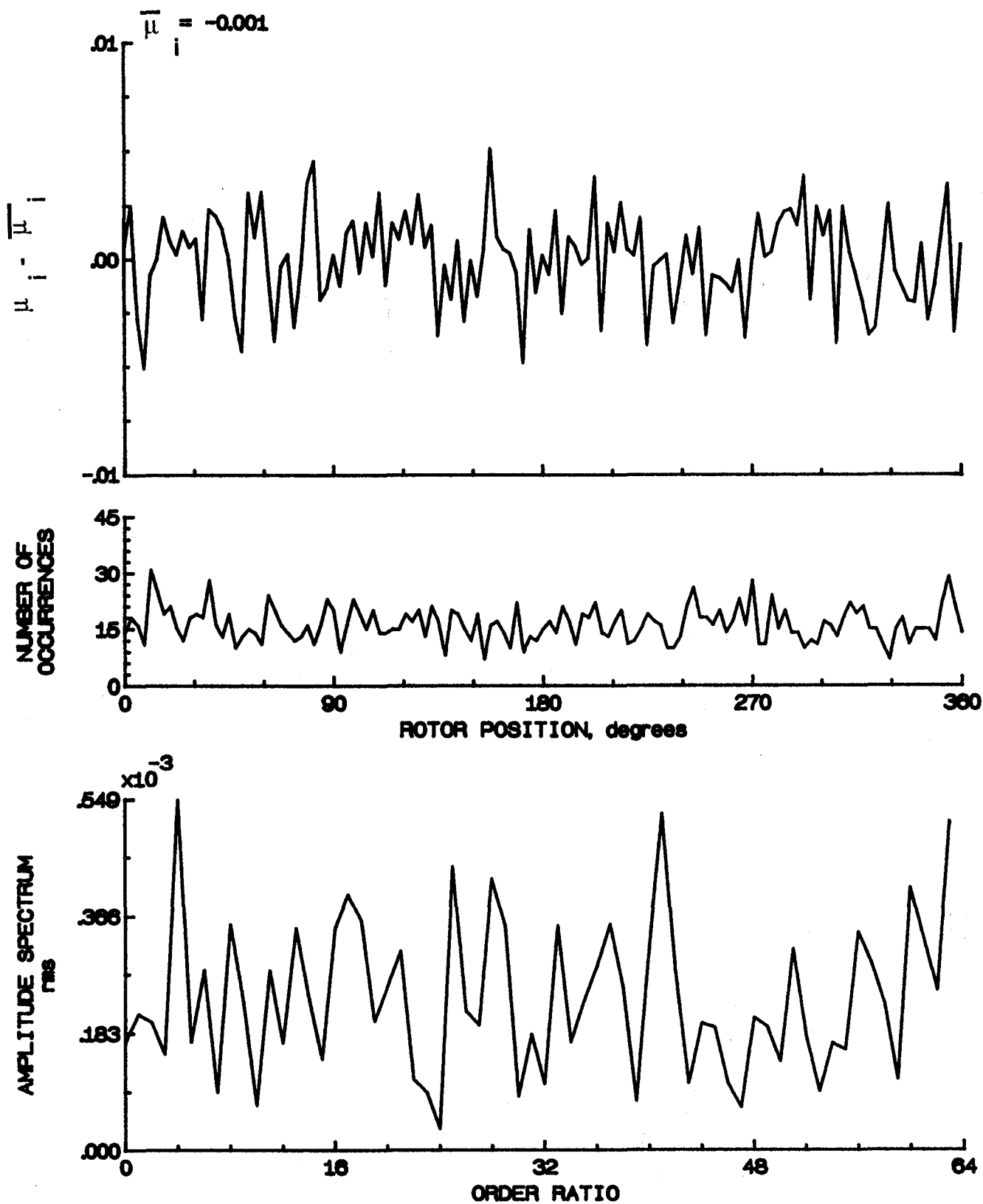


Figure 41.- Induced inflow velocity measured at 30 degrees and  $r/R$  of 1.04.

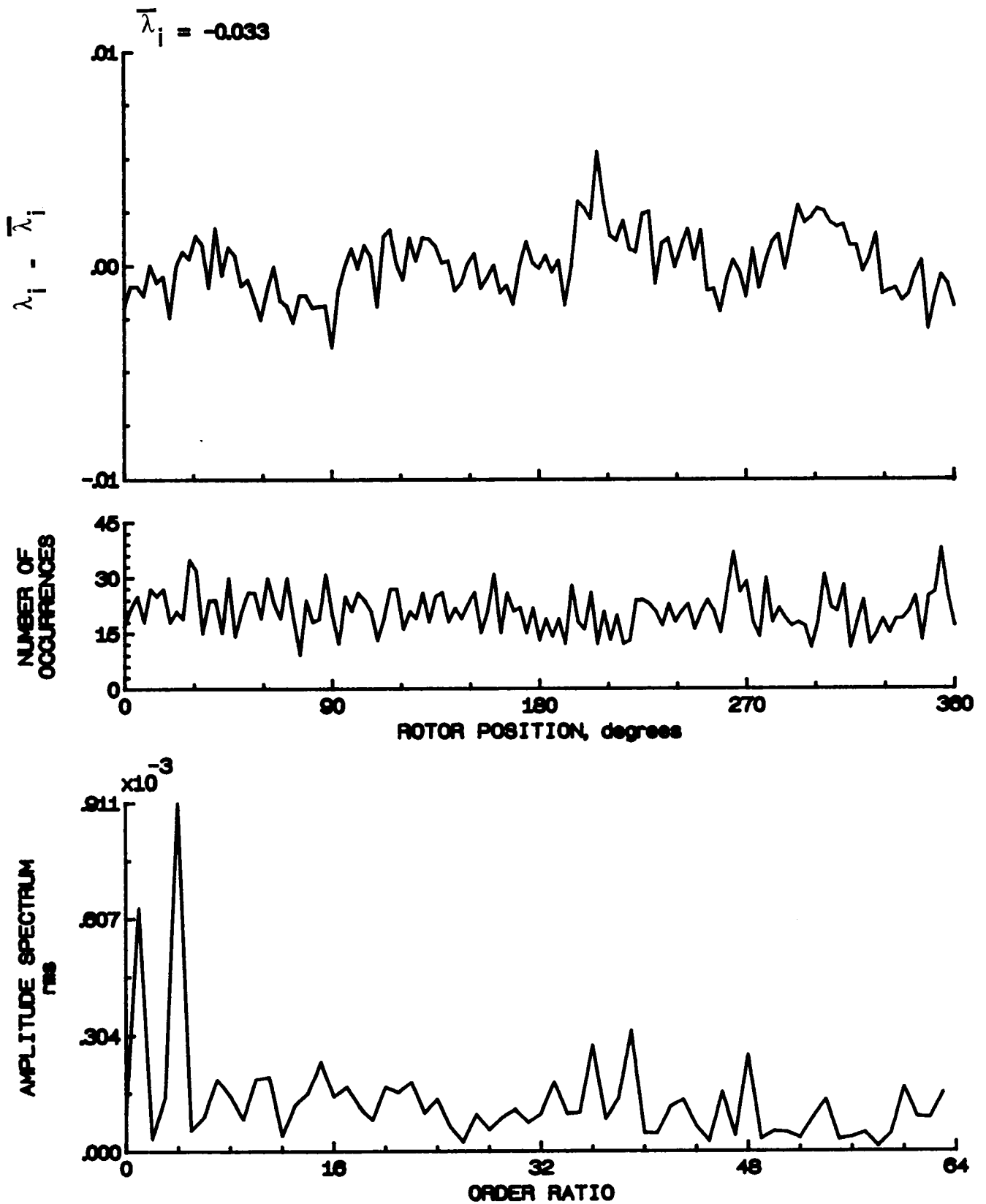


Figure 41.- Concluded.

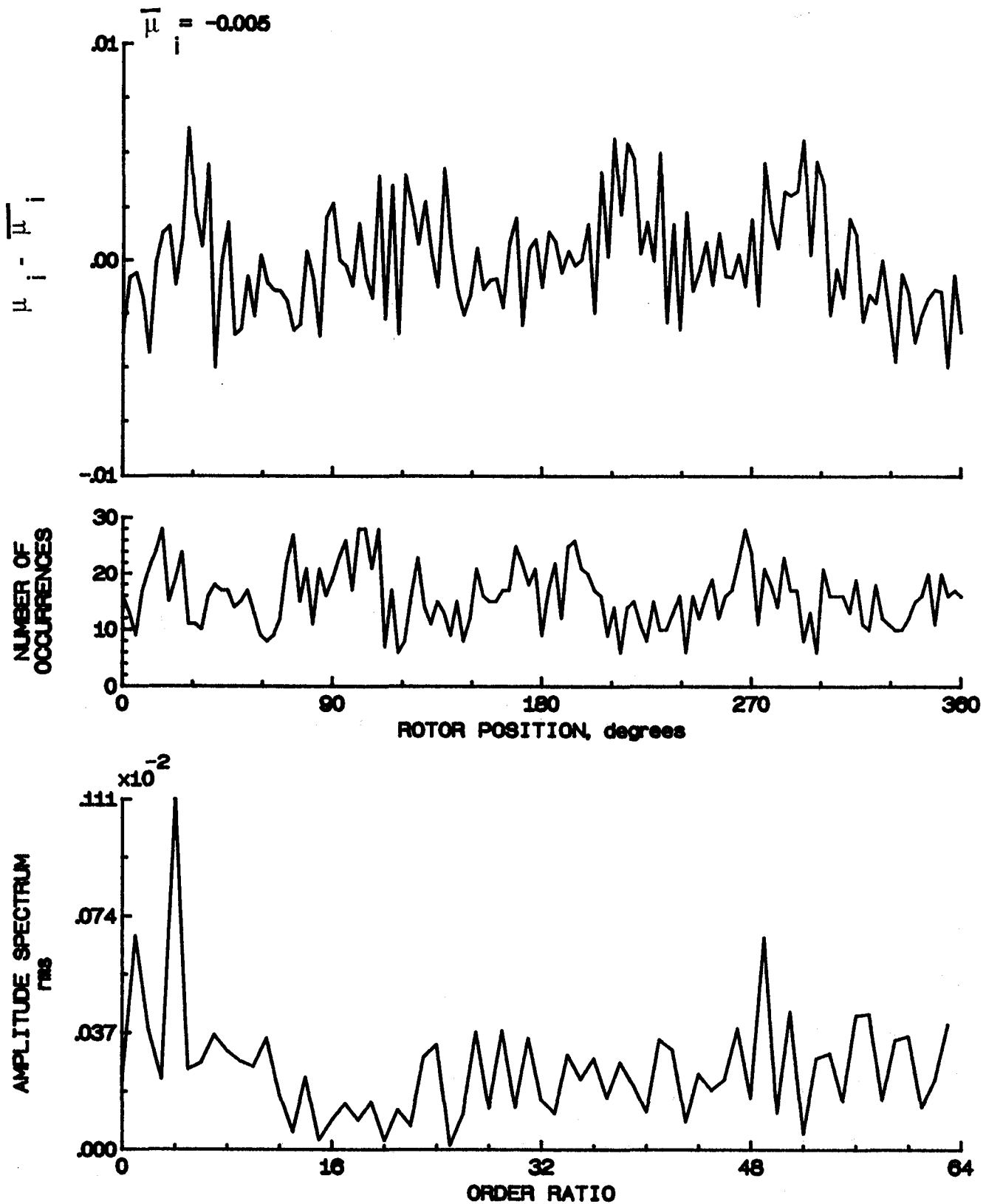


Figure 42.- Induced inflow velocity measured at 30 degrees and r/R of 1.10.

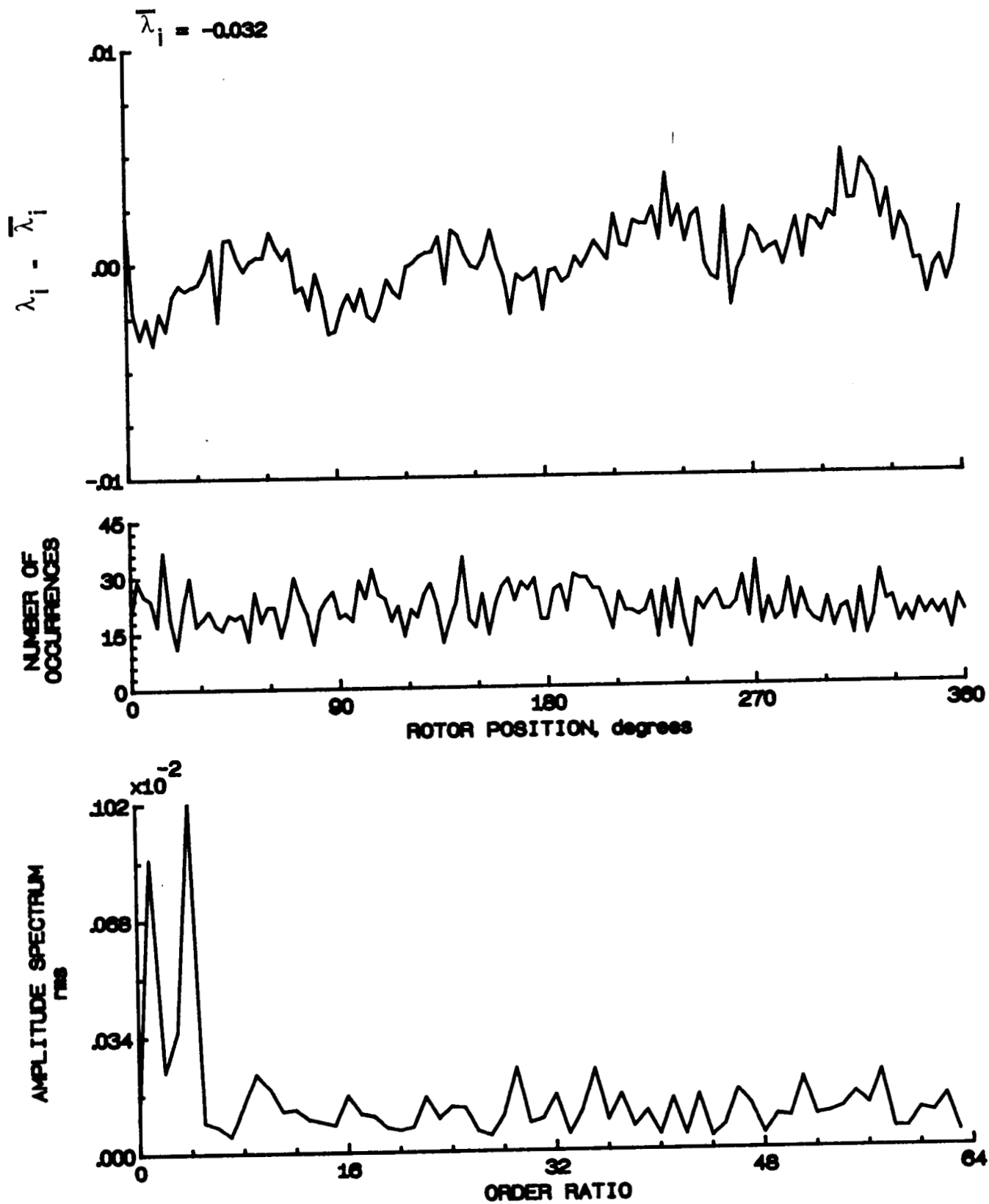


Figure 42.- Concluded.

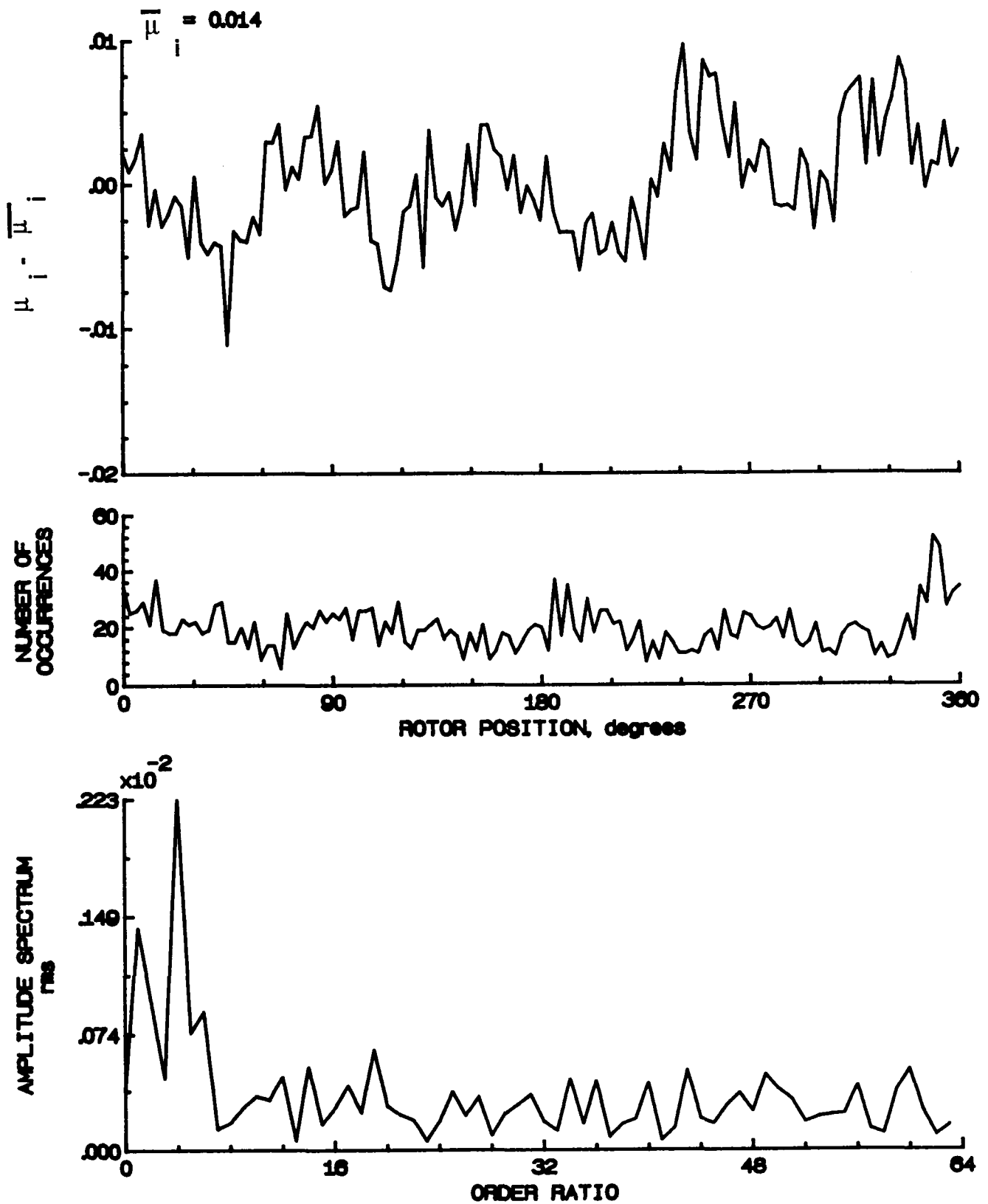


Figure 43.- Induced inflow velocity measured at 60 degrees and r/R of 0.20.

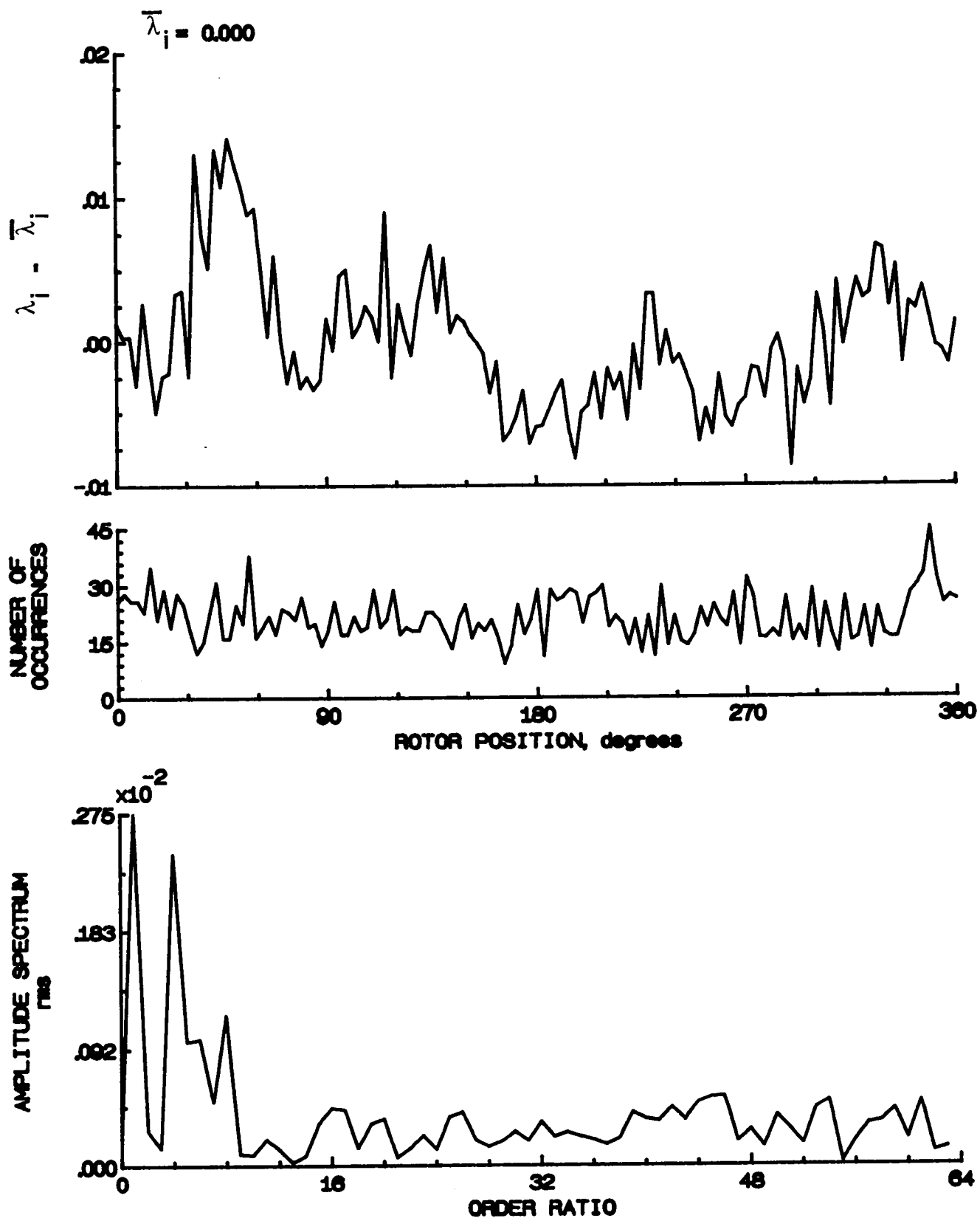


Figure 43.- Concluded.

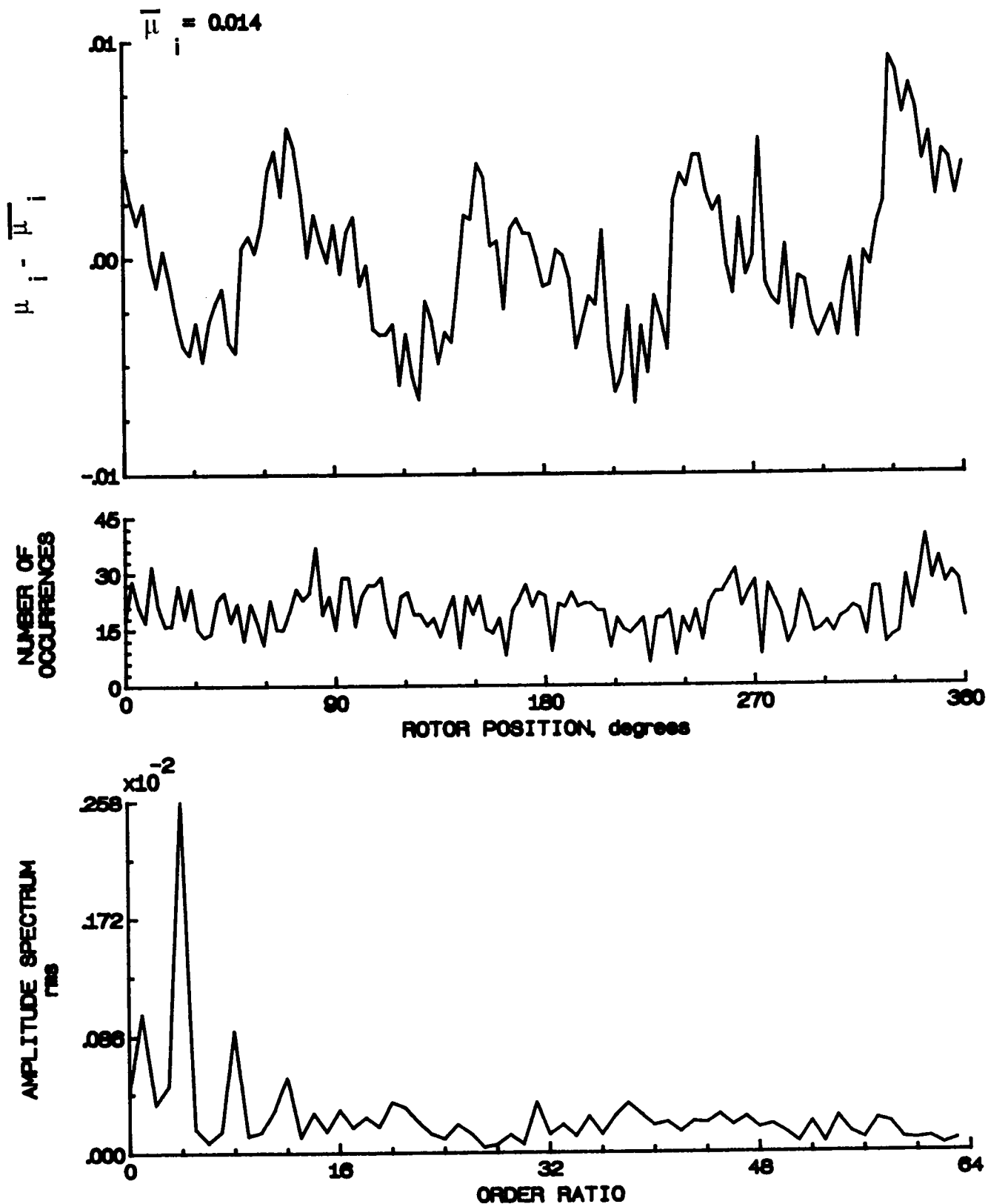


Figure 44.- Induced inflow velocity measured at 60 degrees and r/R of 0.40.



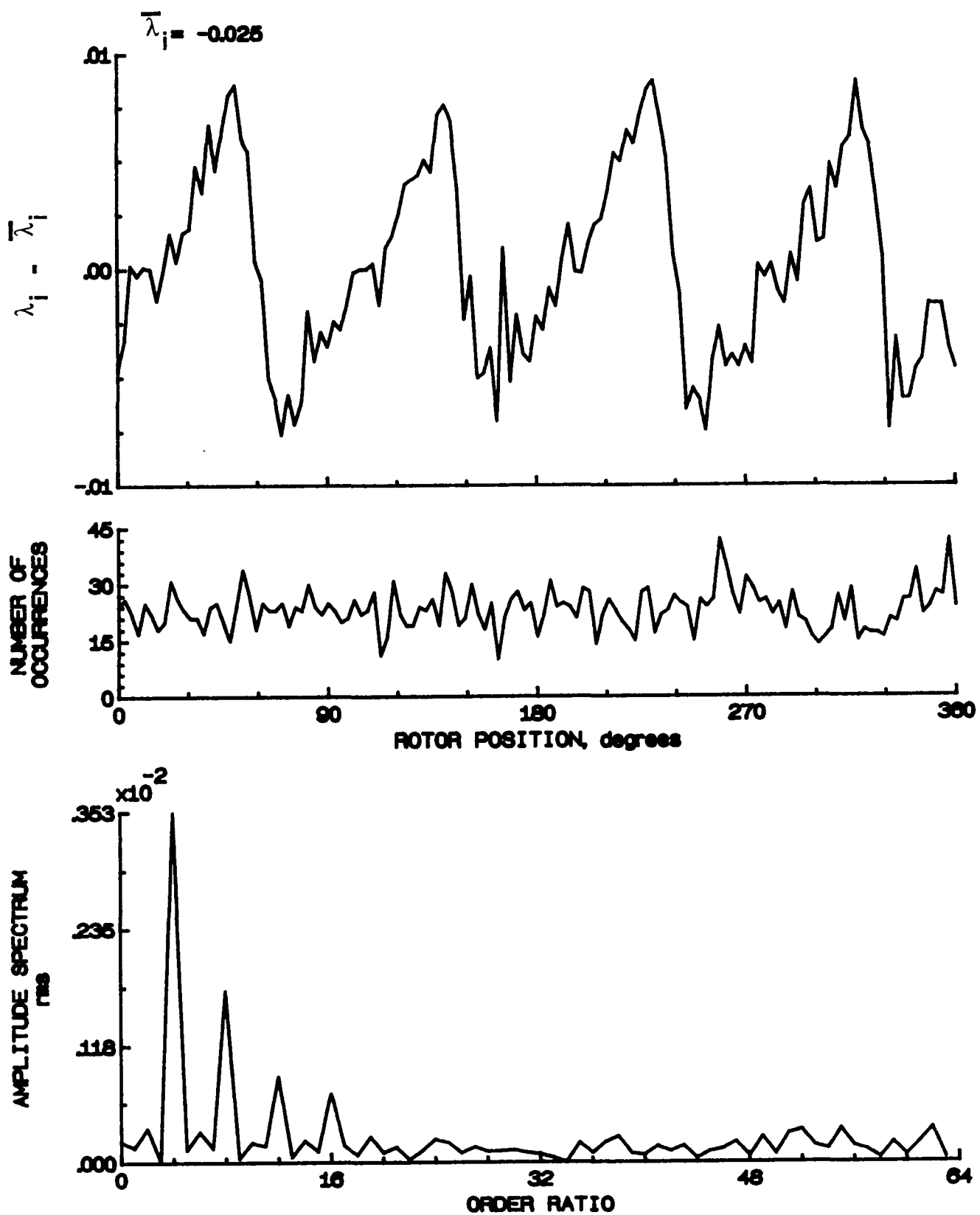


Figure 44.- Concluded.

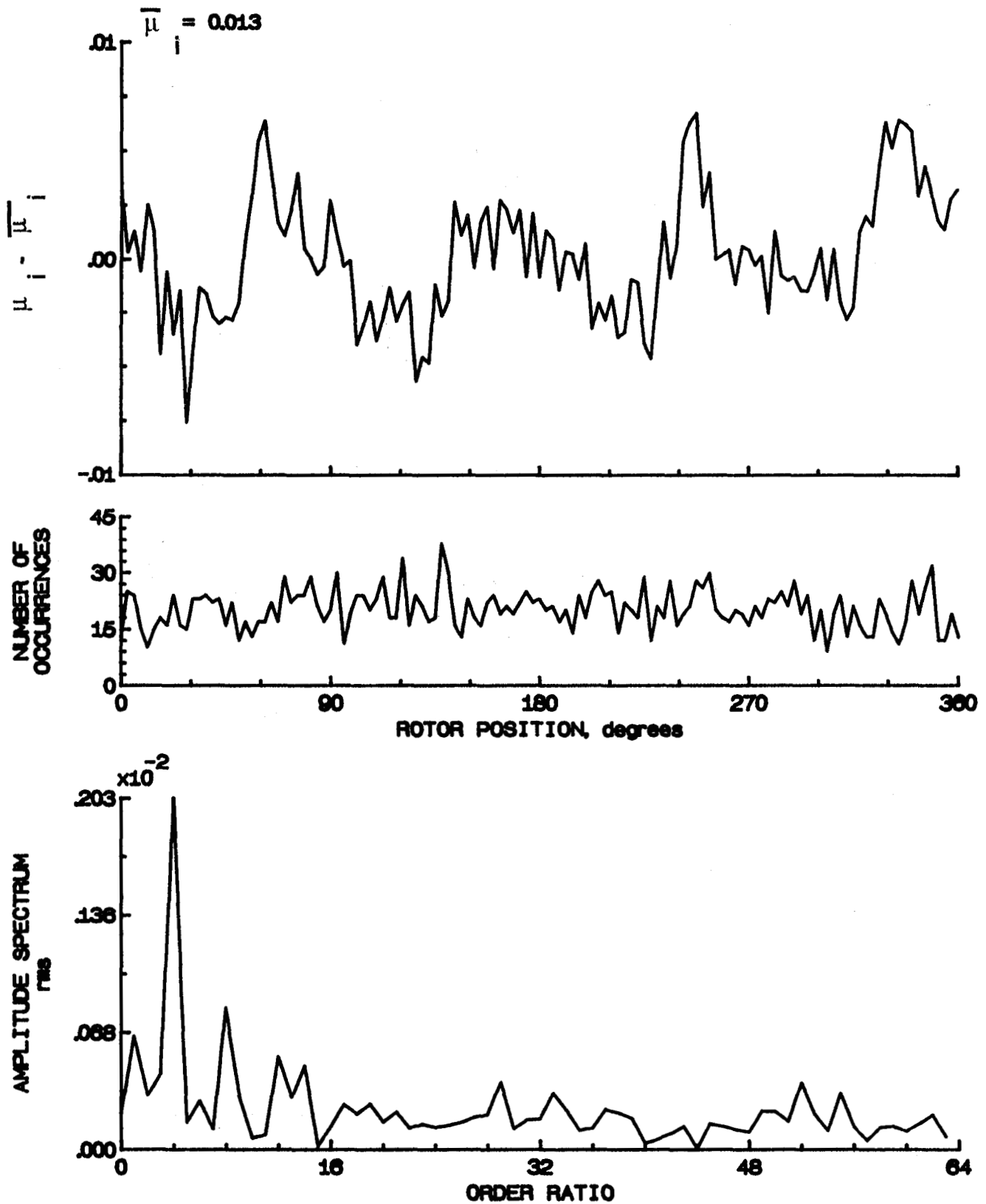


Figure 45.- Induced inflow velocity measured at 60 degrees and r/R of 0.50.

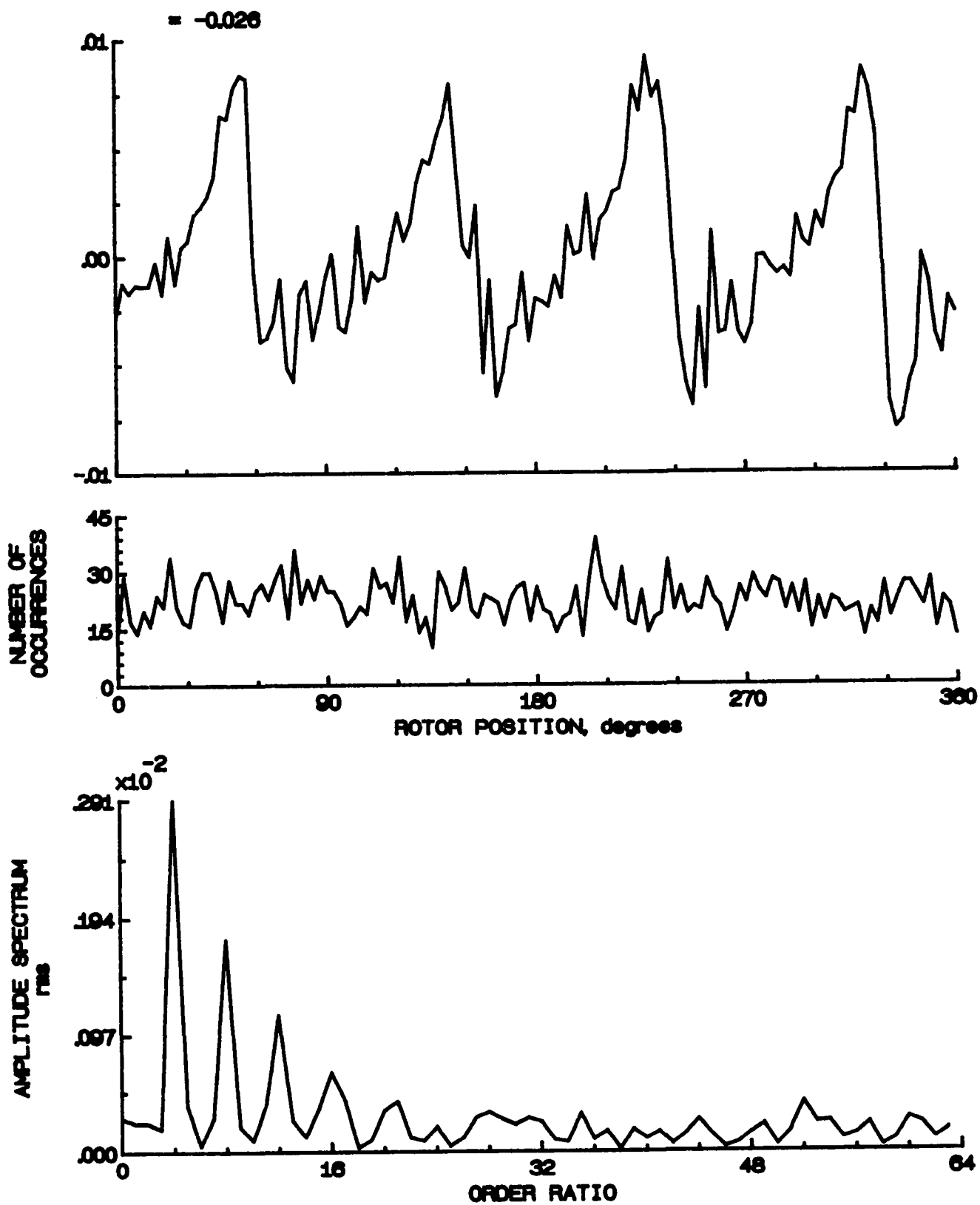


Figure 45.- Concluded.

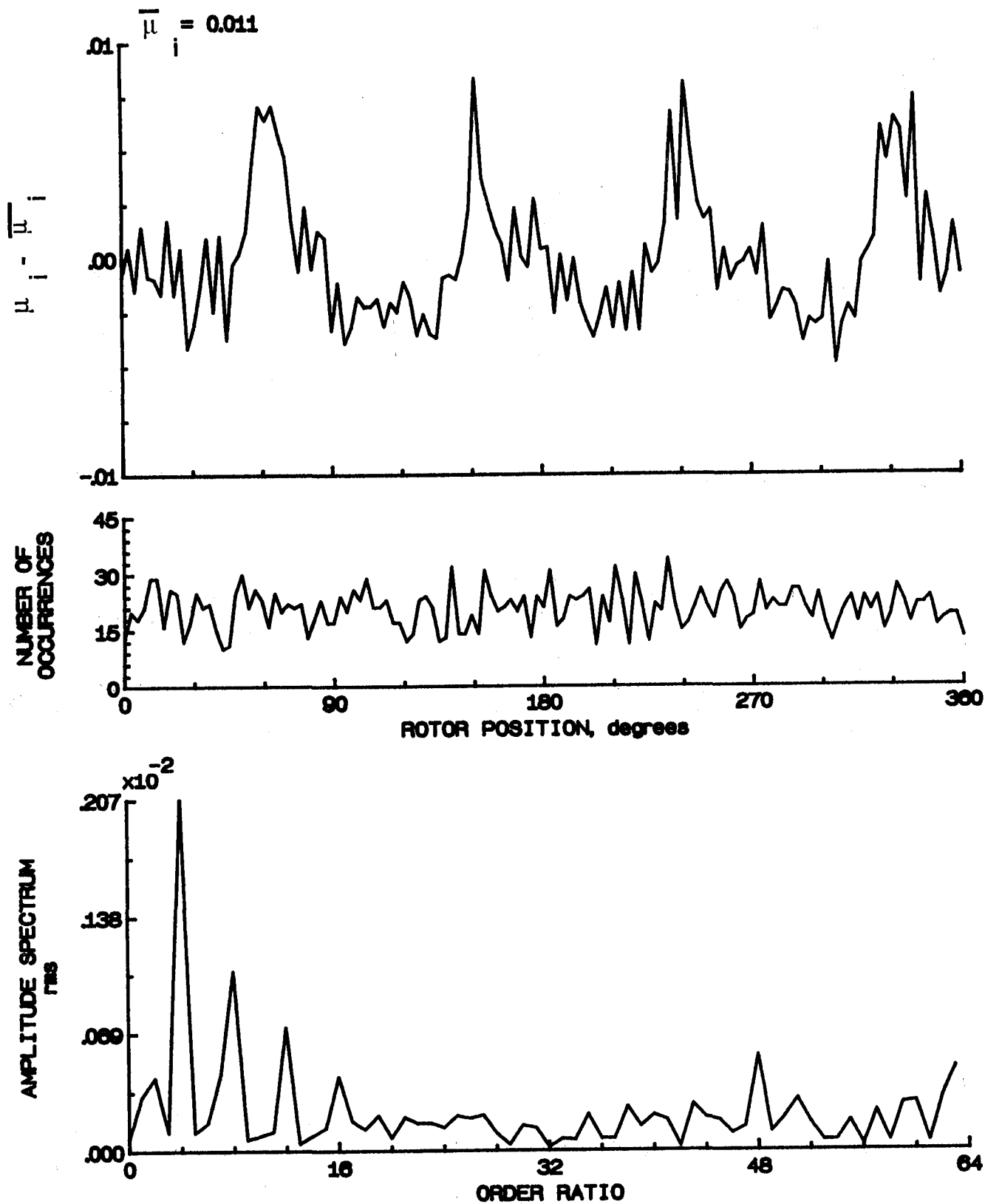


Figure 46.- Induced inflow velocity measured at 60 degrees and r/R of 0.60.

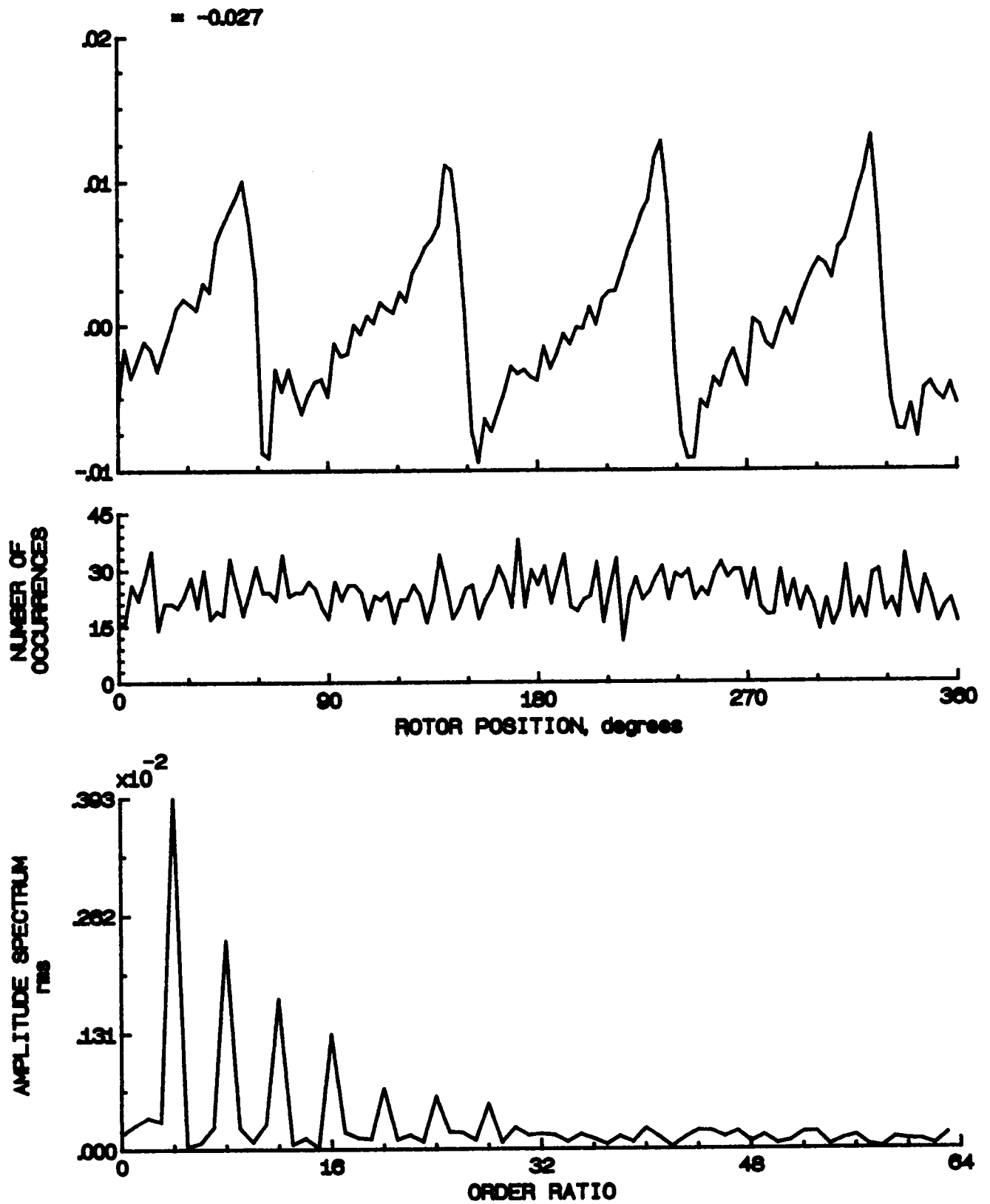


Figure 46.- Concluded.

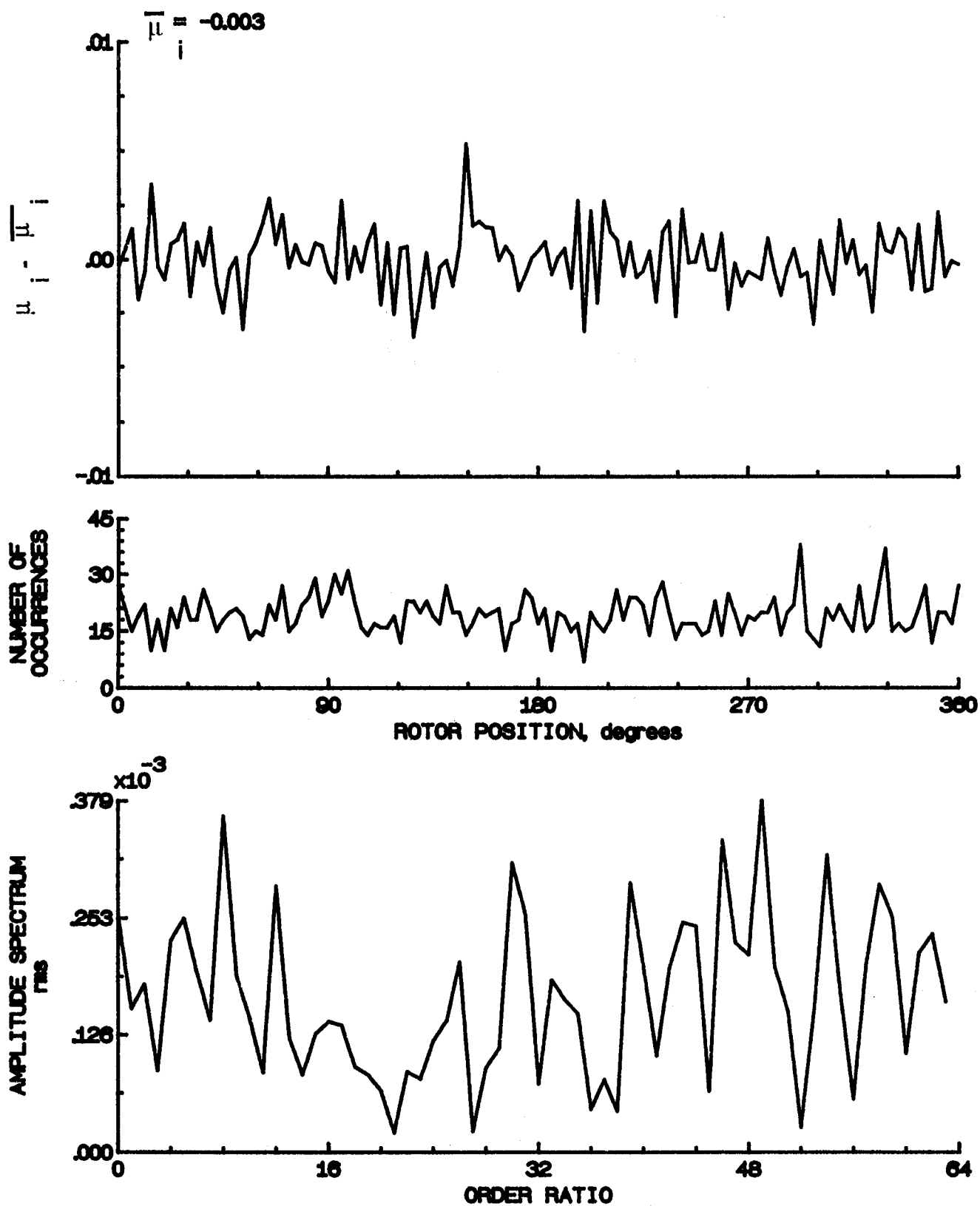


Figure 47.- Induced inflow velocity measured at 60 degrees and r/R of 0.70.

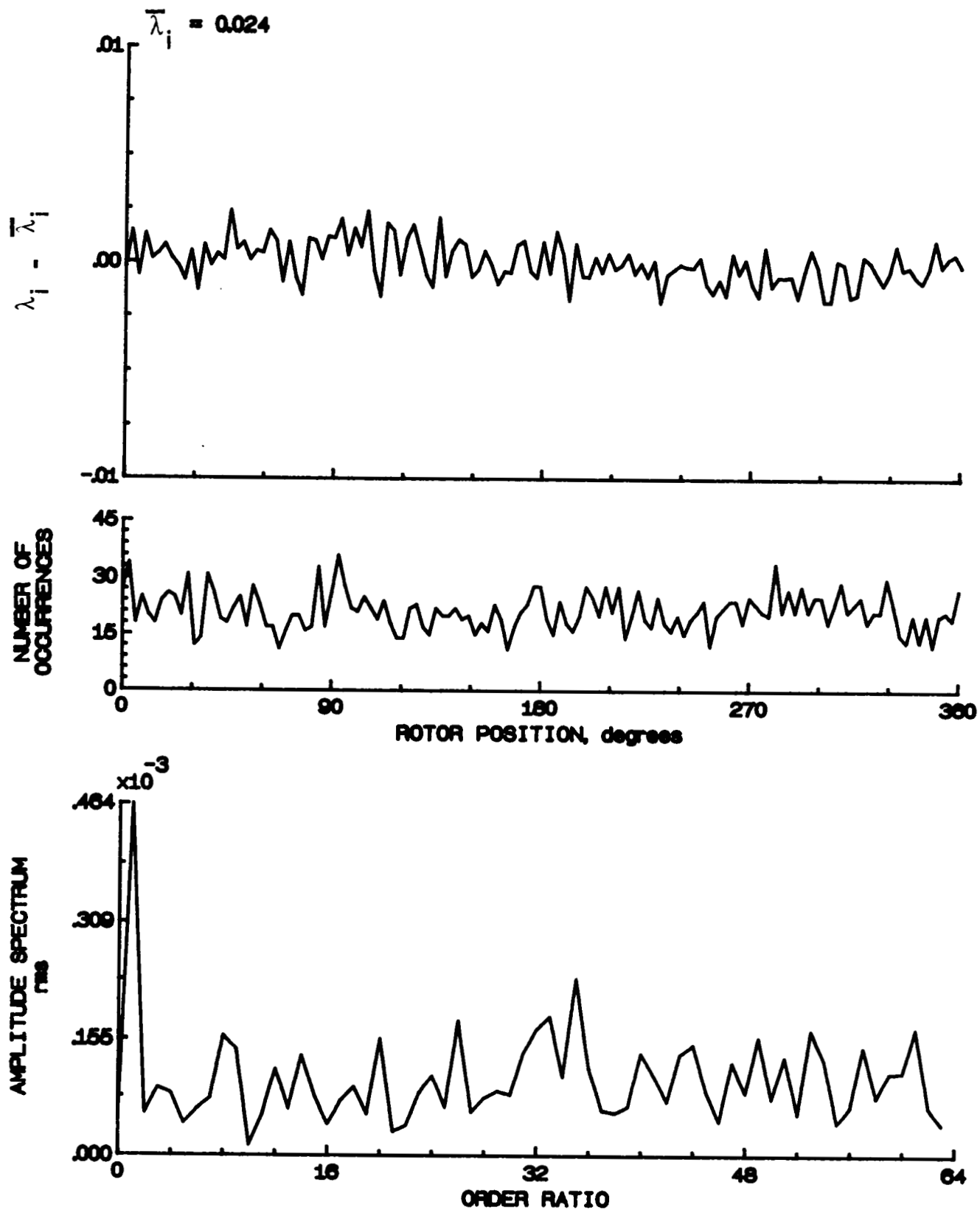


Figure 47.- Concluded.

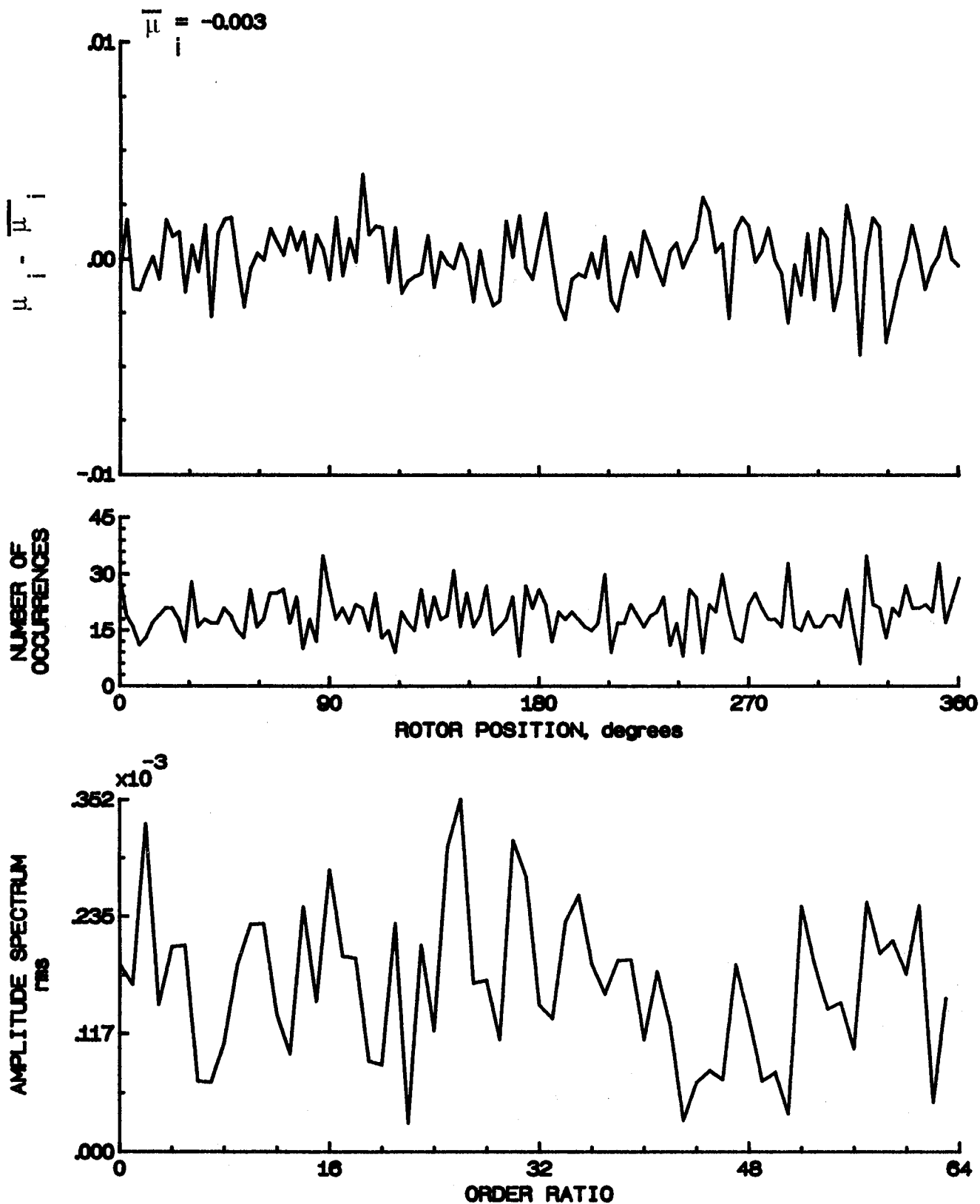


Figure 48.- Induced inflow velocity measured at 60 degrees and r/R of 0.74.



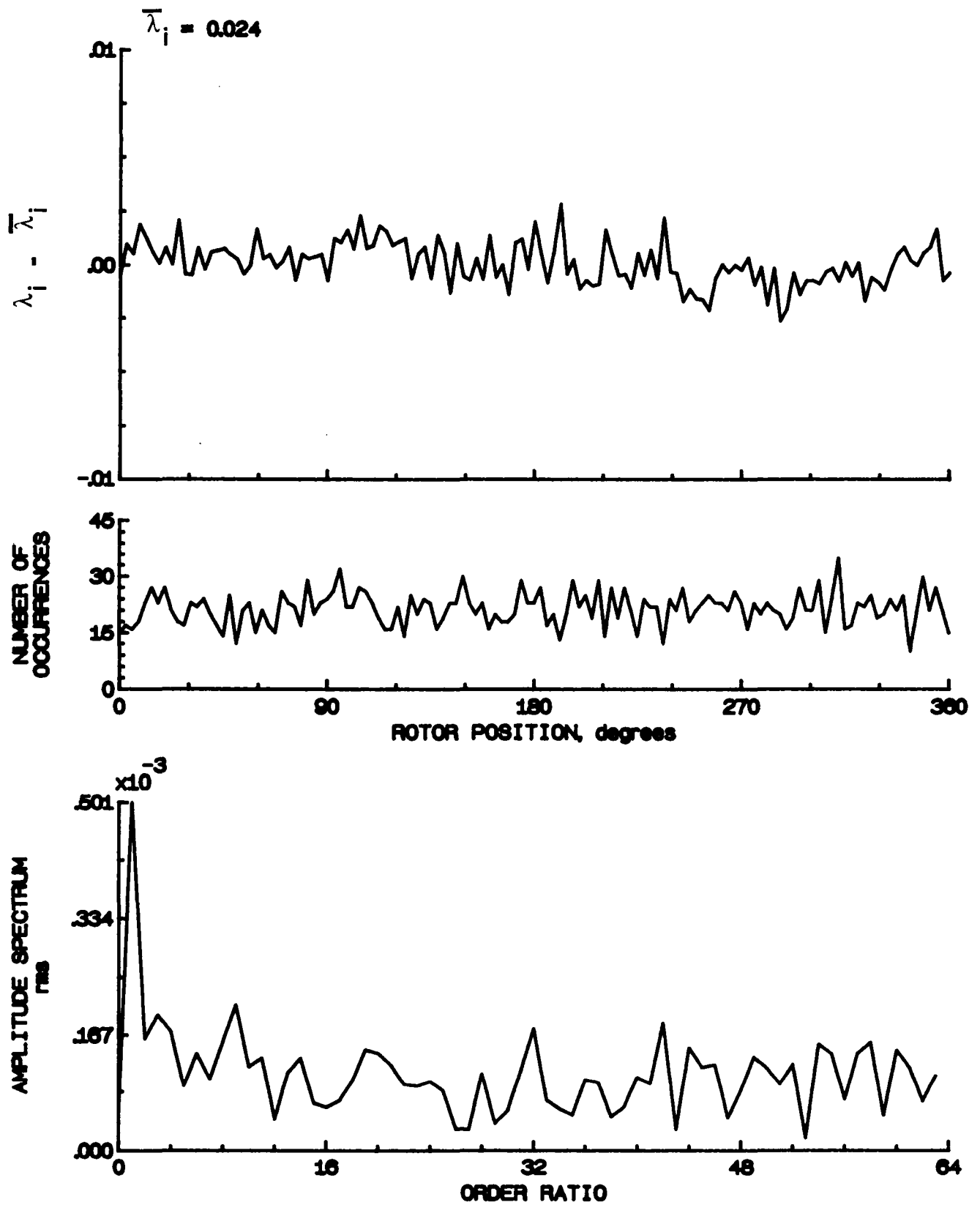


Figure 48.- Concluded.

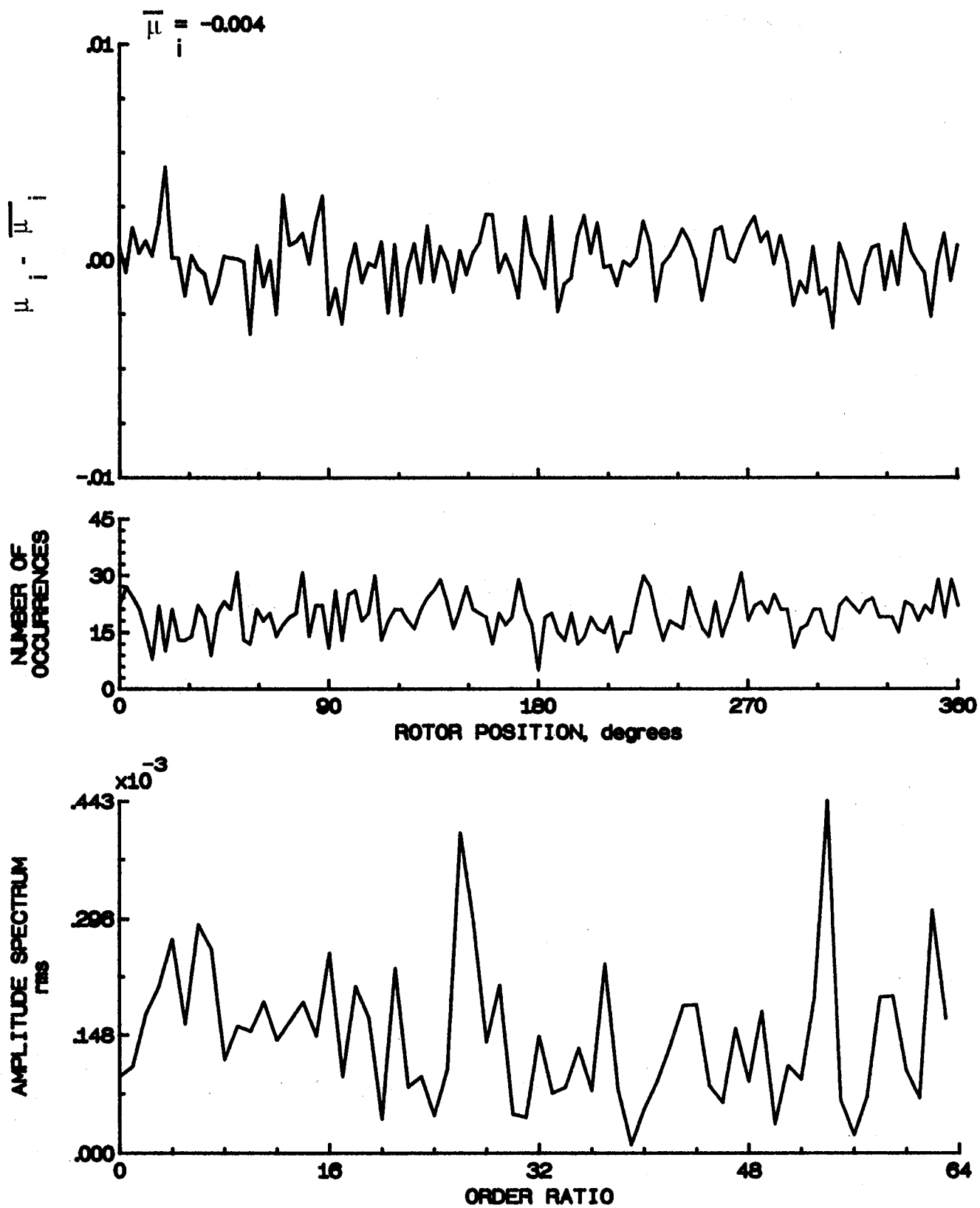


Figure 49.- Induced inflow velocity measured at 60 degrees and r/R of 0.78.

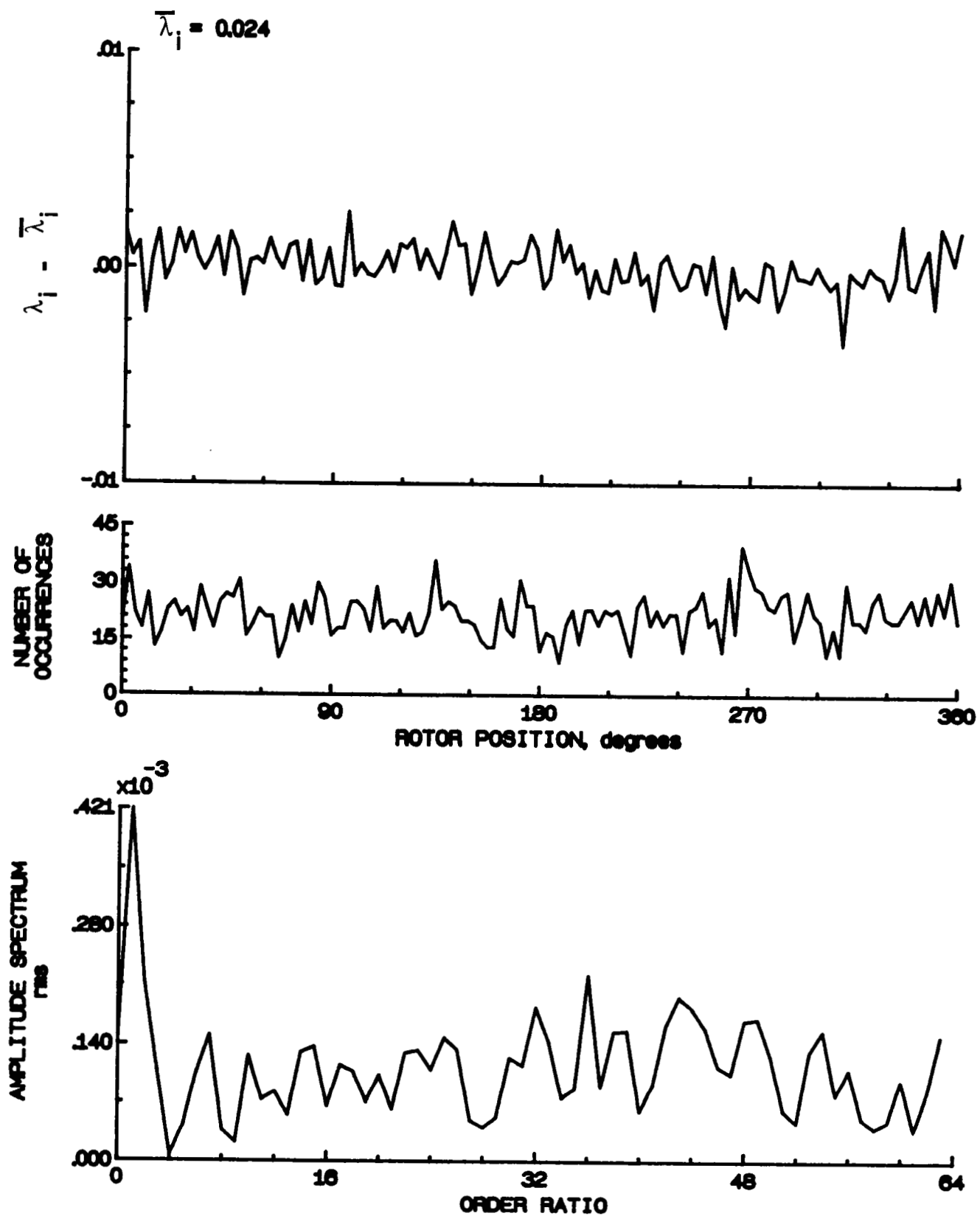


Figure 49.- Concluded.

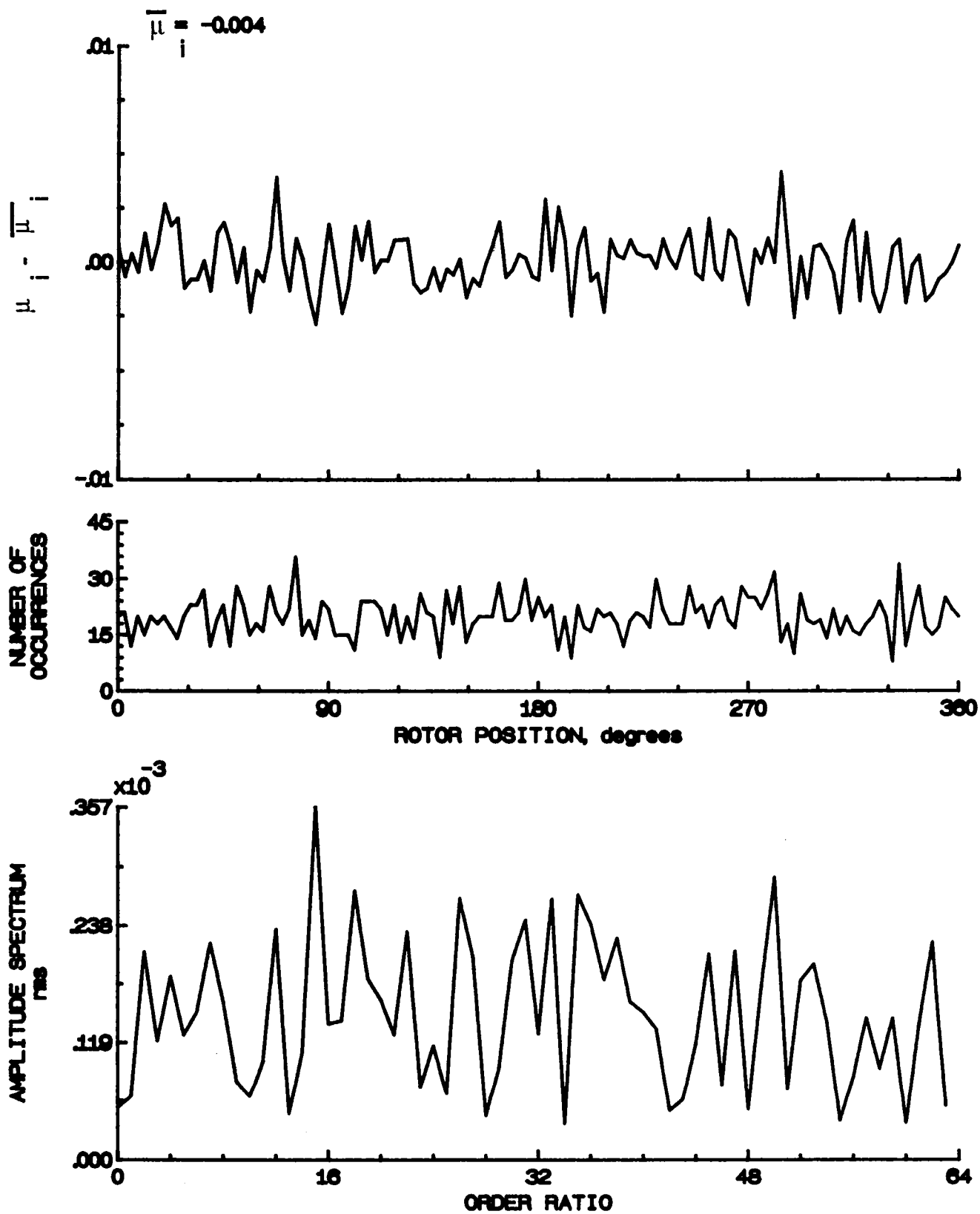


Figure 50.- Induced inflow velocity measured at 60 degrees and r/R of 0.82.

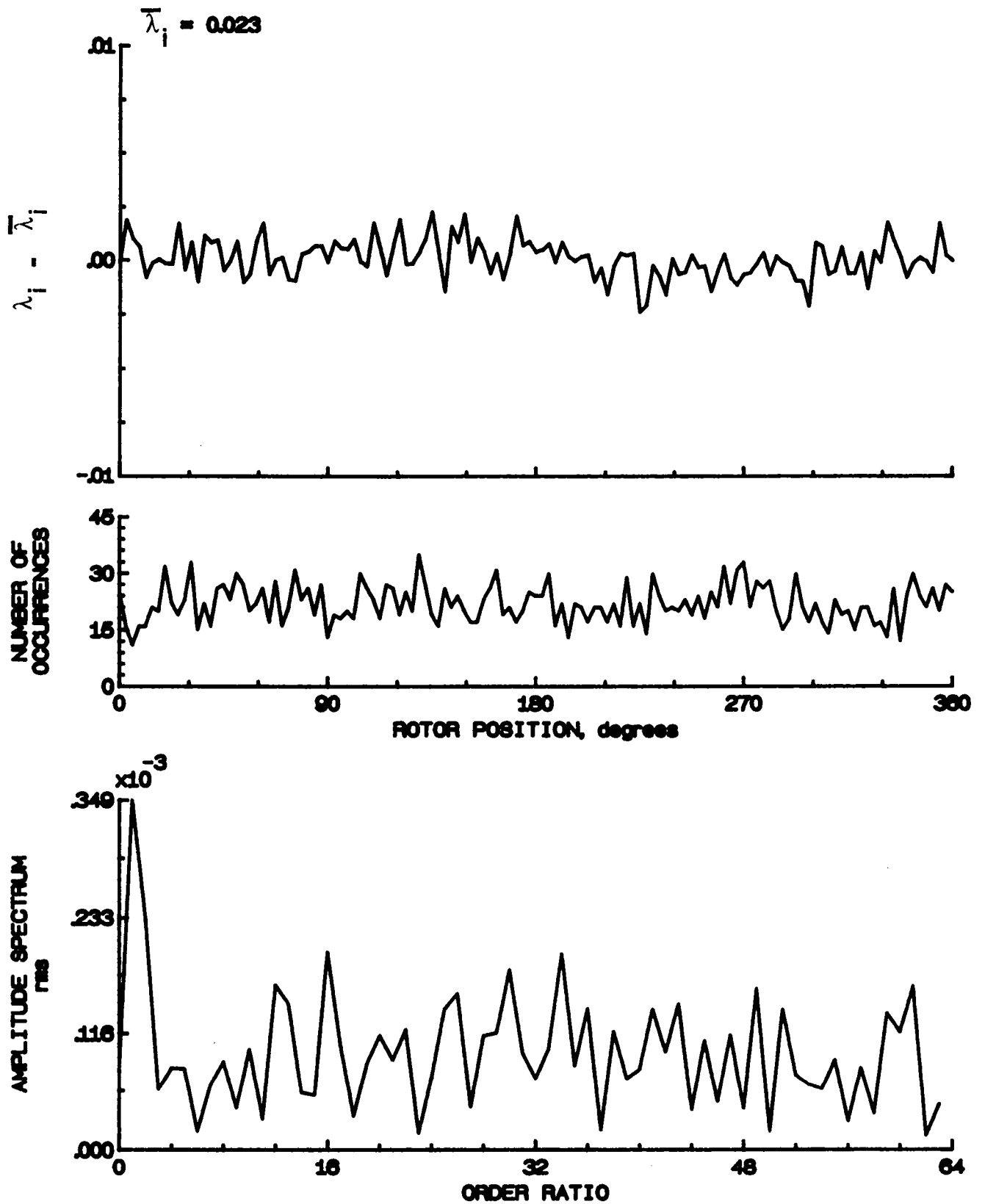


Figure 50.- Concluded.

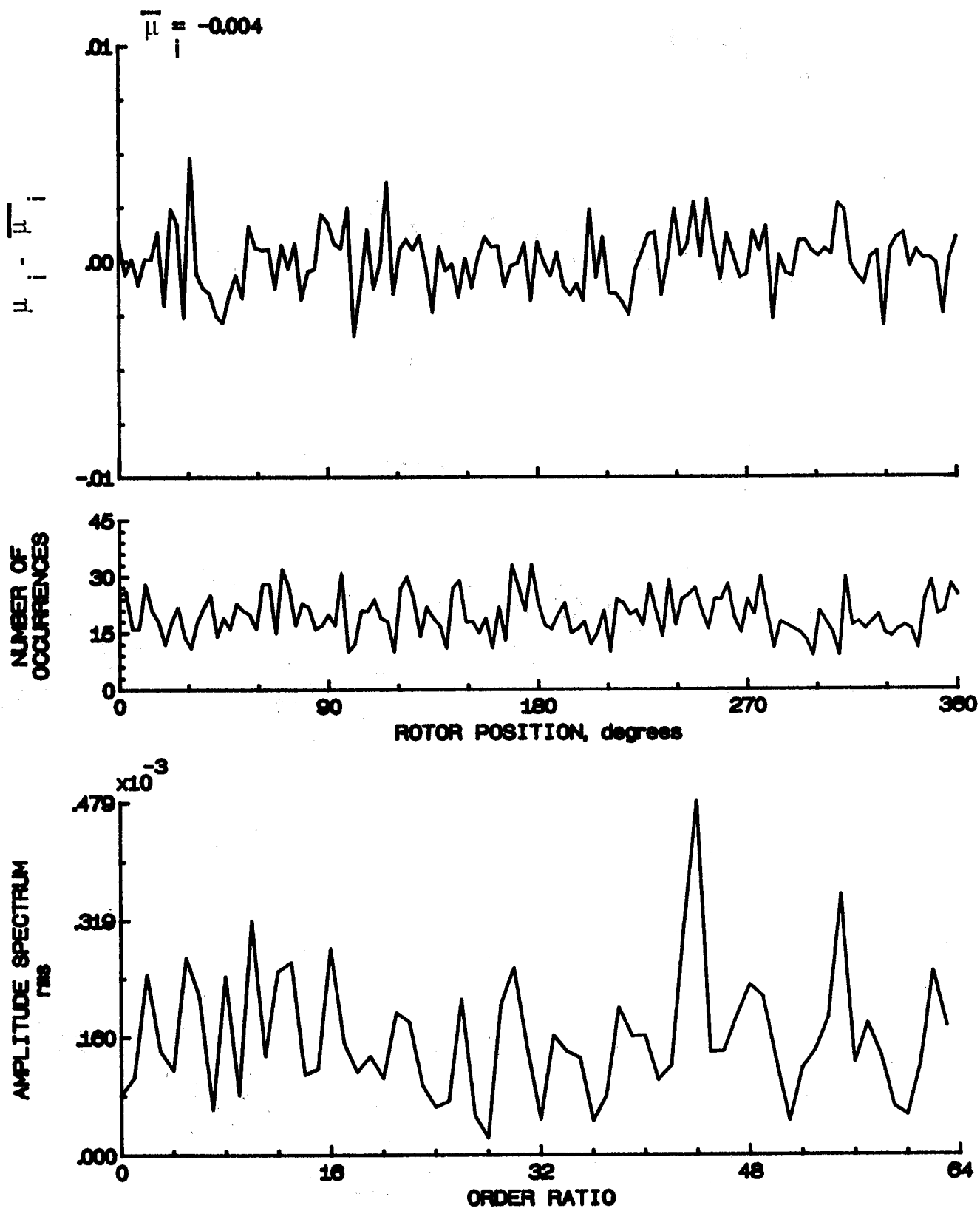


Figure 51- Induced inflow velocity measured at 60 degrees and r/R of 0.86.

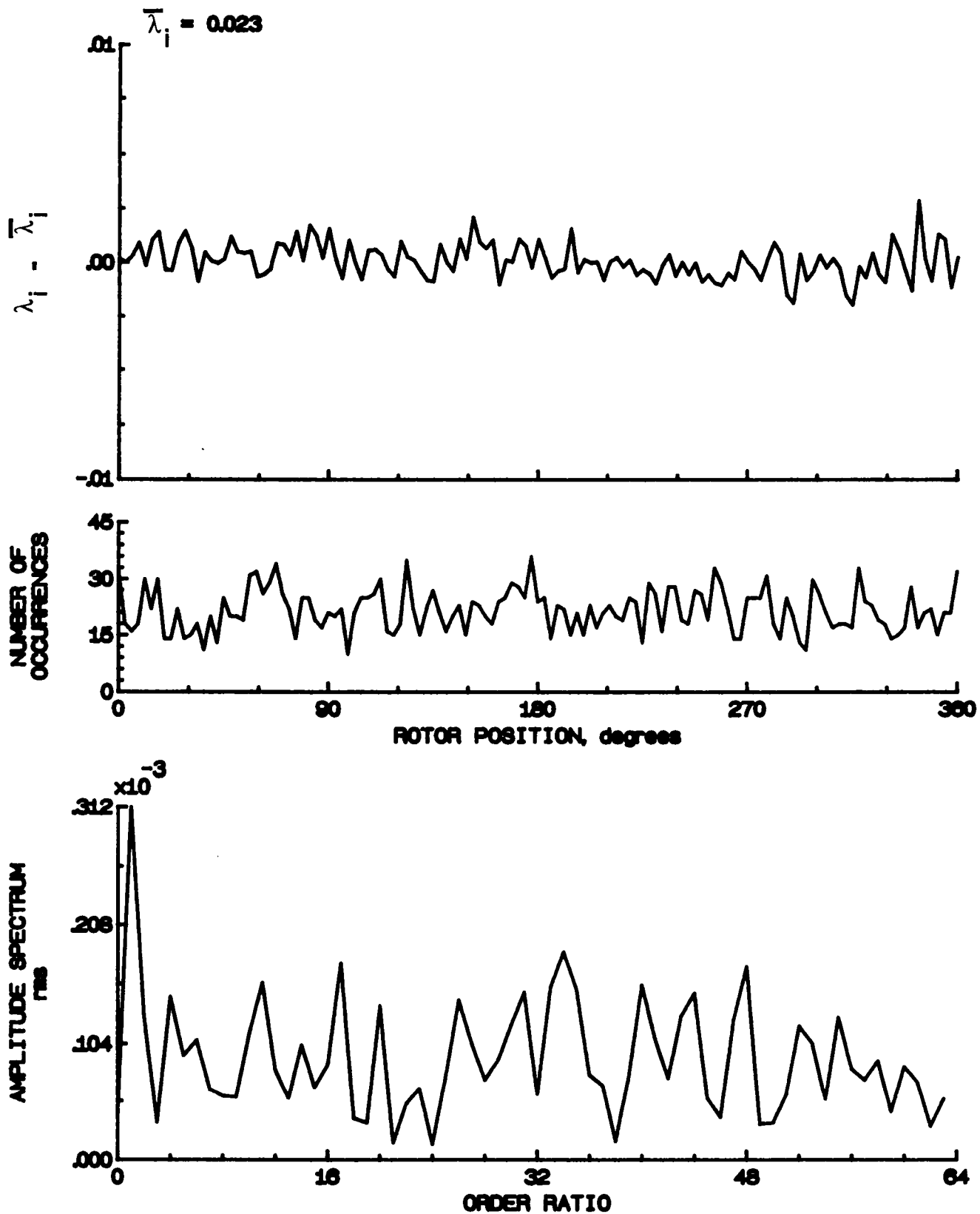


Figure 51- Concluded.

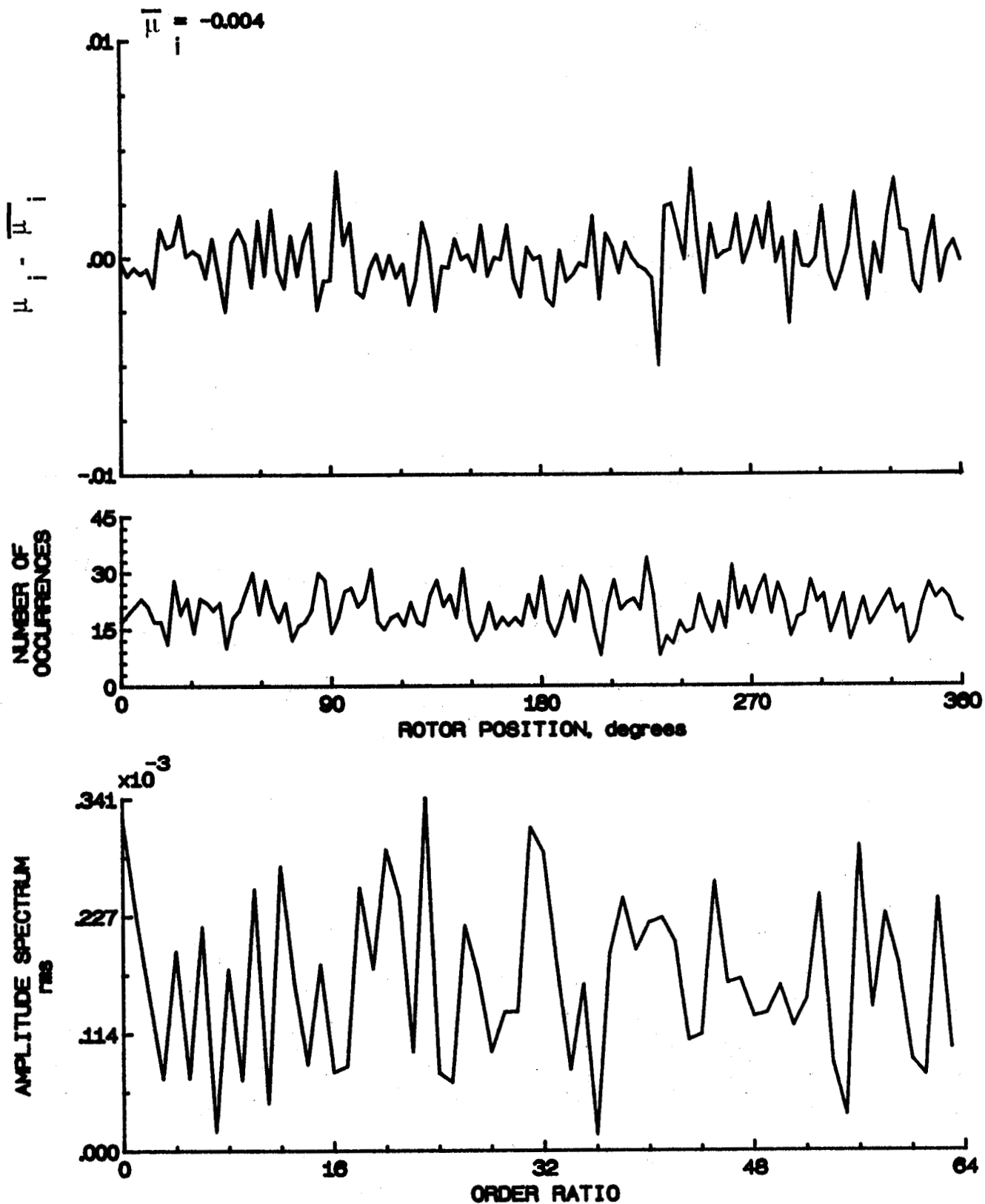


Figure 52.- Induced inflow velocity measured at 60 degrees and r/R of 0.90.



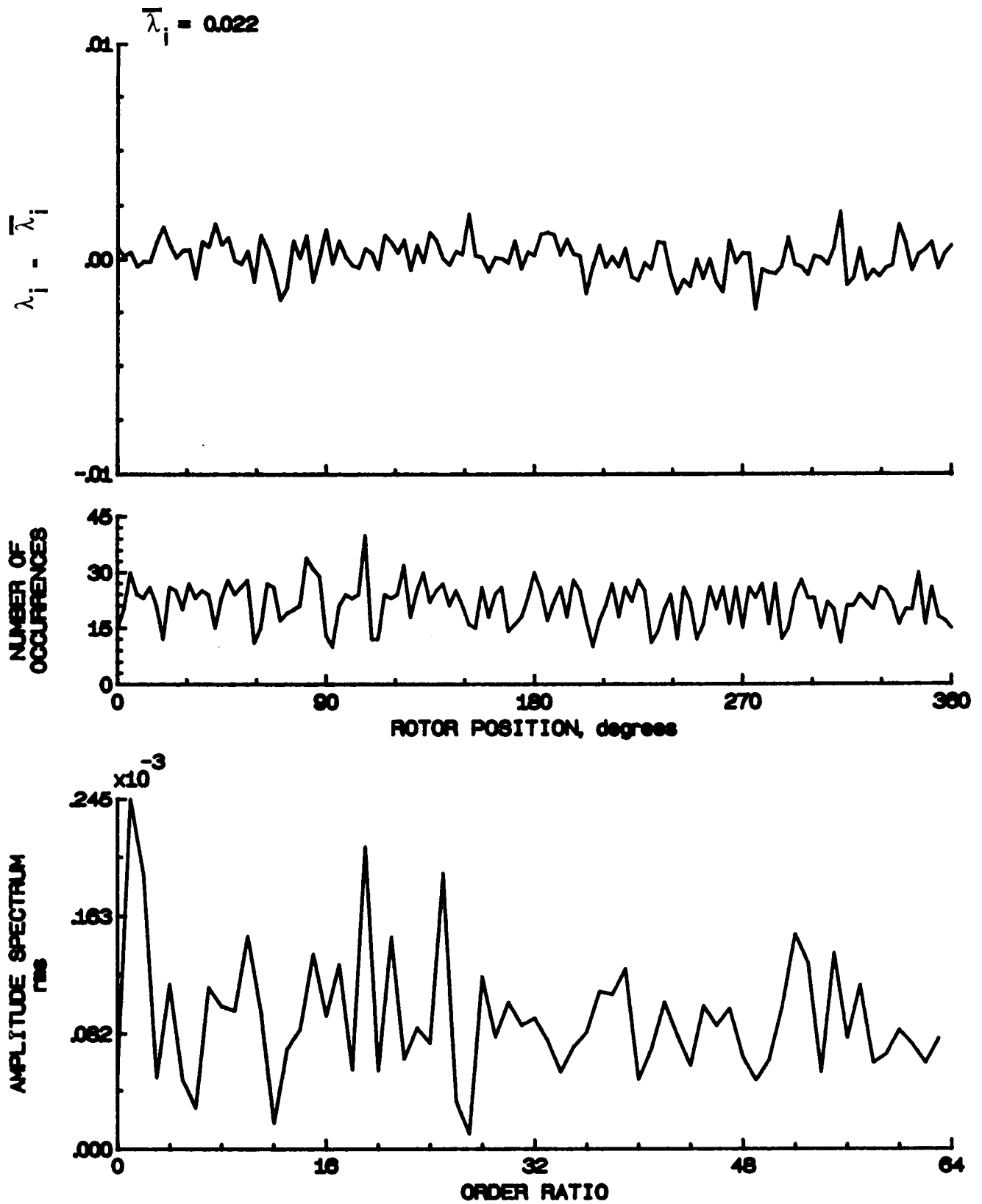


Figure 52.- Concluded.

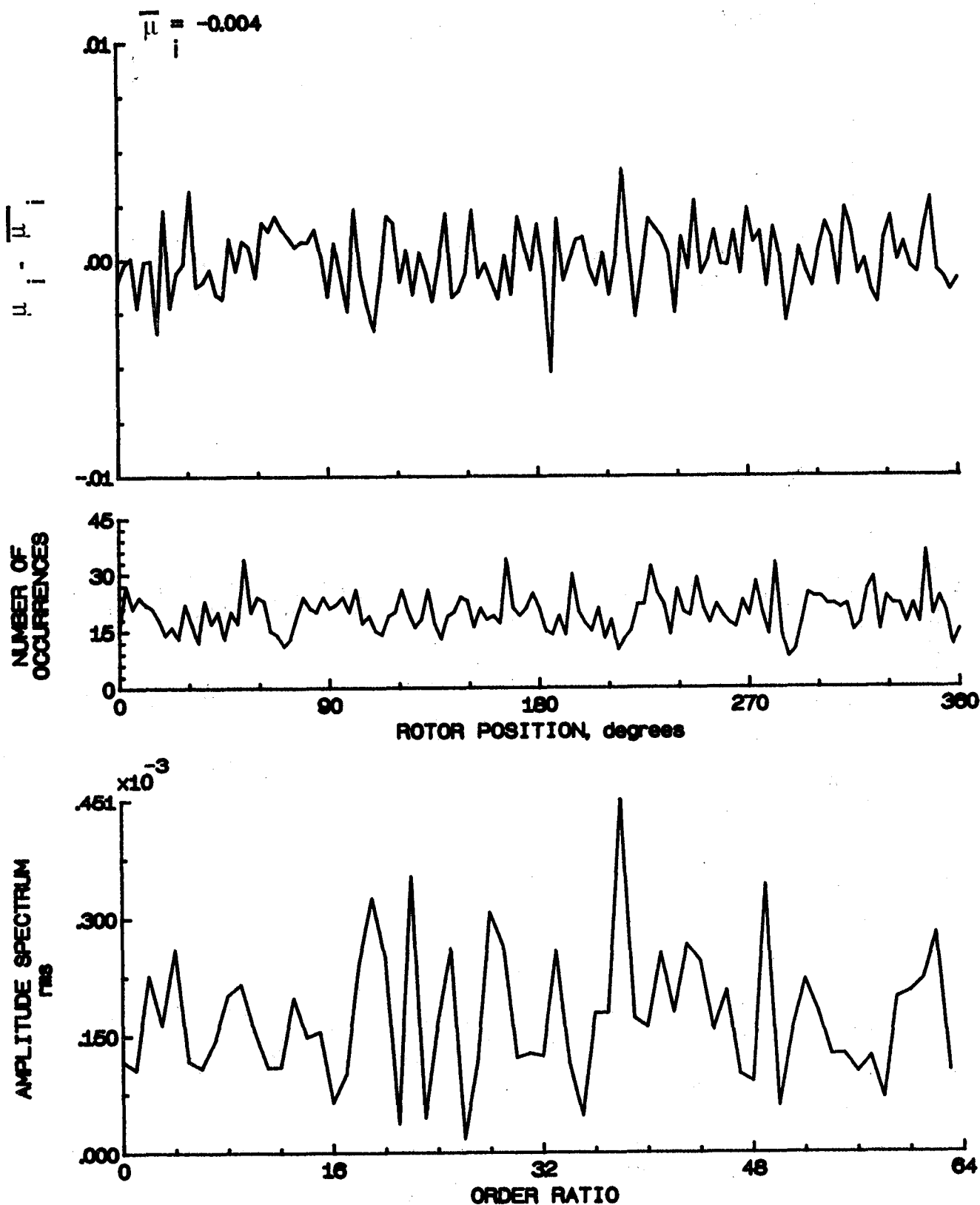


Figure 53.- Induced inflow velocity measured at 60 degrees and  $r/R$  of 0.94.

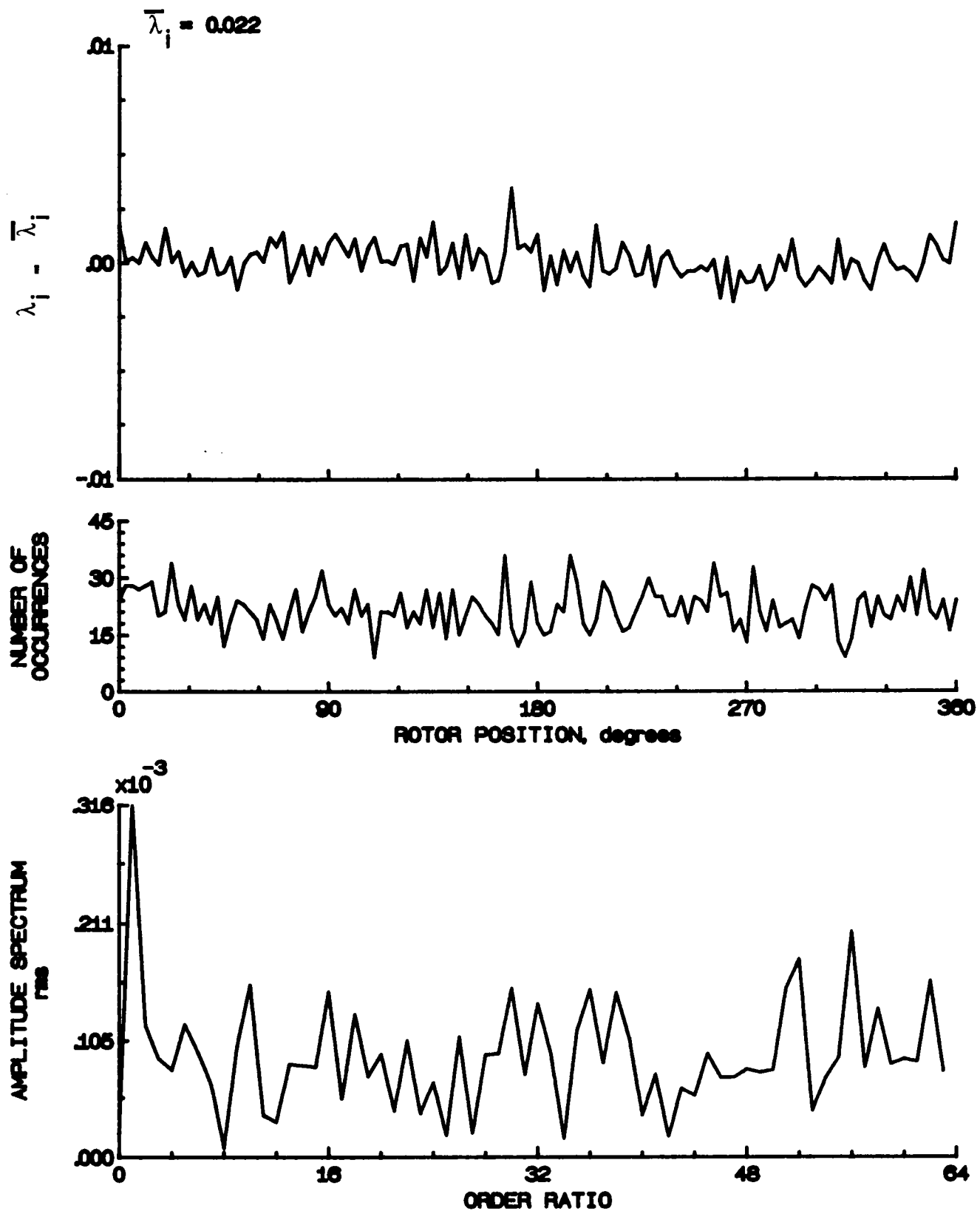


Figure 53.- Concluded.

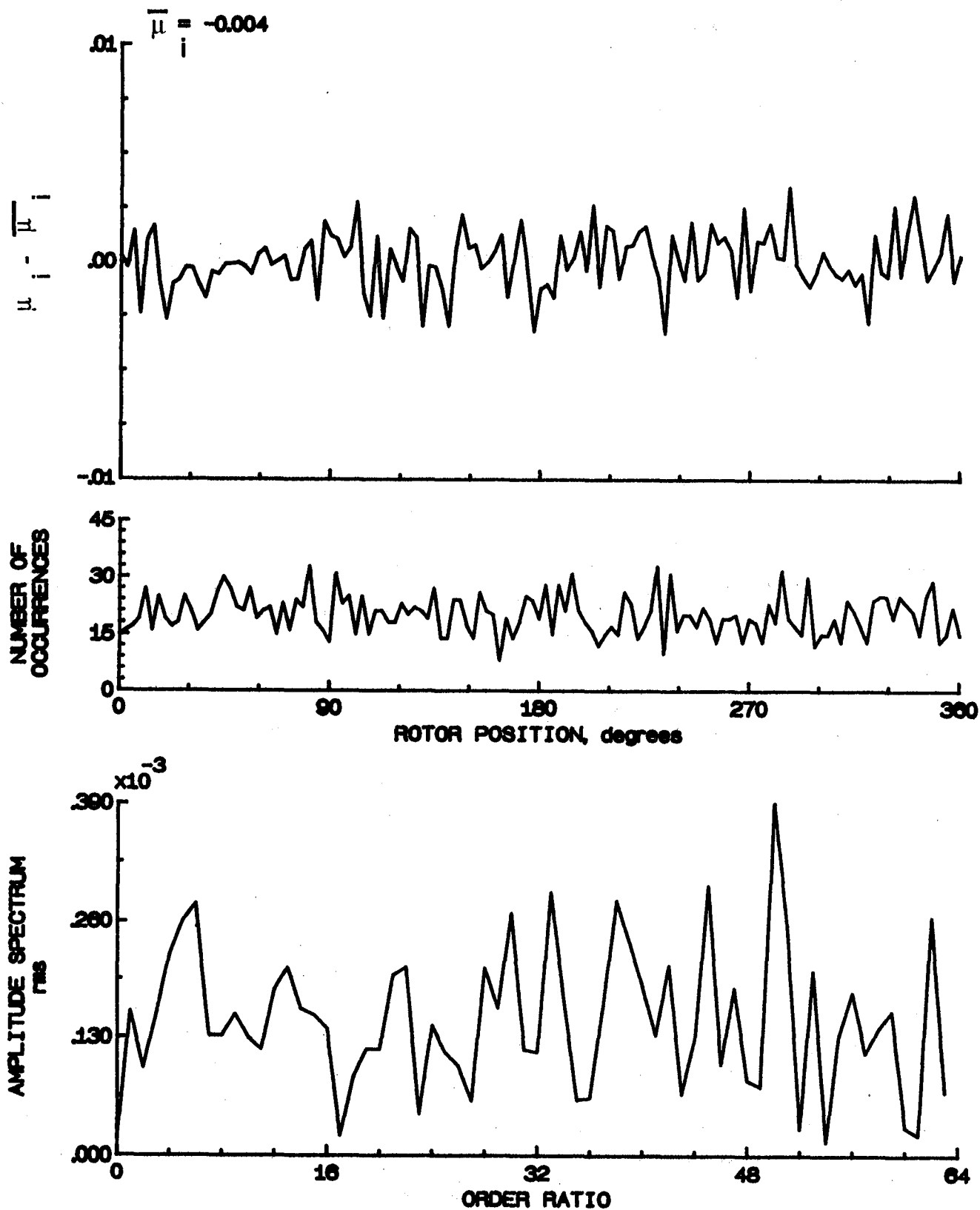


Figure 54.- Induced inflow velocity measured at 60 degrees and r/R of 0.98.

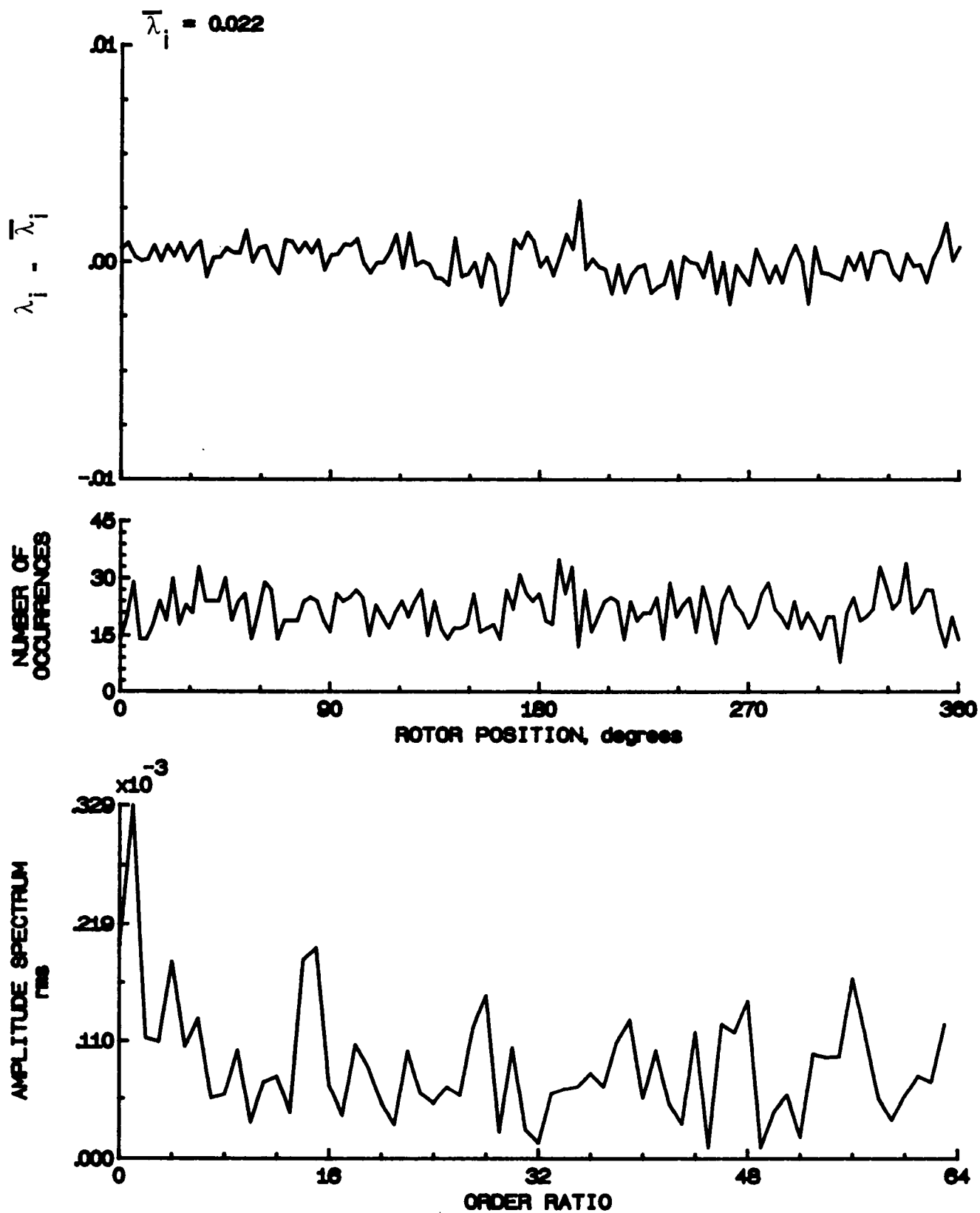


Figure 54.- Concluded.

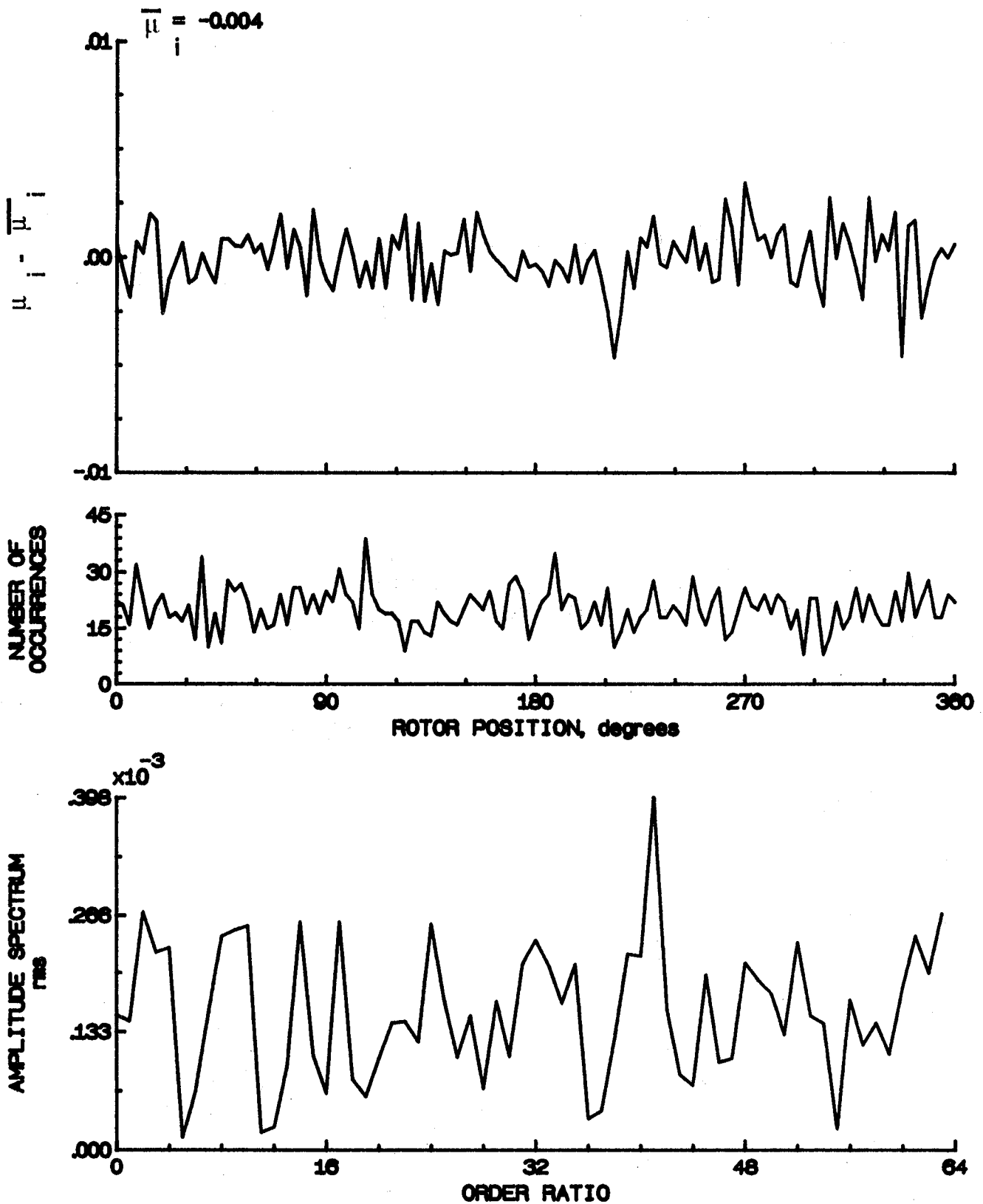


Figure 55.- Induced inflow velocity measured at 60 degrees and r/R of 1.02.

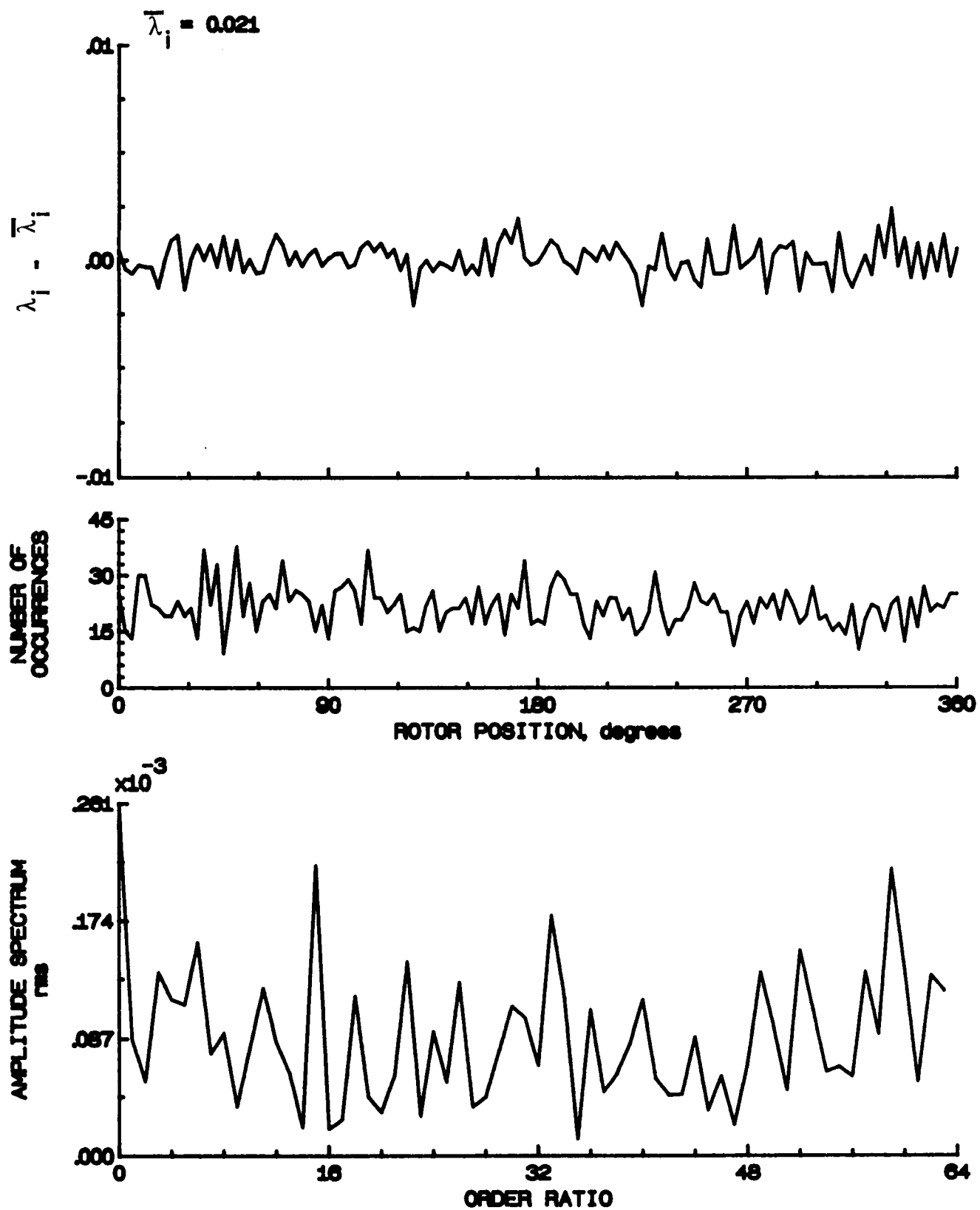


Figure 55.- Concluded.

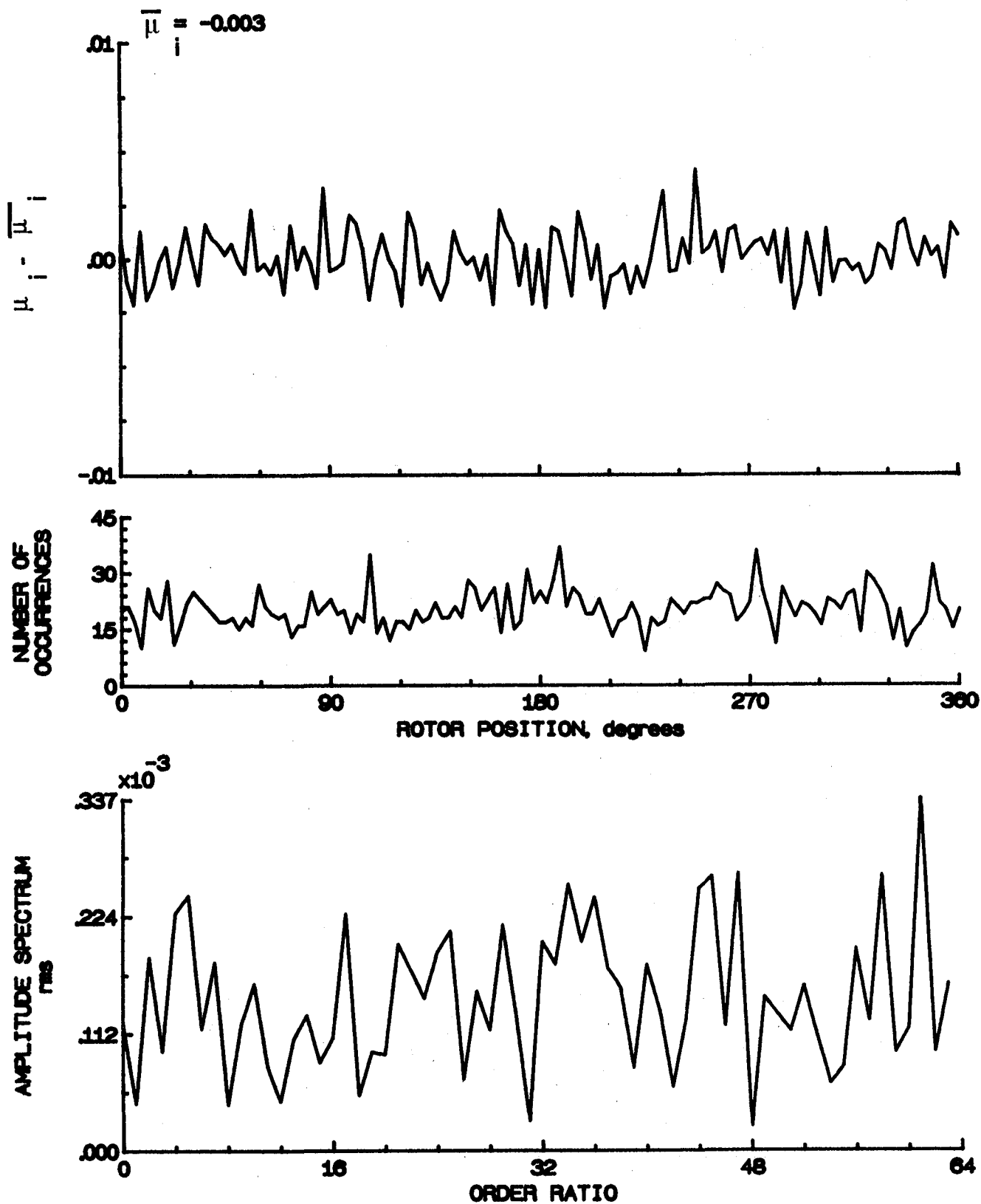


Figure 56.- Induced inflow velocity measured at 60 degrees and  $r/R$  of 1.04.



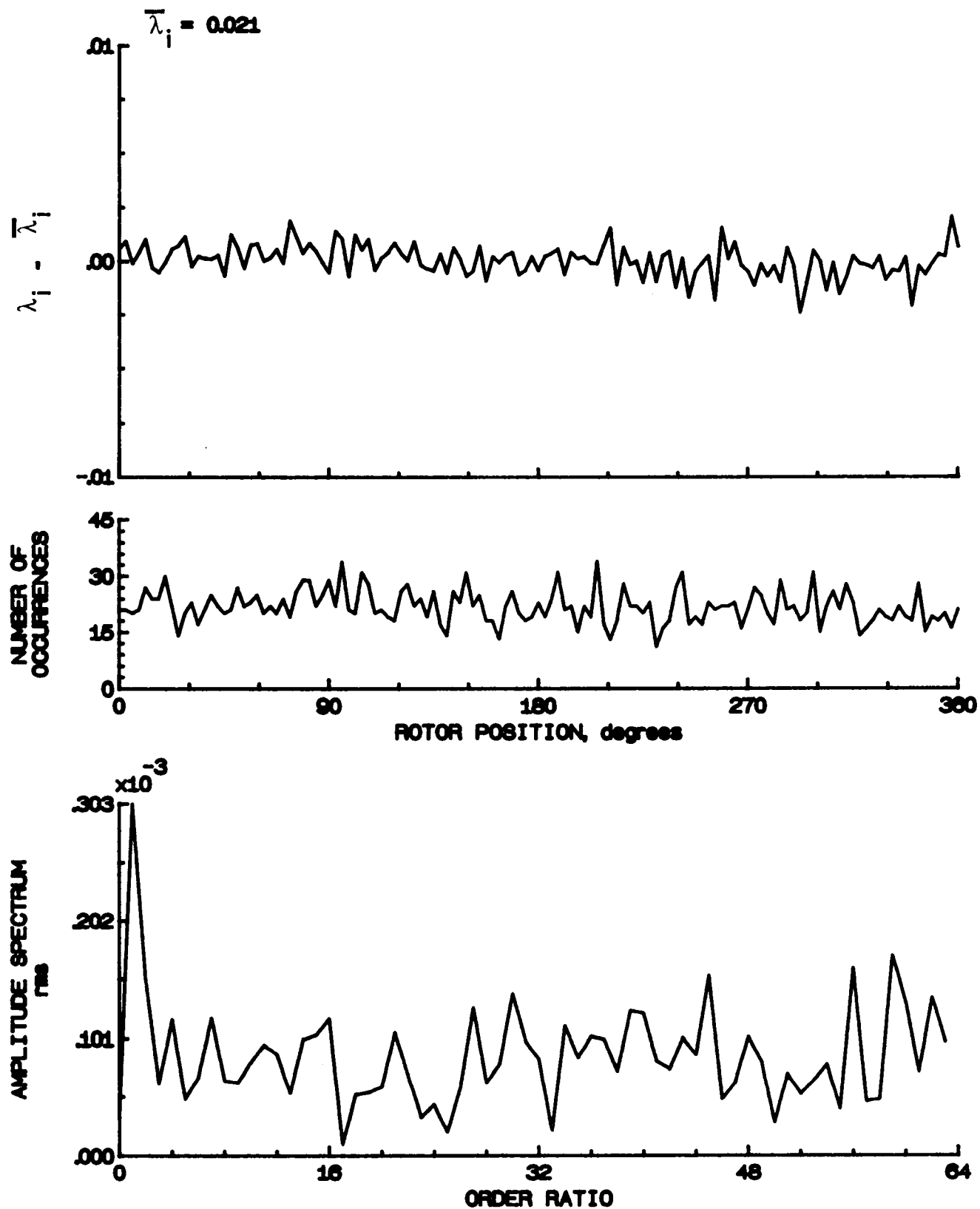


Figure 56.- Concluded.

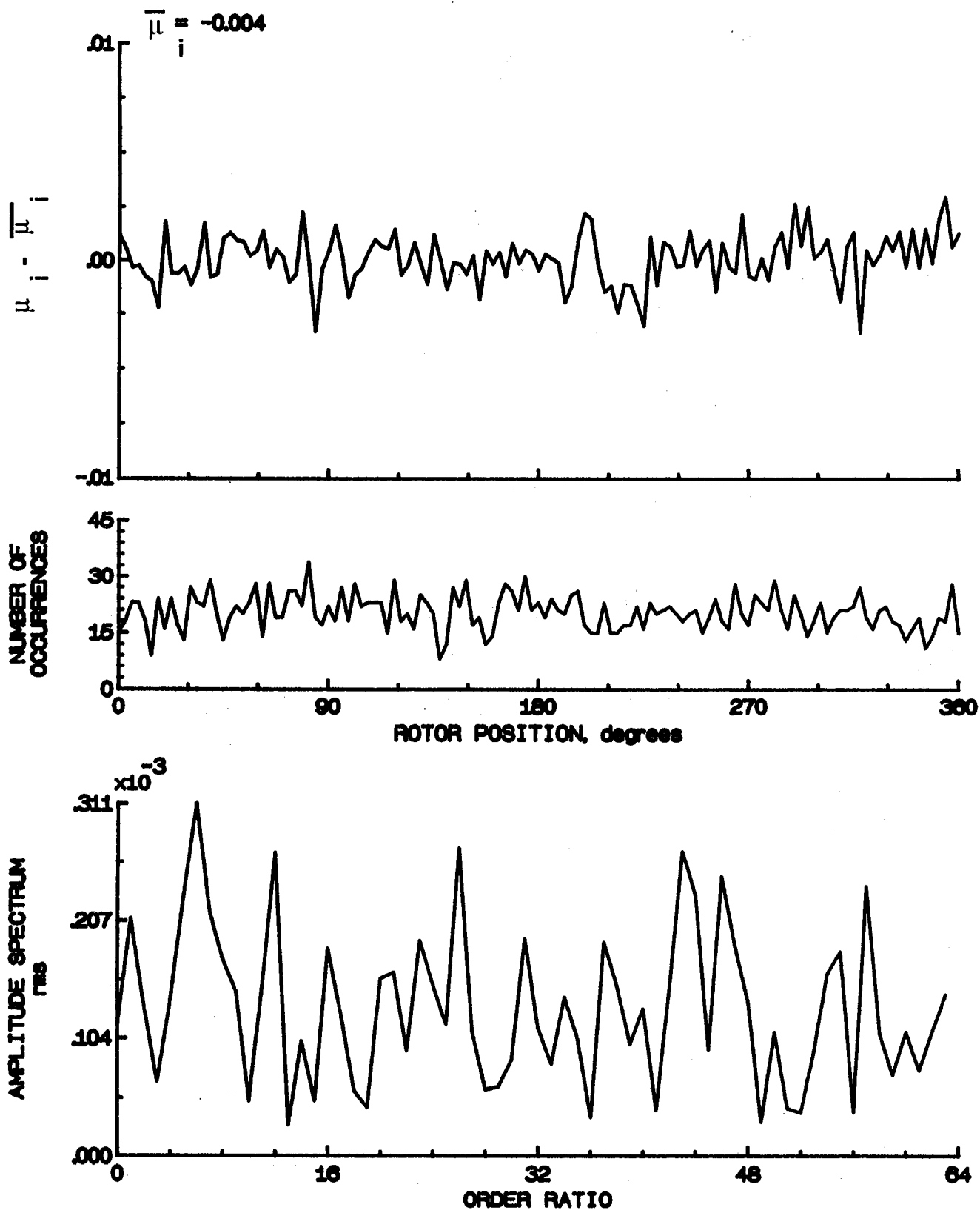


Figure 57.- Induced inflow velocity measured at 60 degrees and  $r/R$  of 1.10.

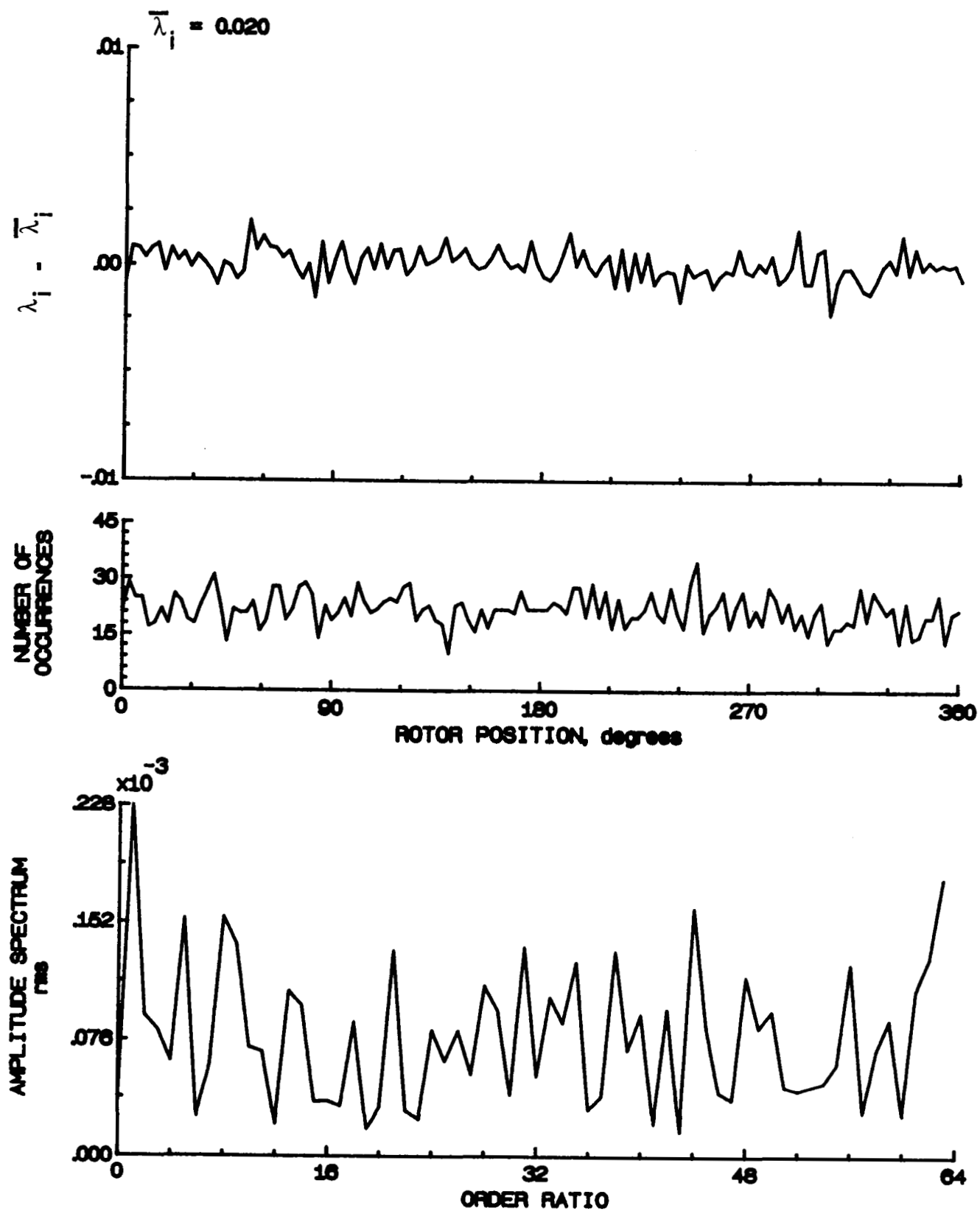


Figure 57.- Concluded.

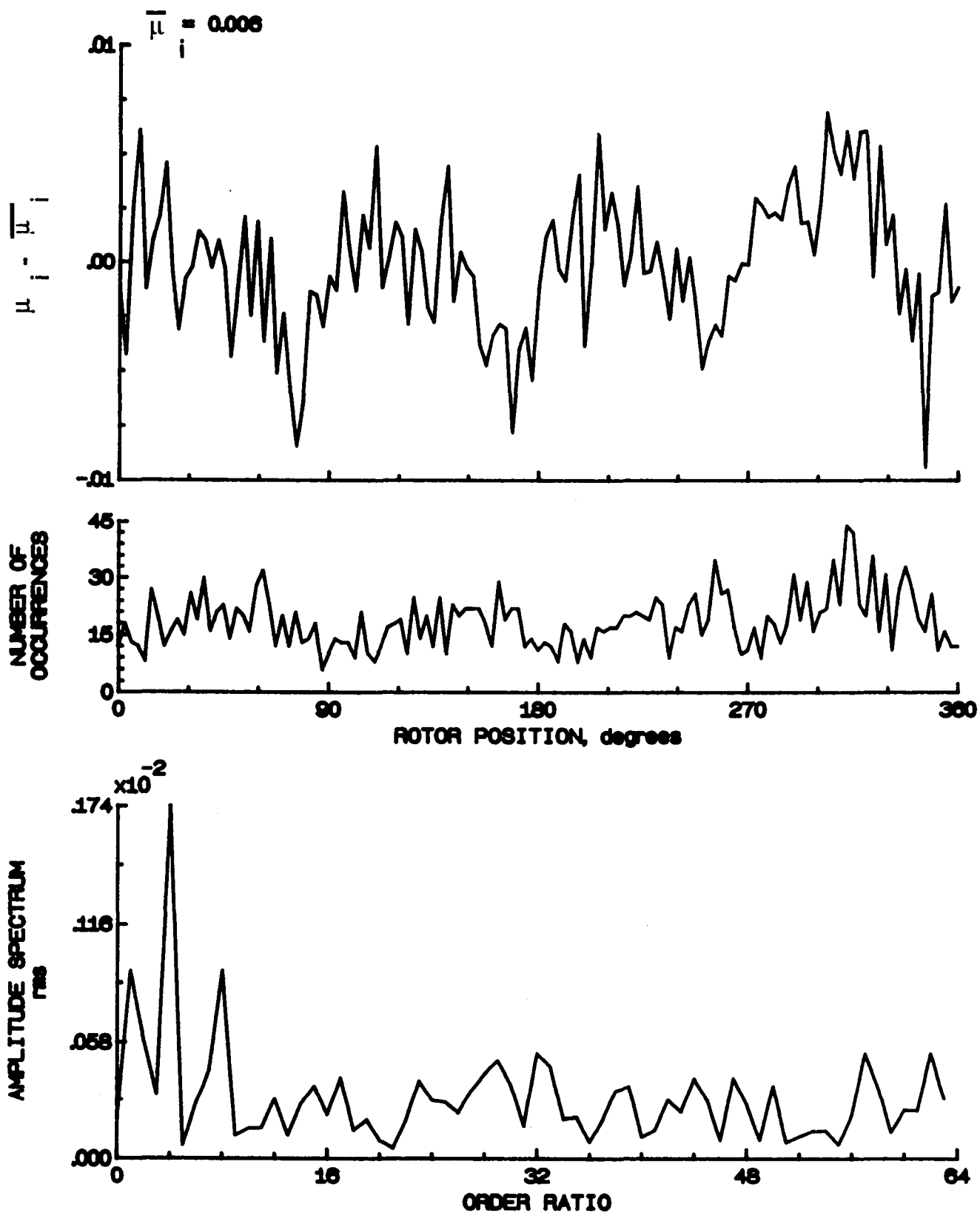


Figure 58.- Induced inflow velocity measured at 90 degrees and  $r/R$  of 0.20.

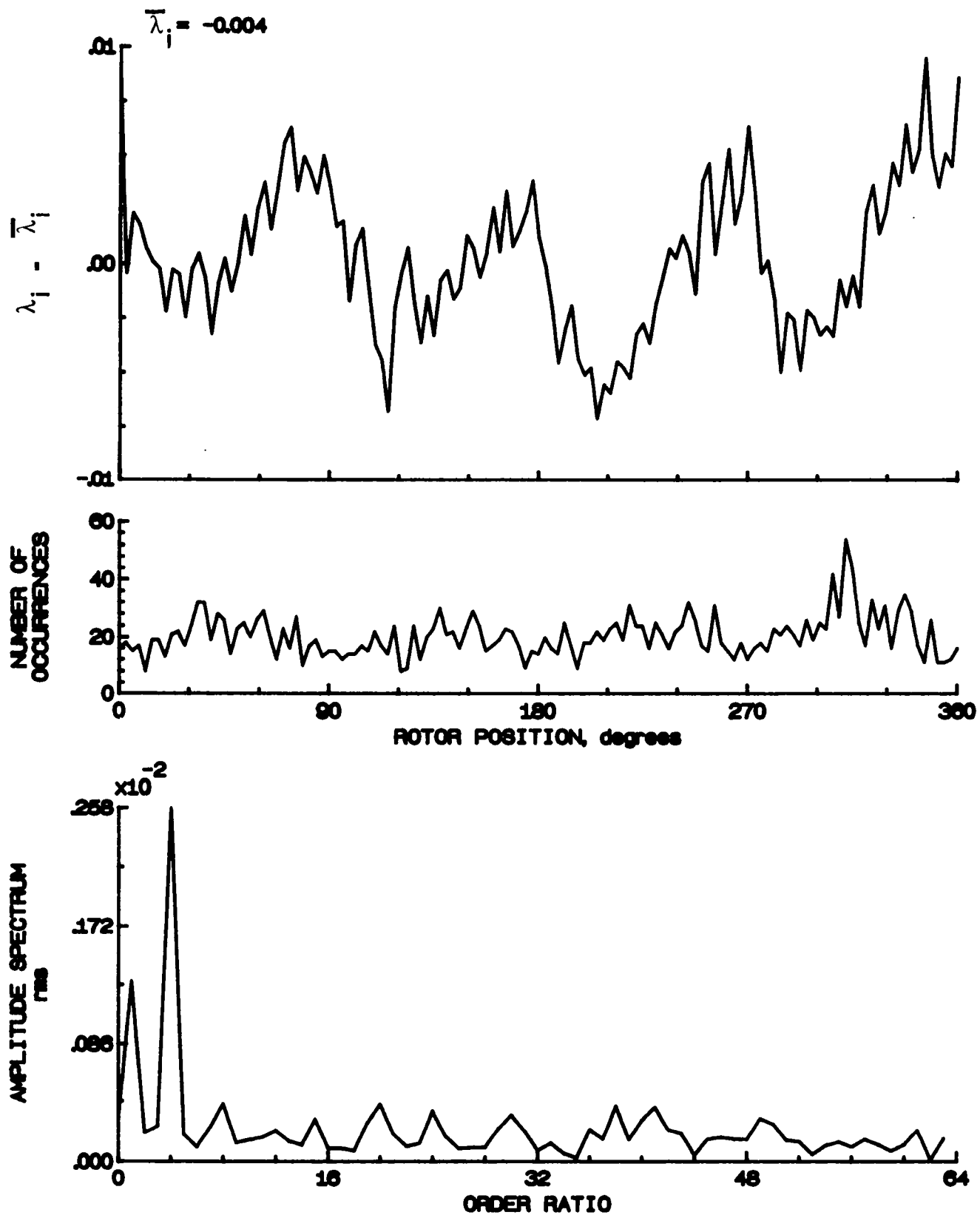


Figure 58.- Concluded.

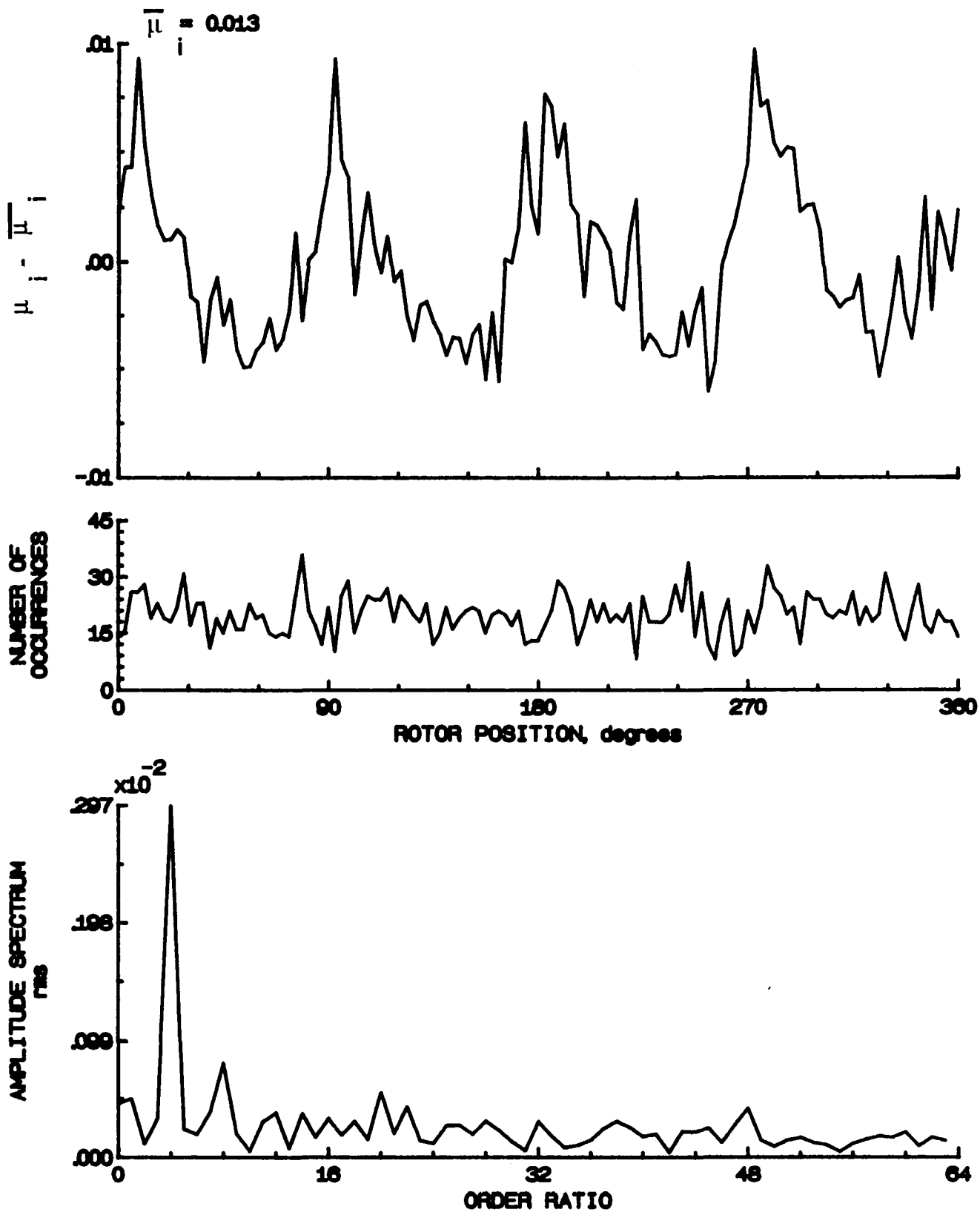


Figure 59.- Induced inflow velocity measured at 90 degrees and  $r/R$  of 0.40.

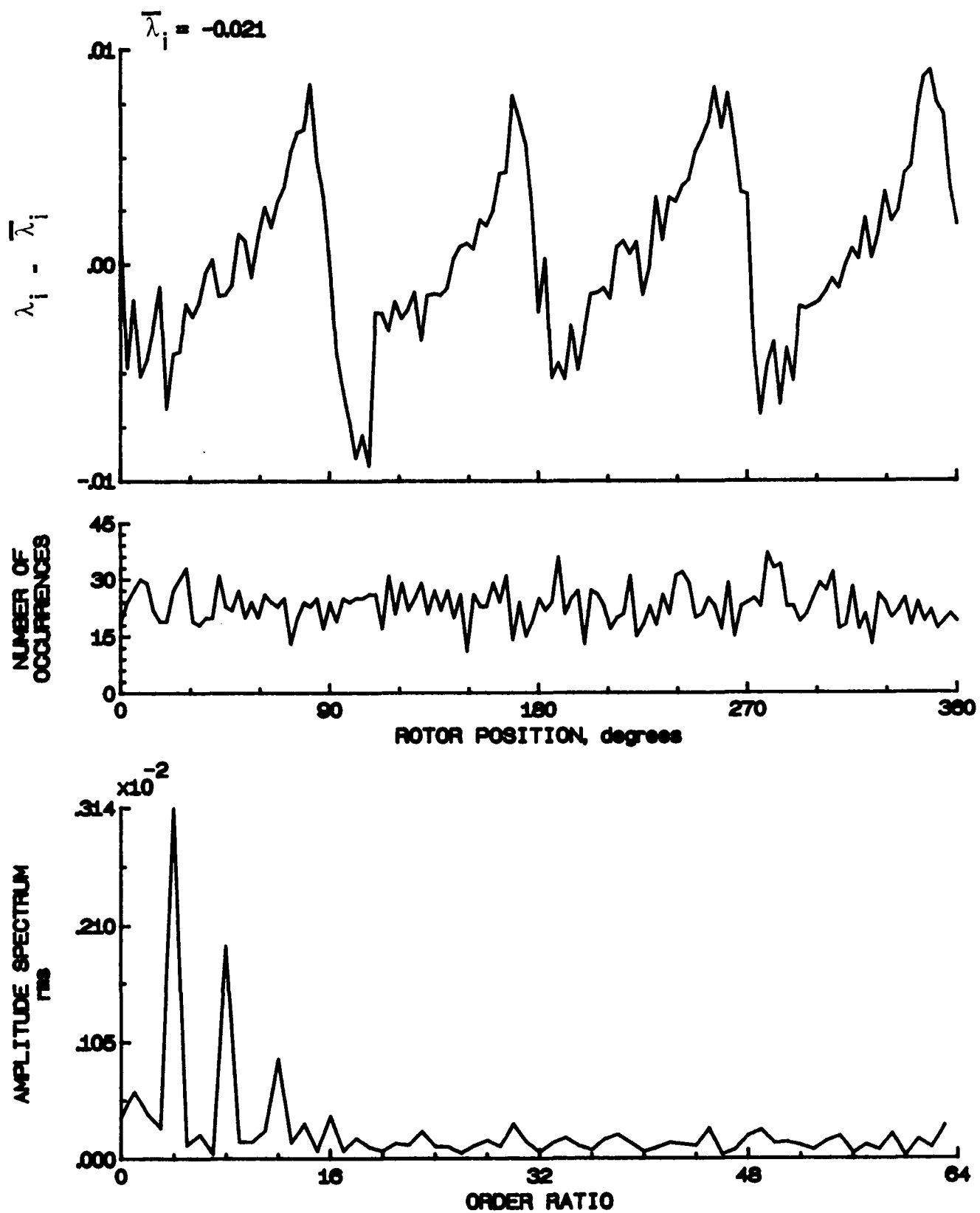


Figure 59.- Concluded.

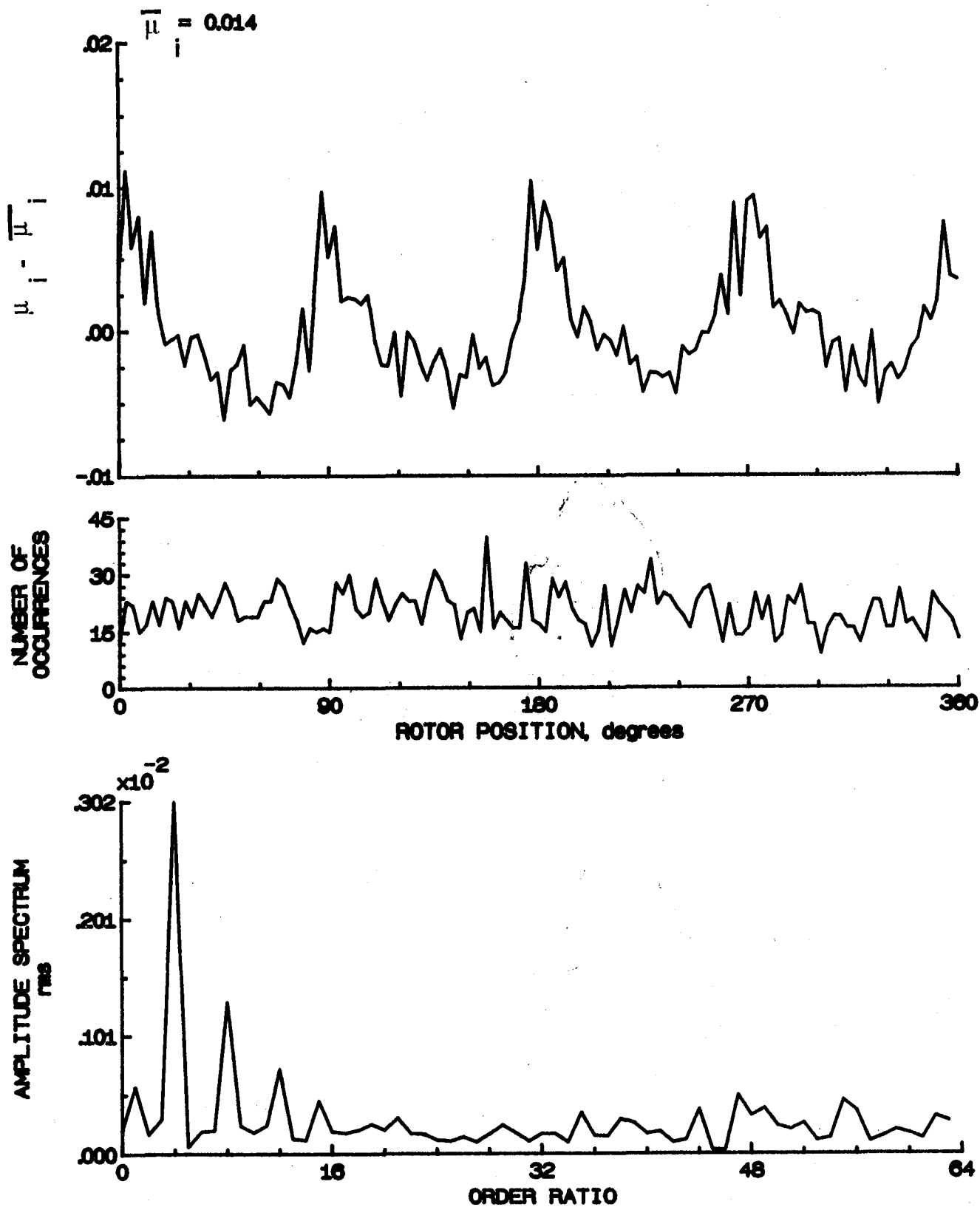


Figure 60.- Induced inflow velocity measured at 90 degrees and  $r/R$  of 0.50.



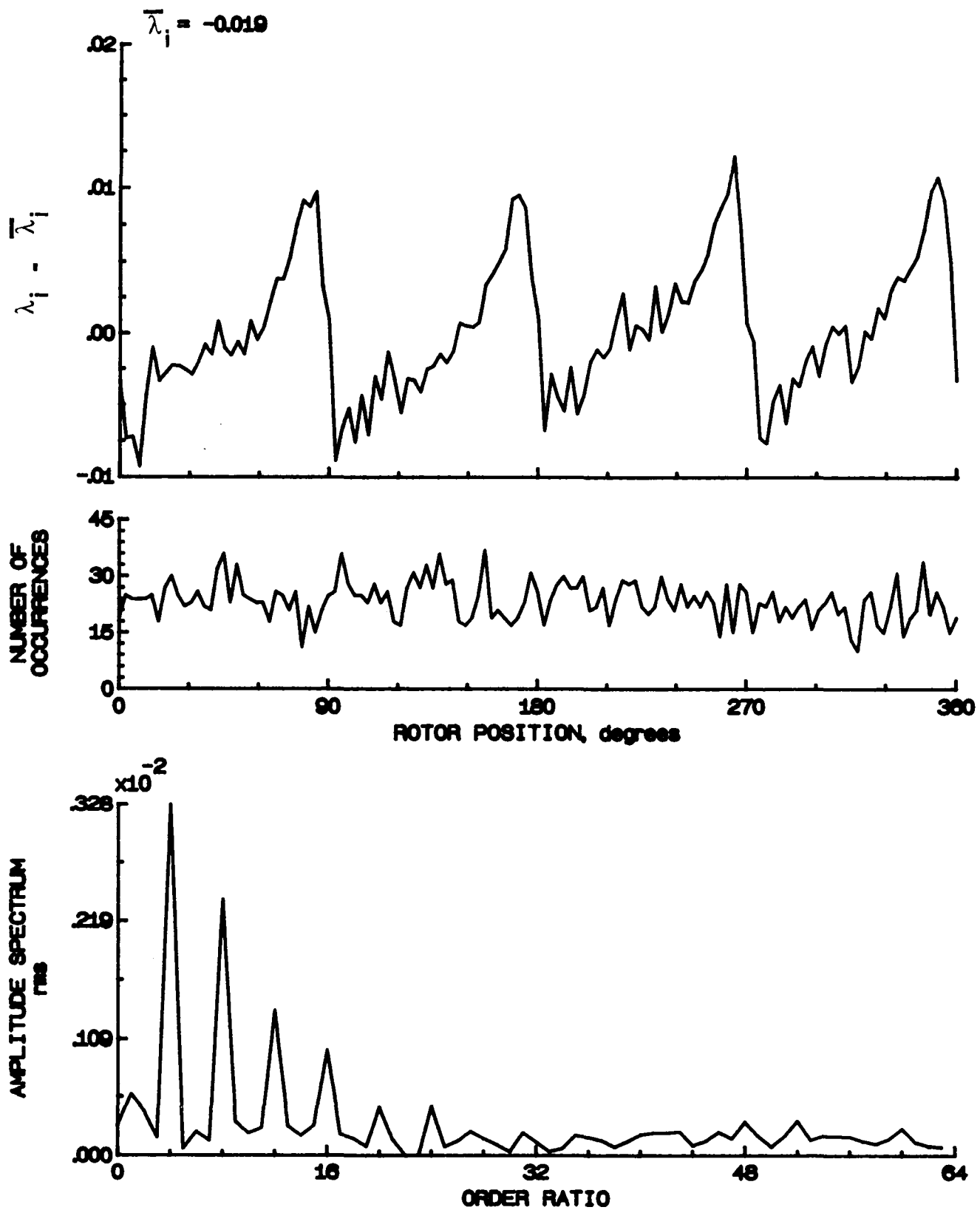


Figure 60.- Concluded.

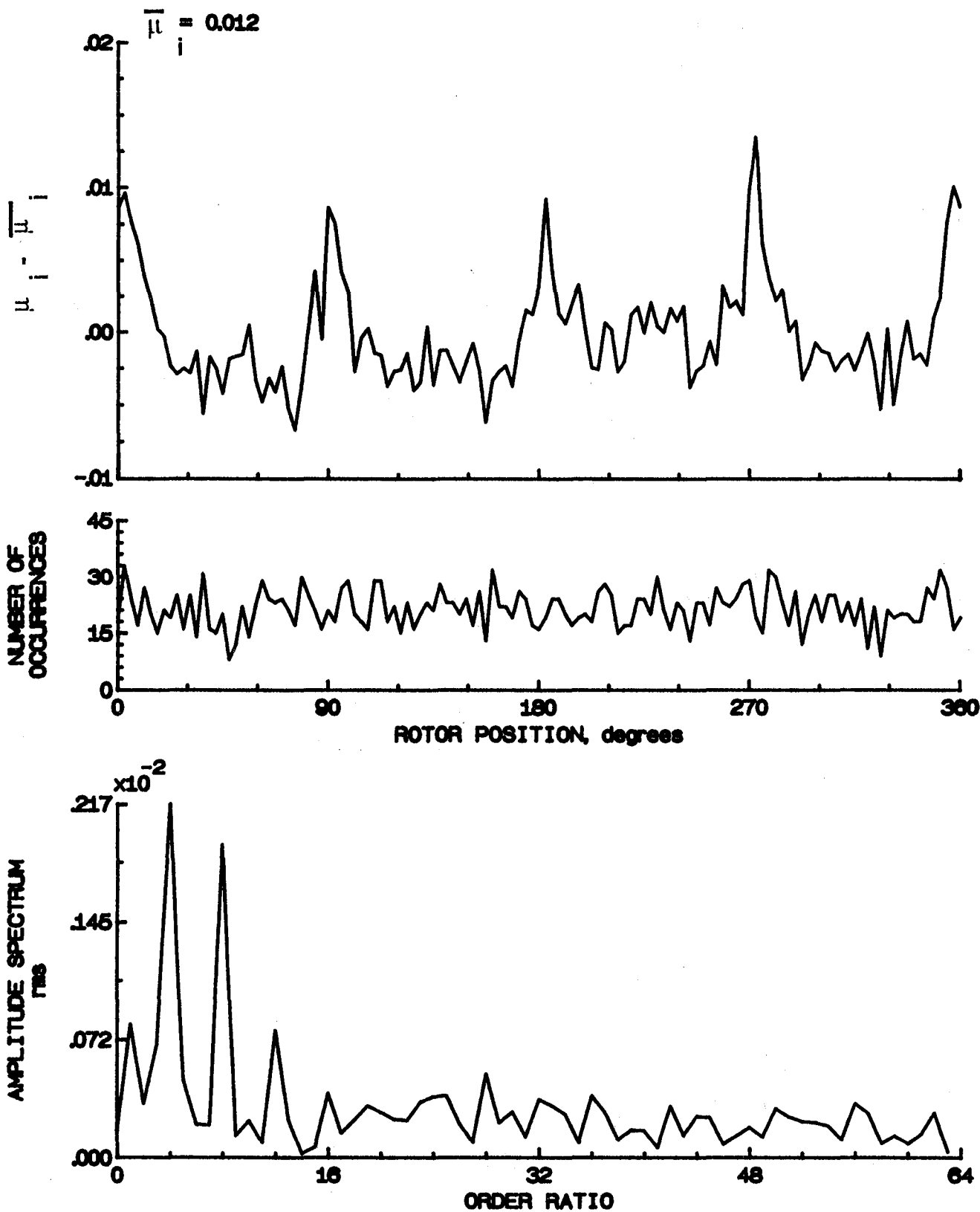


Figure 61- Induced inflow velocity measured at 90 degrees and  $r/R$  of 0.60.

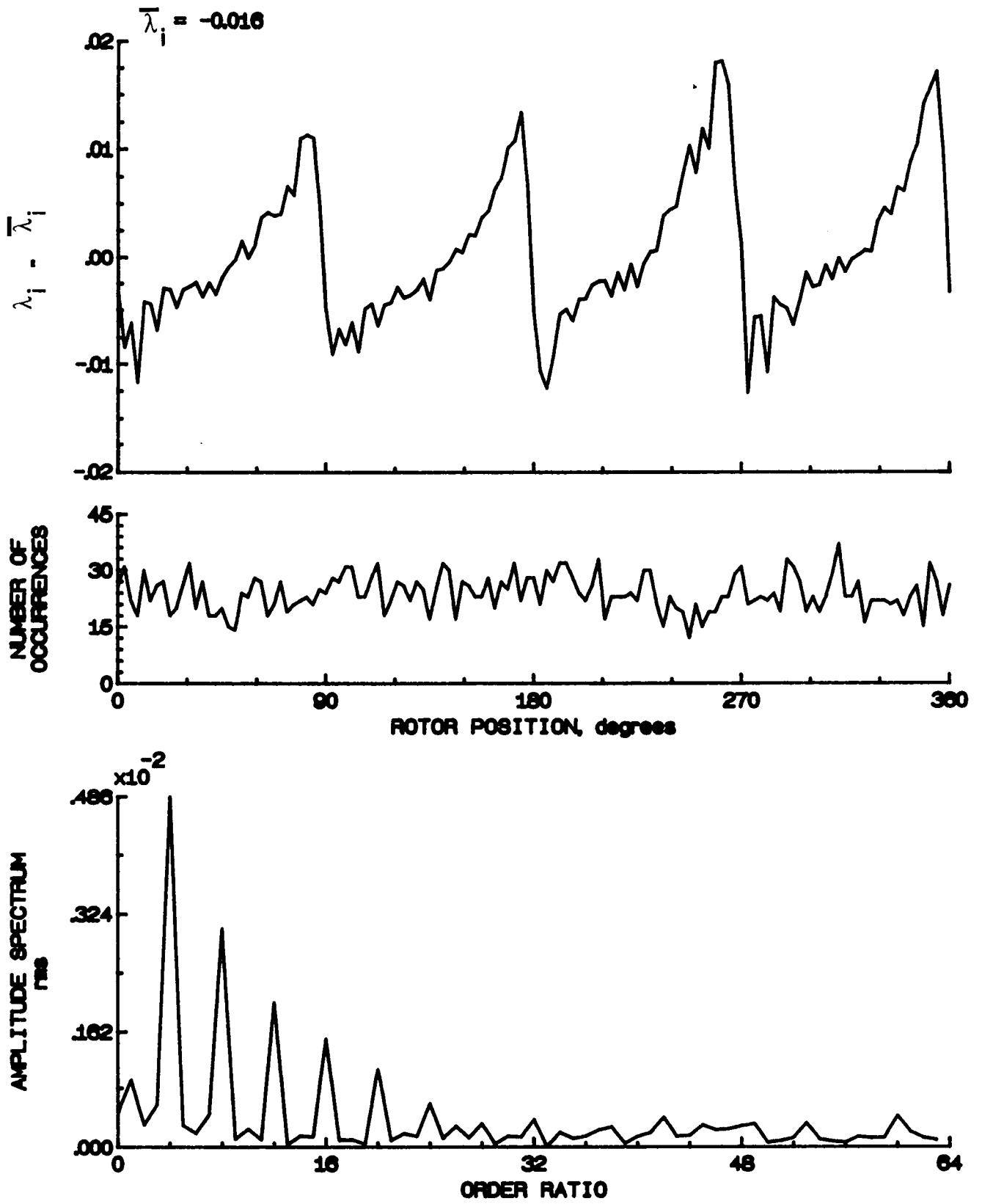


Figure 61.- Concluded.

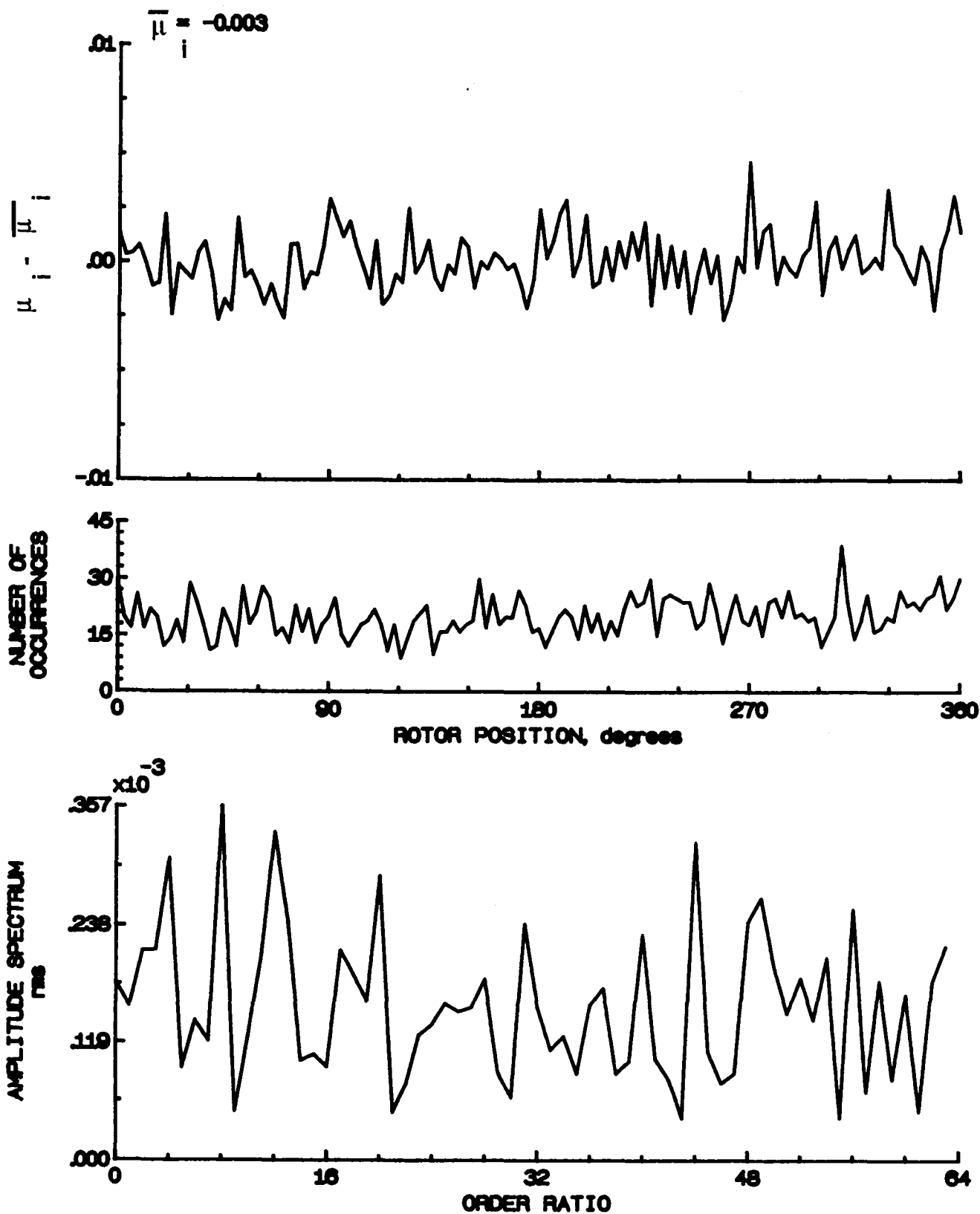


Figure 62.- Induced inflow velocity measured at 90 degrees and  $r/R$  of 0.70.

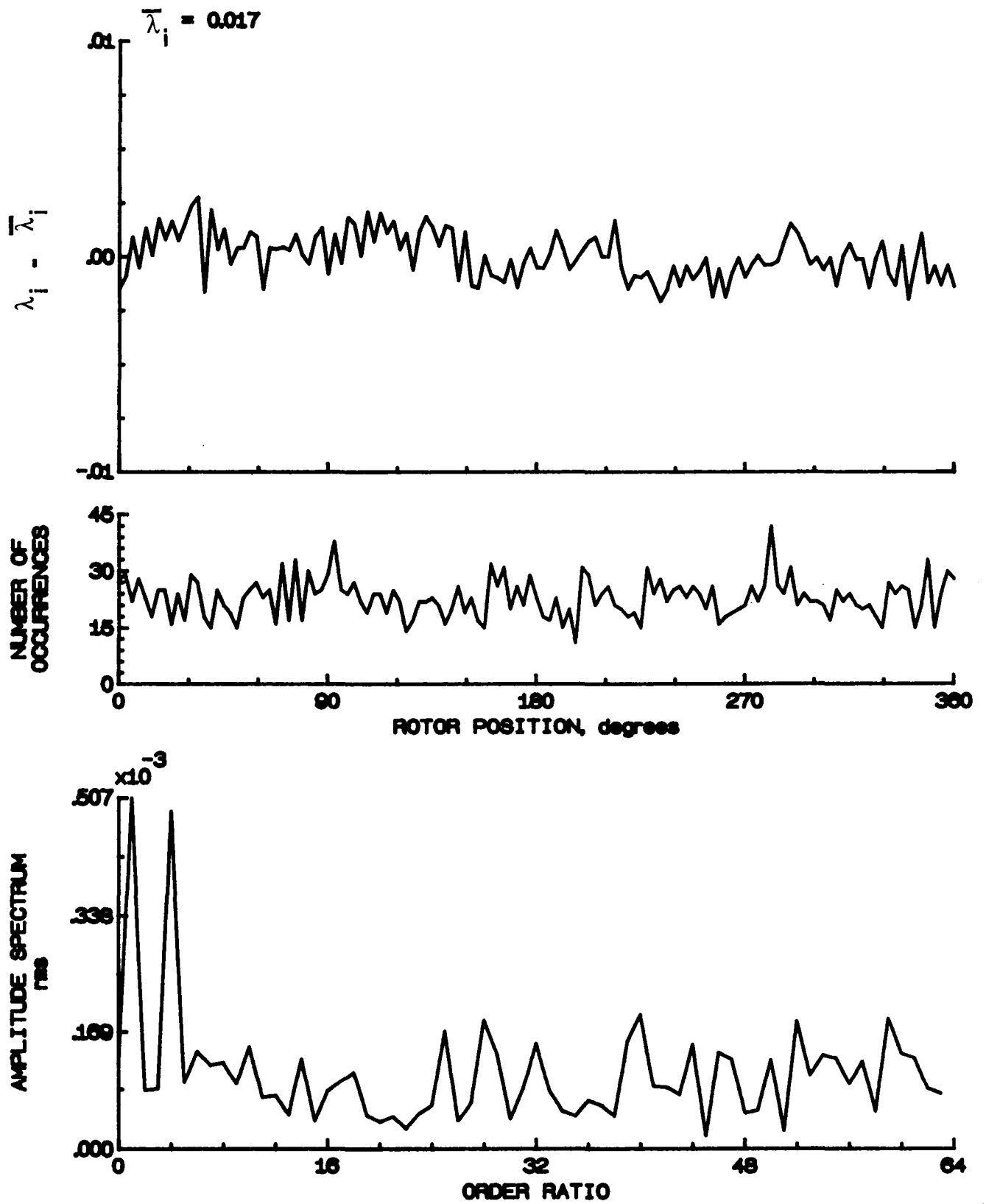


Figure 62- Concluded.

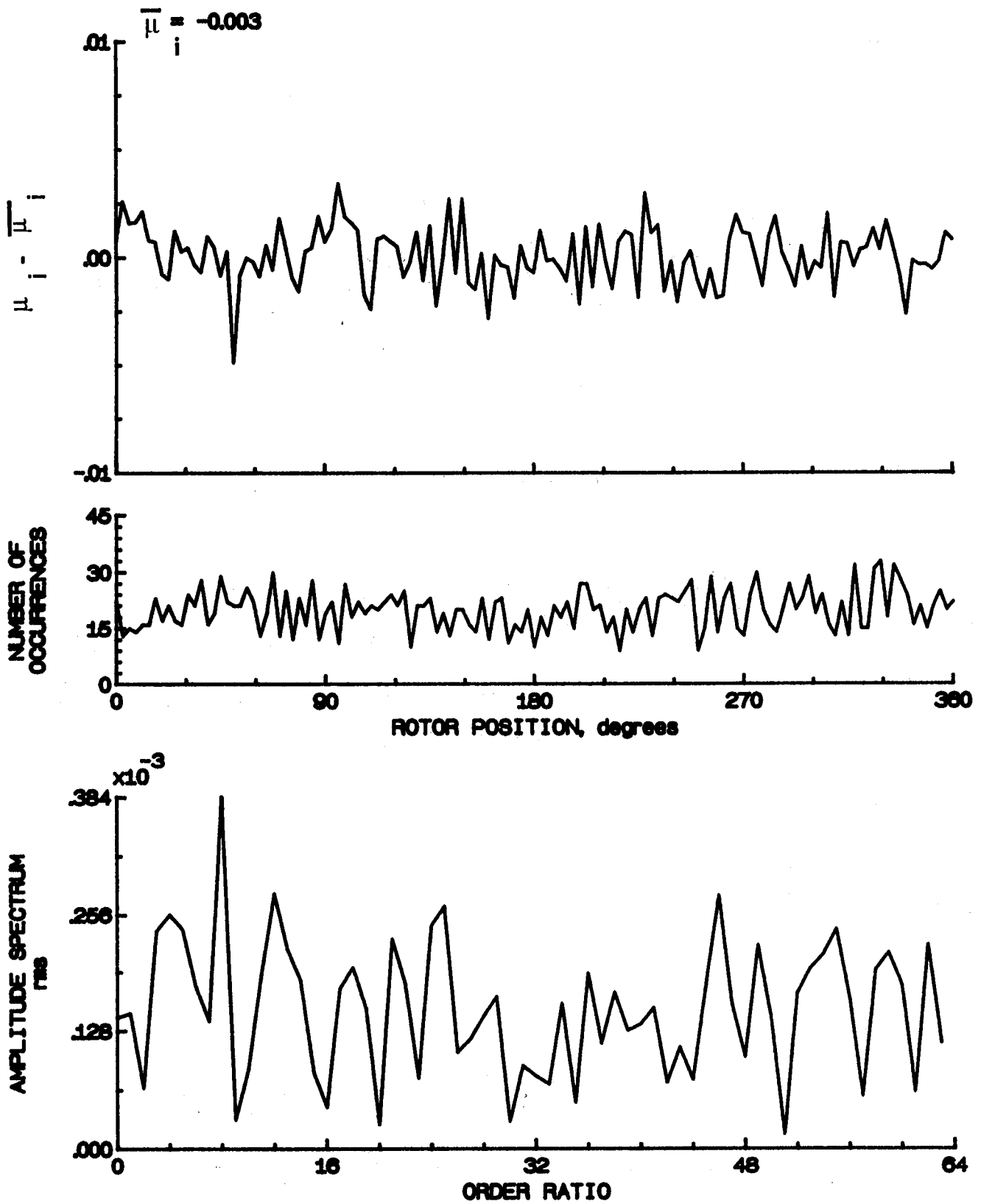


Figure 63.- Induced inflow velocity measured at 90 degrees and  $r/R$  of 0.74.

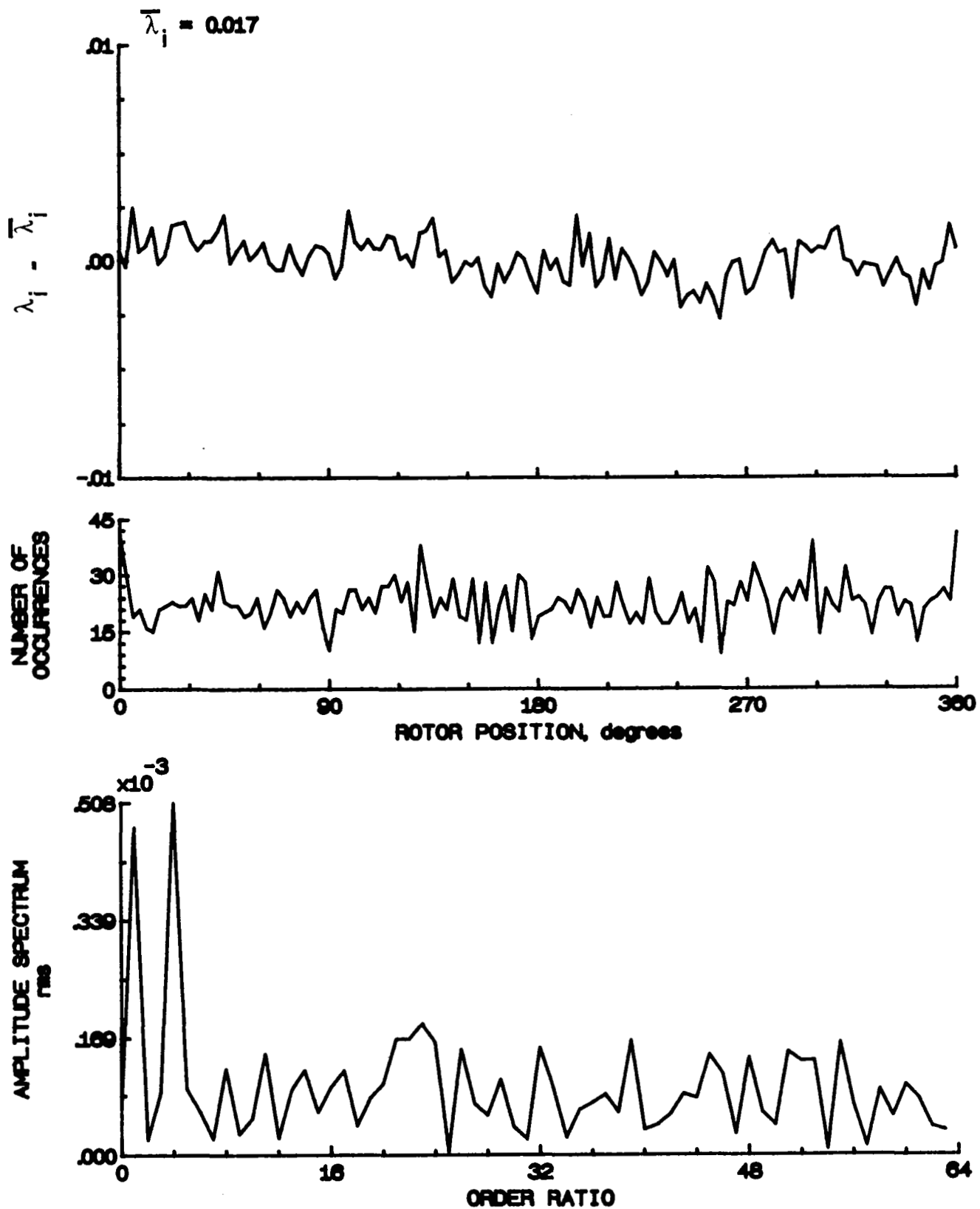


Figure 63.- Concluded.

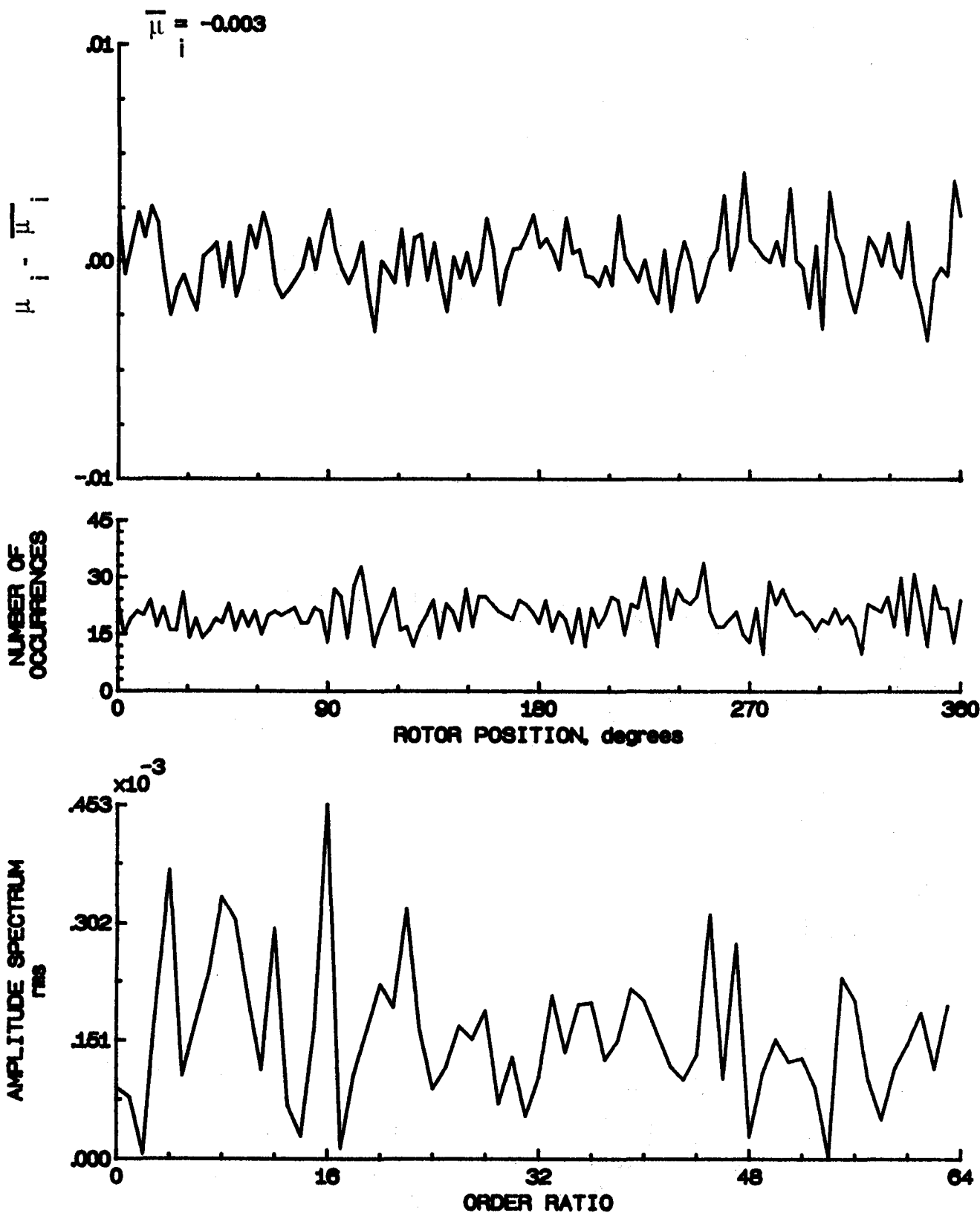


Figure 64.- Induced inflow velocity measured at 90 degrees and r/R of 0.78.



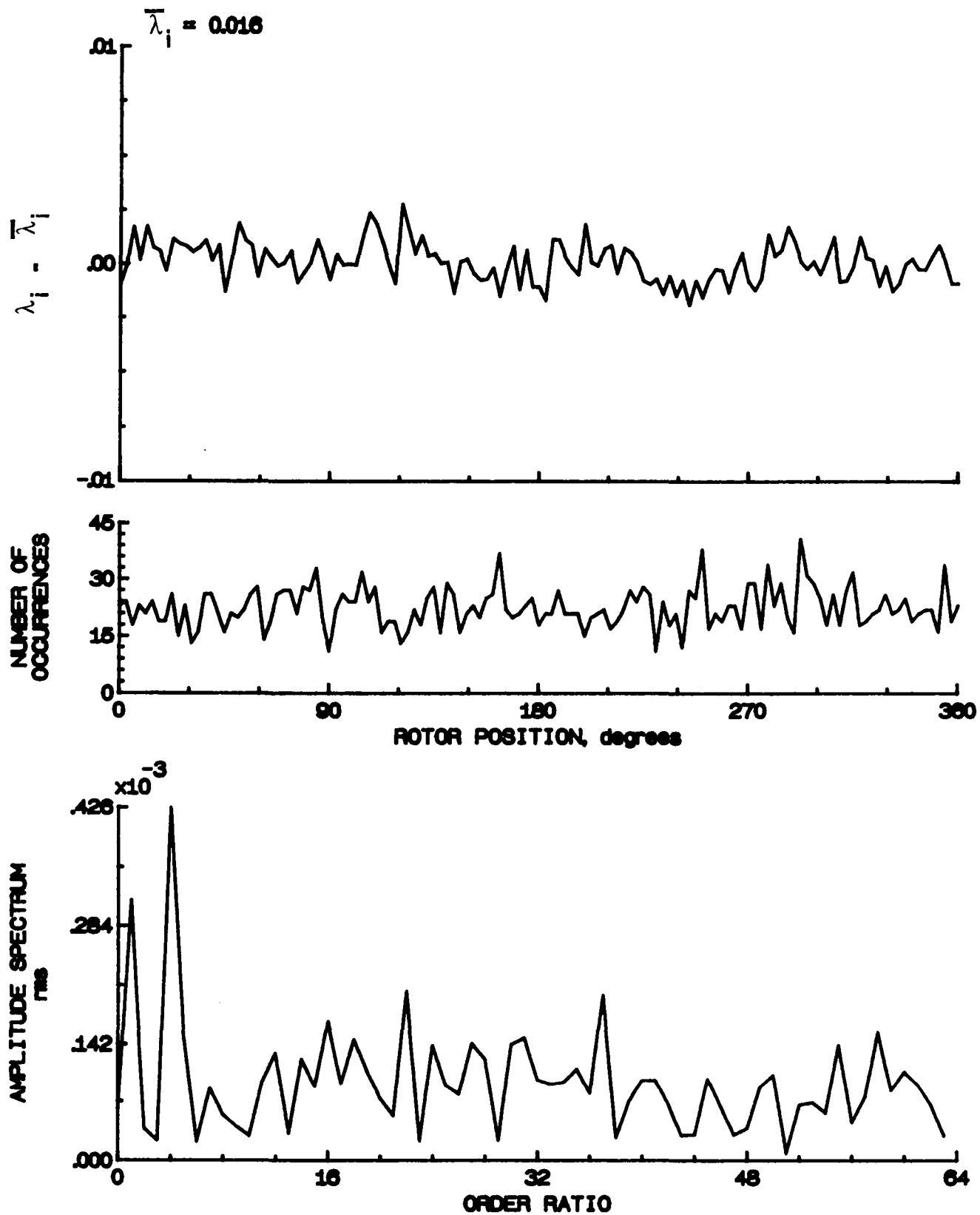


Figure 64.- Concluded.

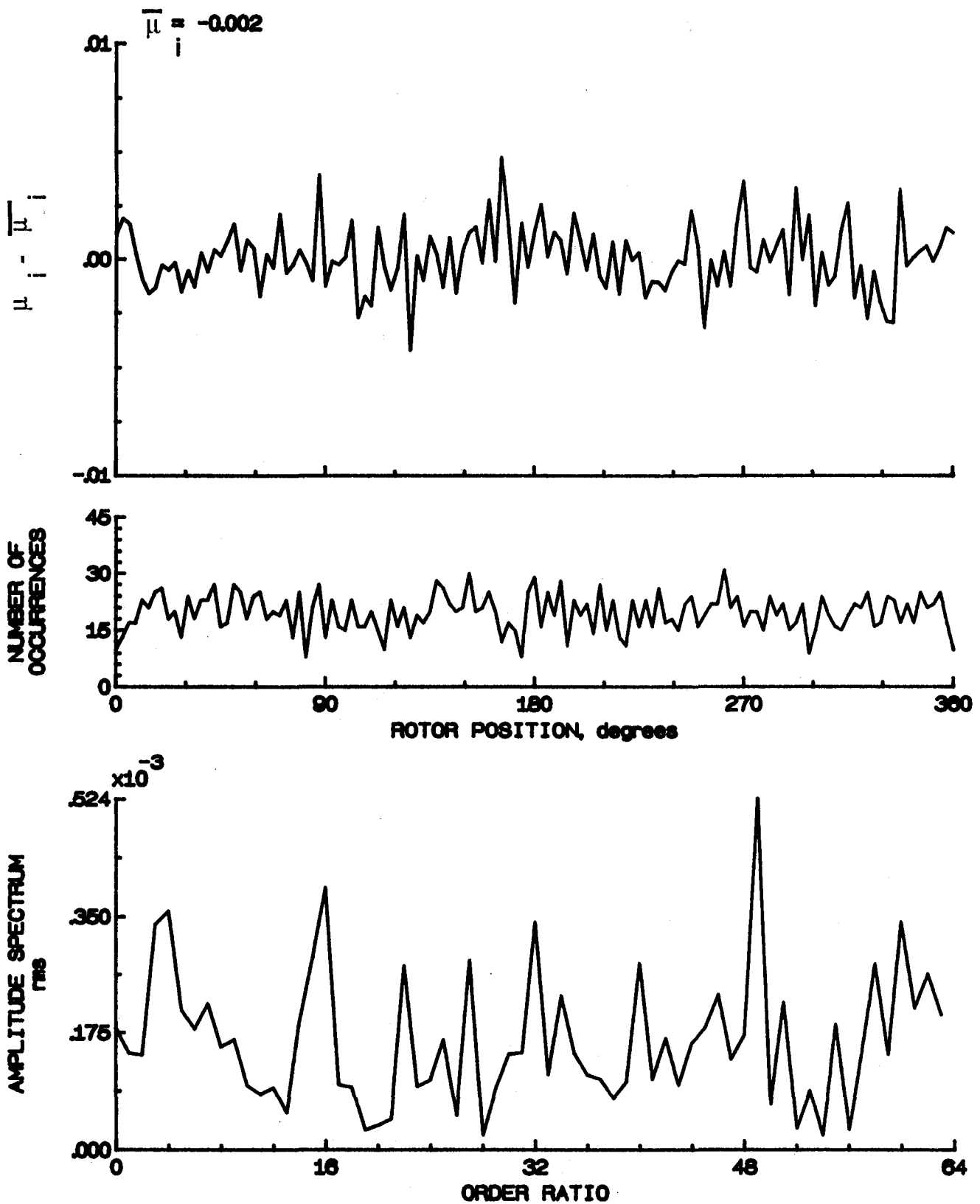


Figure 65.- Induced inflow velocity measured at 90 degrees and r/R of 0.82.

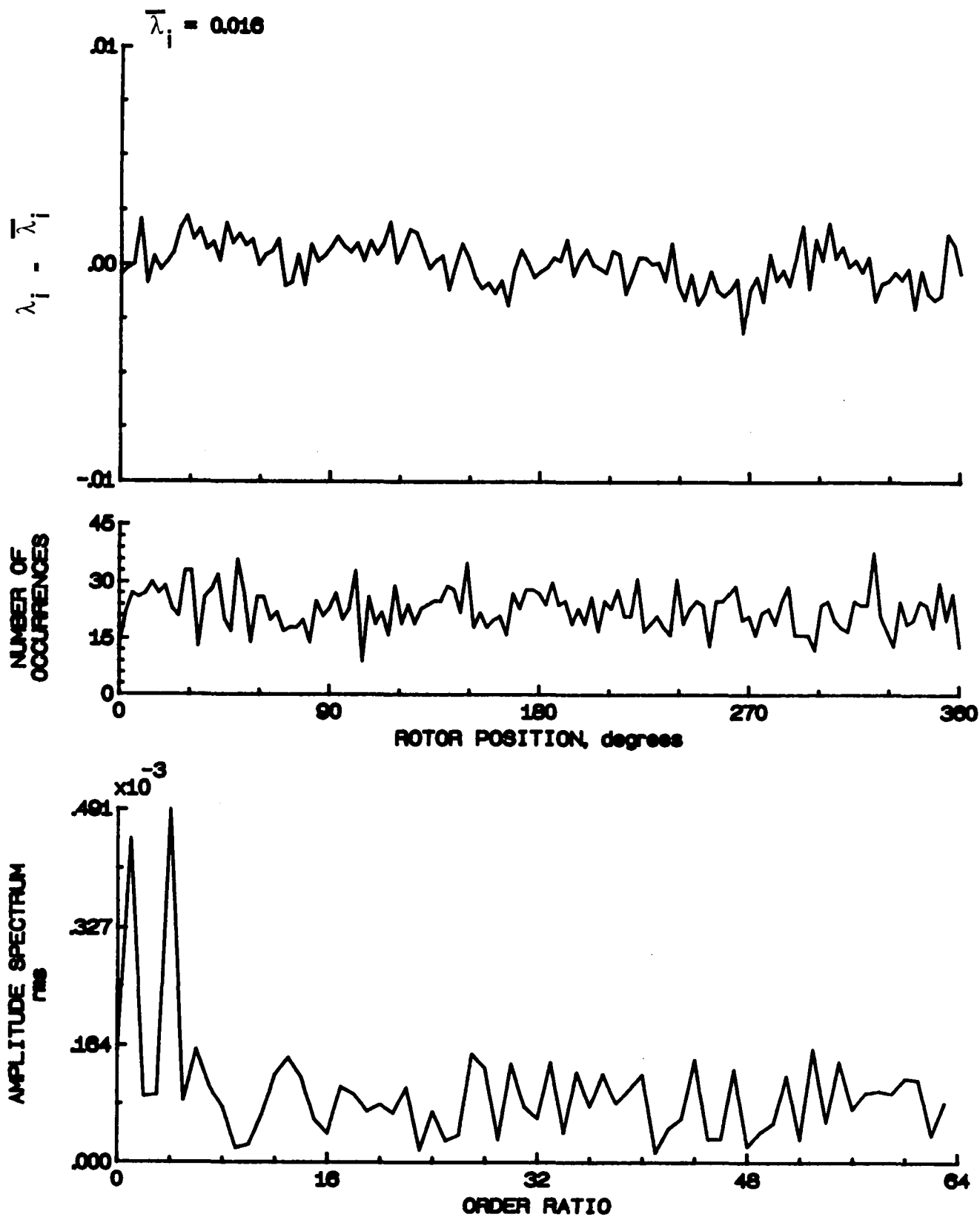


Figure 65.- Concluded.

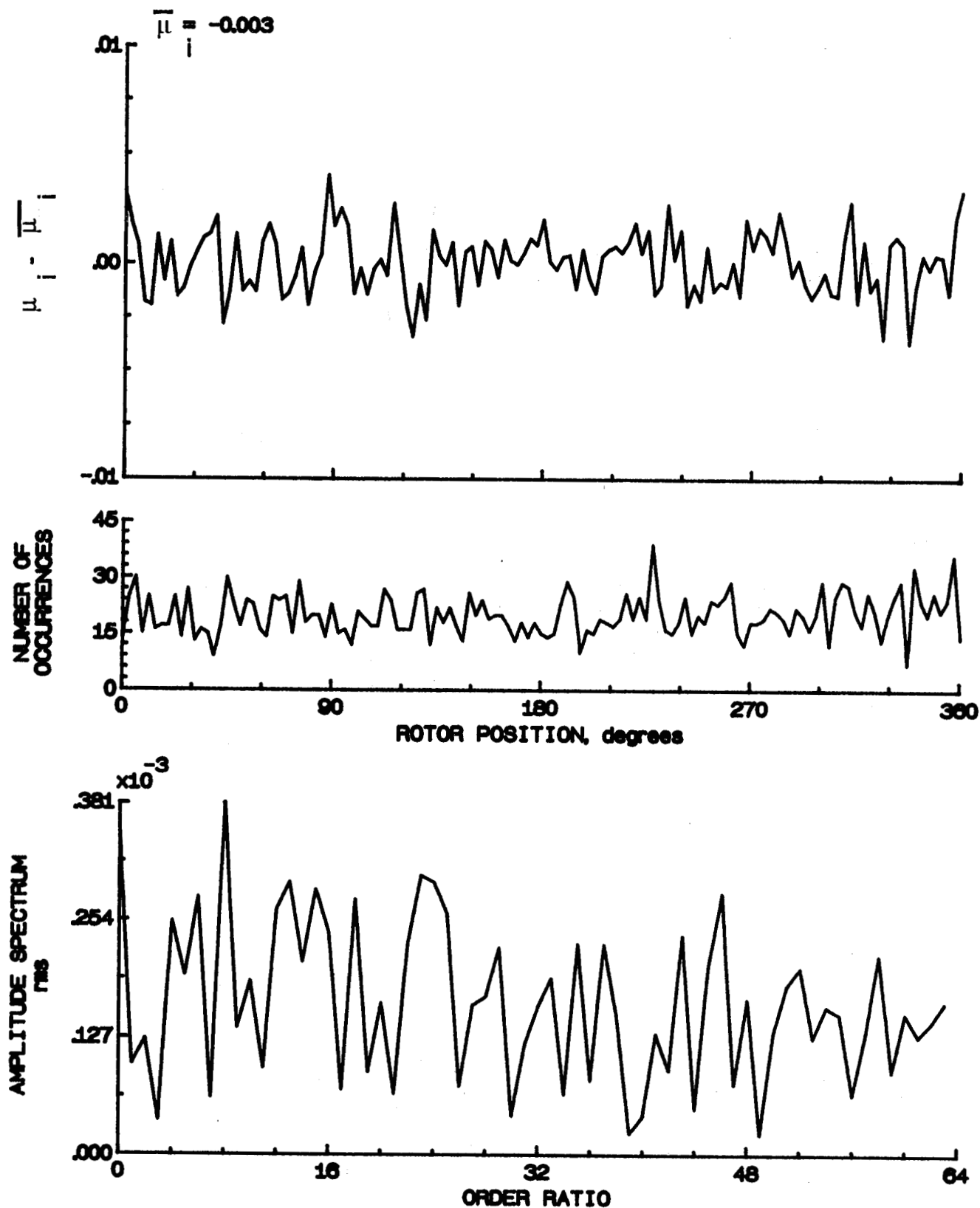


Figure 66.- Induced inflow velocity measured at 90 degrees and  $r/R$  of 0.86.

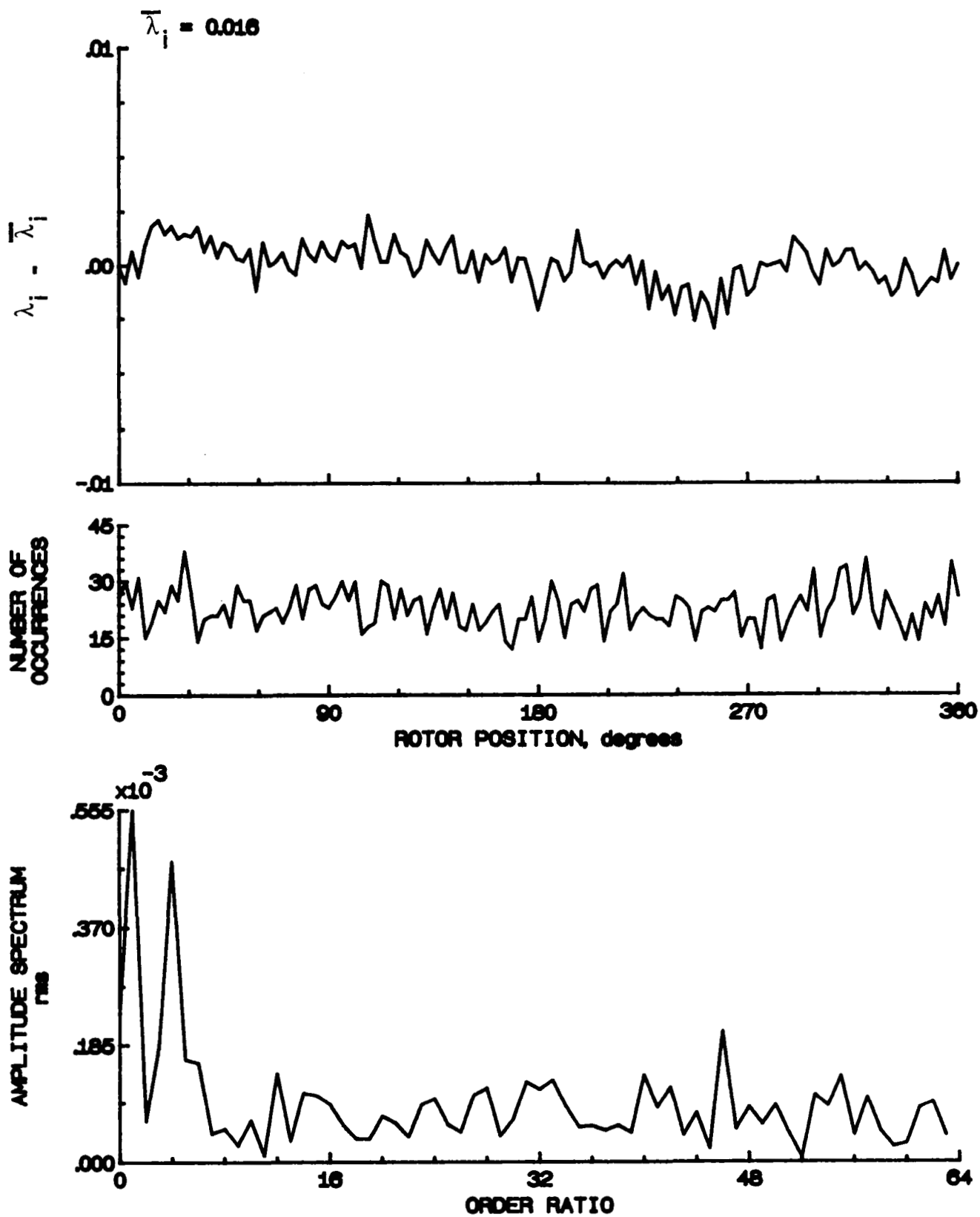


Figure 66.- Concluded.

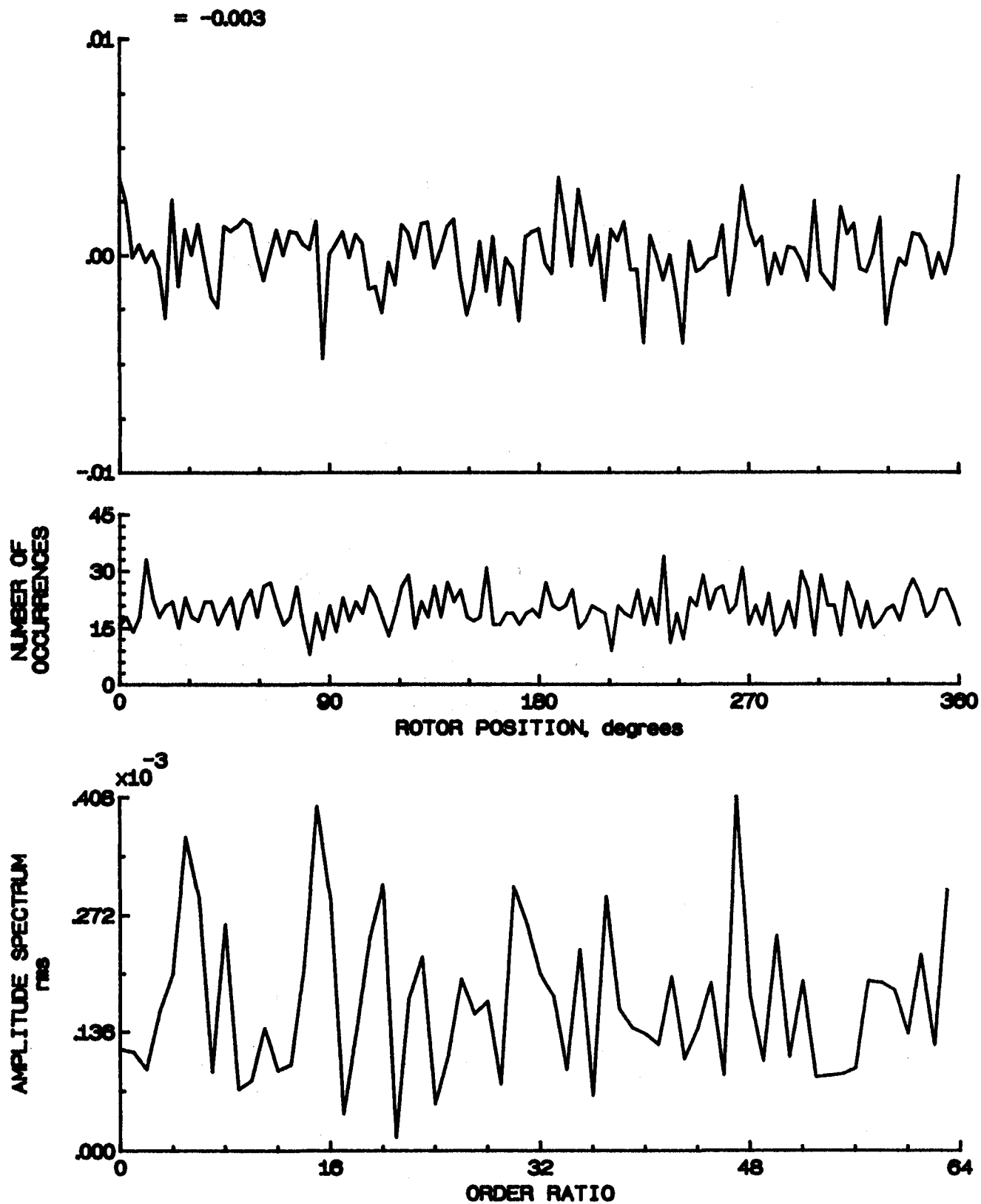


Figure 67.- Induced inflow velocity measured at 90 degrees and r/R of 0.90.

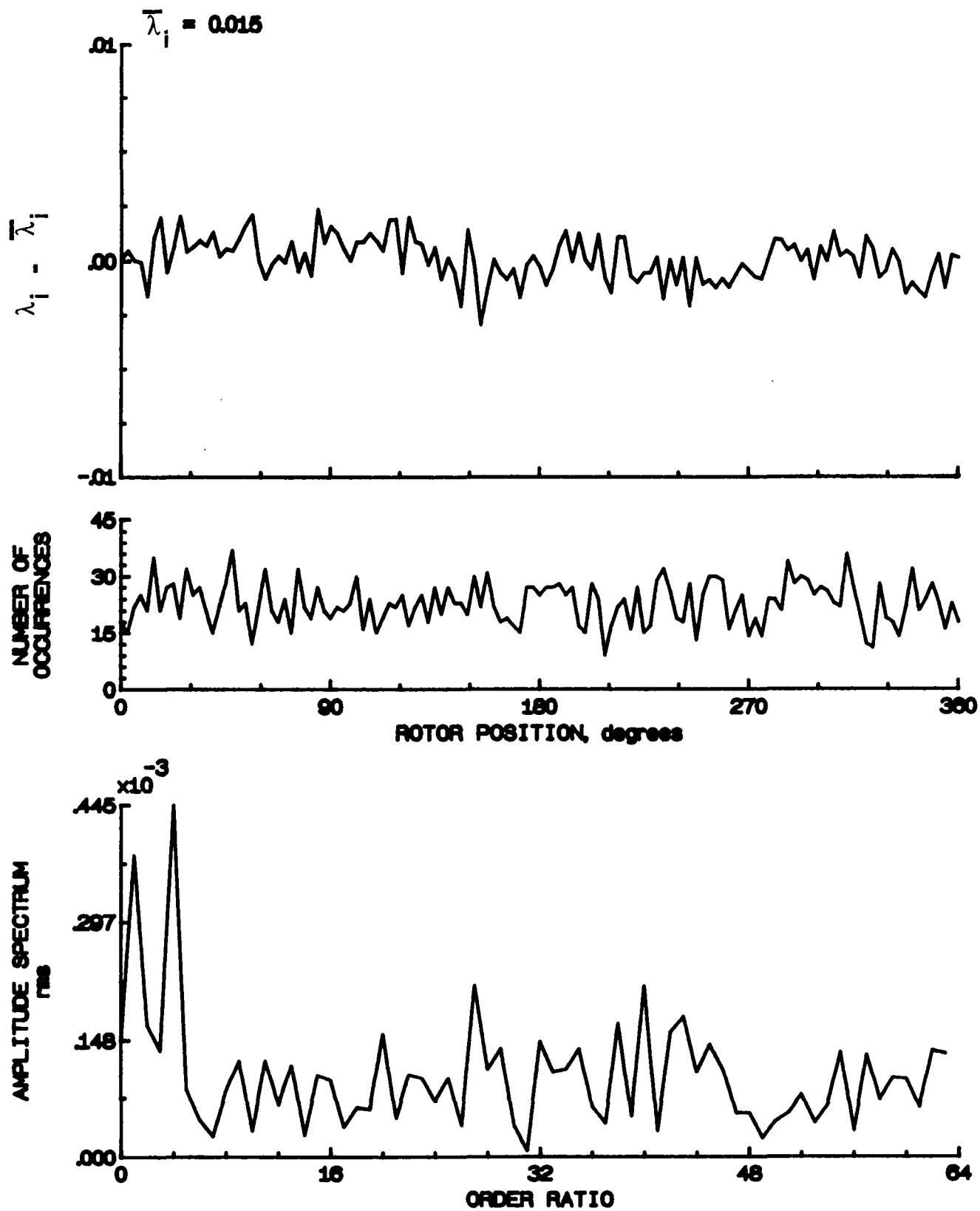


Figure 67.- Concluded.

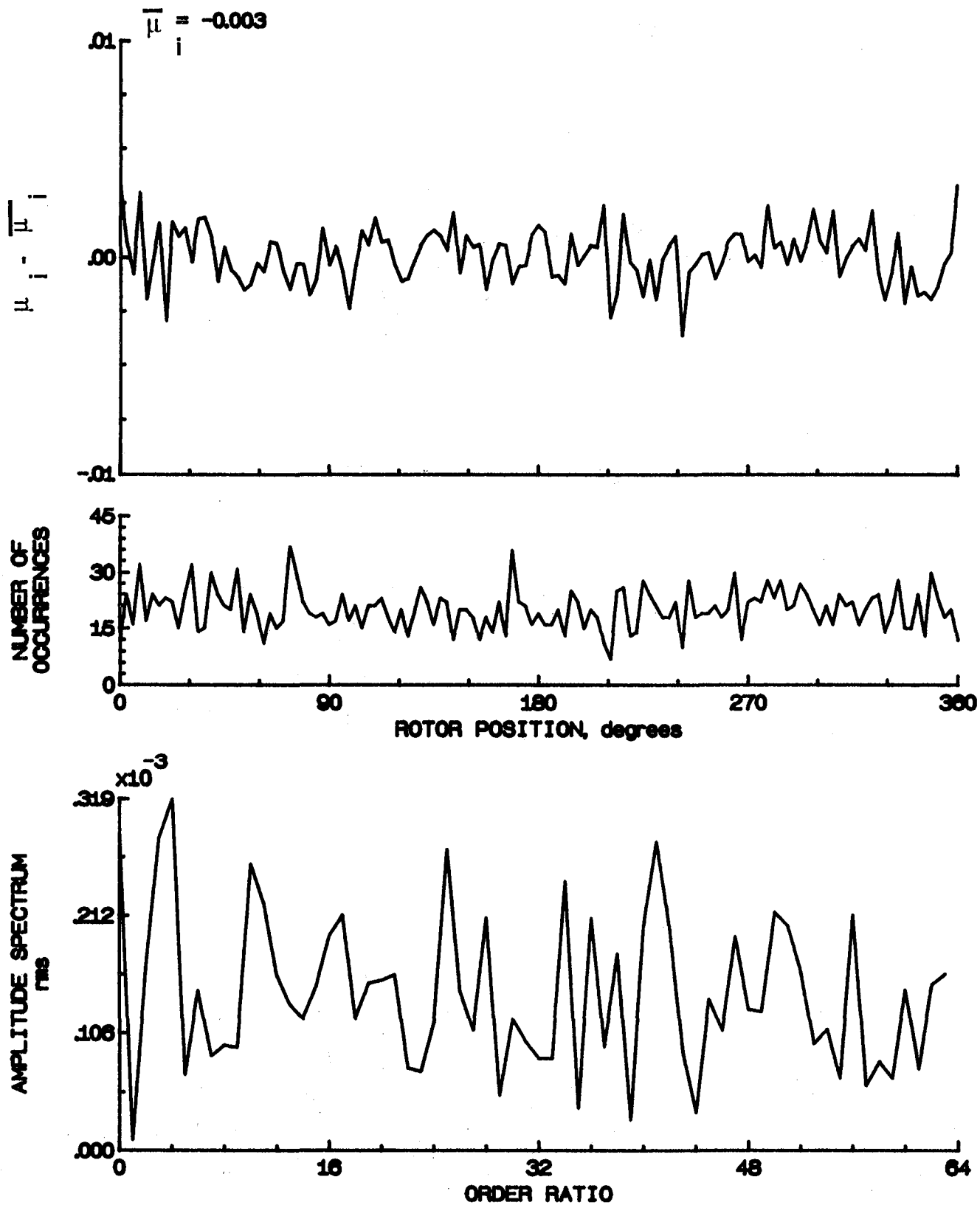


Figure 68.- Induced inflow velocity measured at 90 degrees and  $r/R$  of 0.94.



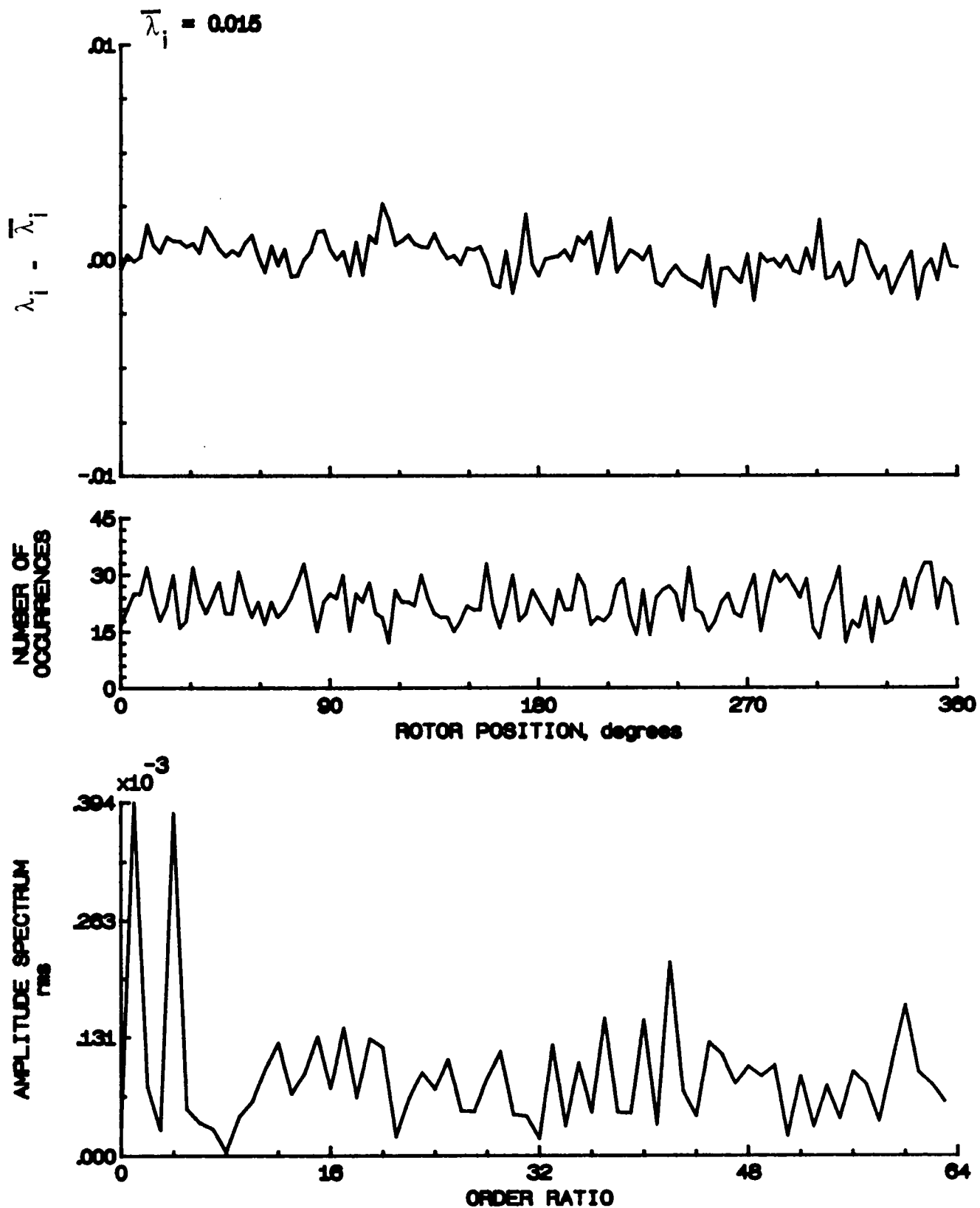


Figure 68.- Concluded.

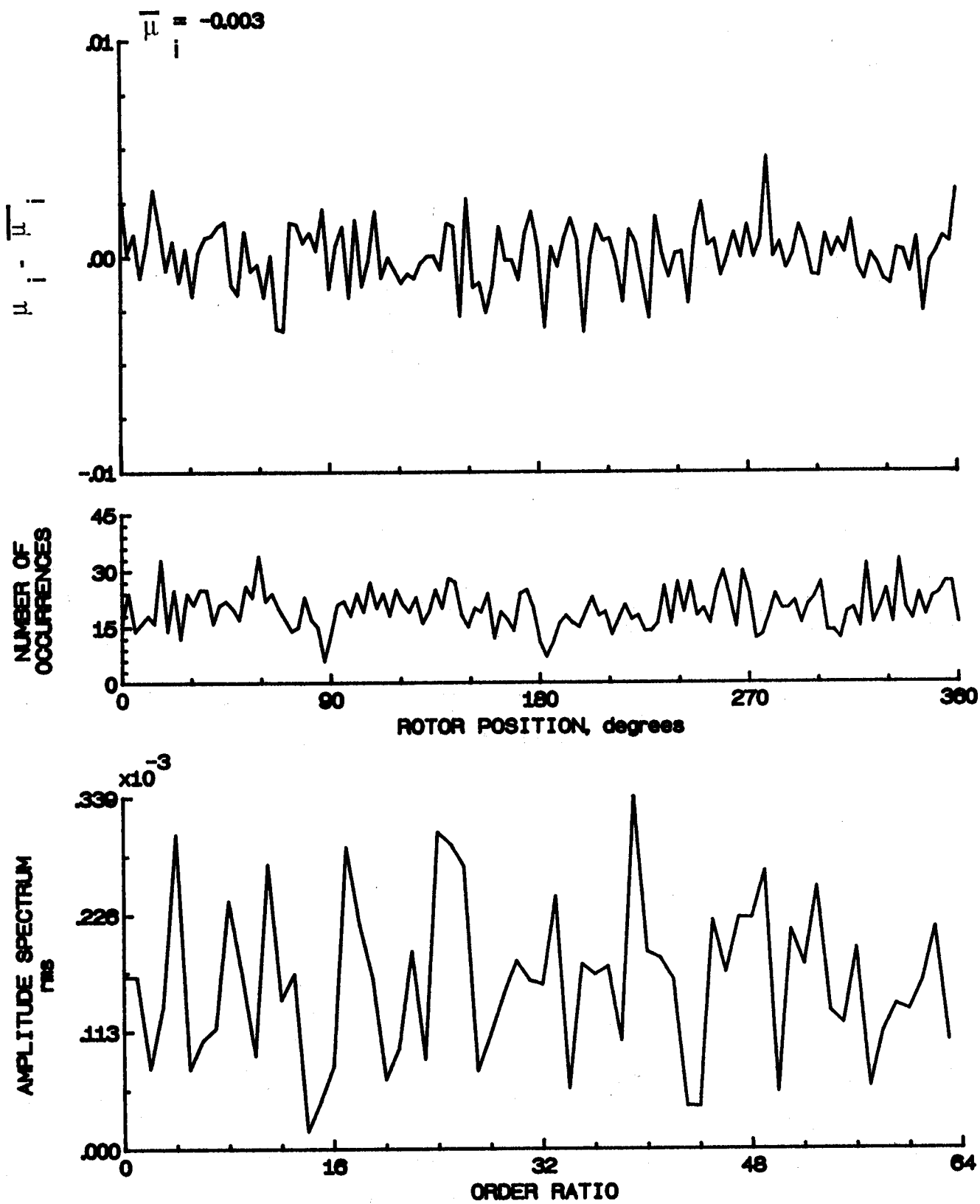


Figure 69.- Induced inflow velocity measured at 90 degrees and  $r/R$  of 0.98.

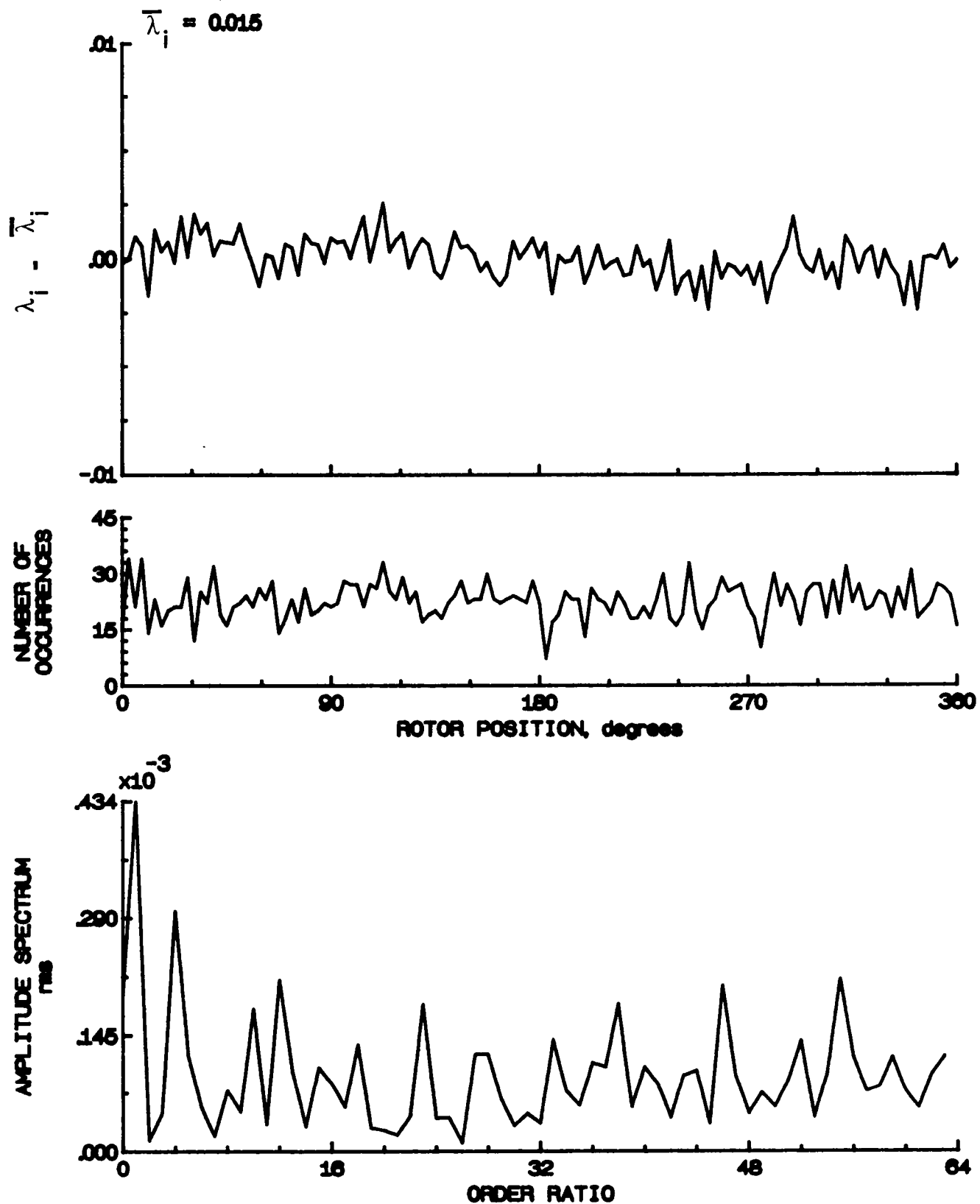


Figure 69.- Concluded.

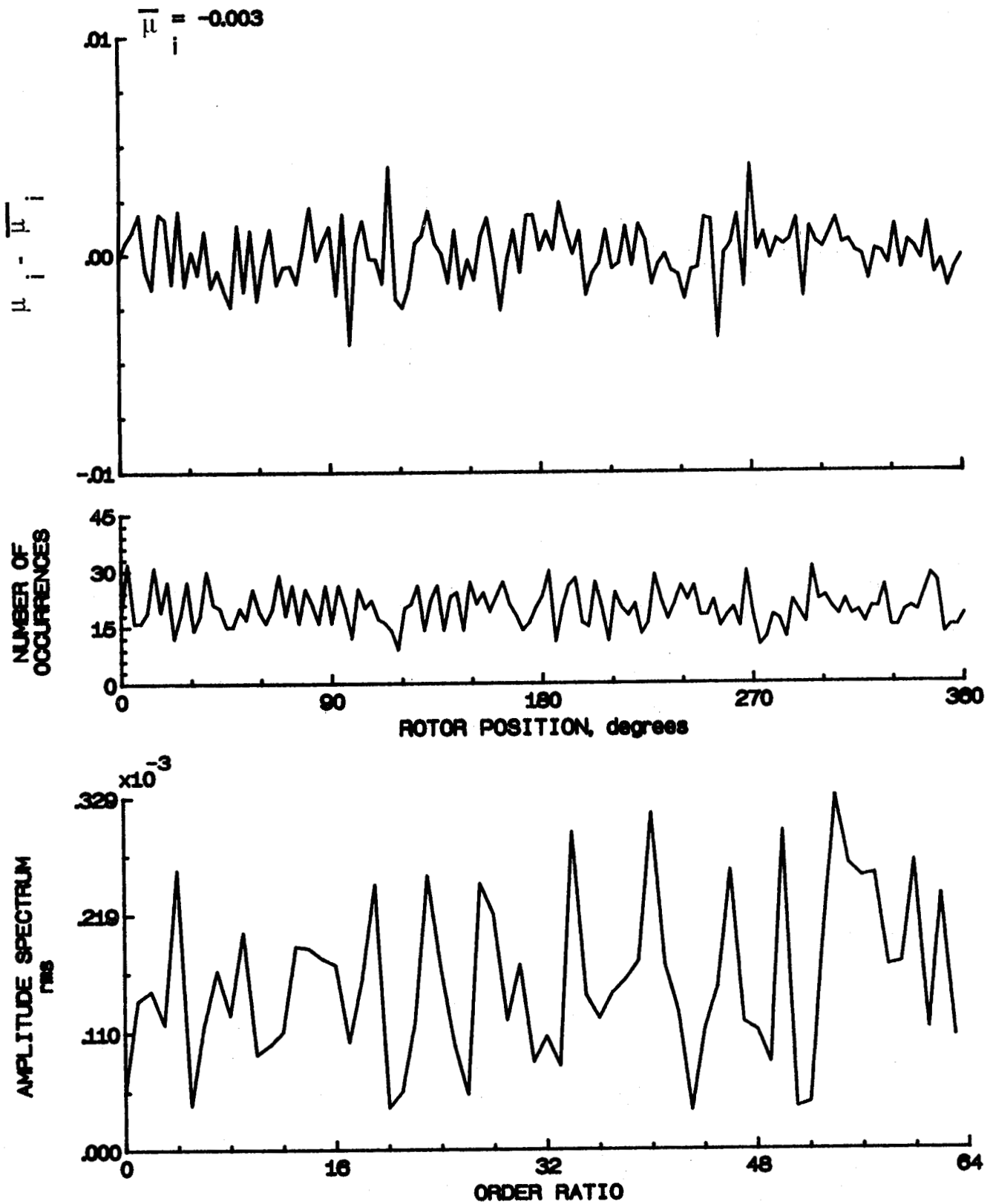


Figure 70.- Induced inflow velocity measured at 90 degrees and r/R of 1.02.

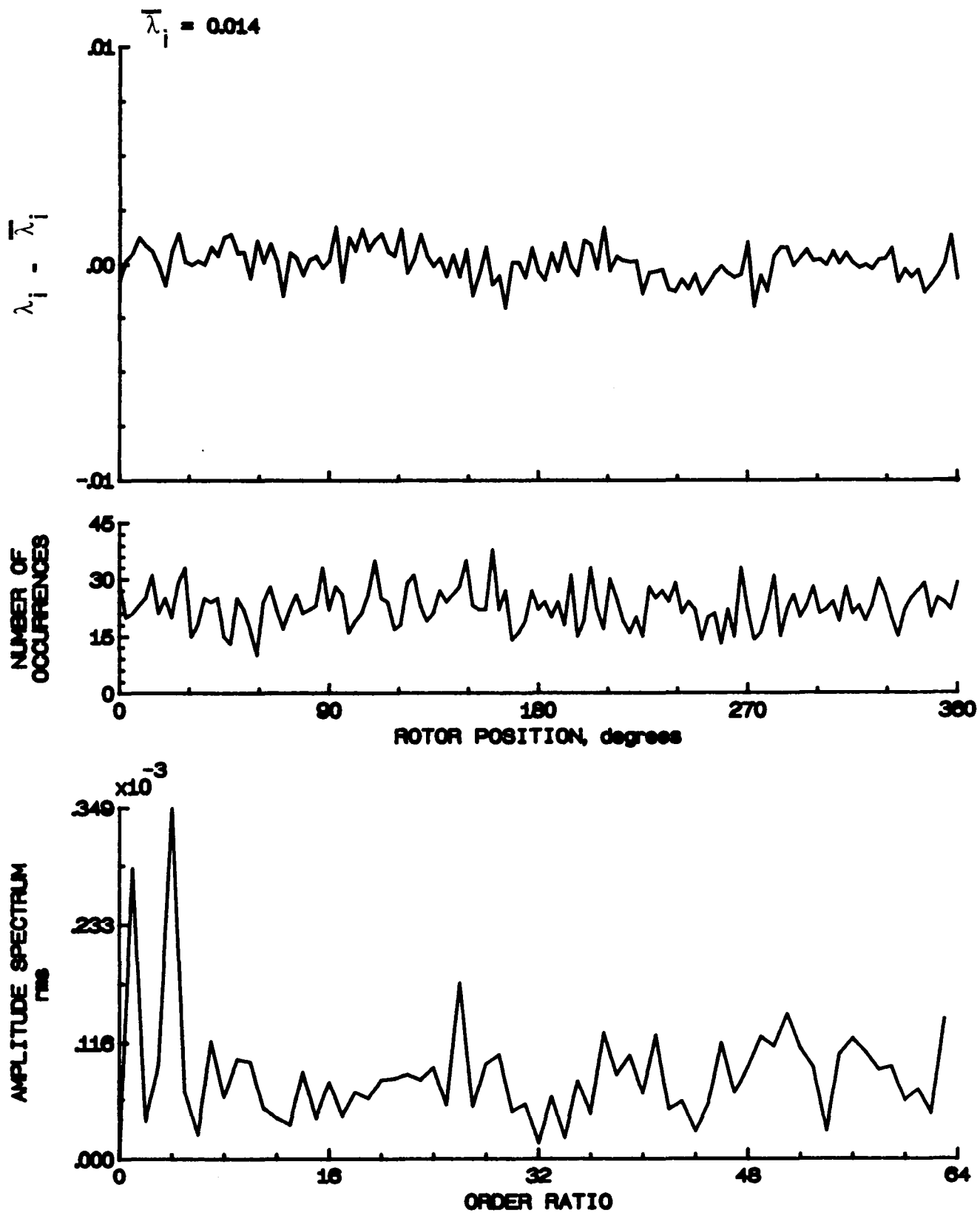


Figure 70.- Concluded.

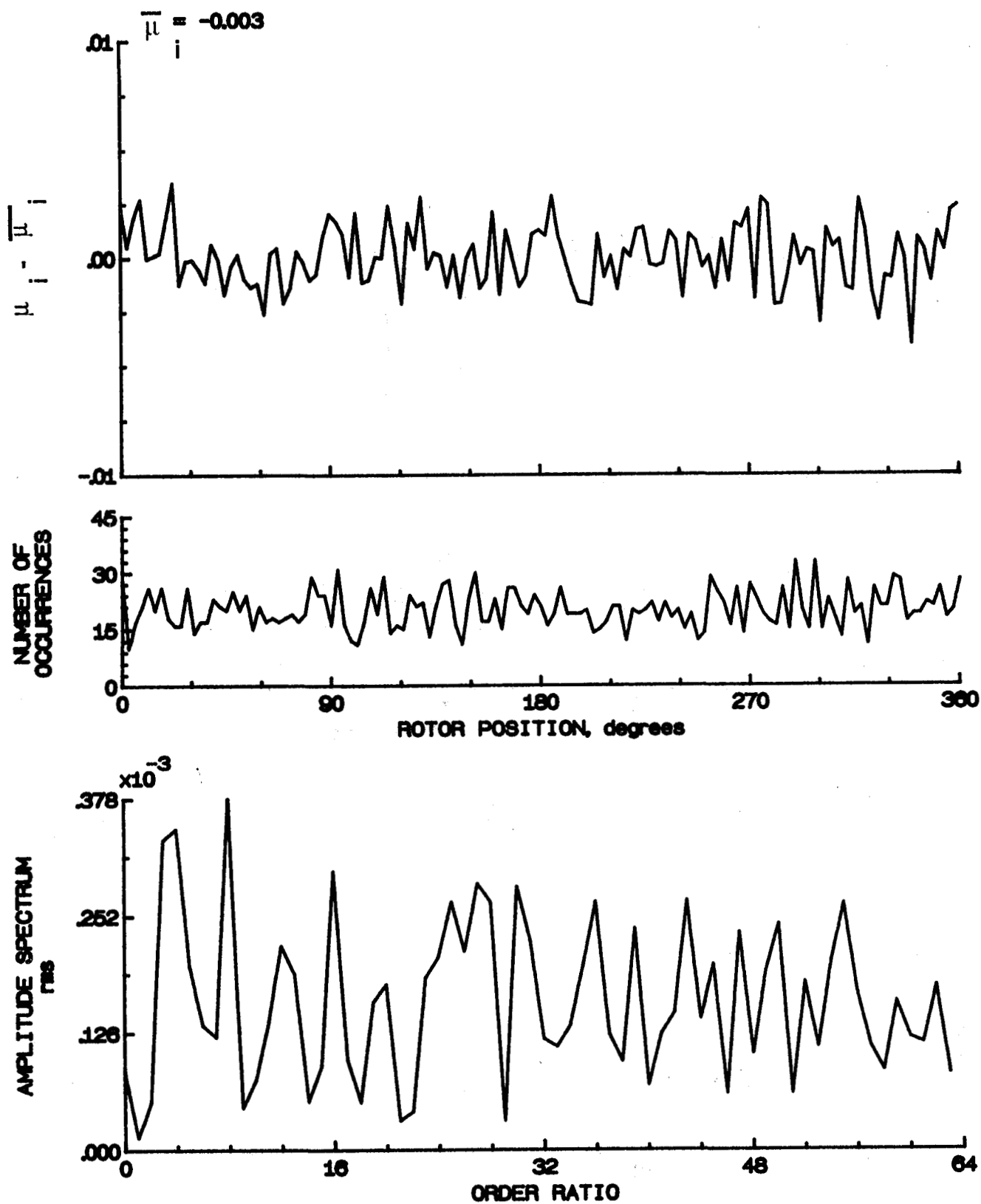


Figure 71.- Induced inflow velocity measured at 90 degrees and  $r/R$  of 1.04.

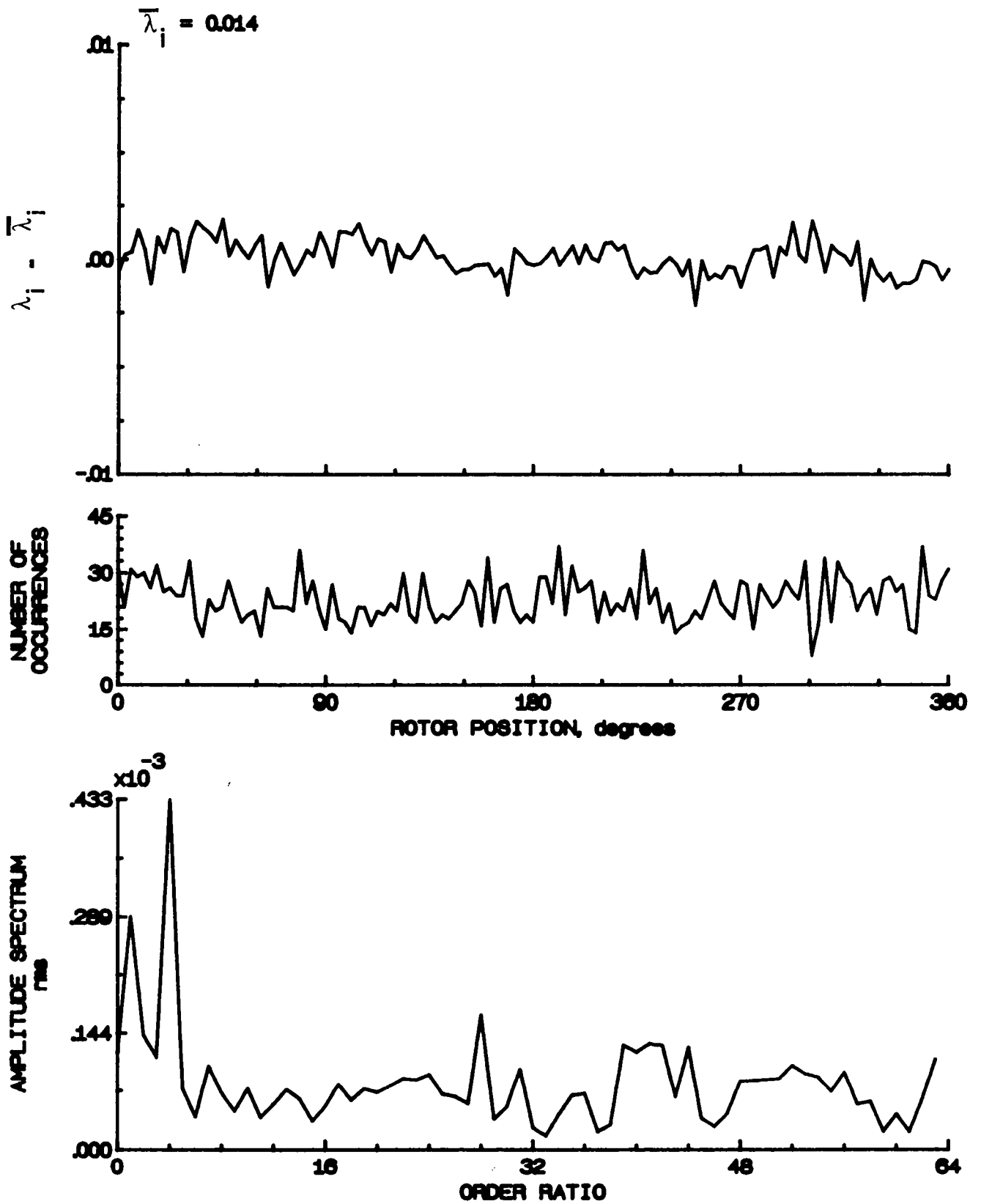


Figure 71- Concluded.

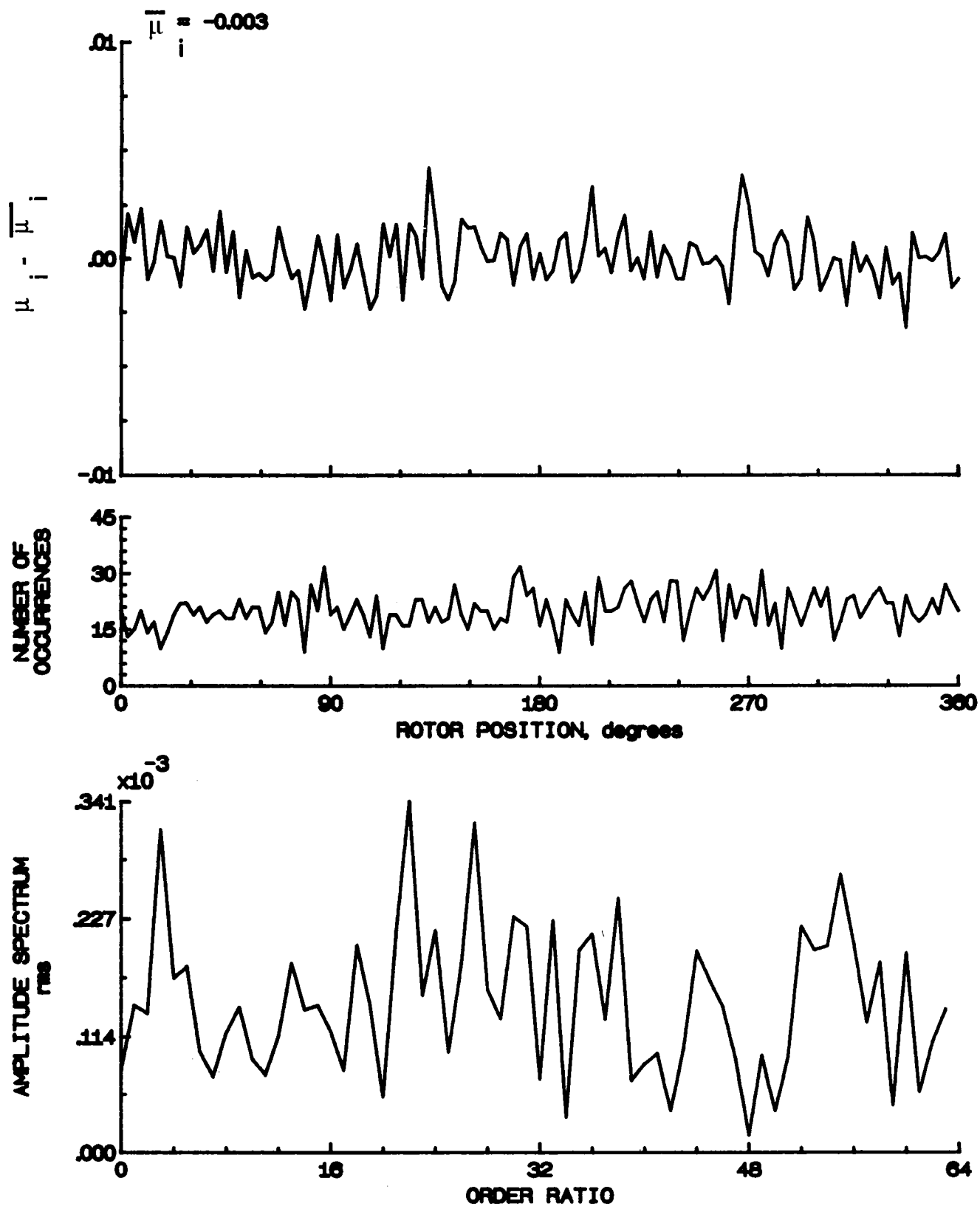


Figure 72.- Induced inflow velocity measured at 90 degrees and  $r/R$  of 1.10.



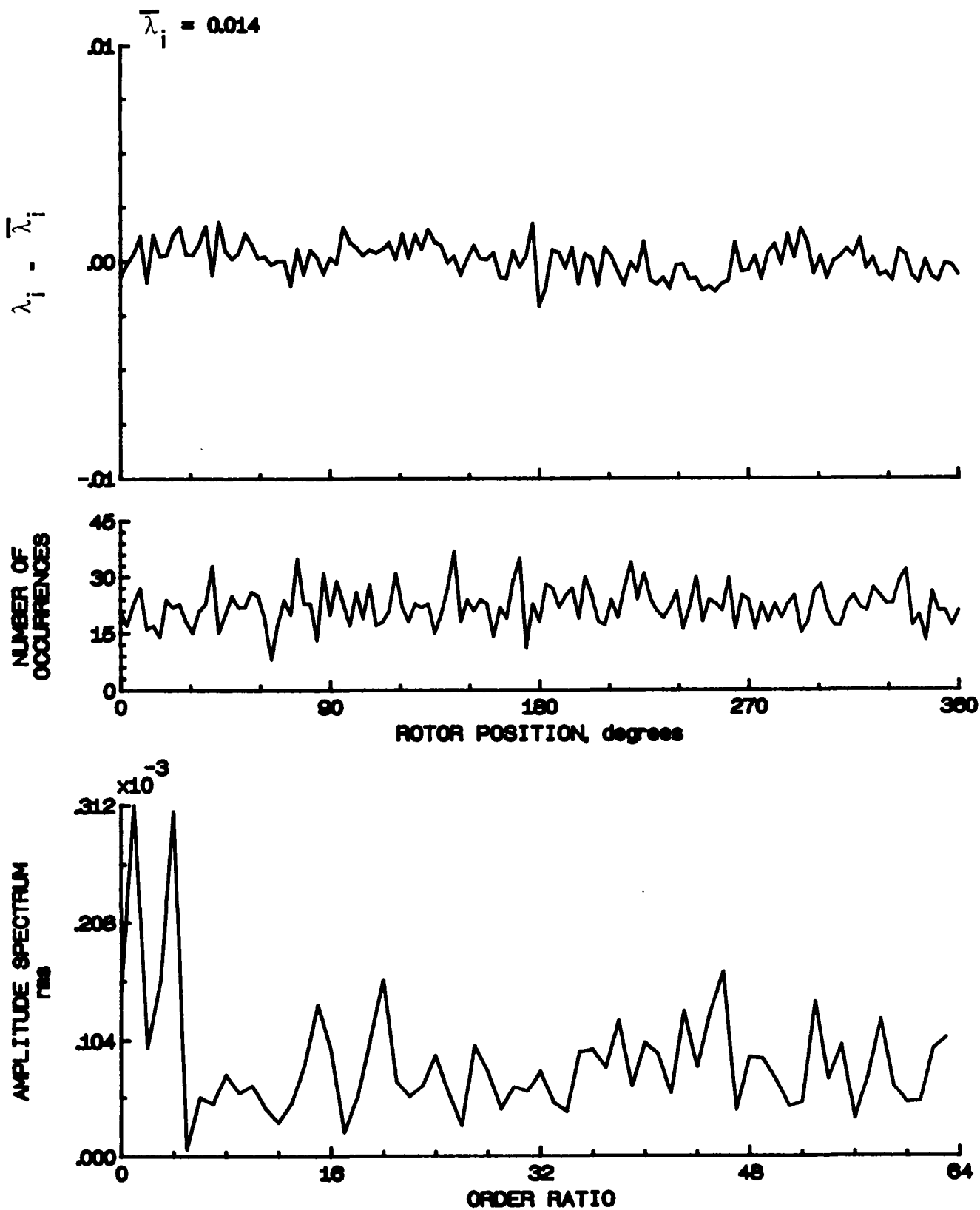


Figure 72- Concluded.

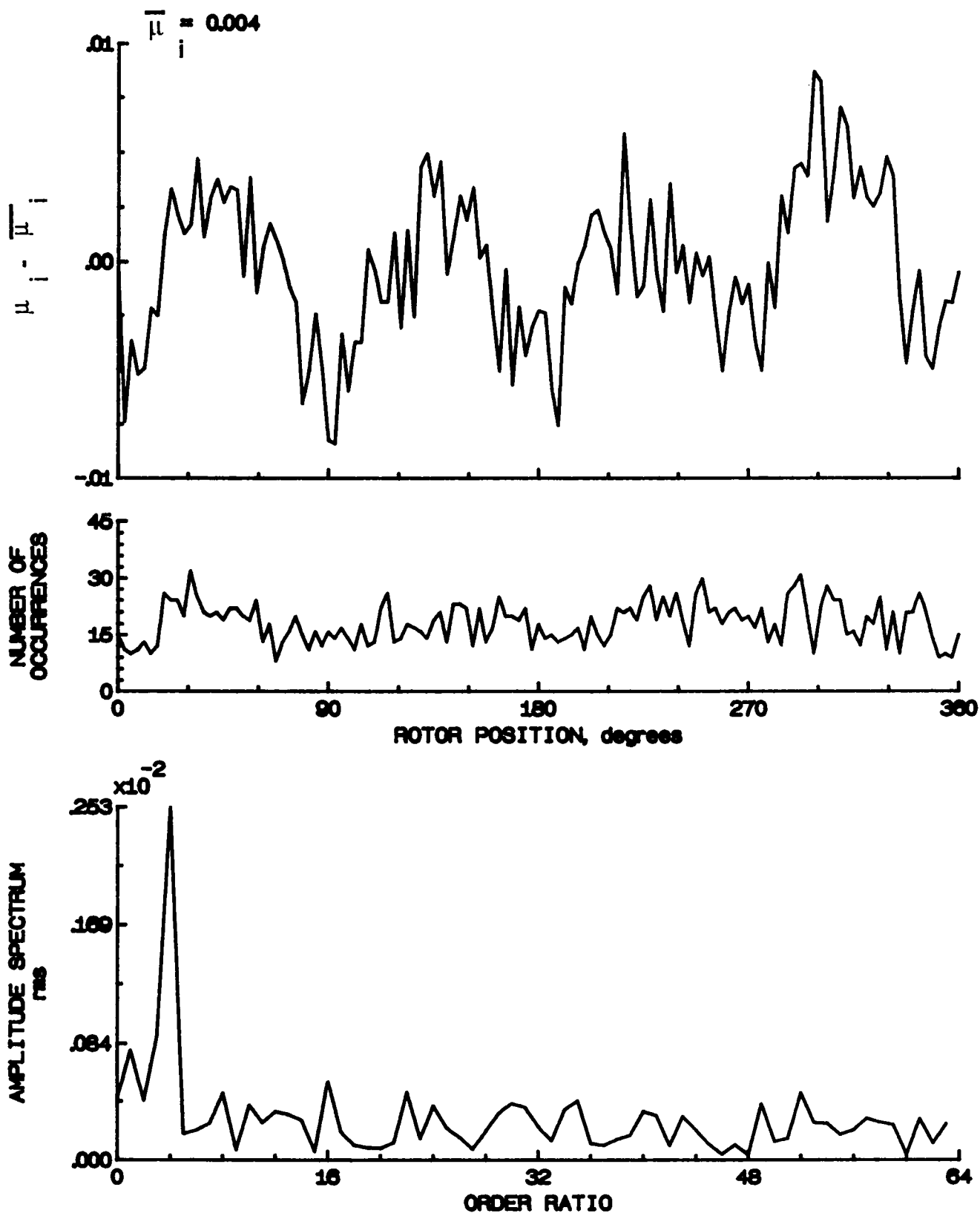


Figure 73.- Induced inflow velocity measured at 120 degrees and  $r/R$  of 0.20.

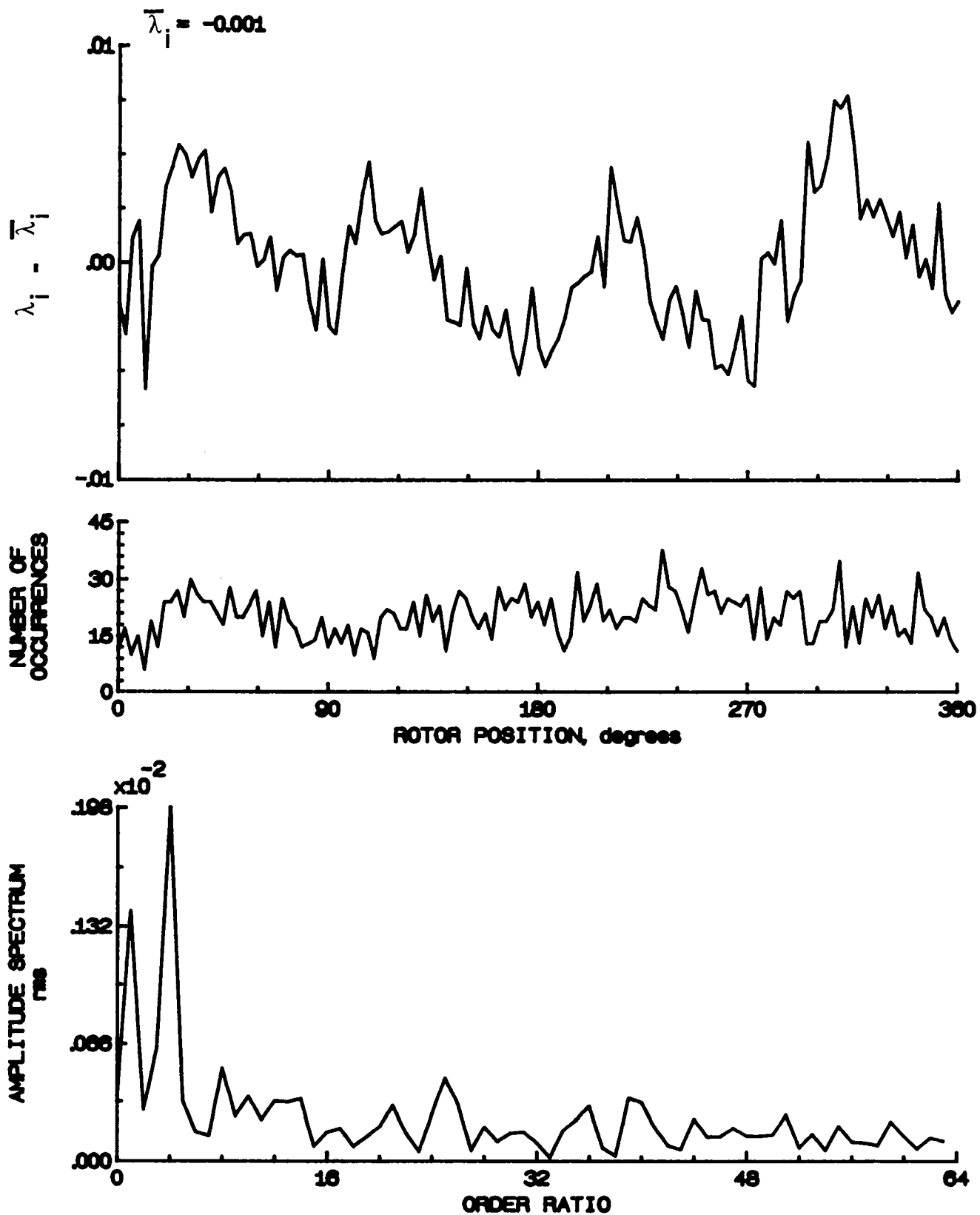


Figure 73- Concluded.

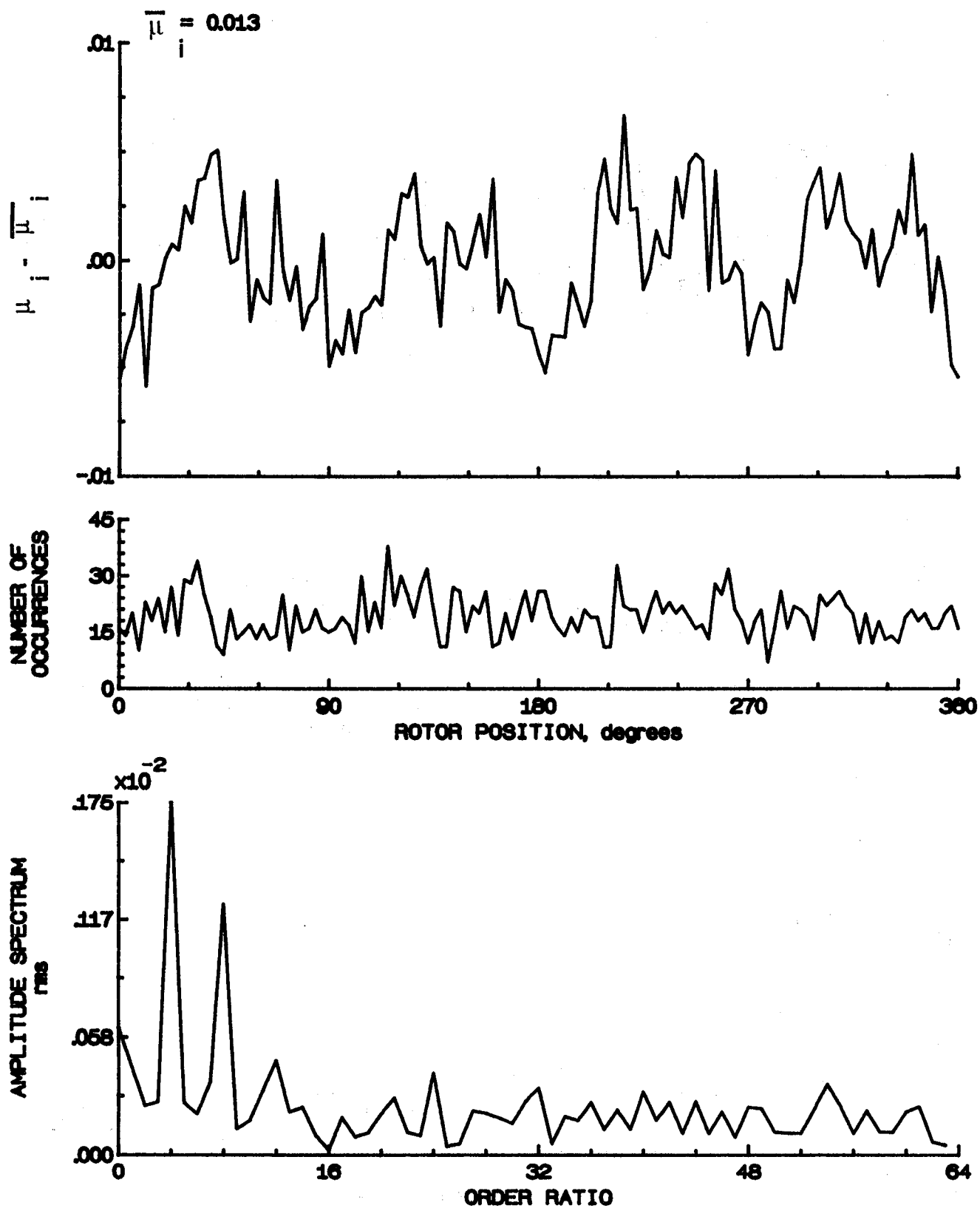


Figure 74.- Induced inflow velocity measured at 120 degrees and r/R of 0.40.

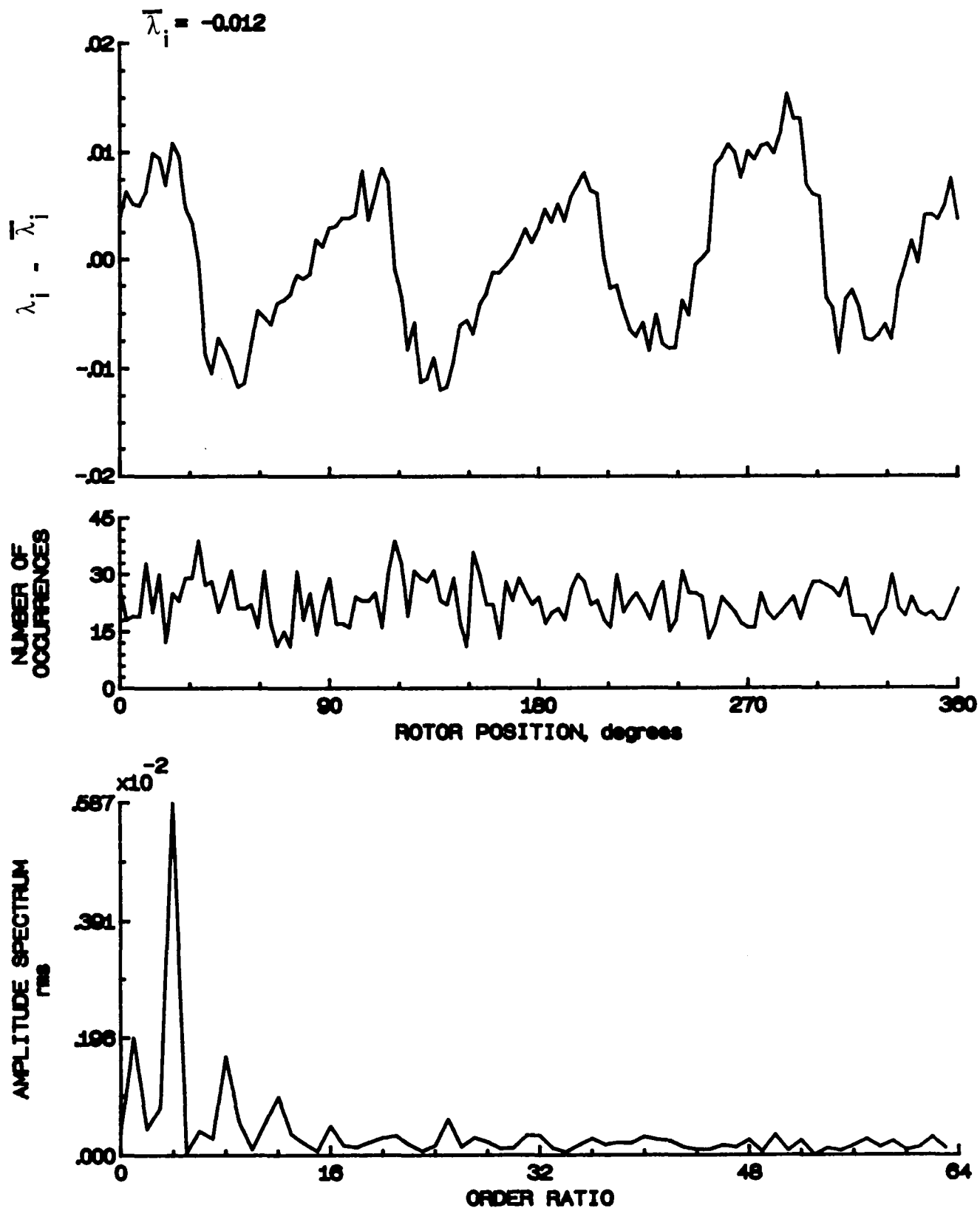


Figure 74.- Concluded.

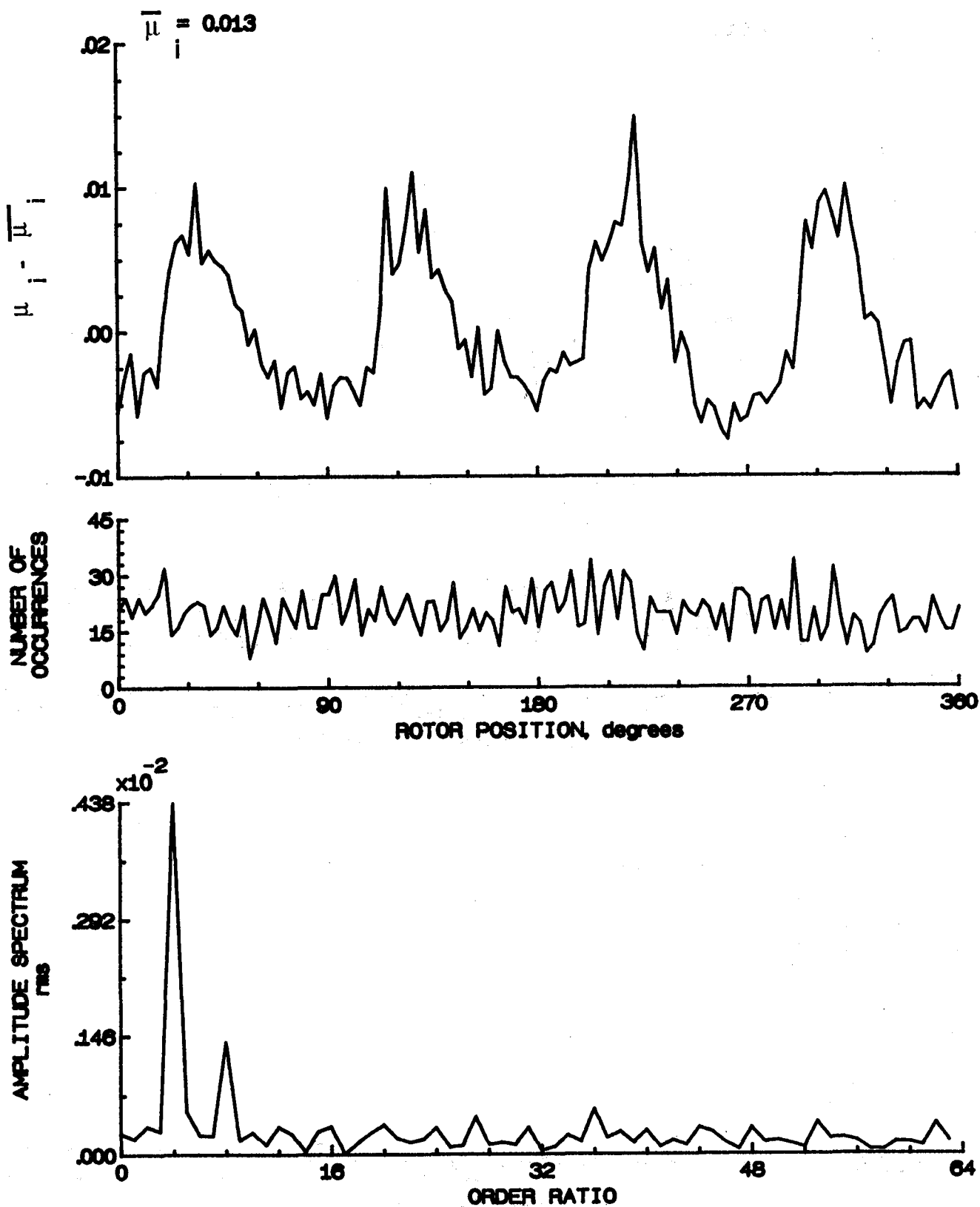


Figure 75.- Induced inflow velocity measured at 120 degrees and  $r/R$  of 0.50.

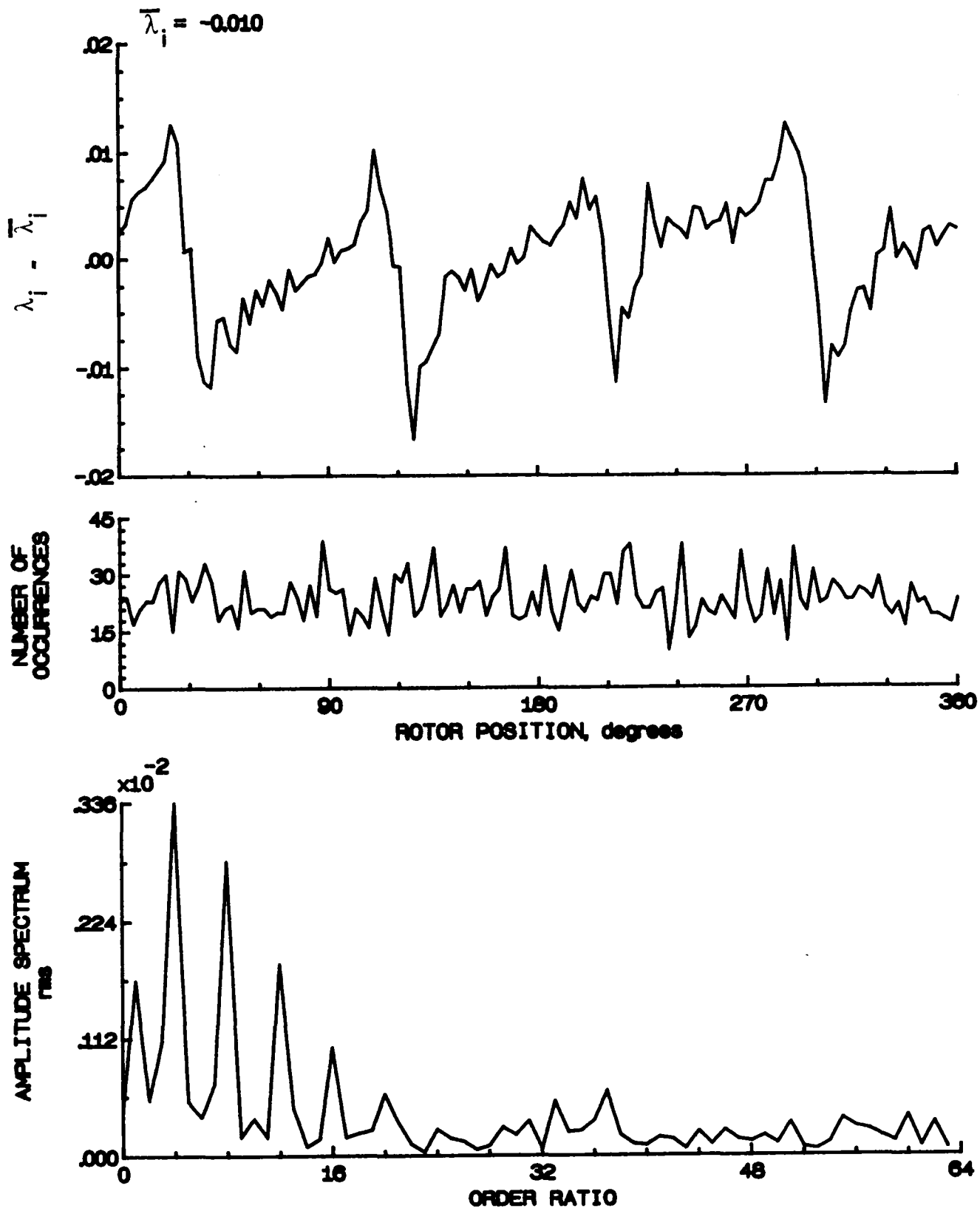


Figure 75.- Concluded.

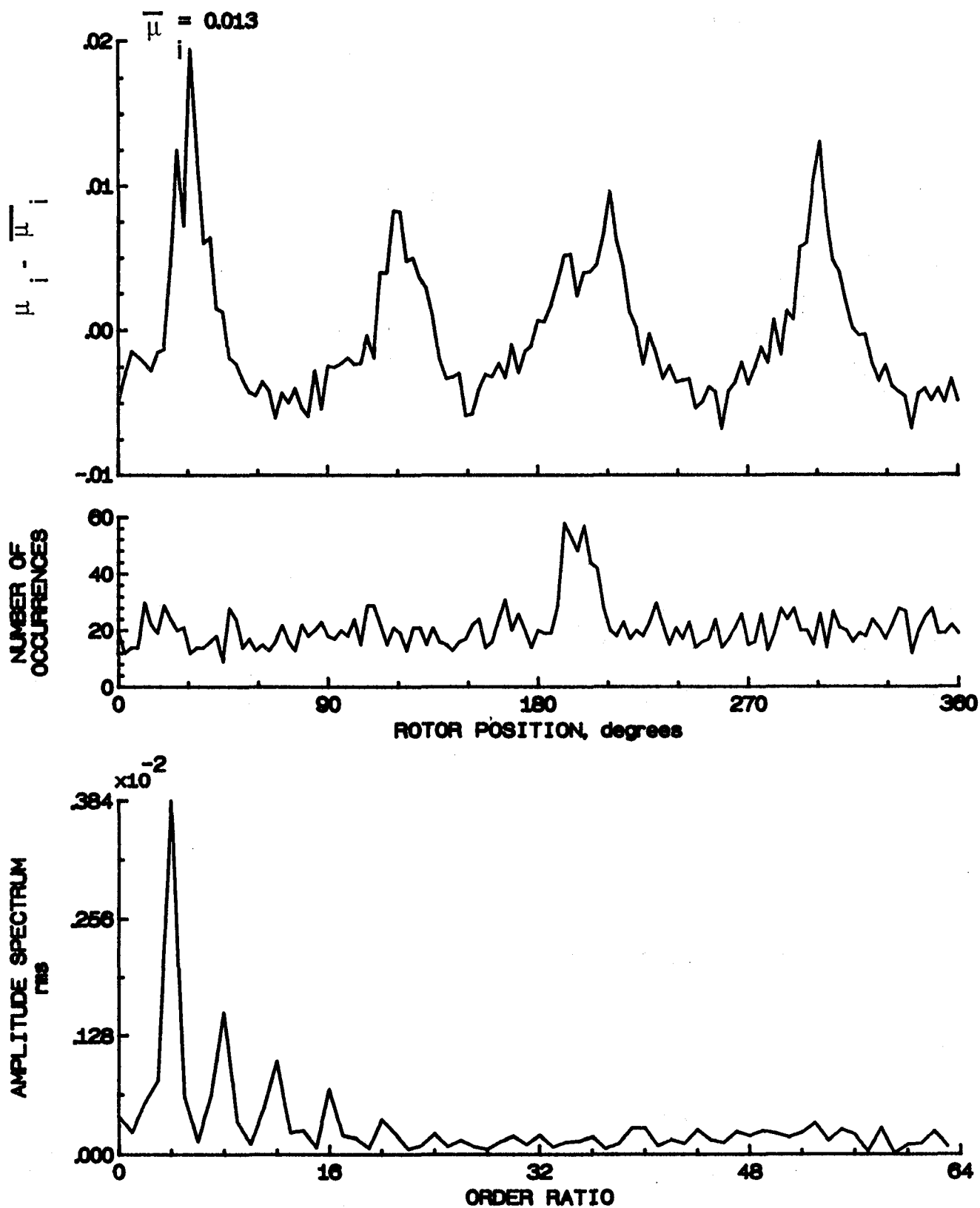


Figure 76.- Induced inflow velocity measured at 120 degrees and r/R of 0.60.



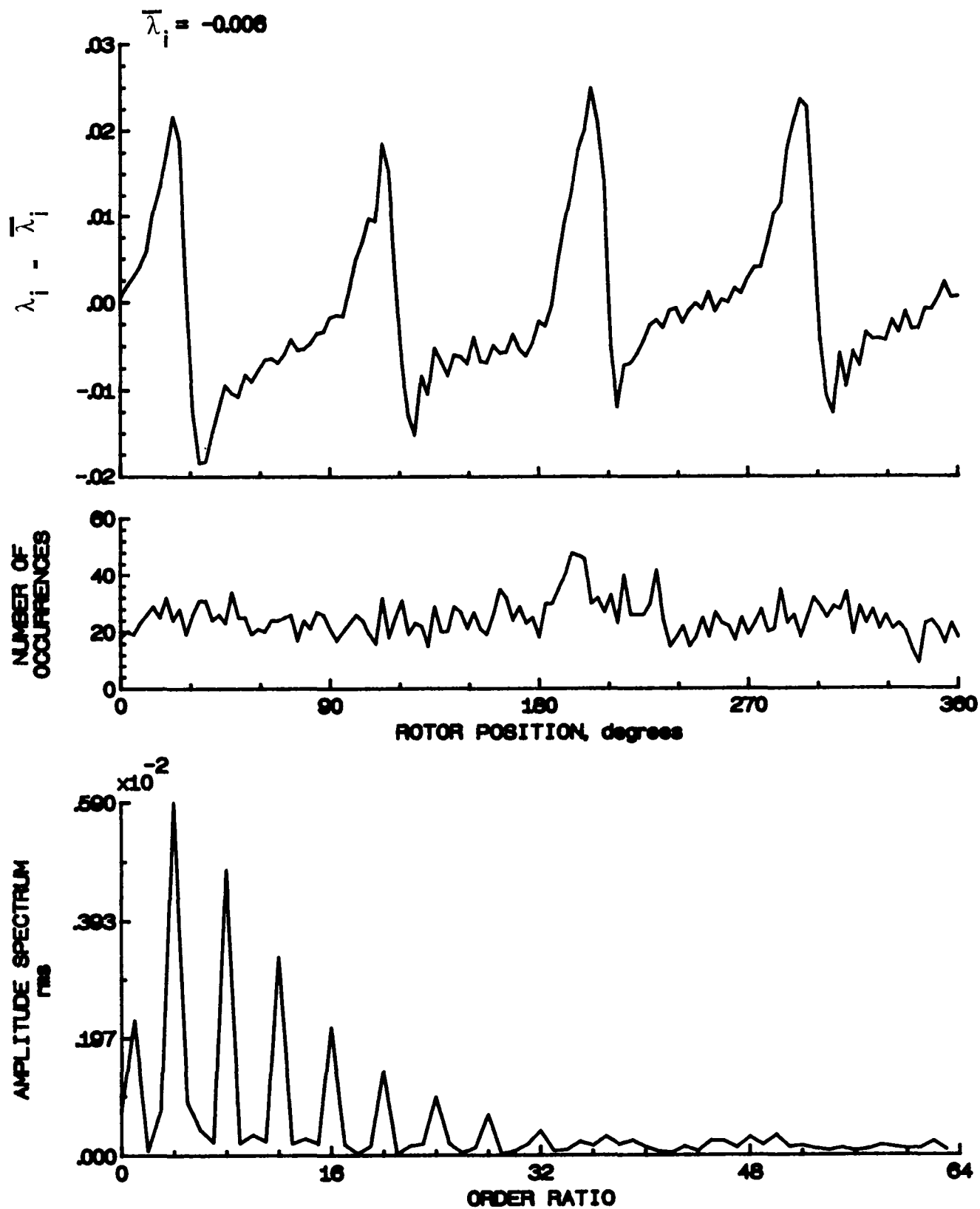


Figure 76.- Concluded.

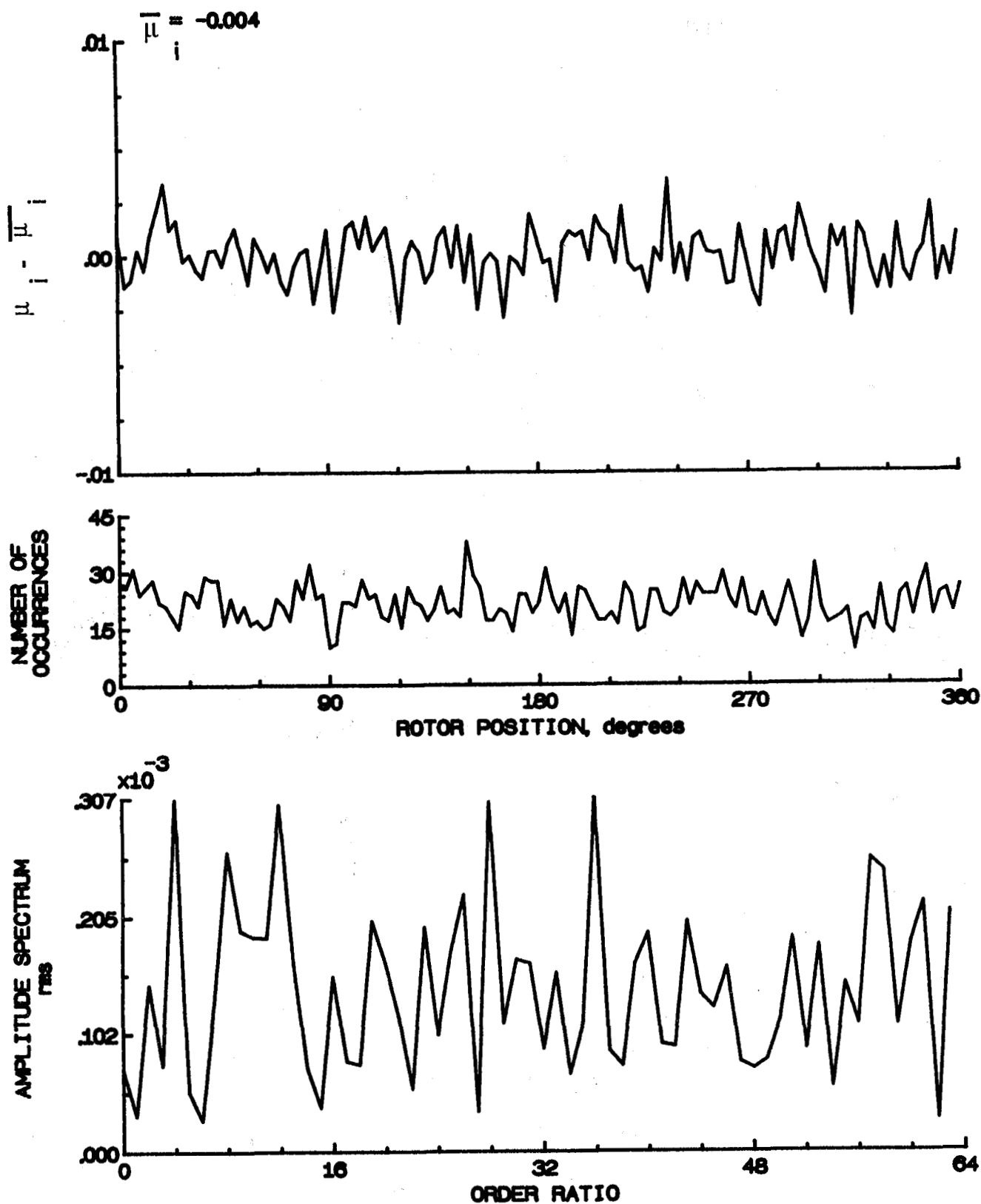


Figure 77.- Induced inflow velocity measured at 120 degrees and  $r/R$  of 0.70.

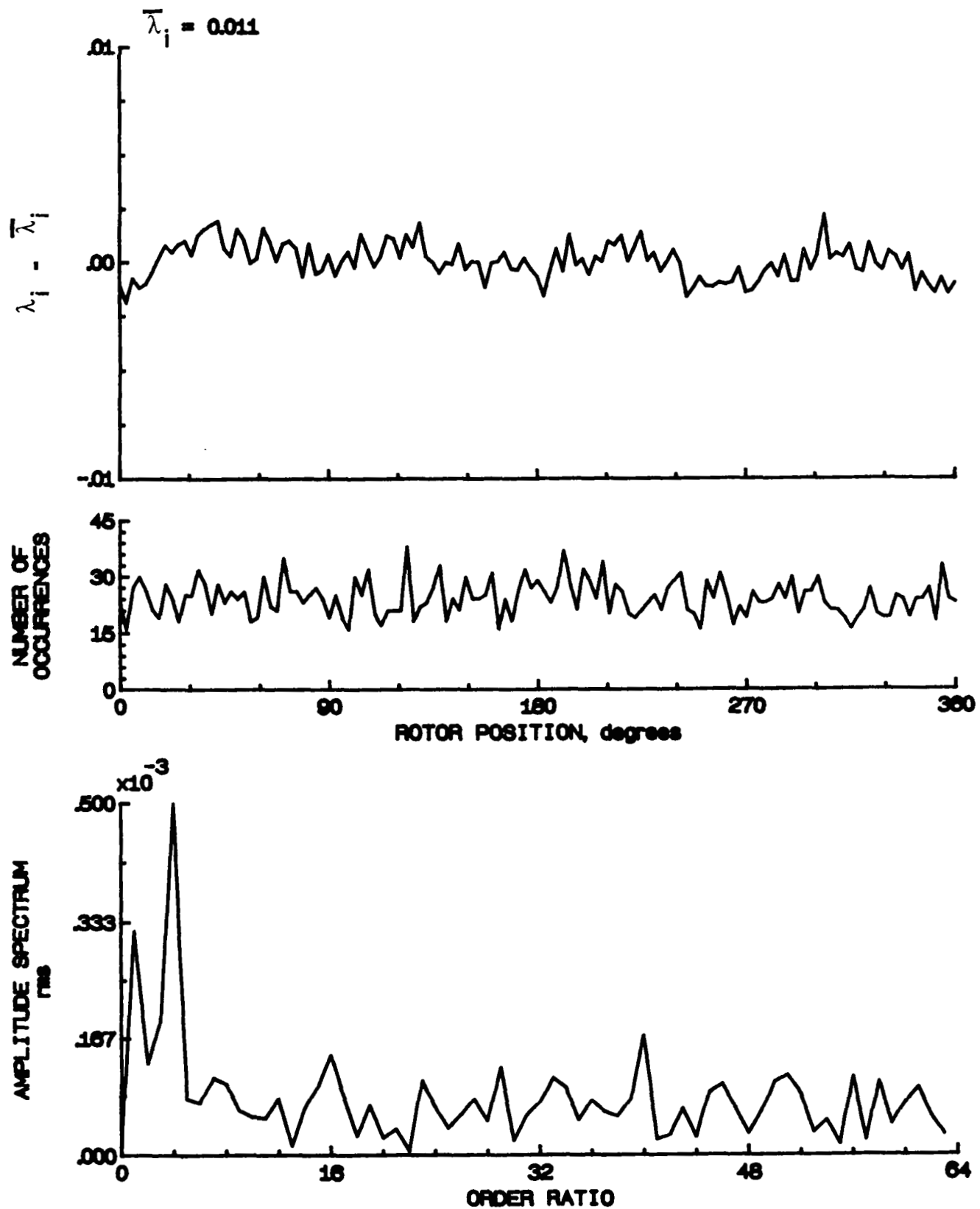


Figure 77.- Concluded.

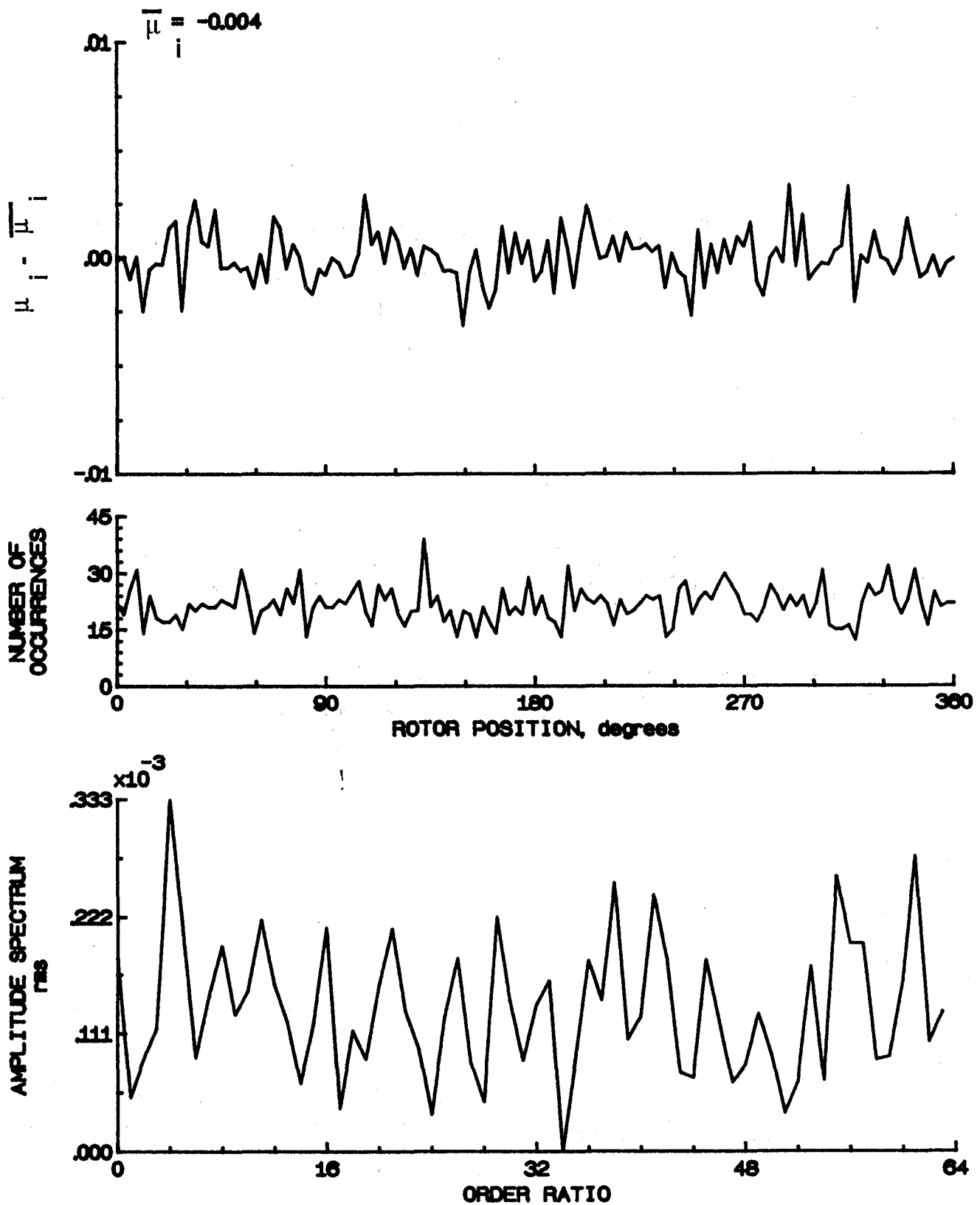


Figure 78.- Induced inflow velocity measured at 120 degrees and r/R of 0.74.

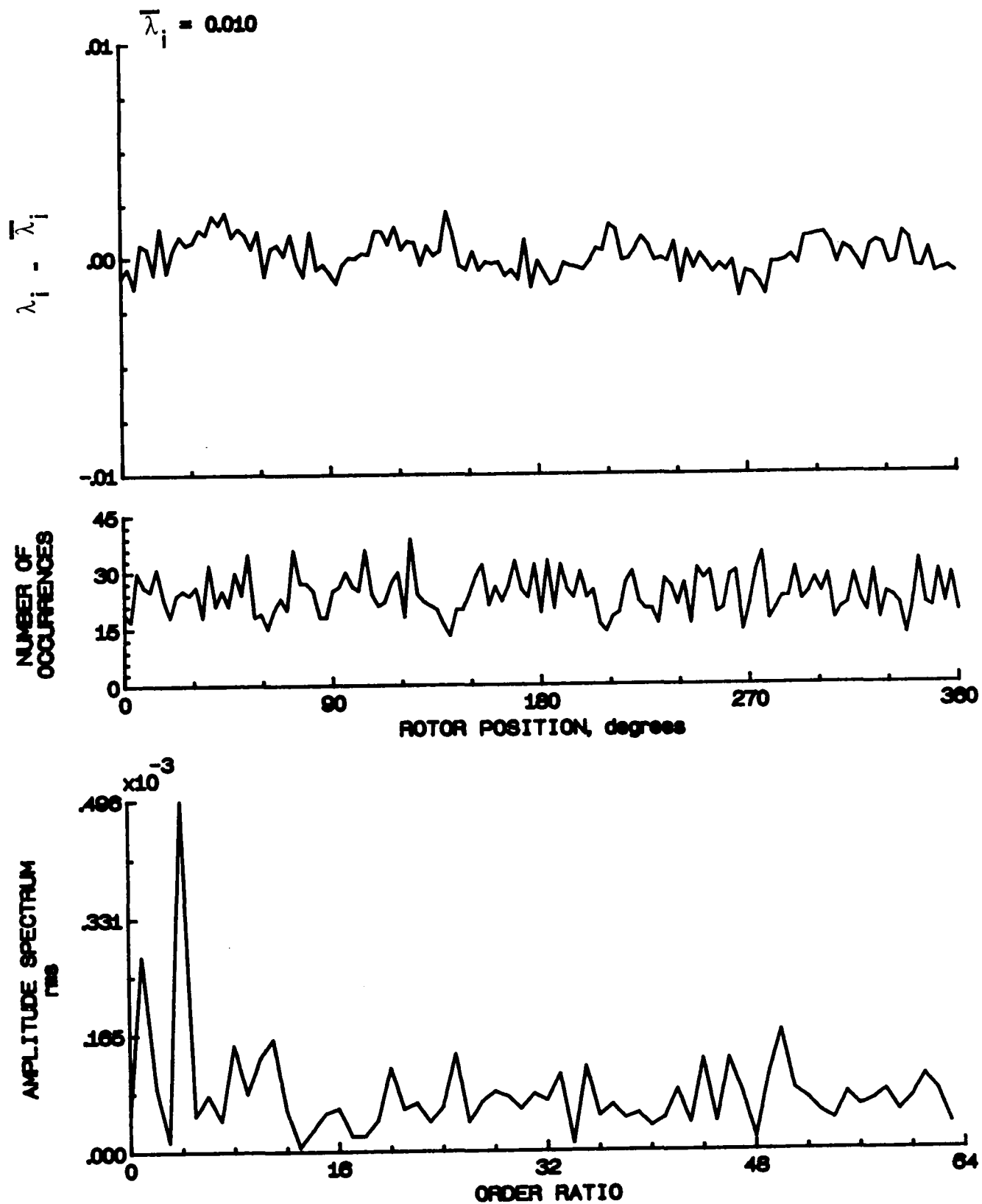


Figure 78.- Concluded.

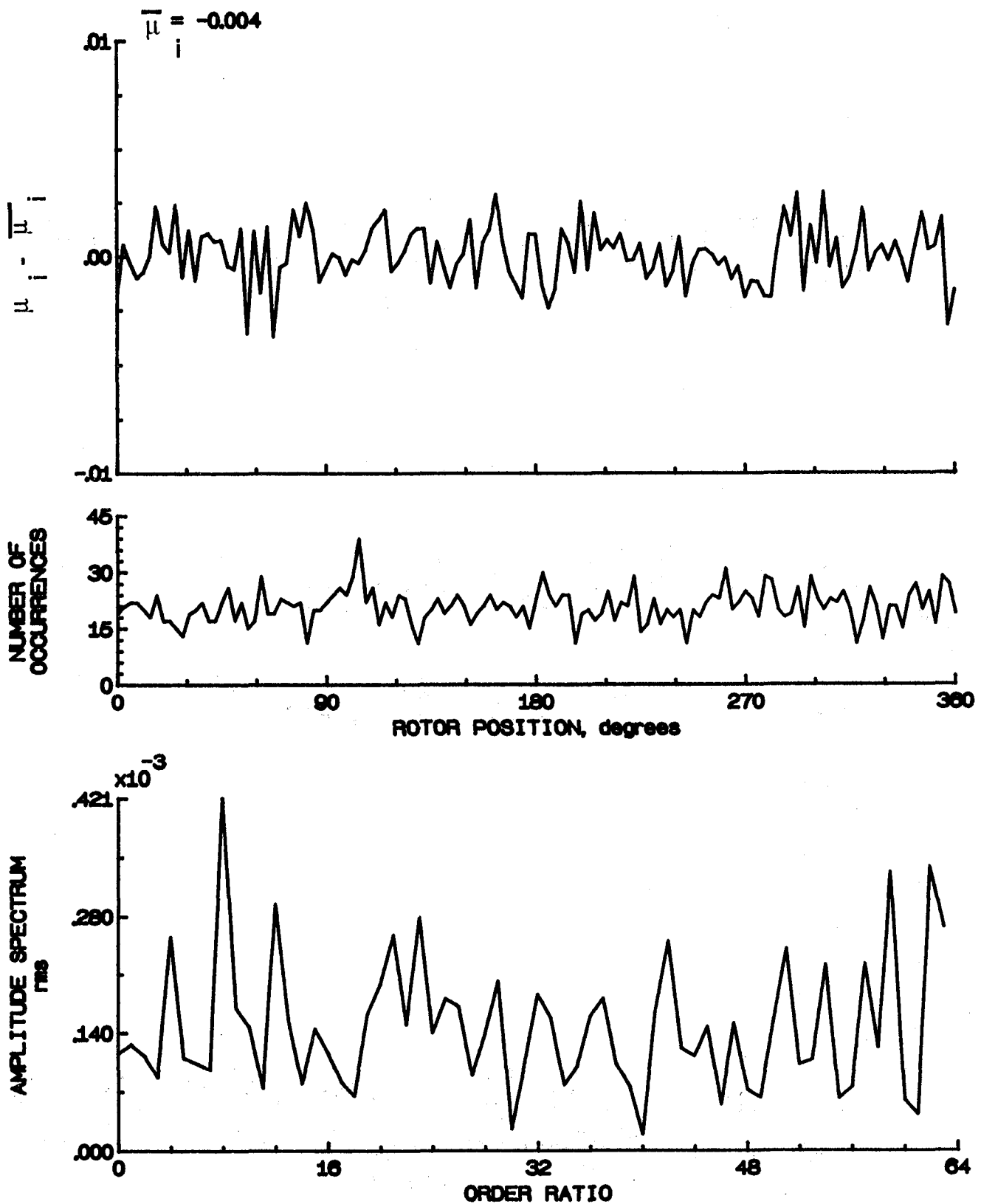


Figure 79.- Induced inflow velocity measured at 120 degrees and  $r/R$  of 0.78.

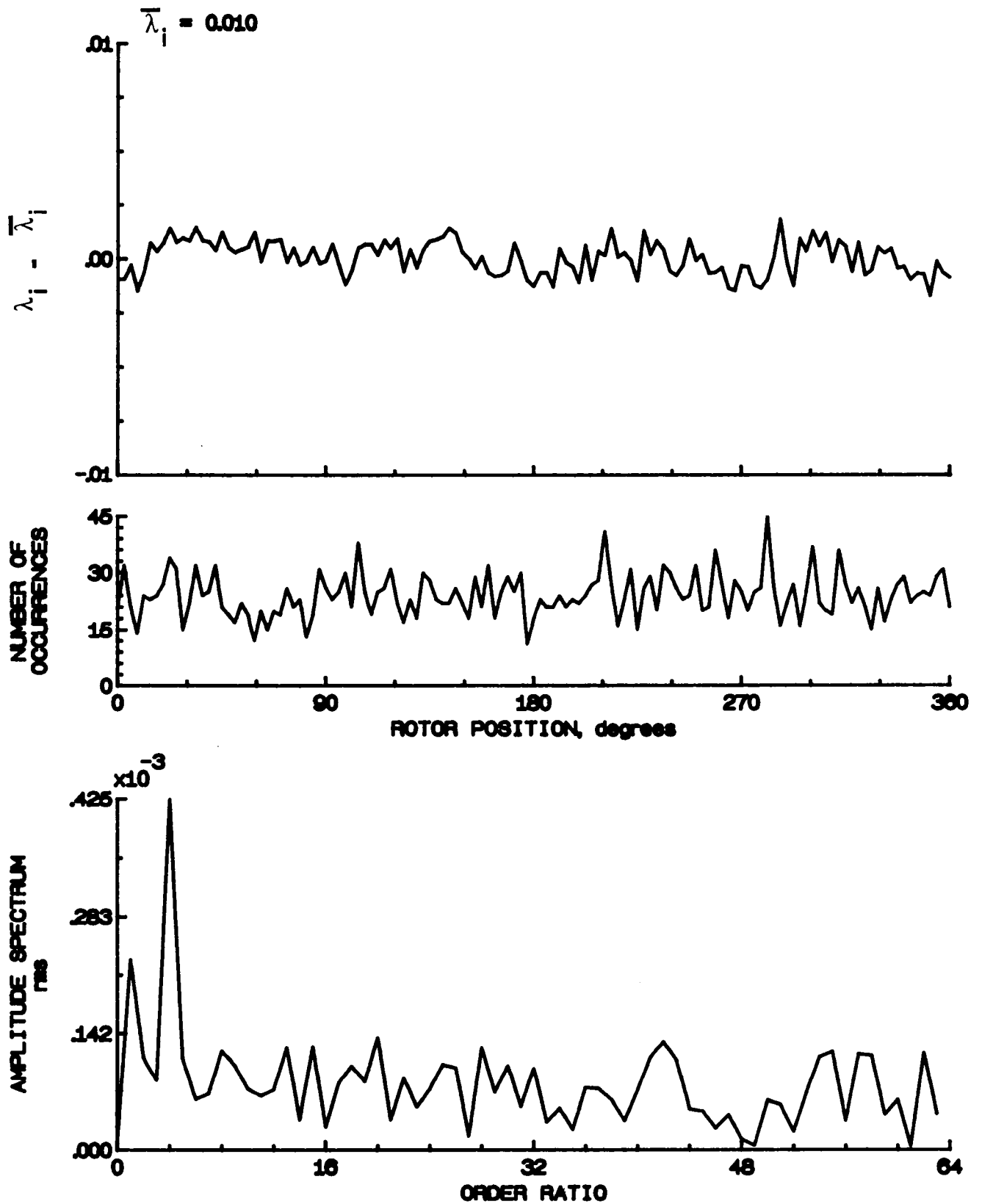


Figure 79.- Concluded.

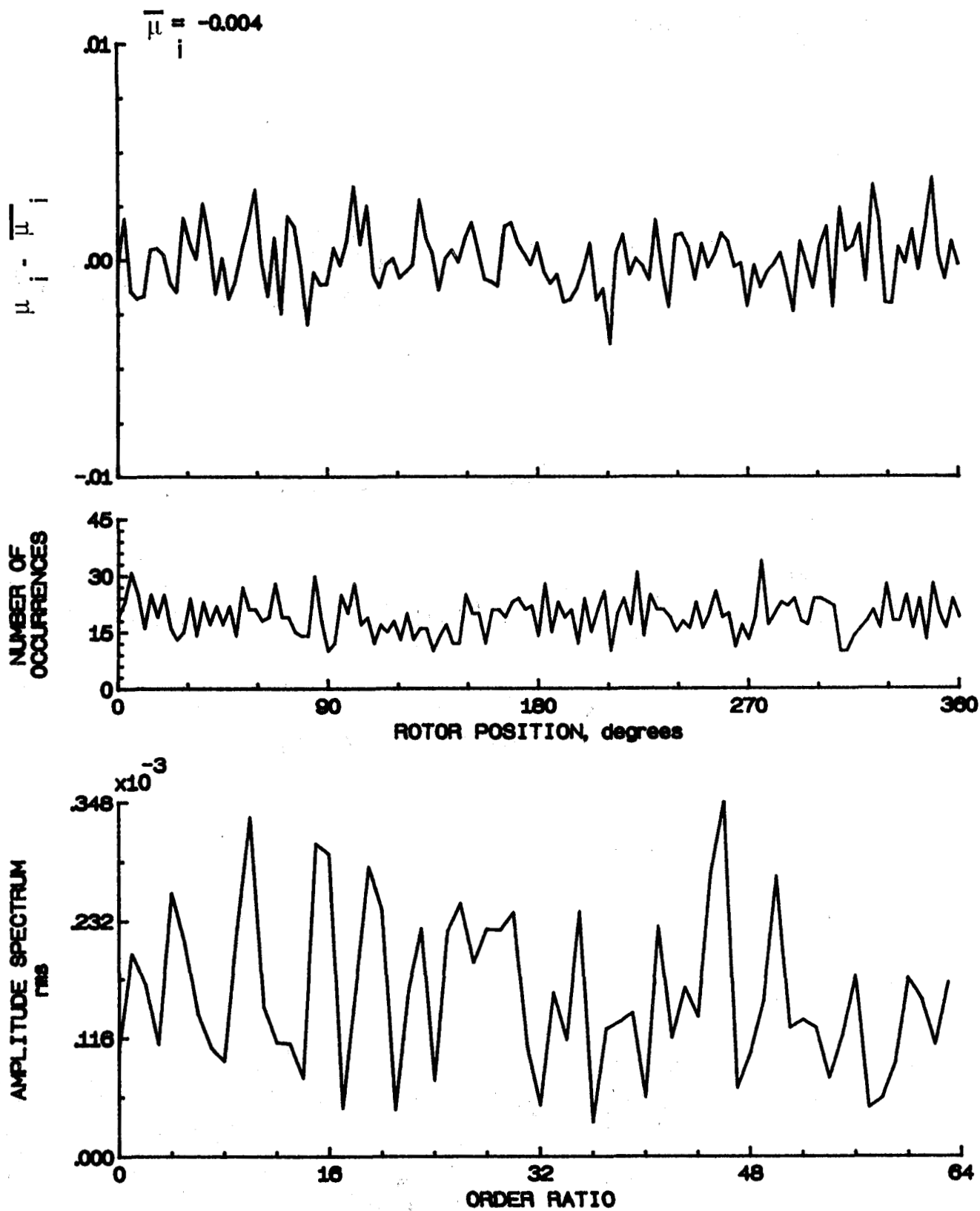


Figure 80.- Induced inflow velocity measured at 120 degrees and r/R of 0.82.



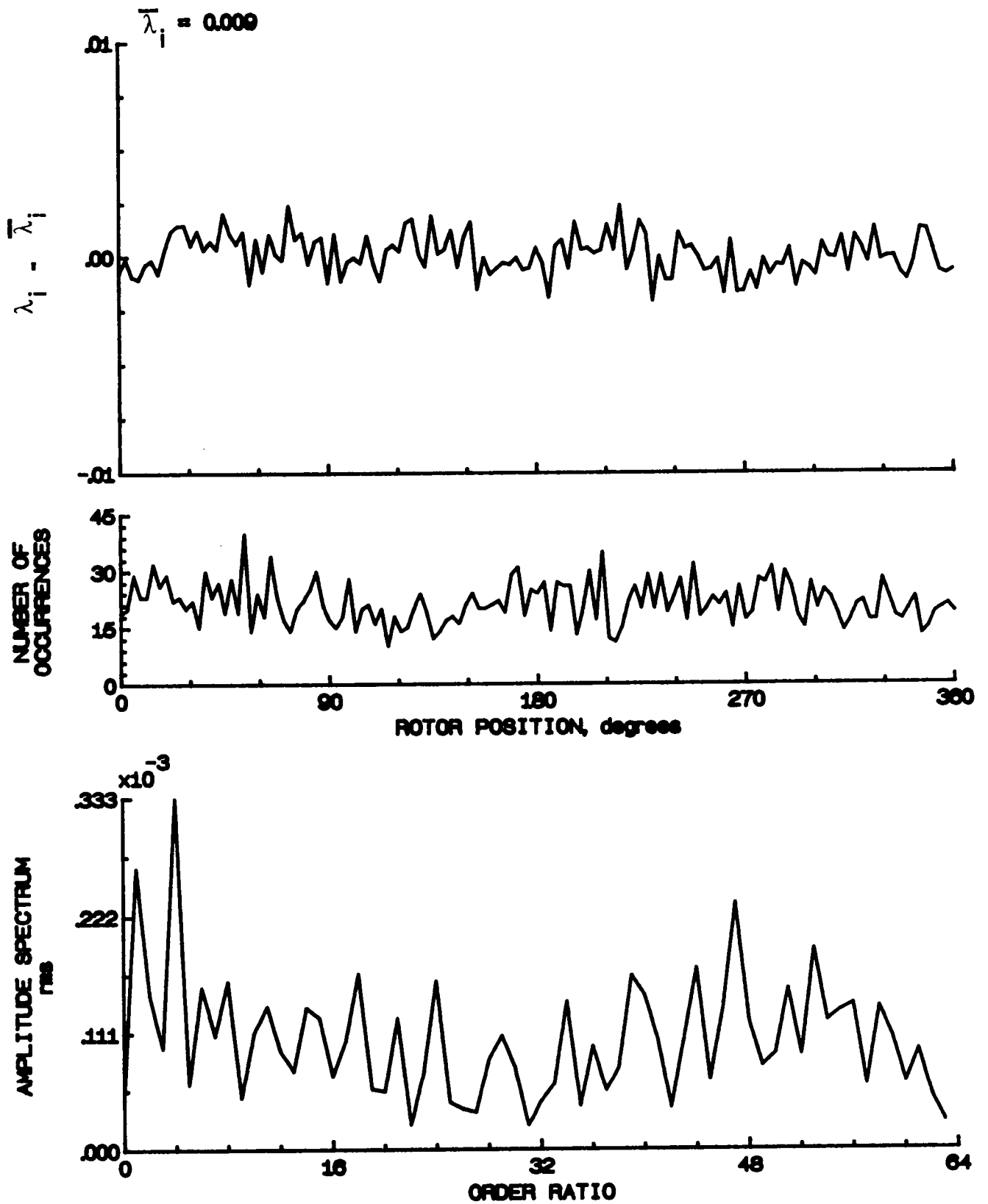


Figure 80.- Concluded.

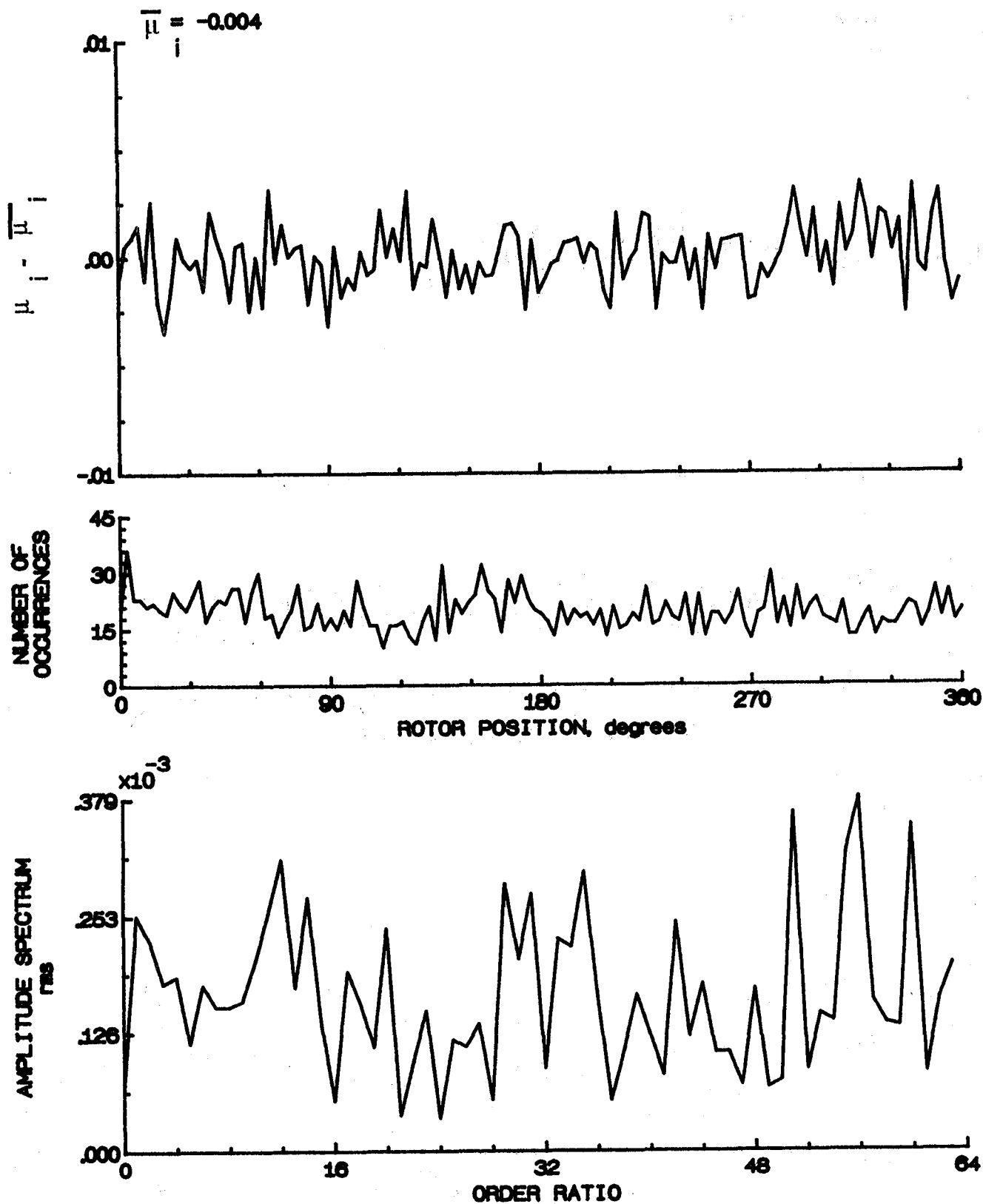


Figure 81- Induced inflow velocity measured at 120 degrees and  $r/R$  of 0.86.

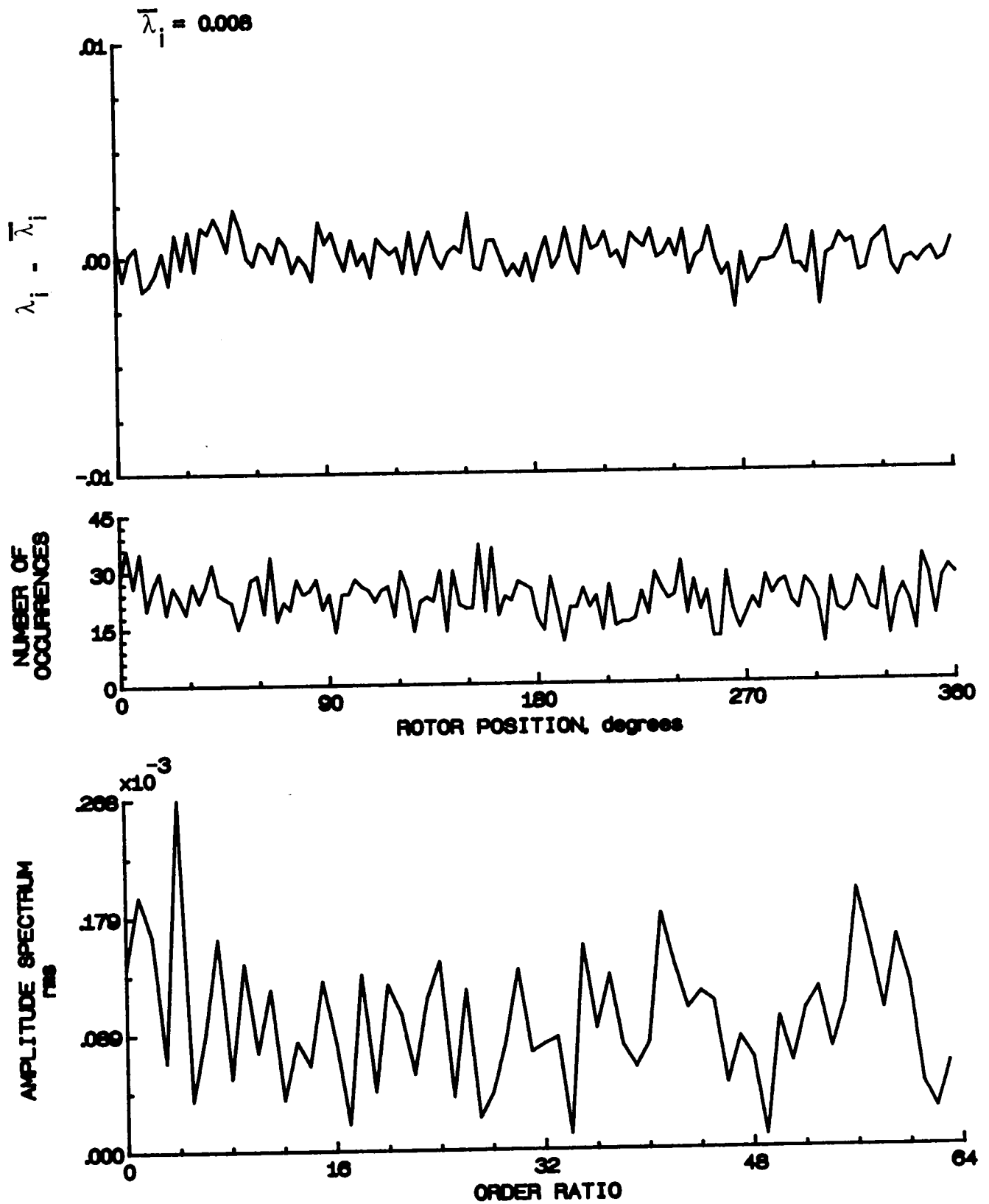


Figure 81- Concluded.

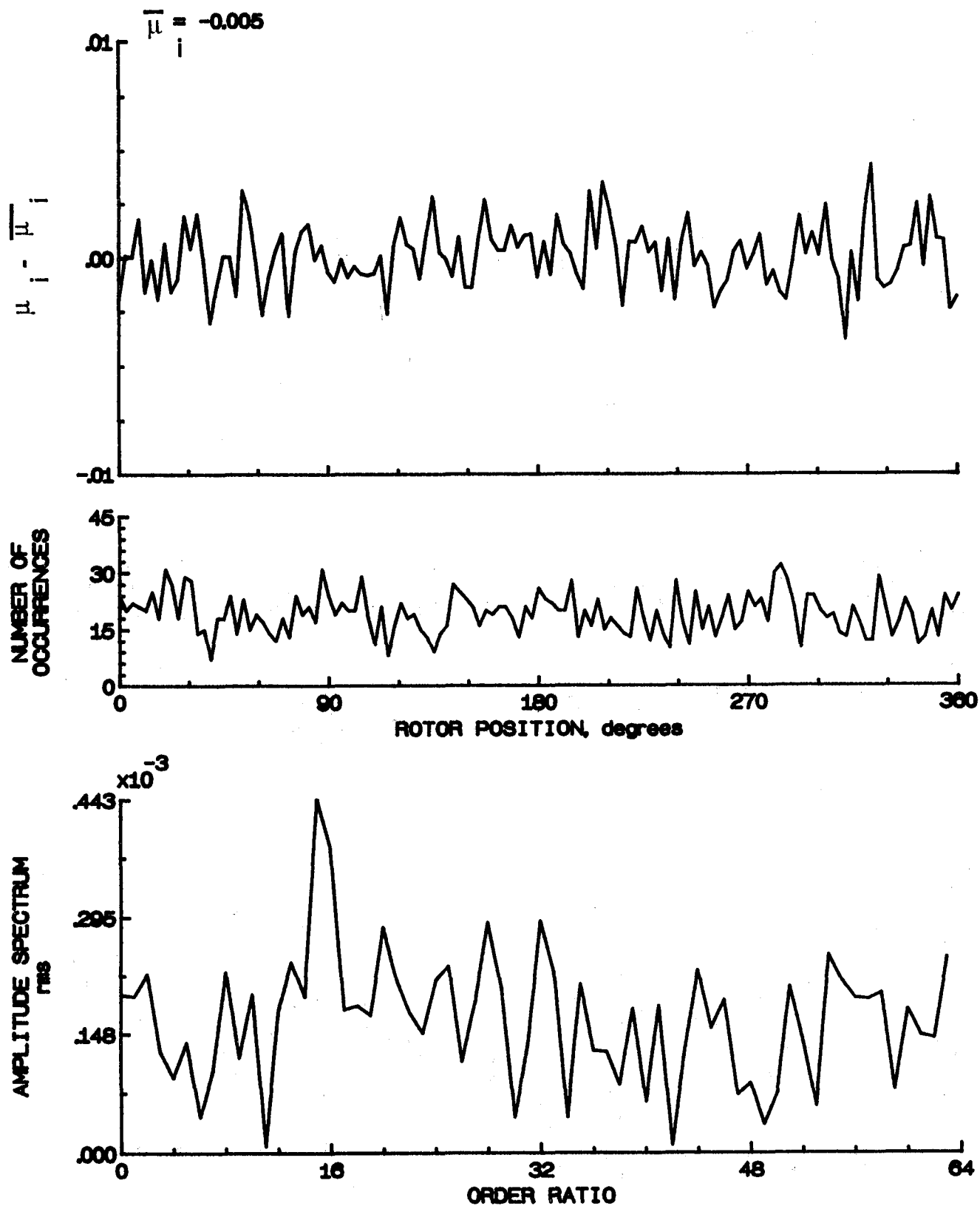


Figure 82.- Induced inflow velocity measured at 120 degrees and  $r/R$  of 0.90.

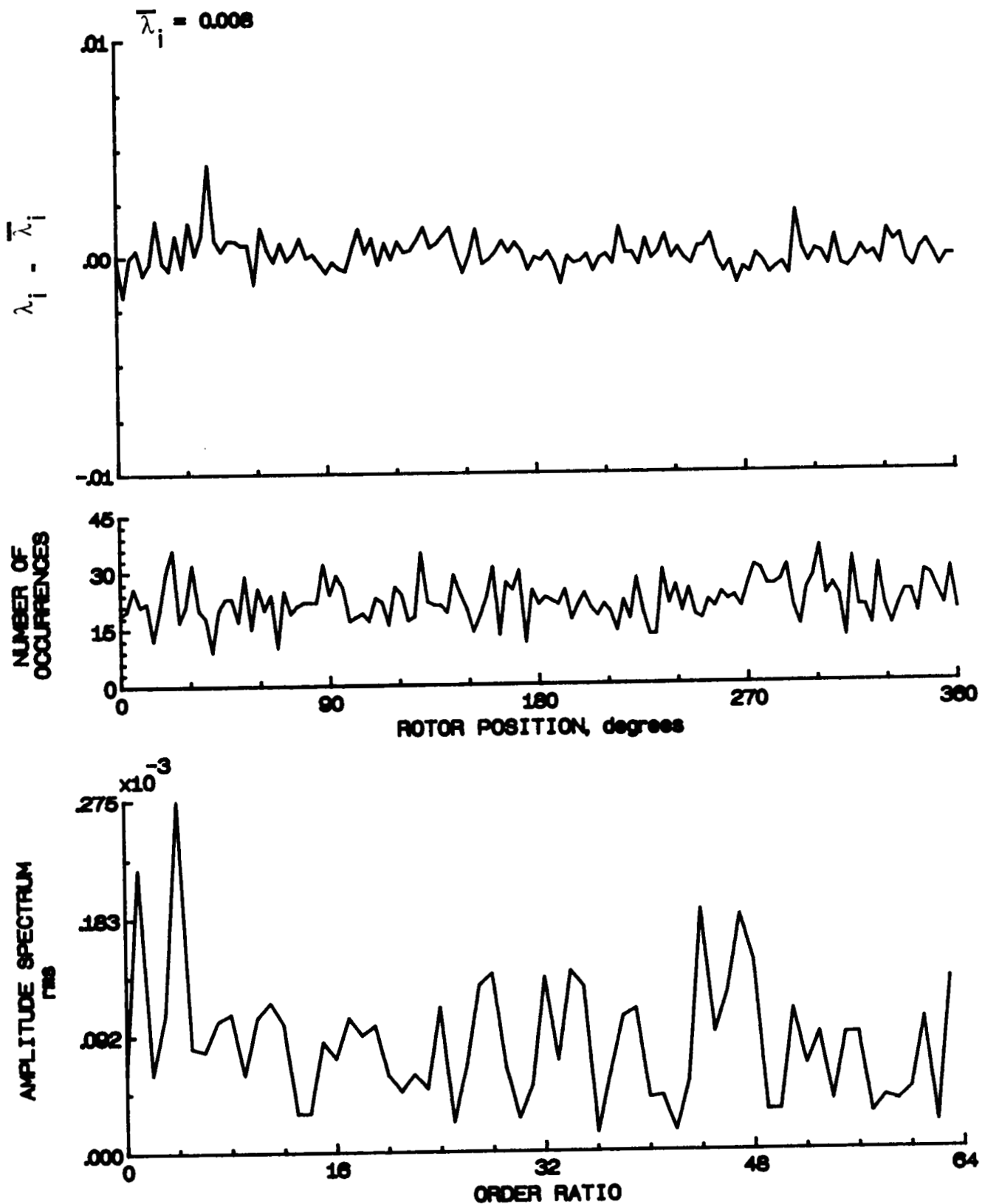


Figure 82.- Concluded.

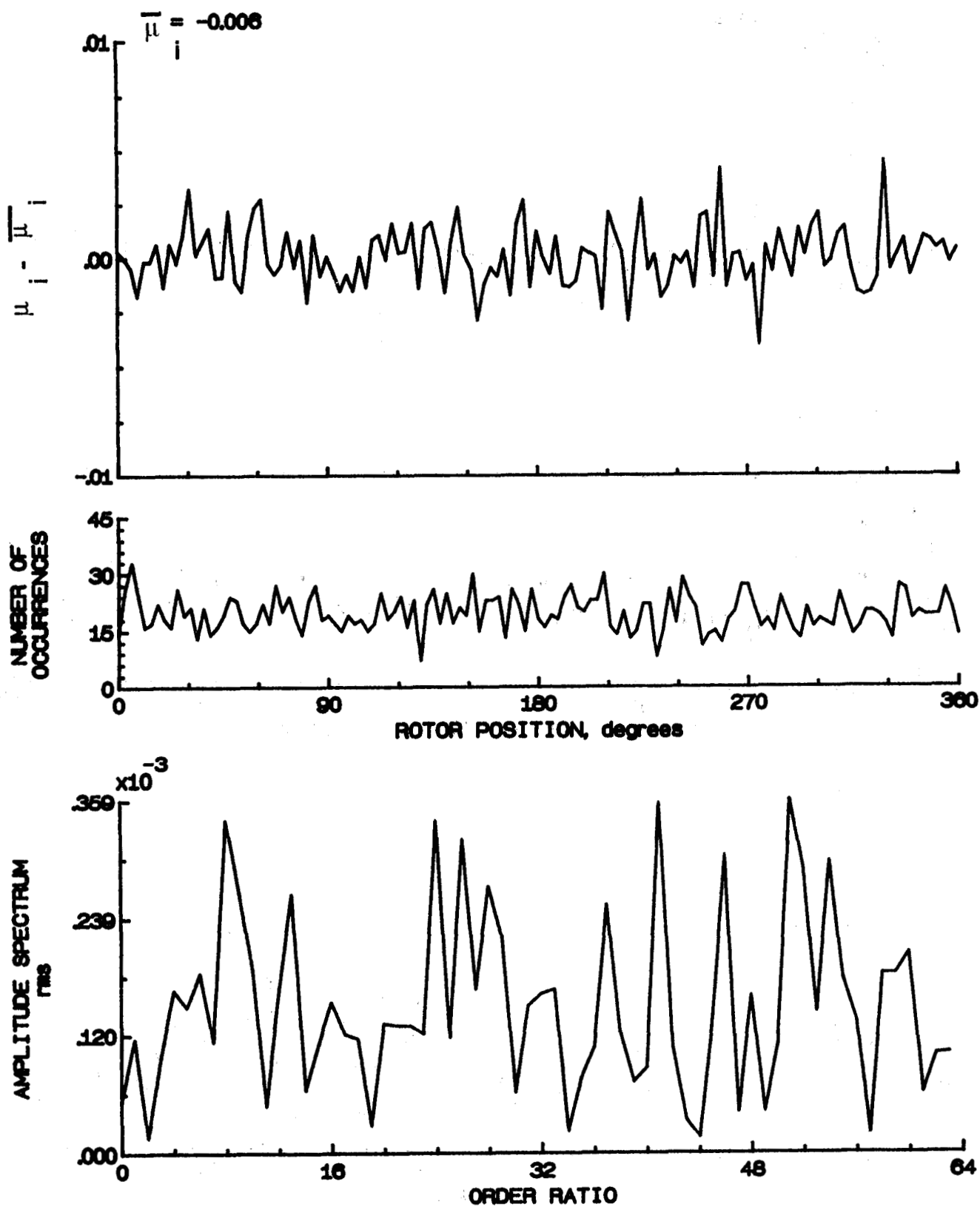


Figure 83.- Induced inflow velocity measured at 120 degrees and r/R of 0.94.

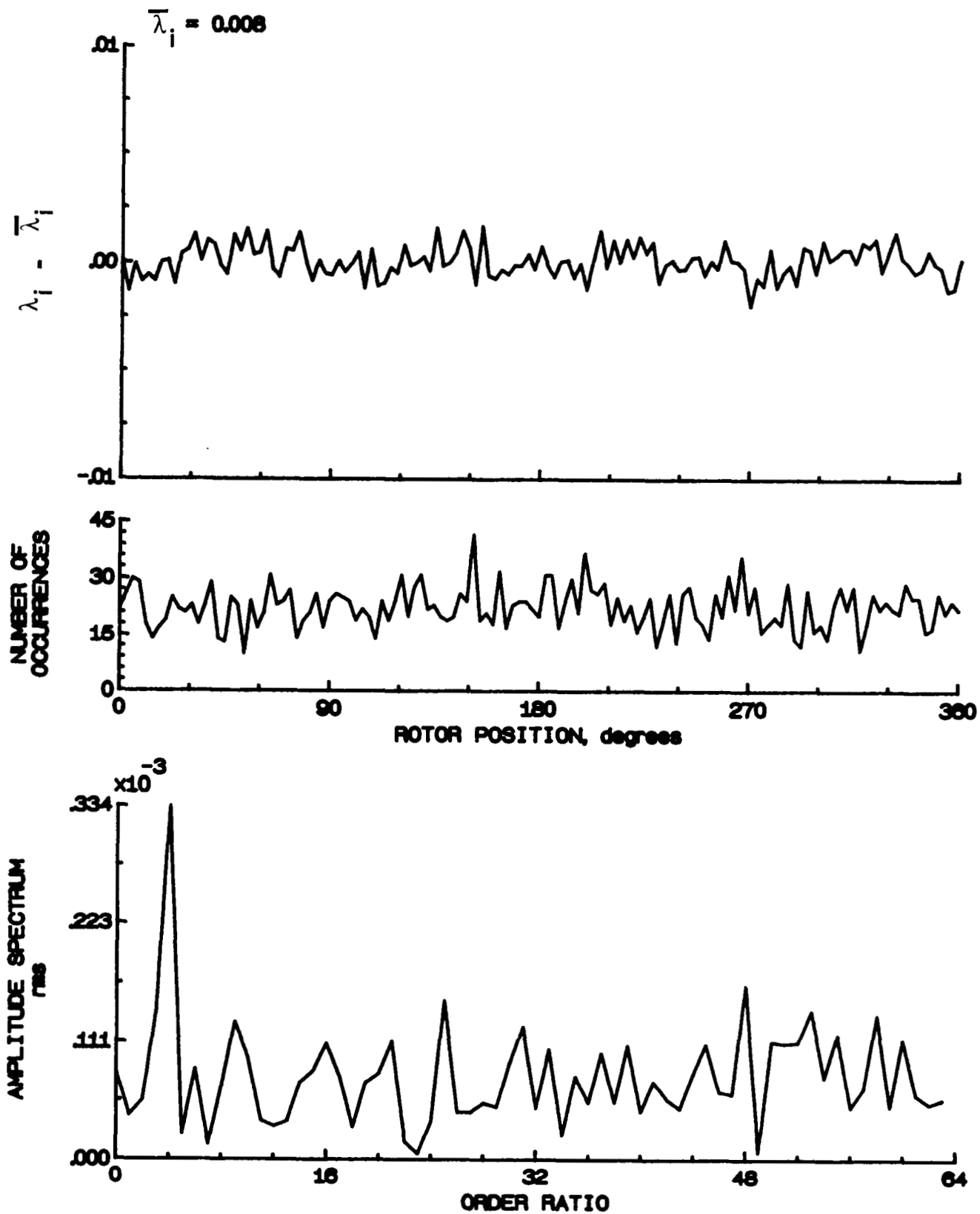


Figure 83.- Concluded.

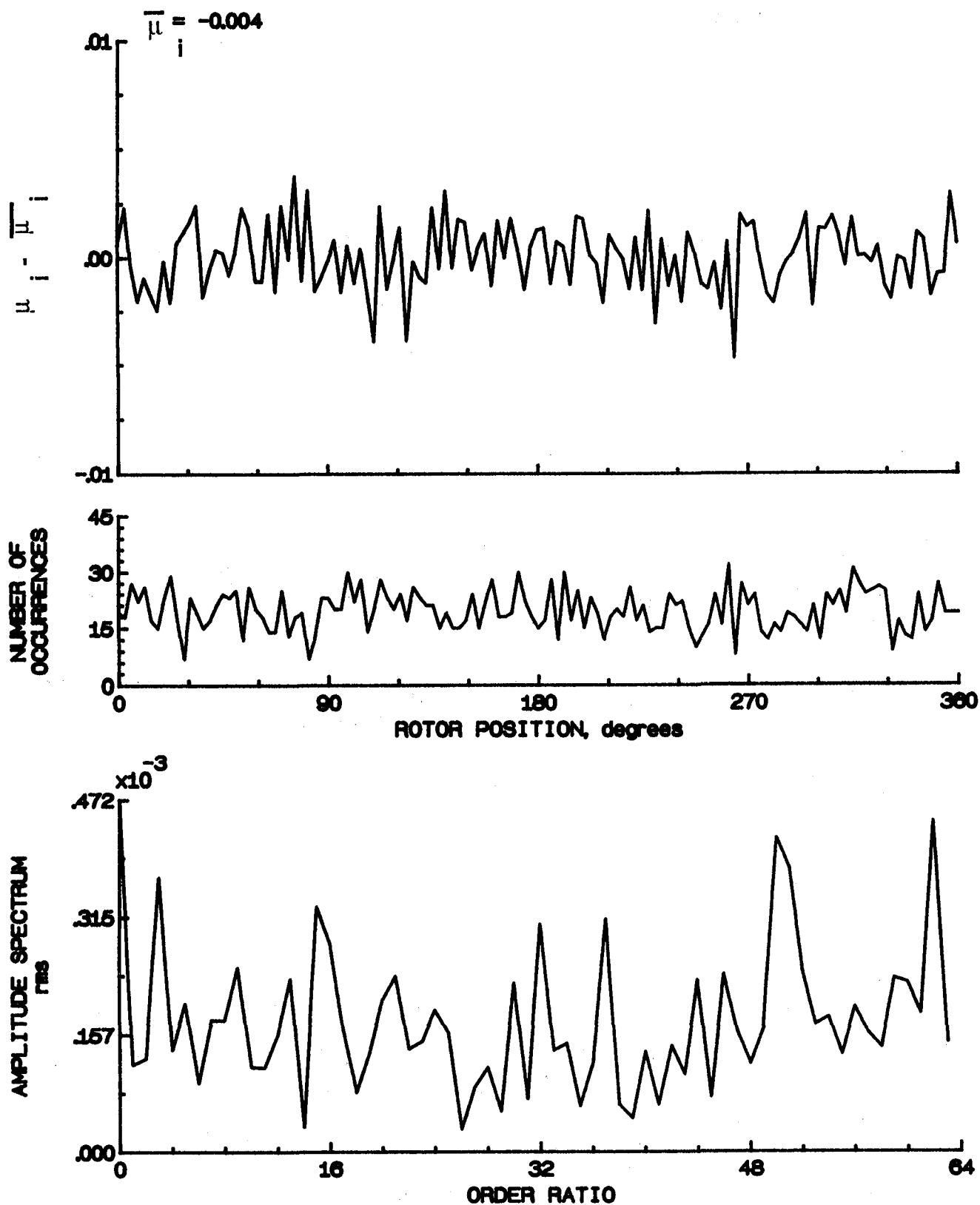


Figure 84.- Induced inflow velocity measured at 120 degrees and r/R of 0.98.



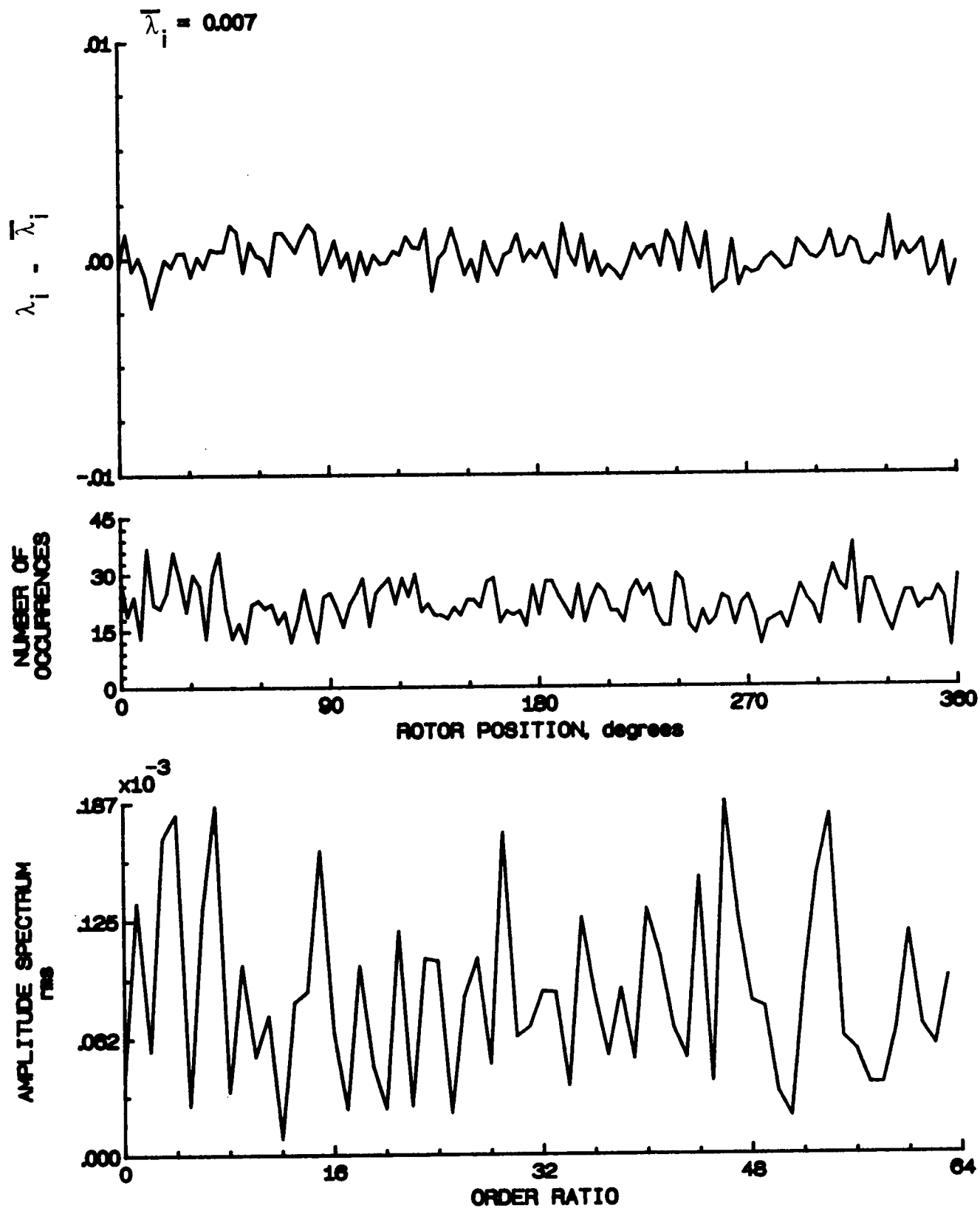


Figure 84.- Concluded.

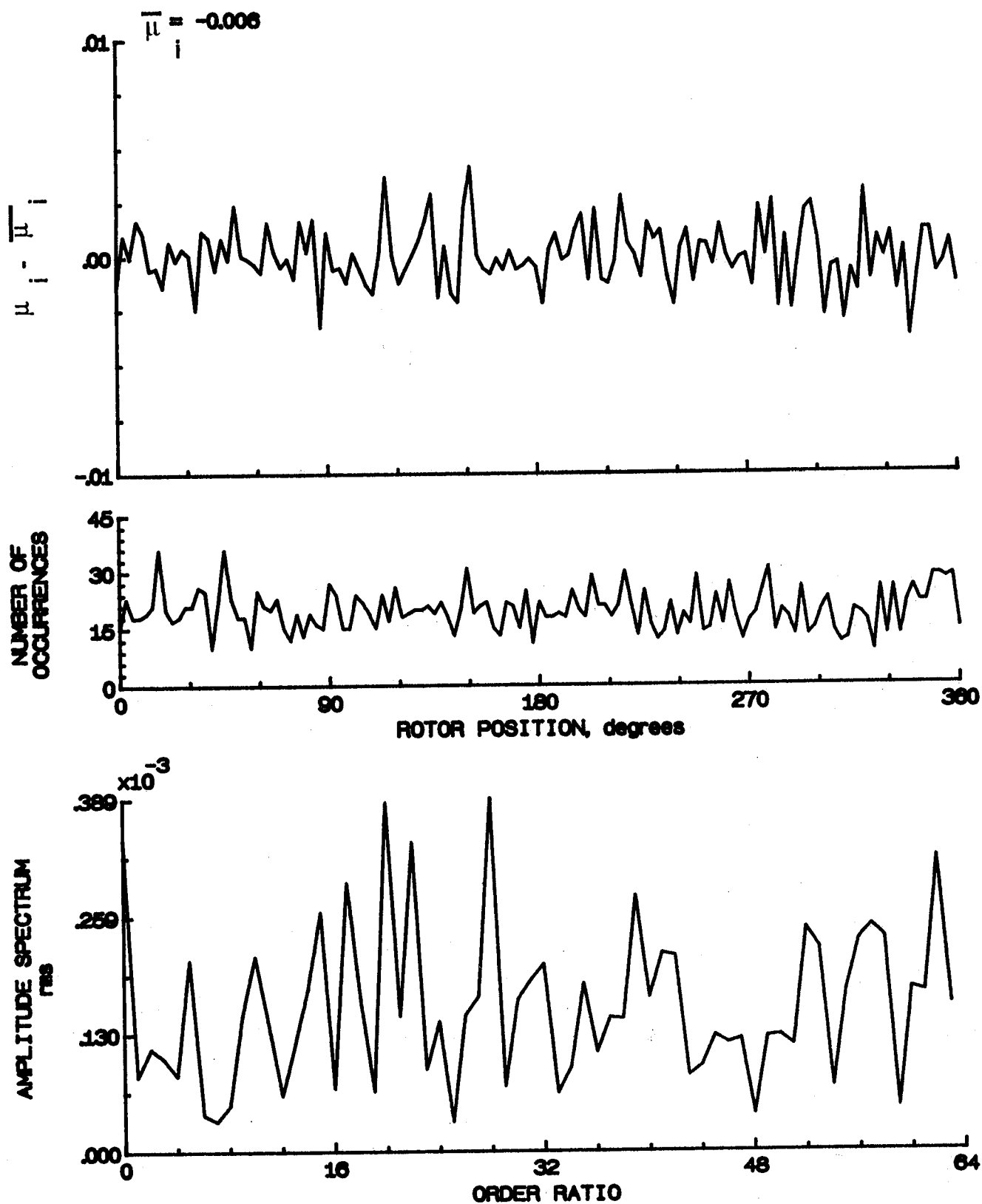


Figure 85.- Induced inflow velocity measured at 120 degrees and r/R of 1.02.

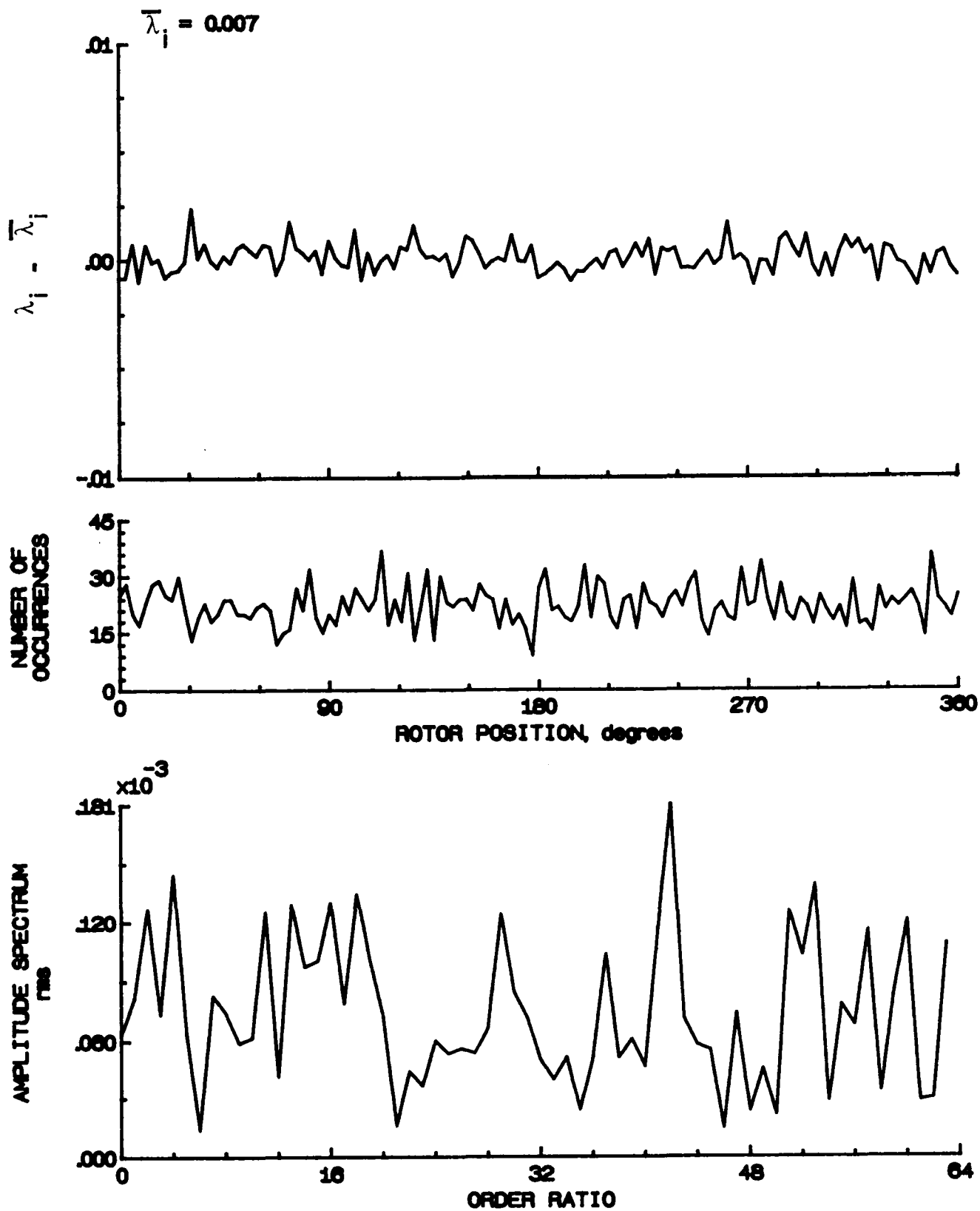


Figure 85.- Concluded.

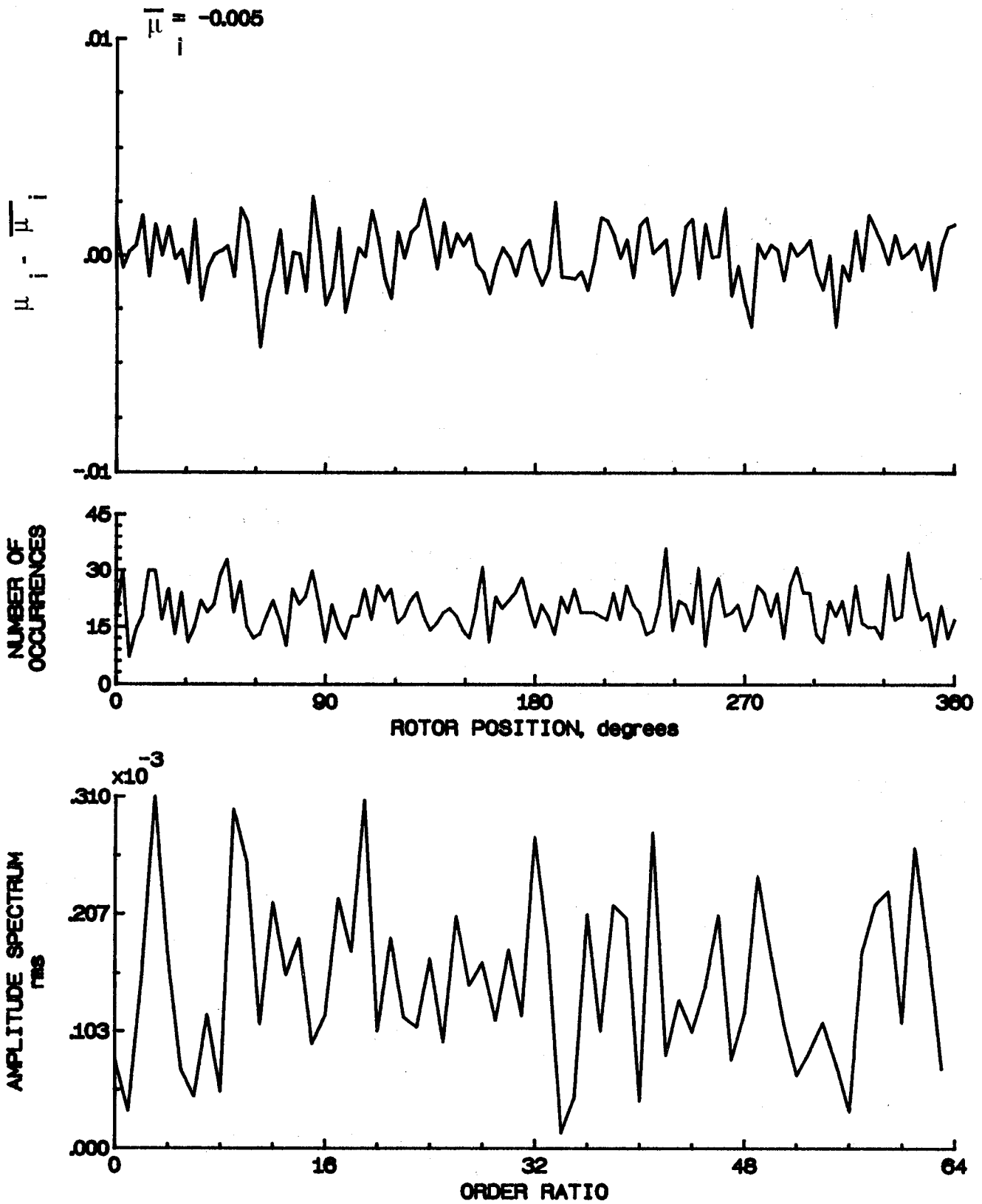


Figure 86.- Induced inflow velocity measured at 120 degrees and  $r/R$  of 1.04.

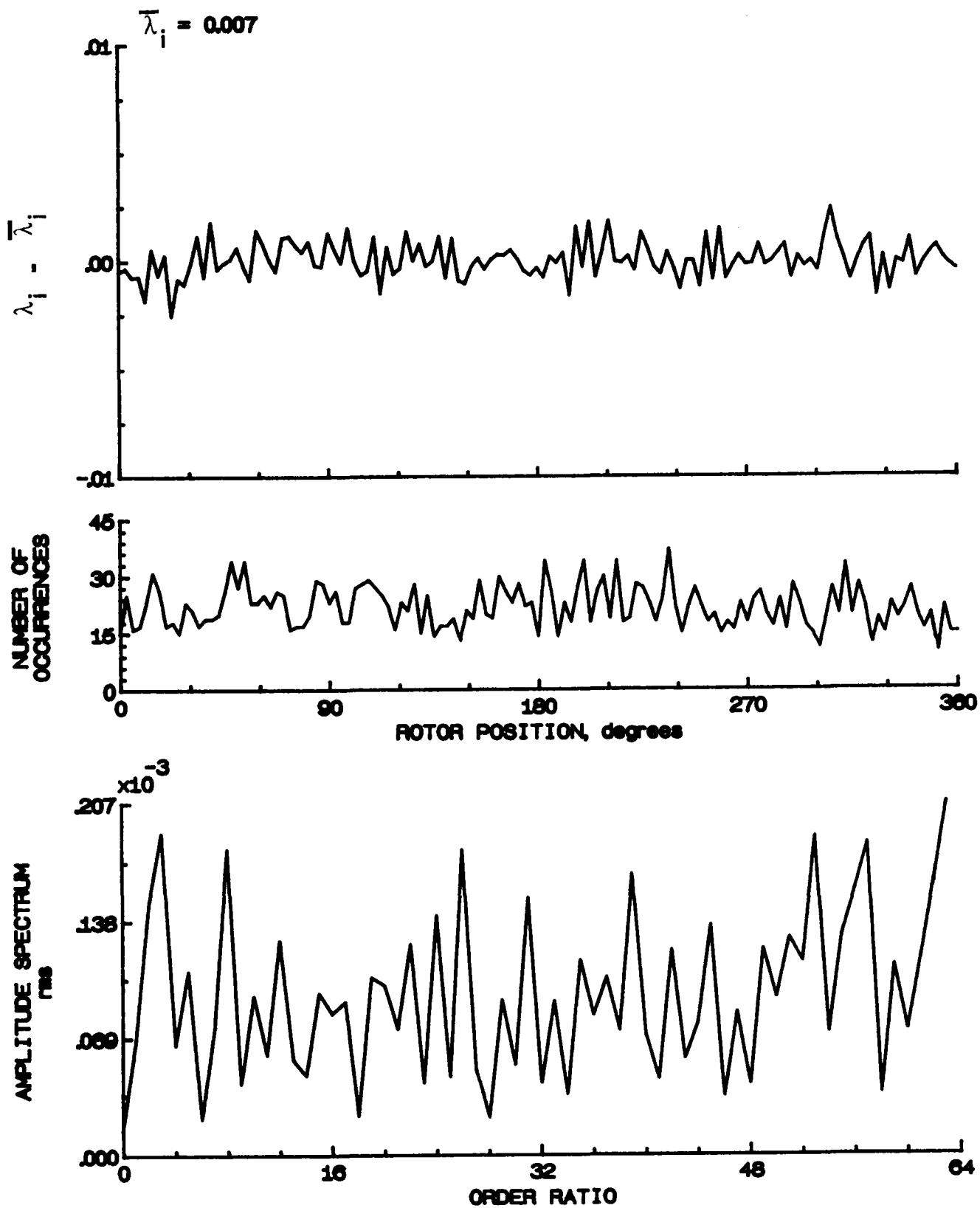


Figure 86.- Concluded.

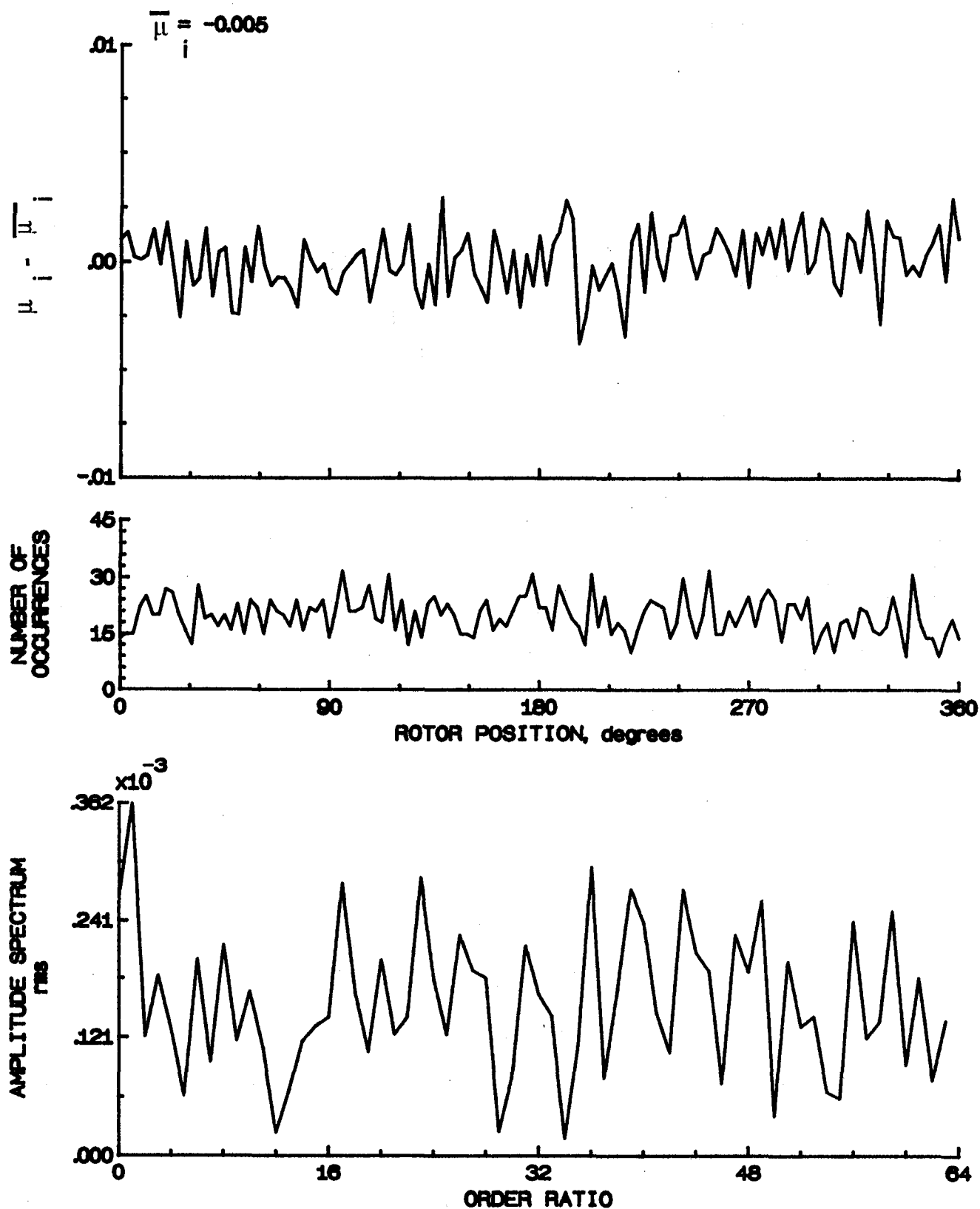


Figure 87.- Induced inflow velocity measured at 120 degrees and r/R of 1.10.

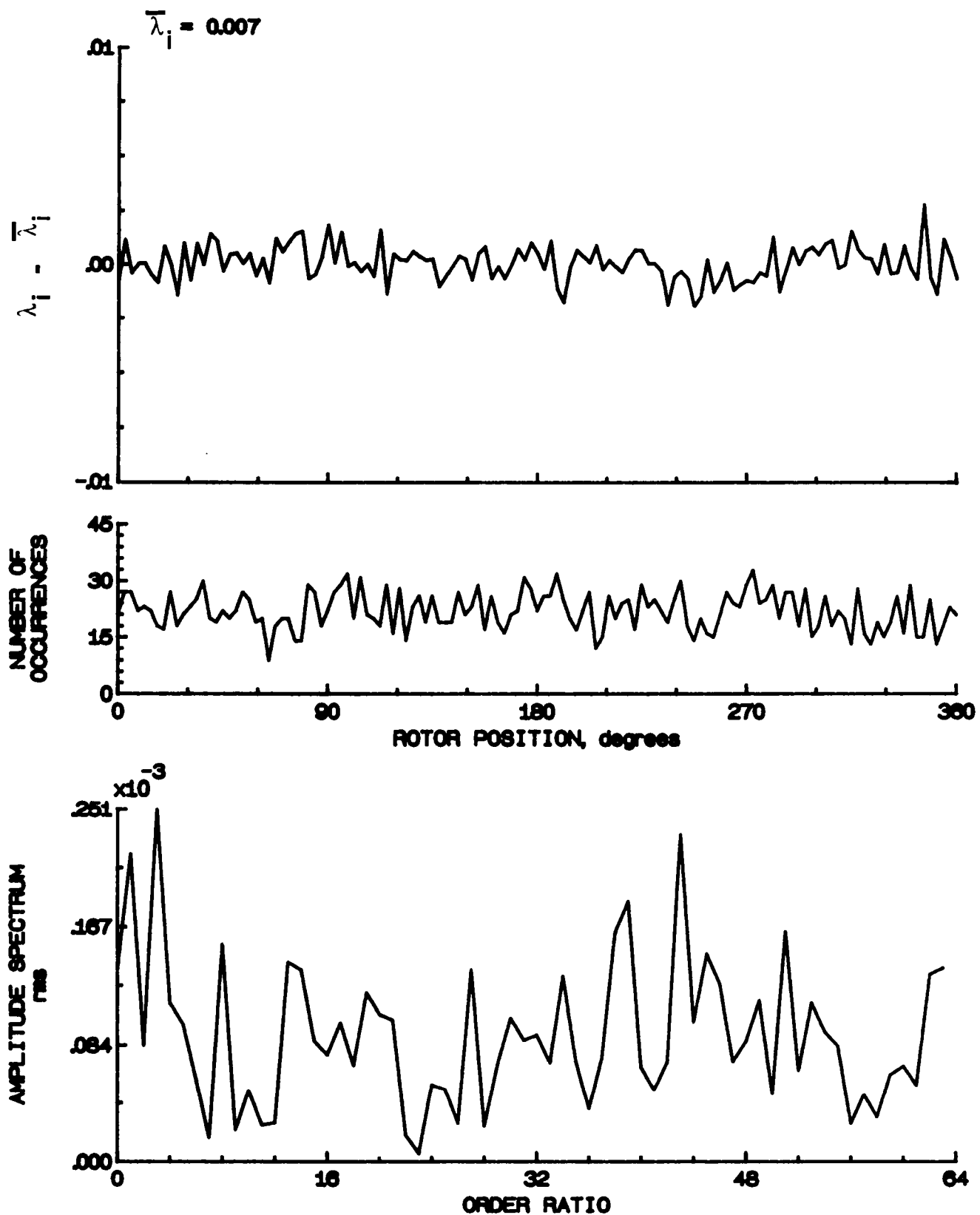


Figure 87.- Concluded.

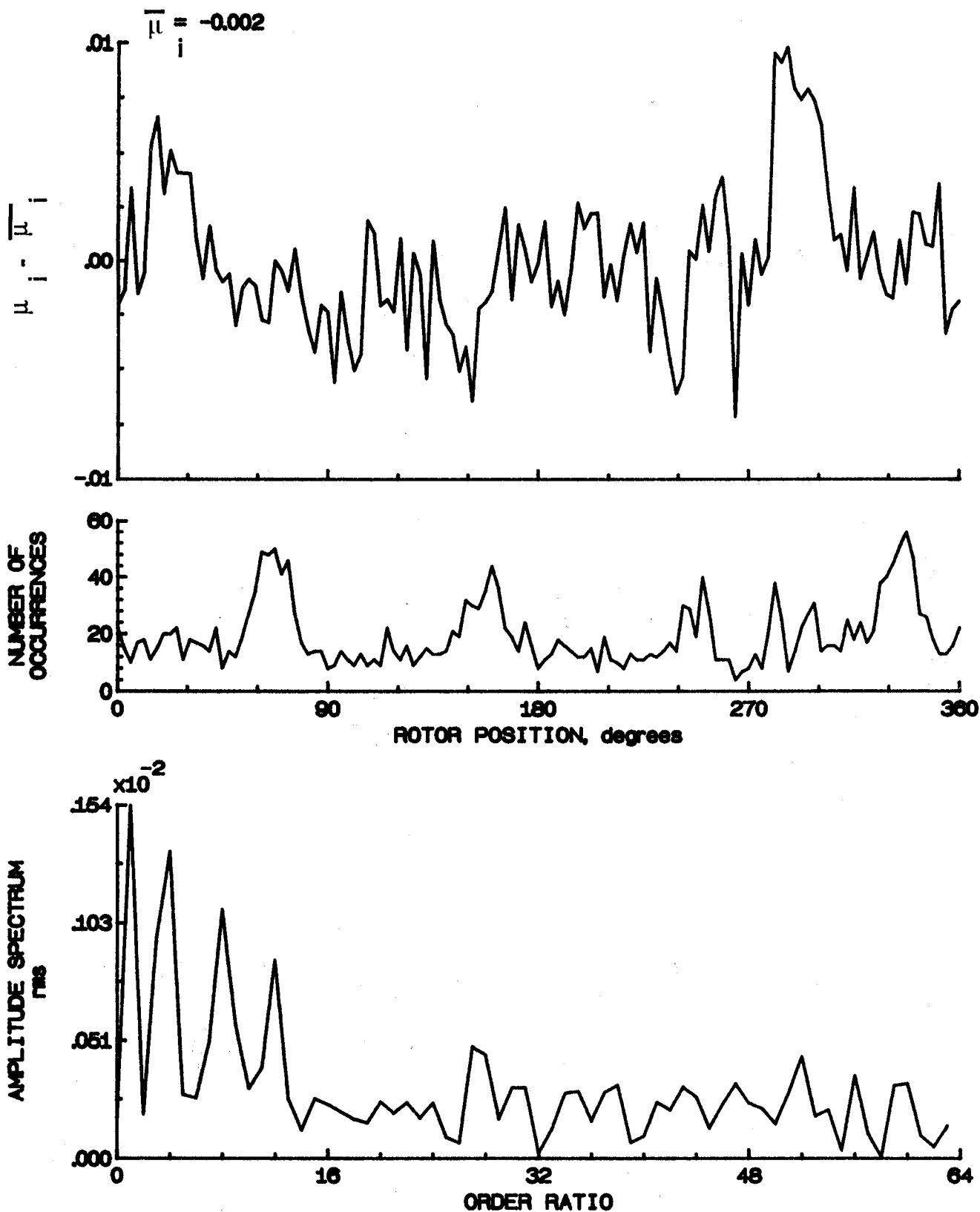


Figure 88.- Induced inflow velocity measured at 150 degrees and r/R of 0.20.



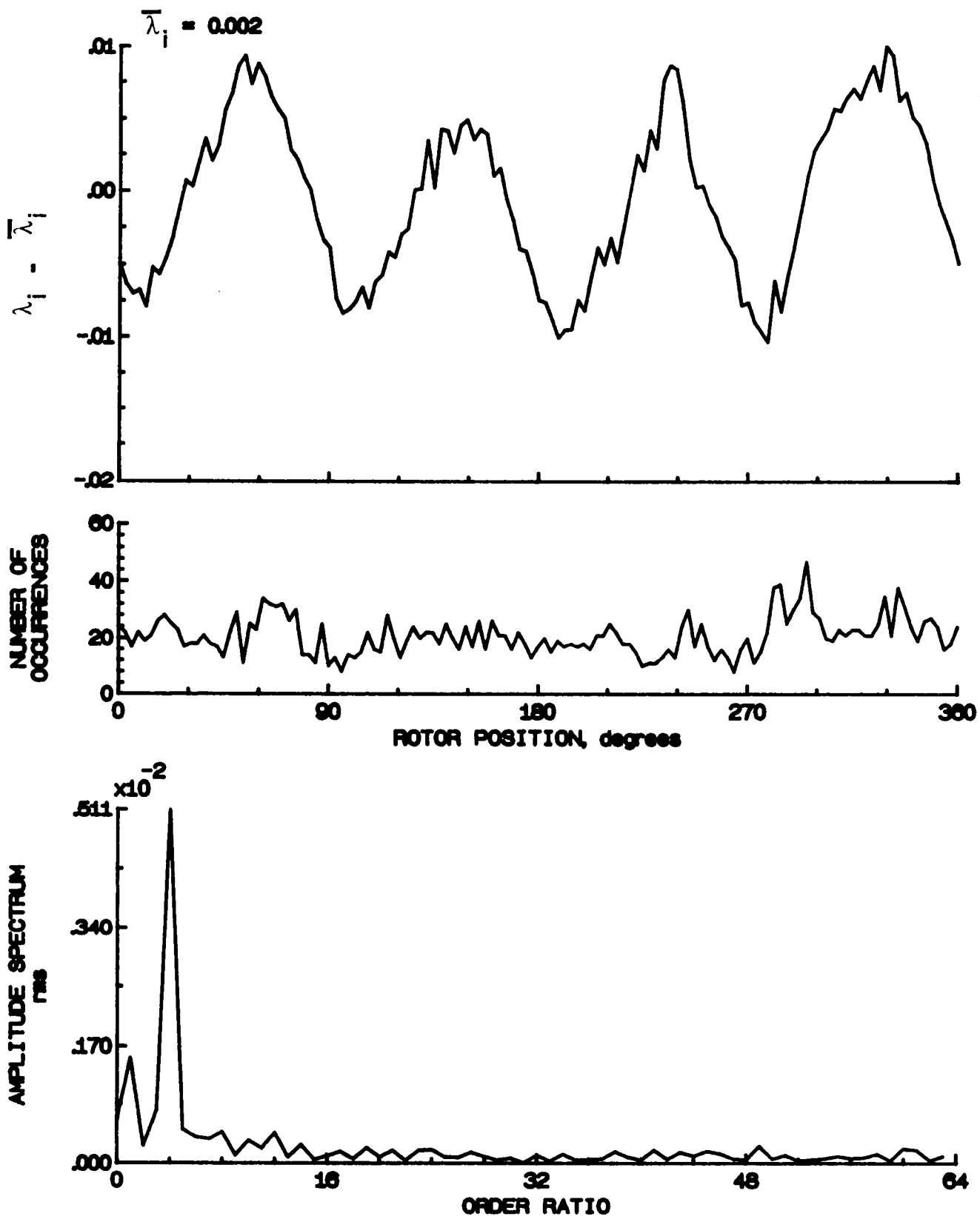


Figure 88.- Concluded.

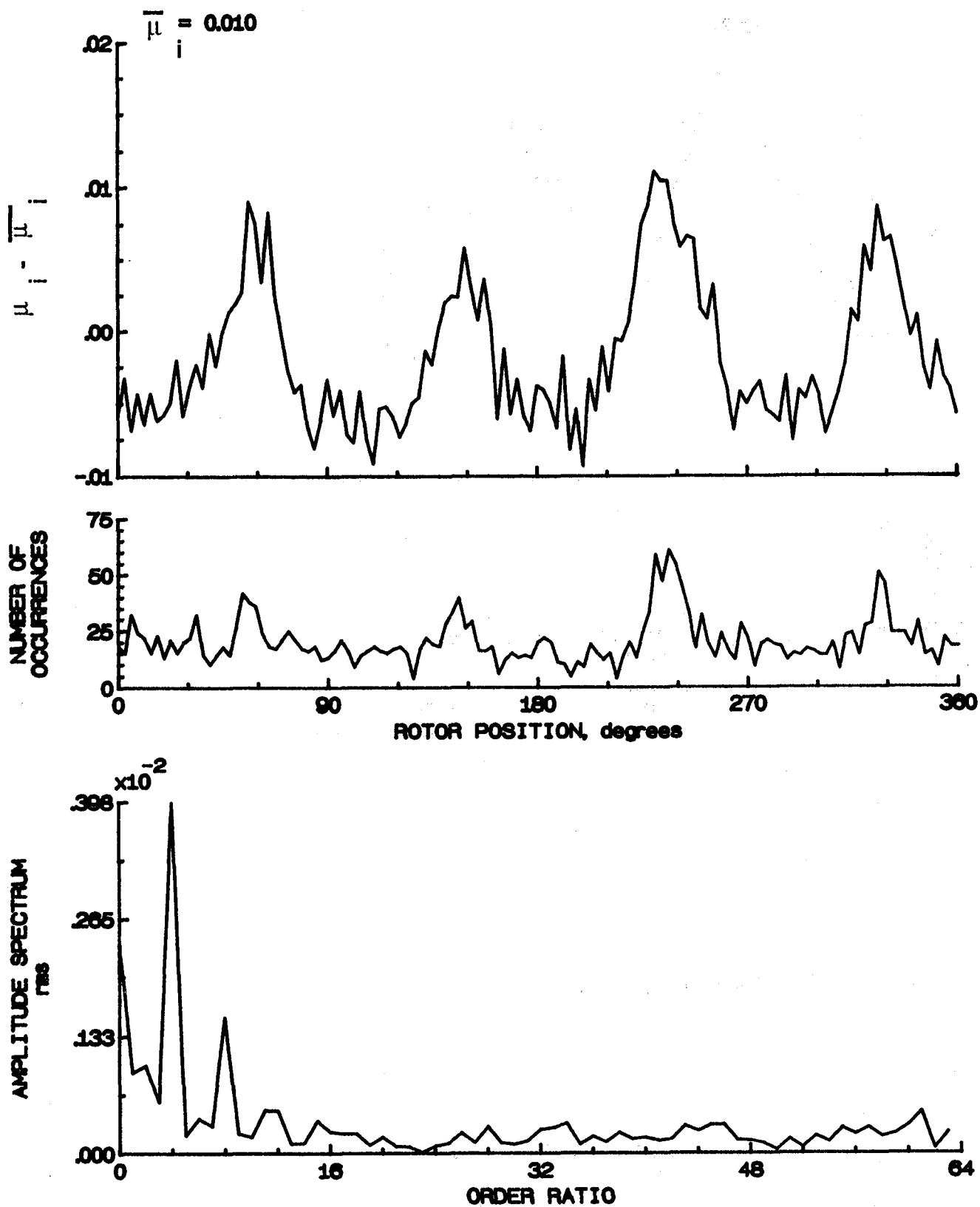


Figure 89.- Induced inflow velocity measured at 150 degrees and r/R of 0.40.

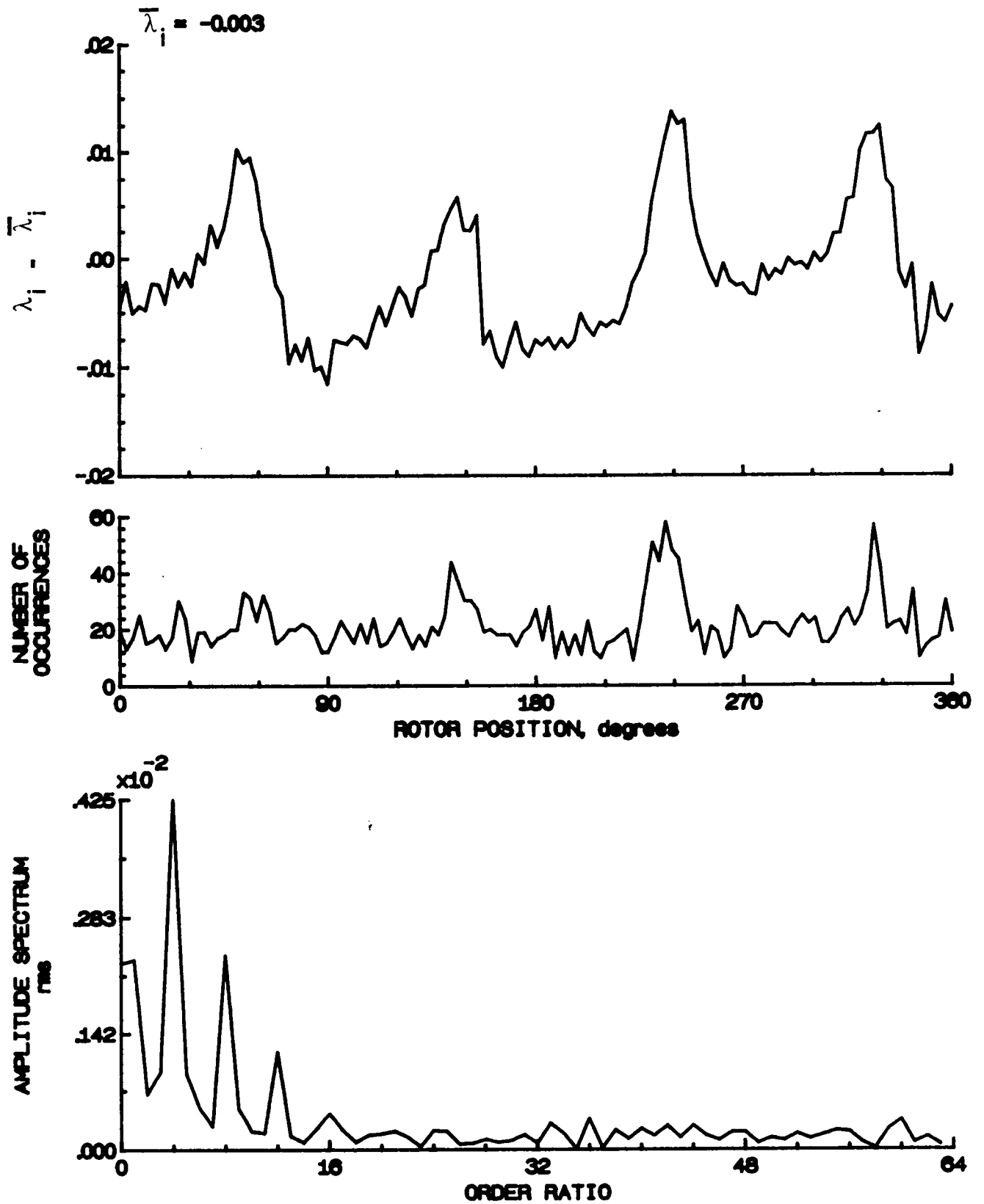


Figure 89.- Concluded.

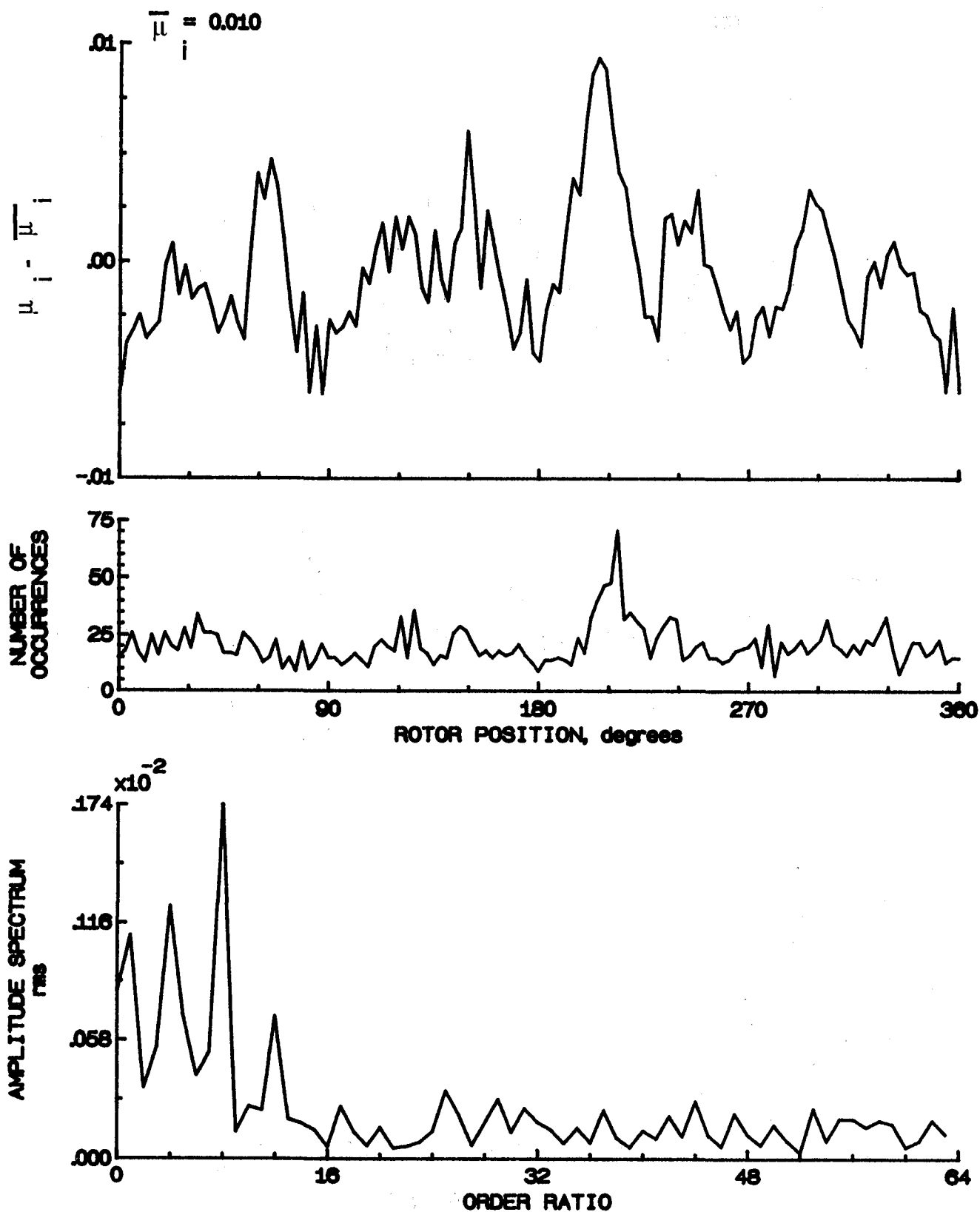


Figure 90.- Induced inflow velocity measured at 150 degrees and r/R of 0.50.

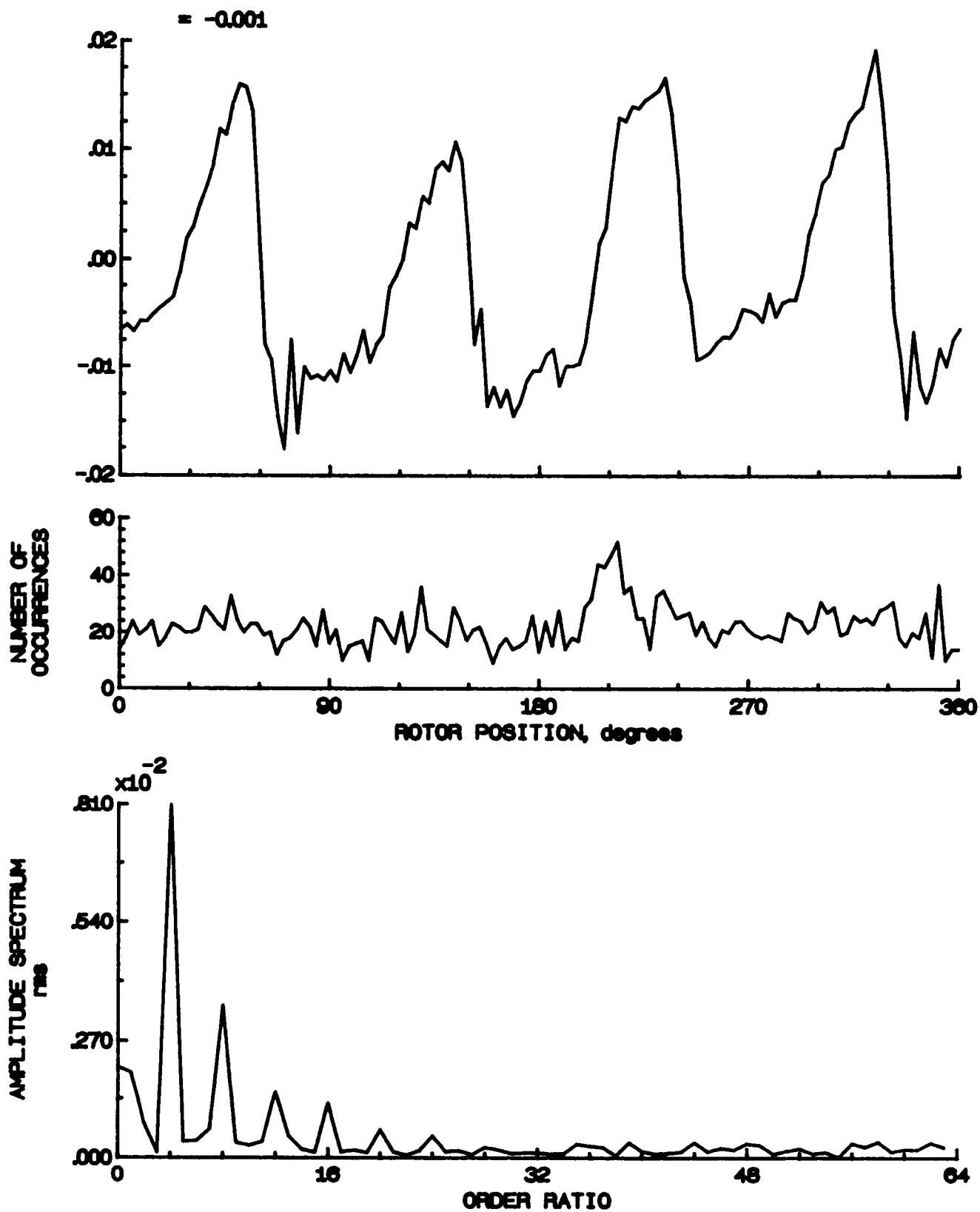


Figure 90.- Concluded.

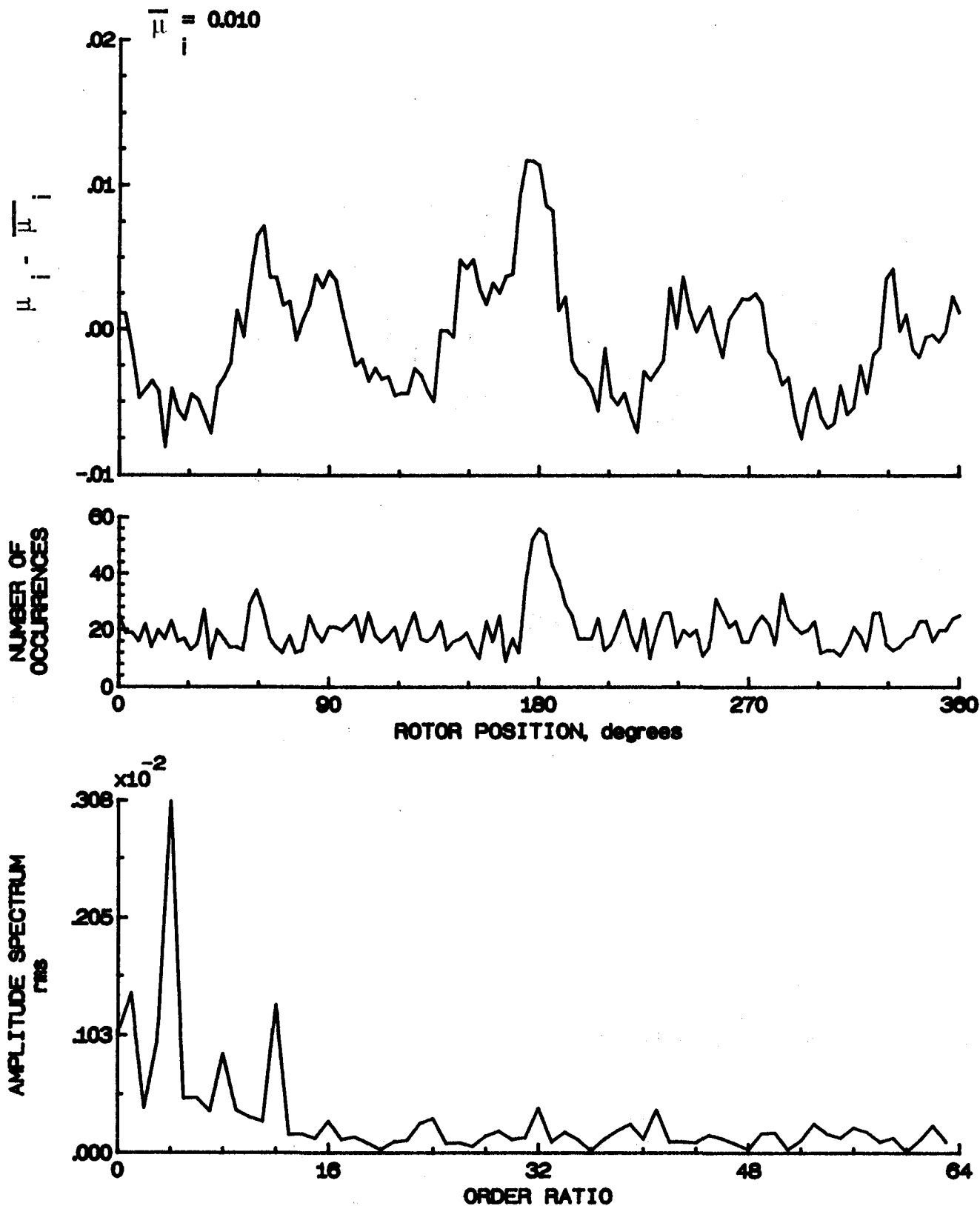


Figure 9L- Induced inflow velocity measured at 150 degrees and r/R of 0.60.

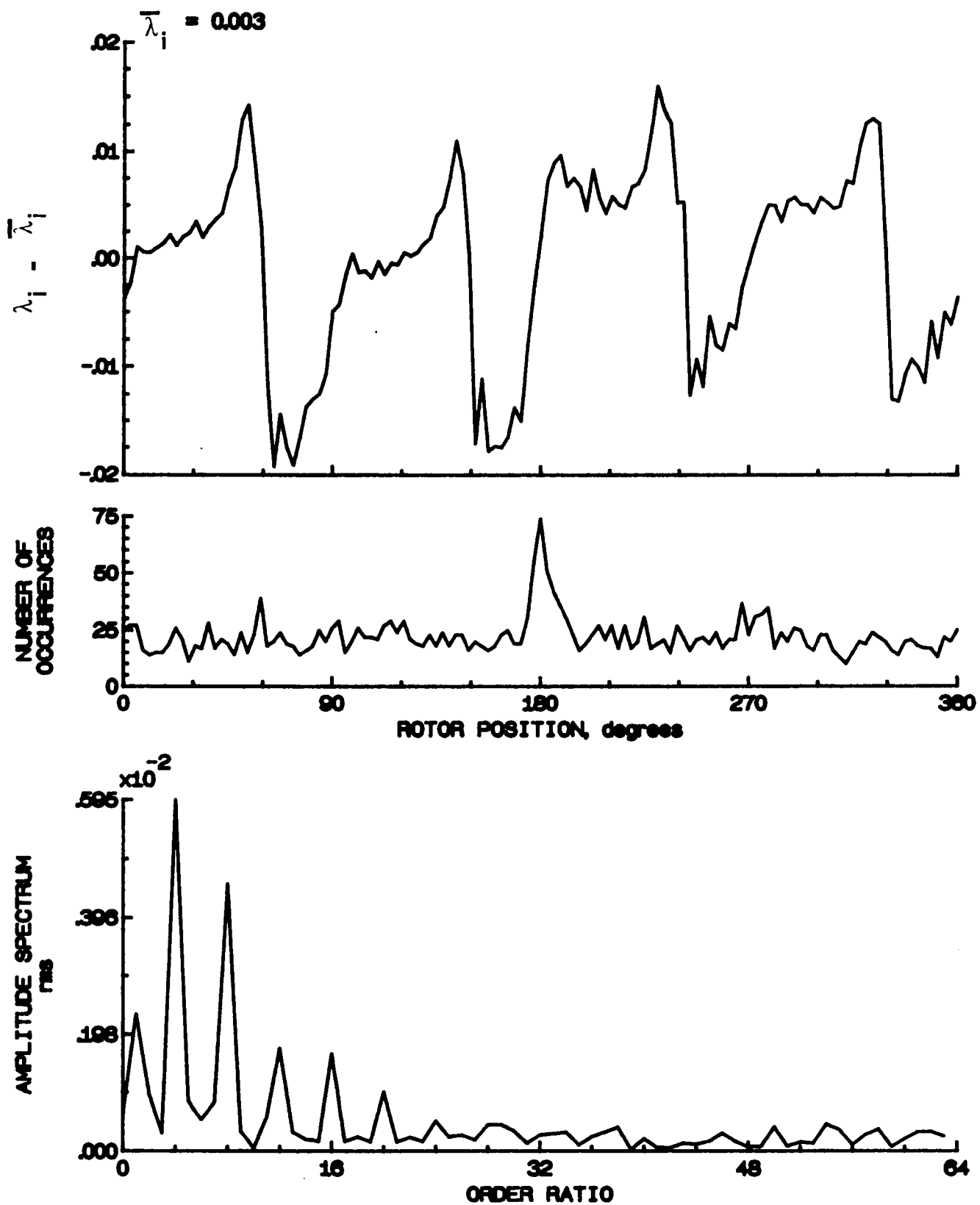


Figure 91.- Concluded.

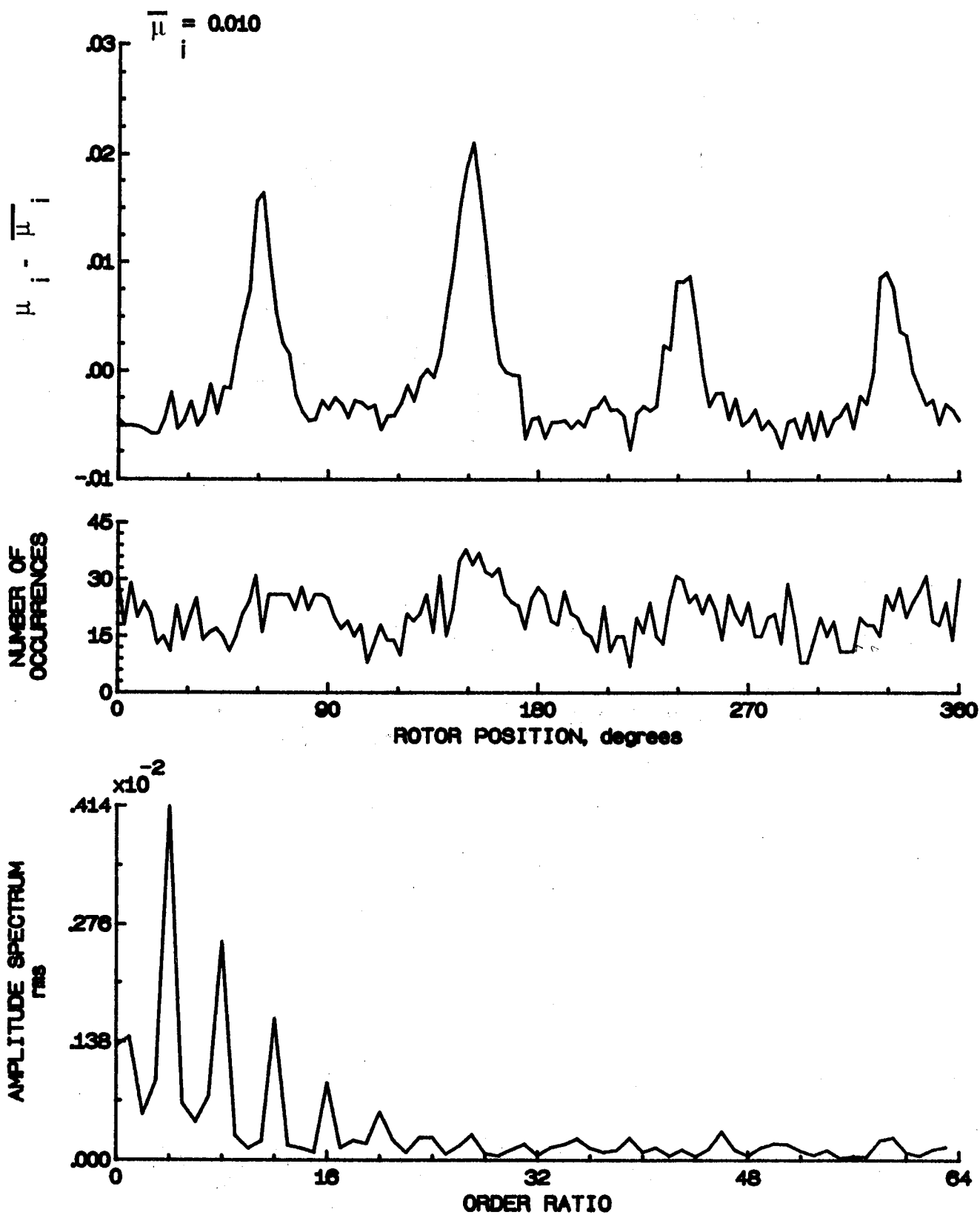


Figure 92.- Induced inflow velocity measured at 150 degrees and r/R of 0.70.



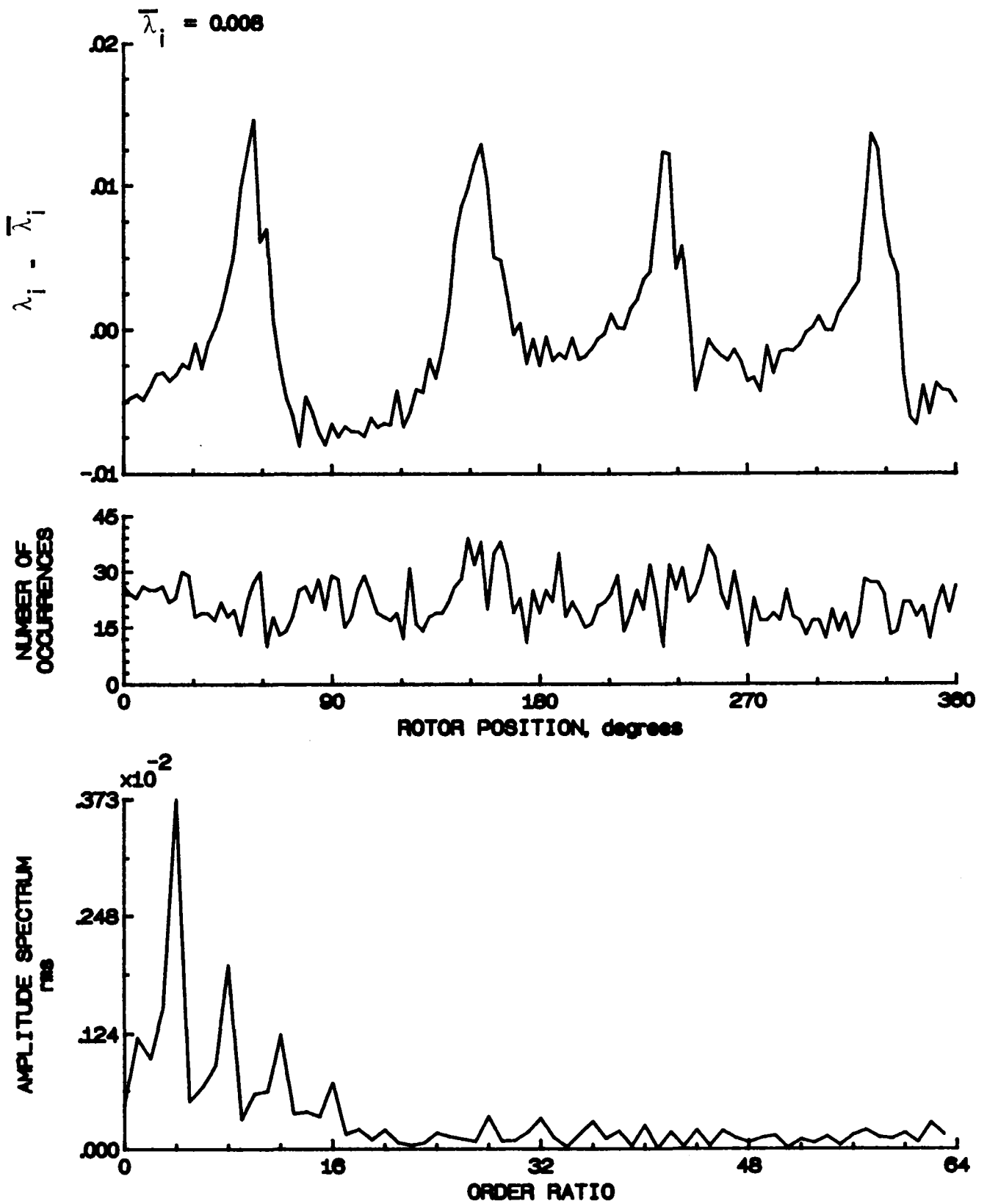


Figure 92.- Concluded.

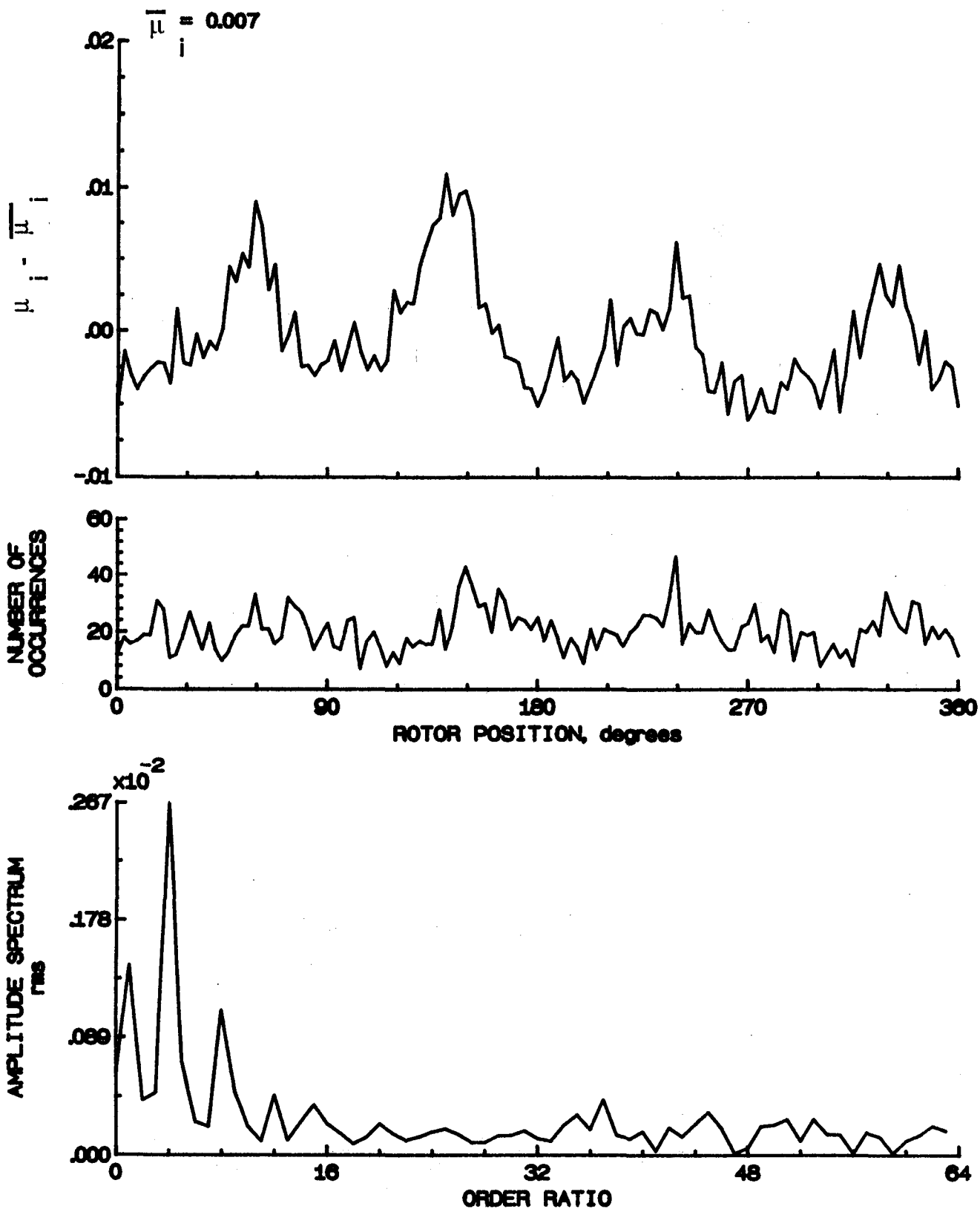


Figure 93.- Induced inflow velocity measured at 150 degrees and r/R of 0.74.

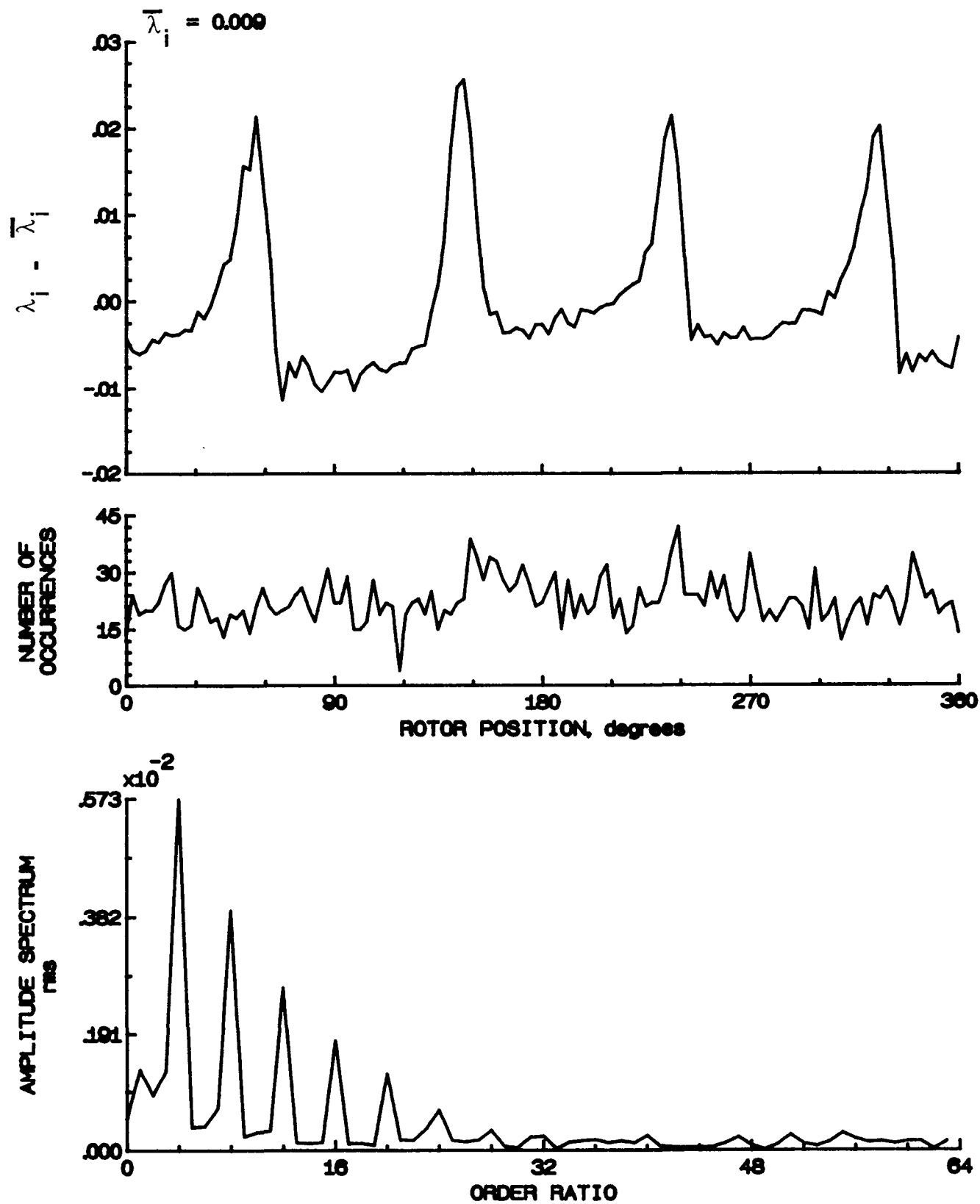


Figure 93.- Concluded.

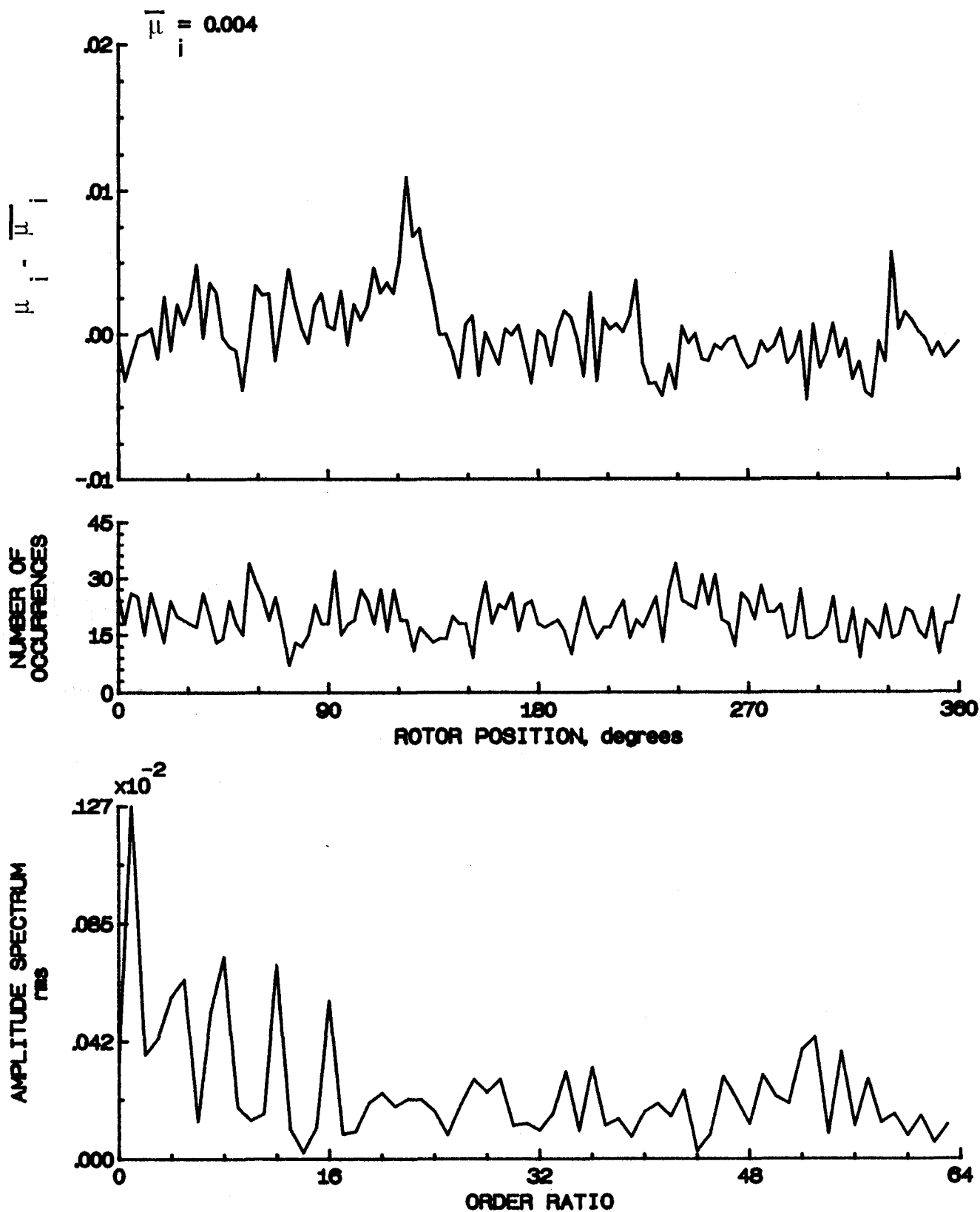


Figure 94.- Induced inflow velocity measured at 150 degrees and r/R of 0.78.

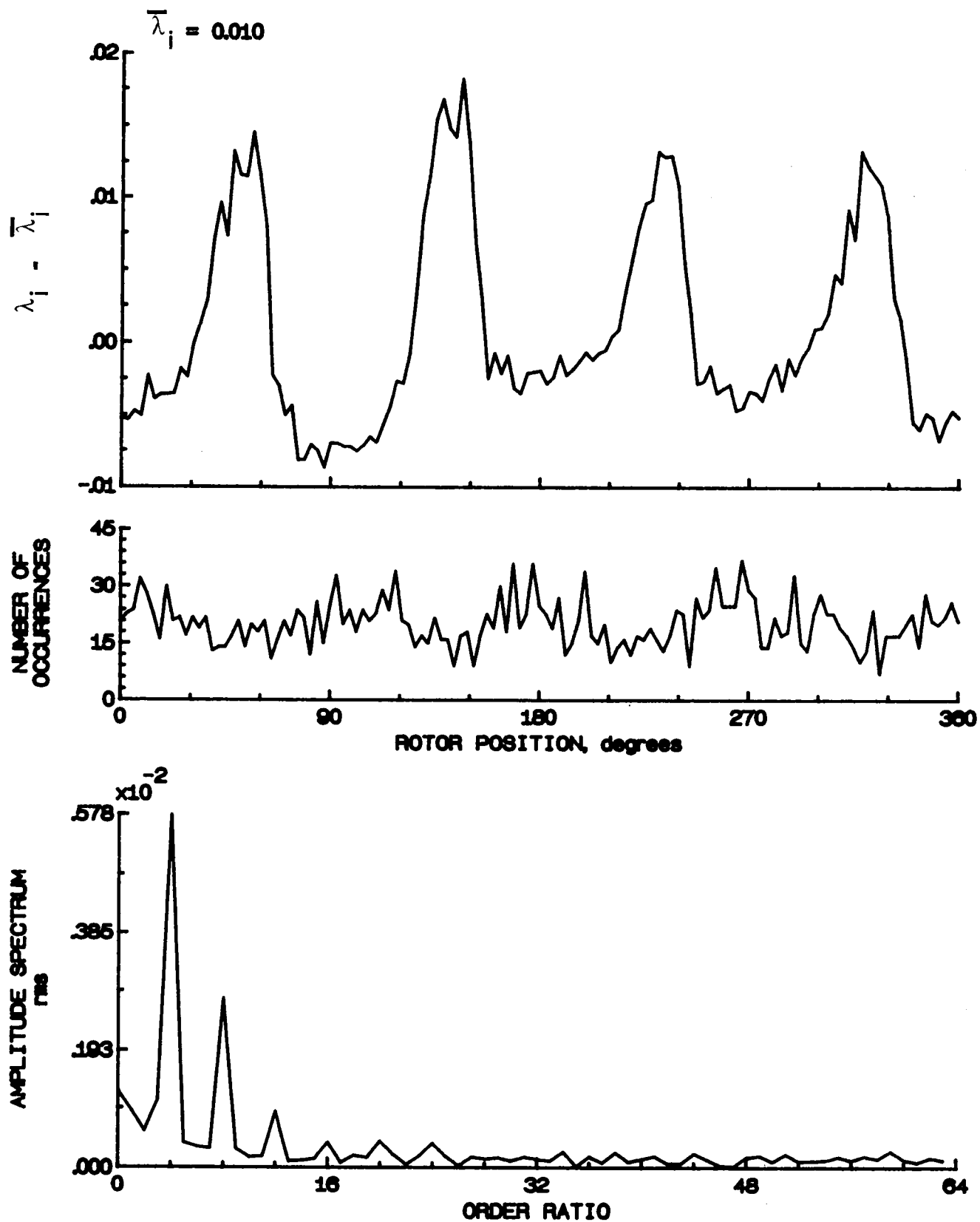


Figure 94.- Concluded.

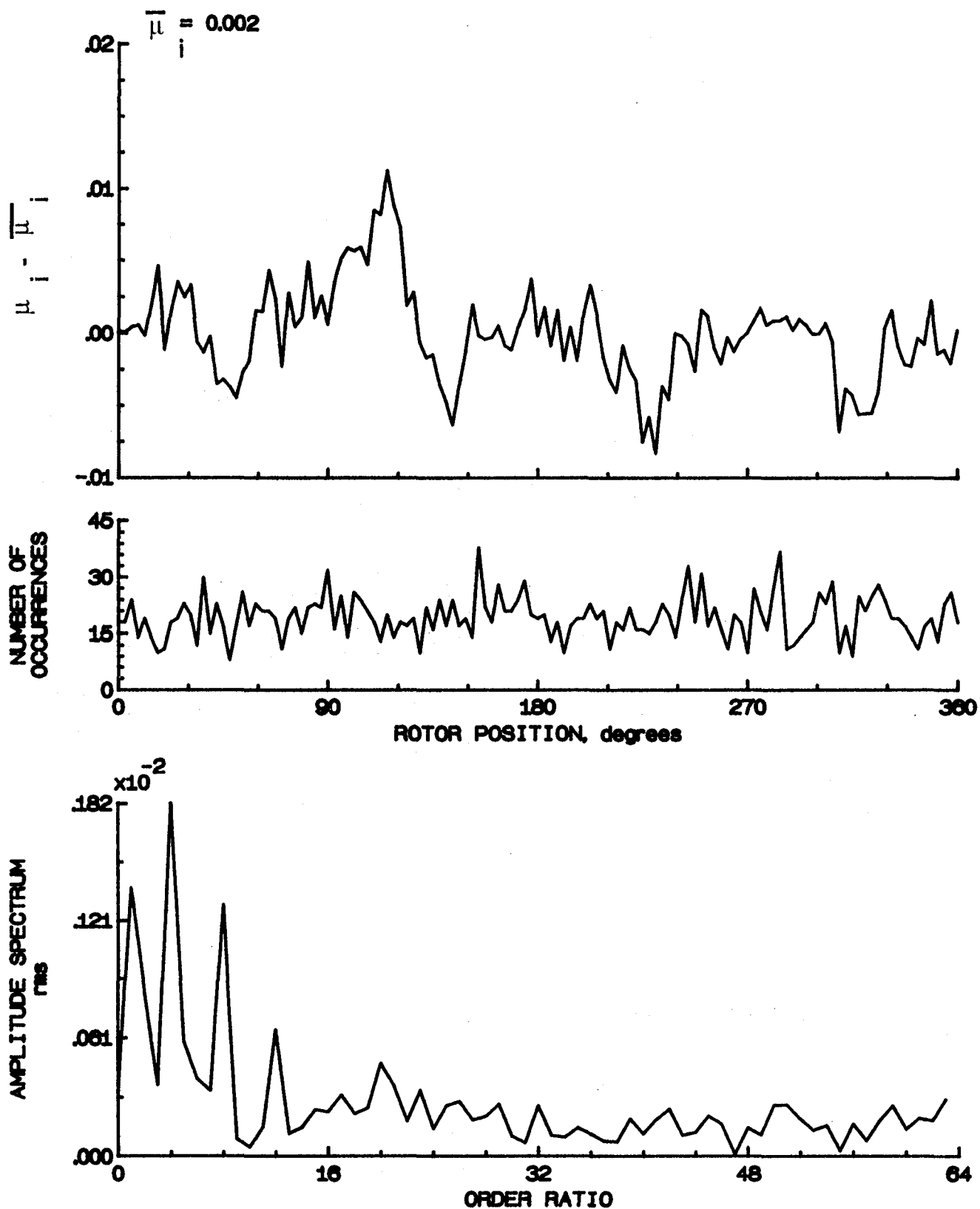


Figure 95.- Induced inflow velocity measured at 150 degrees and  $r/R$  of 0.82.

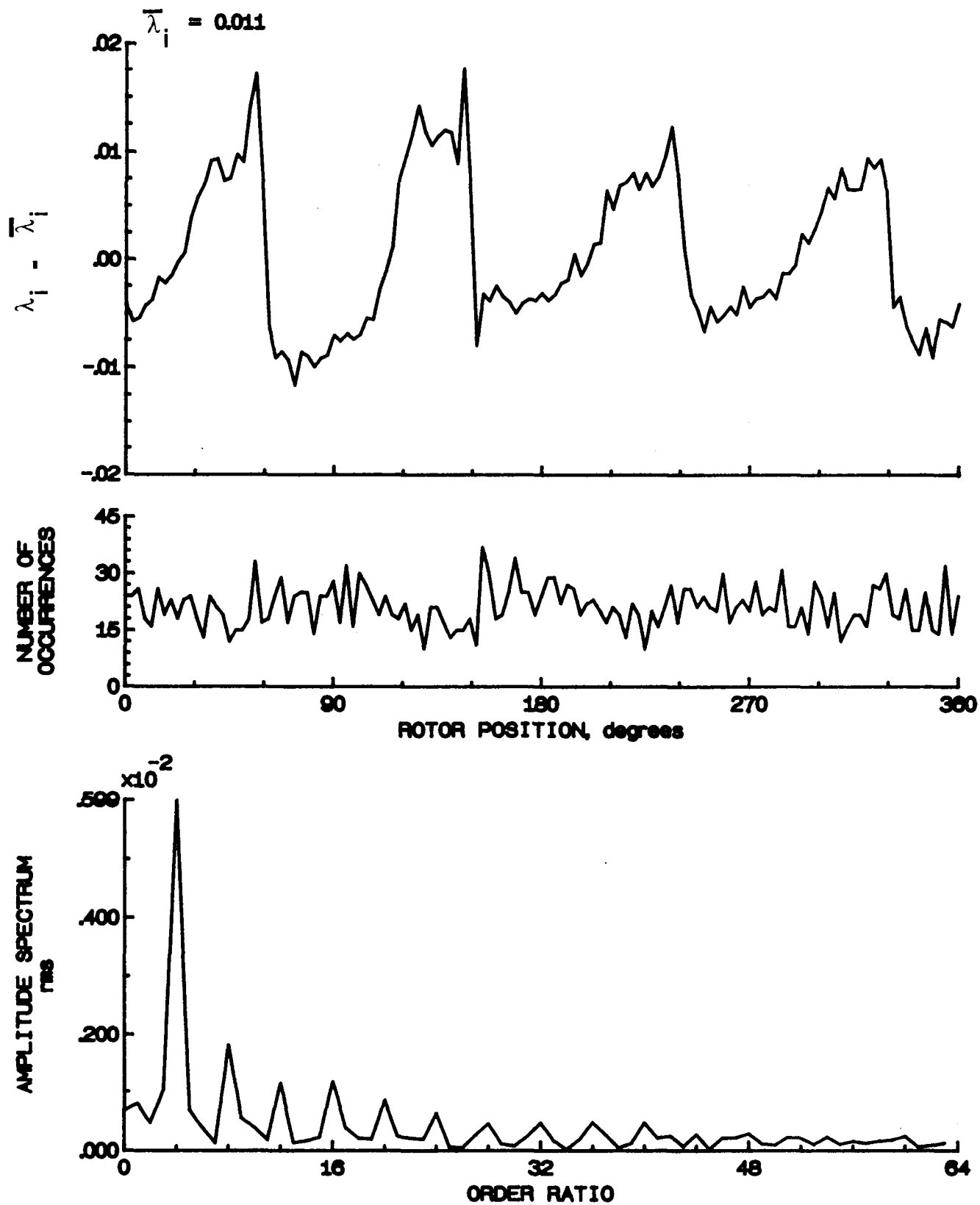


Figure 95.- Concluded.

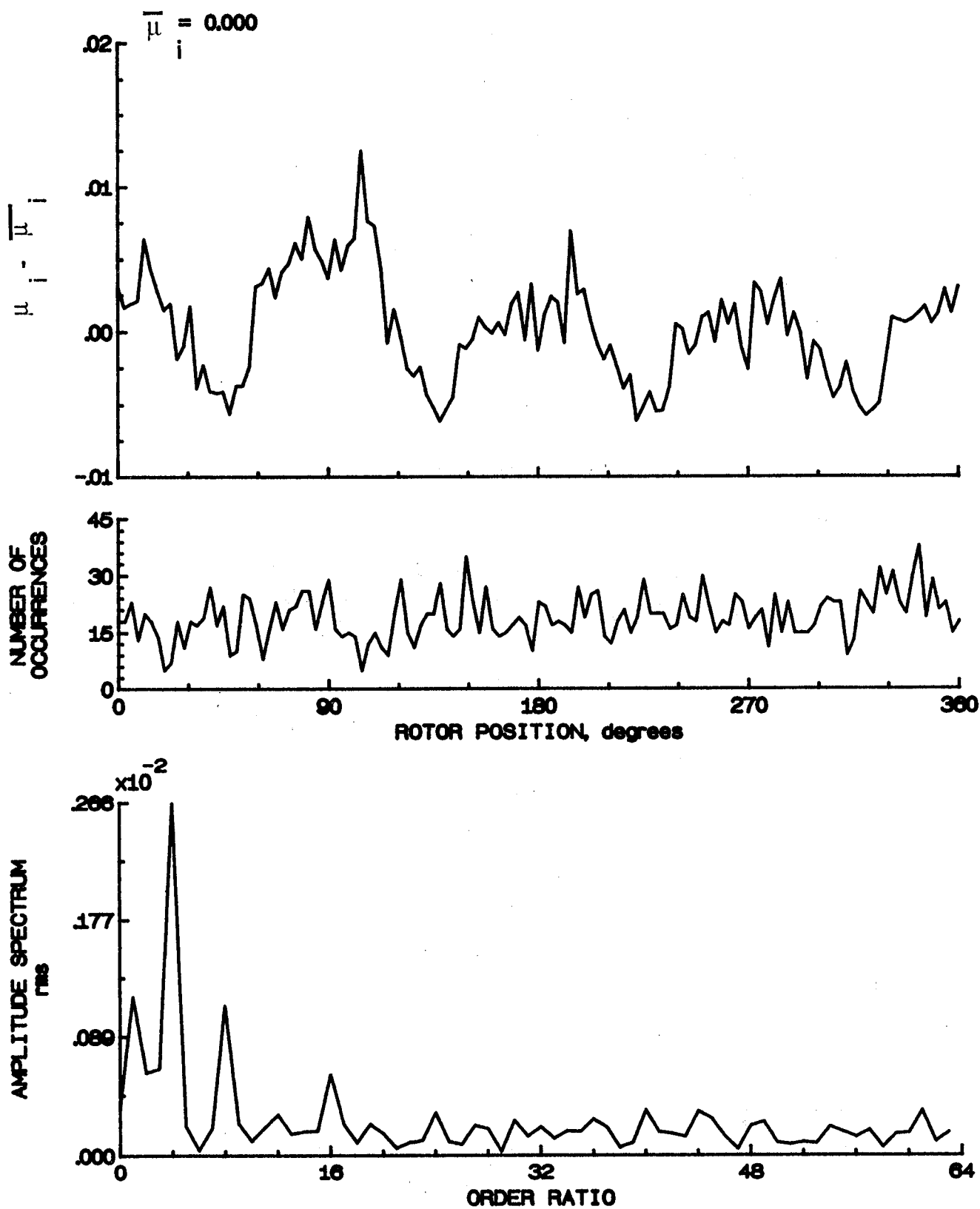


Figure 96.- Induced inflow velocity measured at 150 degrees and r/R of 0.86.



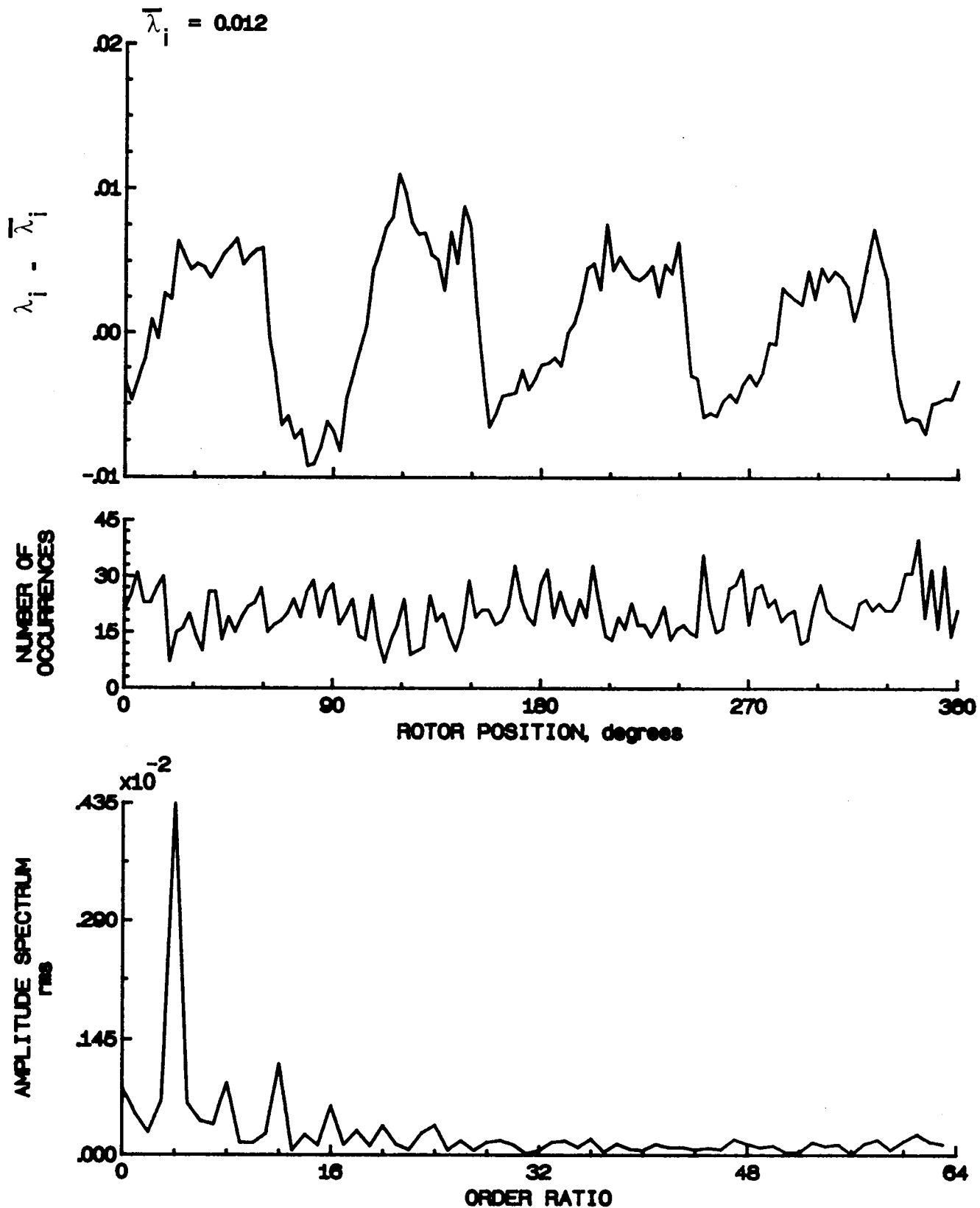


Figure 96.- Concluded.

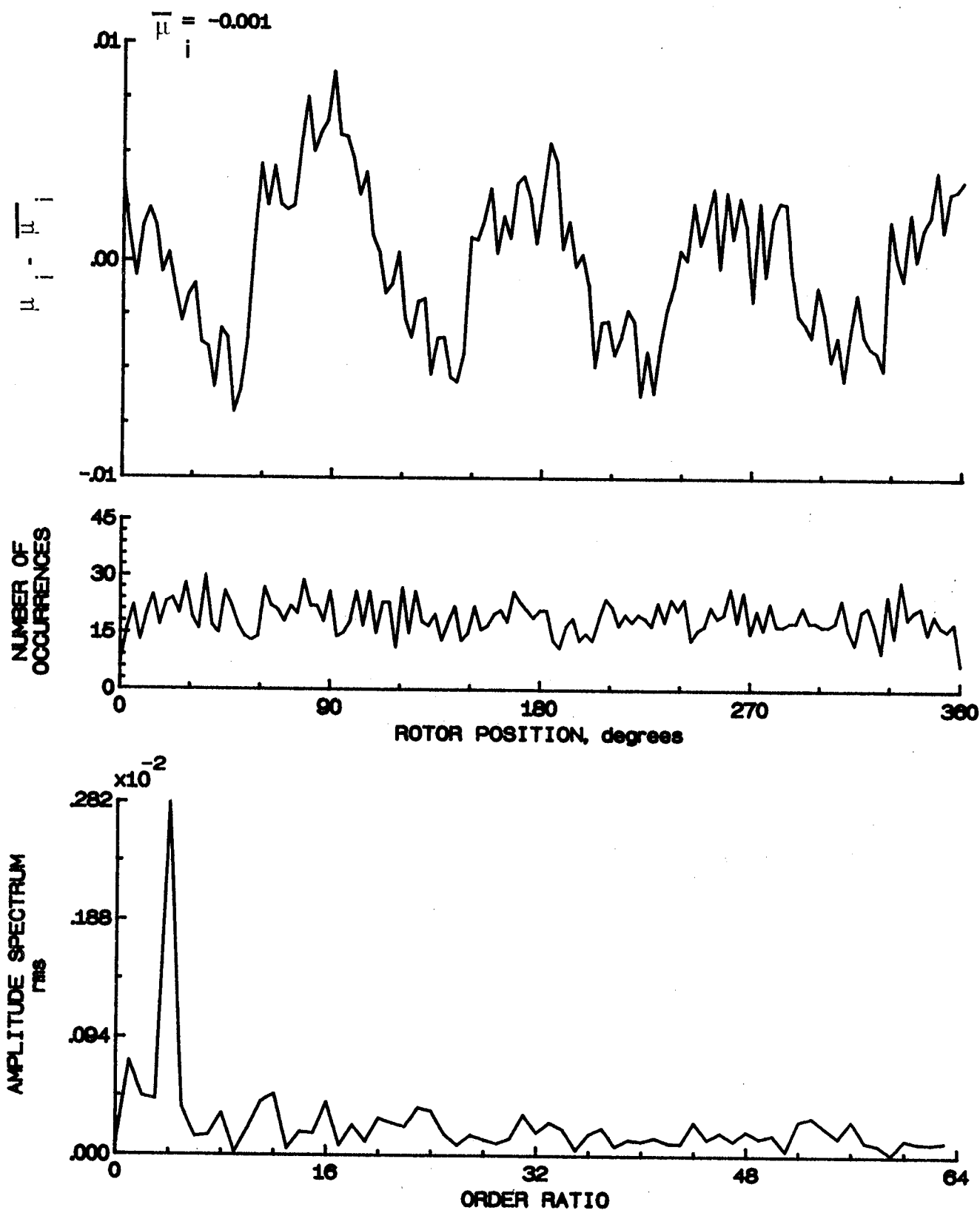


Figure 97.- Induced inflow velocity measured at 150 degrees and r/R of 0.90.

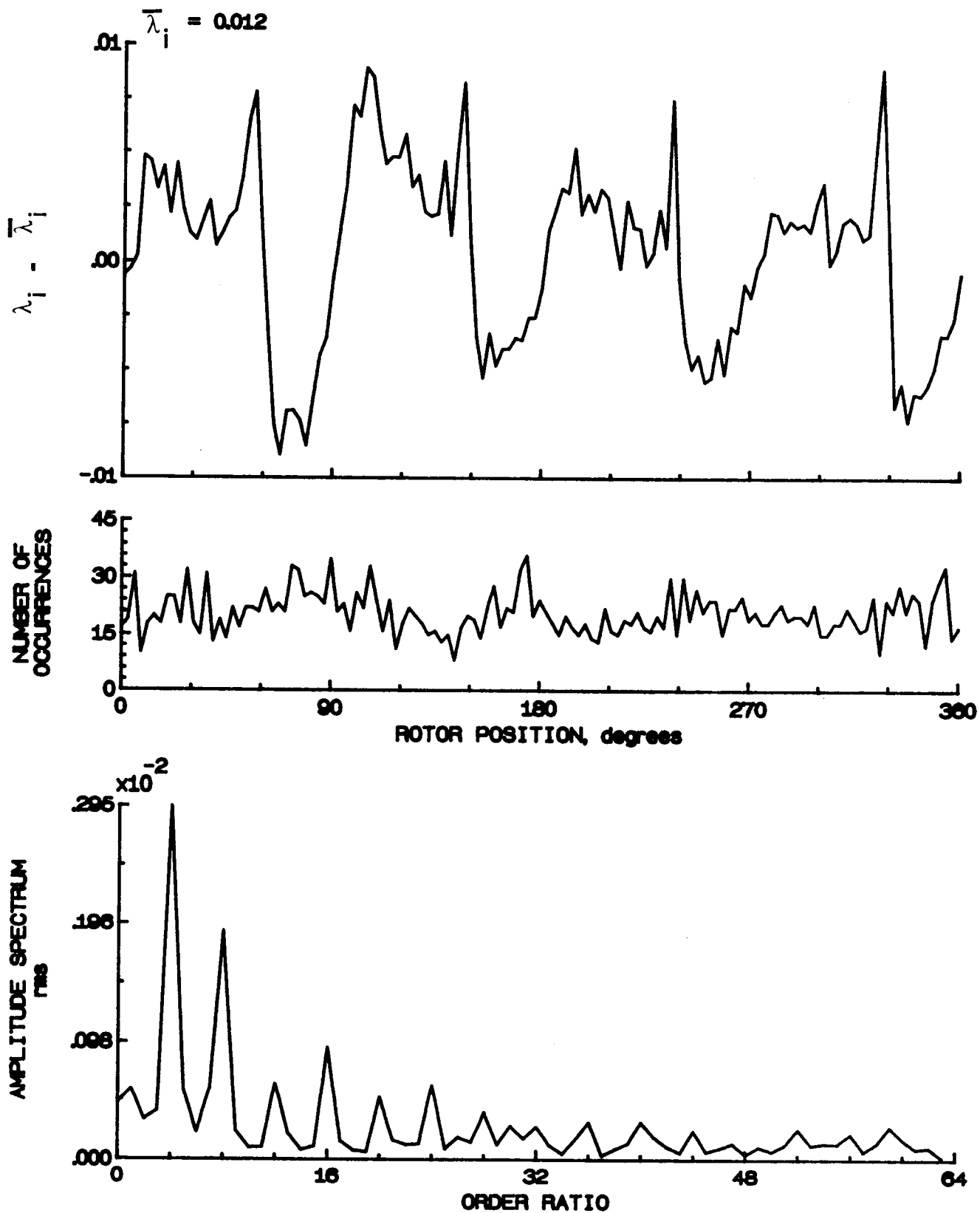


Figure 97.- Concluded.

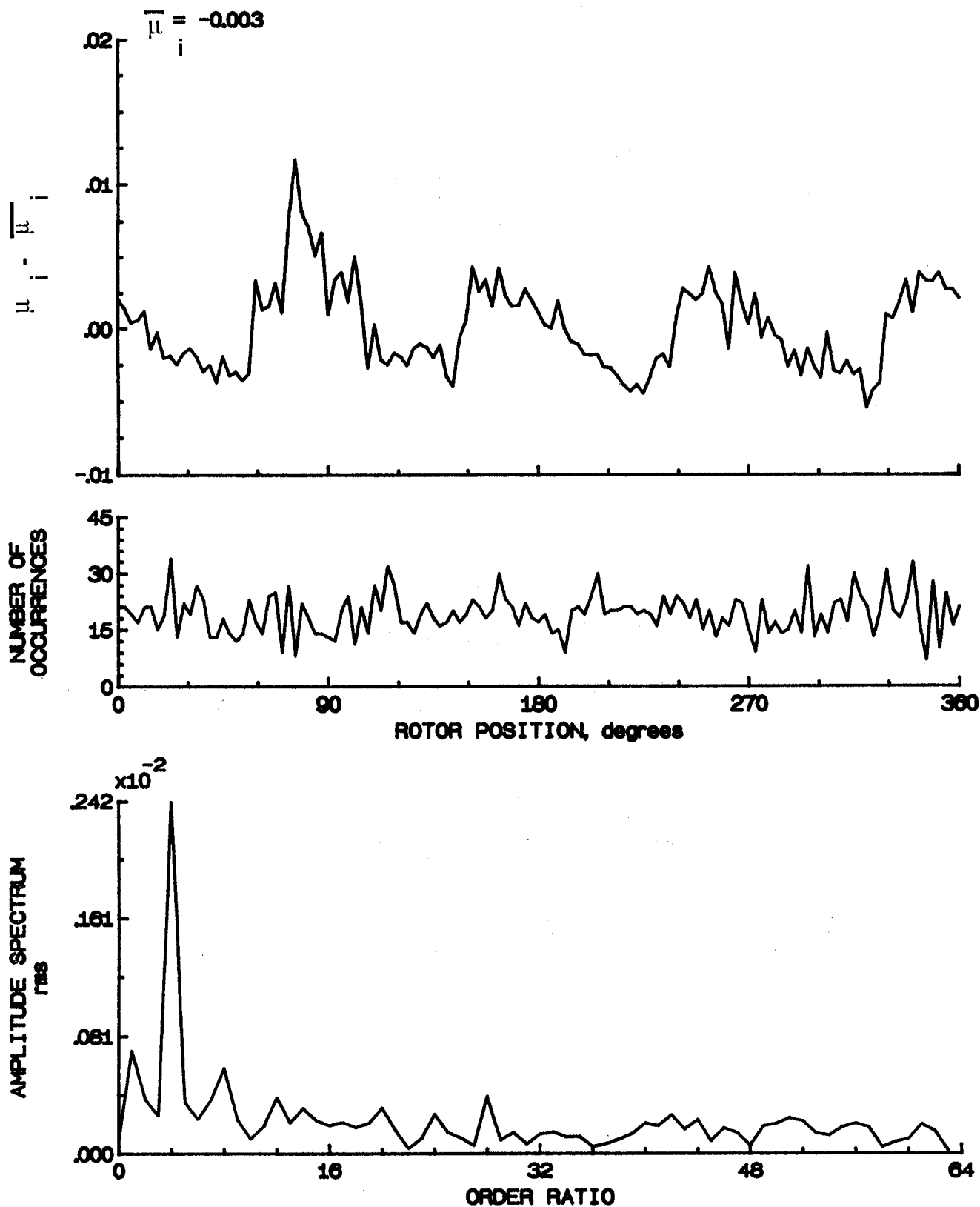


Figure 98.- Induced inflow velocity measured at 150 degrees and r/R of 0.94.

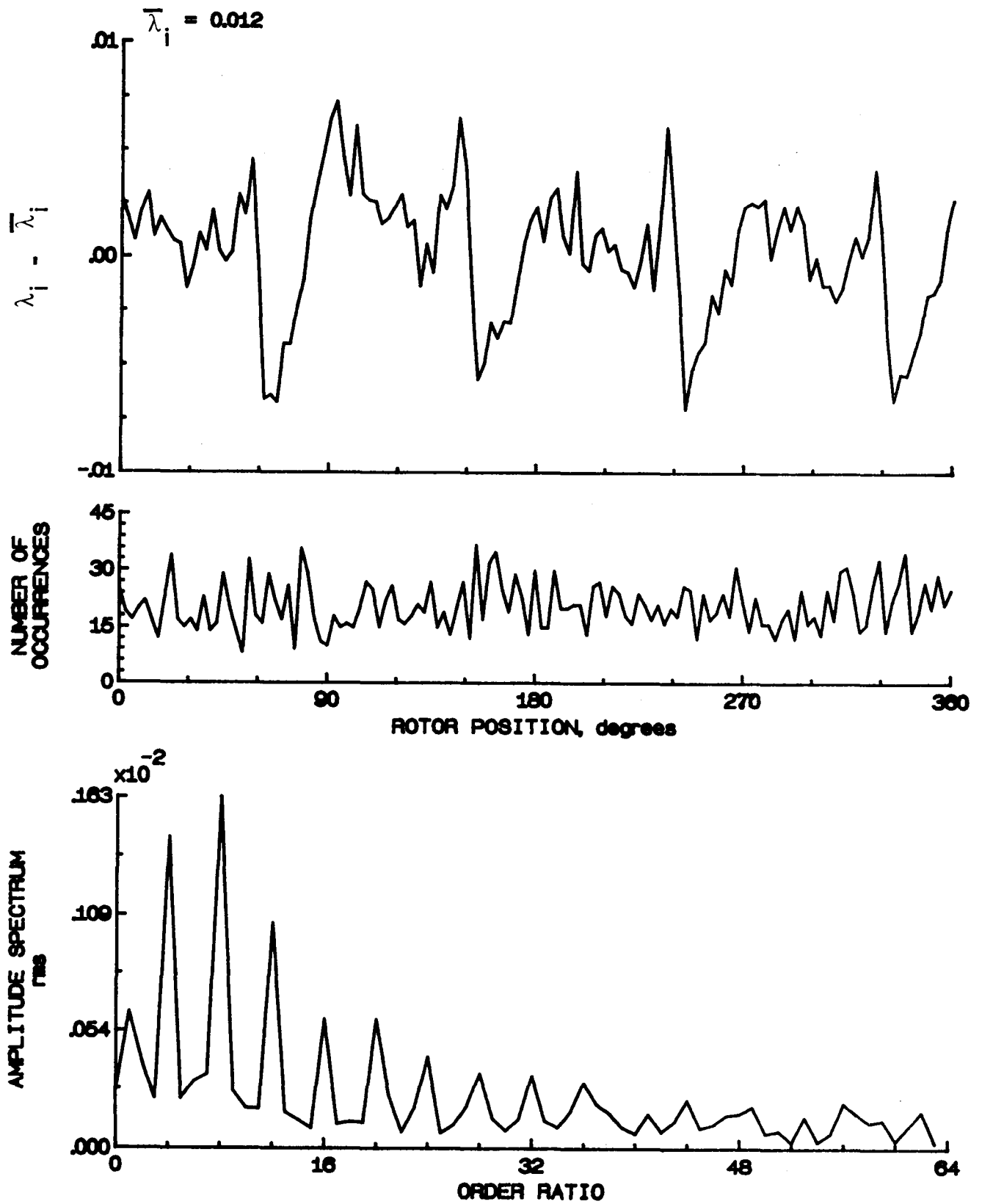


Figure 98.- Concluded.

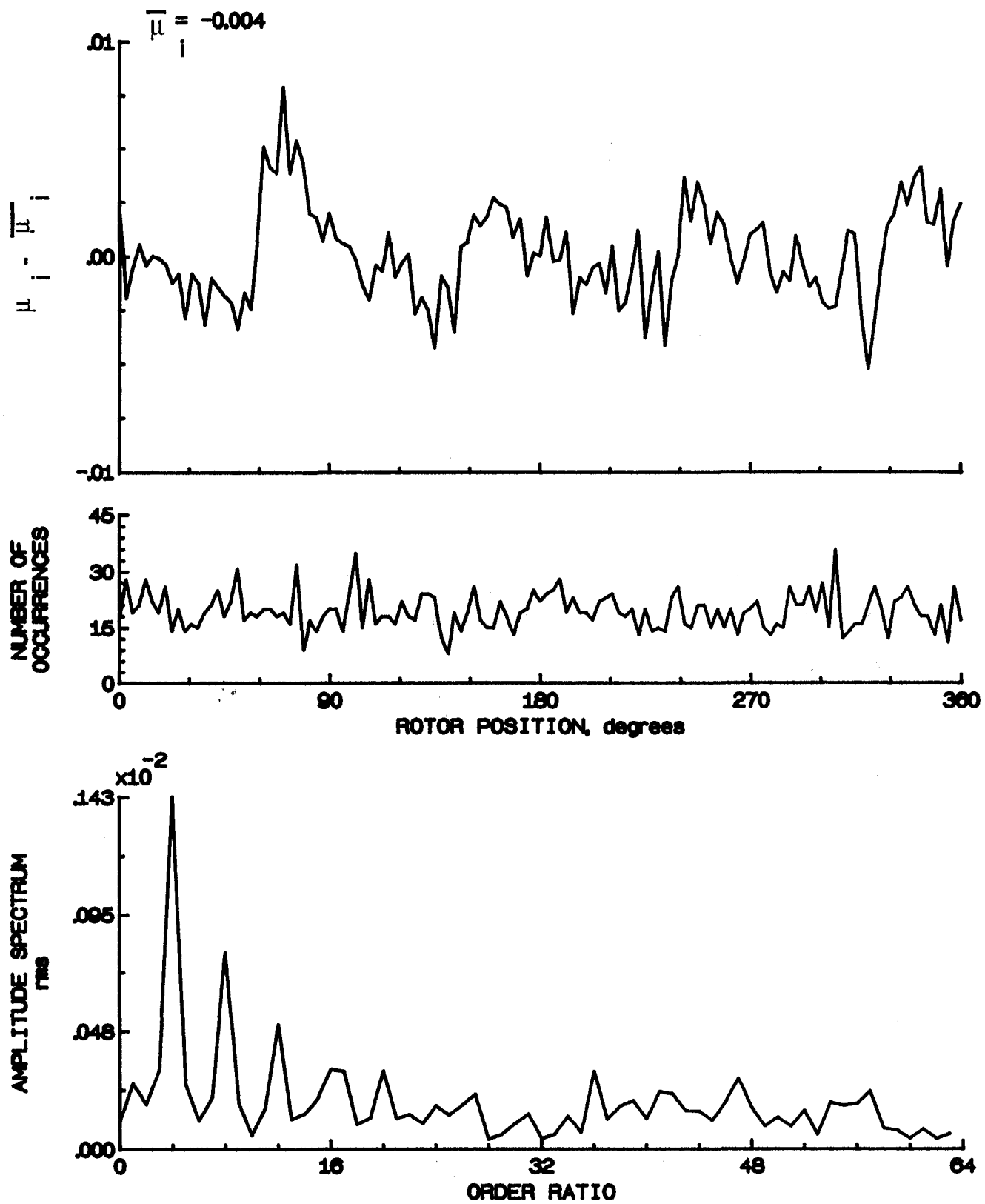


Figure 99.- Induced inflow velocity measured at 150 degrees and r/R of 0.98.

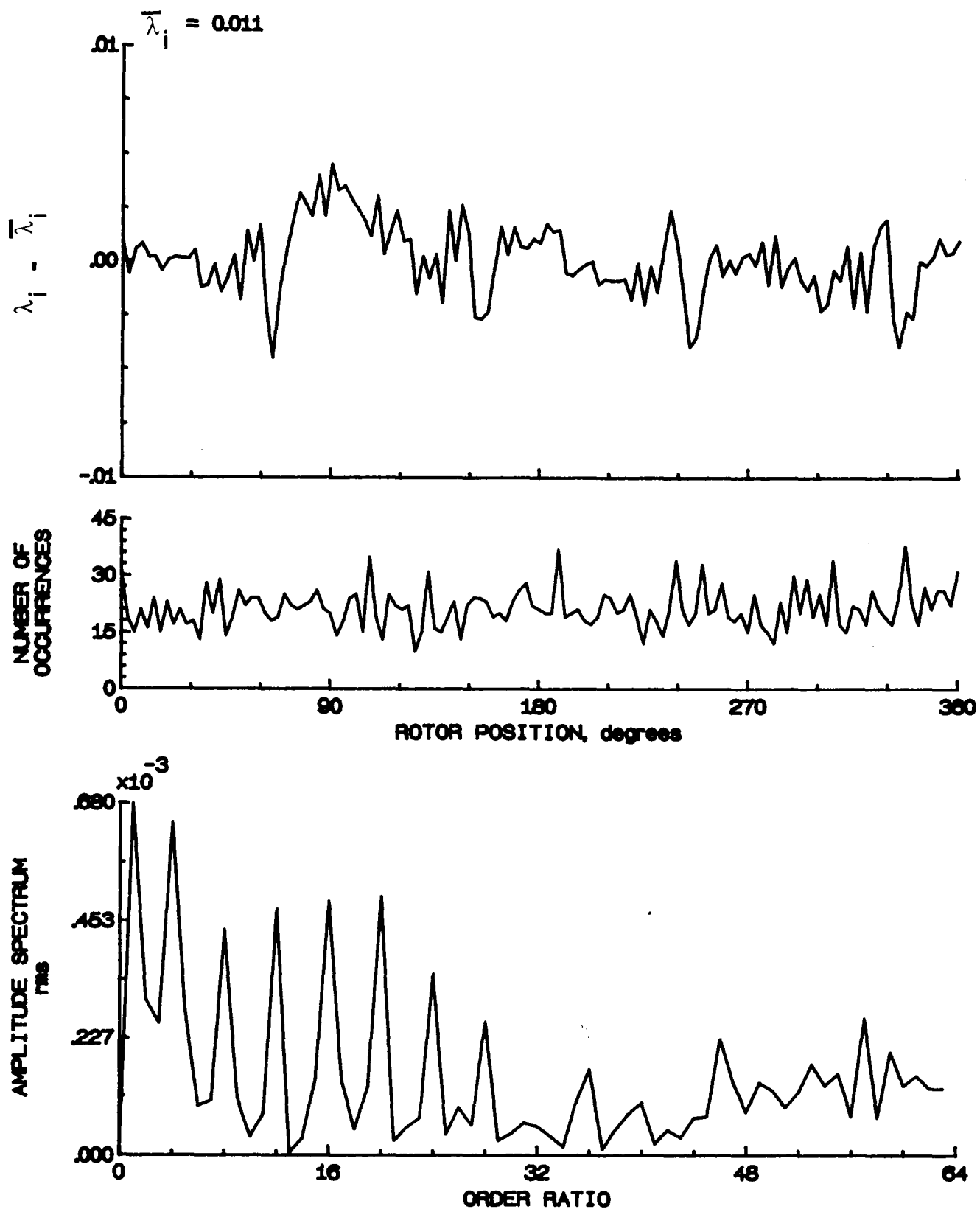


Figure 99.- Concluded.

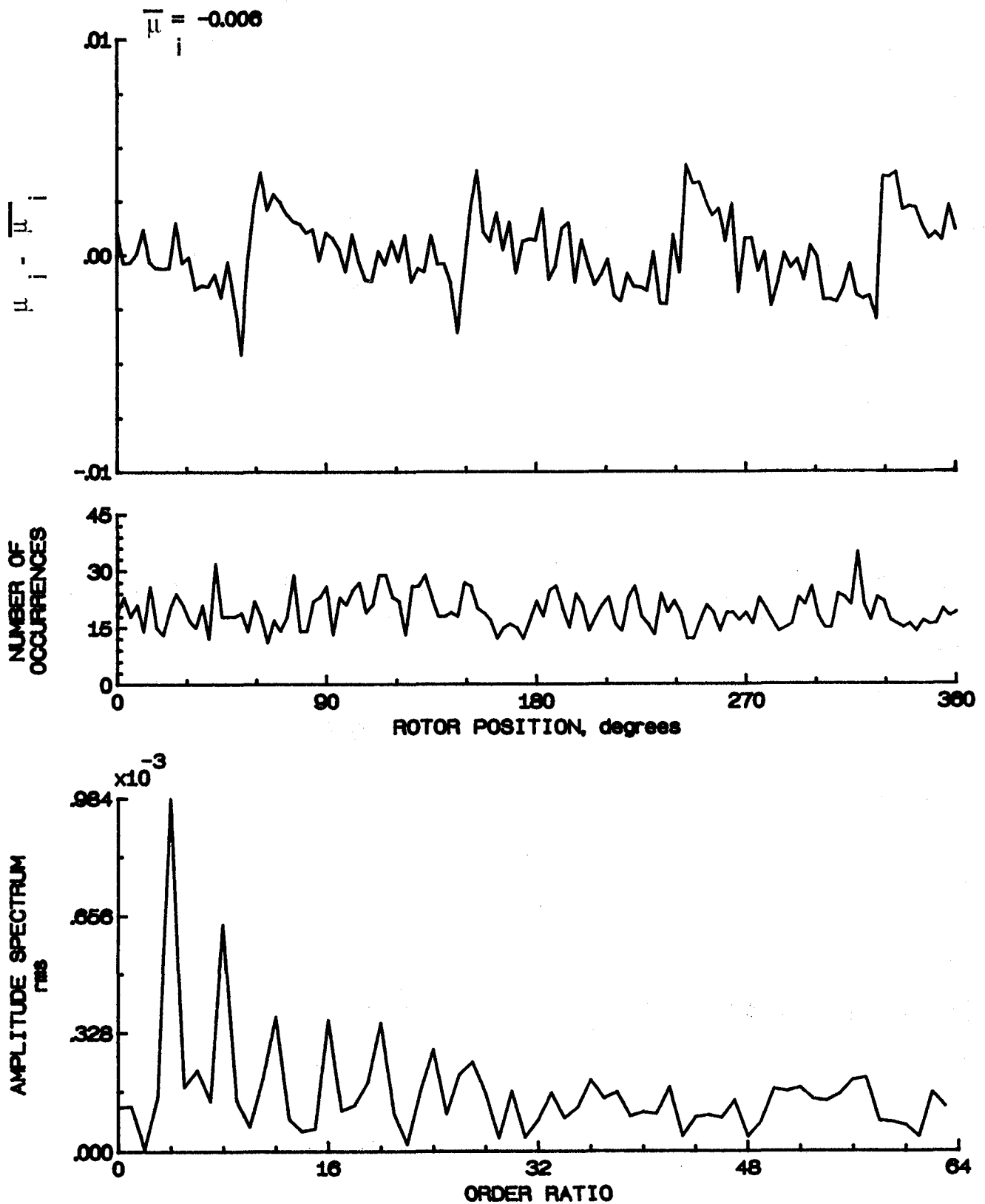


Figure 100.- Induced inflow velocity measured at 150 degrees and r/R of 1.02.



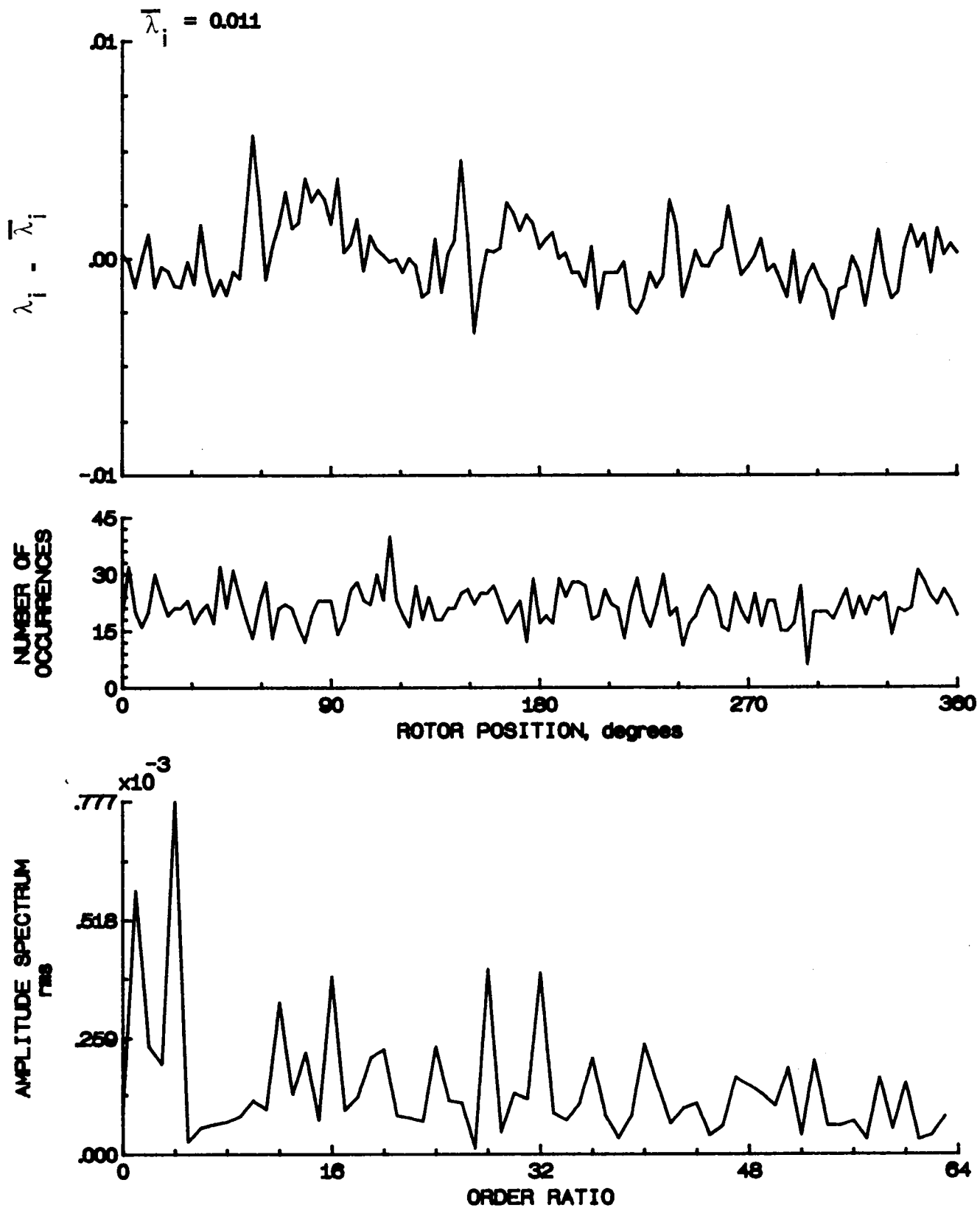


Figure 100.- Concluded.

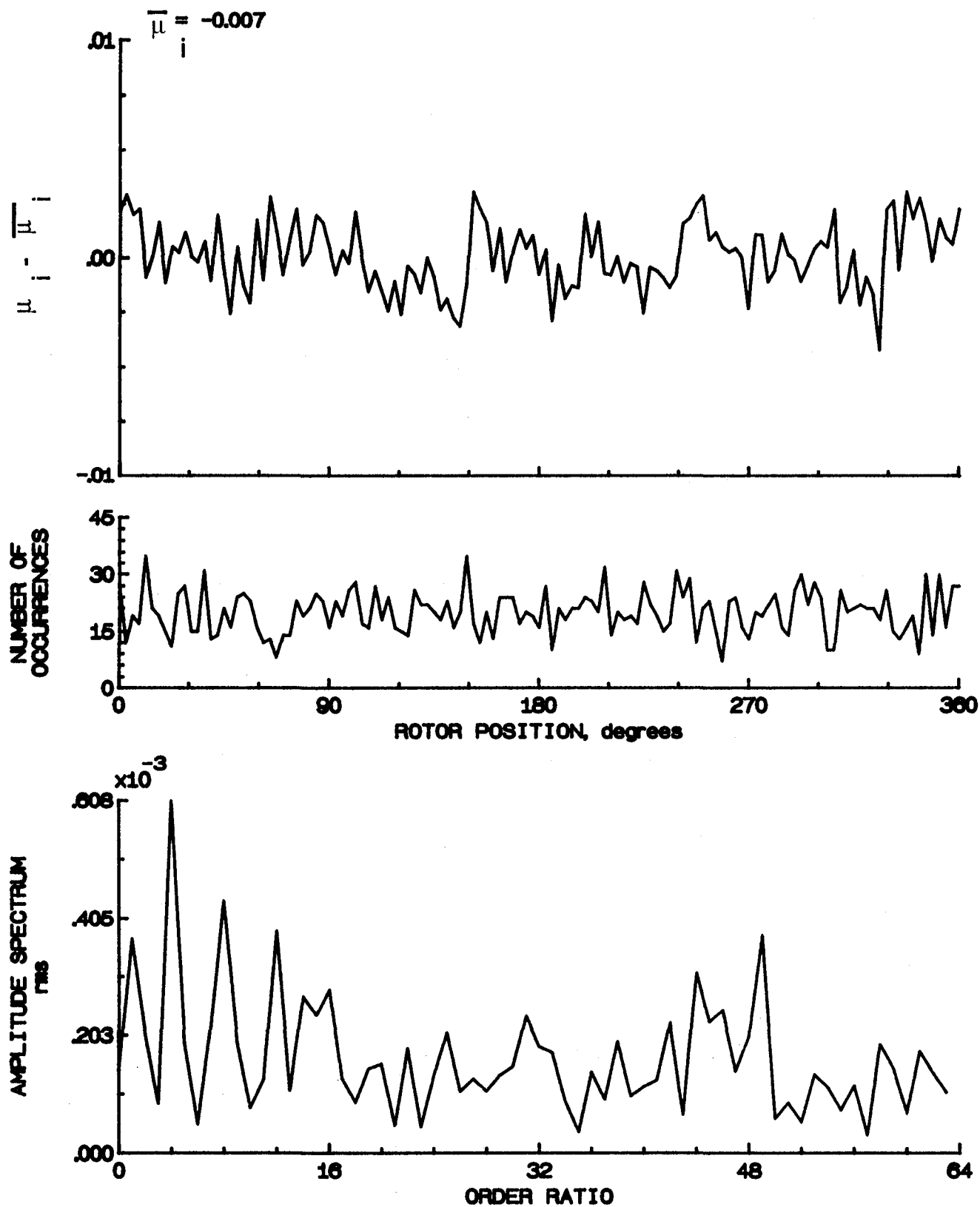


Figure 101.- Induced inflow velocity measured at 150 degrees and r/R of 1.04.

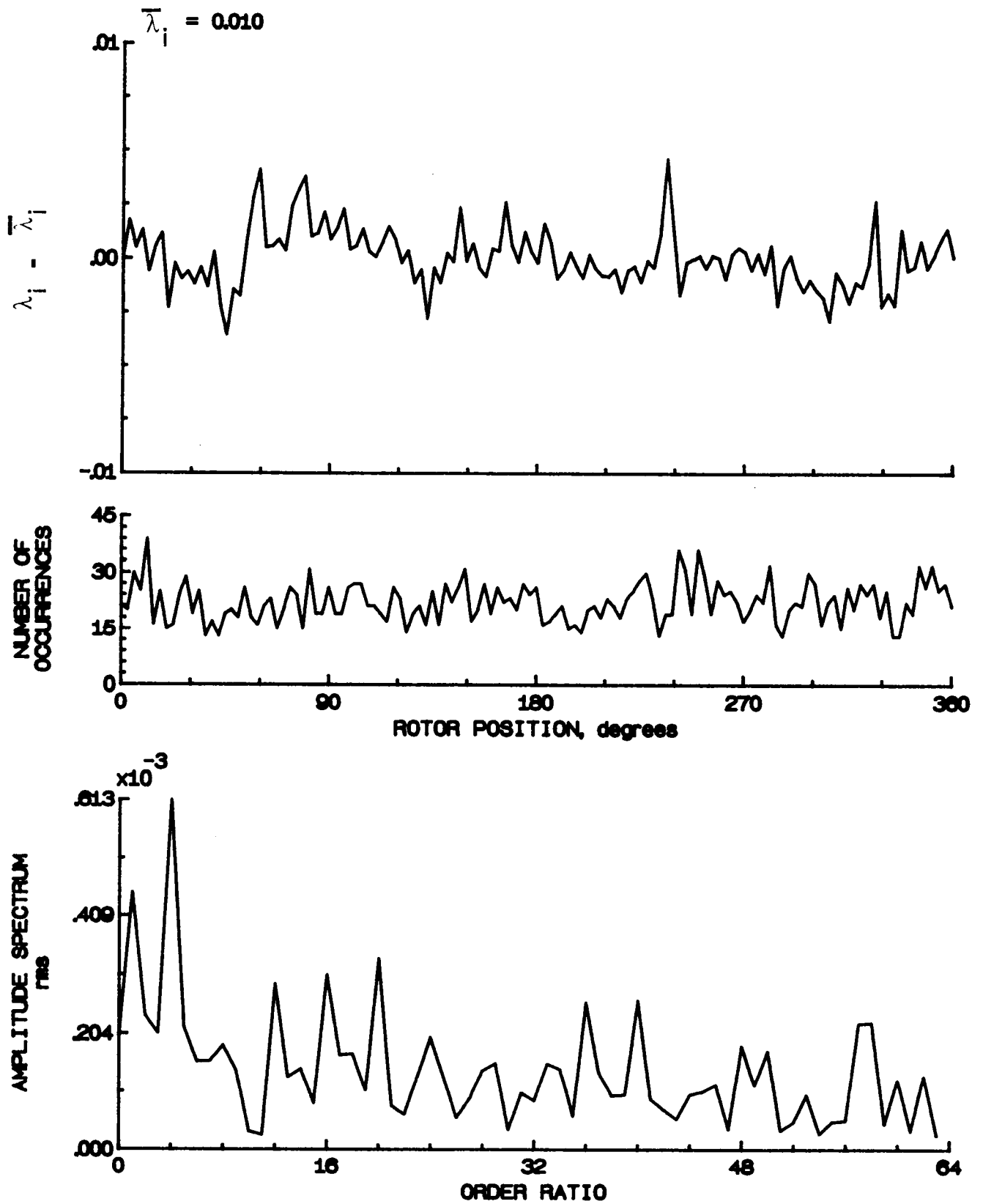


Figure 101.- Concluded.

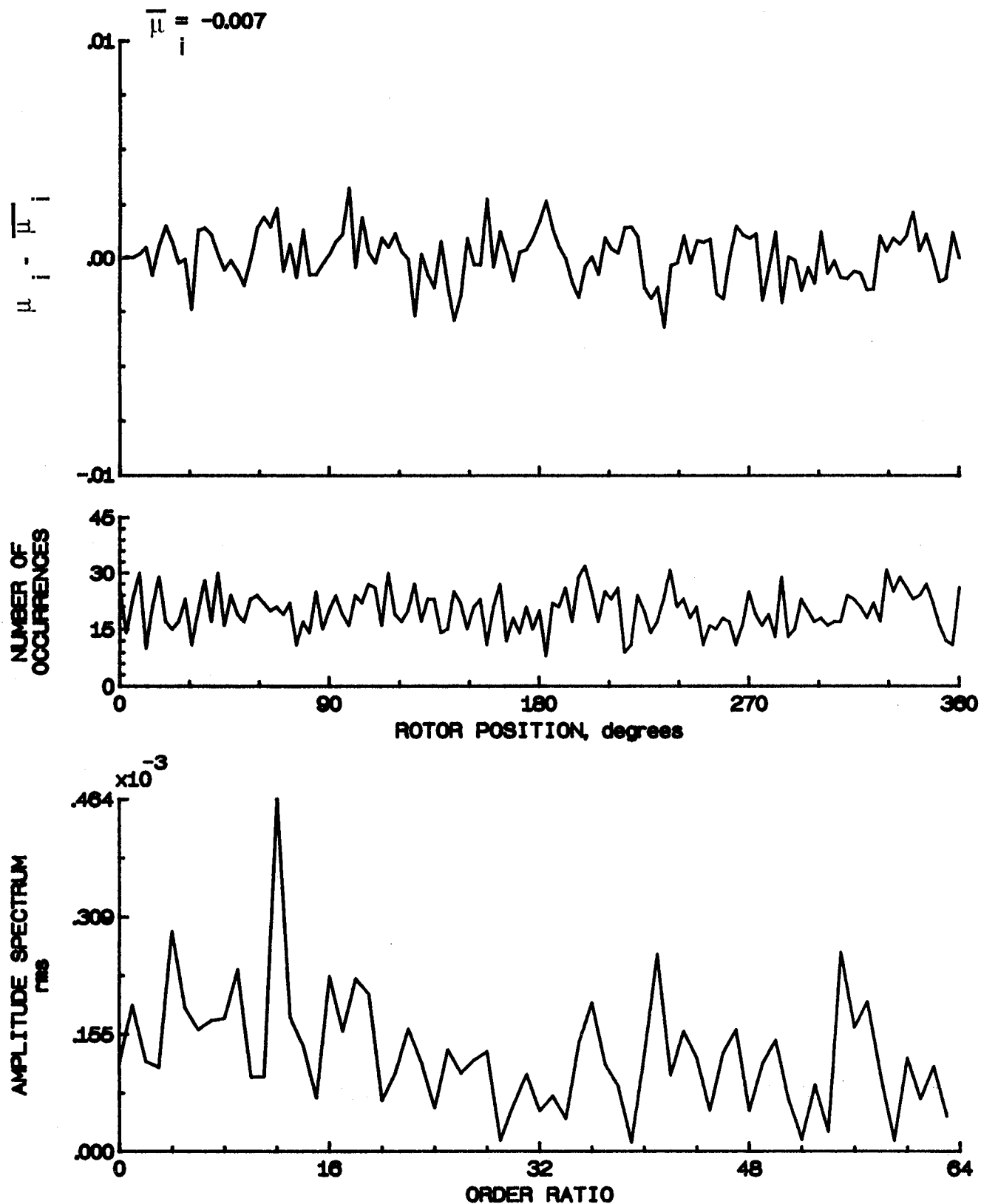


Figure 102.- Induced inflow velocity measured at 150 degrees and r/R of 1.10.

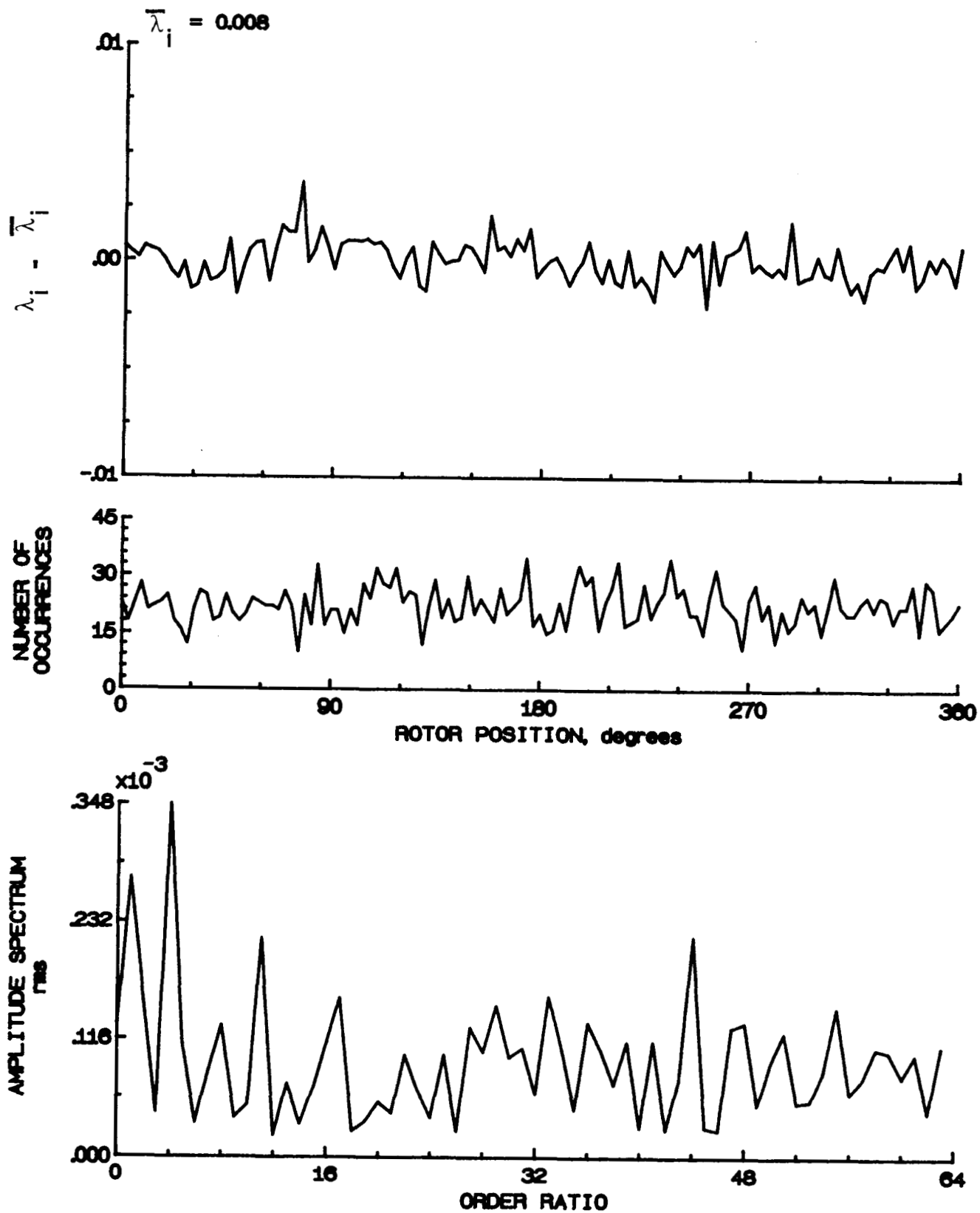


Figure 102.- Concluded.

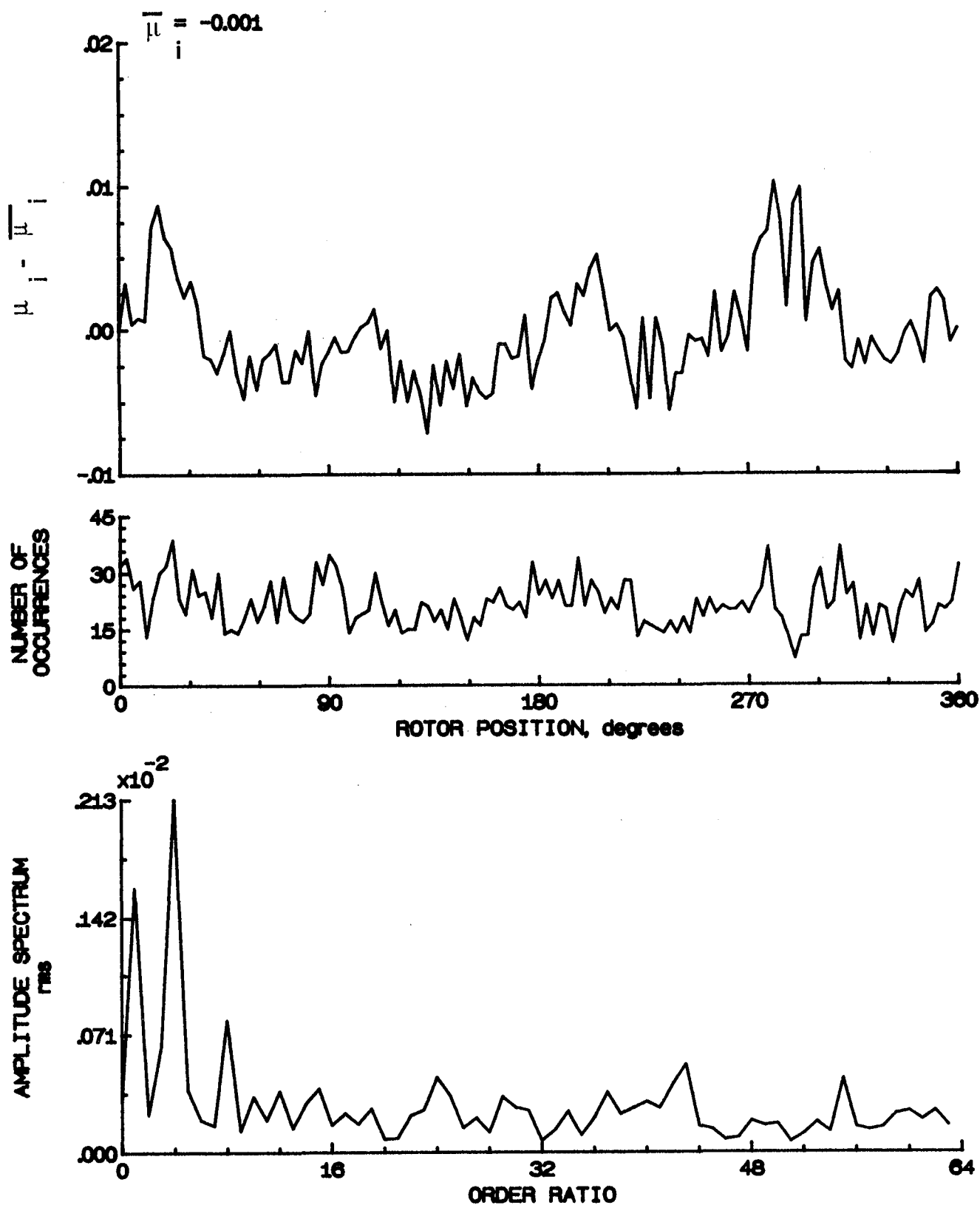


Figure 103.- Induced inflow velocity measured at 180 degrees and r/R of 0.20.

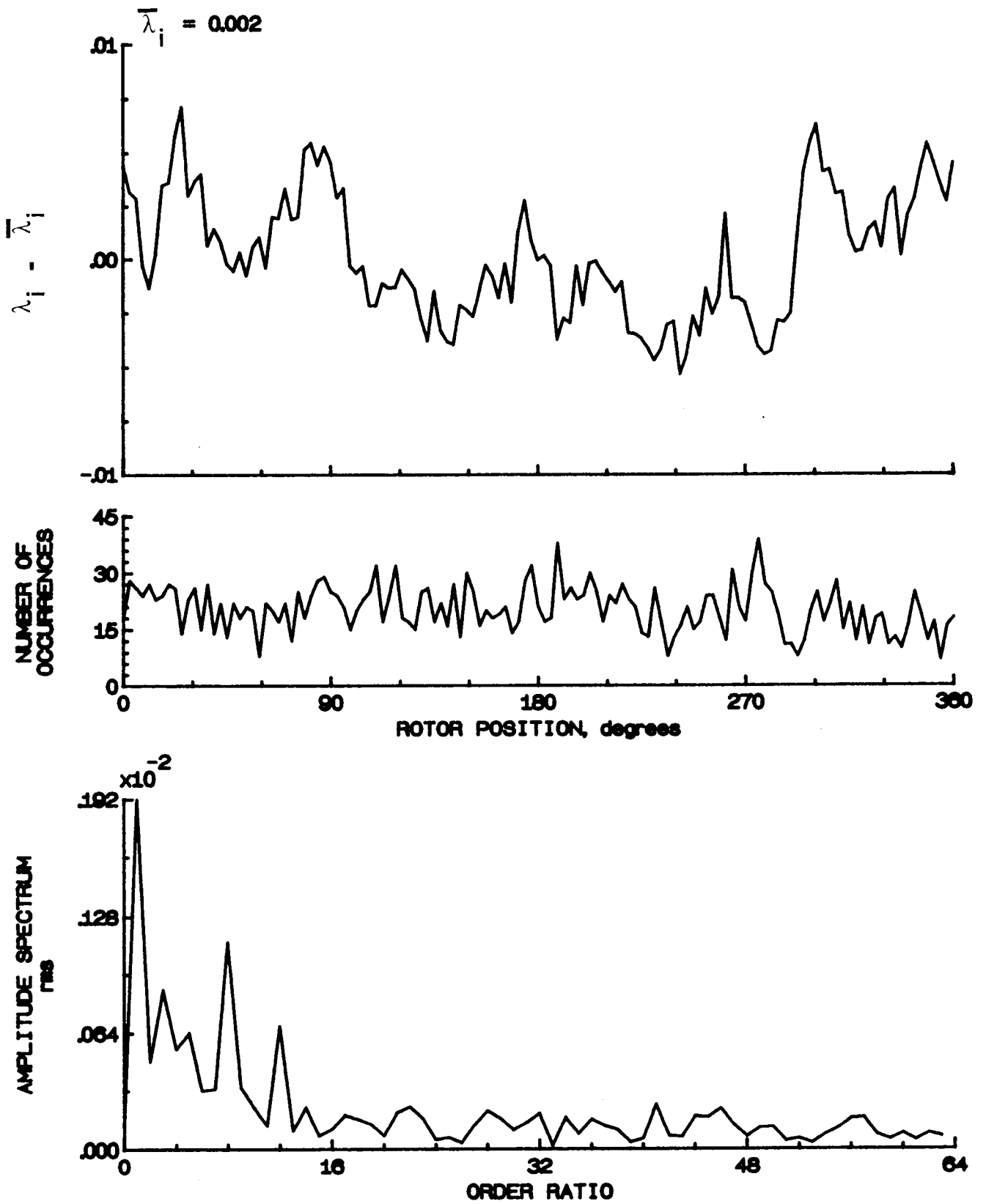


Figure 103.- Concluded.

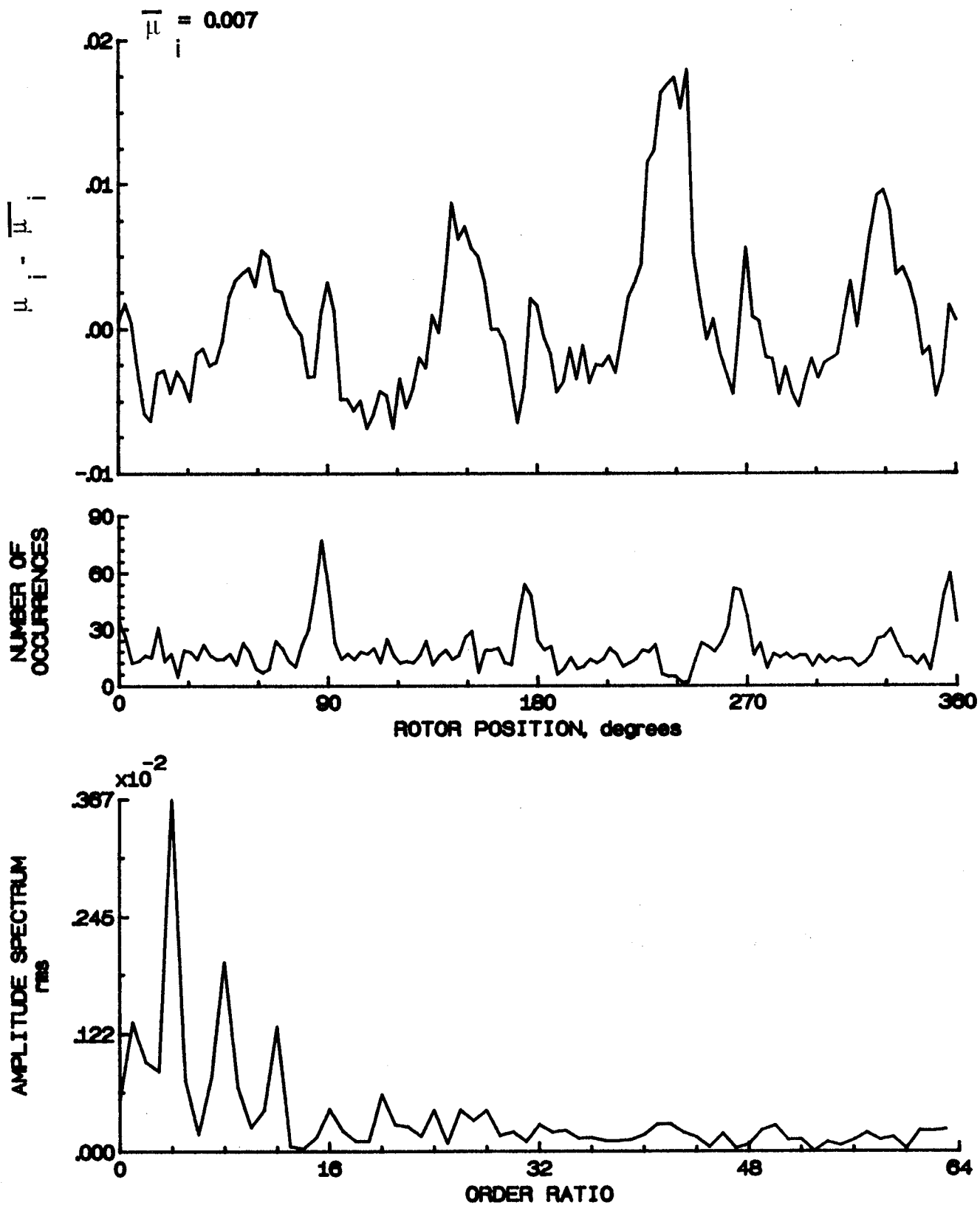


Figure 104.- Induced inflow velocity measured at 180 degrees and  $r/R$  of 0.40.



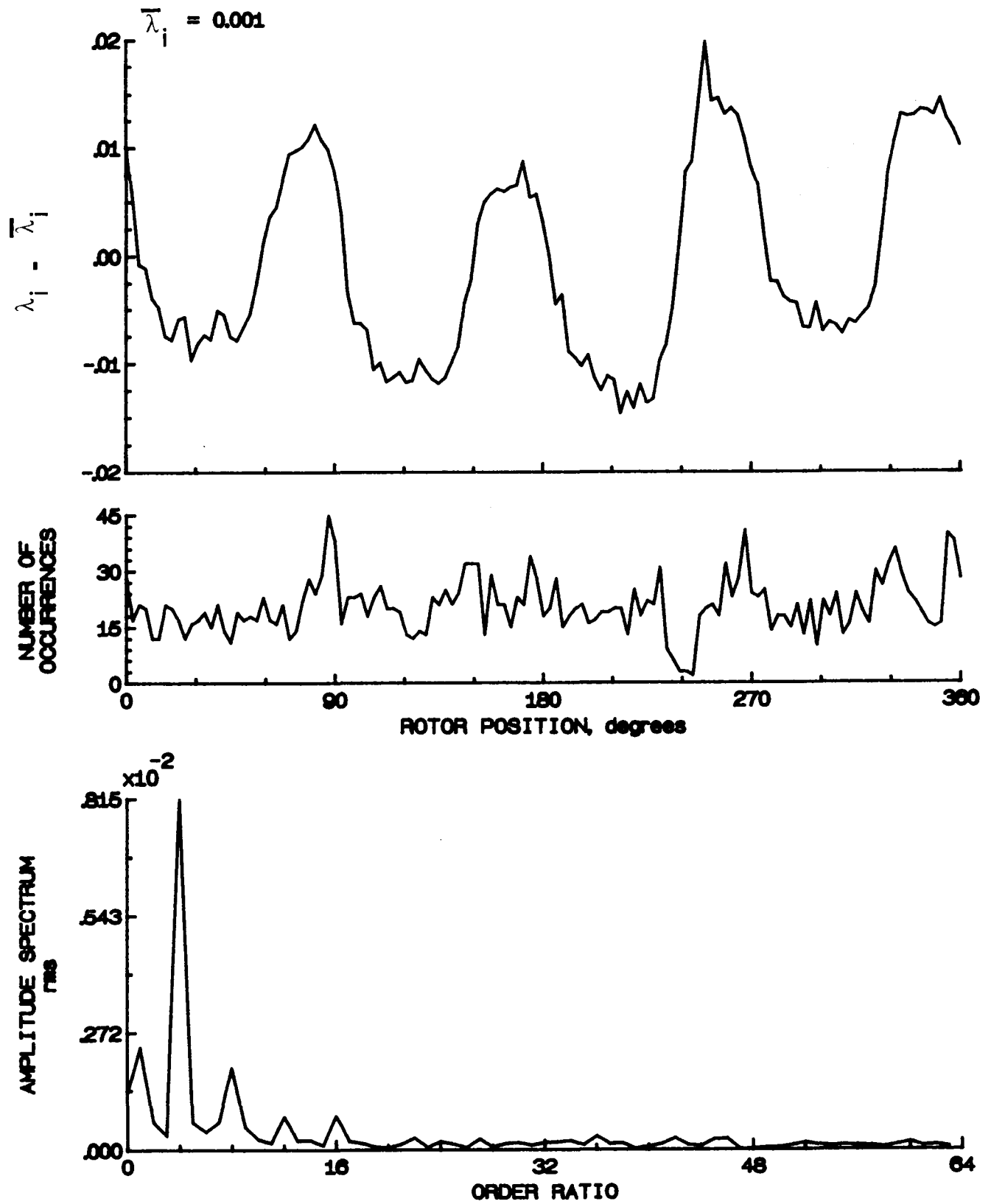


Figure 104.- Concluded.

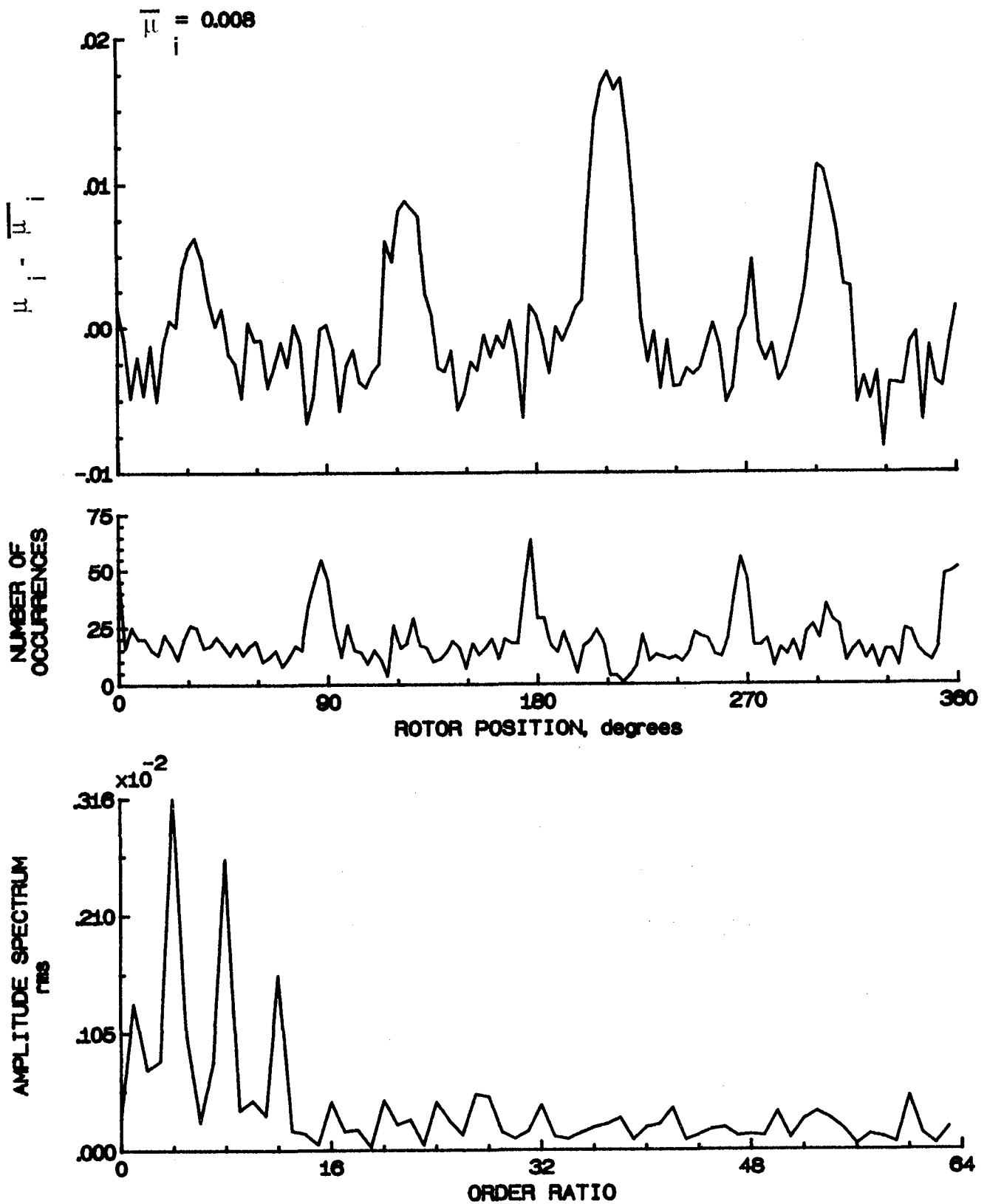


Figure 105.- Induced inflow velocity measured at 180 degrees and  $r/R$  of 0.50.

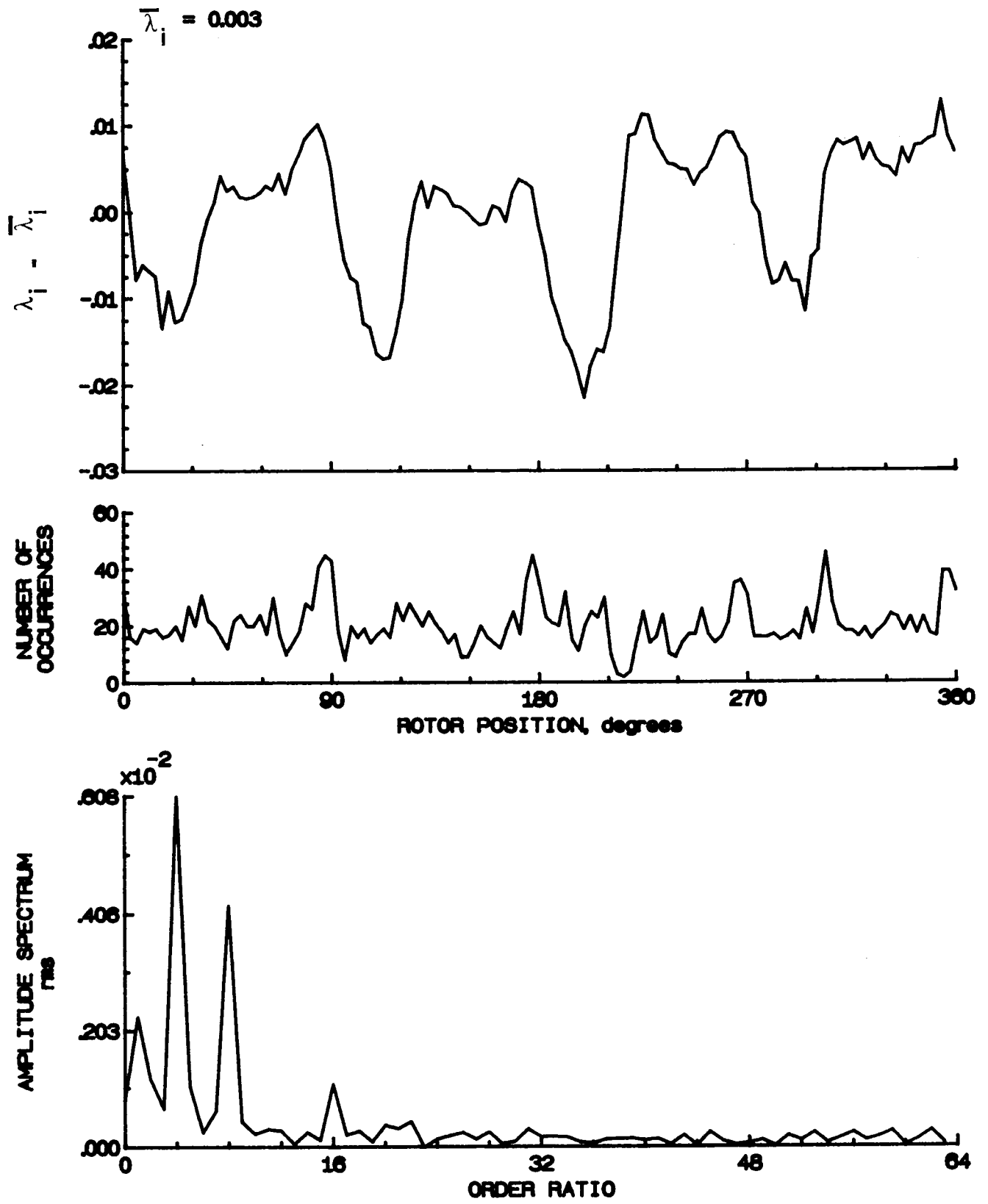


Figure 105.- Concluded.

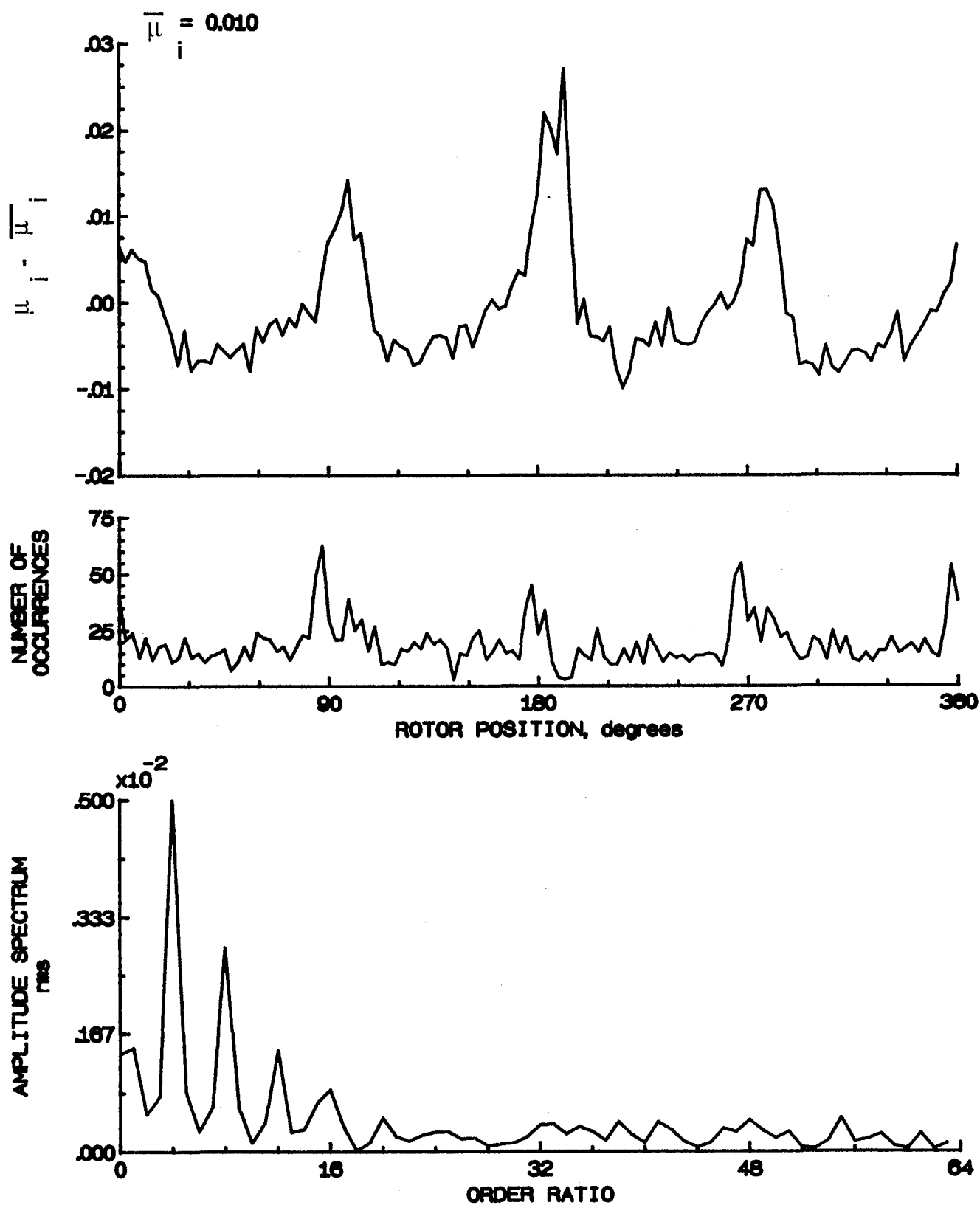


Figure 106.- Induced inflow velocity measured at 180 degrees and  $r/R$  of 0.60.

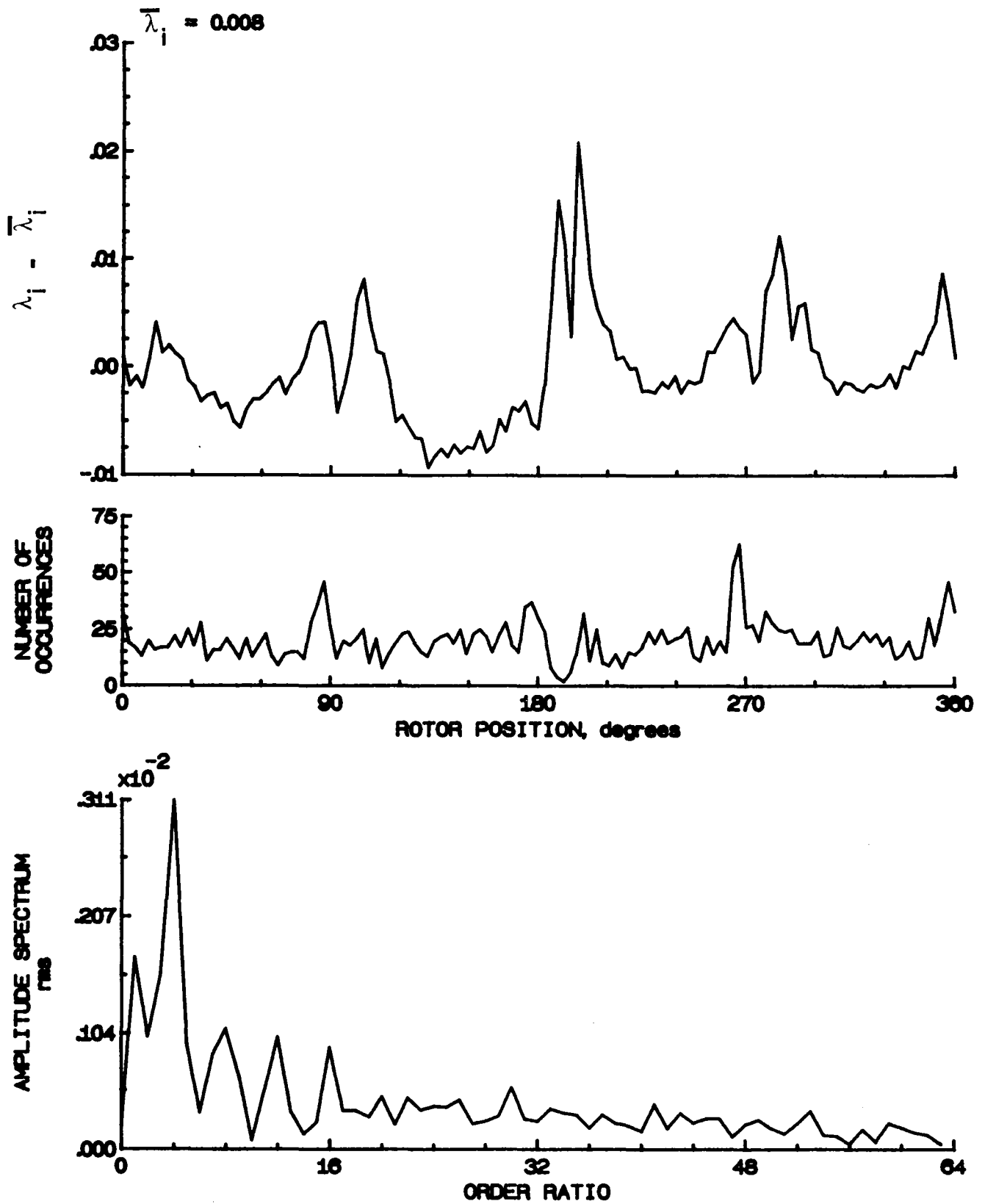


Figure 106.- Concluded.

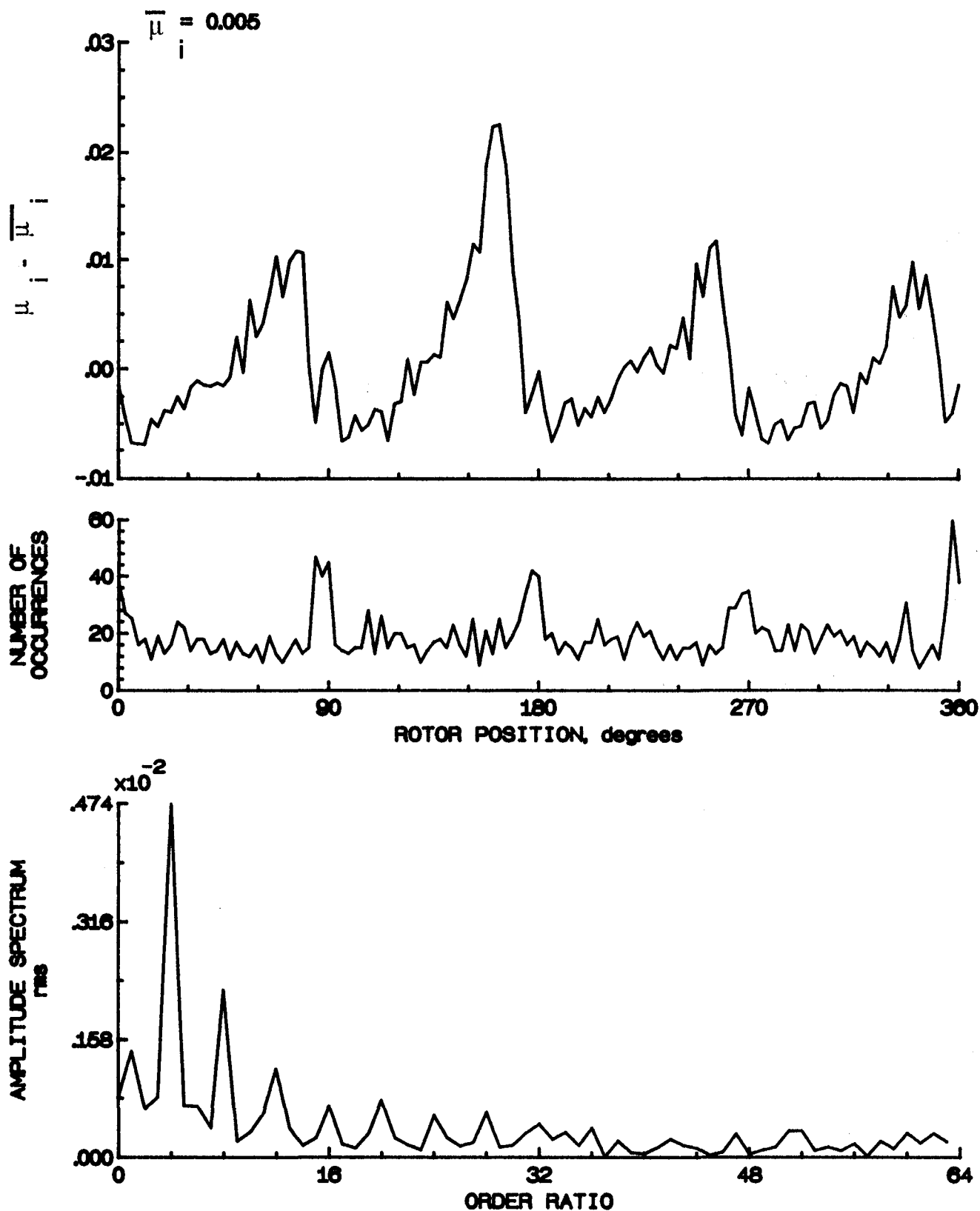


Figure 107.- Induced inflow velocity measured at 180 degrees and r/R of 0.70.

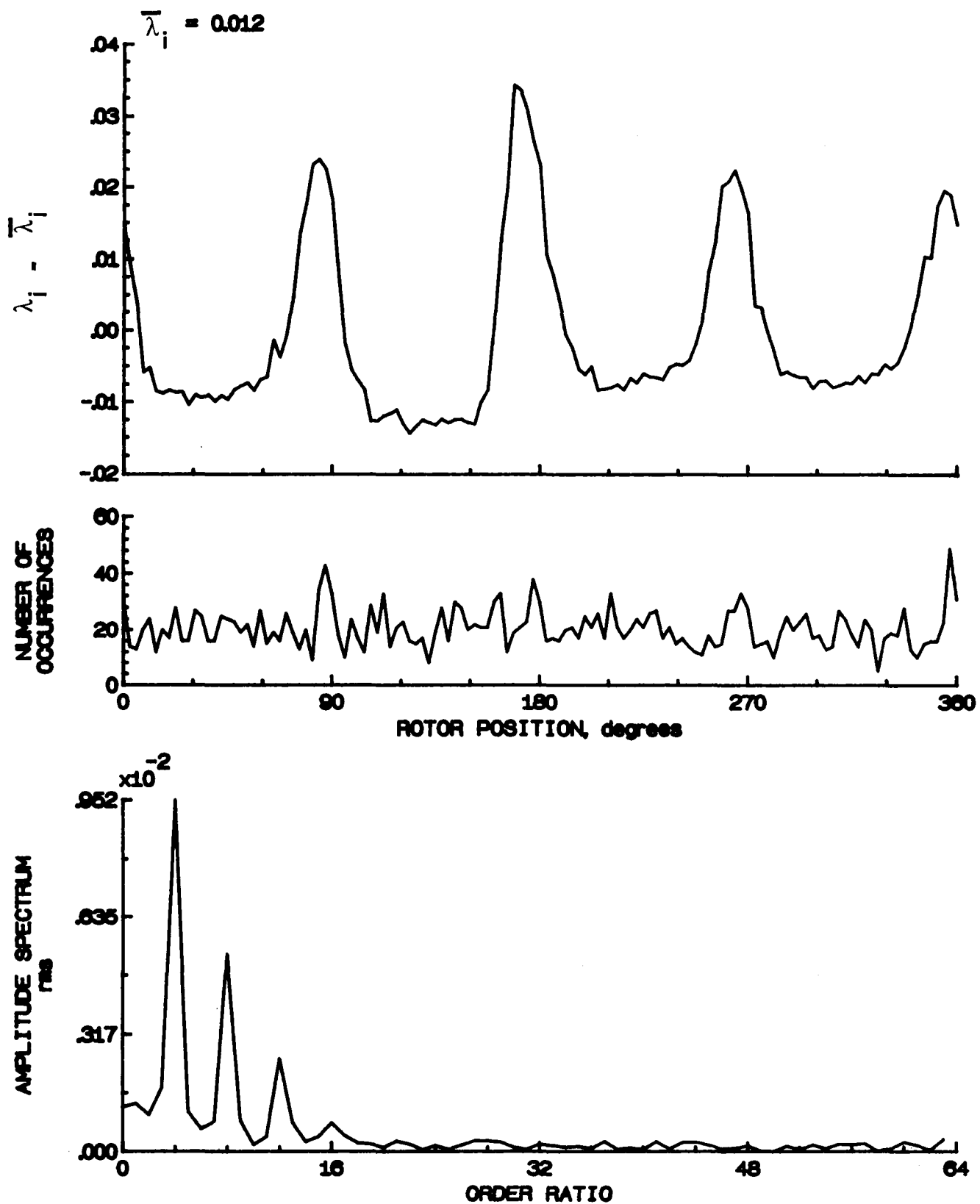


Figure 107.- Concluded.

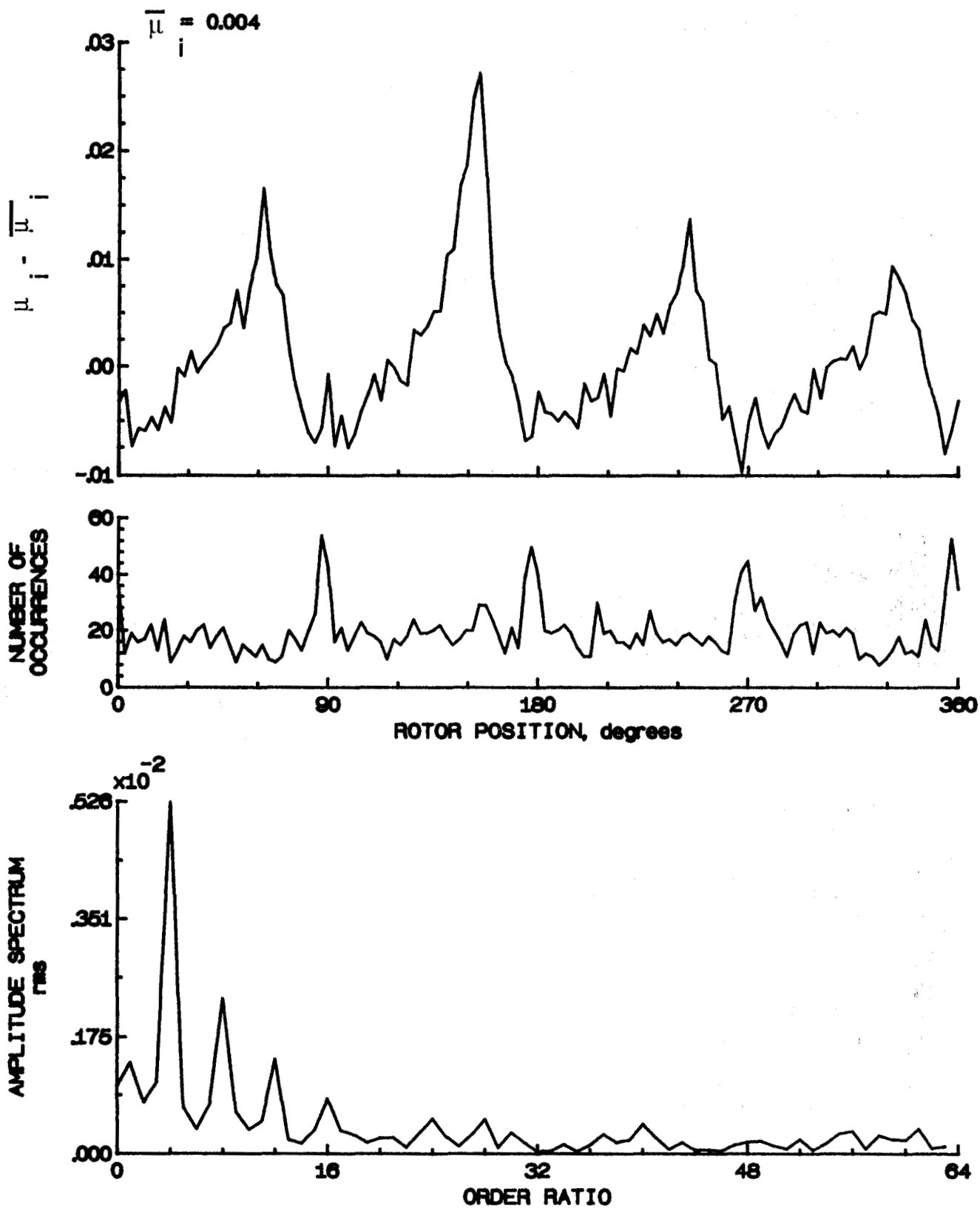


Figure 108.- Induced inflow velocity measured at 180 degrees and  $r/R$  of 0.74.



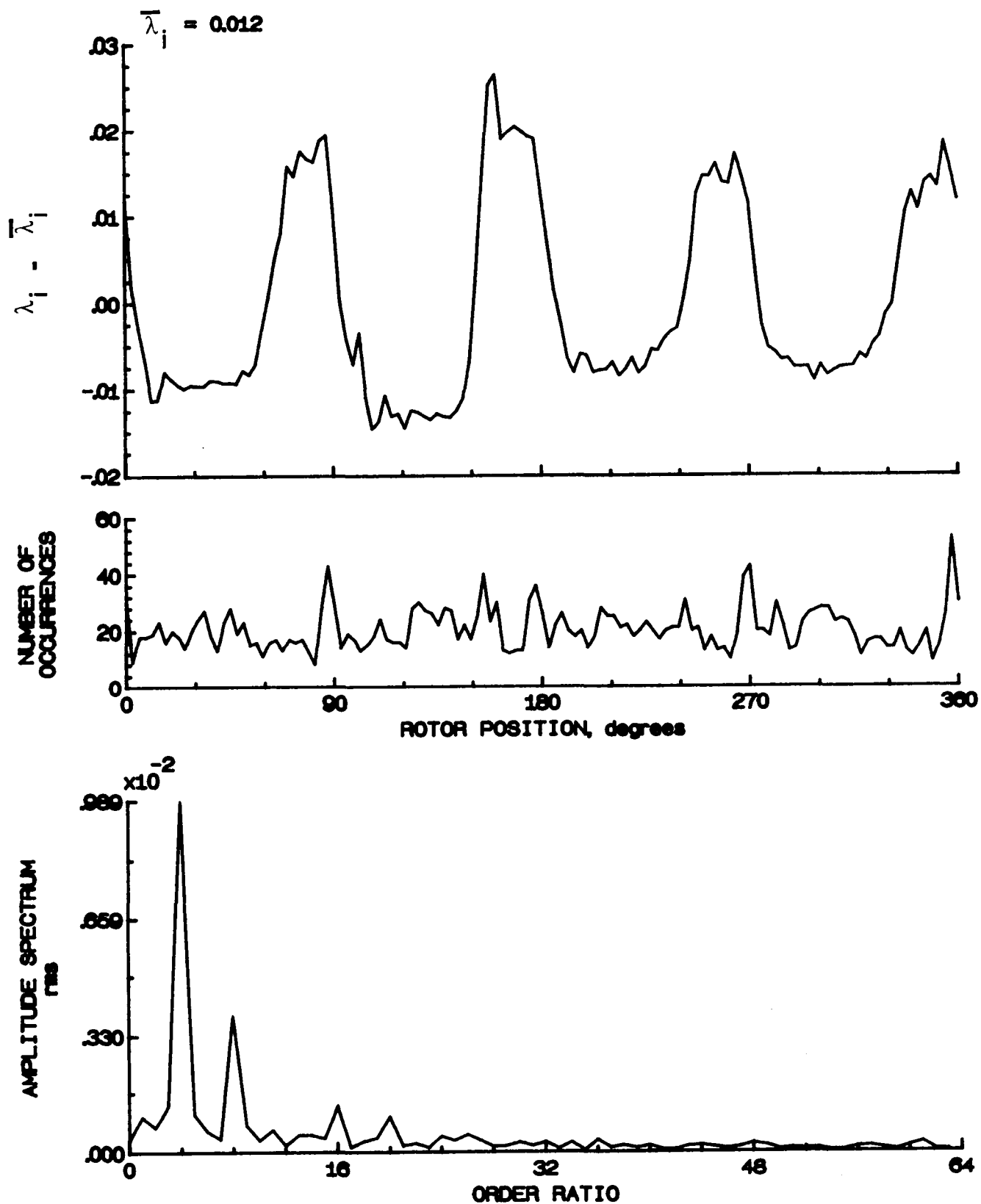


Figure 108.- Concluded.

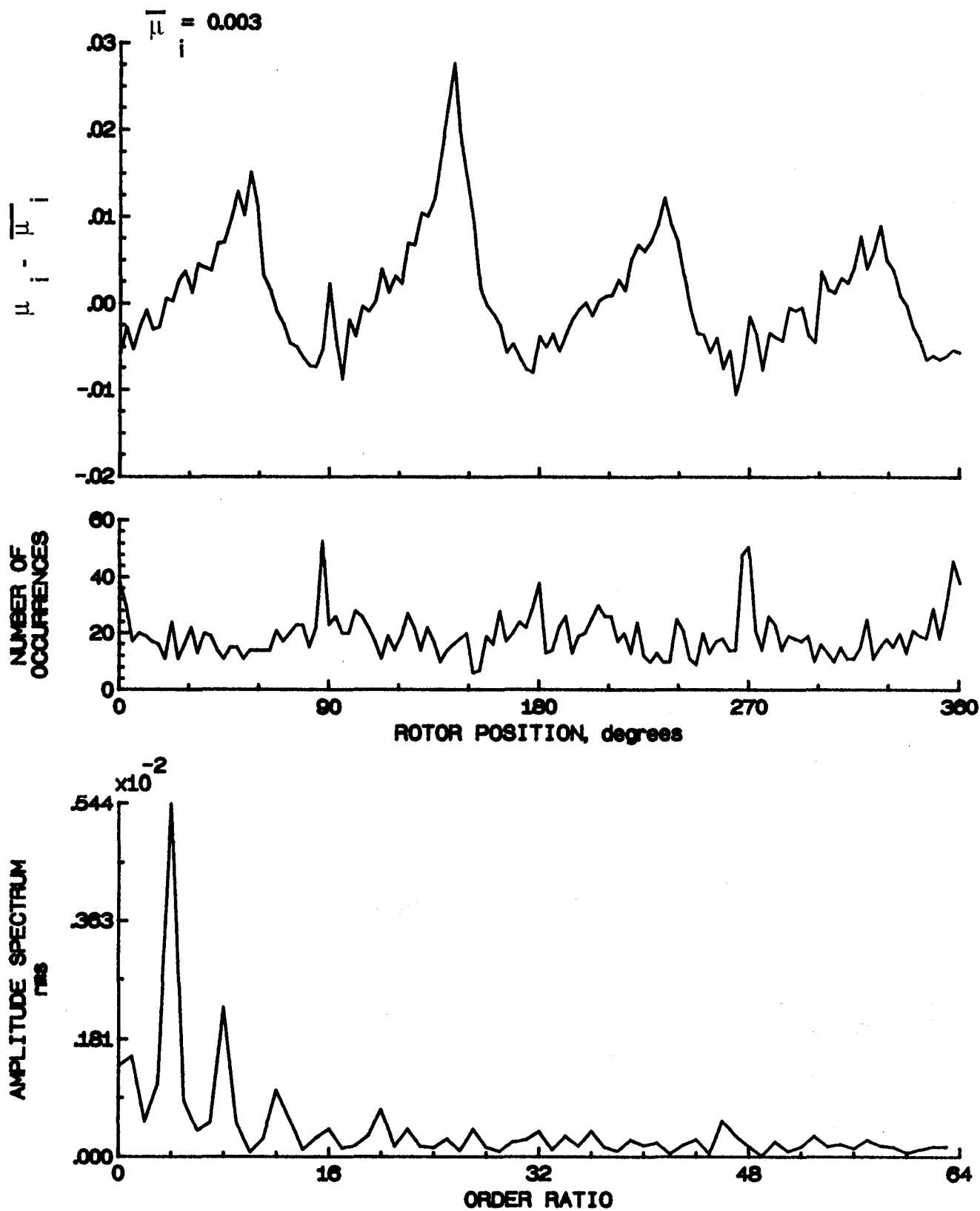


Figure 109.- Induced inflow velocity measured at 180 degrees and r/R of 0.78.

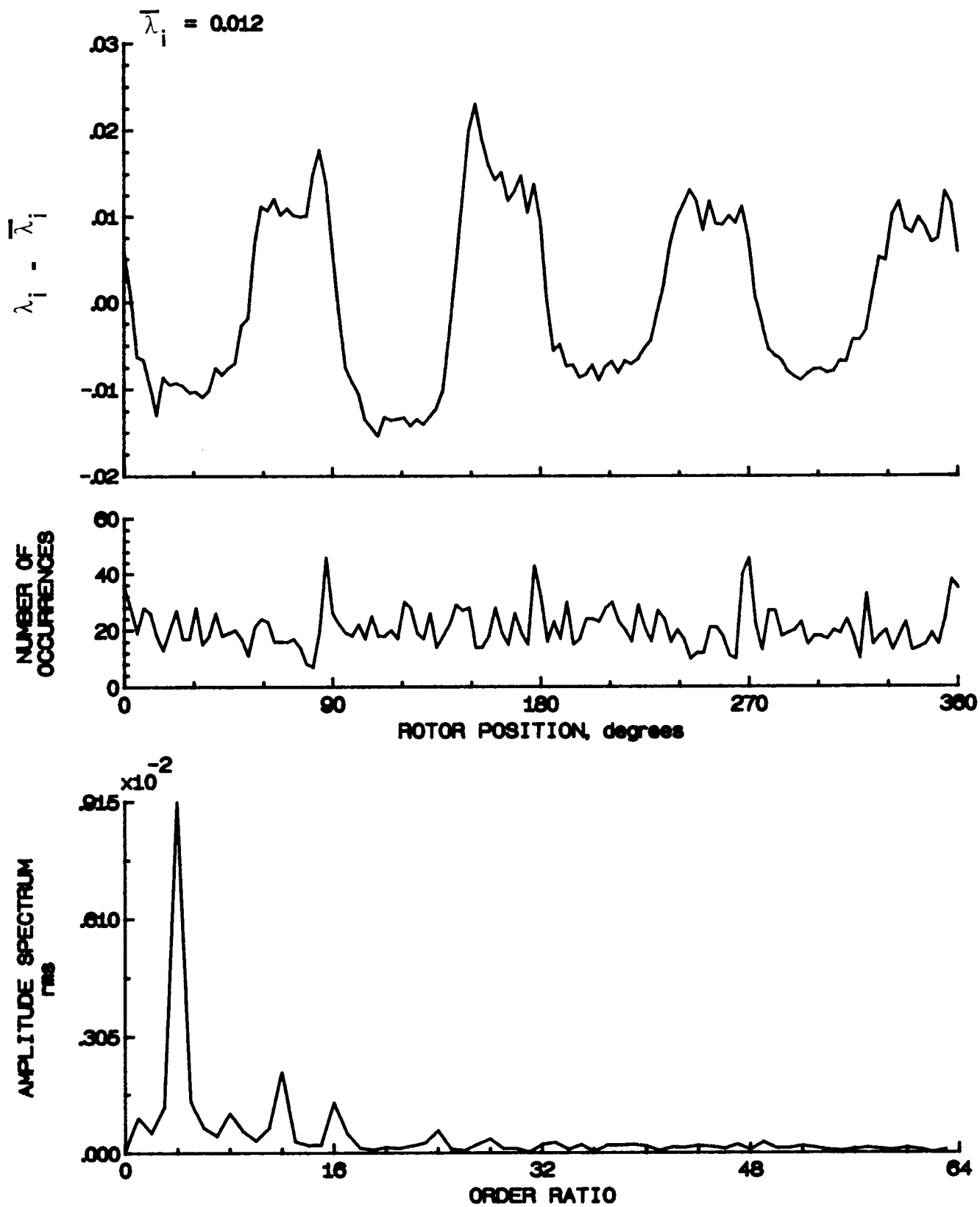


Figure 109.- Concluded.

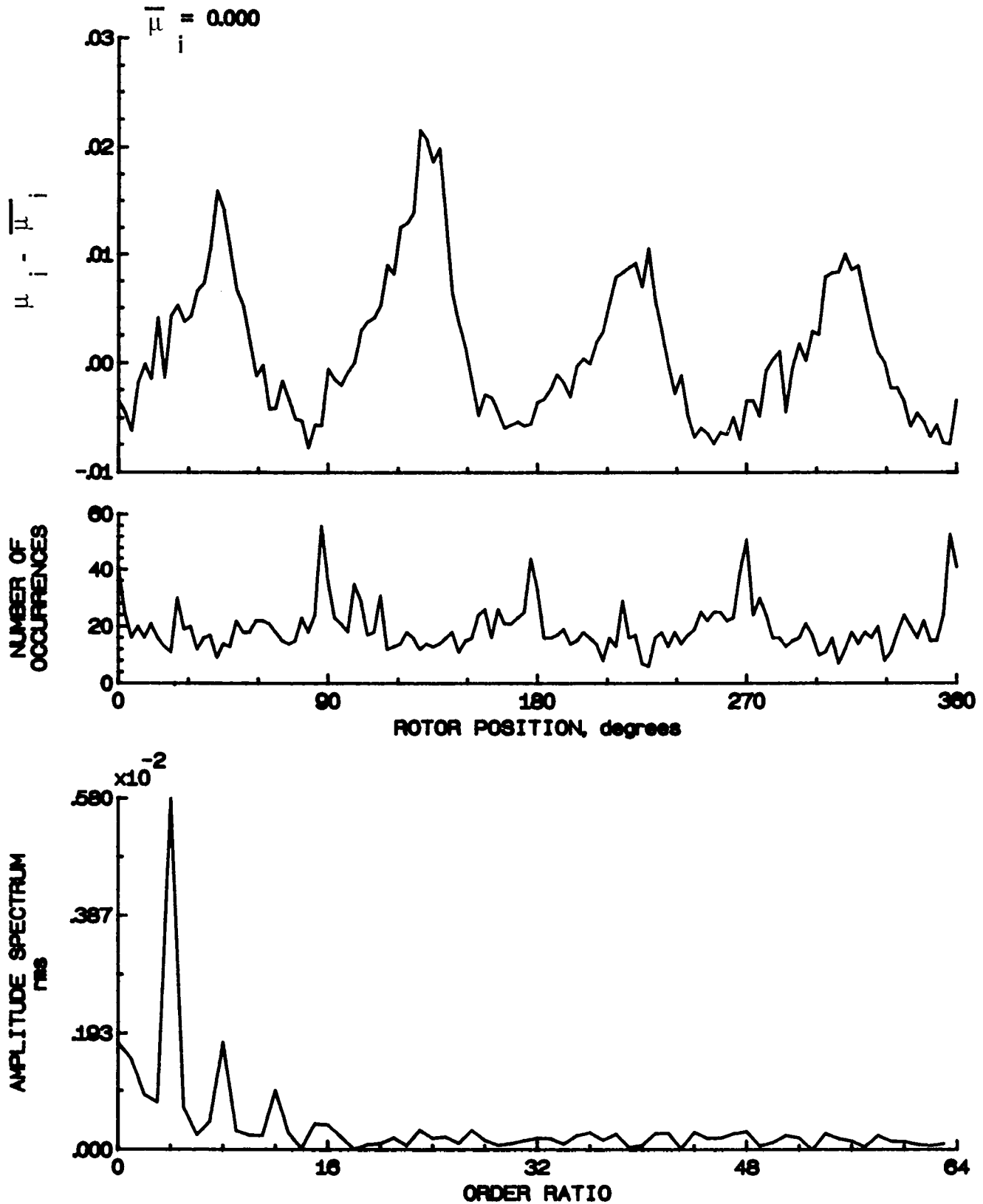


Figure 110.- Induced inflow velocity measured at 180 degrees and  $r/R$  of 0.82.

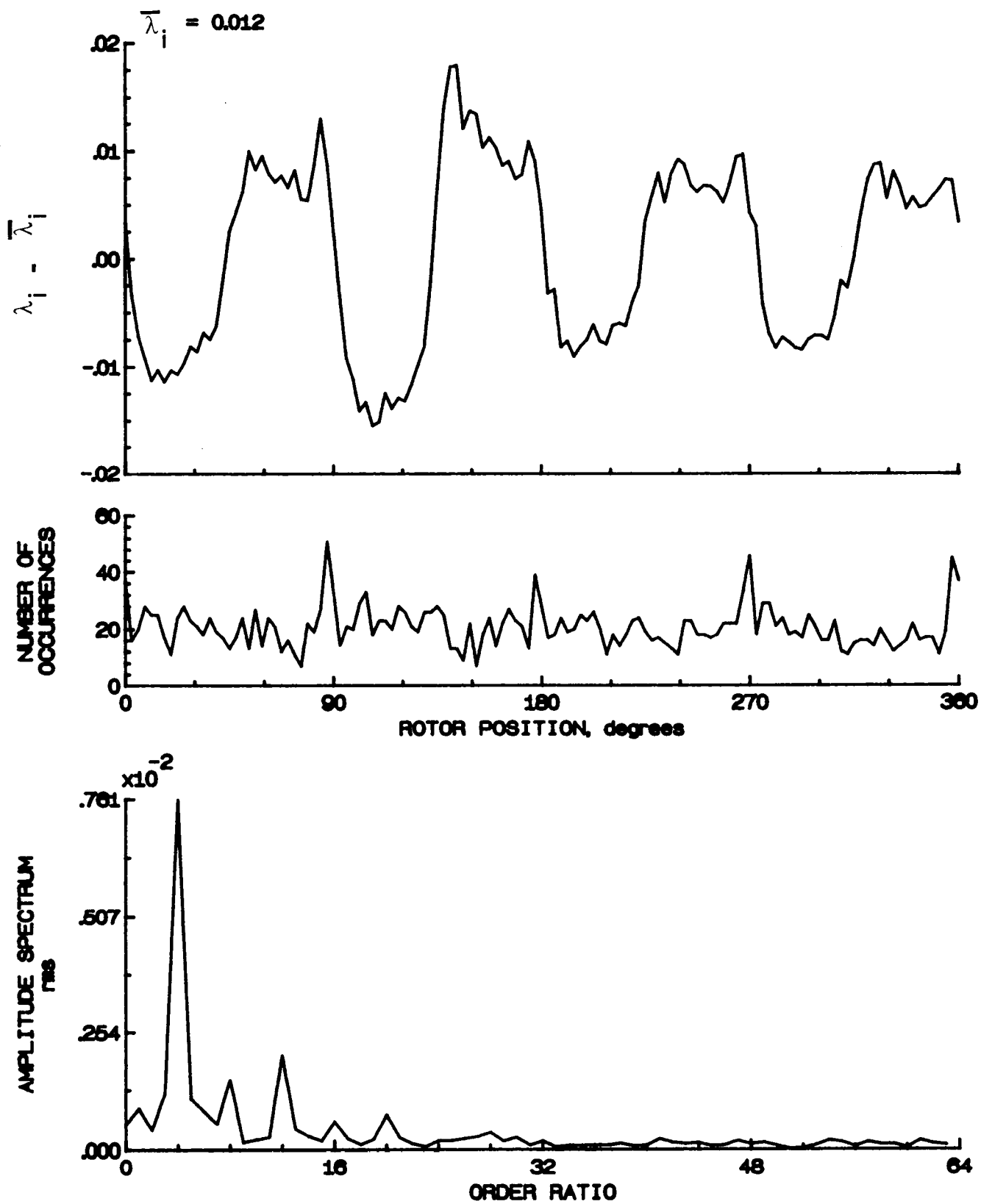


Figure 110.- Concluded.

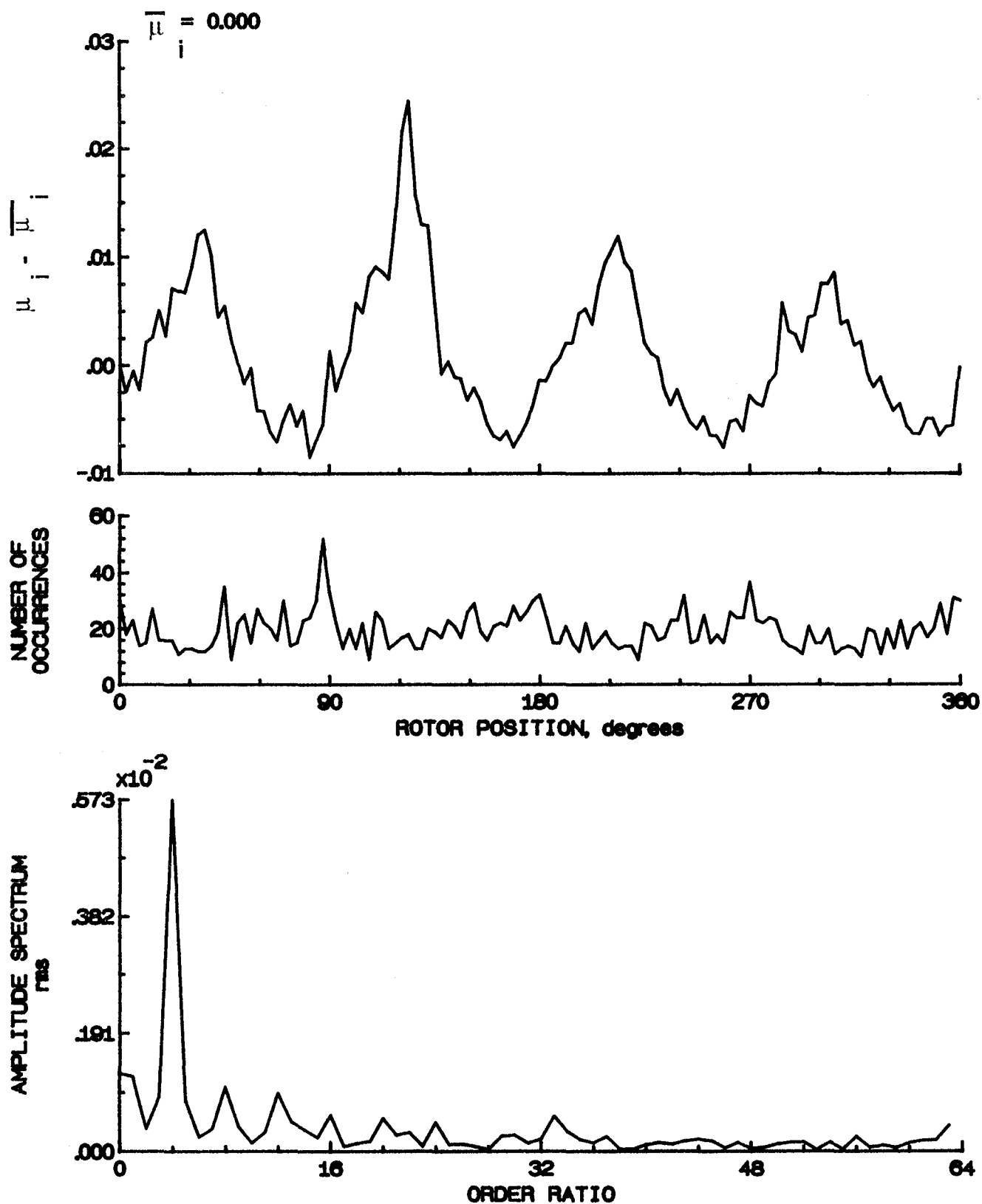


Figure 111.- Induced inflow velocity measured at 180 degrees and r/R of 0.86.

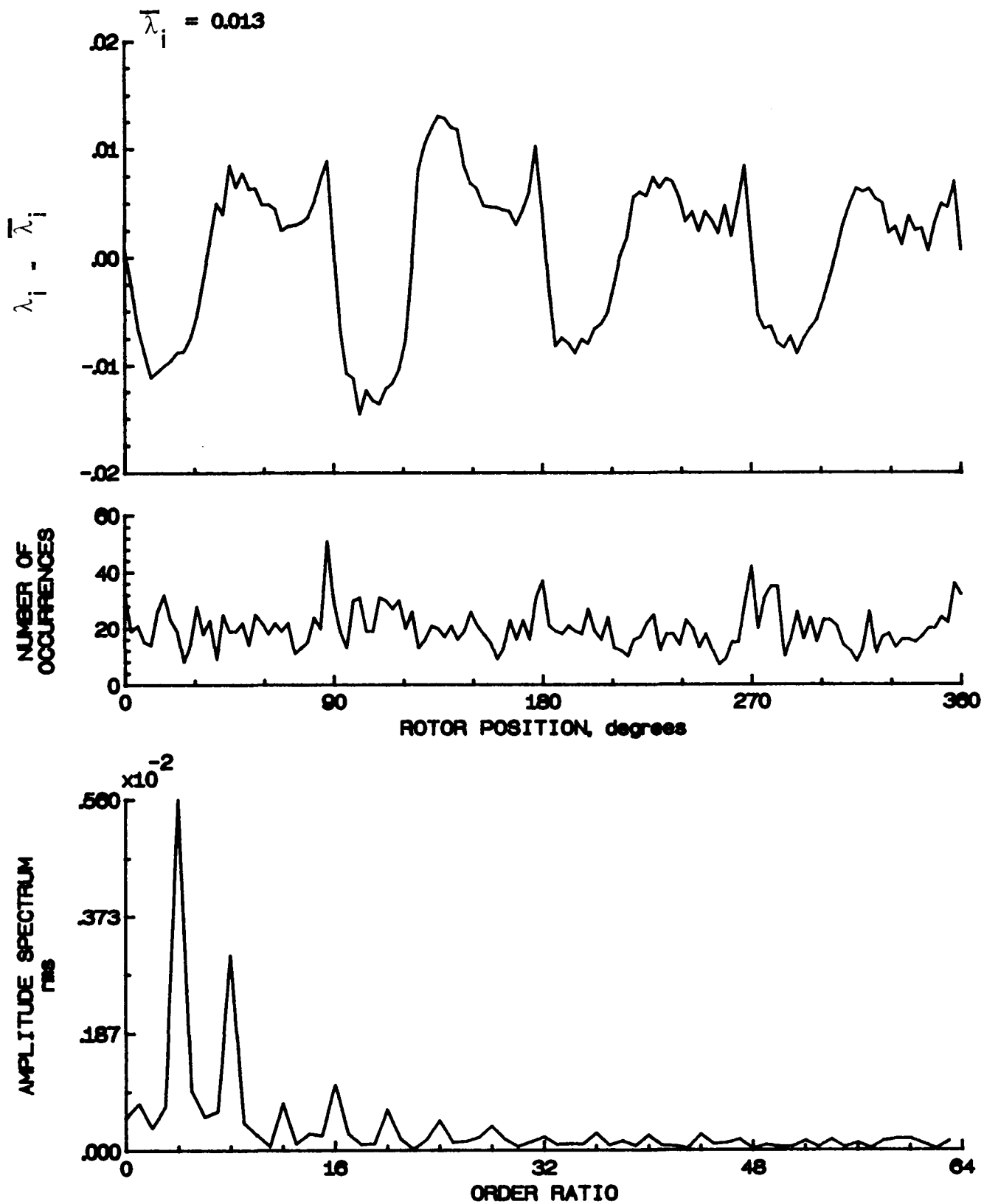


Figure 111.- Concluded.

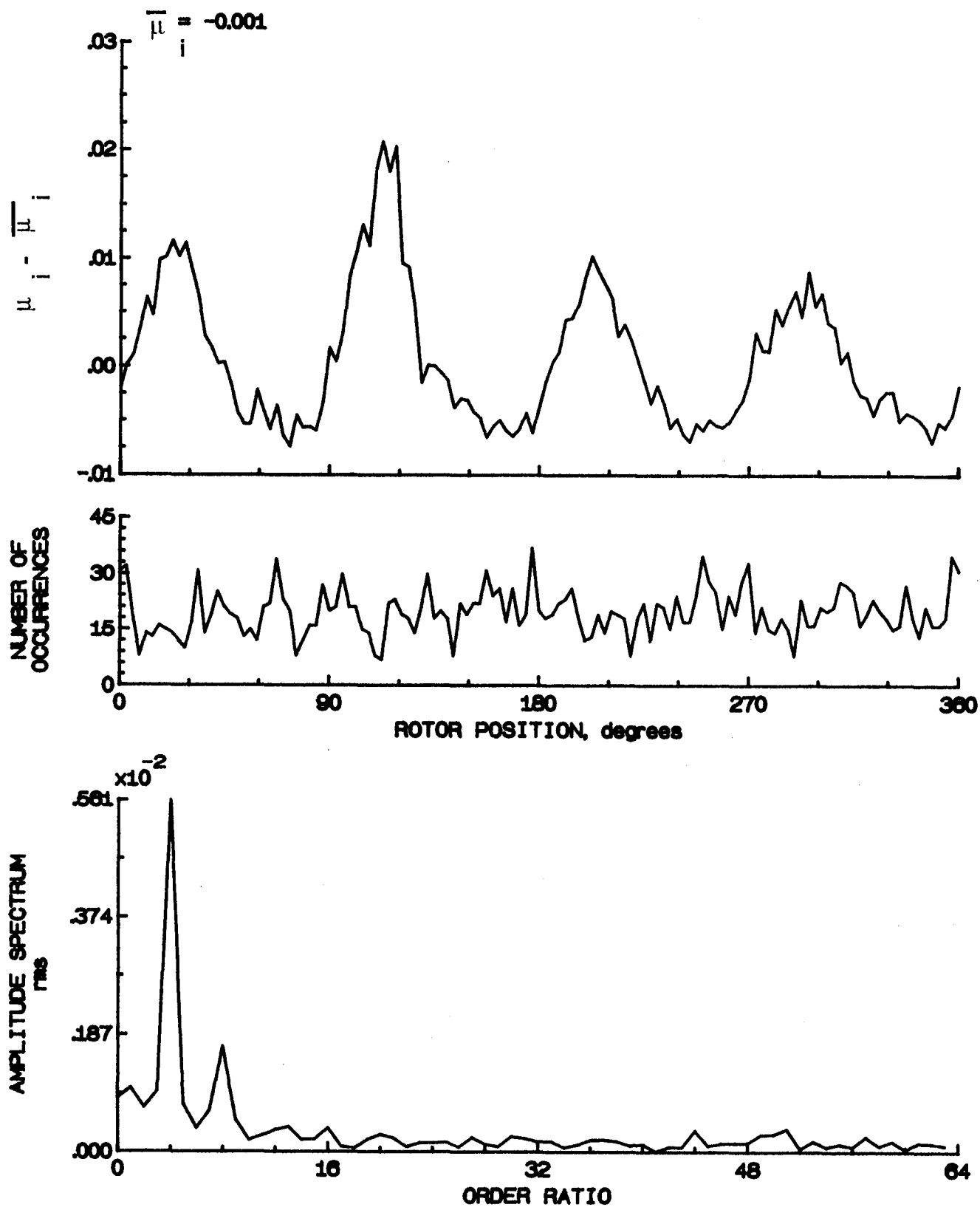


Figure 112.- Induced inflow velocity measured at 180 degrees and r/R of 0.90.



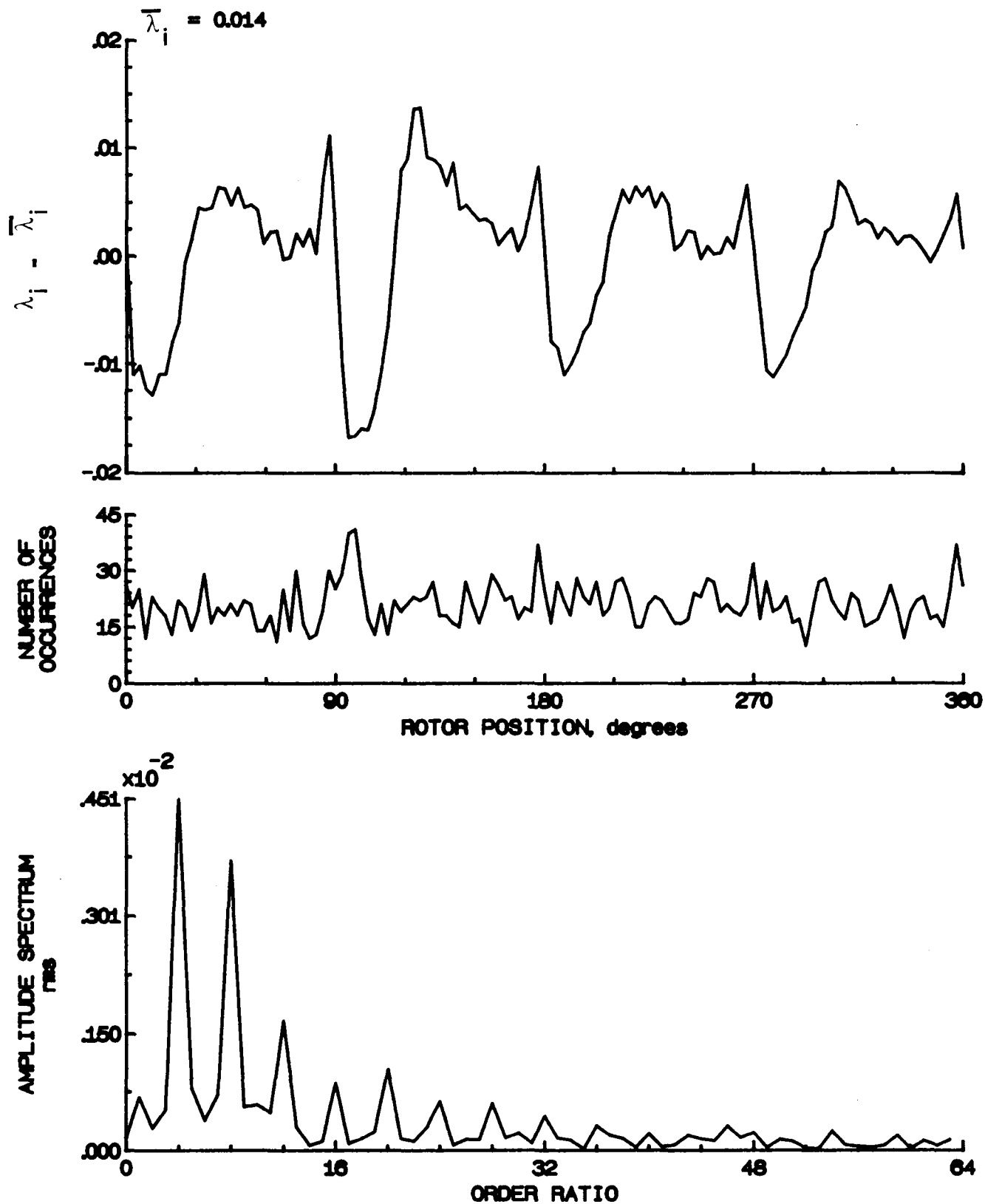


Figure 112.- Concluded.

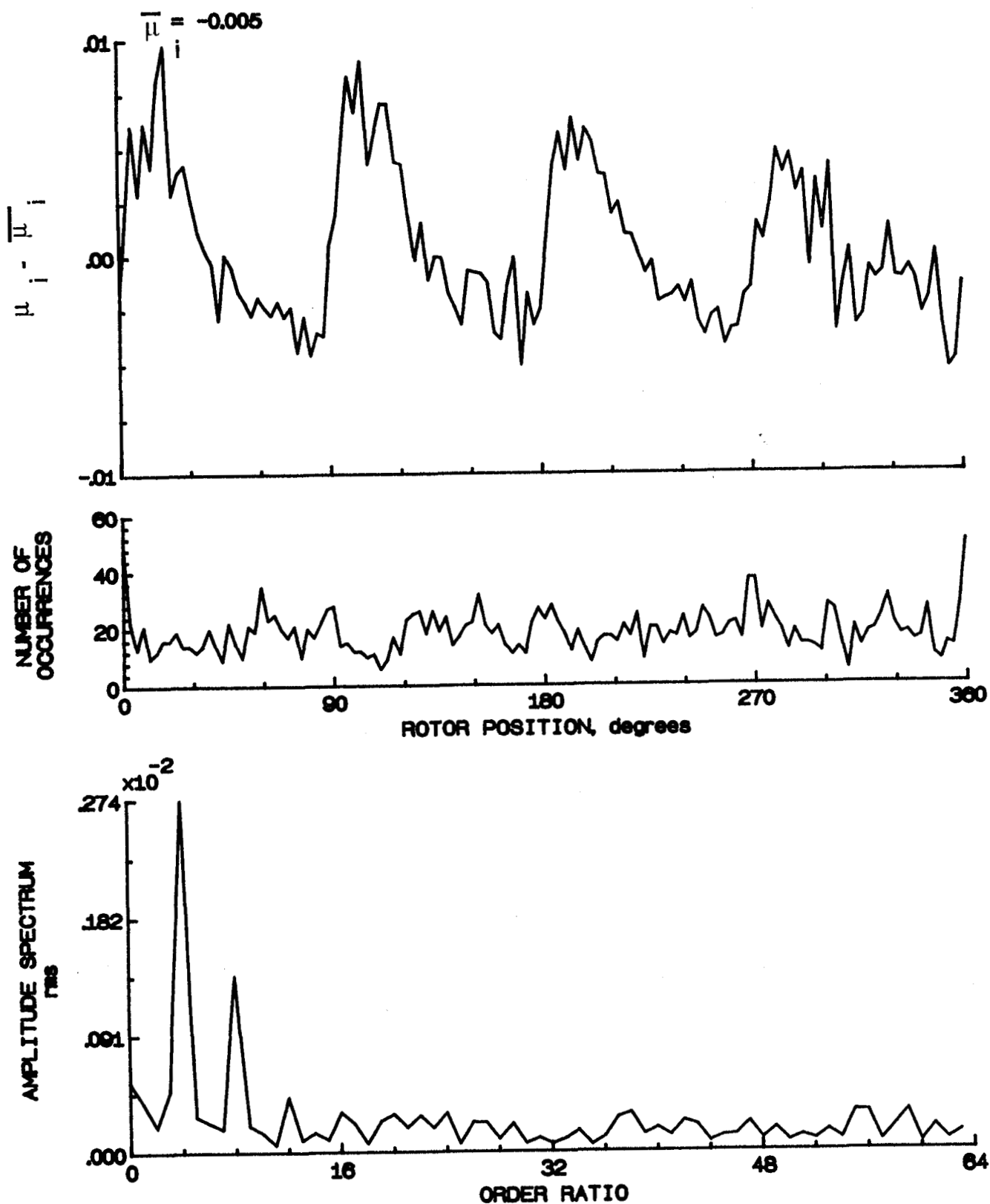


Figure 113.- Induced inflow velocity measured at 180 degrees and  $r/R$  of 0.94.

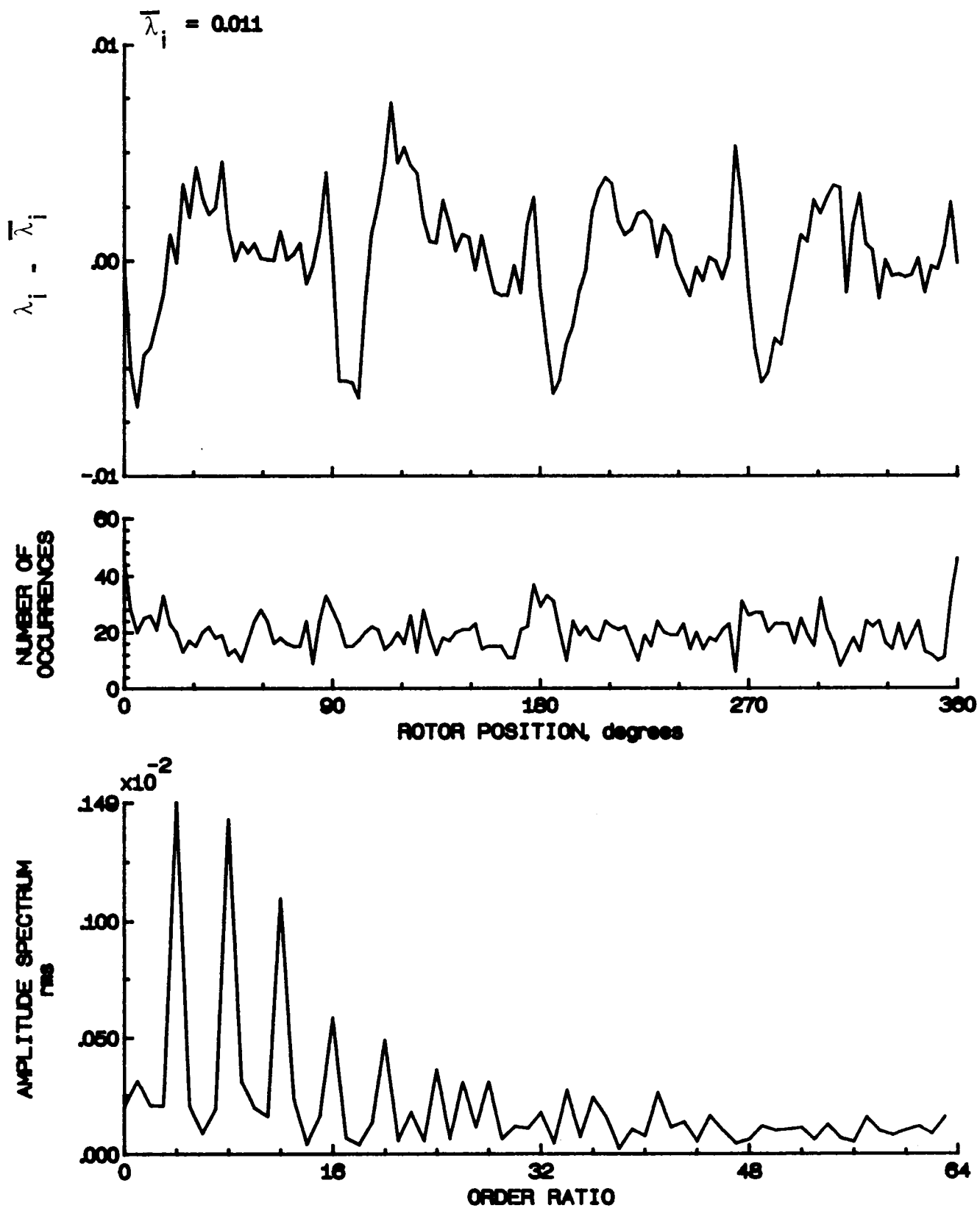


Figure 113.- Concluded.

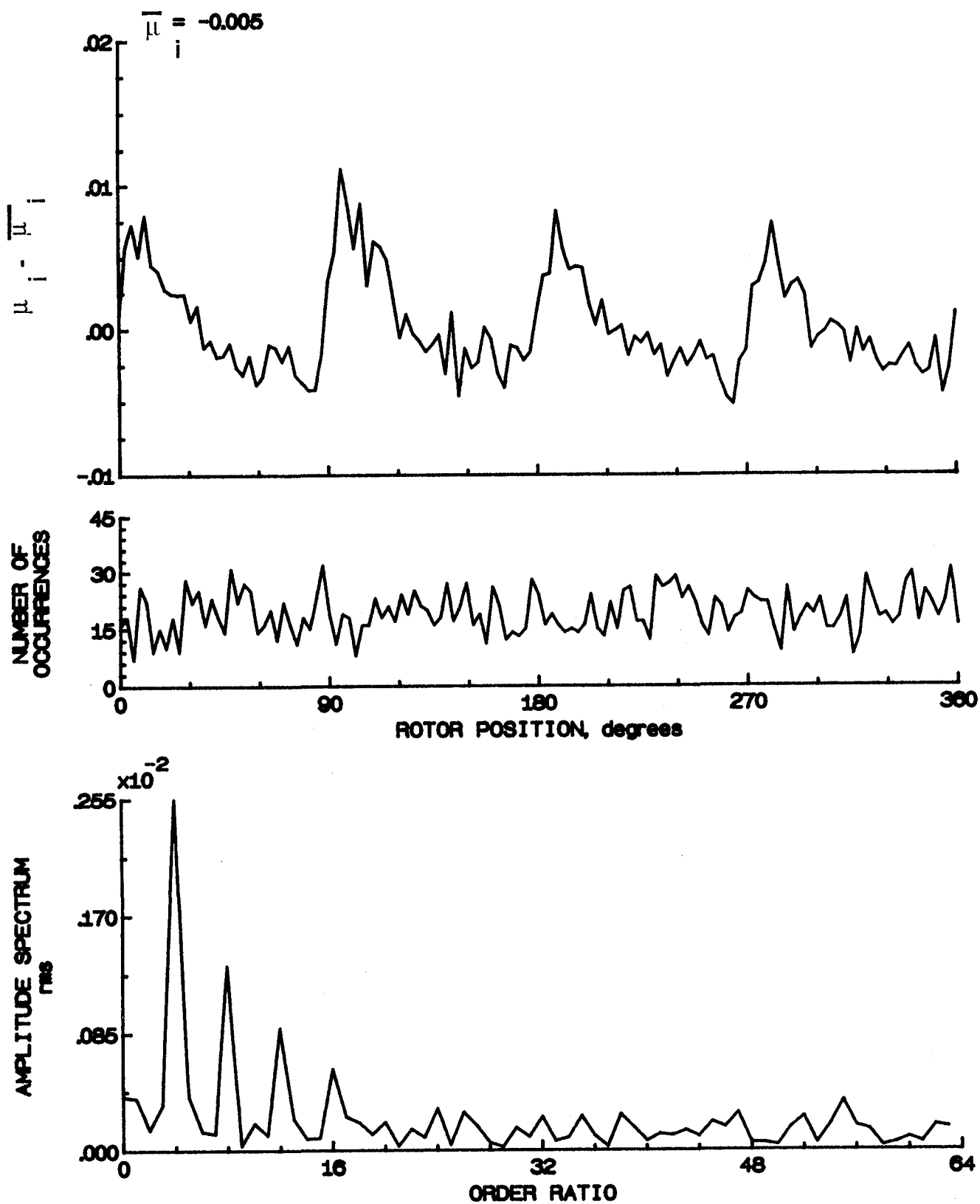


Figure 114.- Induced inflow velocity measured at 180 degrees and  $r/R$  of 0.98.

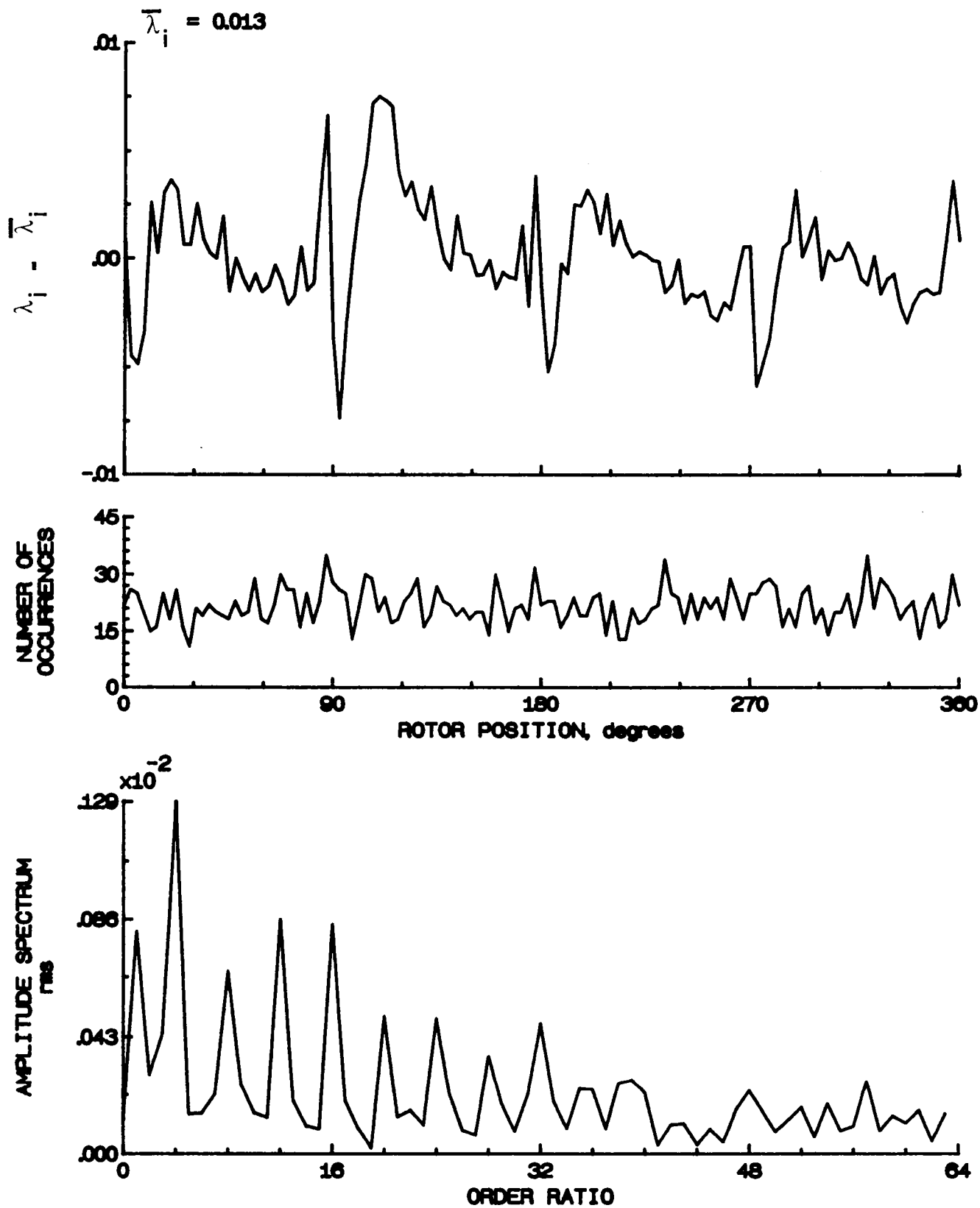


Figure 114.- Concluded.

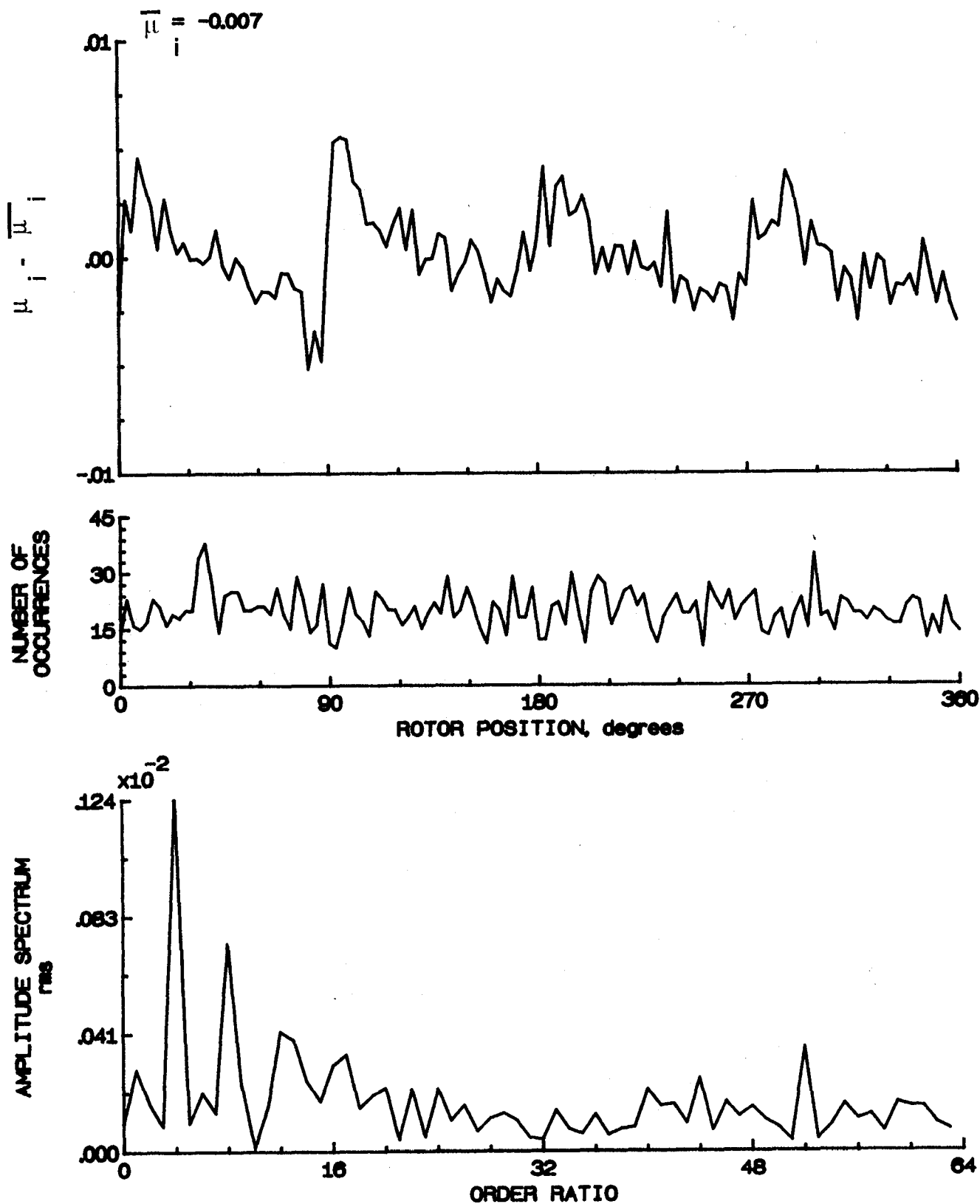


Figure 115.- Induced inflow velocity measured at 180 degrees and r/R of 1.02.

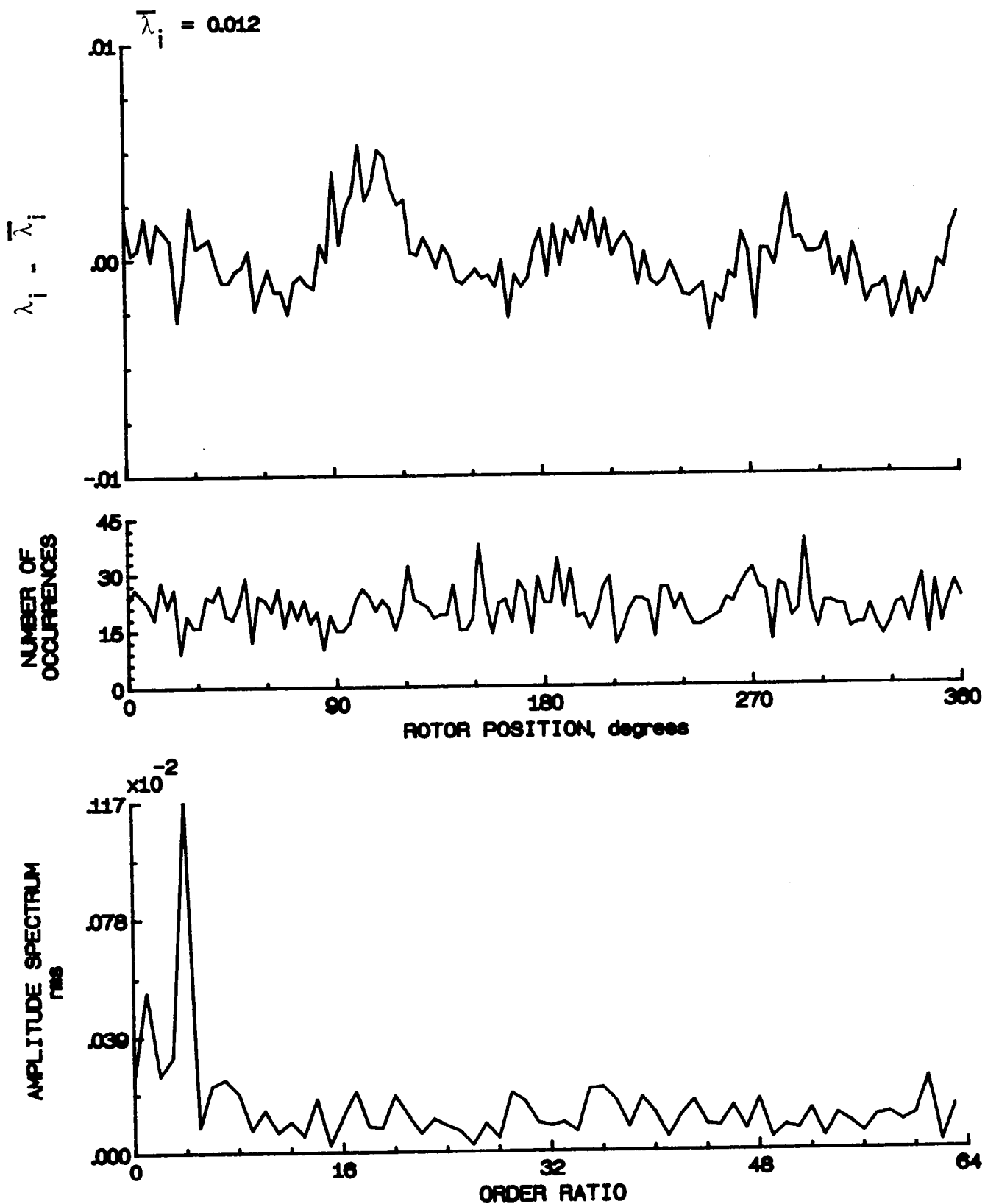


Figure 115.- Concluded.

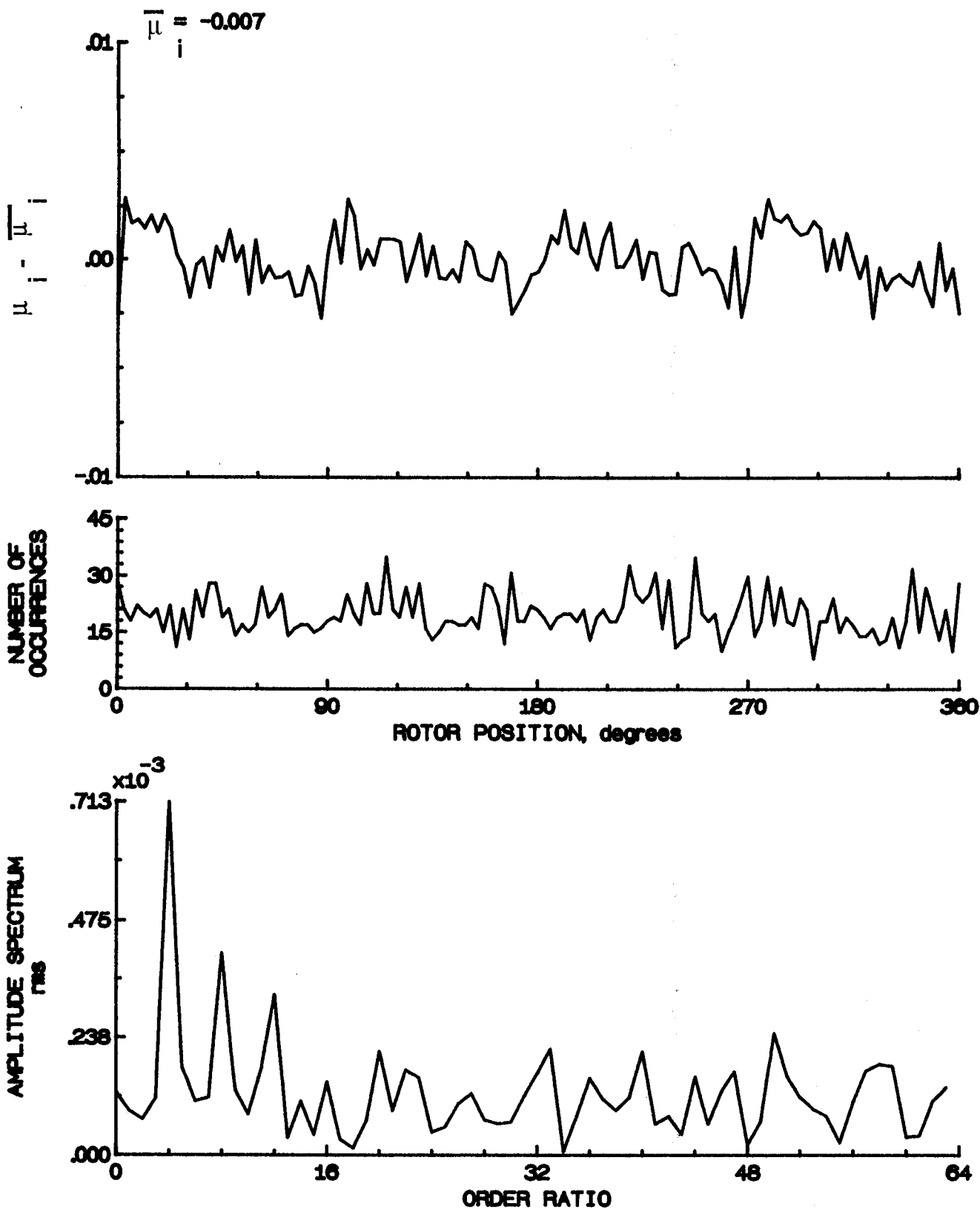


Figure 116.- Induced inflow velocity measured at 180 degrees and  $r/R$  of 1.04.



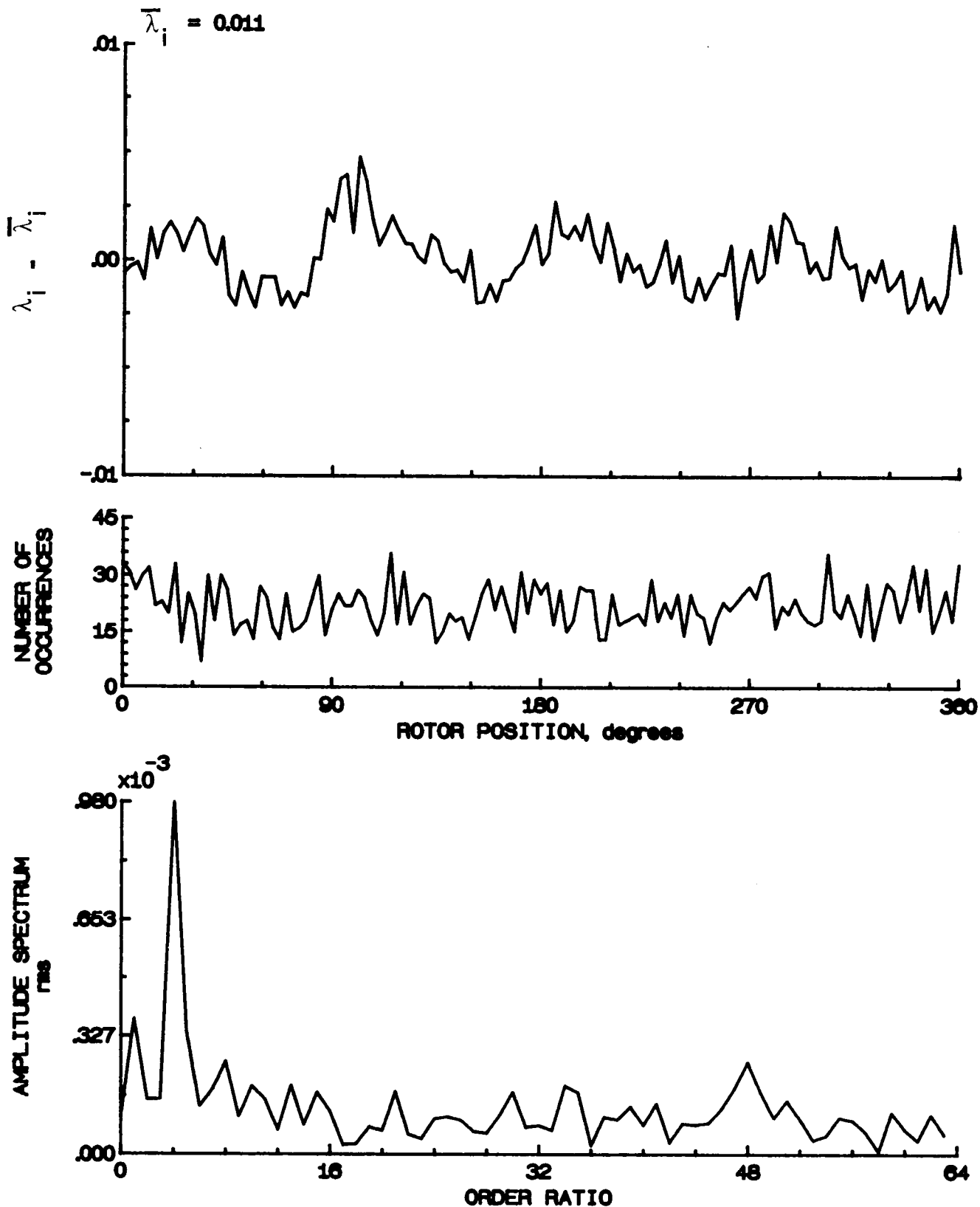


Figure 116.- Concluded.

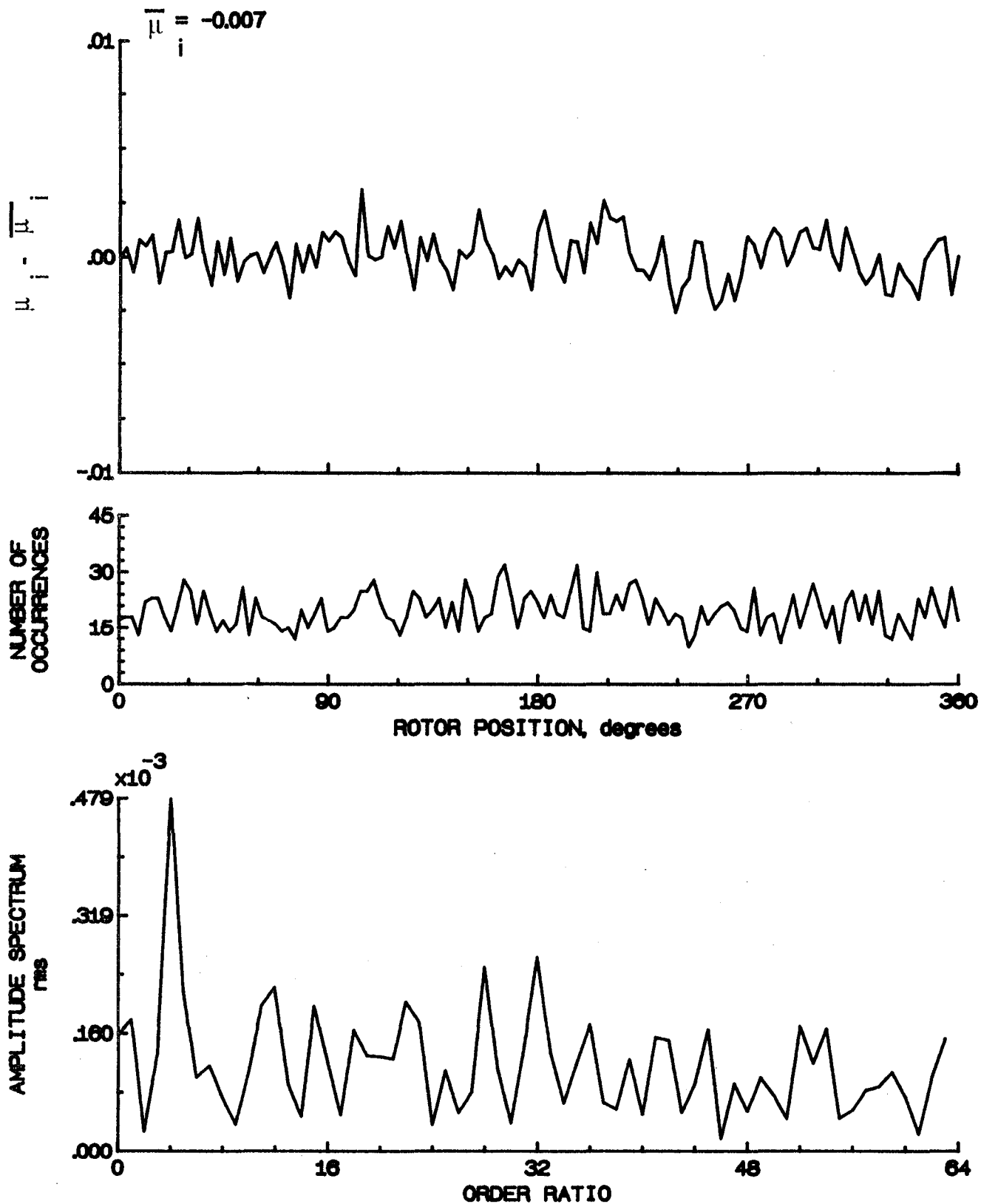


Figure 117.- Induced inflow velocity measured at 180 degrees and r/R of 1.10.

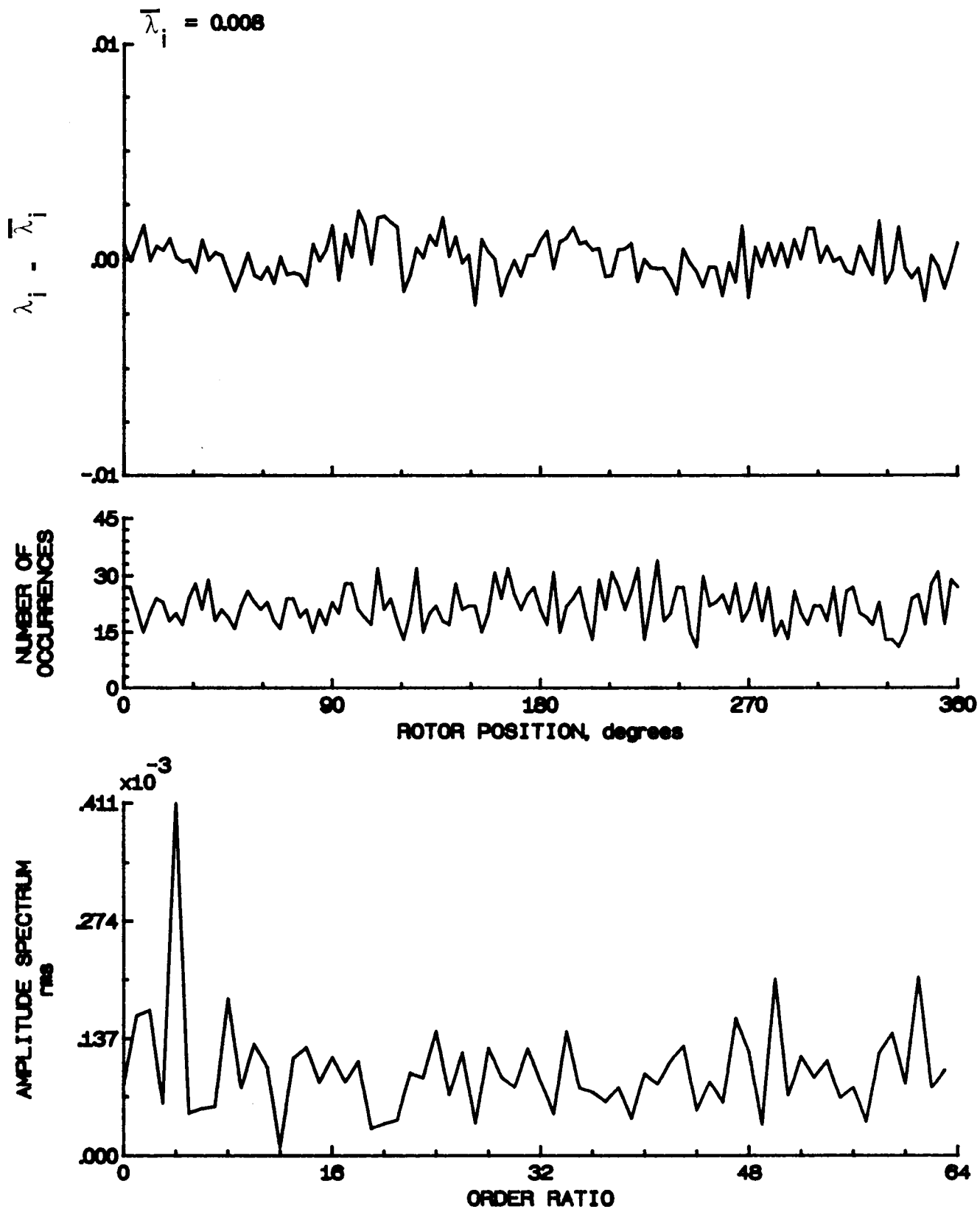


Figure 117.- Concluded.

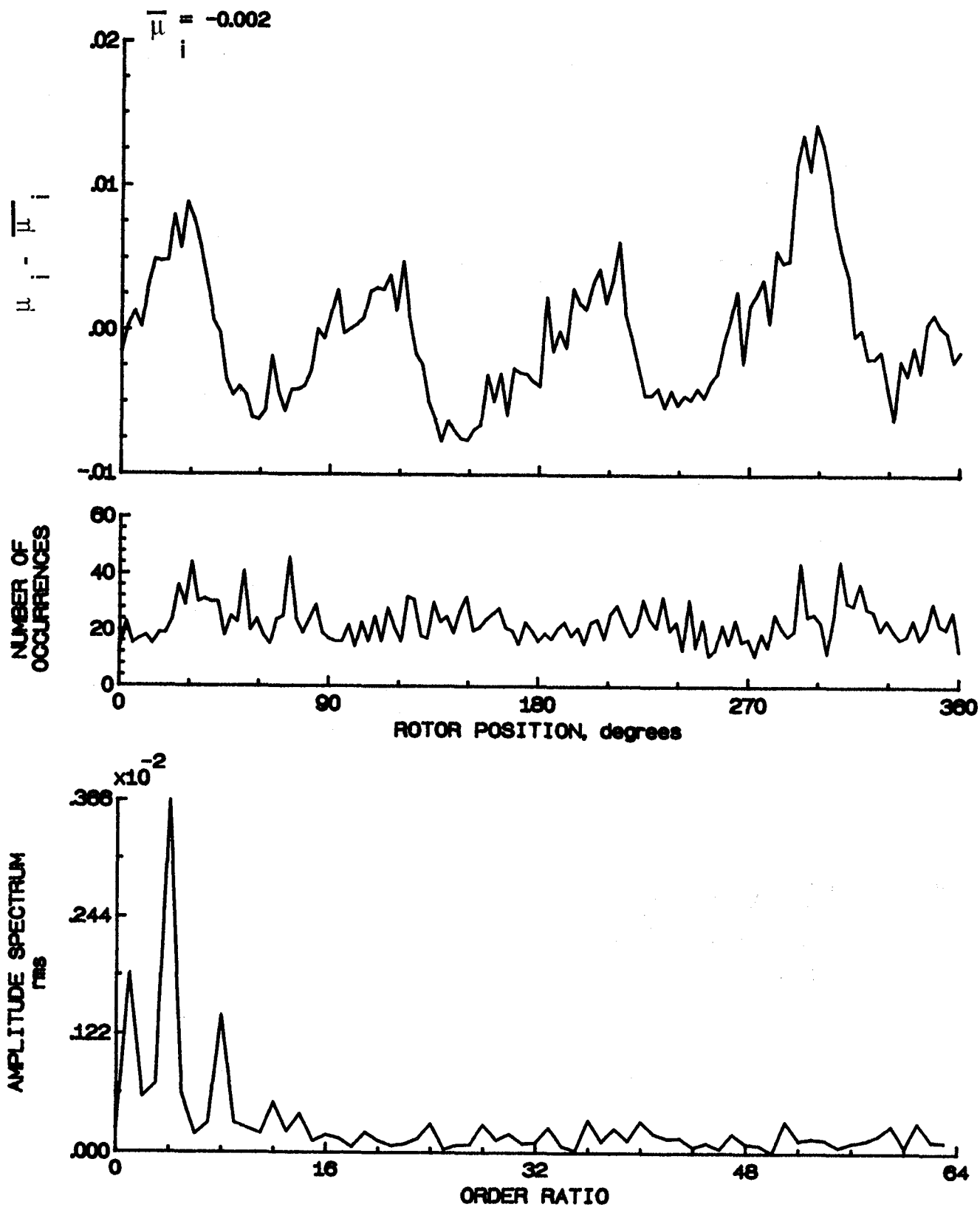


Figure 118.- Induced inflow velocity measured at 210 degrees and r/R of 0.20.

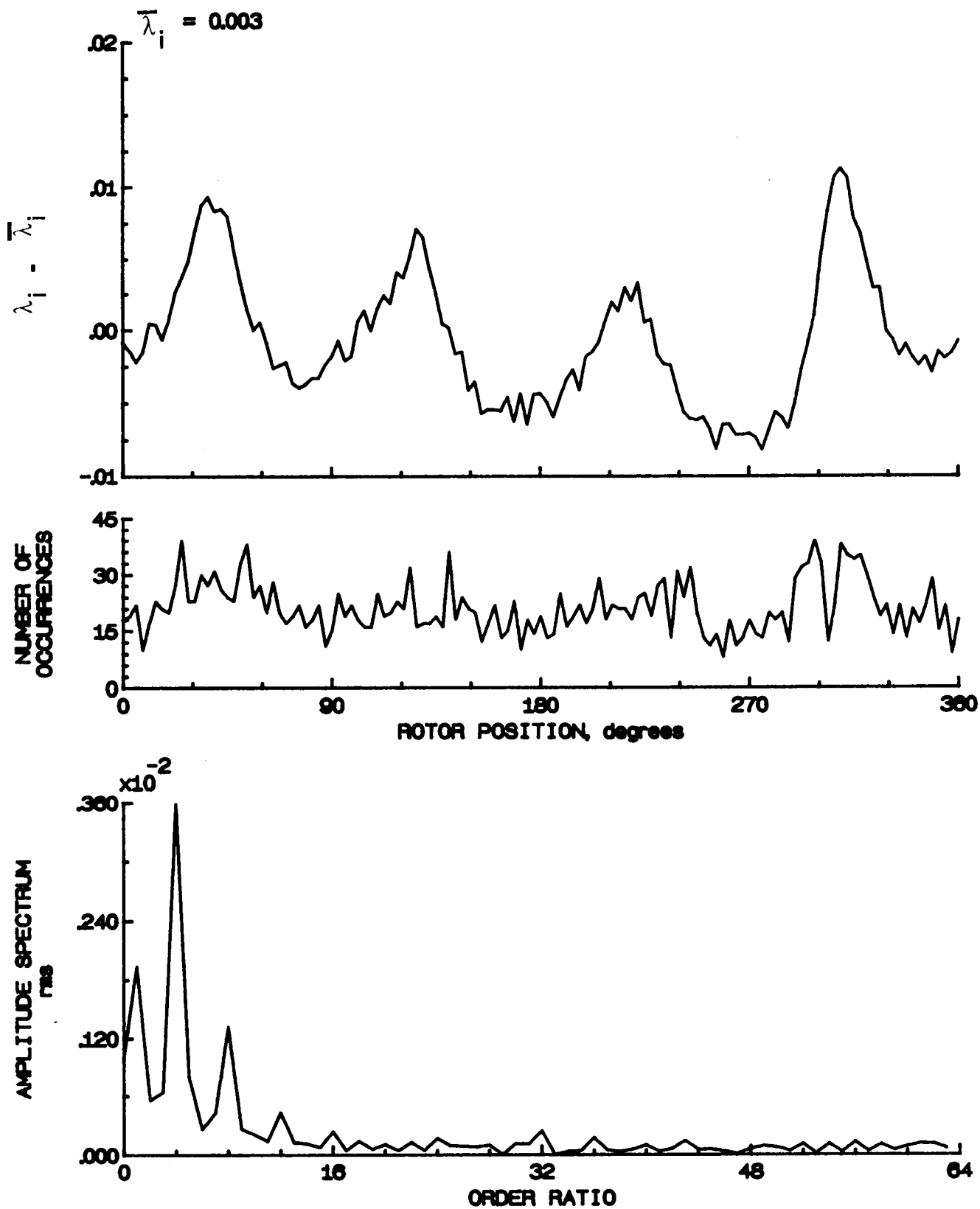


Figure 118.- Concluded.

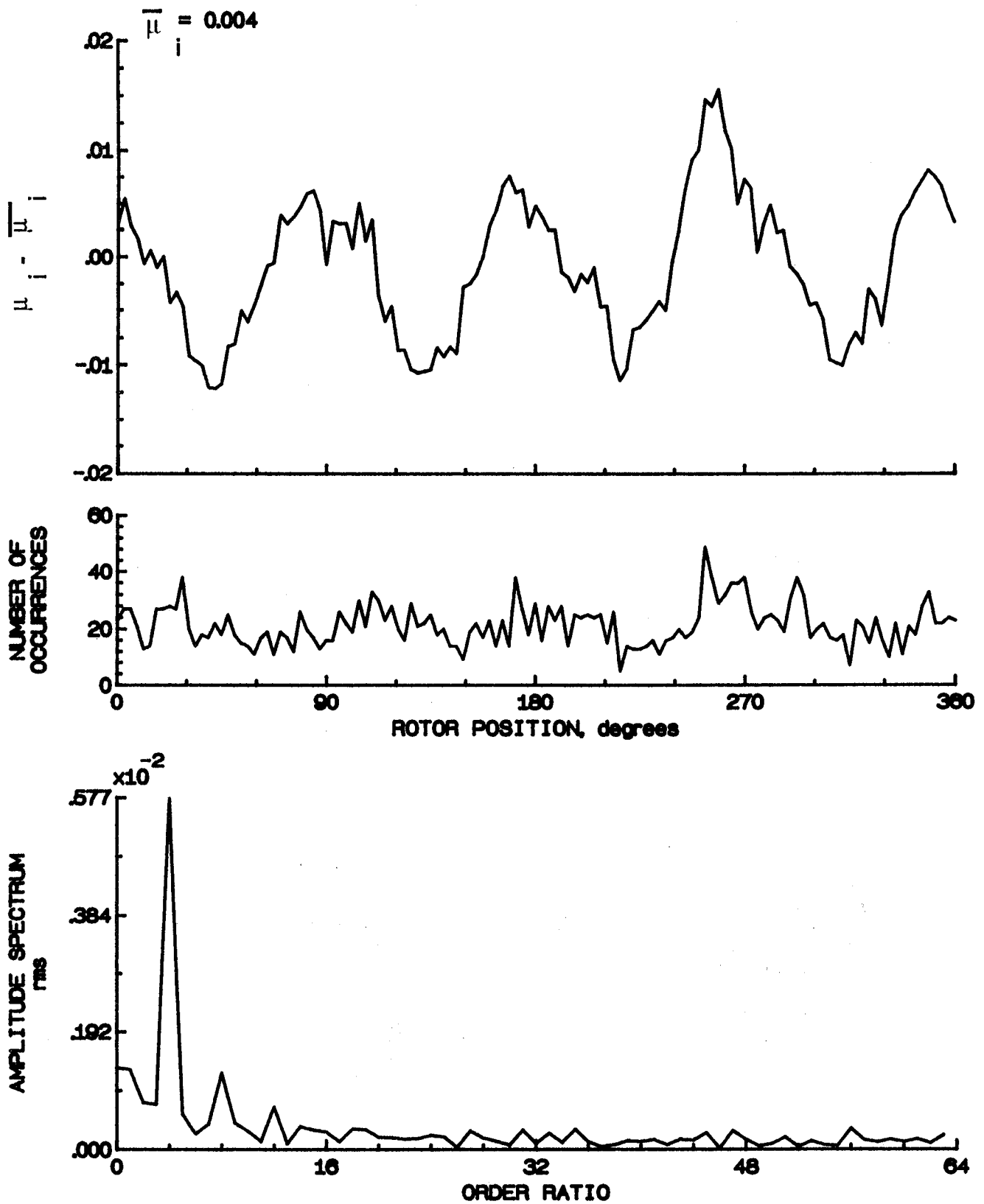


Figure 119.- Induced inflow velocity measured at 210 degrees and r/R of 0.40.

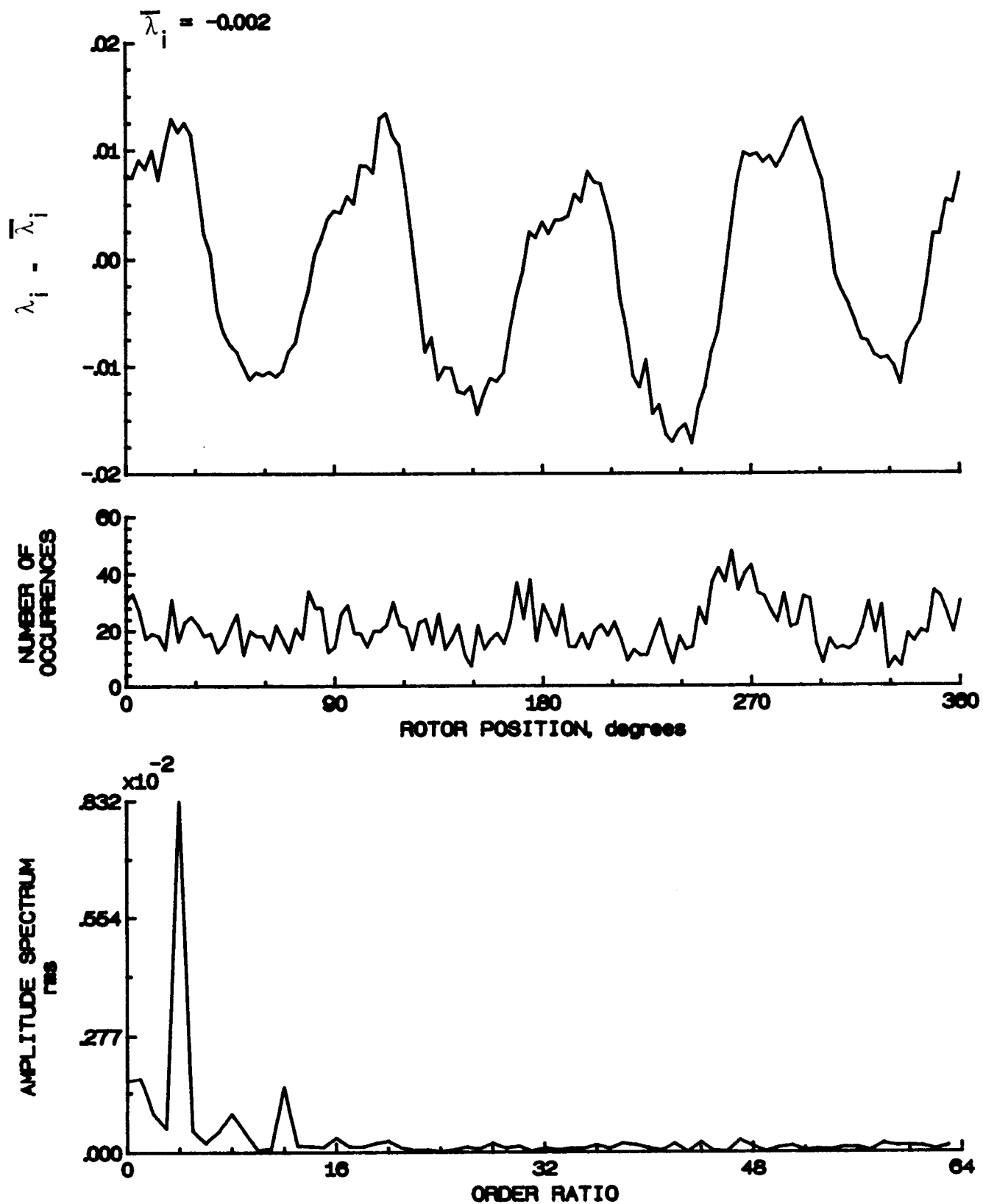


Figure 119.- Concluded.

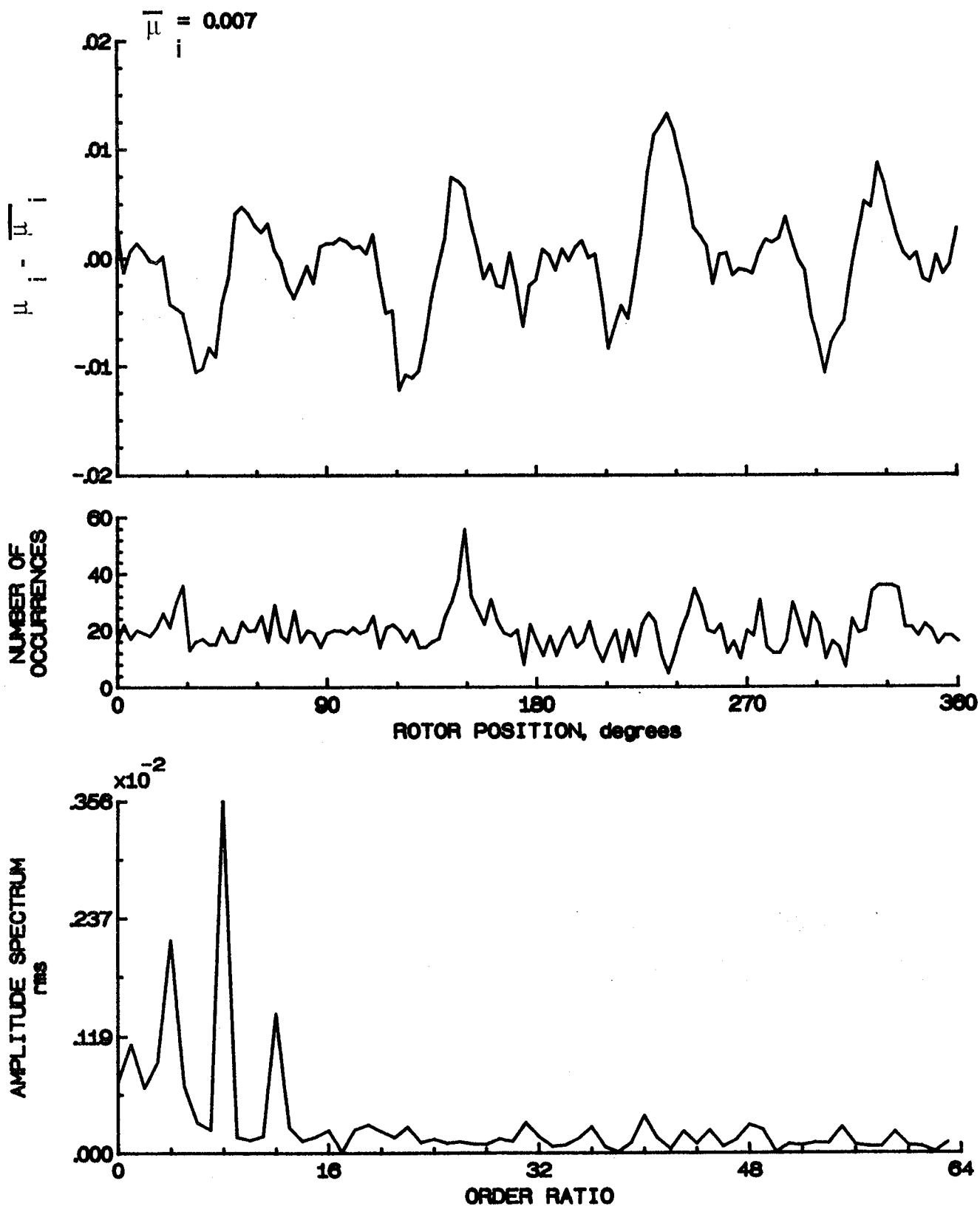


Figure 120.- Induced inflow velocity measured at 210 degrees and r/R of 0.50.



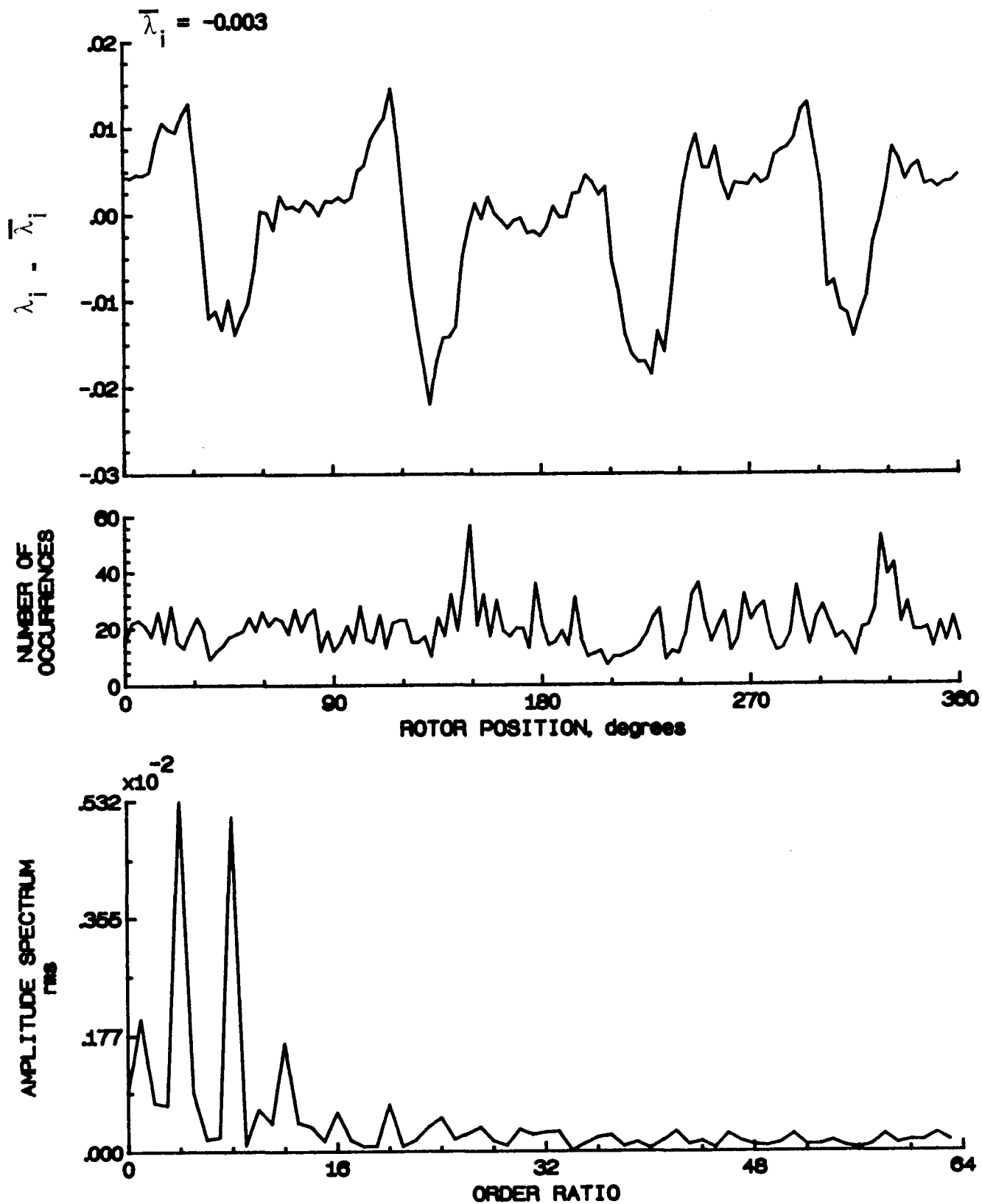


Figure 120.- Concluded.

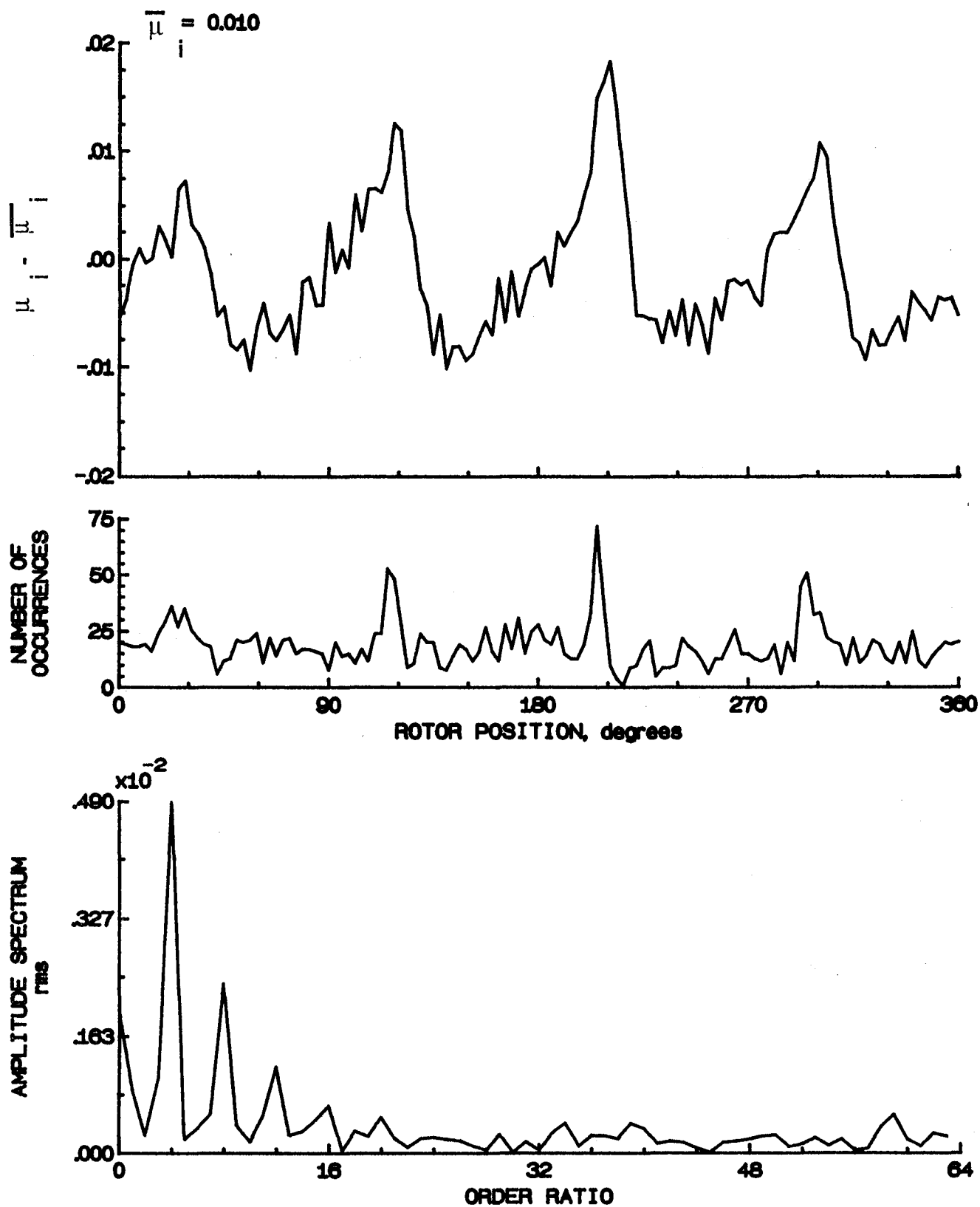


Figure 121.- Induced inflow velocity measured at 210 degrees and r/R of 0.60.

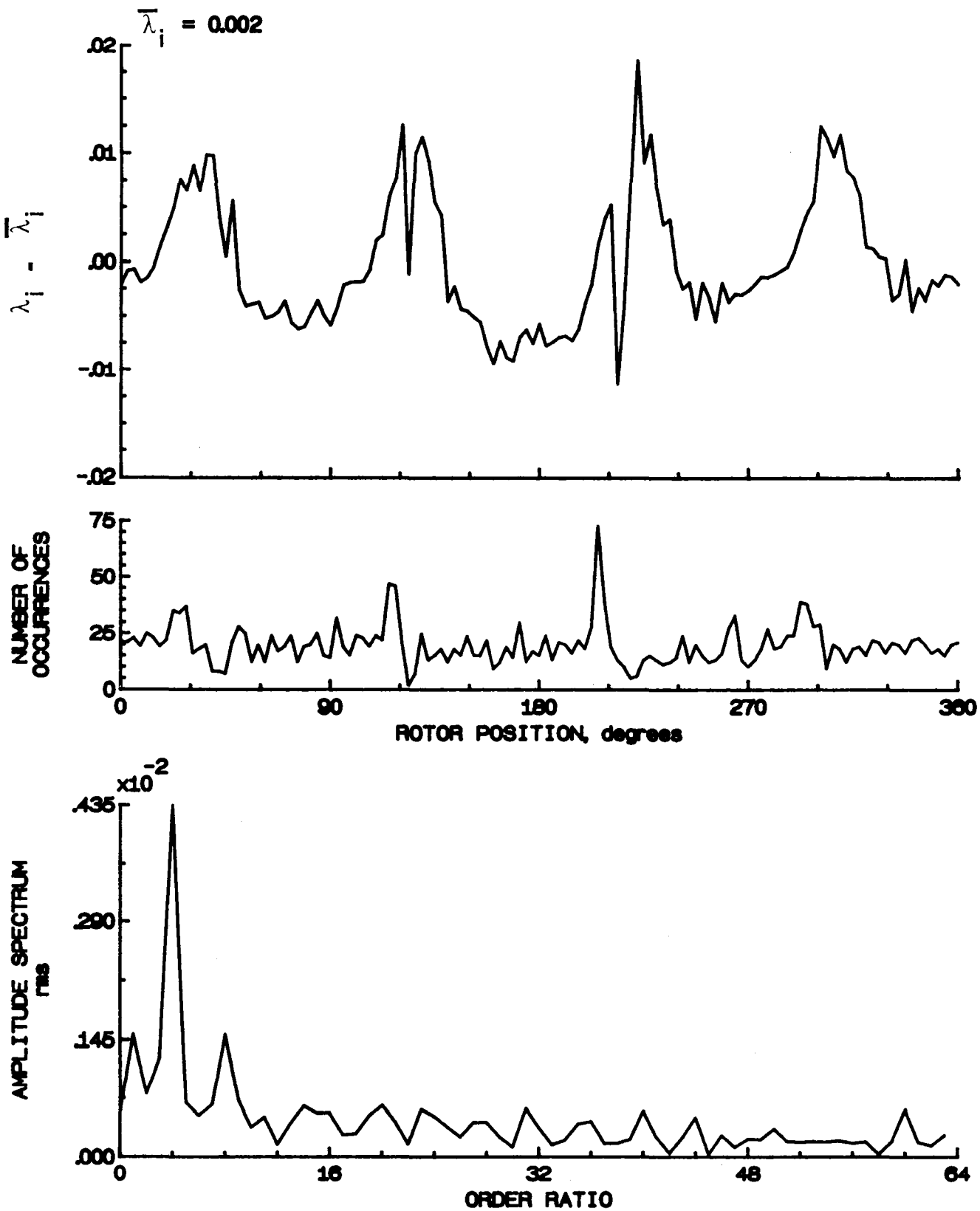


Figure 121- Concluded.

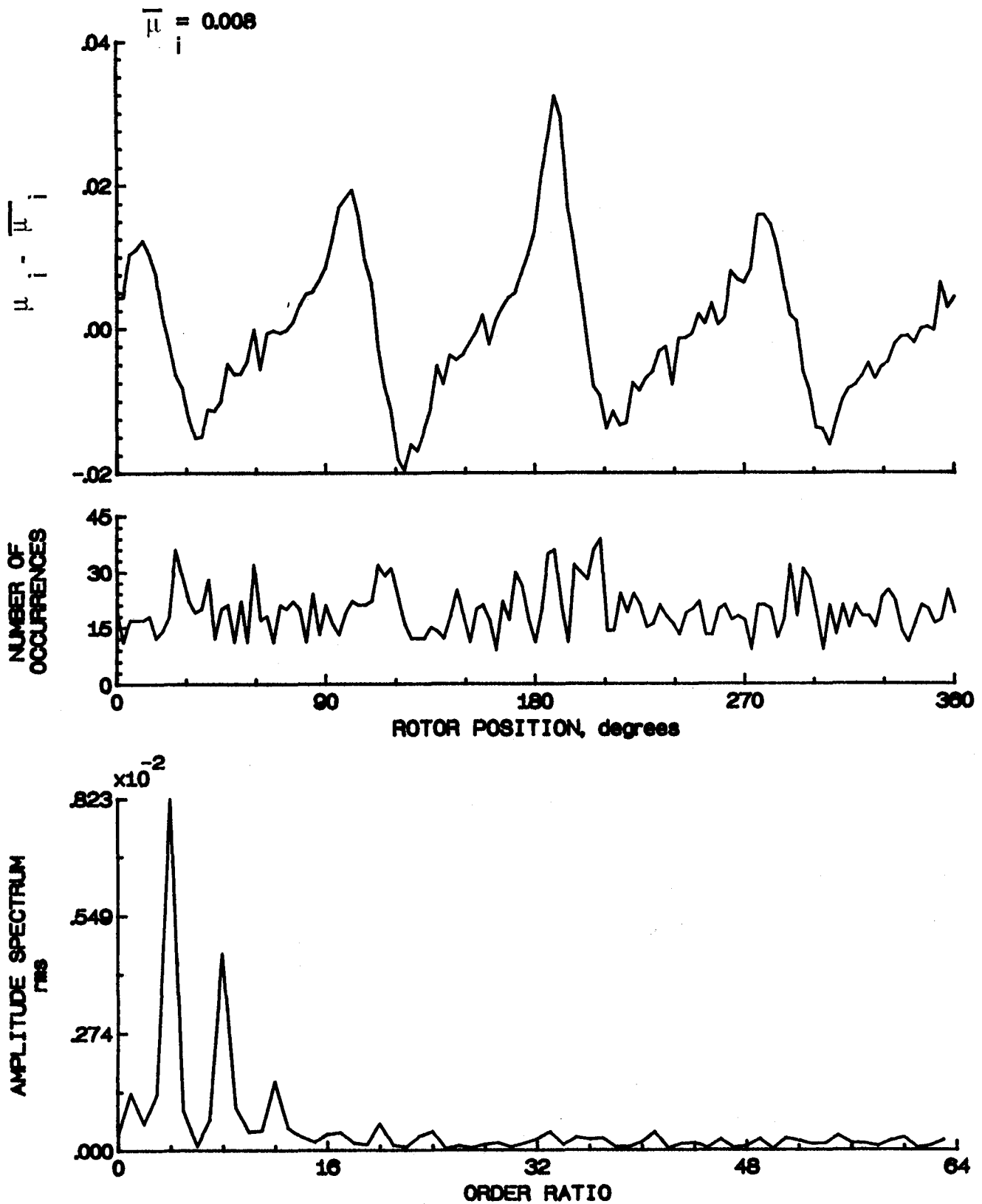


Figure 122.- Induced inflow velocity measured at 210 degrees and r/R of 0.70.

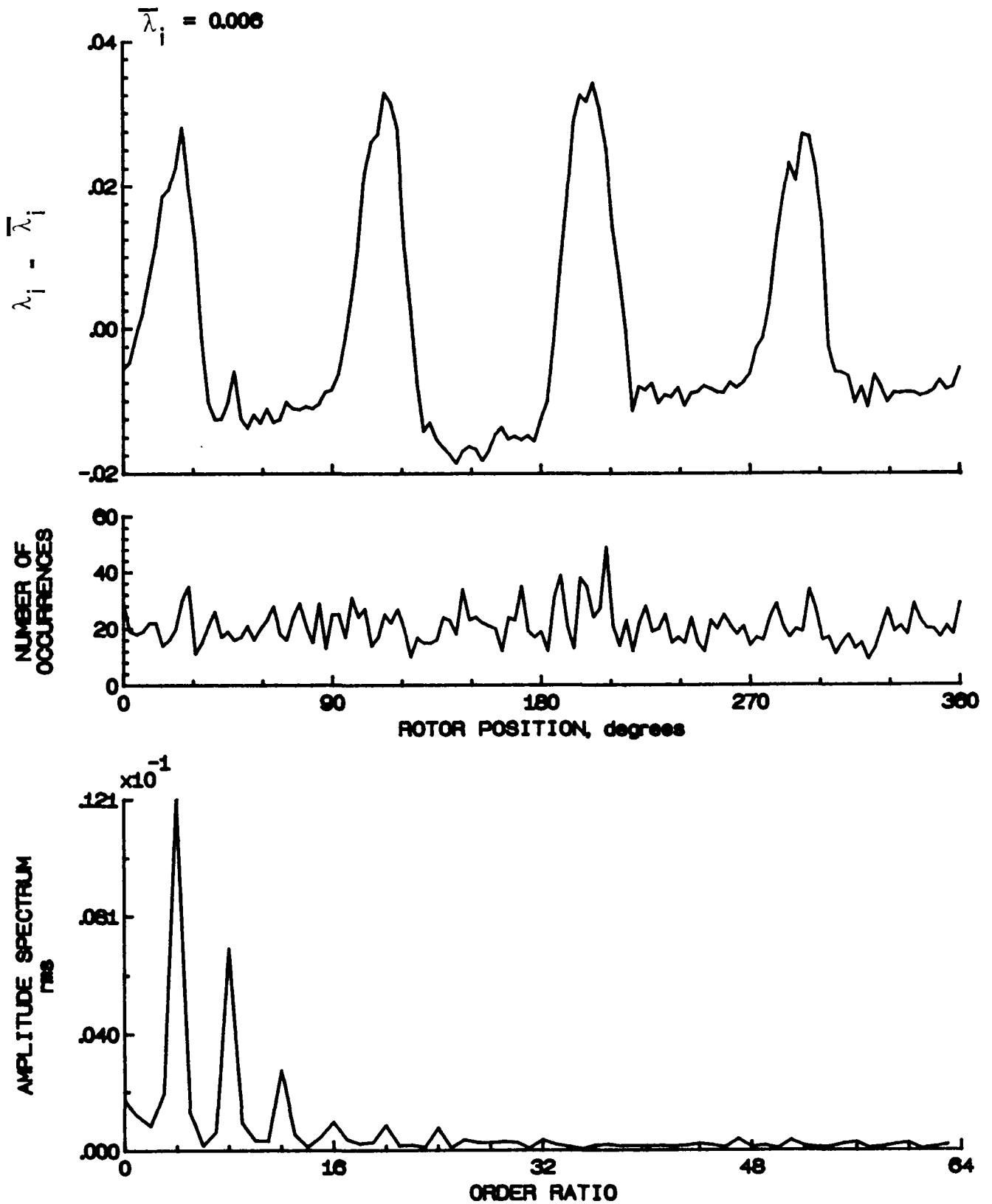


Figure 122.- Concluded.

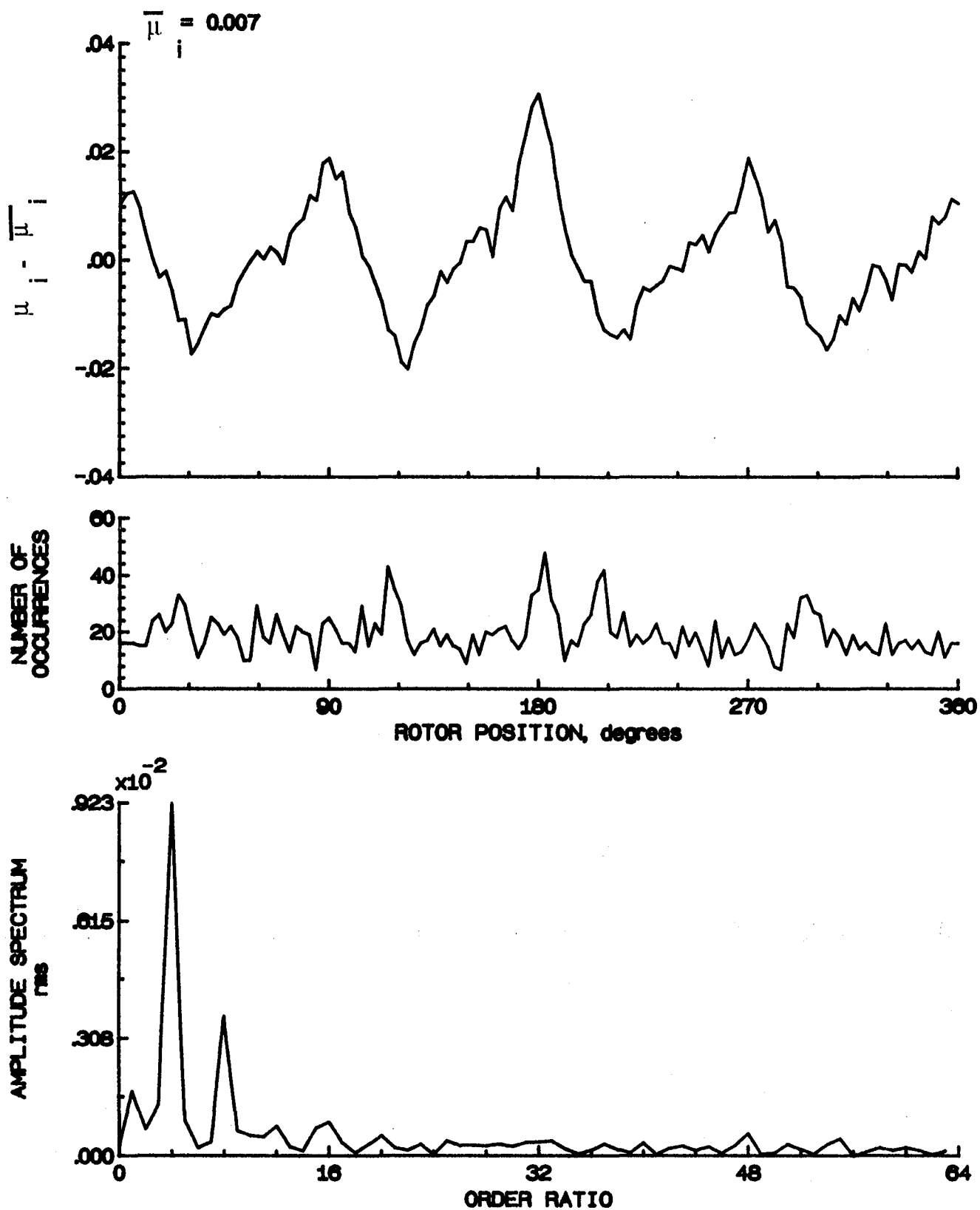


Figure 123.- Induced inflow velocity measured at 210 degrees and r/R of 0.74.

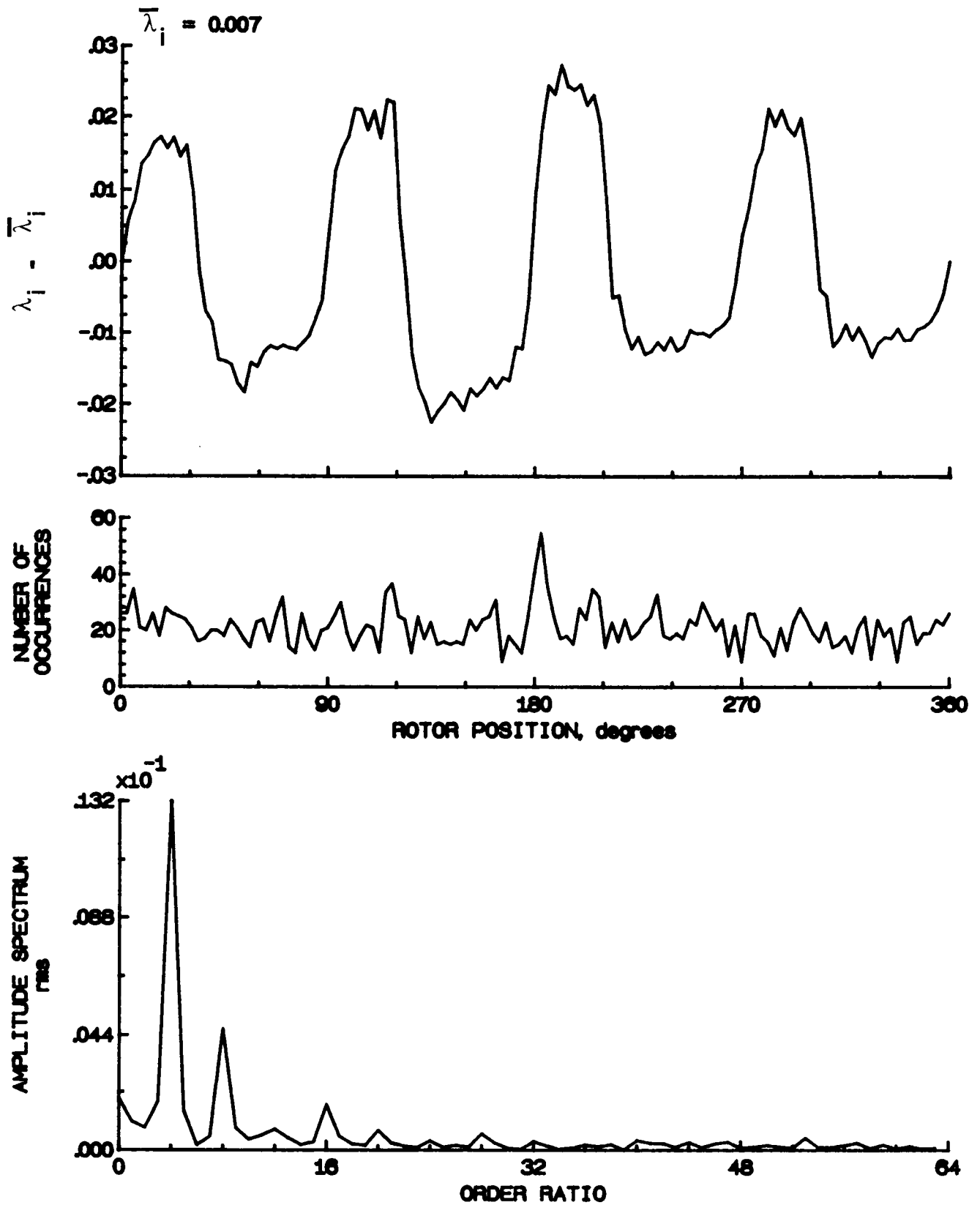


Figure 123.- Concluded.

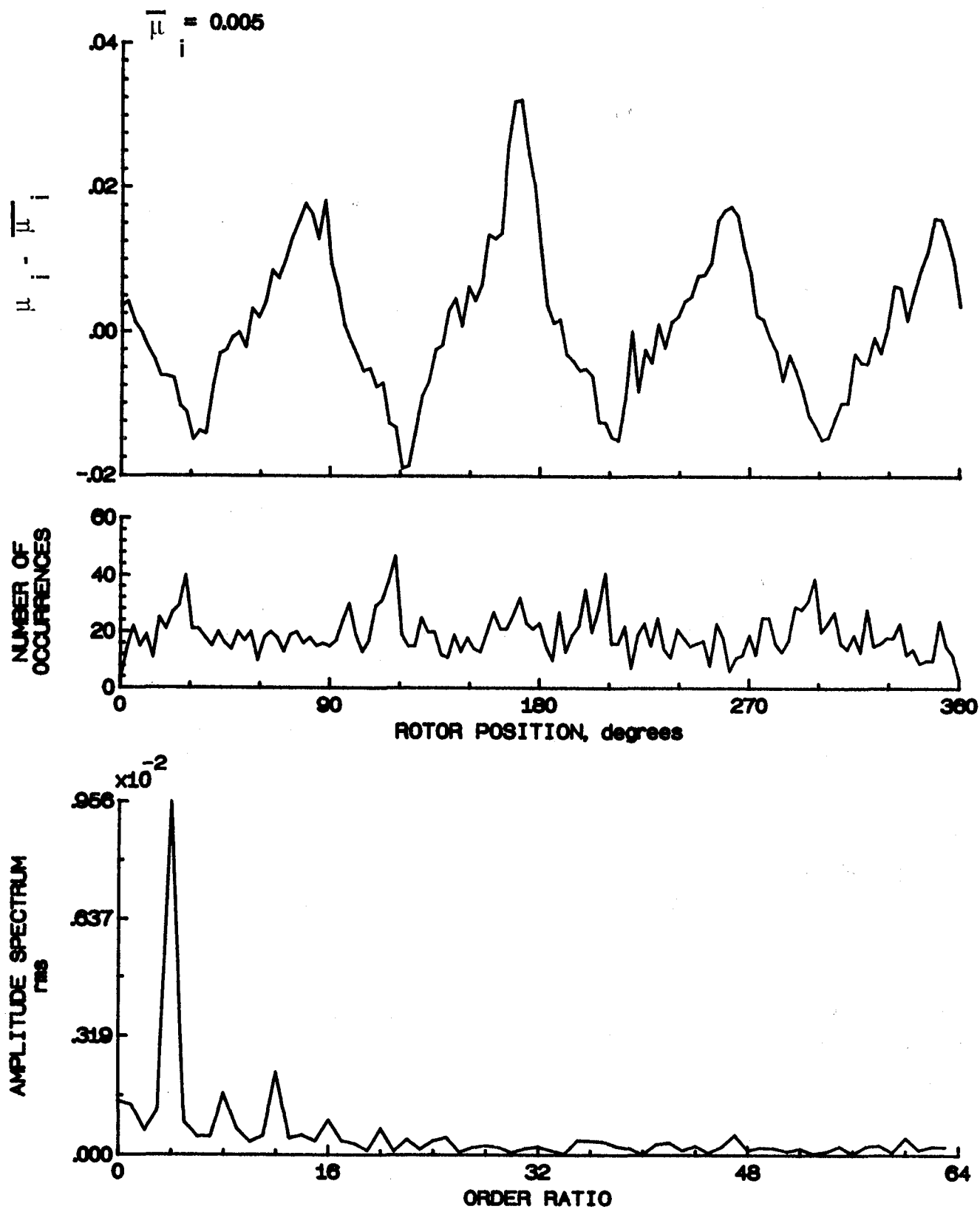


Figure 124.- Induced inflow velocity measured at 210 degrees and  $r/R$  of 0.78.



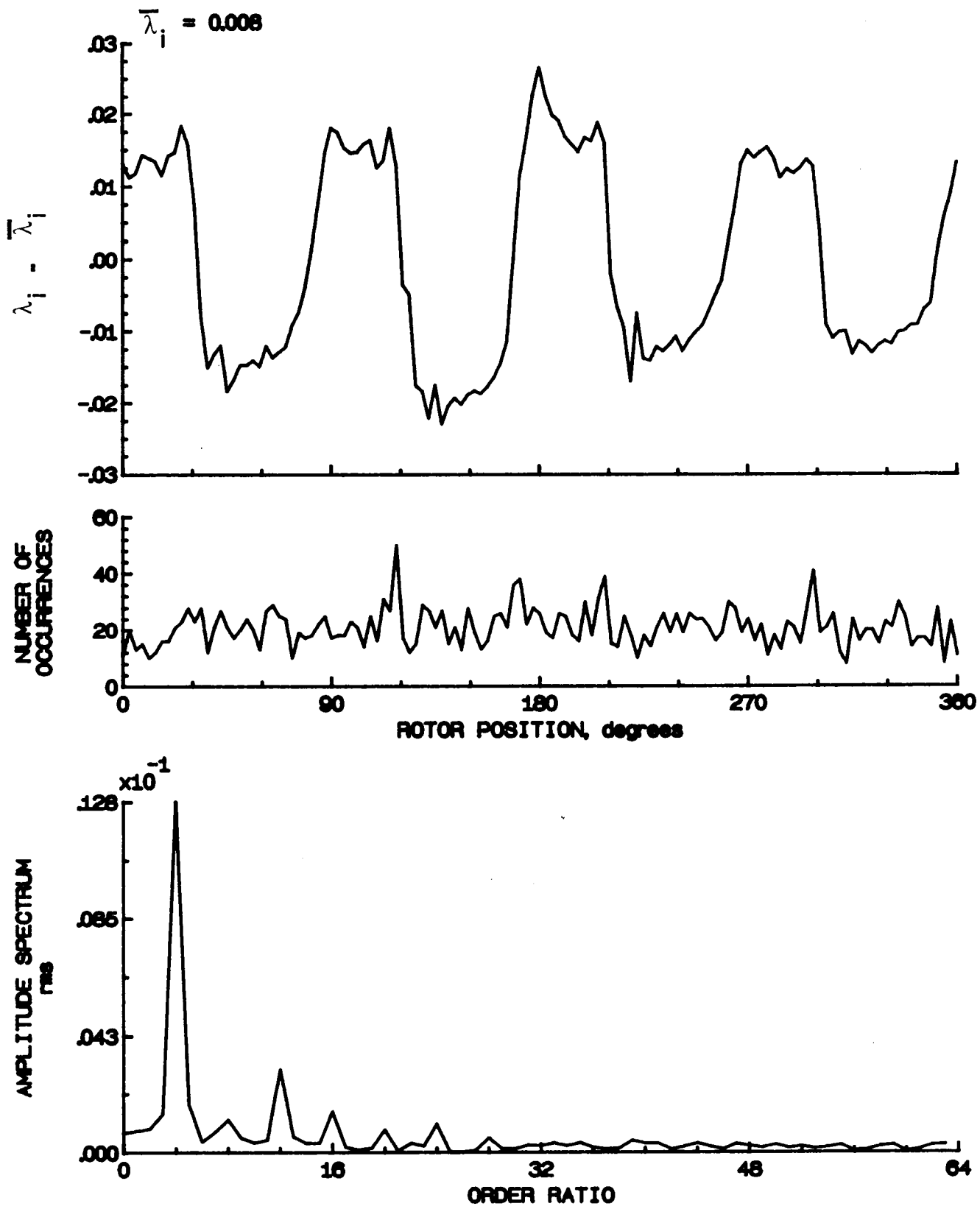


Figure 124.- Concluded.

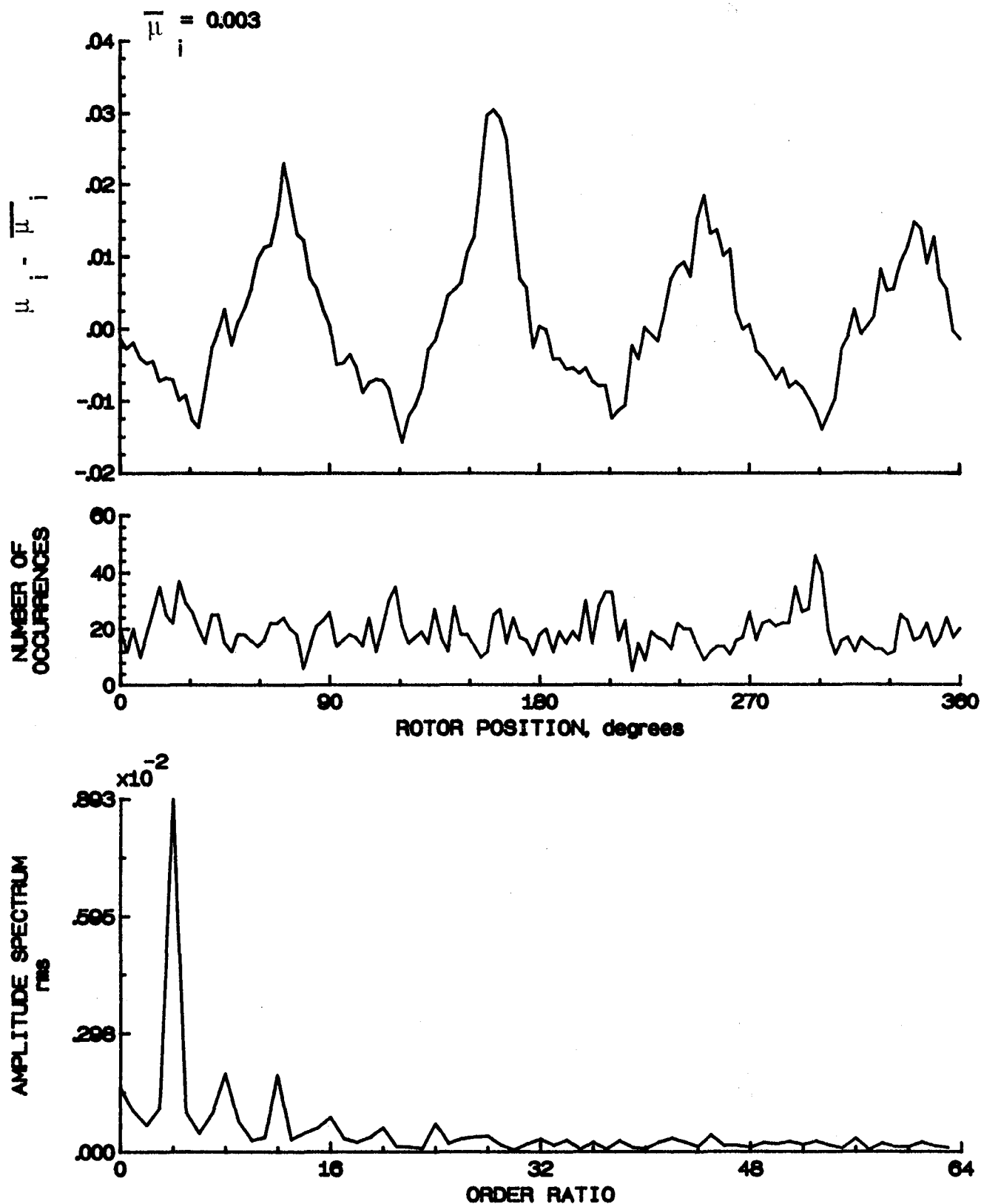


Figure 125.- Induced inflow velocity measured at 210 degrees and  $r/R$  of 0.82.

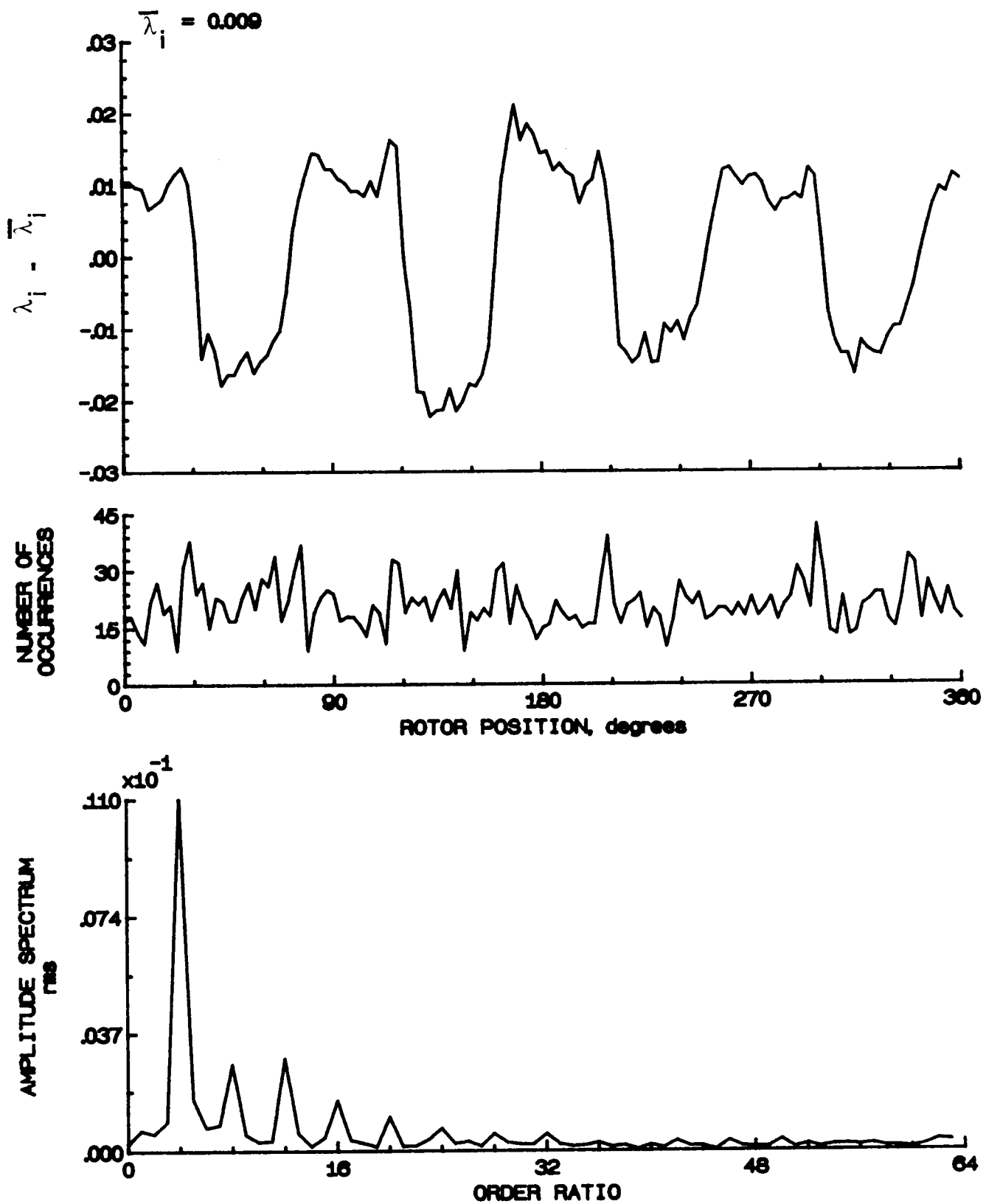


Figure 125.- Concluded.

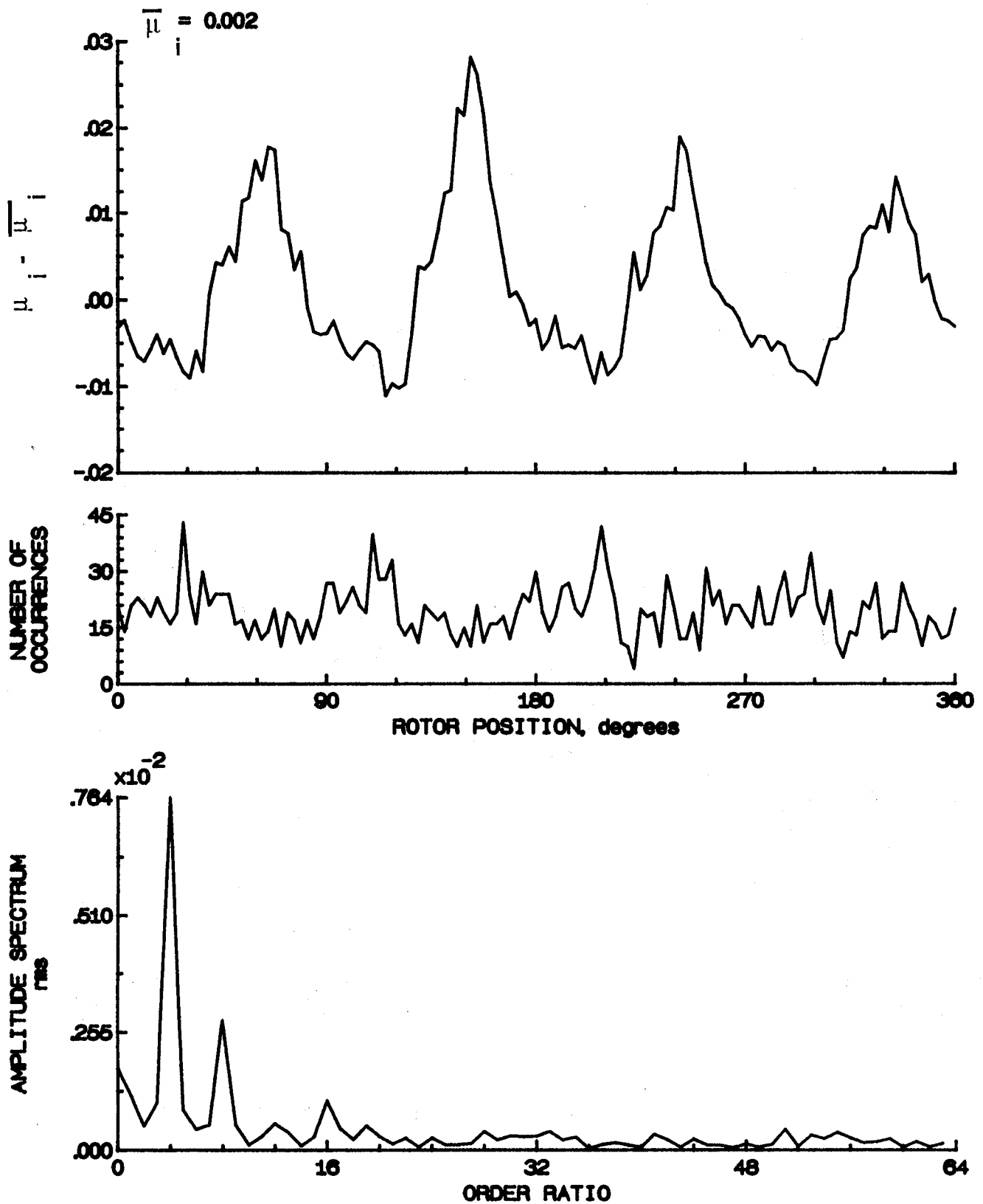


Figure 126.- Induced inflow velocity measured at 210 degrees and  $r/R$  of 0.86.

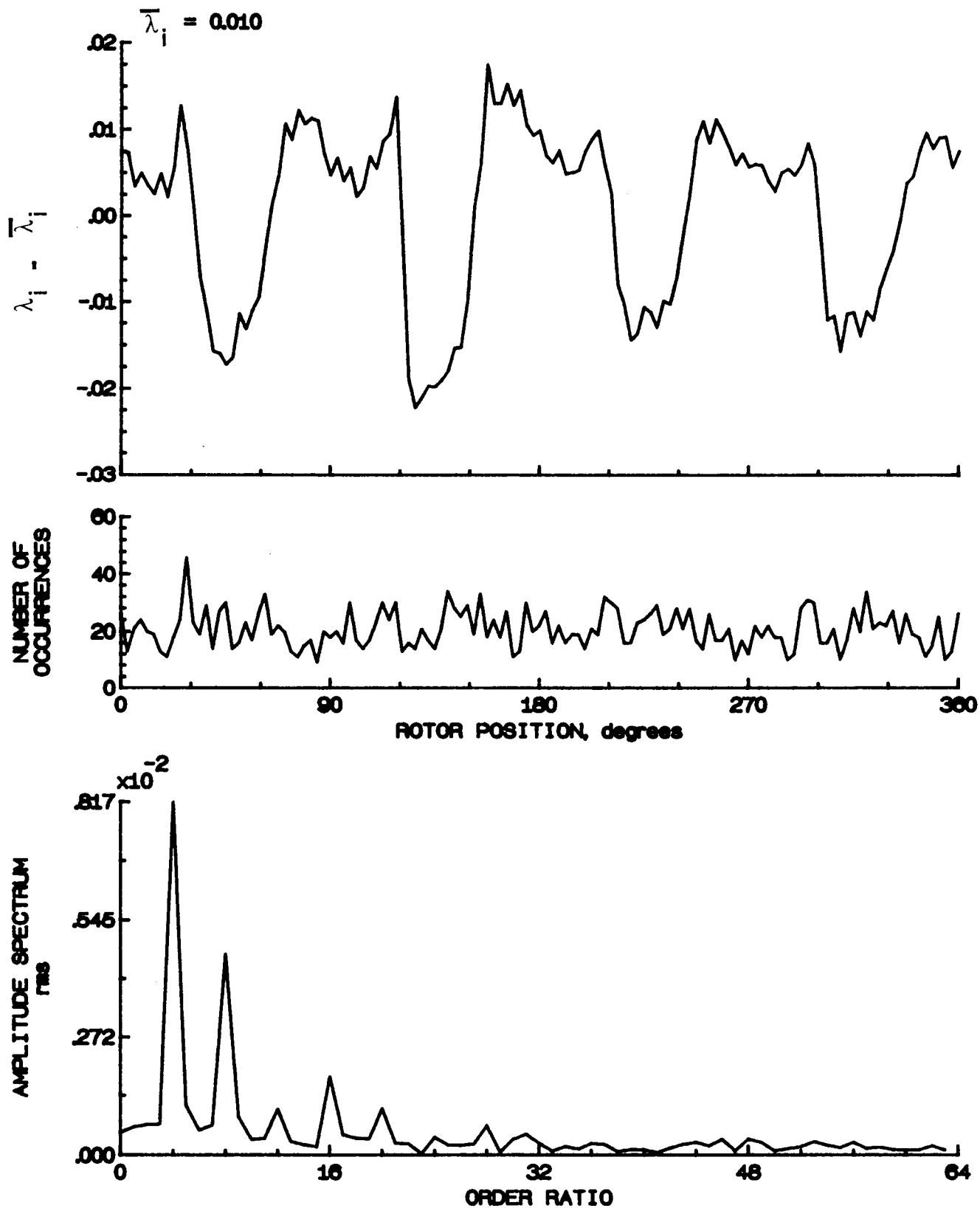


Figure 126.- Concluded.

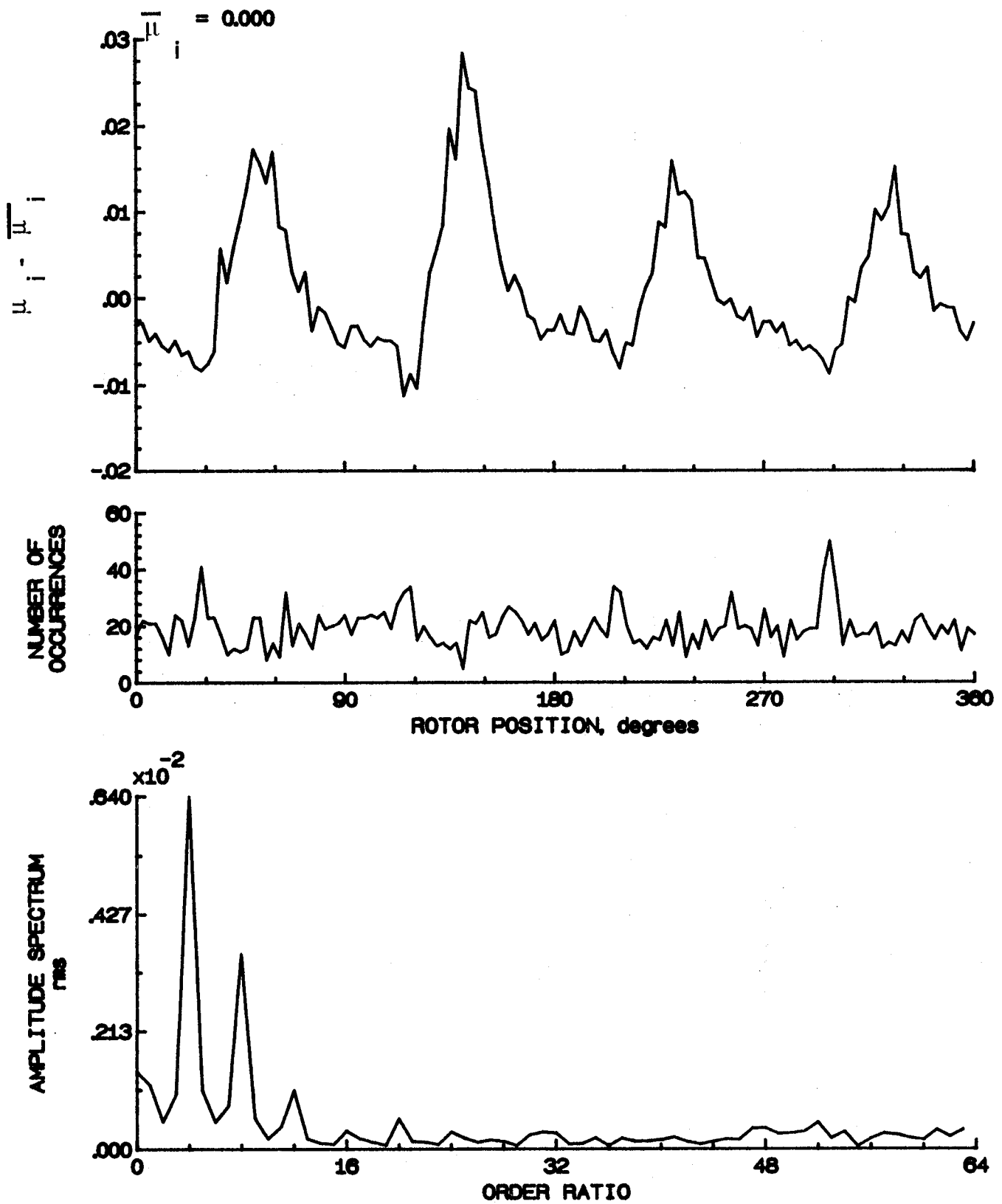


Figure 127.- Induced inflow velocity measured at 210 degrees and r/R of 0.90.

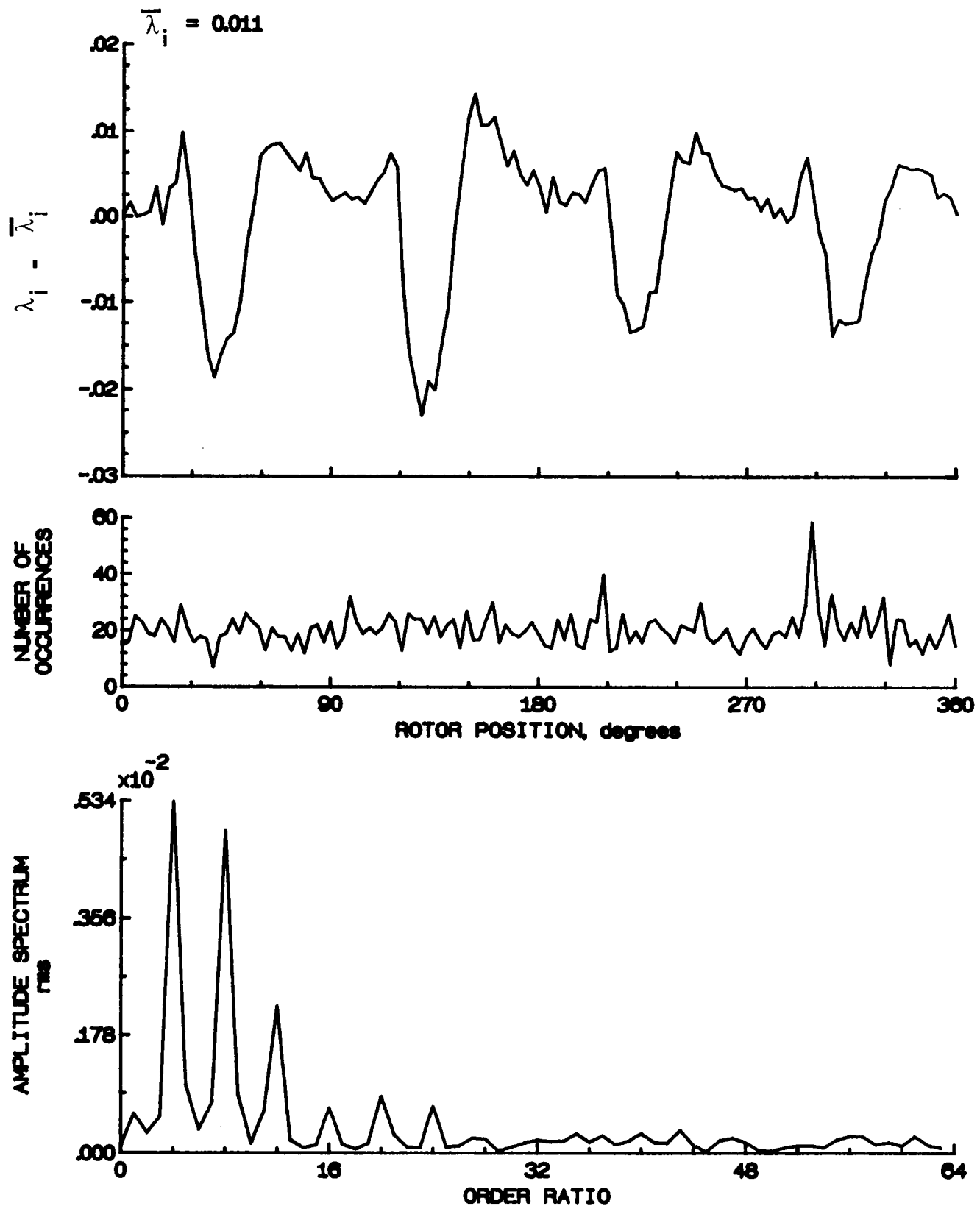


Figure 127.- Concluded.

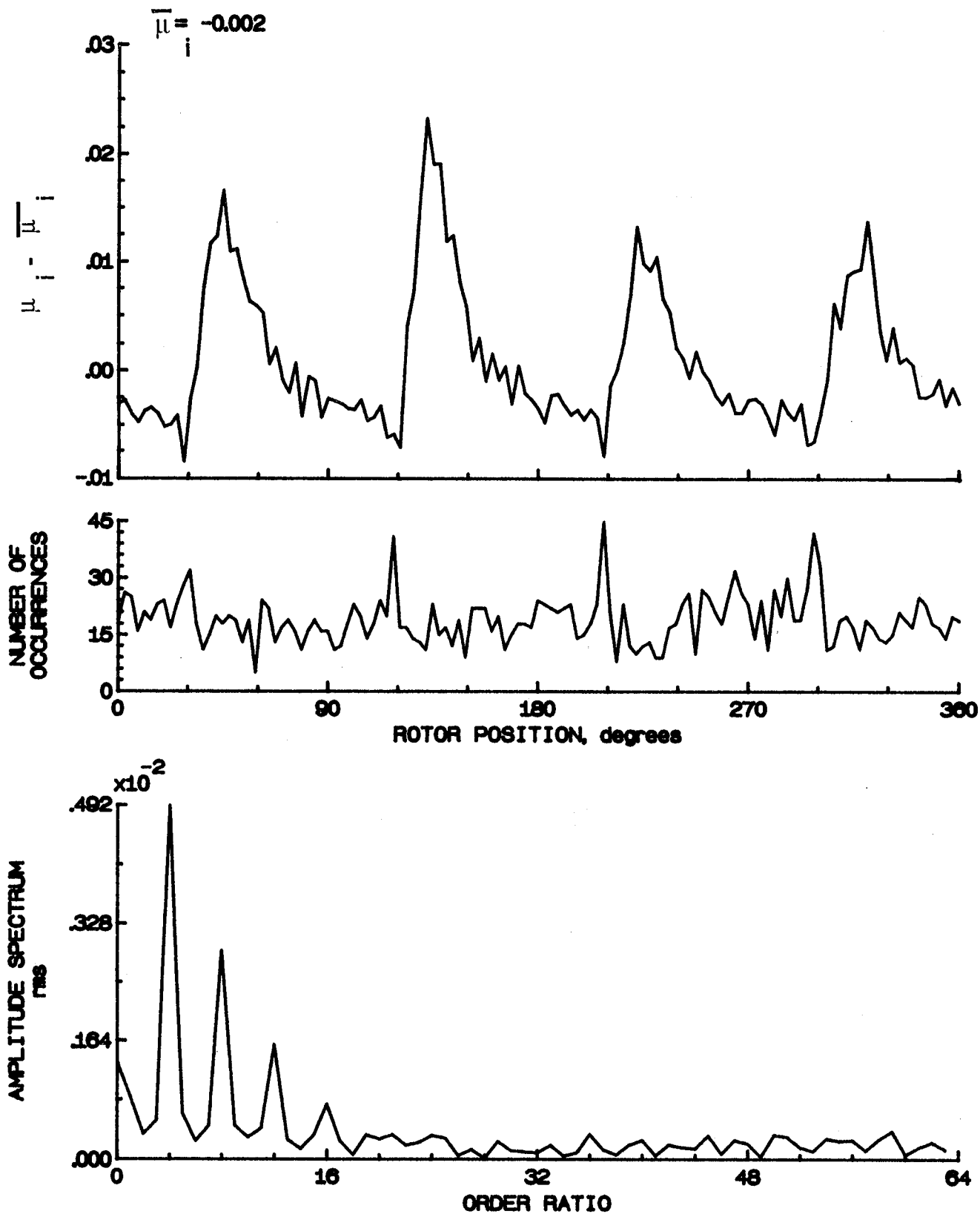


Figure 128.- Induced inflow velocity measured at 210 degrees and  $r/R$  of 0.94.



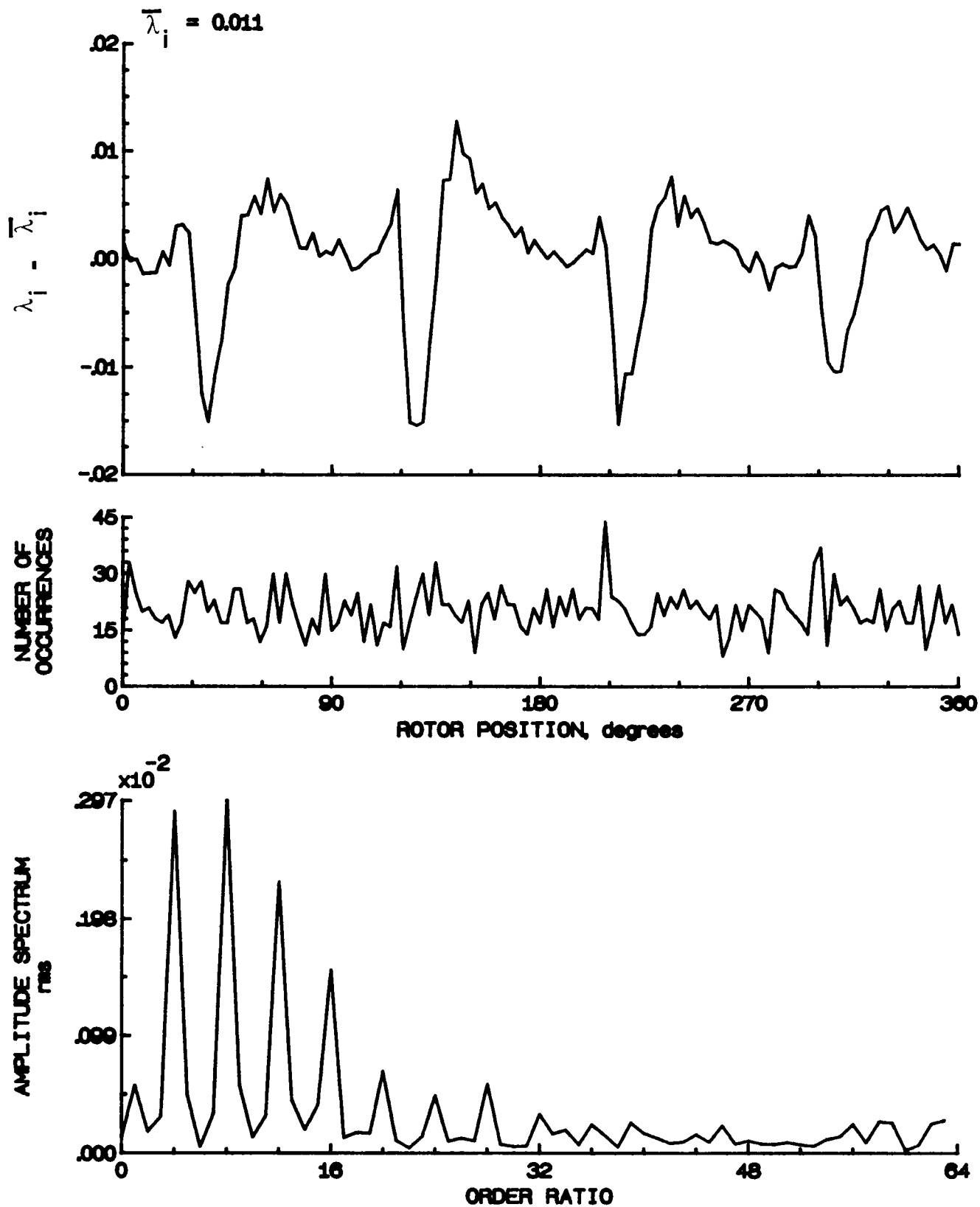


Figure 128.- Concluded.

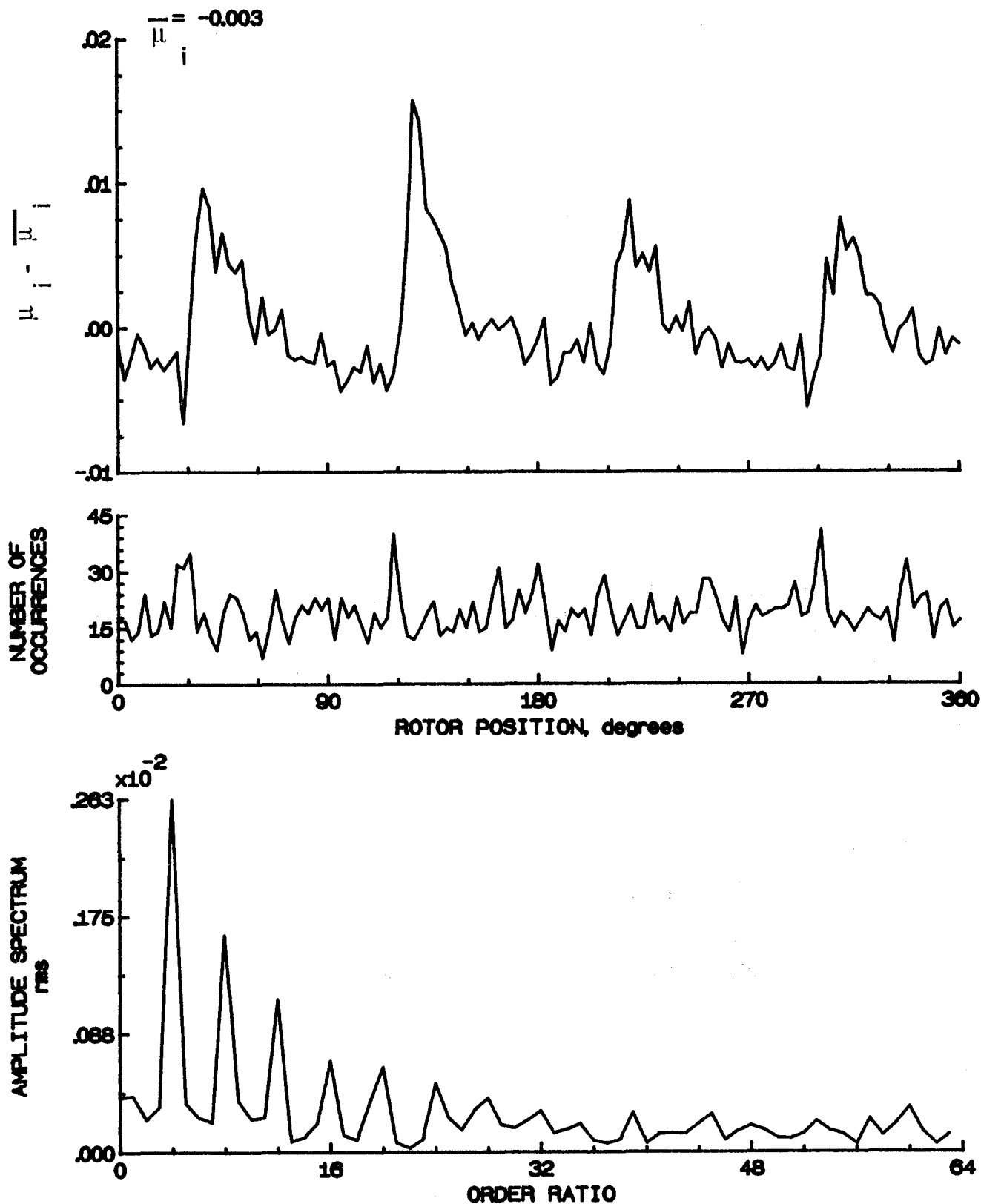


Figure 129.- Induced inflow velocity measured at 210 degrees and r/R of 0.98.

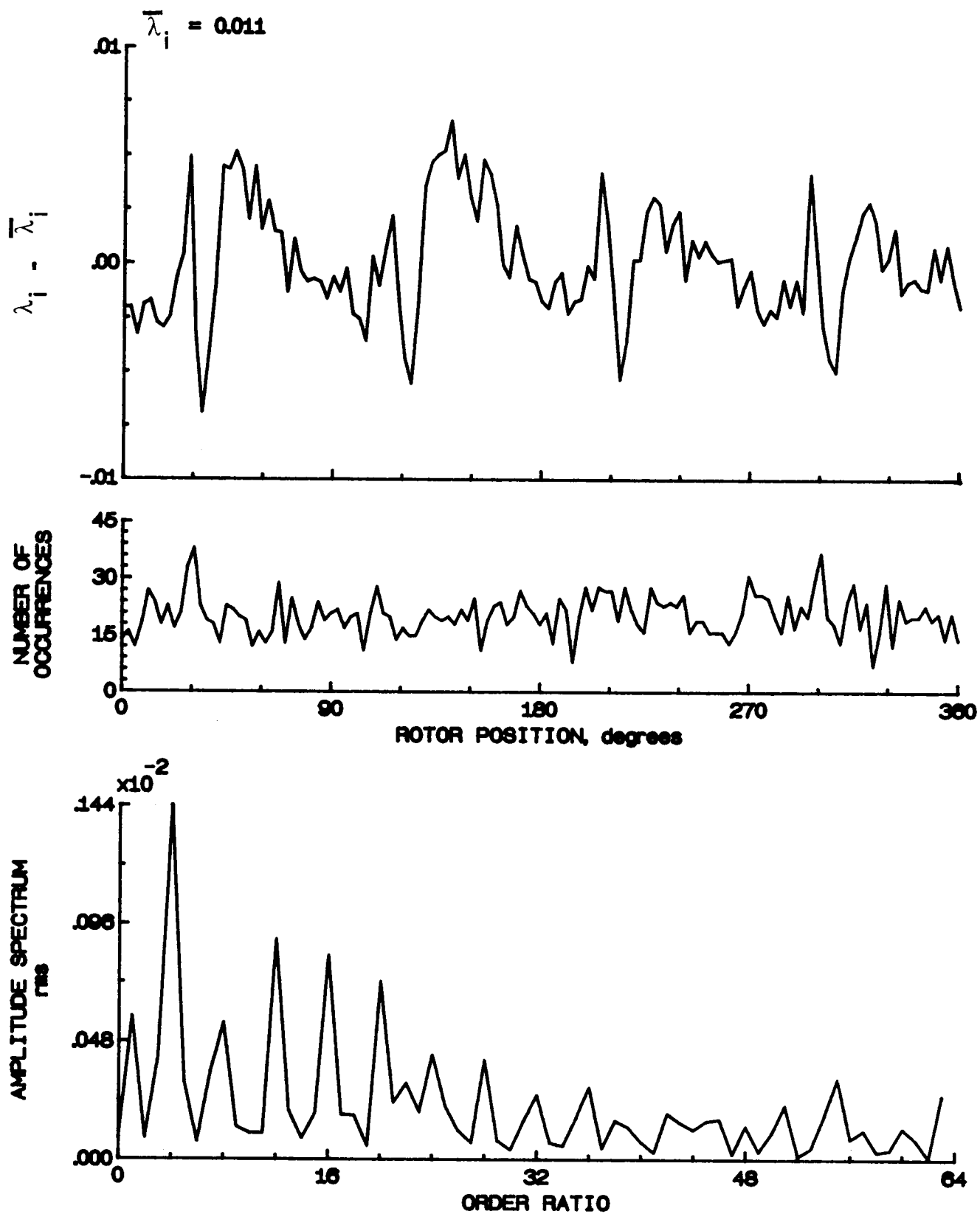


Figure 129.- Concluded.

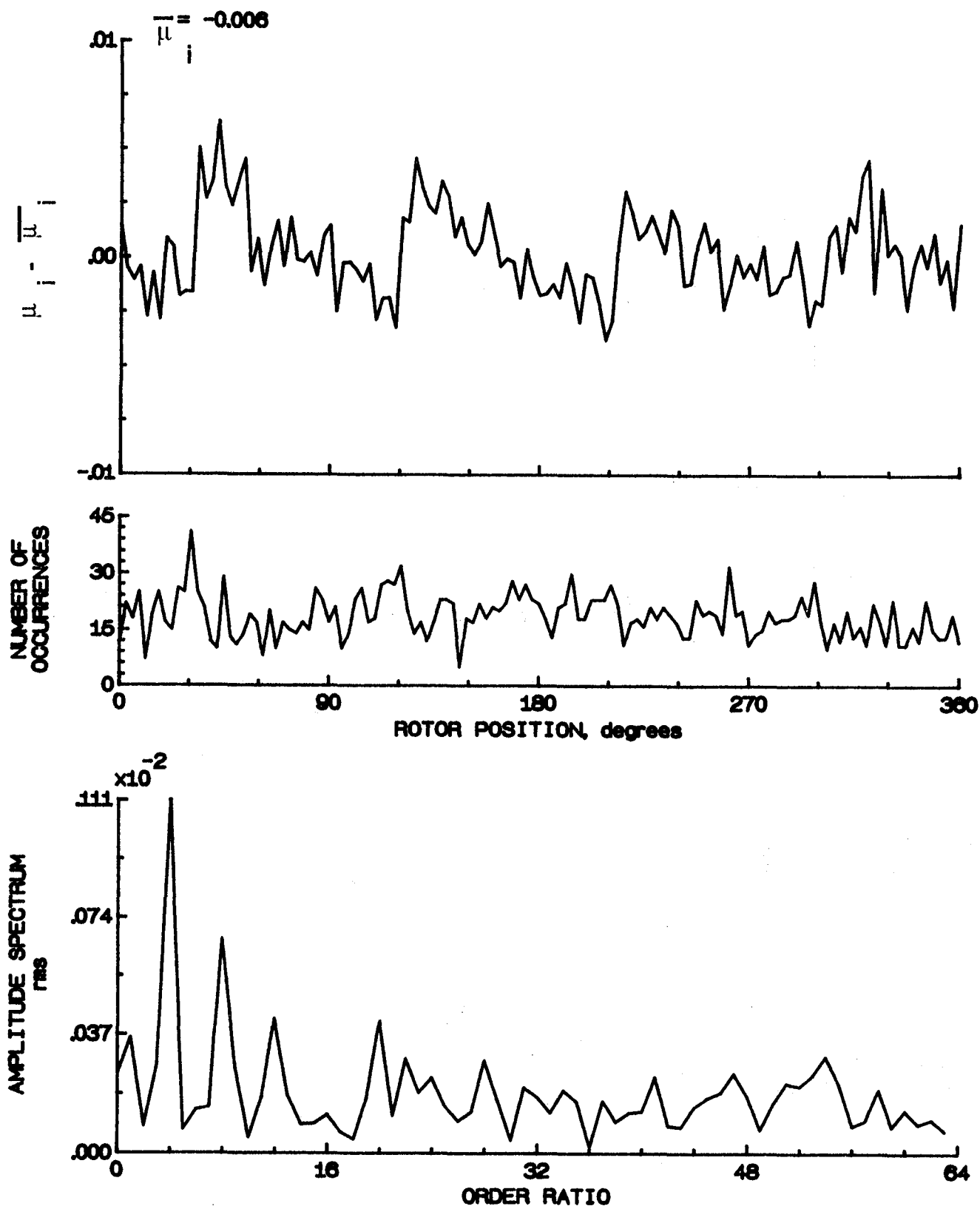


Figure 130.- Induced inflow velocity measured at 210 degrees and r/R of 1.02.

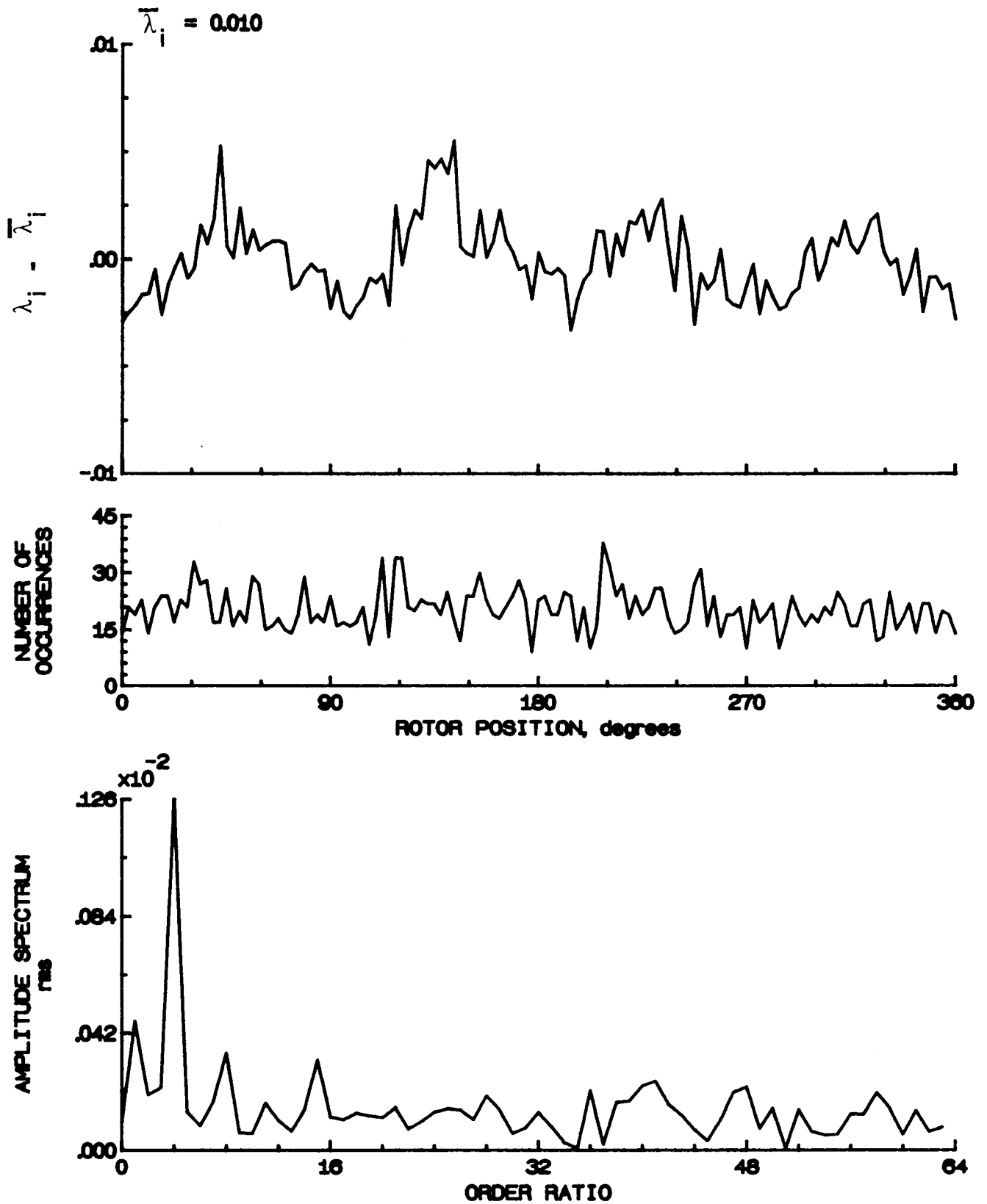


Figure 130.- Concluded.

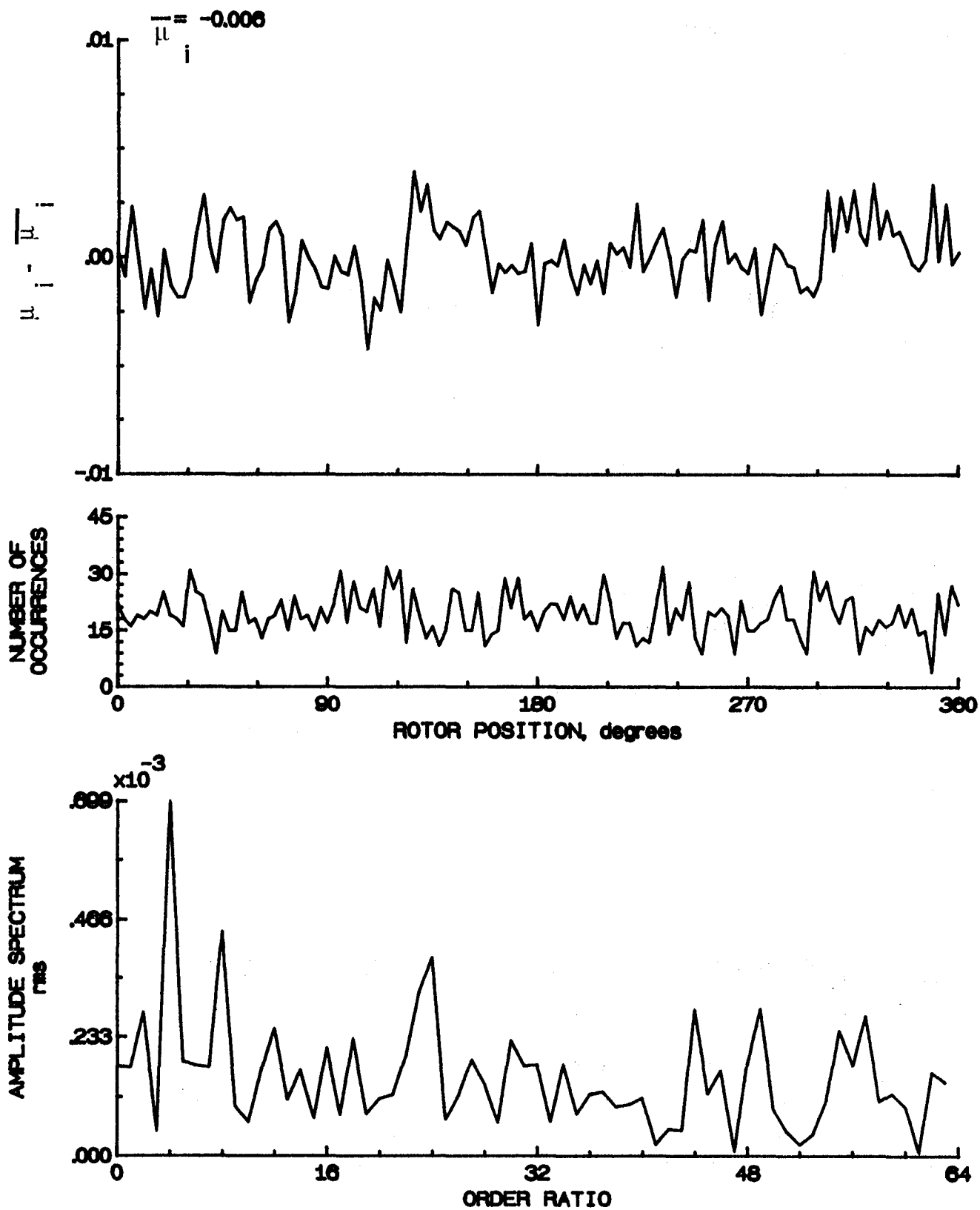


Figure 131.- Induced inflow velocity measured at 210 degrees and r/R of 1.04.

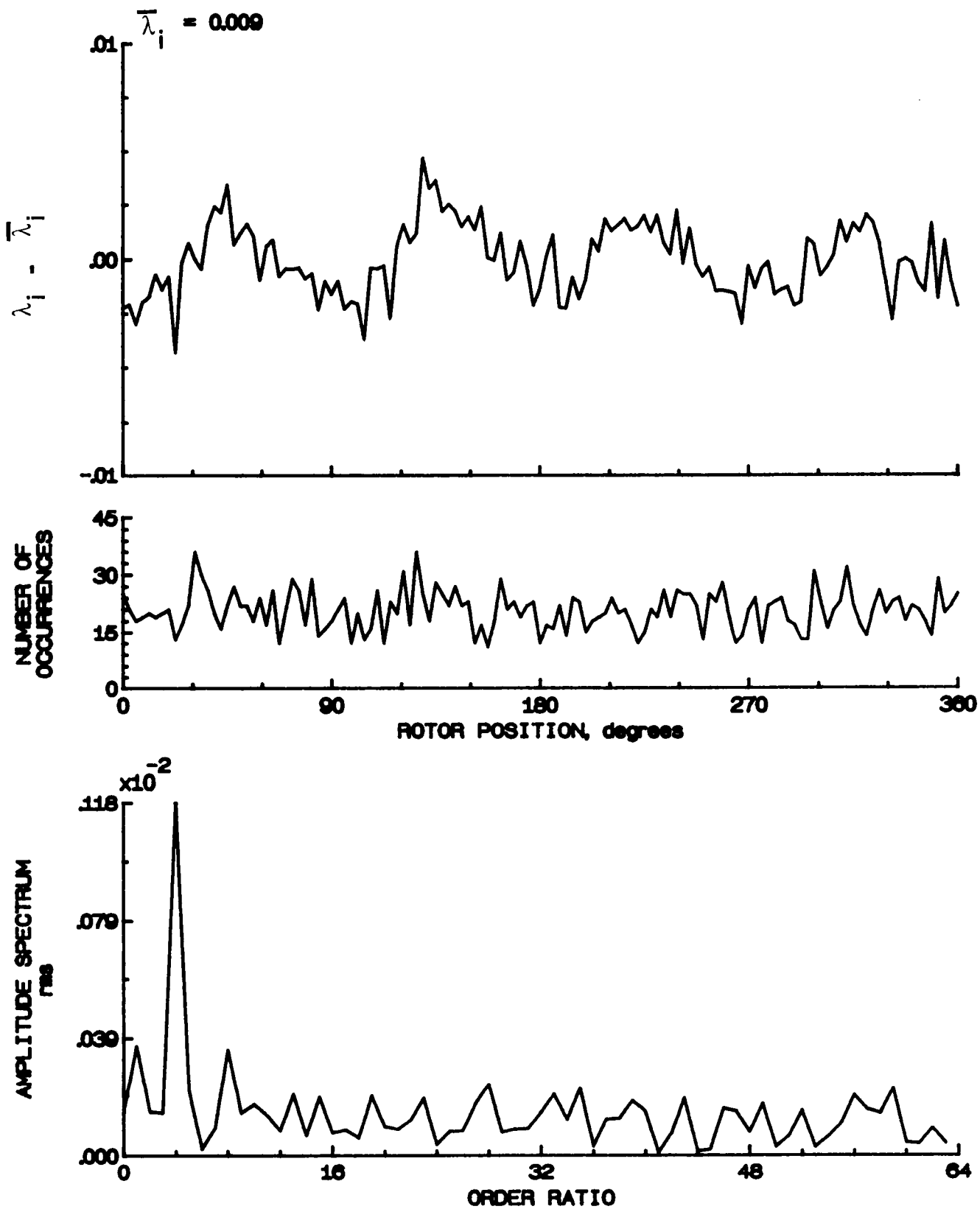


Figure 131- Concluded.

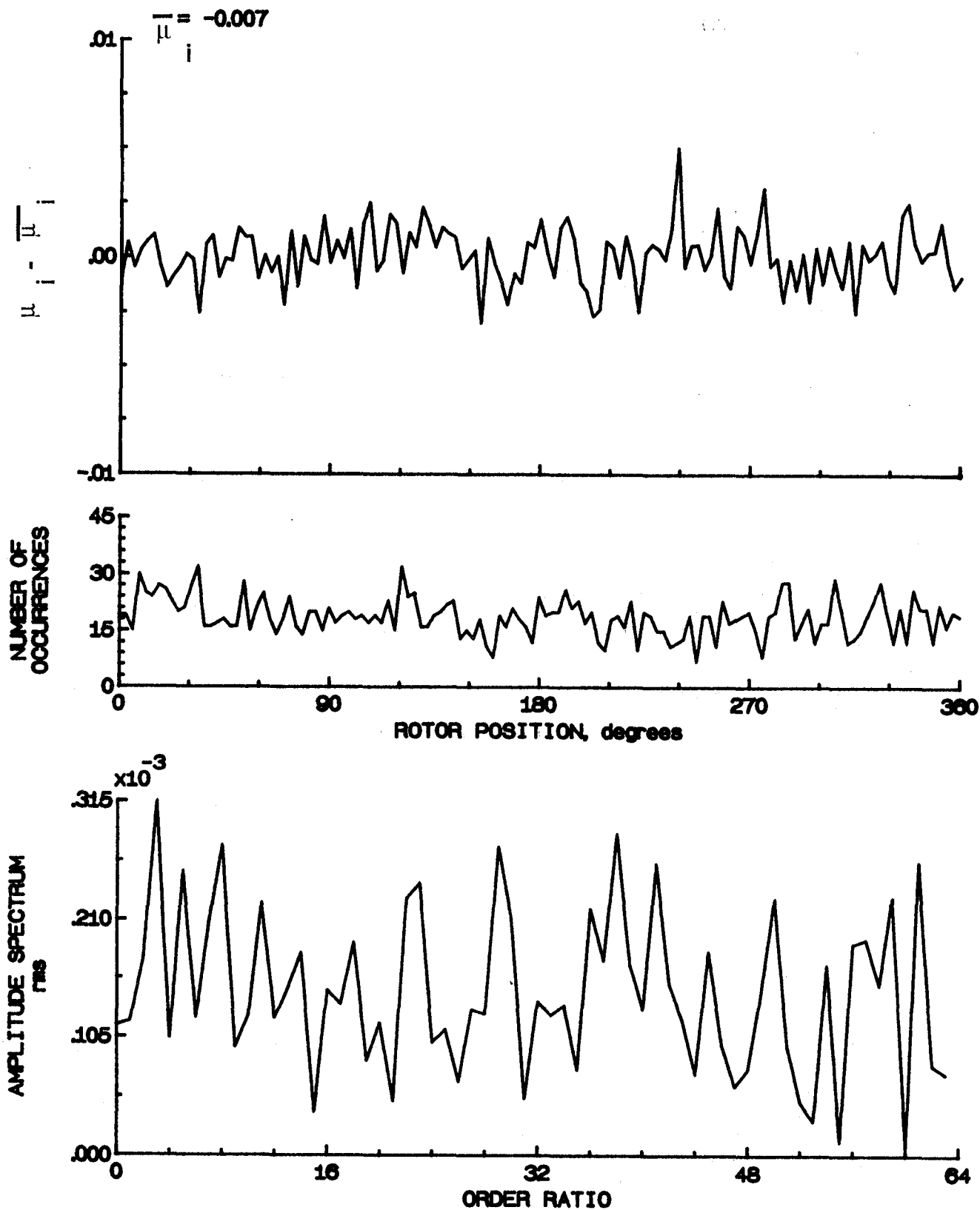


Figure 132.- Induced inflow velocity measured at 210 degrees and r/R of 1.10.



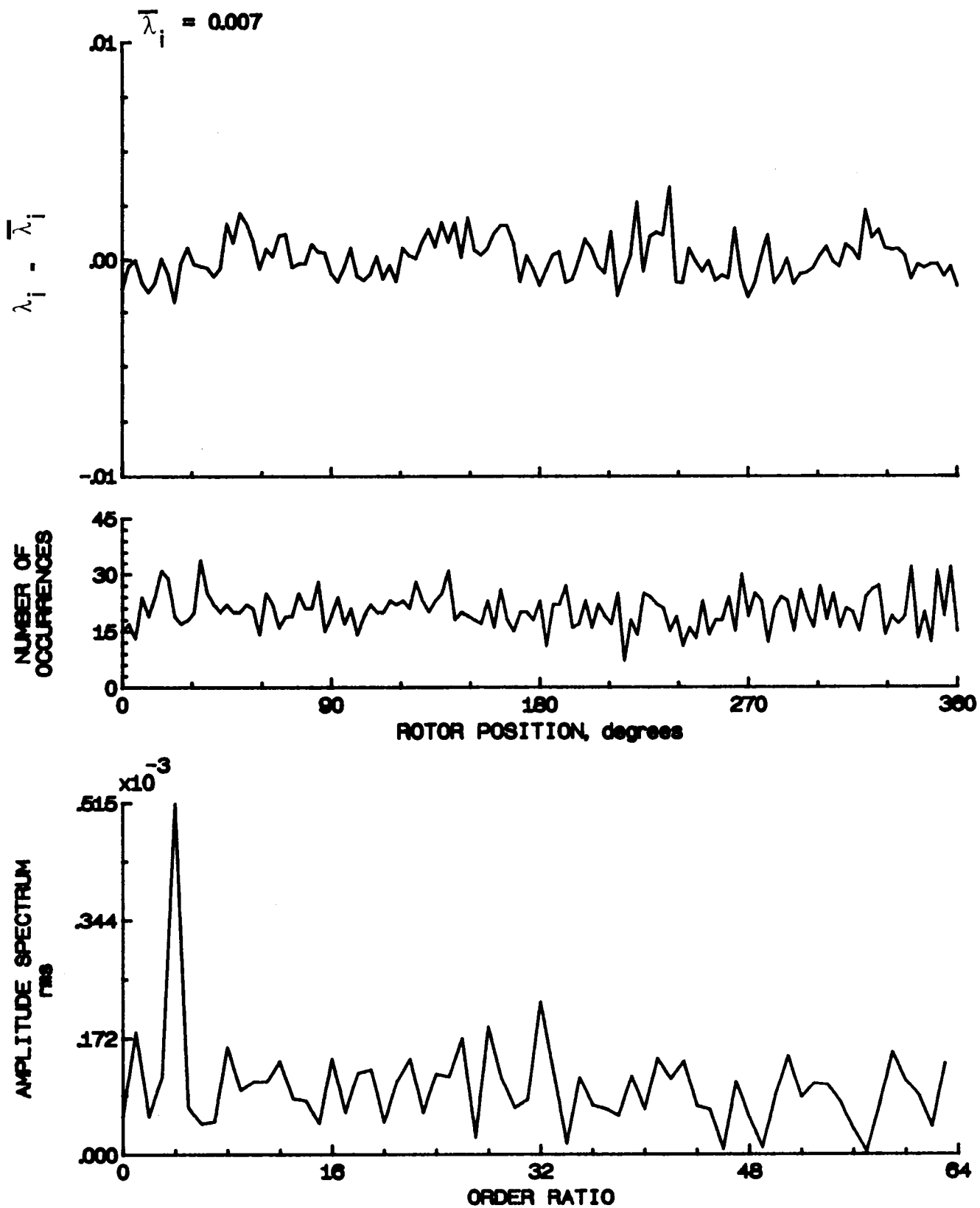


Figure 132.- Concluded.

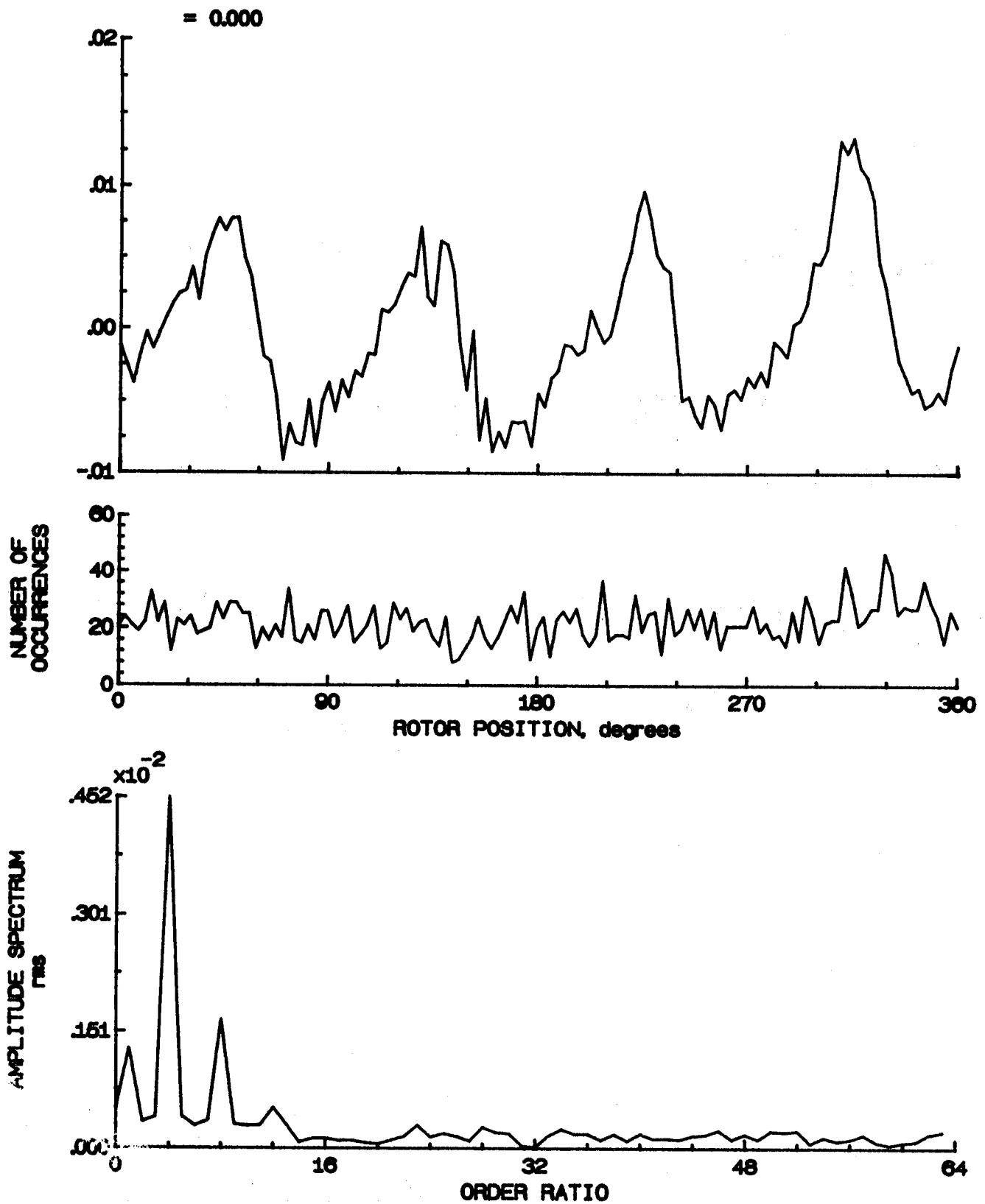


Figure 133.- Induced inflow velocity measured at 240 degrees and  $r/R$  of 0.20.

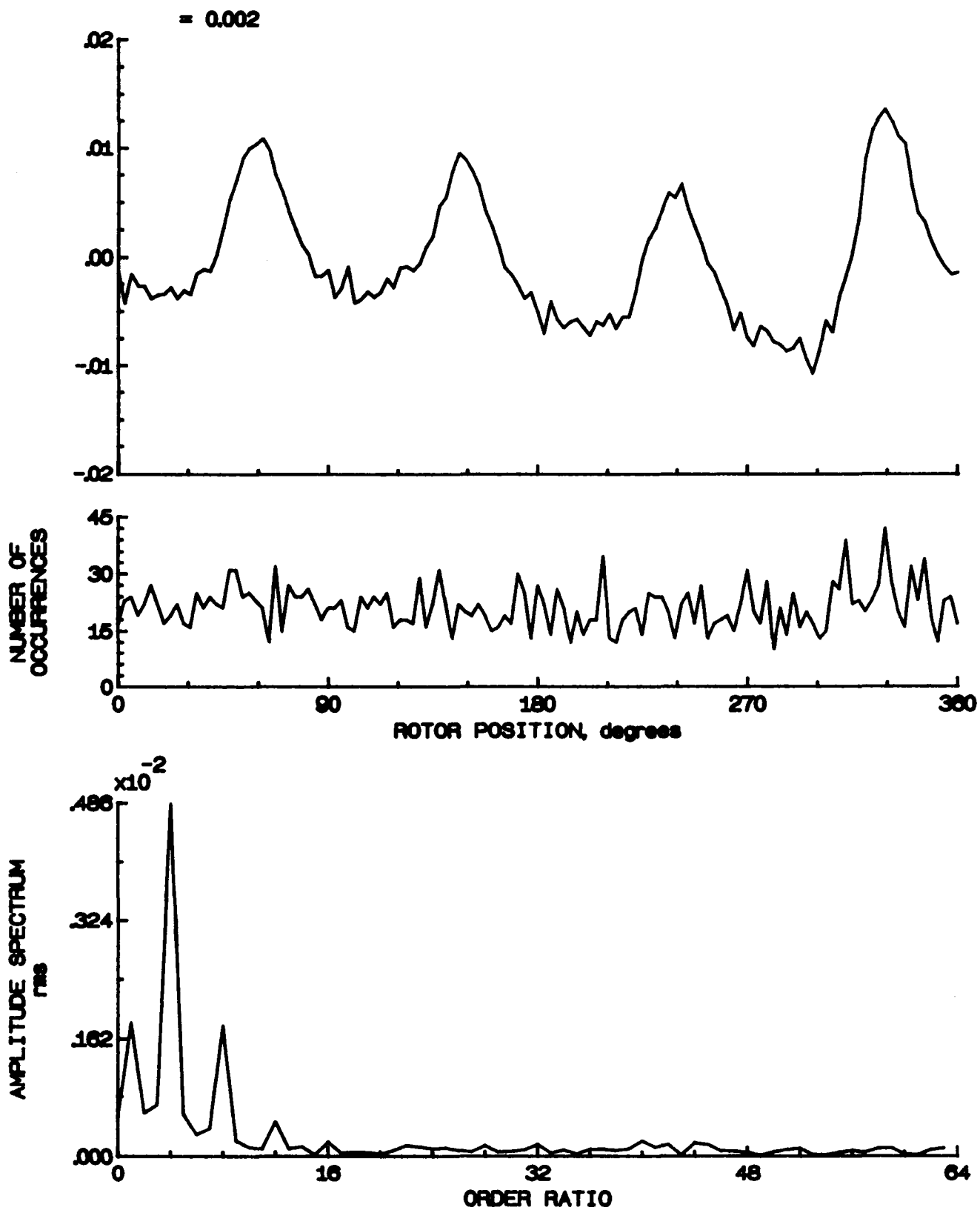


Figure 133.- Concluded.

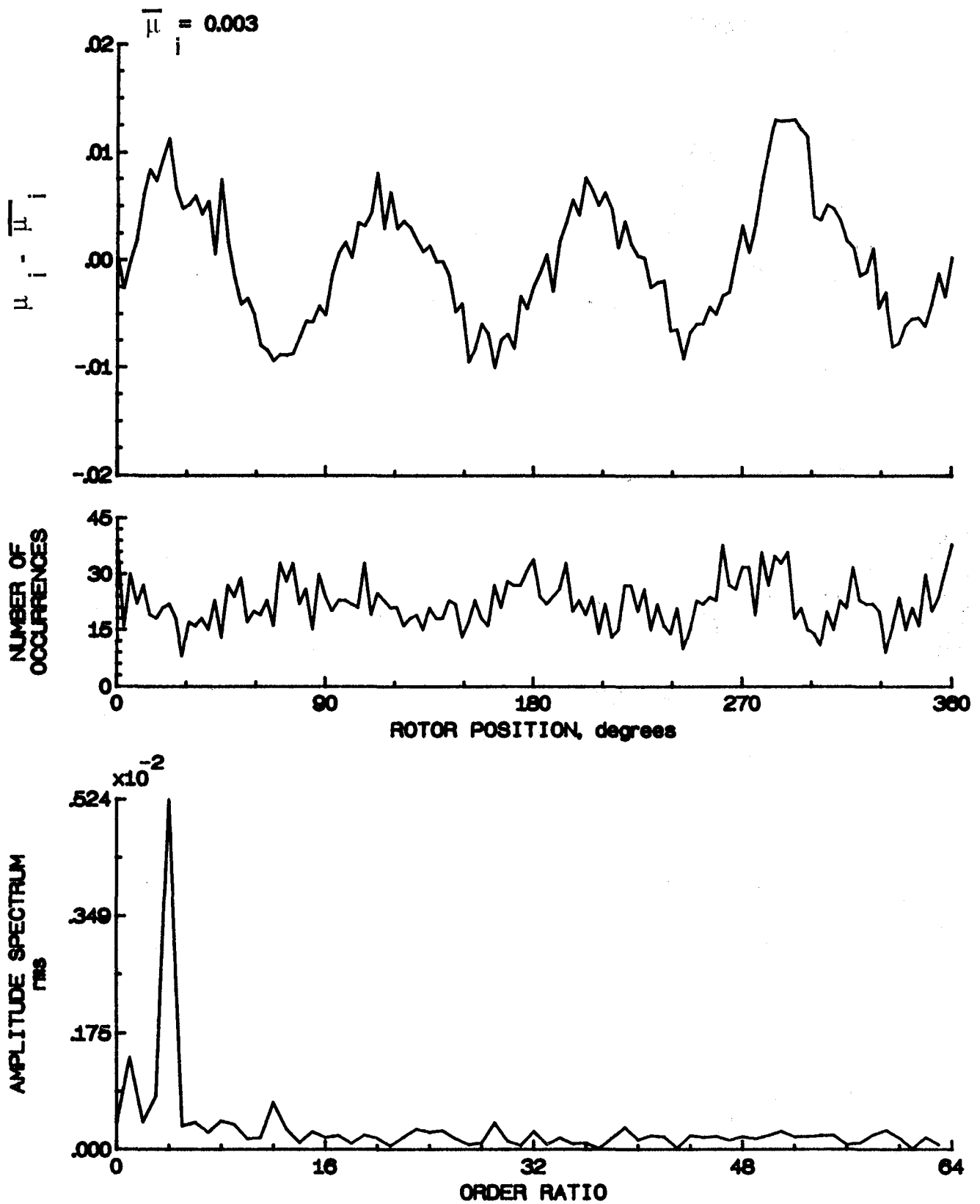


Figure 134.- Induced inflow velocity measured at 240 degrees and r/R of 0.40.

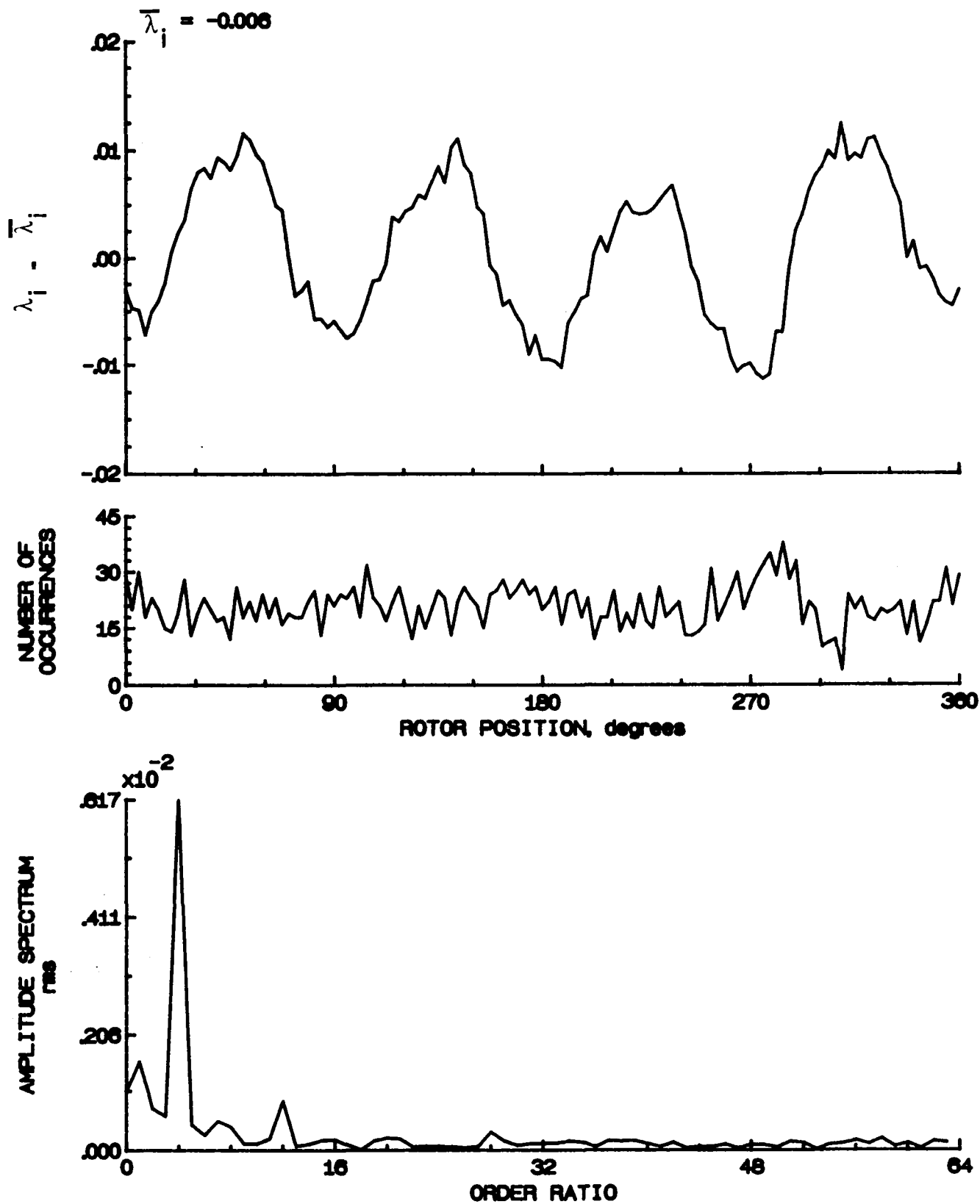


Figure 134.- Concluded.

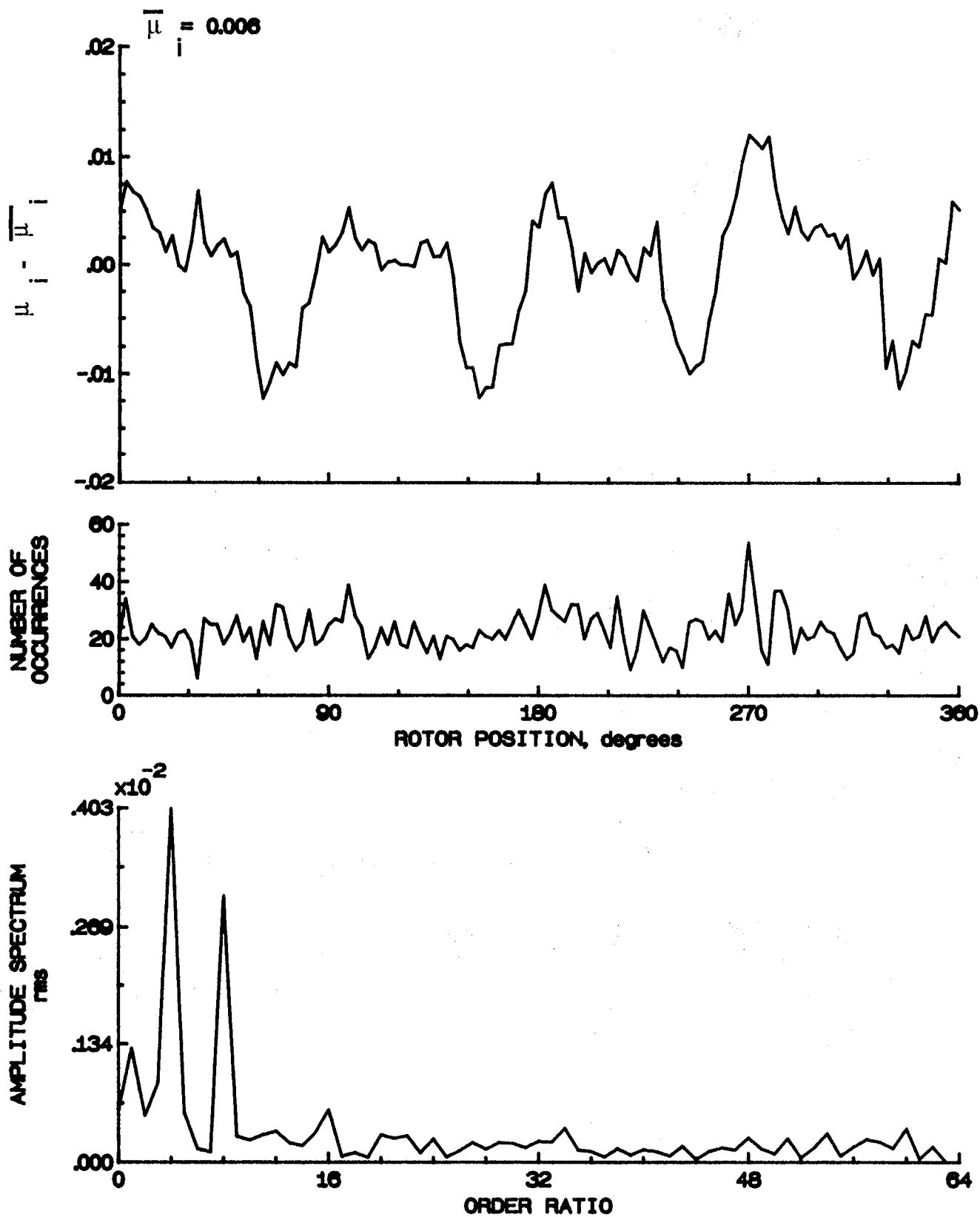


Figure 135.- Induced inflow velocity measured at 240 degrees and  $r/R$  of 0.50.

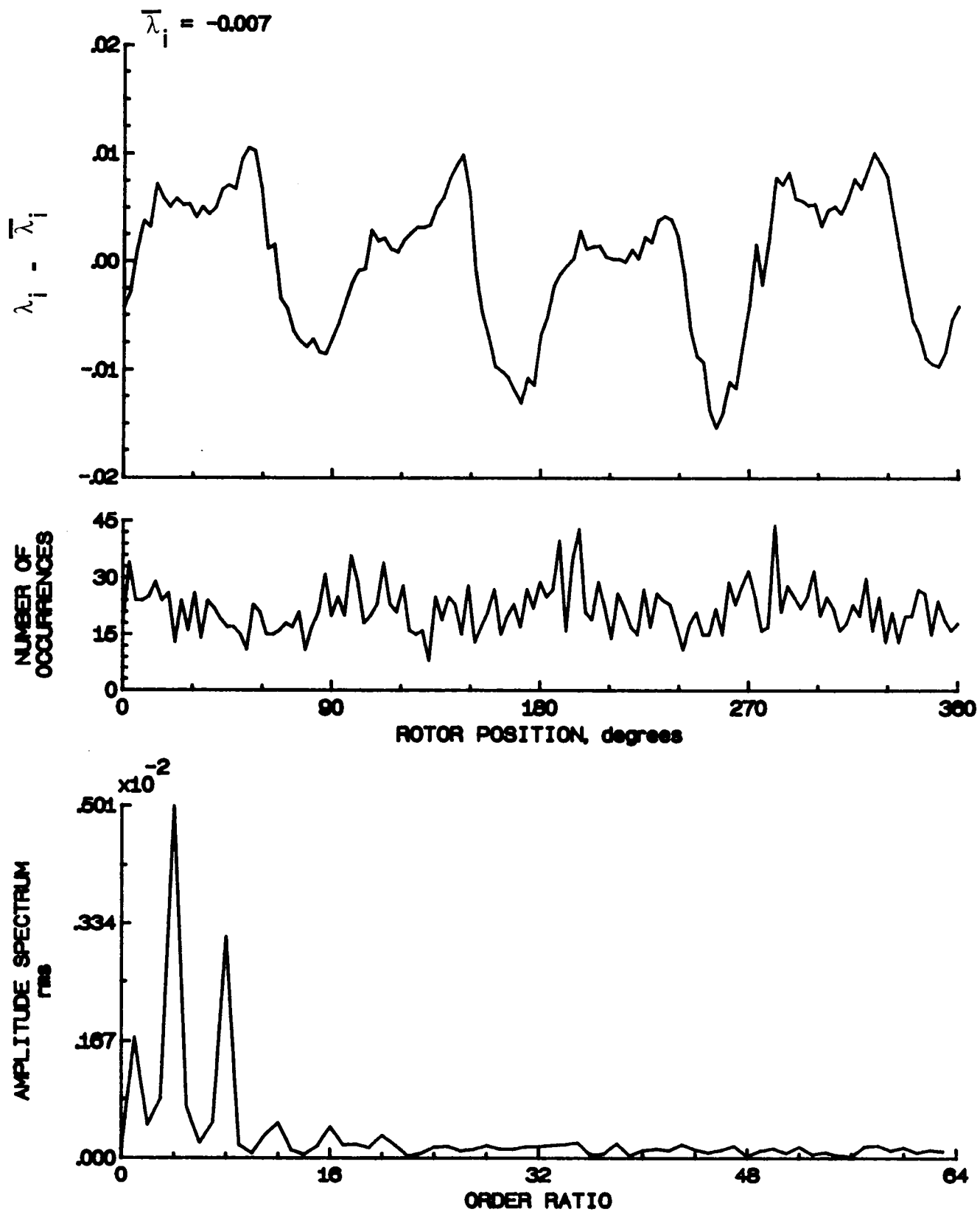


Figure 135.- Concluded.

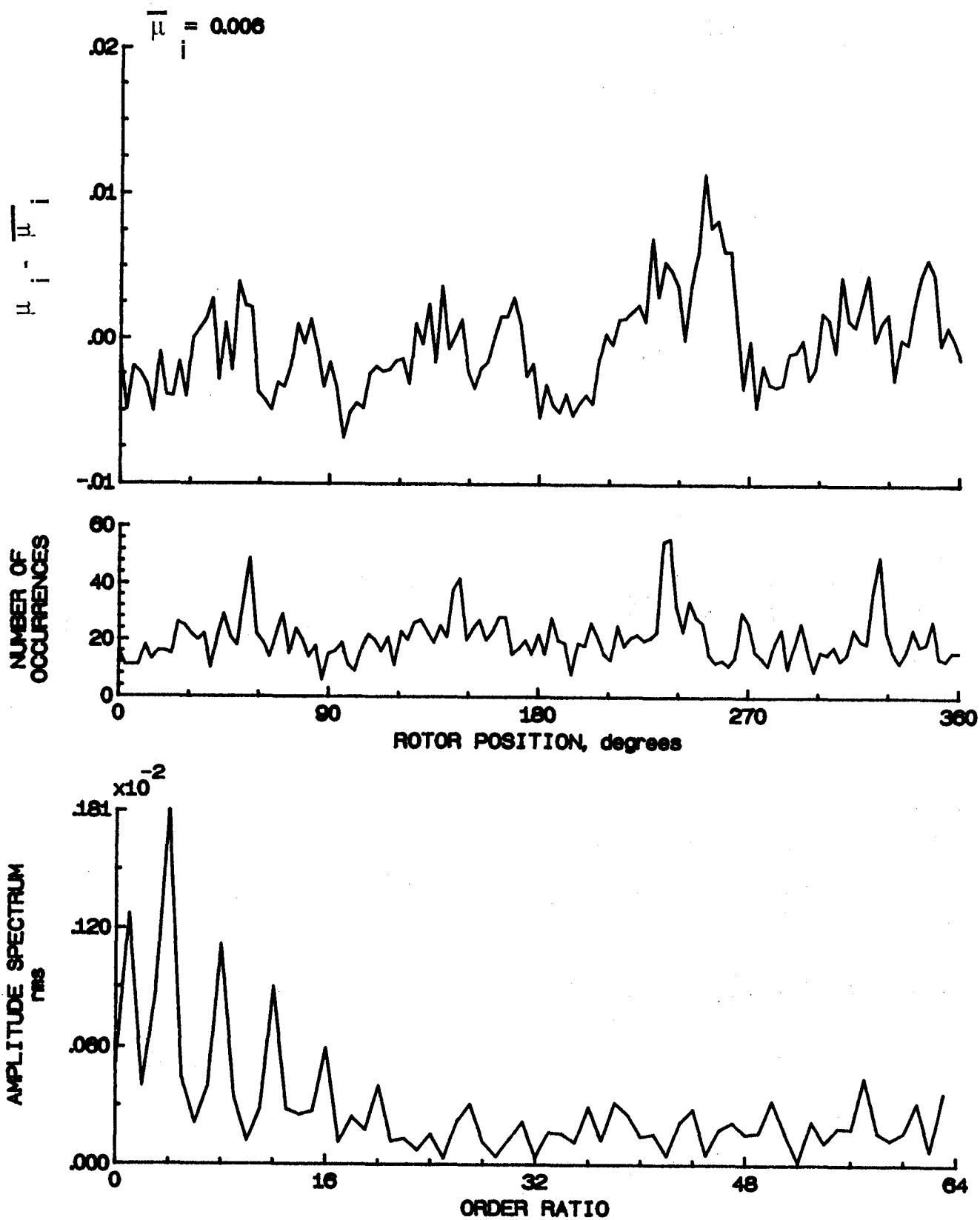


Figure 136.- Induced inflow velocity measured at 240 degrees and  $r/R$  of 0.60.



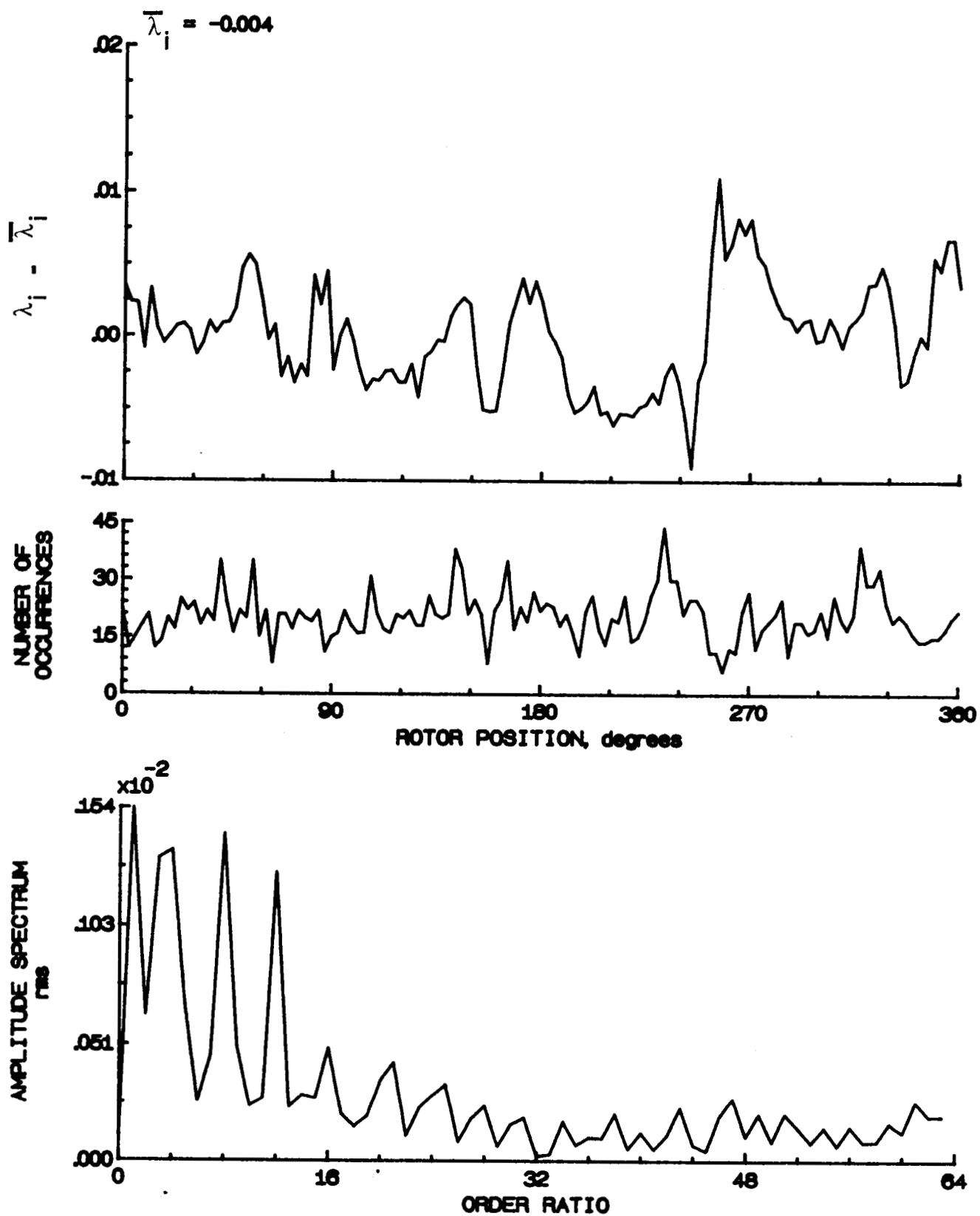


Figure 136.- Concluded.

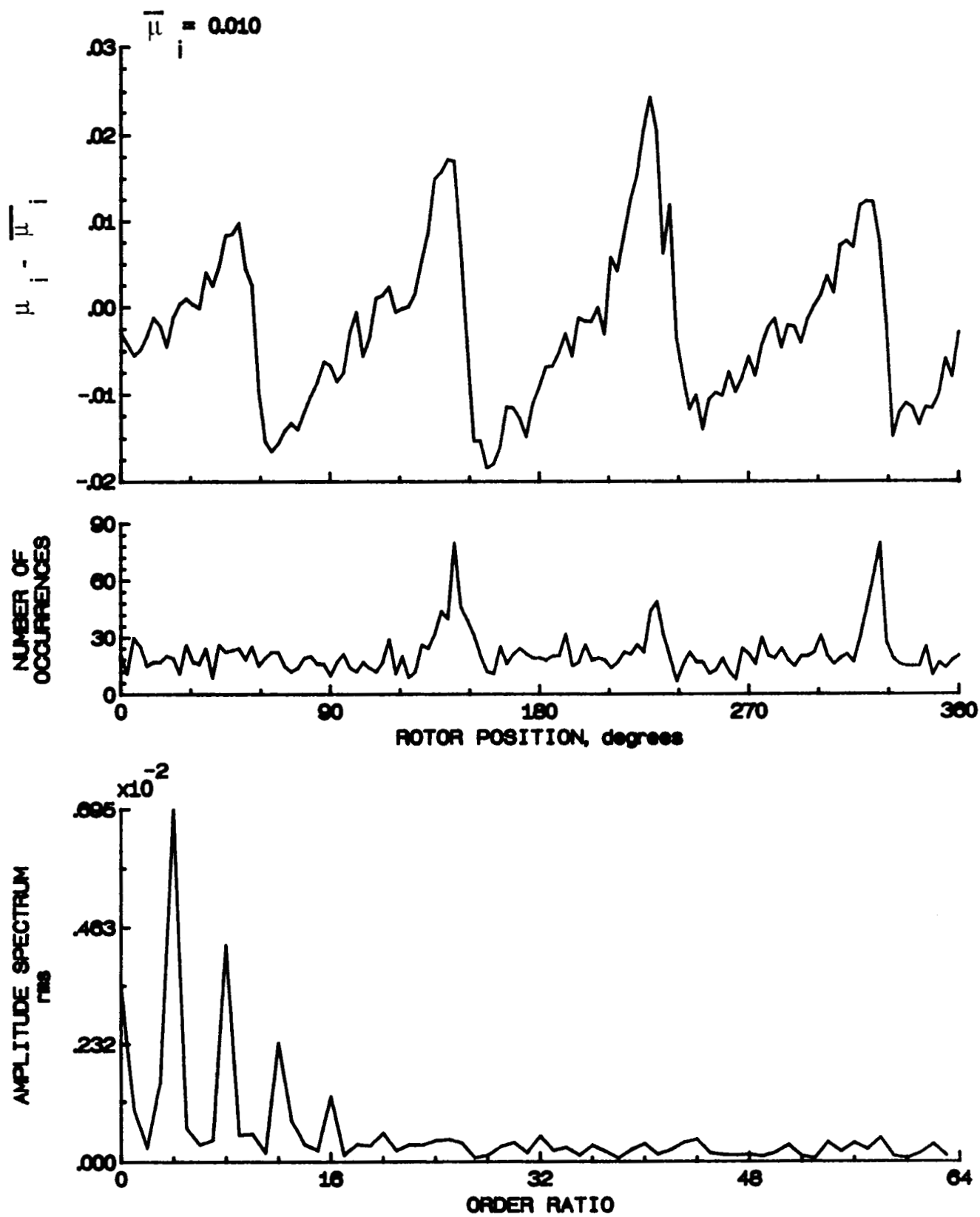


Figure 137.- Induced inflow velocity measured at 240 degrees and  $r/R$  of 0.70.

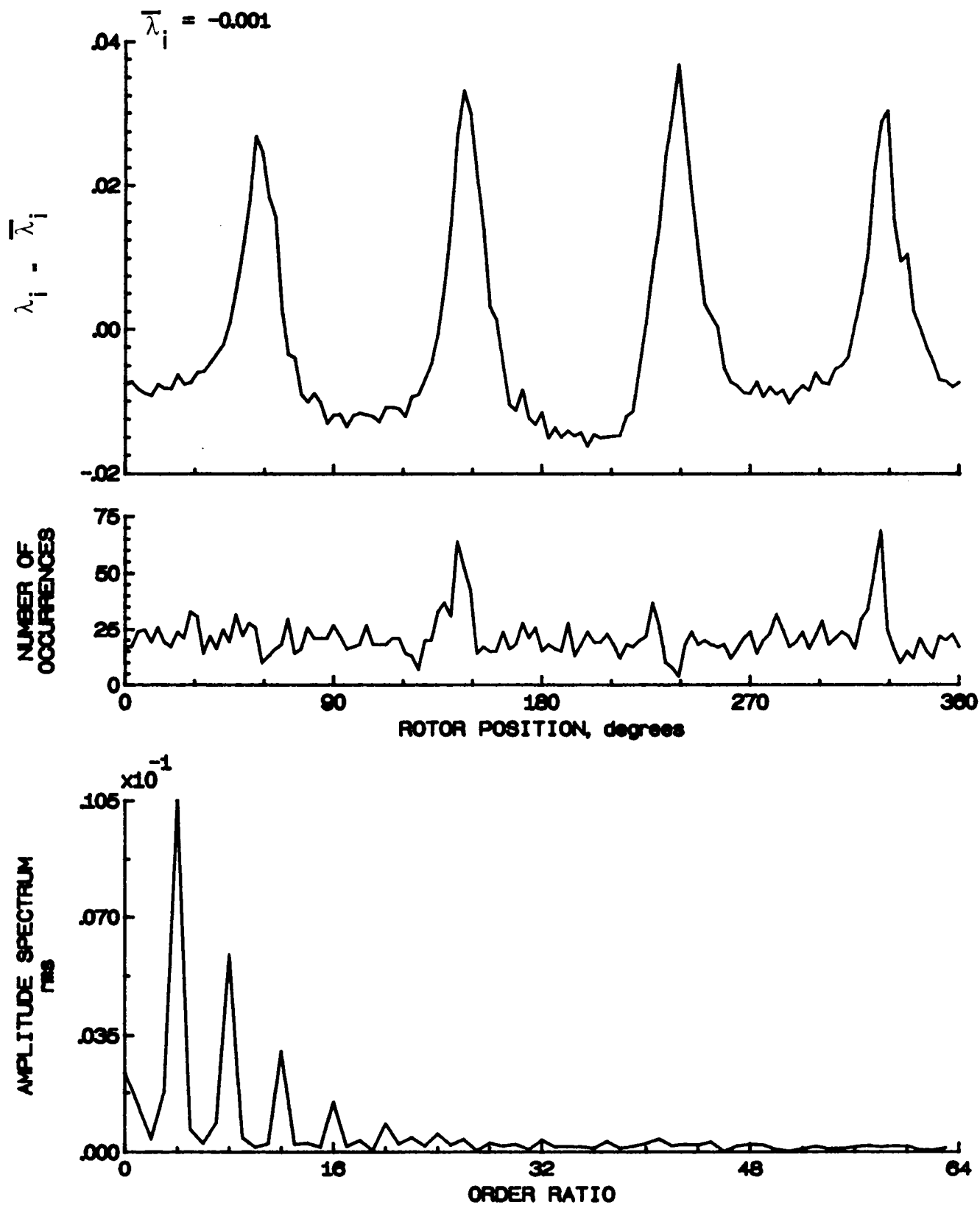


Figure 137.- Concluded.

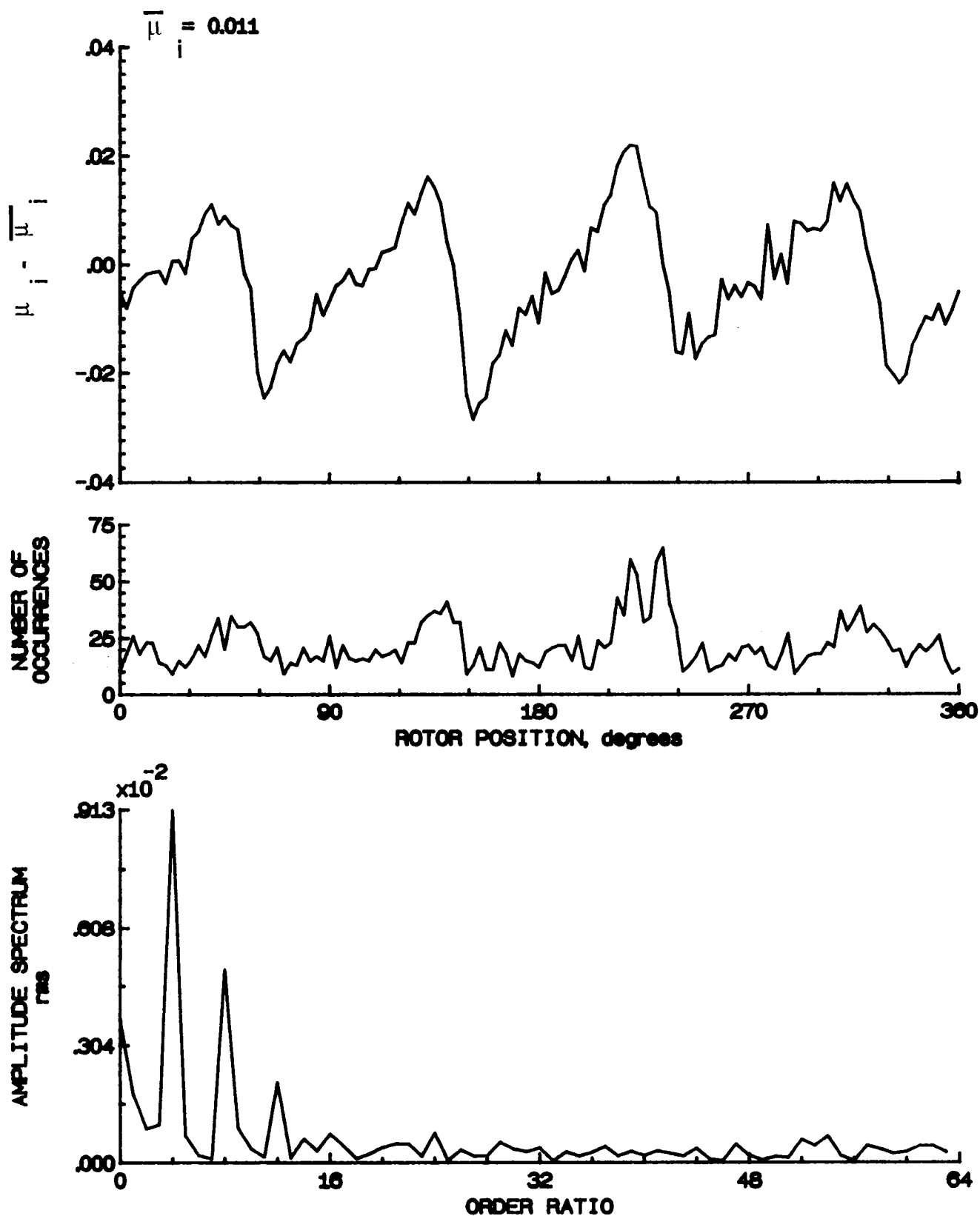


Figure 138.- Induced inflow velocity measured at 240 degrees and r/R of 0.74.

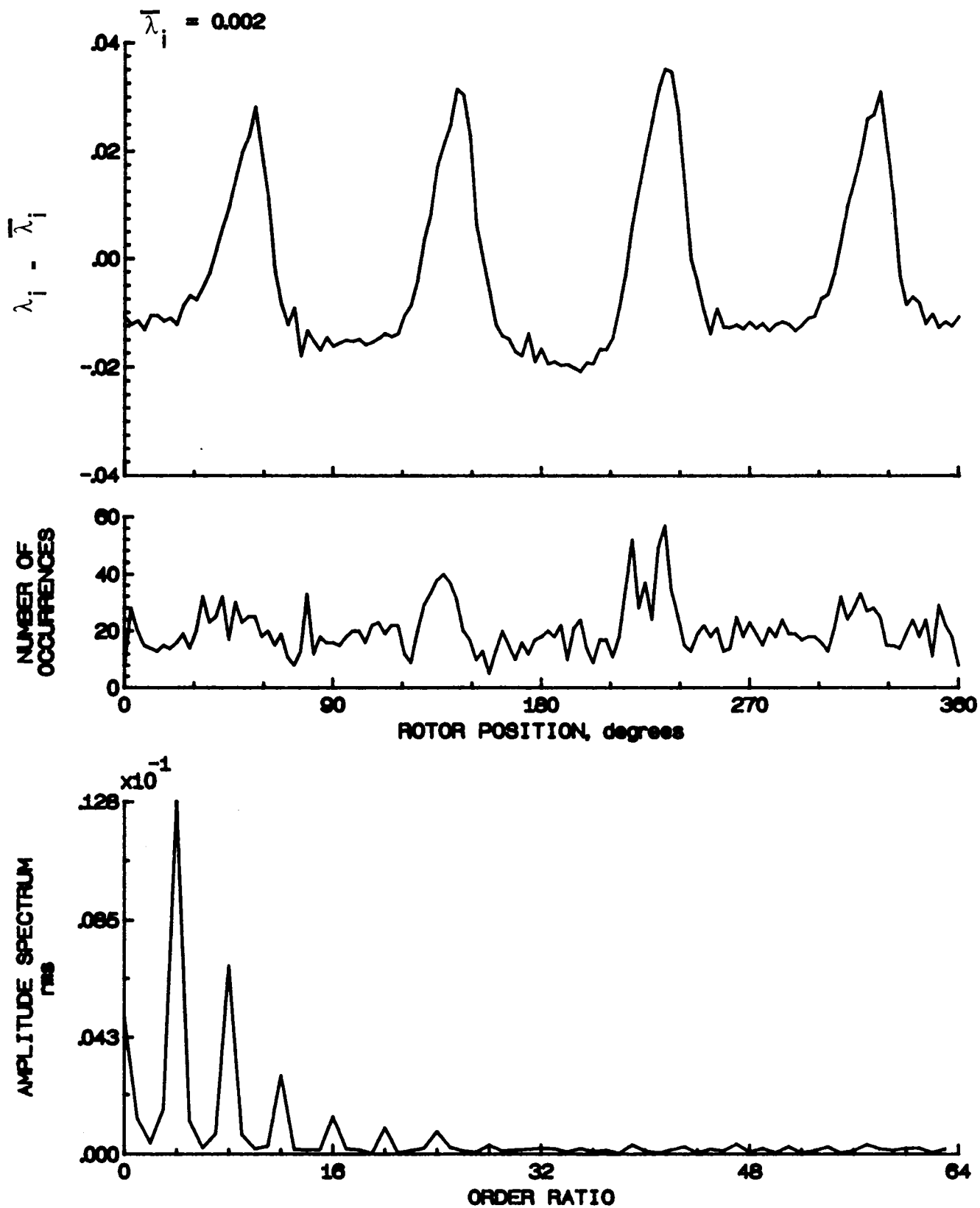


Figure 138.- Concluded.

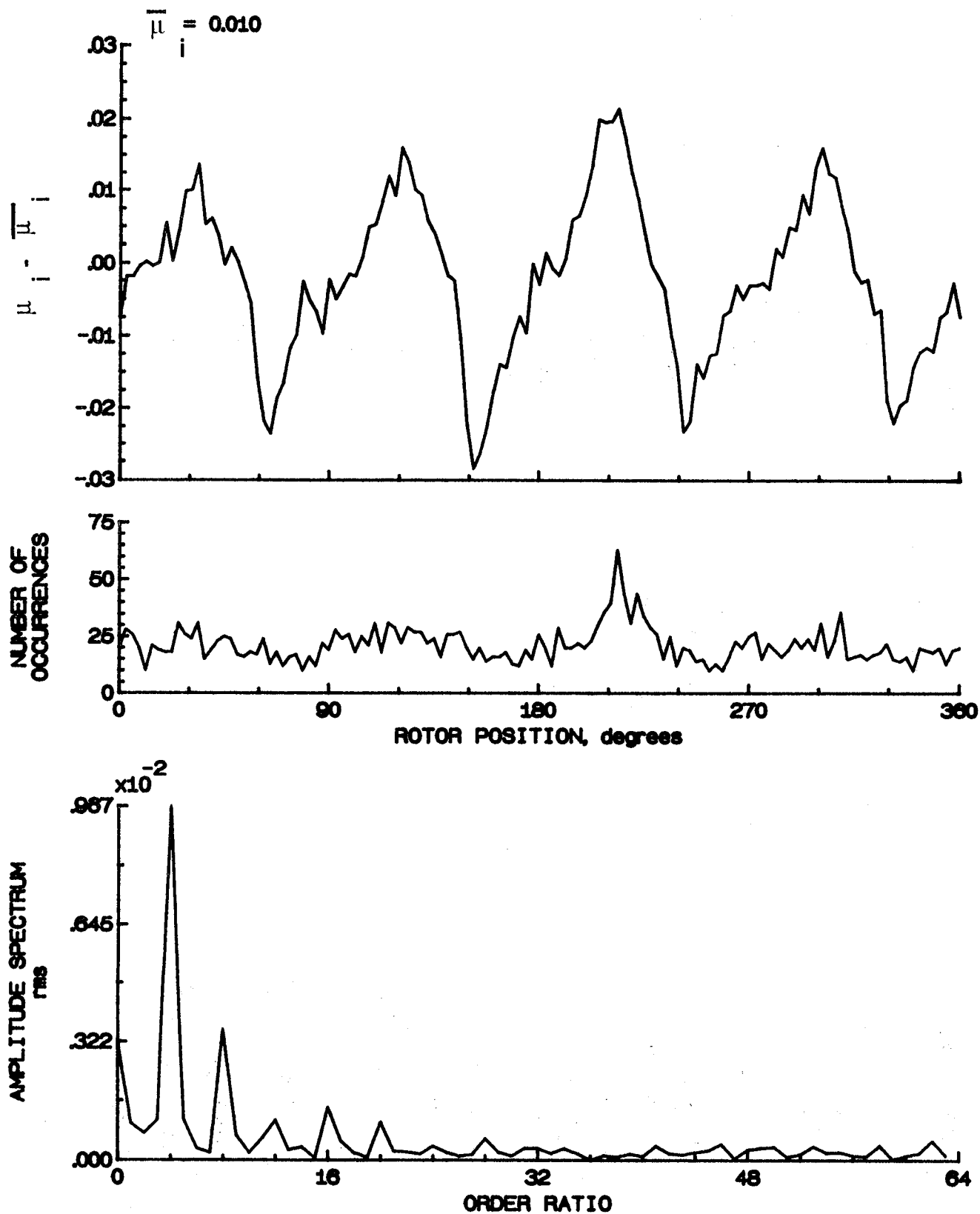


Figure 139.- Induced inflow velocity measured at 240 degrees and  $r/R$  of 0.78.

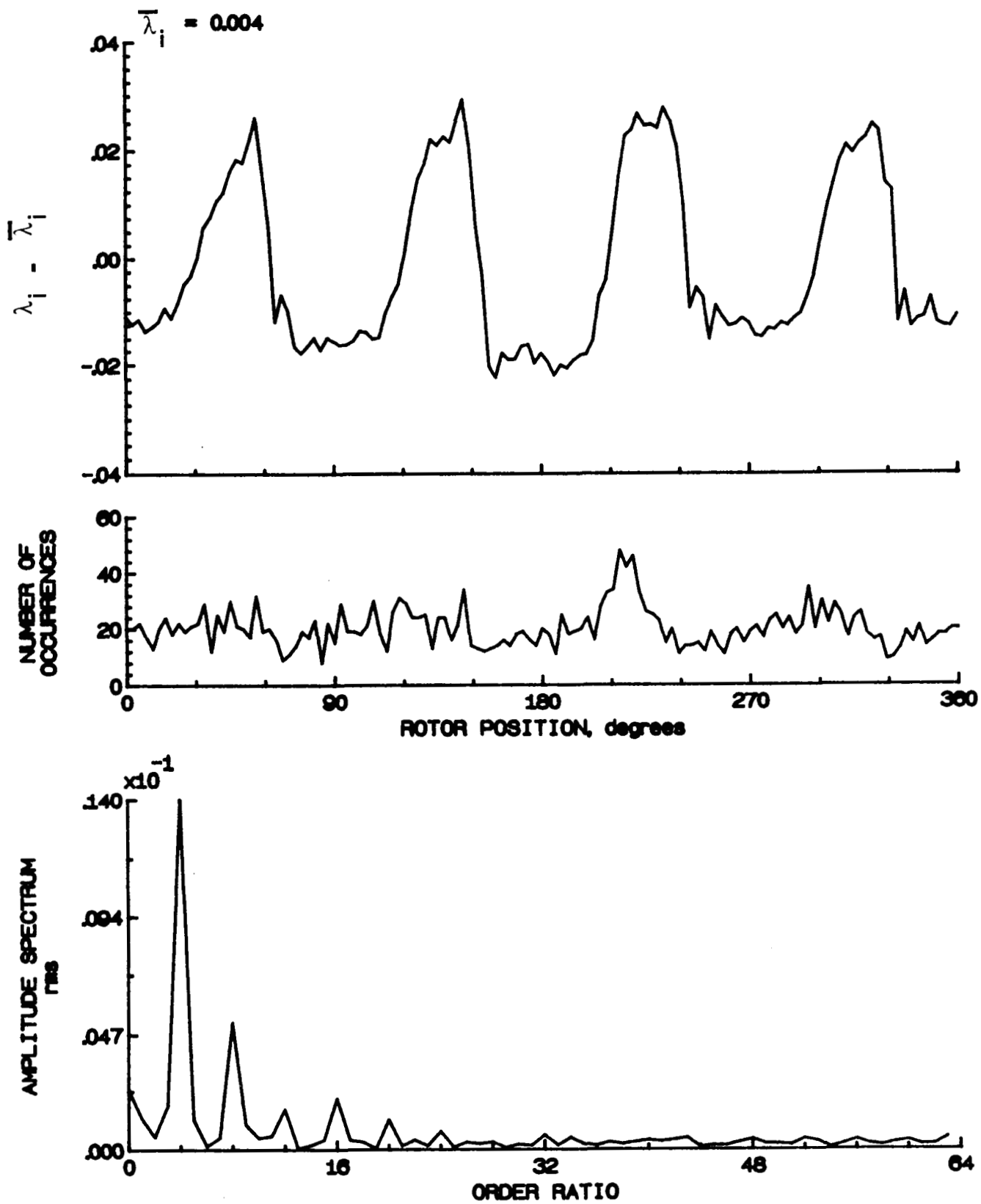


Figure 139.- Concluded.

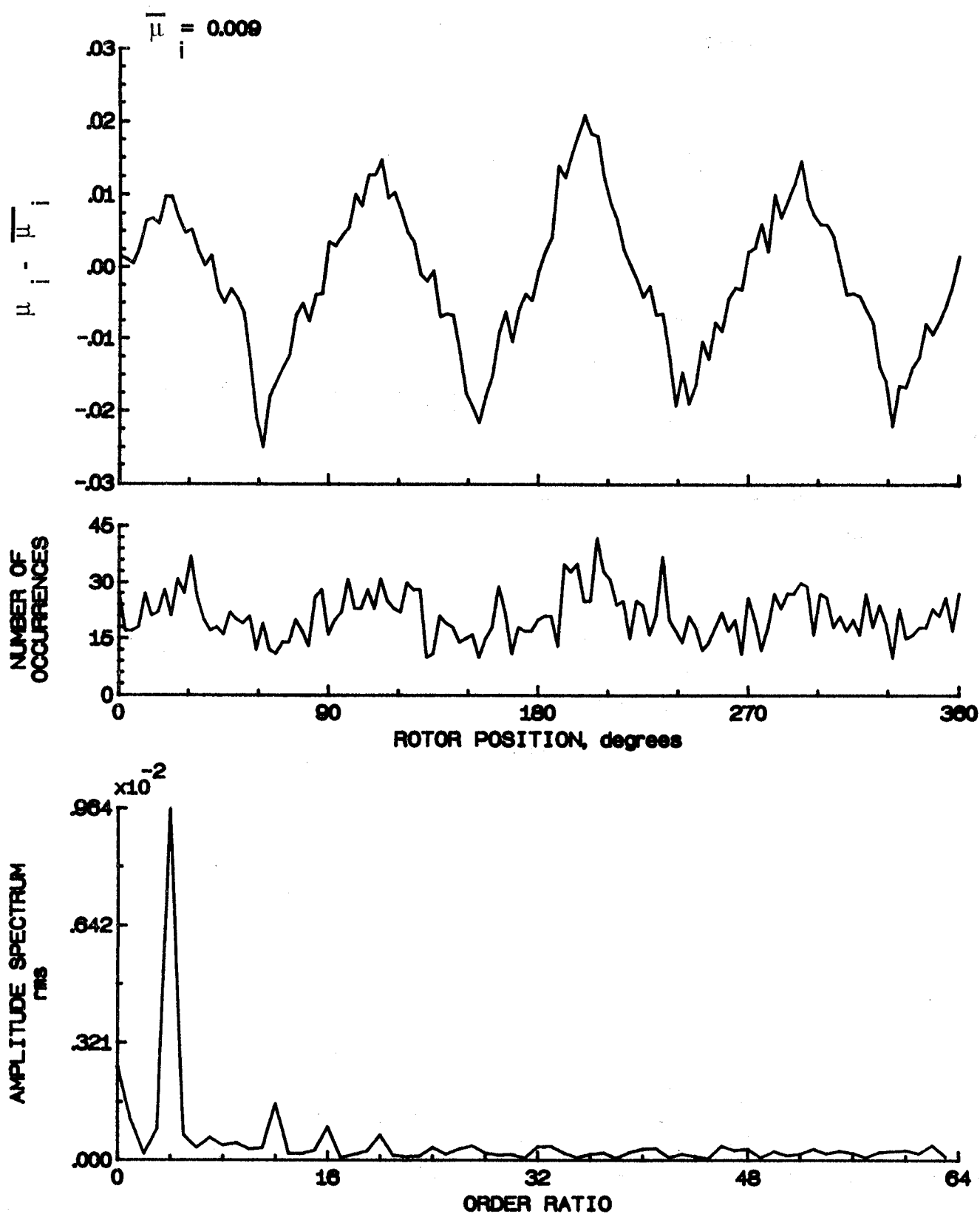


Figure 140.- Induced inflow velocity measured at 240 degrees and r/R of 0.82.



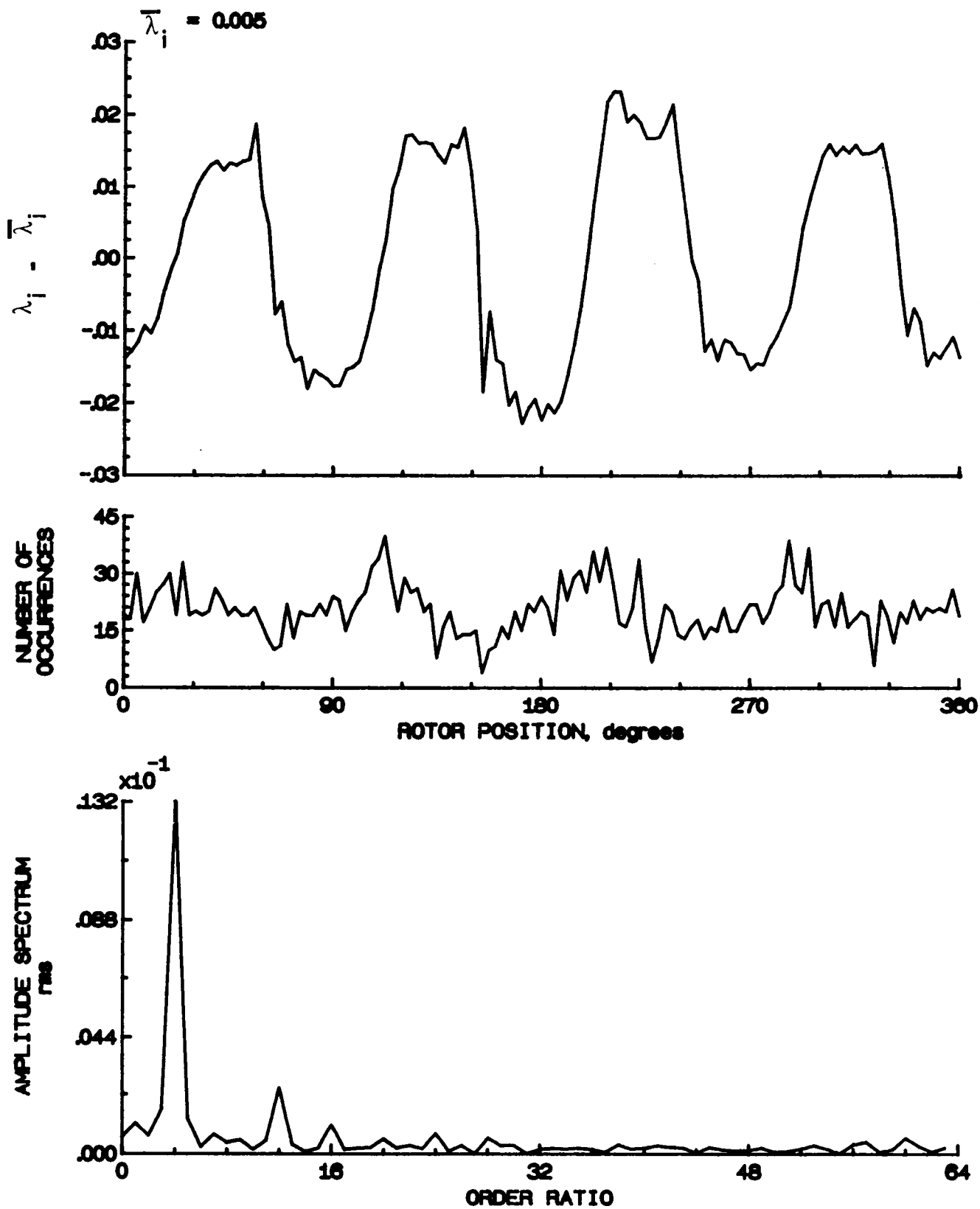


Figure 140.- Concluded.

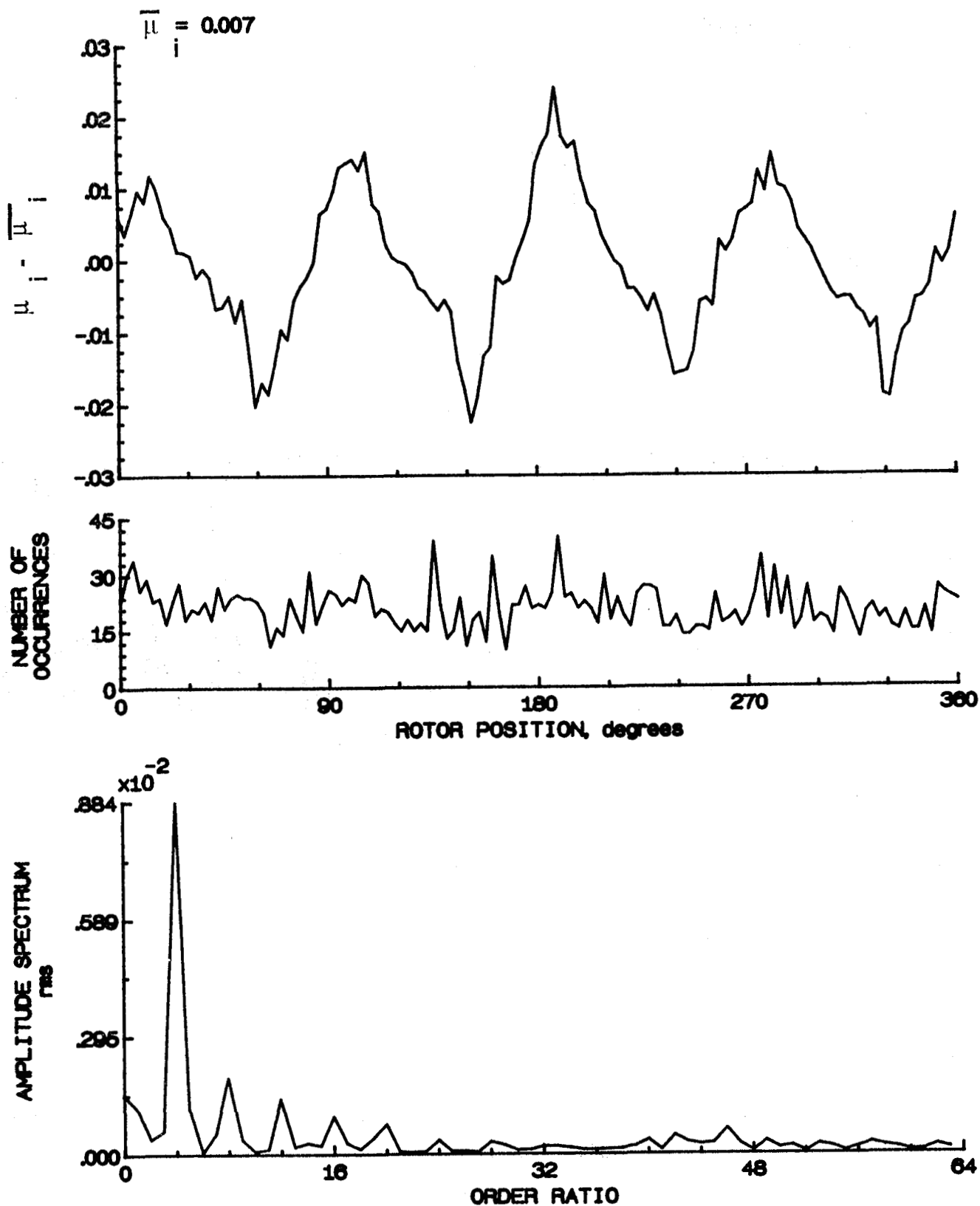


Figure 141.- Induced inflow velocity measured at 240 degrees and r/R of 0.86.

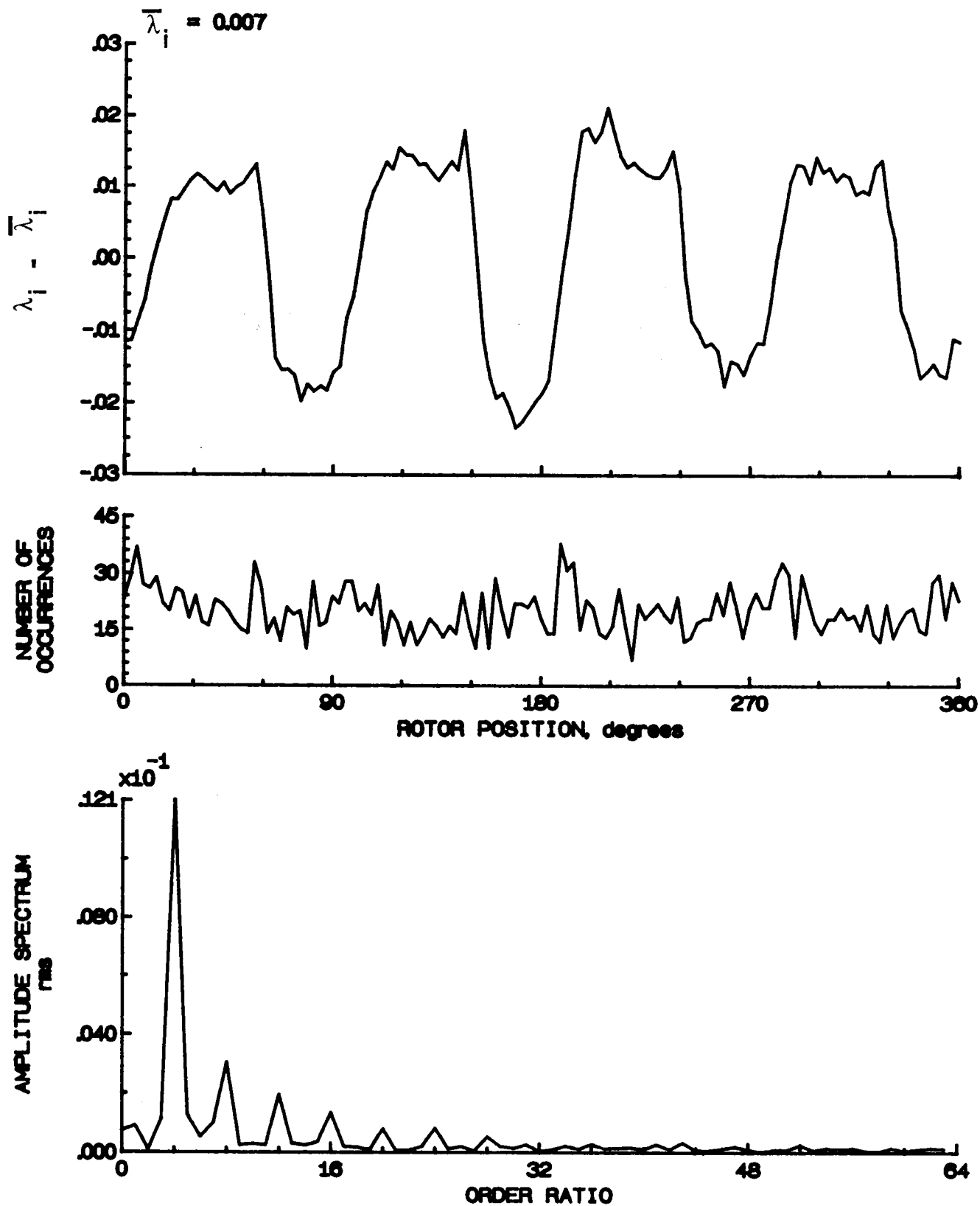


Figure 141.- Concluded.

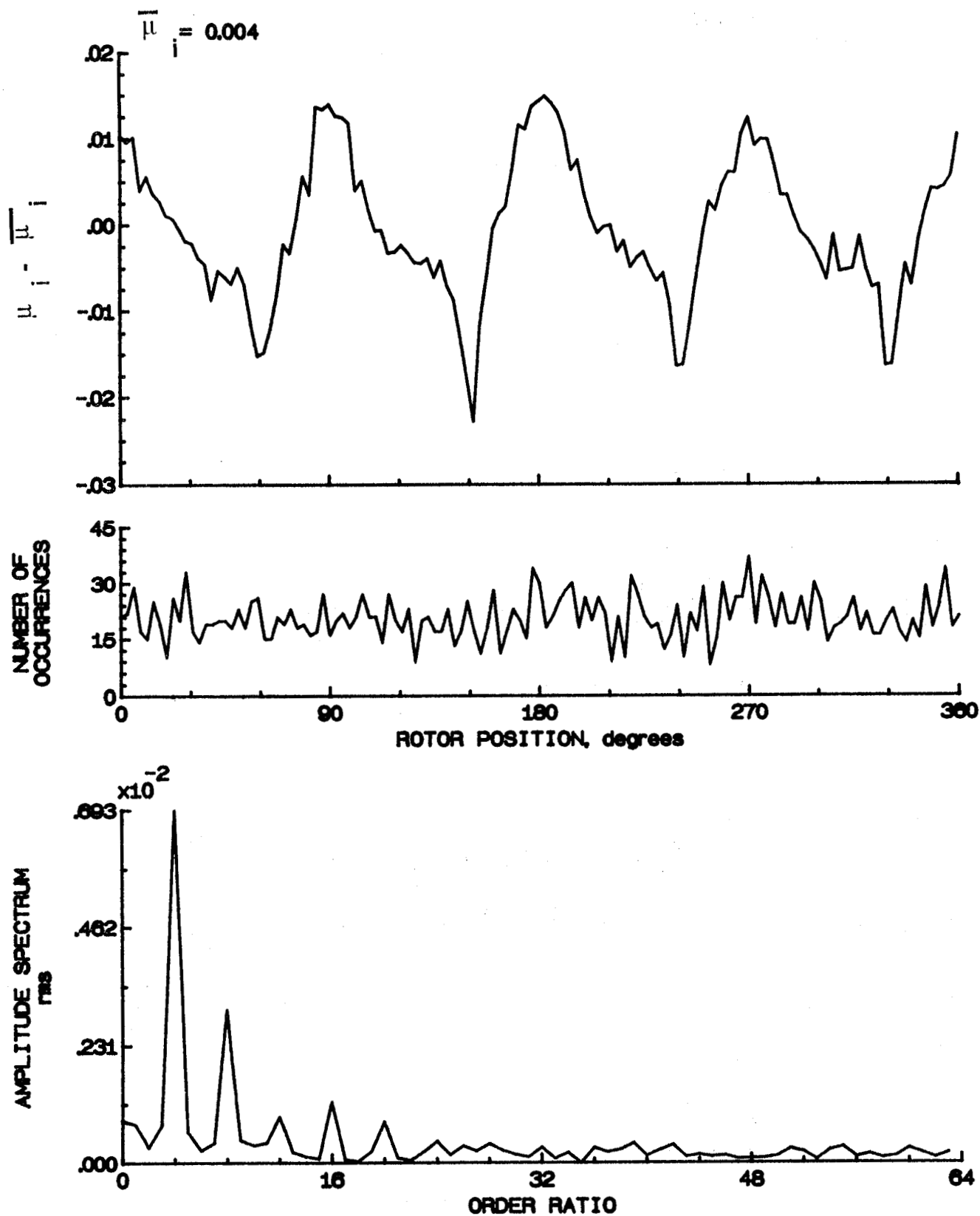


Figure 142.- Induced inflow velocity measured at 240 degrees and  $r/R$  of 0.90.

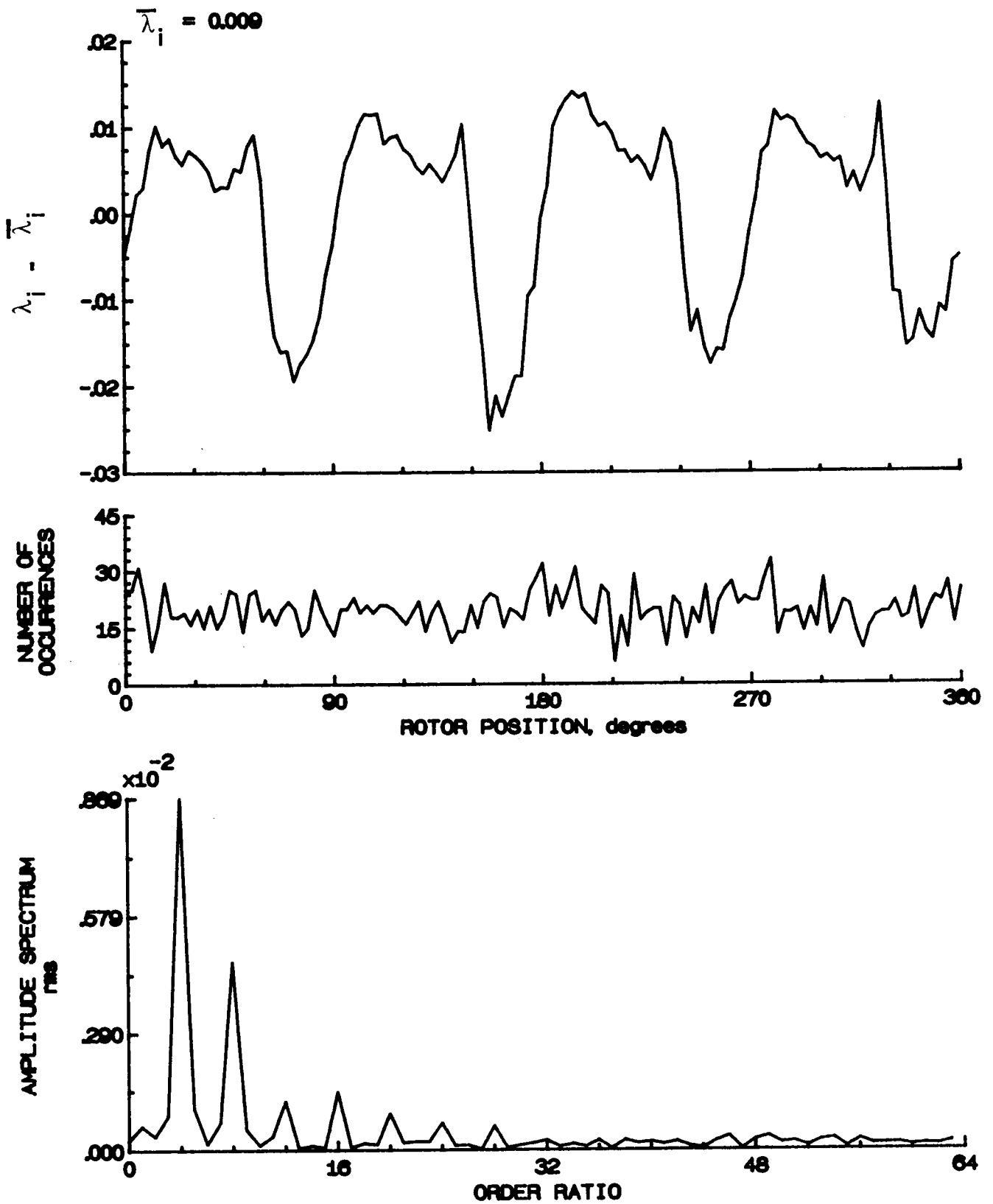


Figure 142.- Concluded.

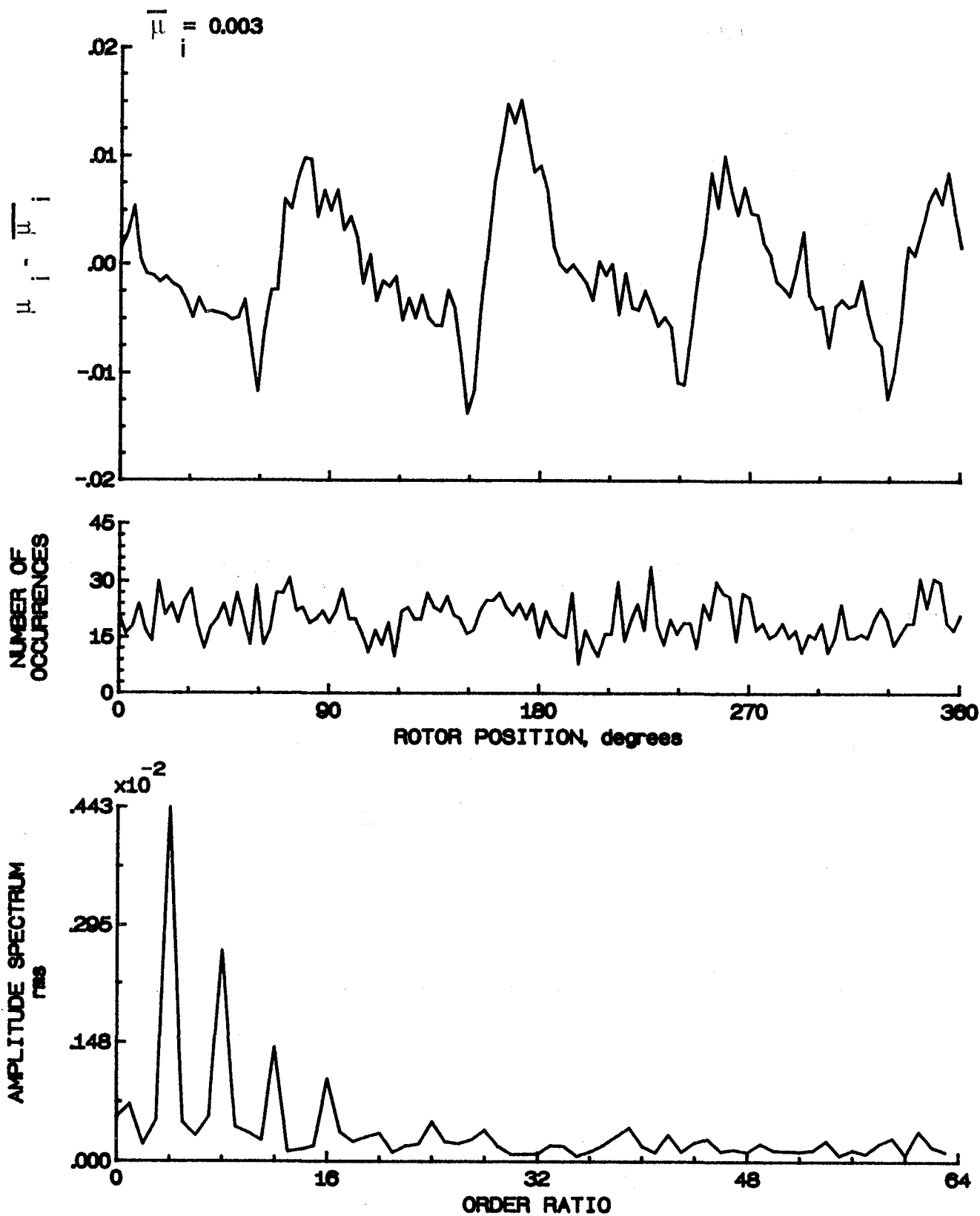


Figure 143.- Induced inflow velocity measured at 240 degrees and r/R of 0.94.

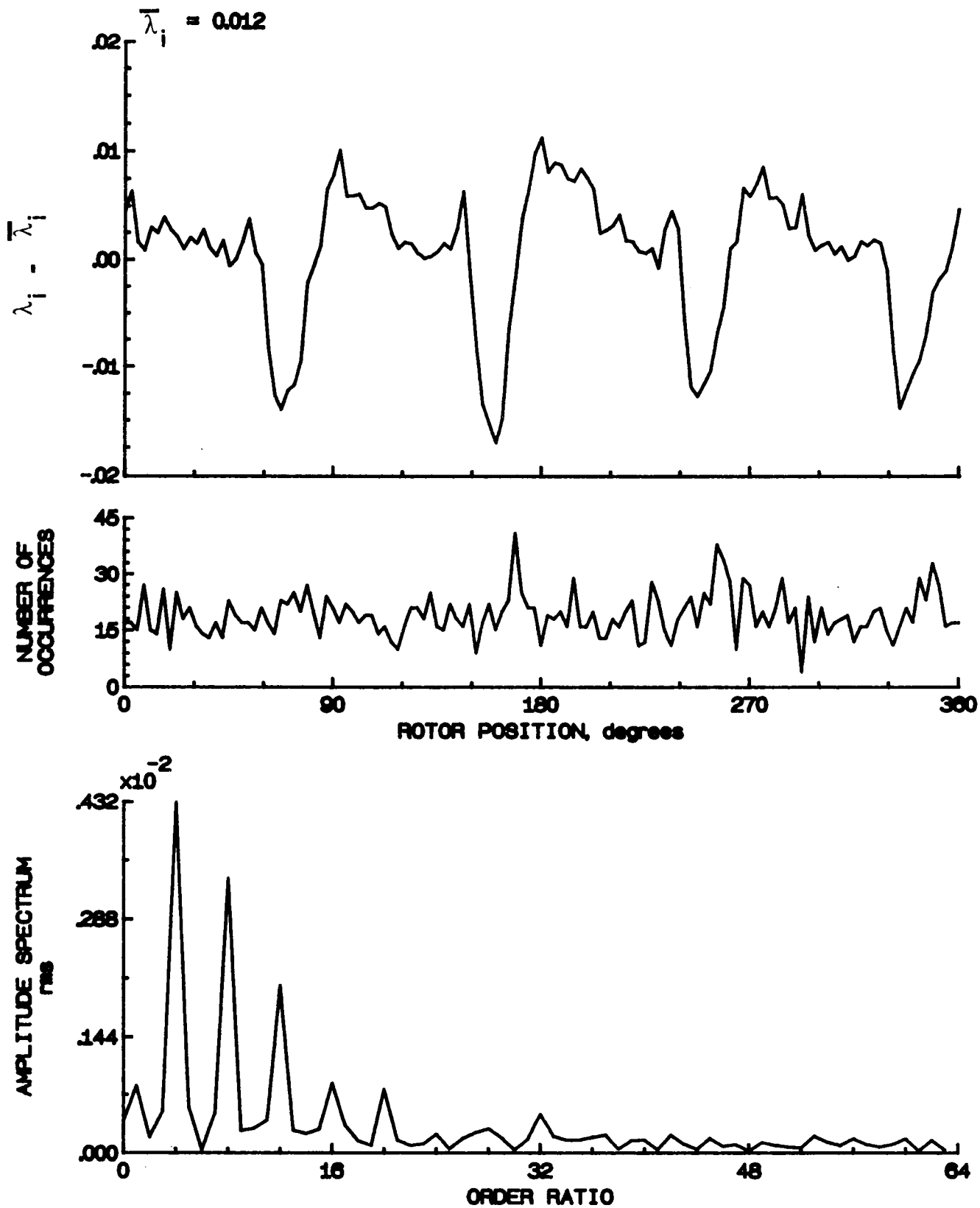


Figure 143.- Concluded.

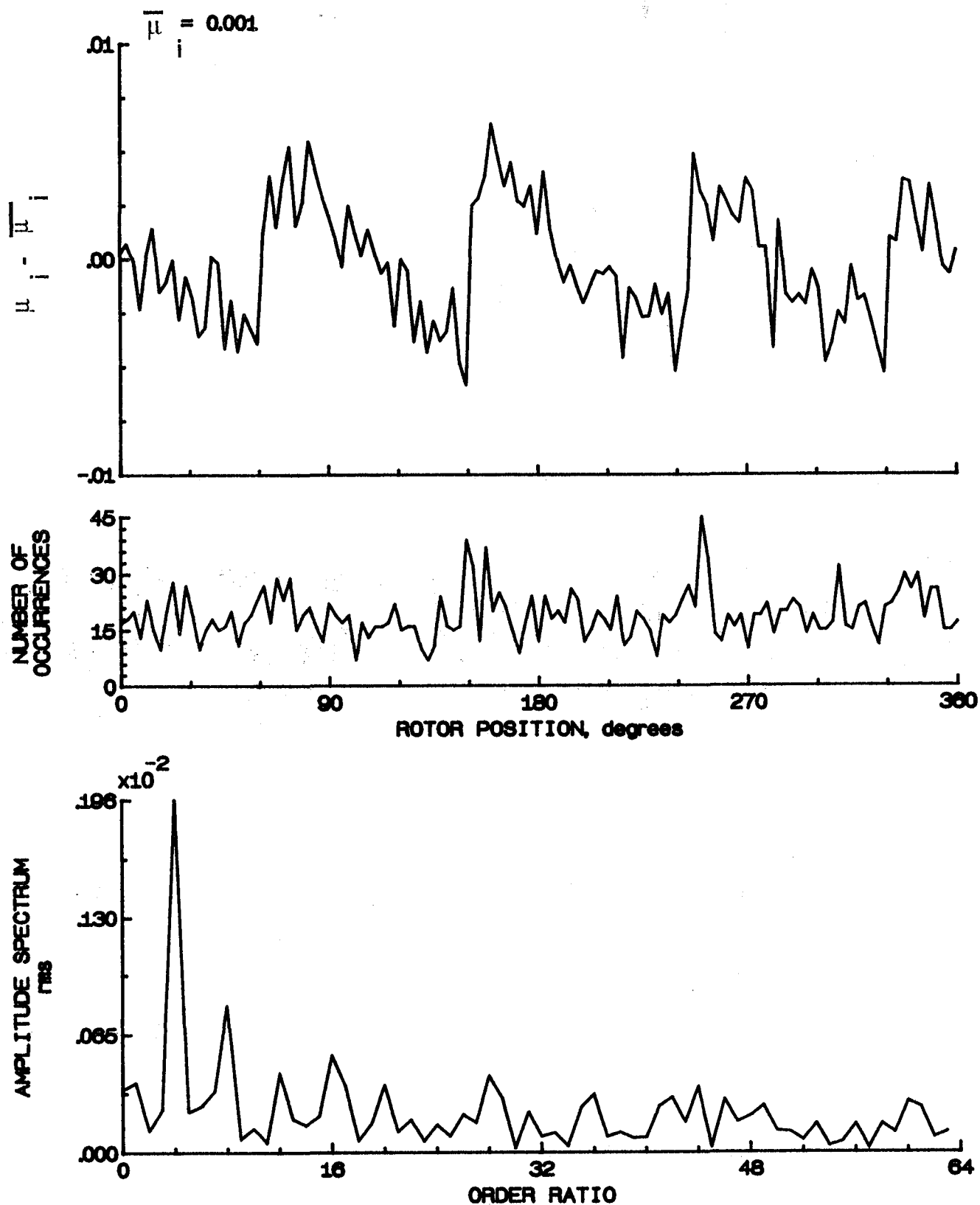


Figure 144.- Induced inflow velocity measured at 240 degrees and  $r/R$  of 0.98.



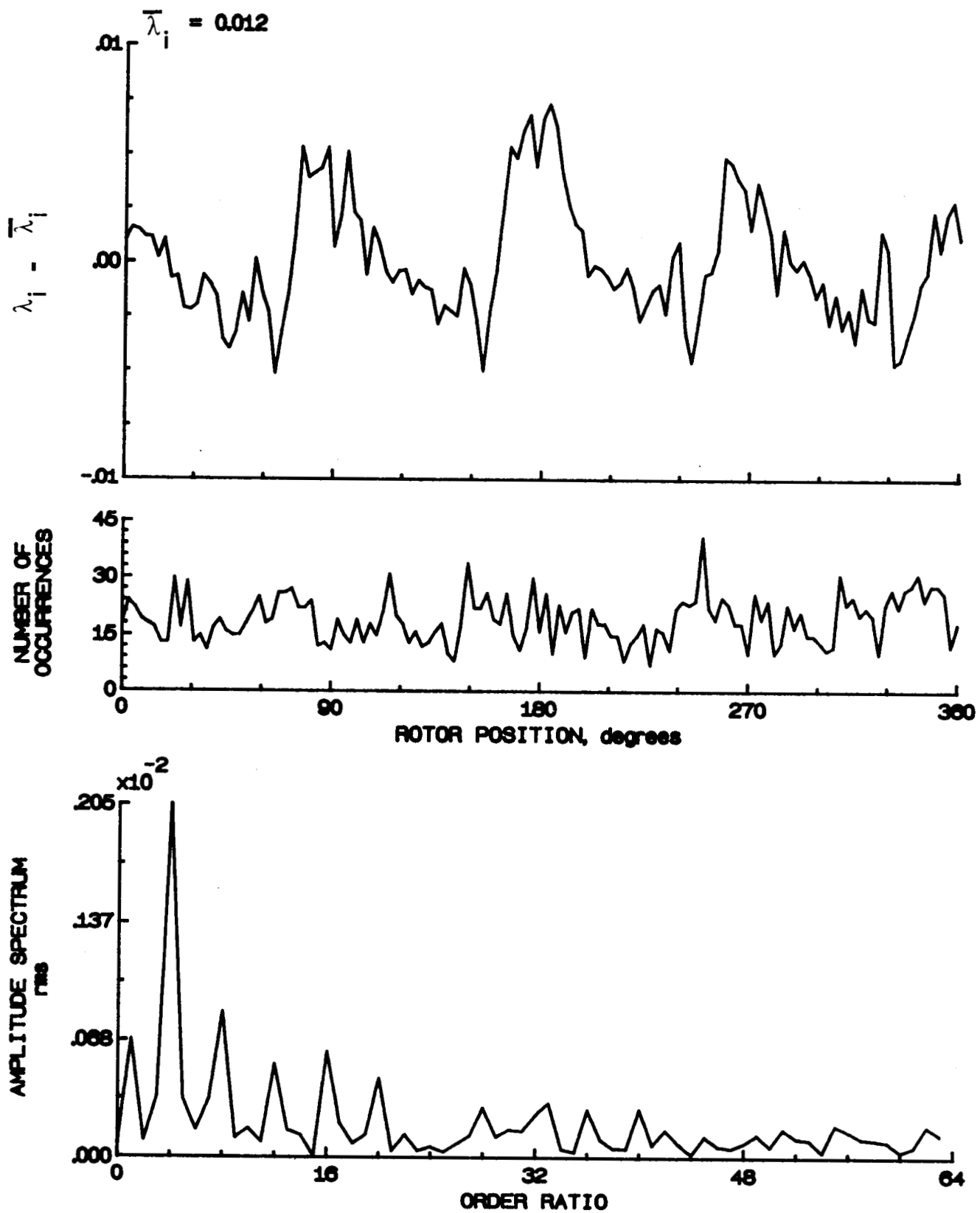


Figure 144.- Concluded.

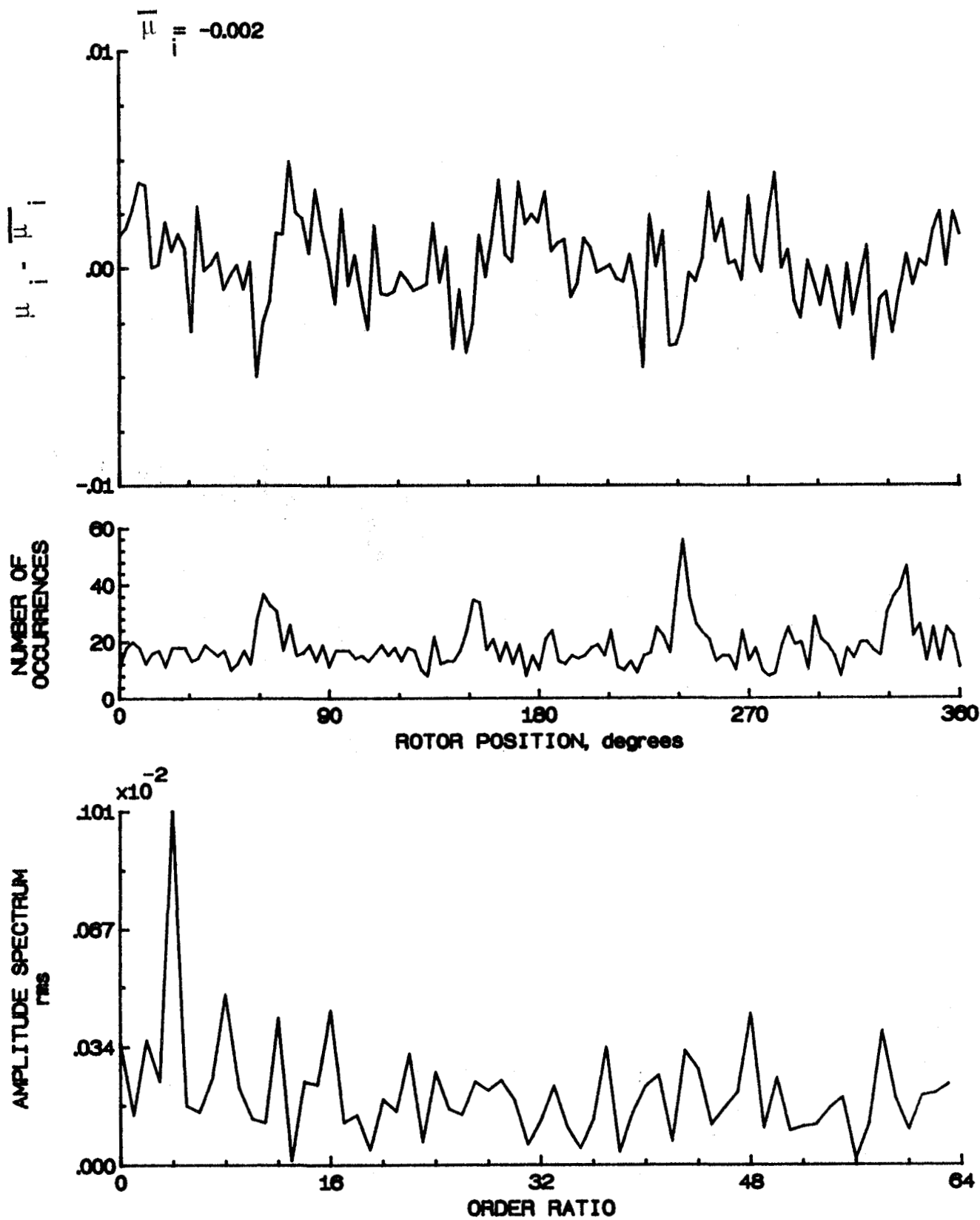


Figure 145.- Induced inflow velocity measured at 240 degrees and r/R of 1.02.

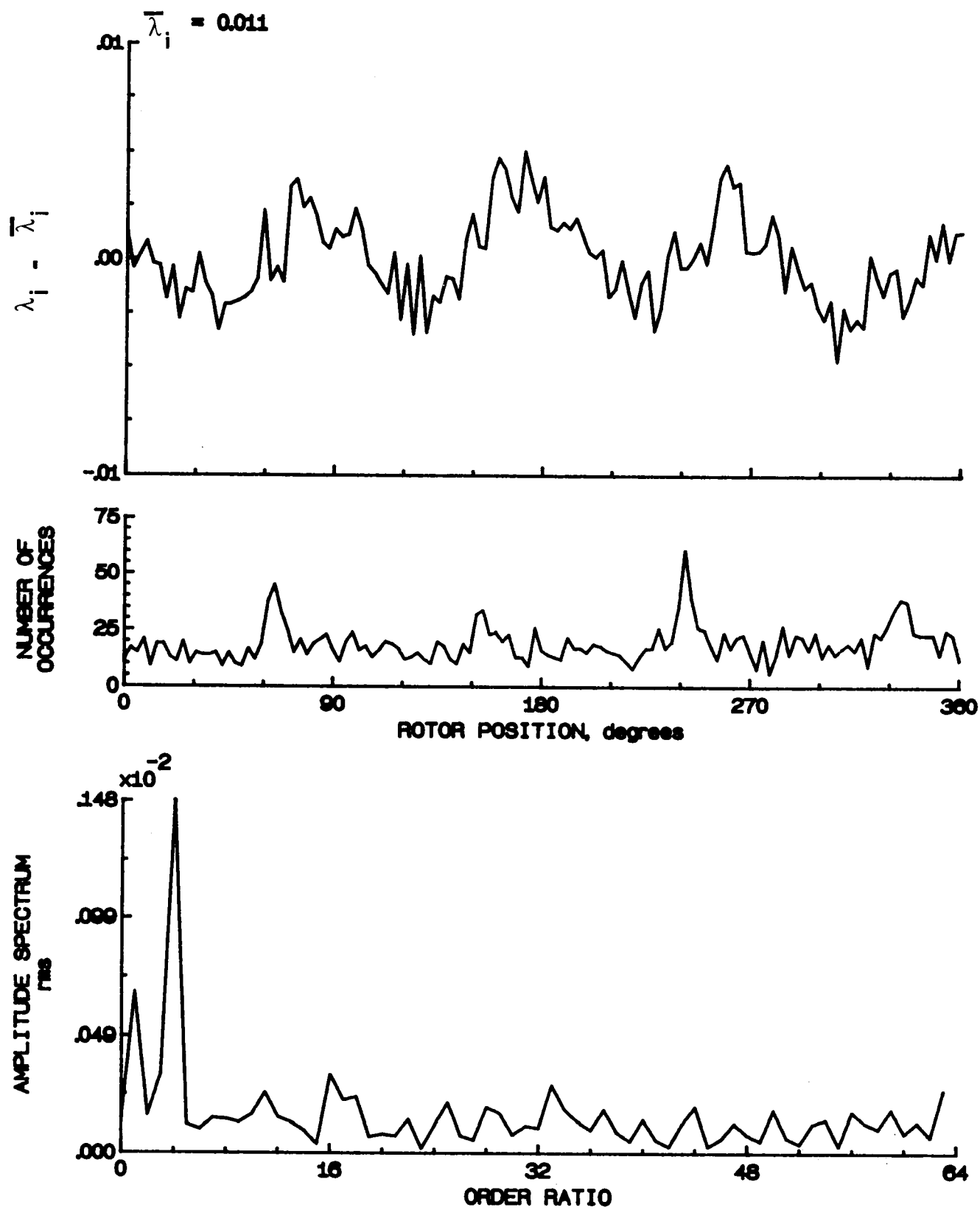


Figure 145.- Concluded.

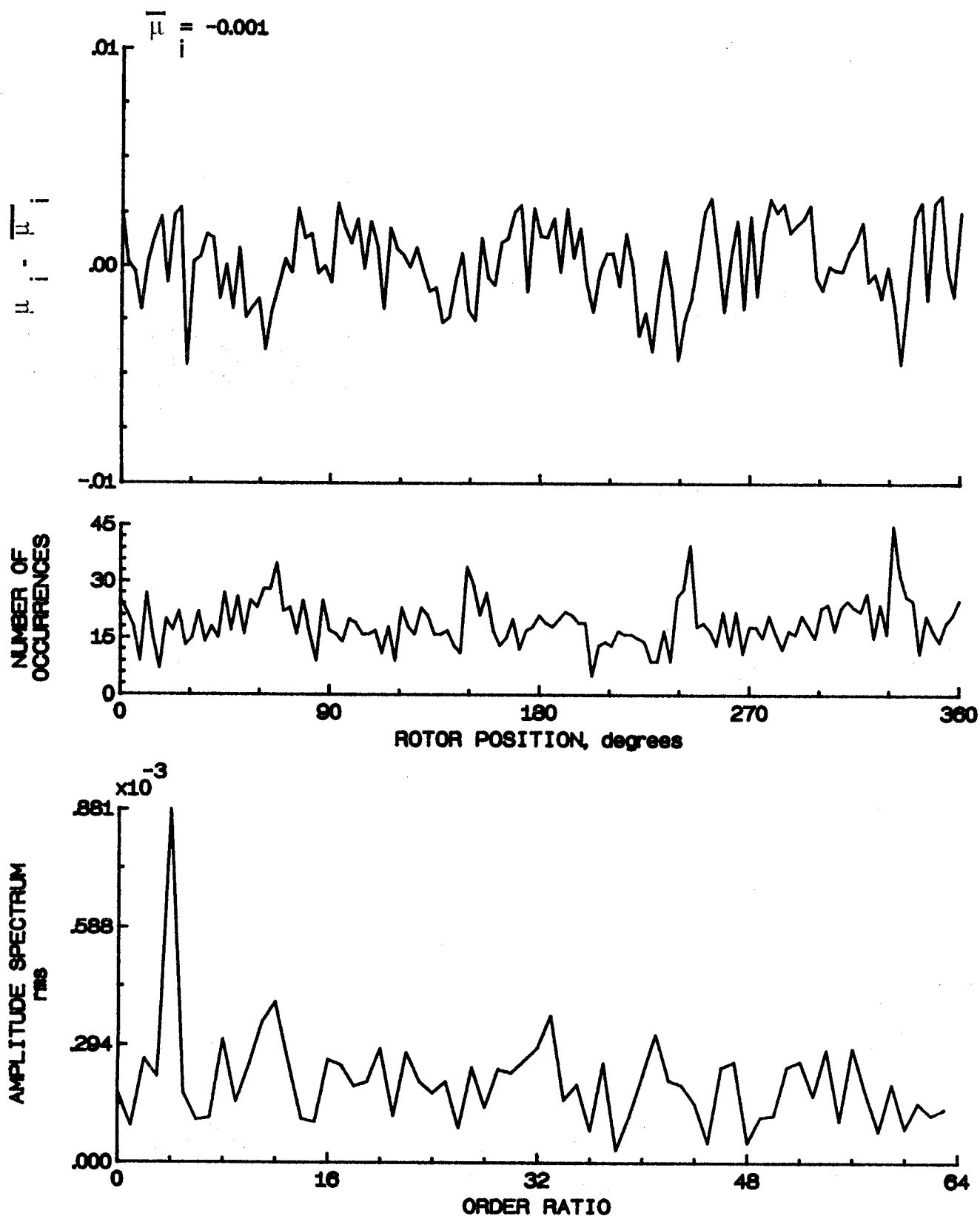


Figure 146.- Induced inflow velocity measured at 240 degrees and  $r/R$  of 1.04.

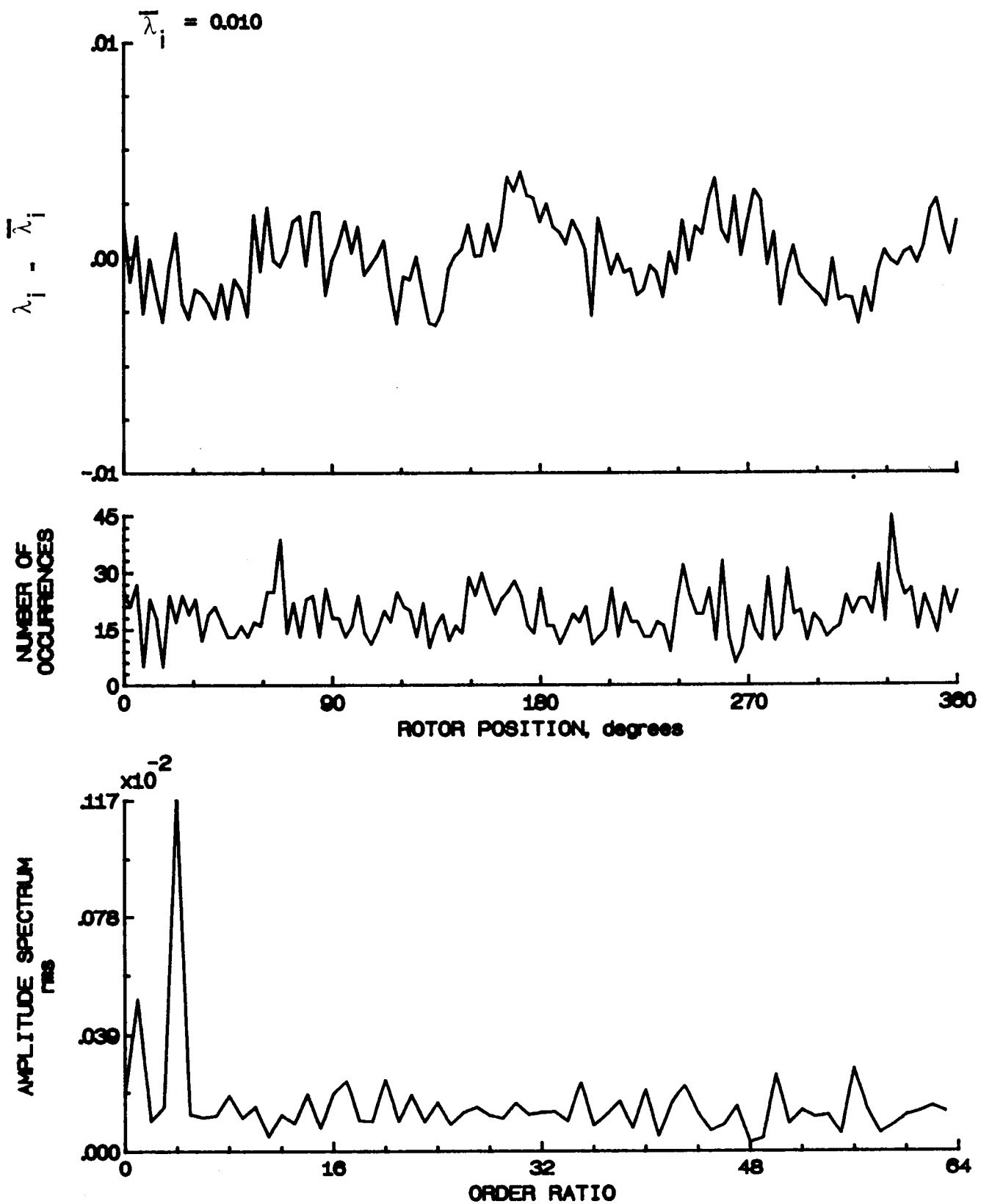


Figure 148.- Concluded.

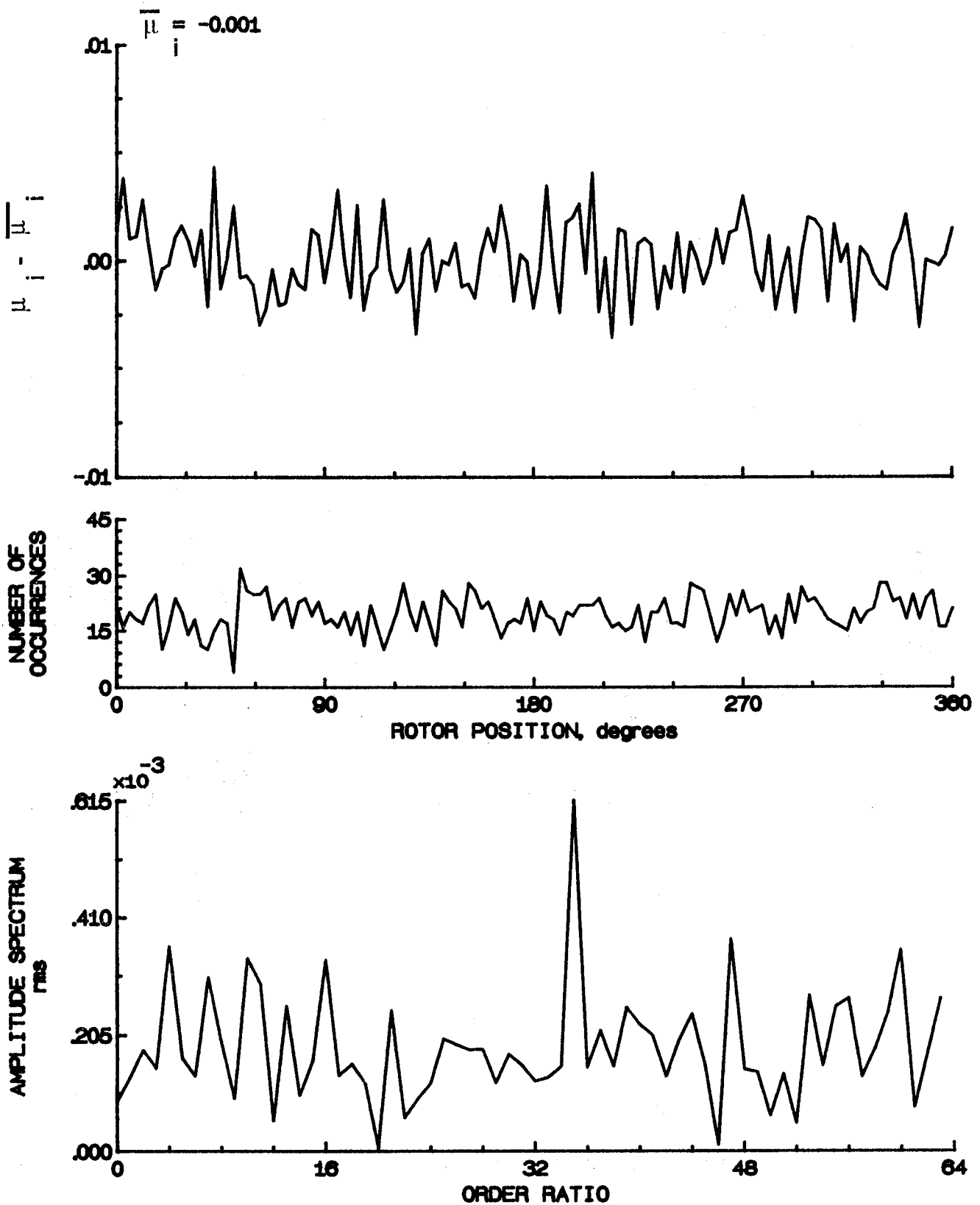


Figure 147.- Induced inflow velocity measured at 240 degrees and r/R of 1.10.

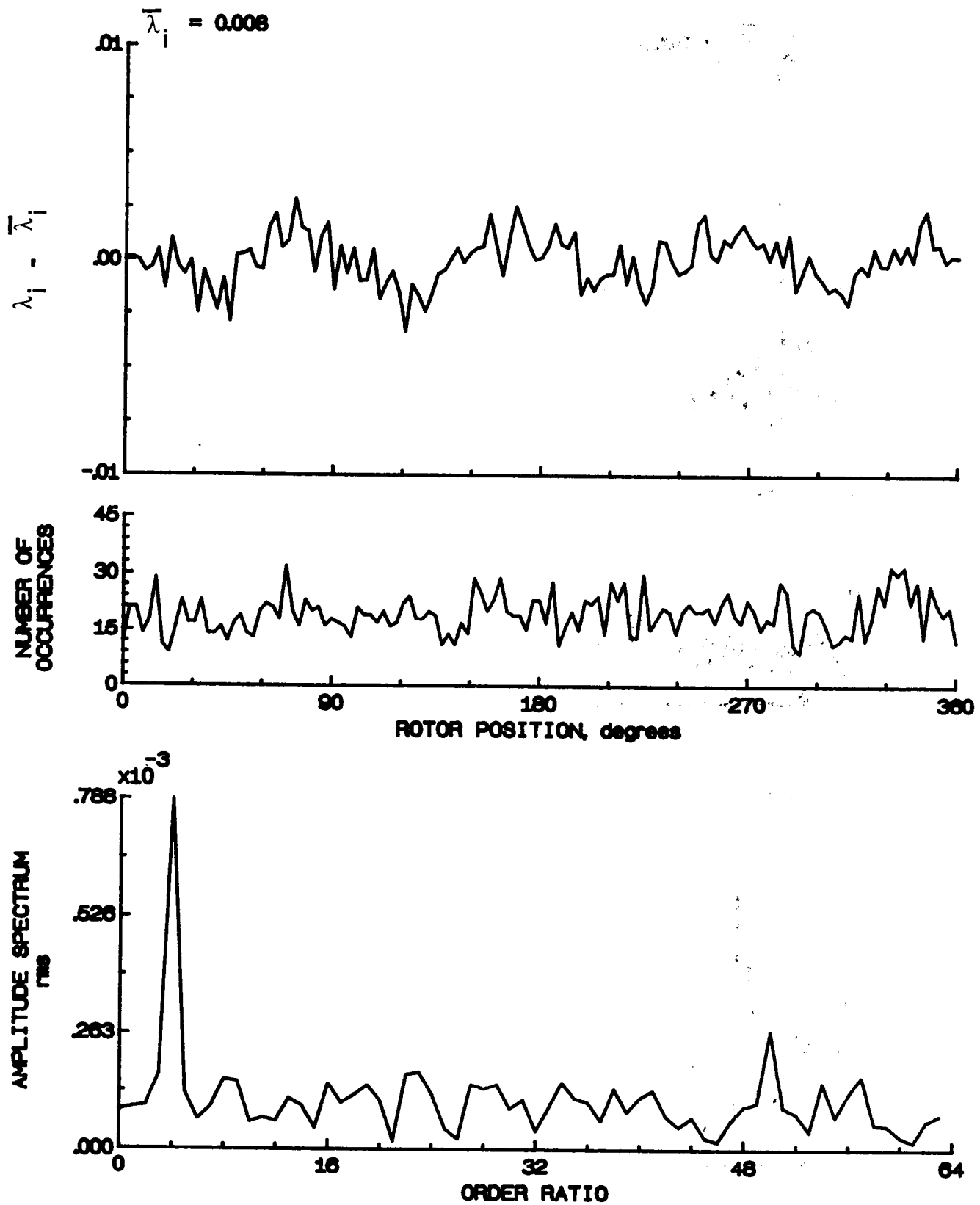


Figure 147.- Concluded.

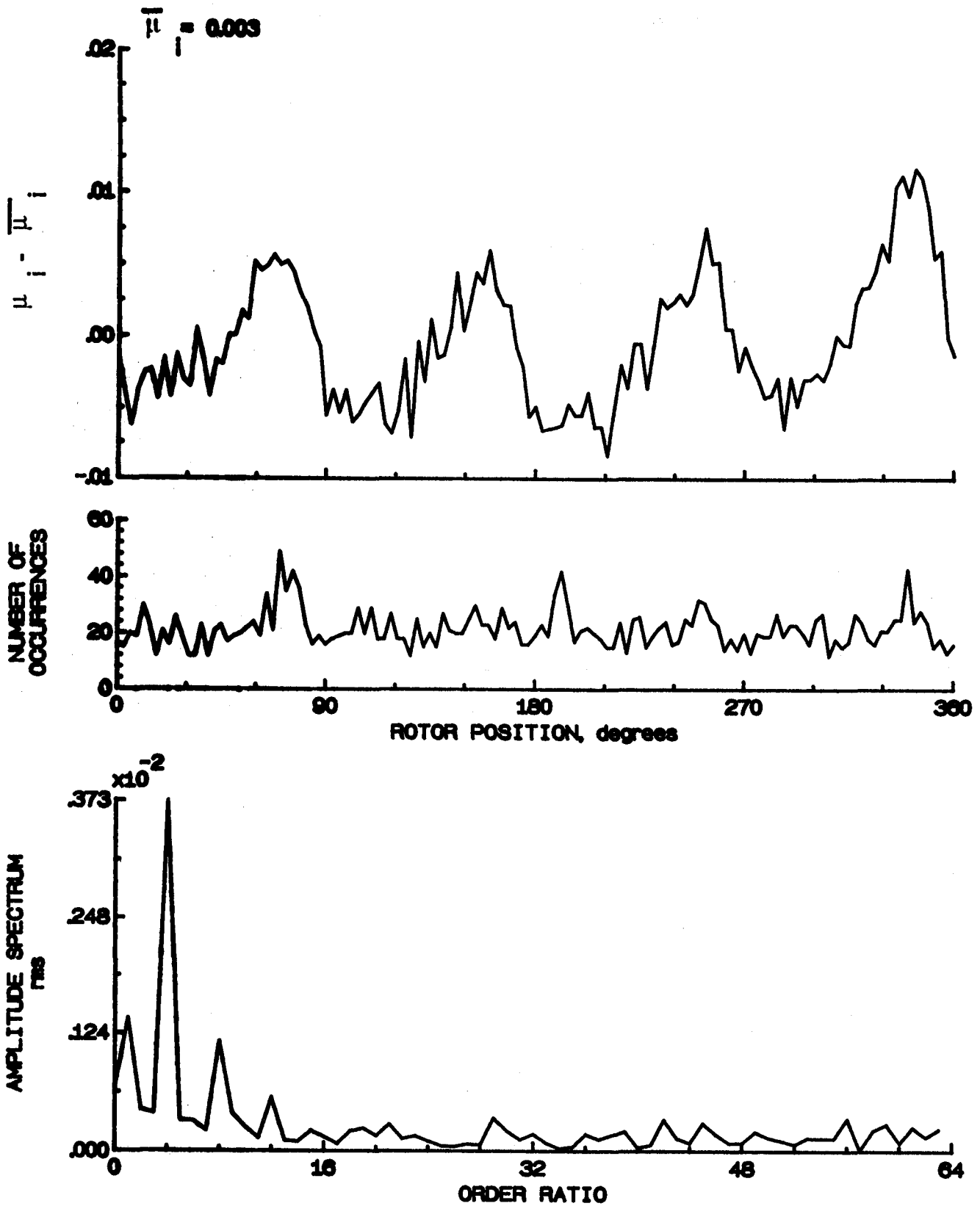


Figure 148.- Induced inflow velocity measured at 270 degrees and r/R of 0.20.



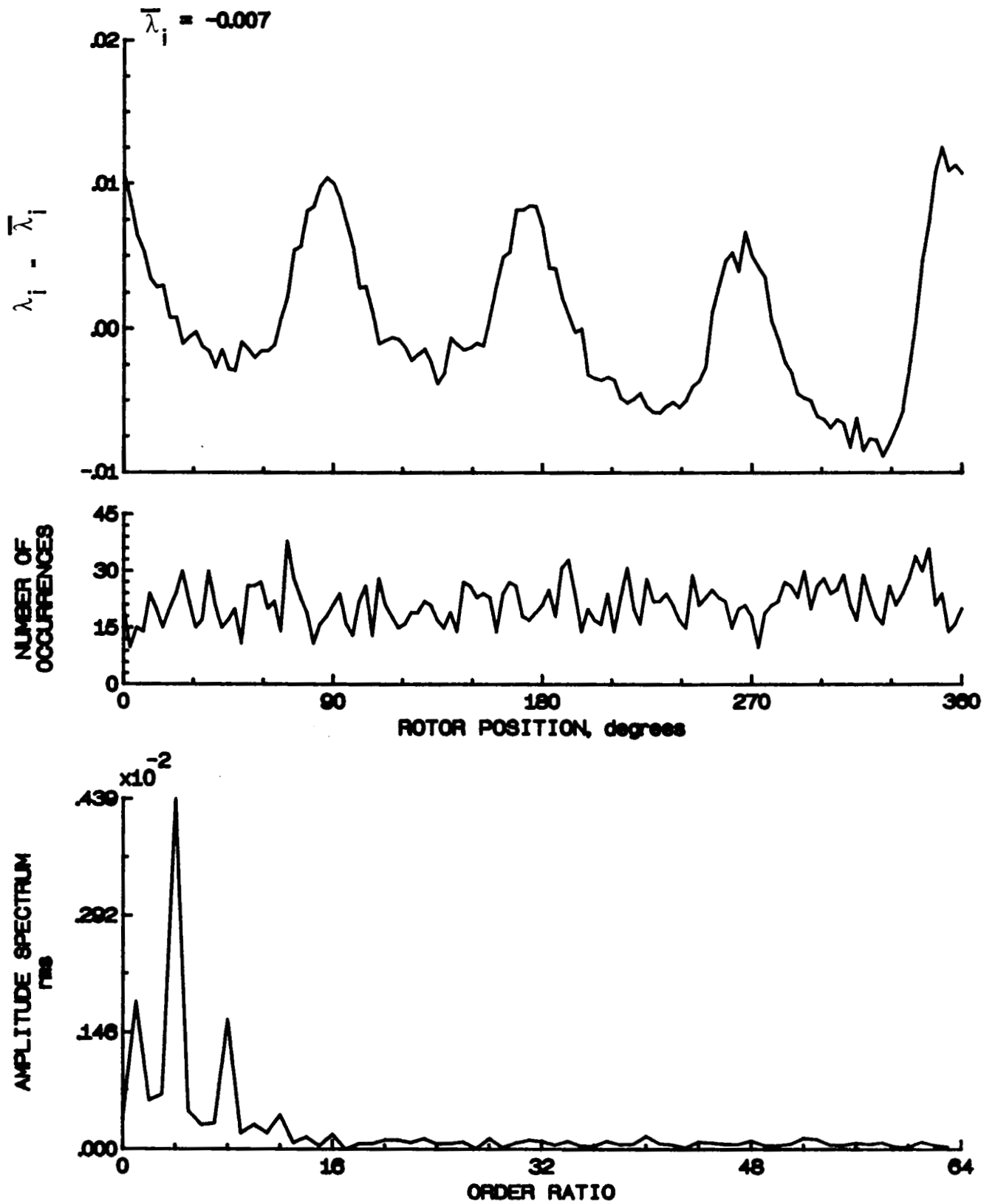


Figure 148.- Concluded.

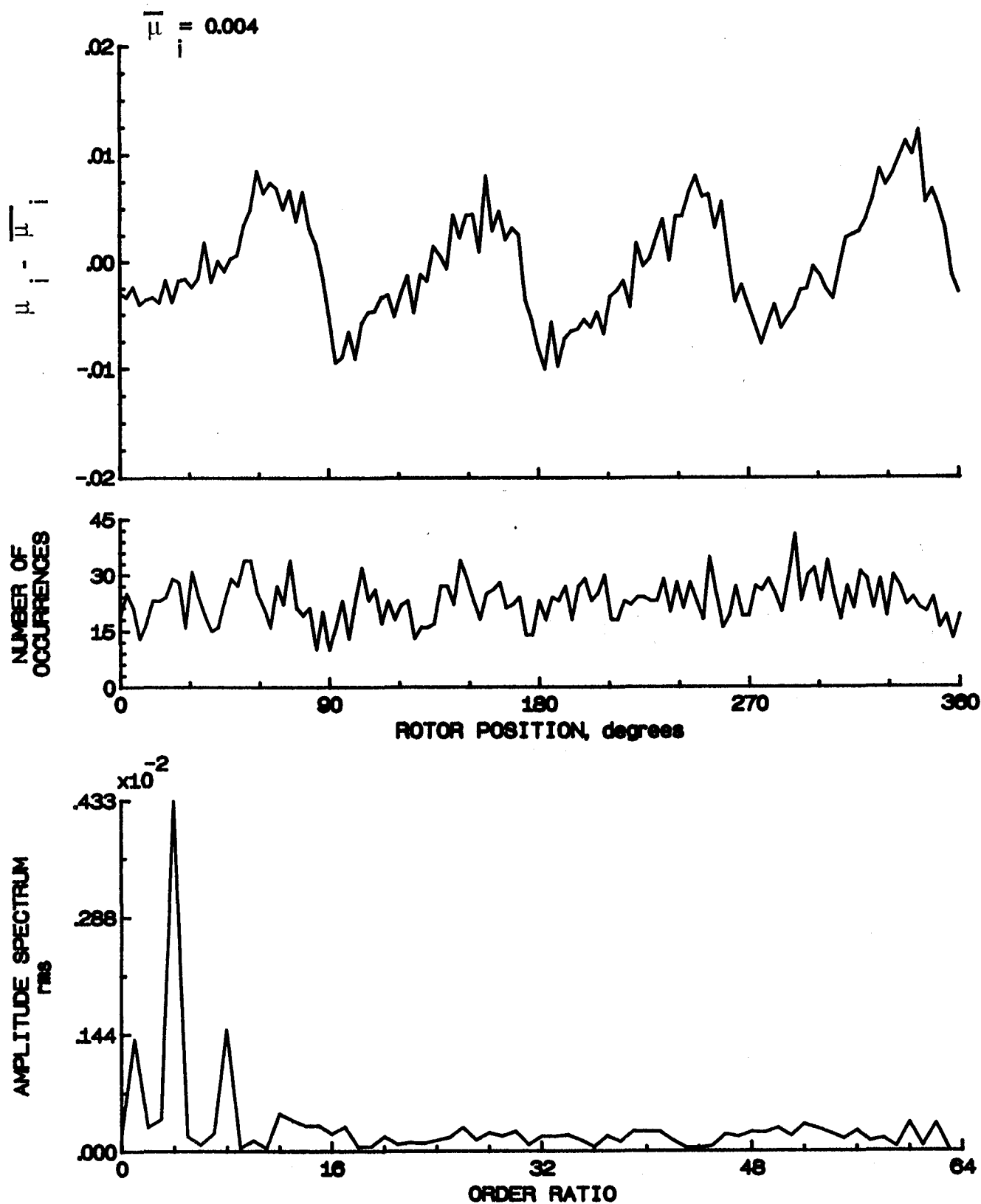


Figure 149.- Induced inflow velocity measured at 270 degrees and r/R of 0.40.

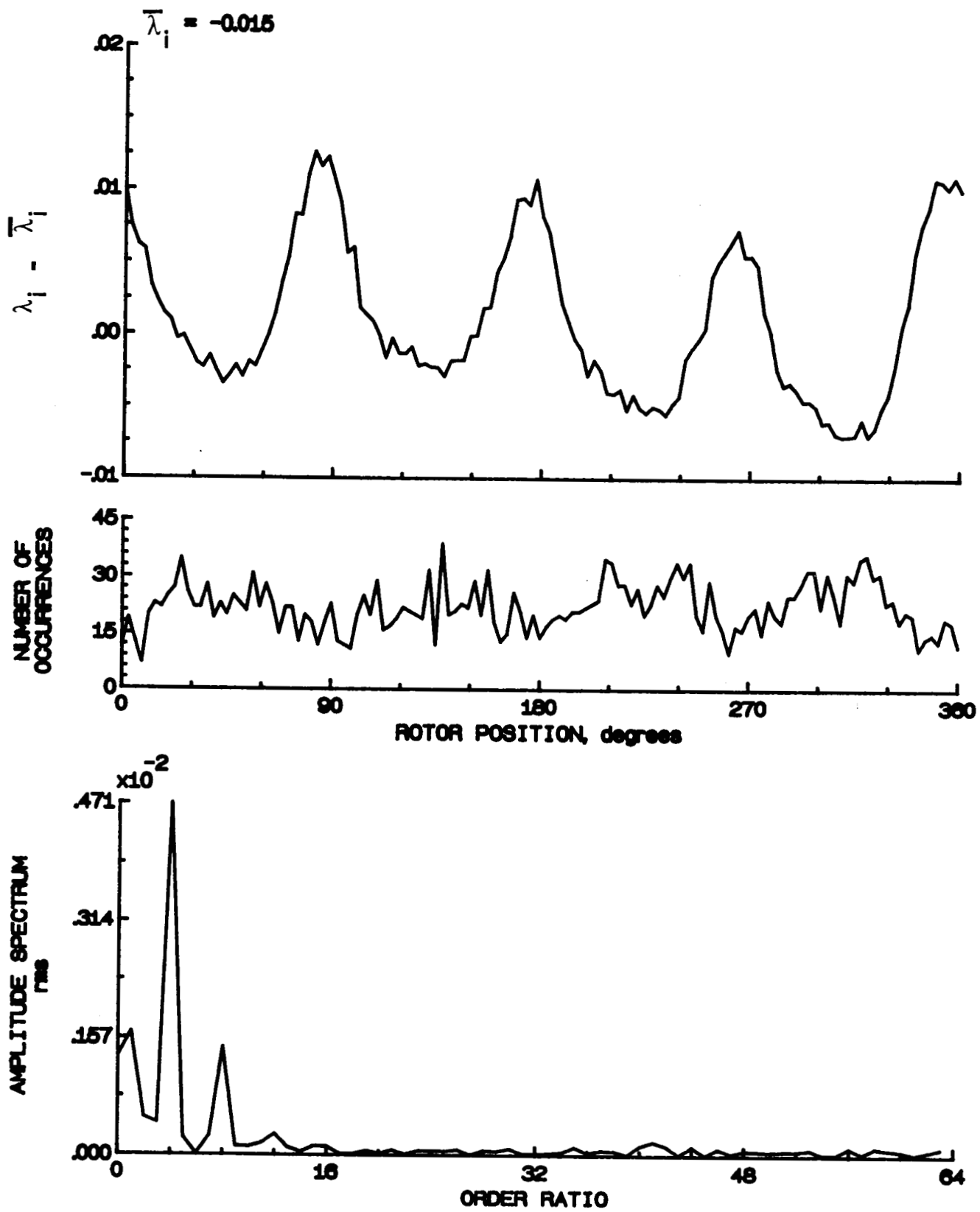


Figure 149.- Concluded.

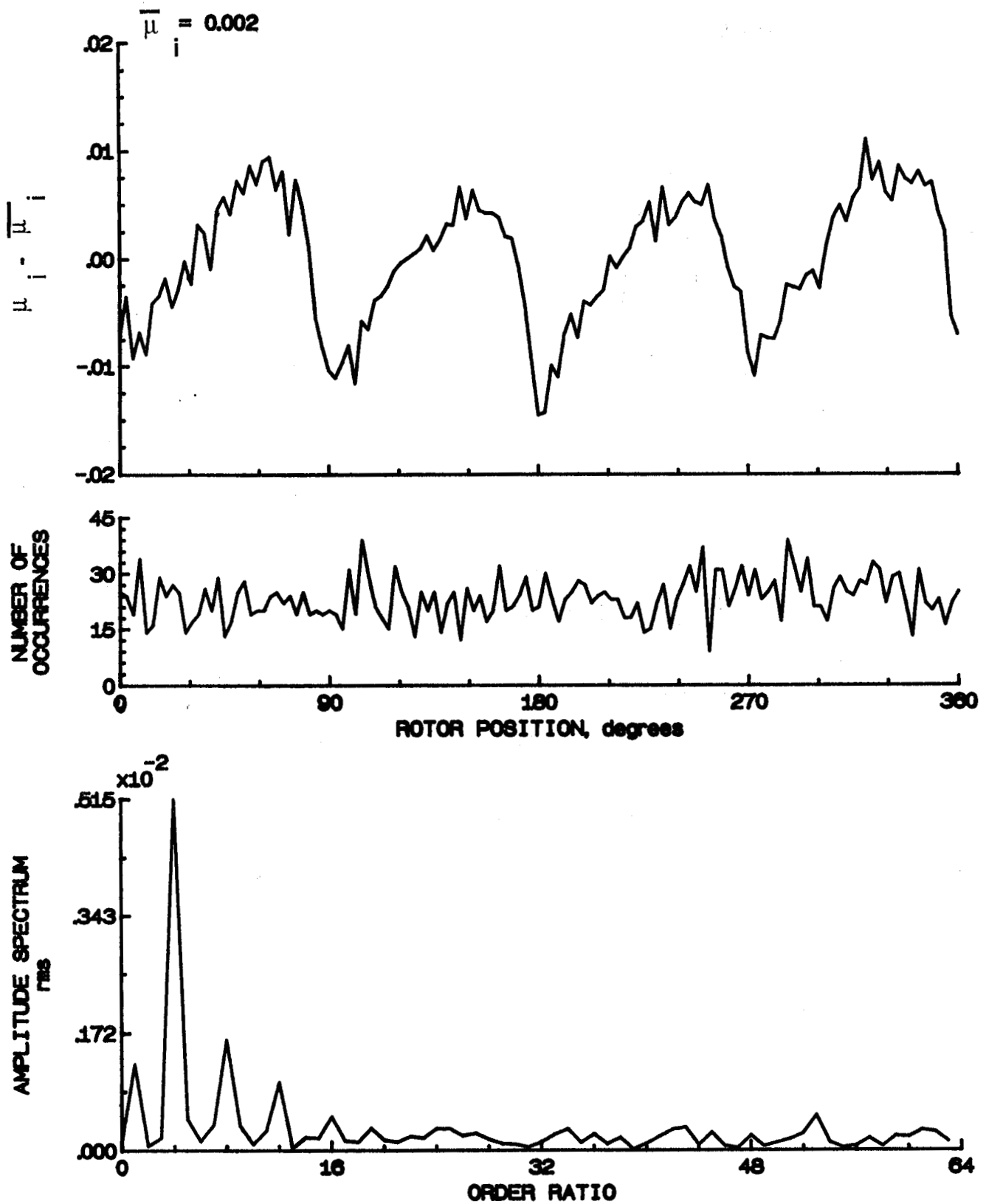


Figure 150.- Induced inflow velocity measured at 270 degrees and r/R of 0.50.

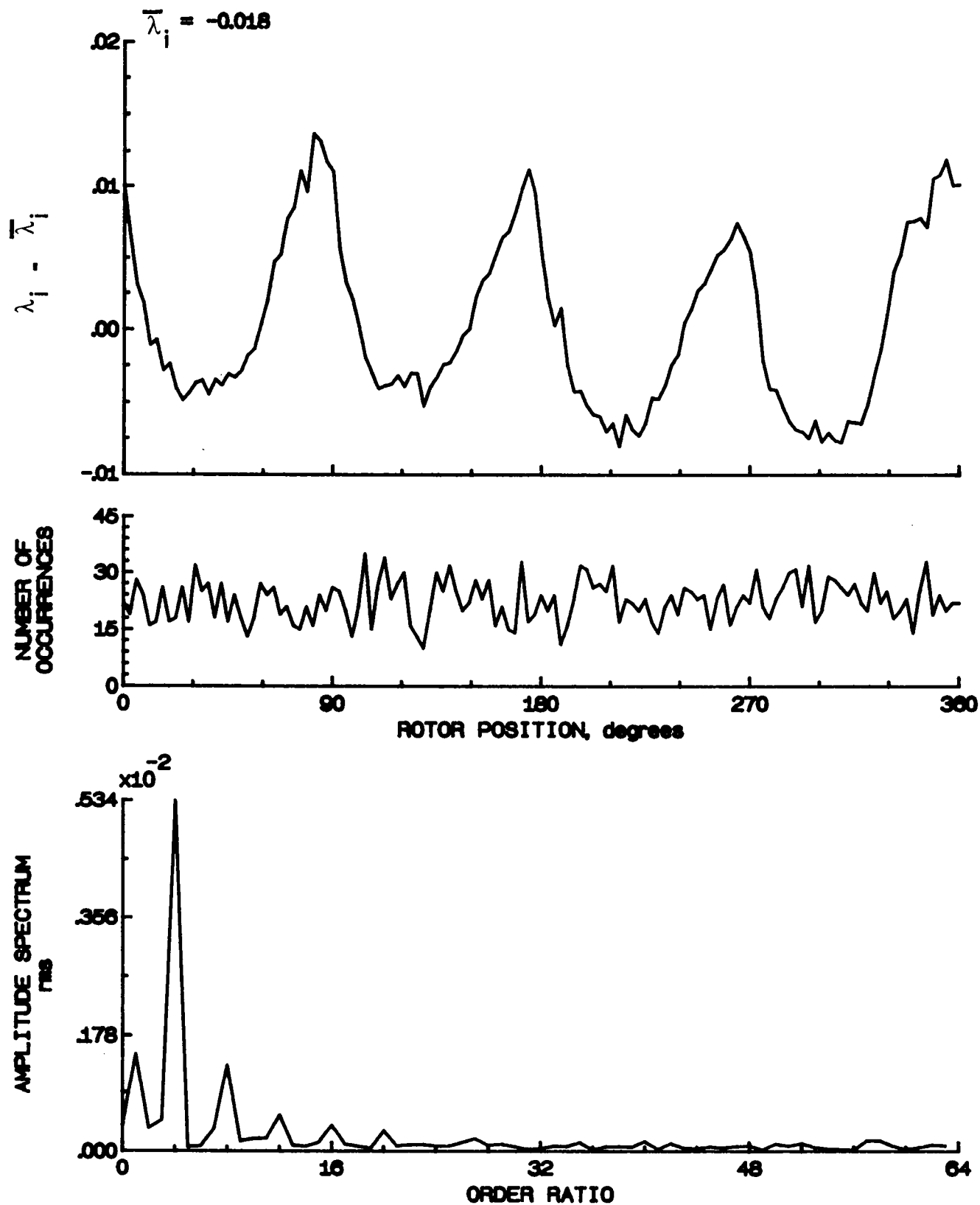


Figure 150.- Concluded.

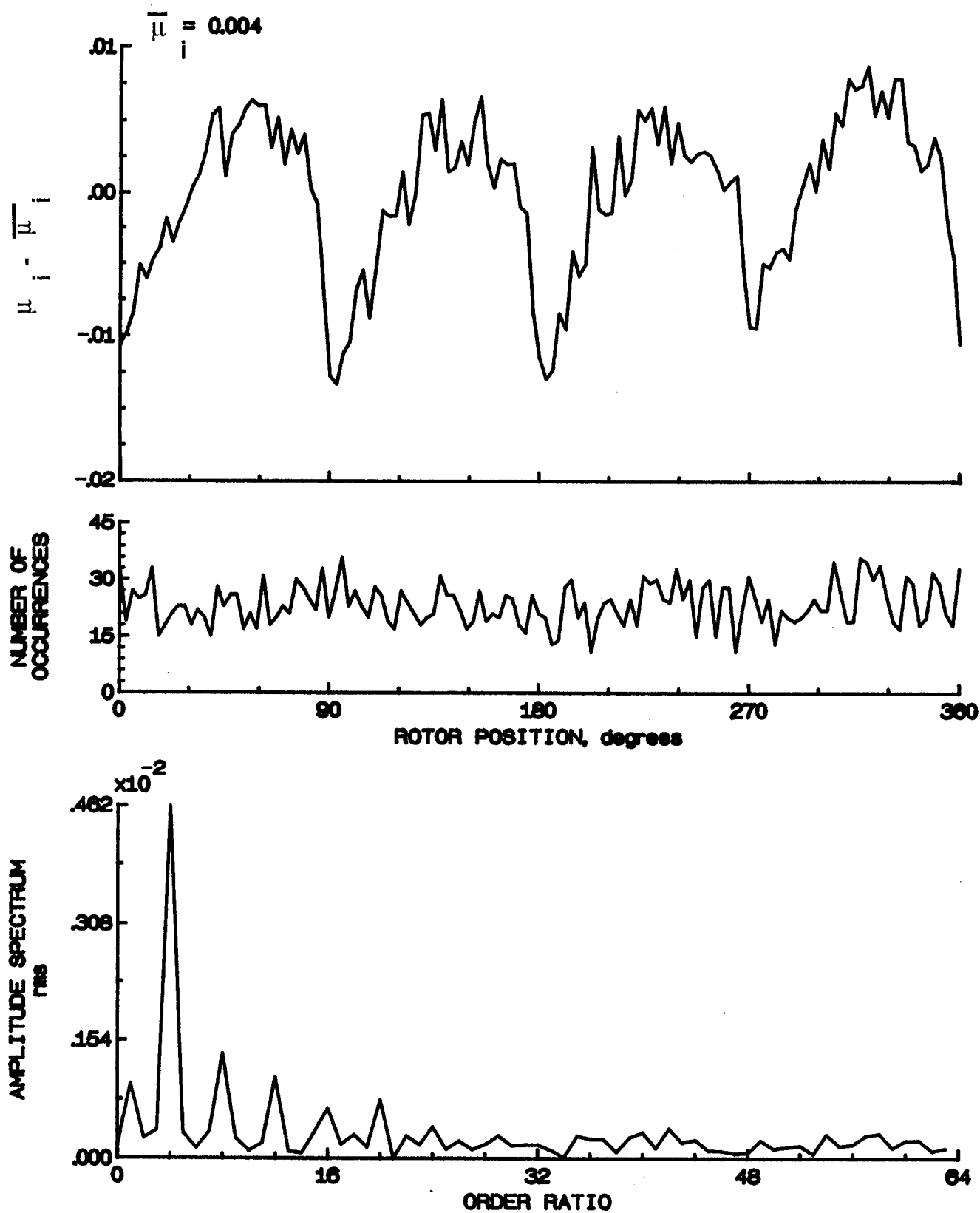


Figure 151.- Induced inflow velocity measured at 270 degrees and r/R of 0.60.

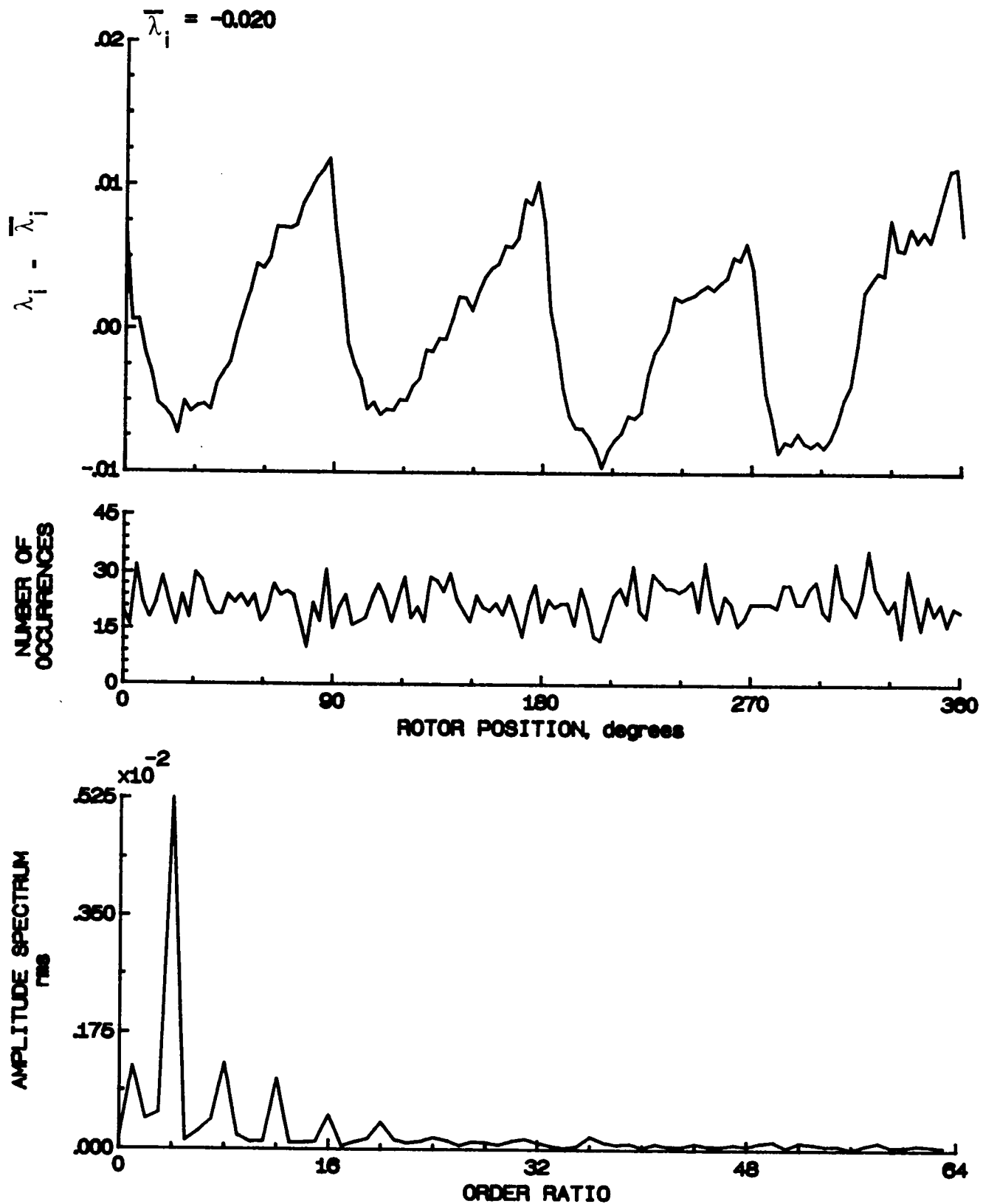


Figure 151.- Concluded.

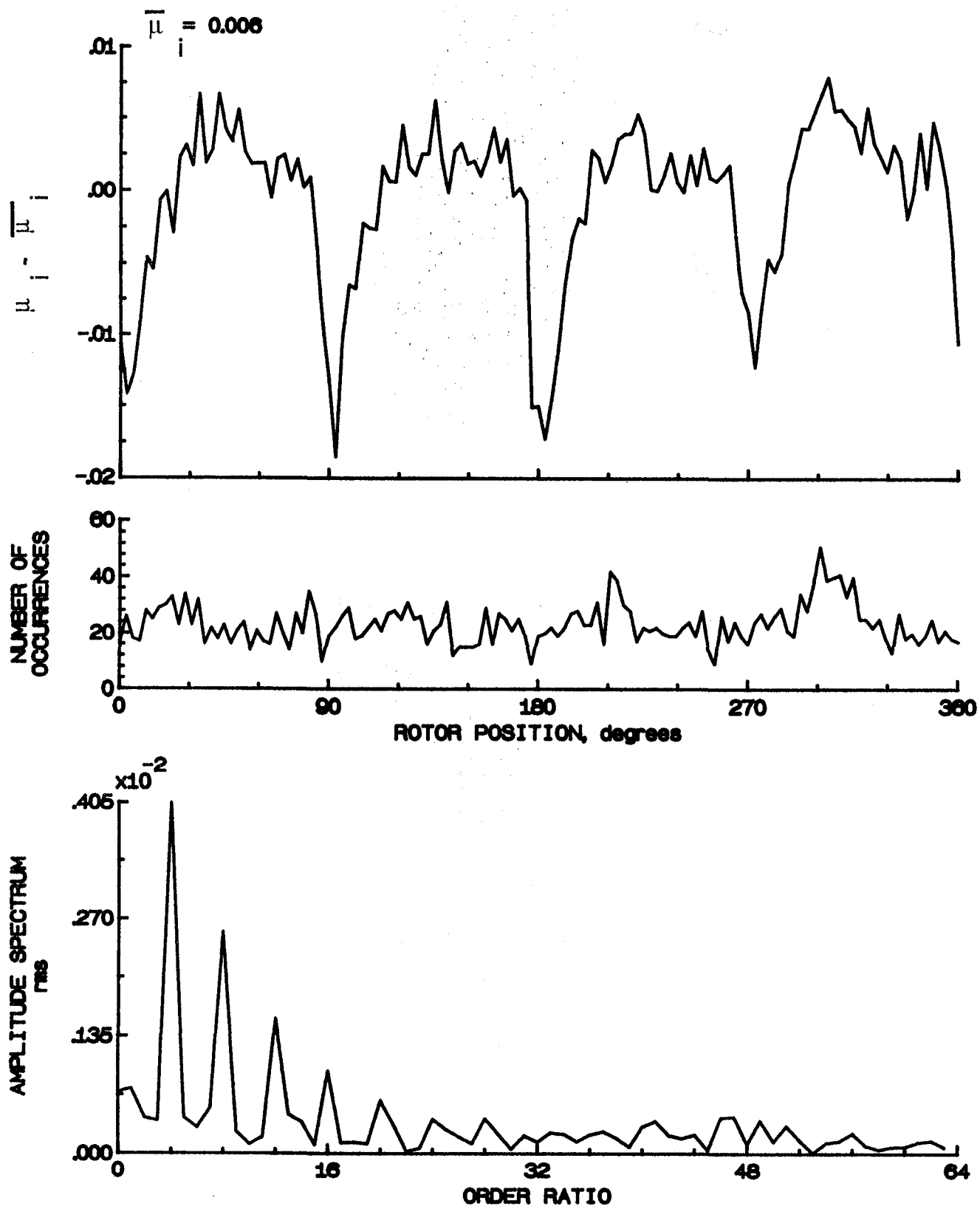


Figure 152.- Induced inflow velocity measured at 270 degrees and r/R of 0.70.



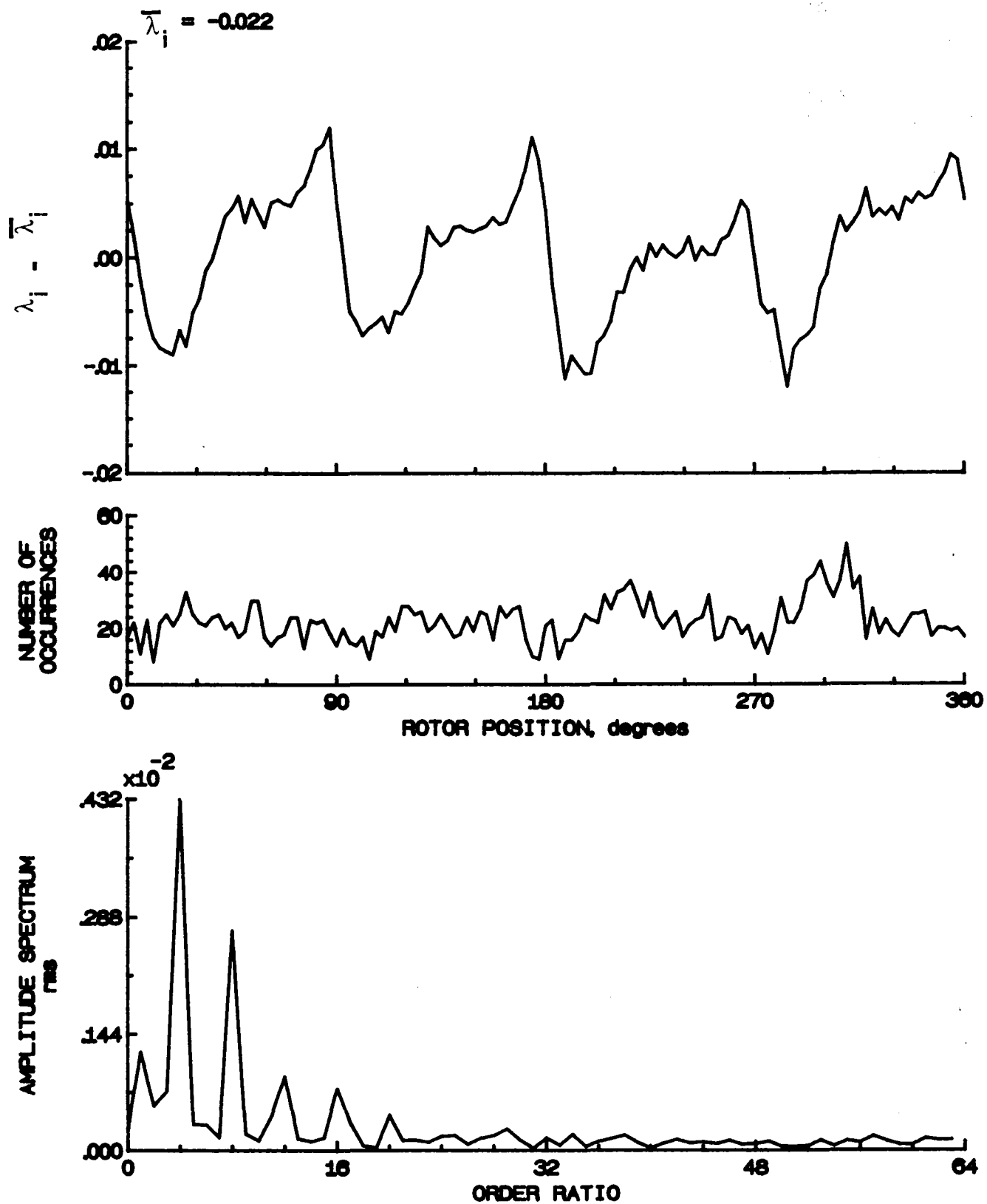


Figure 152.- Concluded.

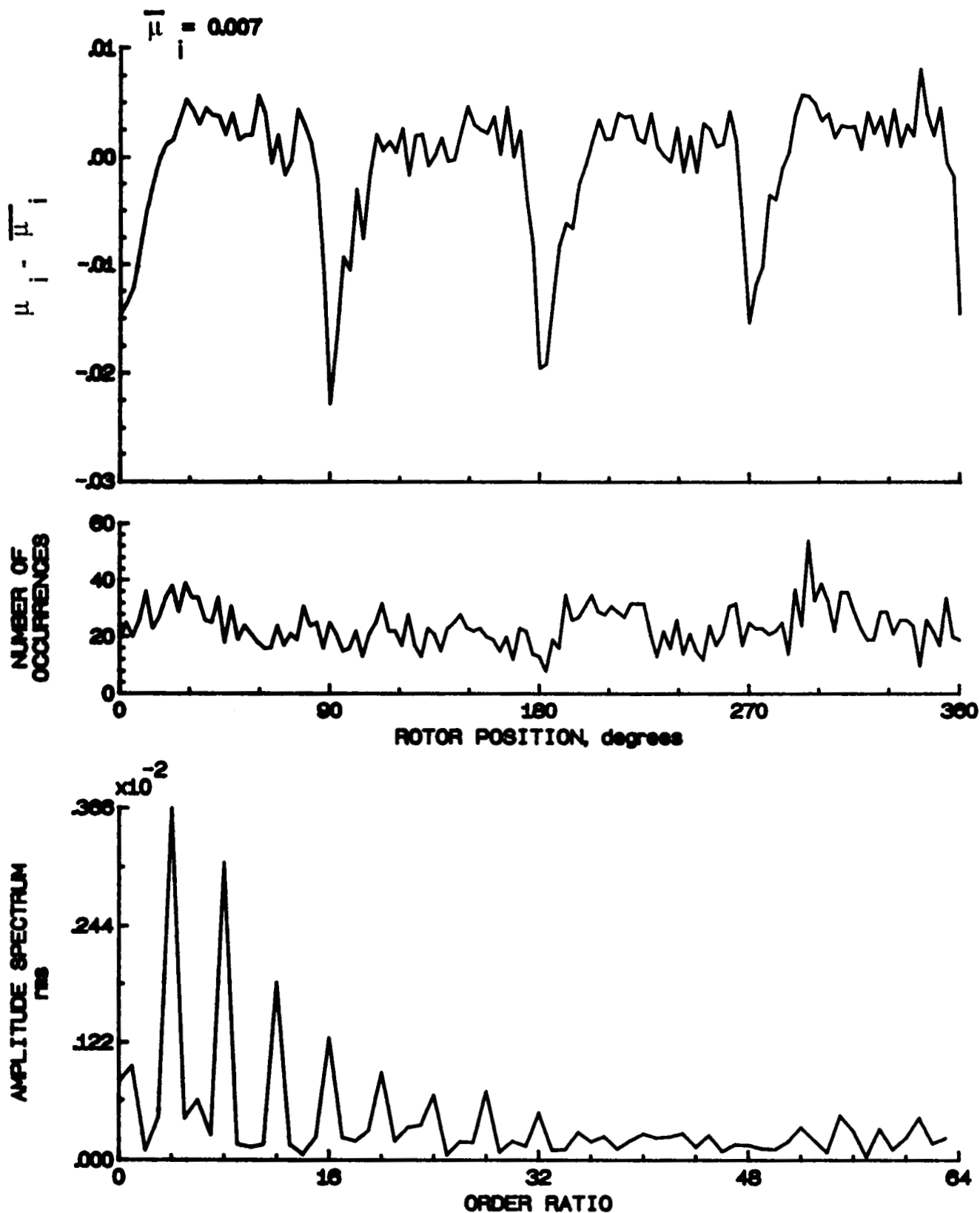


Figure 153.- Induced inflow velocity measured at 270 degrees and r/R of 0.74.

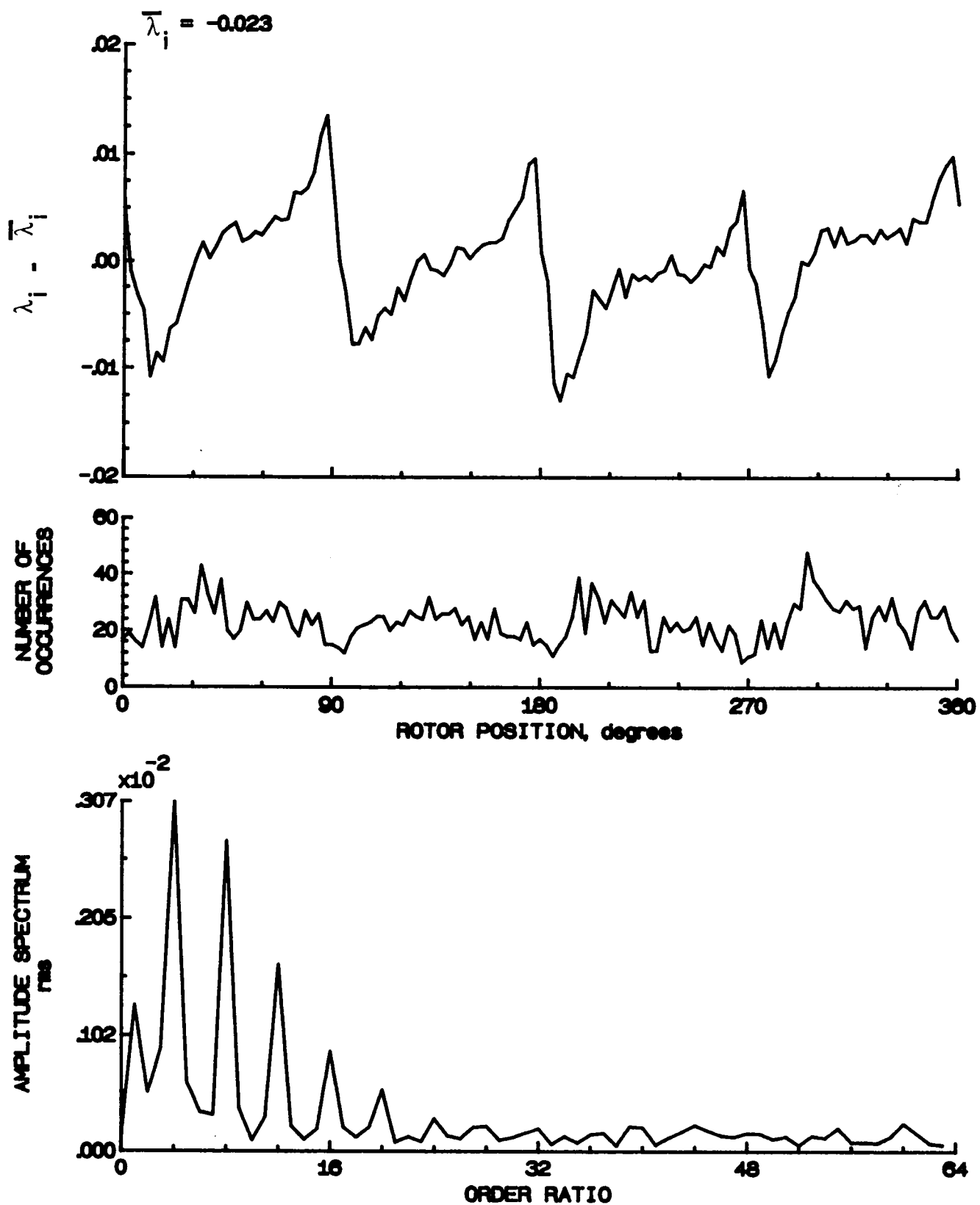


Figure 153.- Concluded.

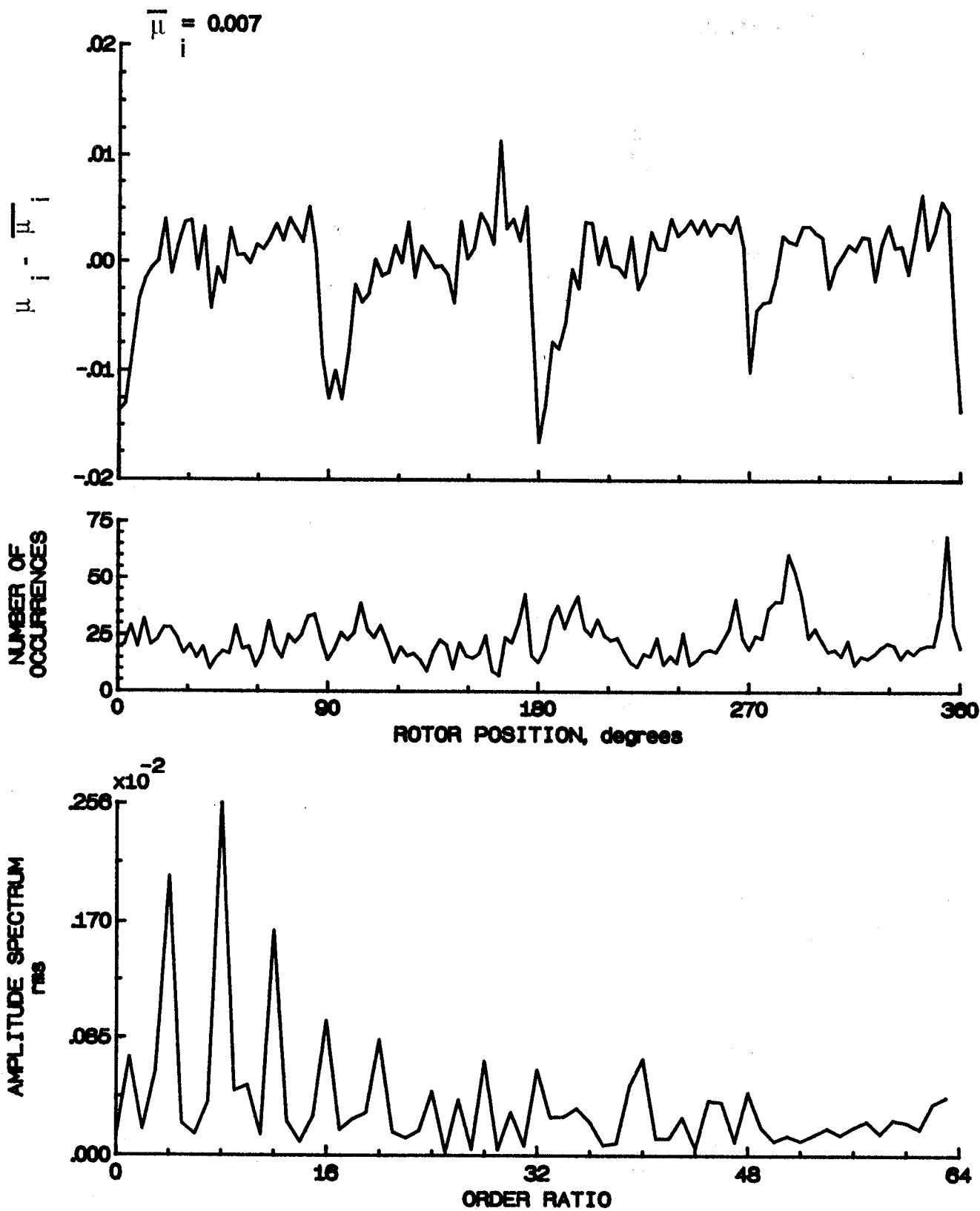


Figure 154.- Induced inflow velocity measured at 270 degrees and  $r/R$  of 0.78.

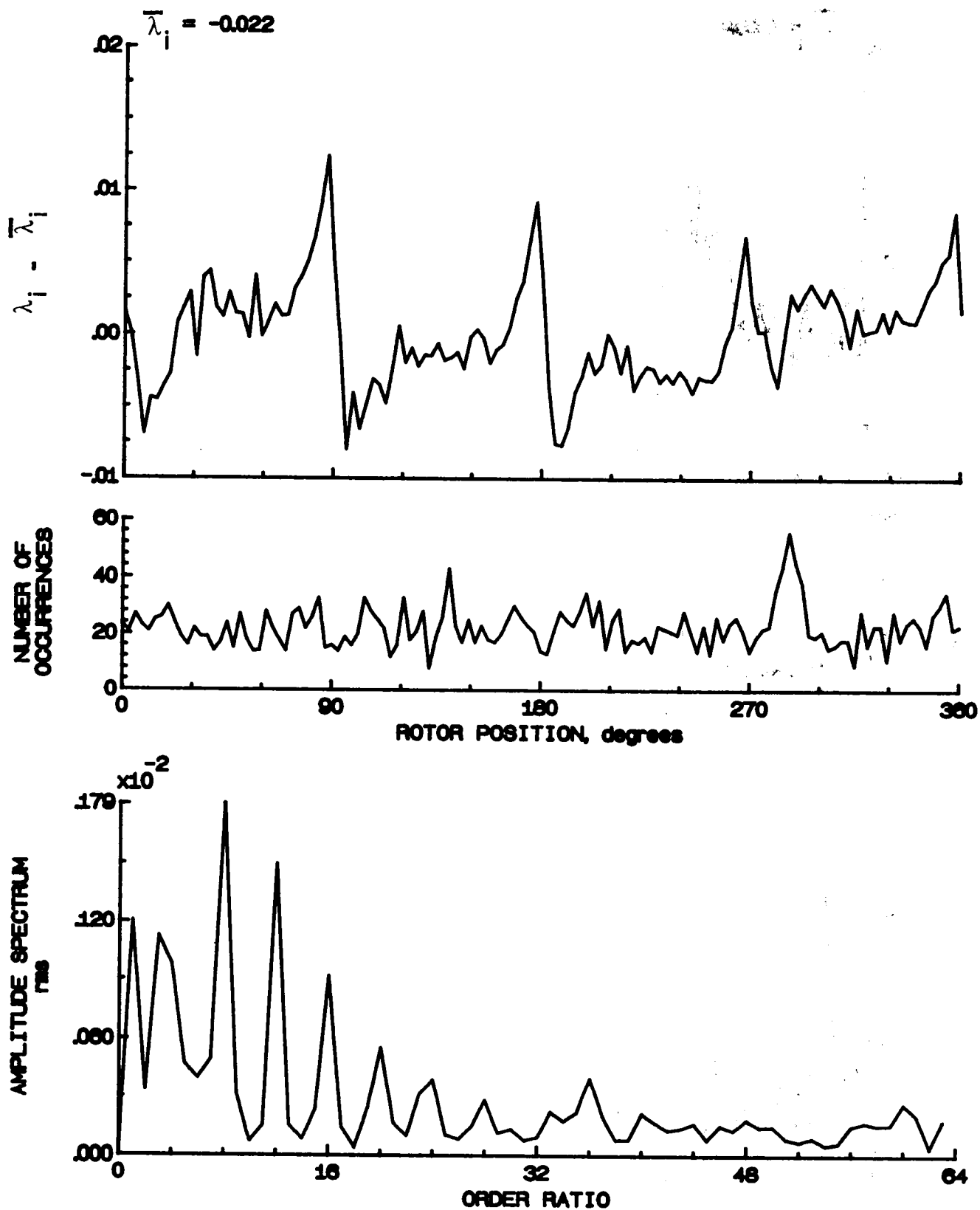


Figure 154.- Concluded.

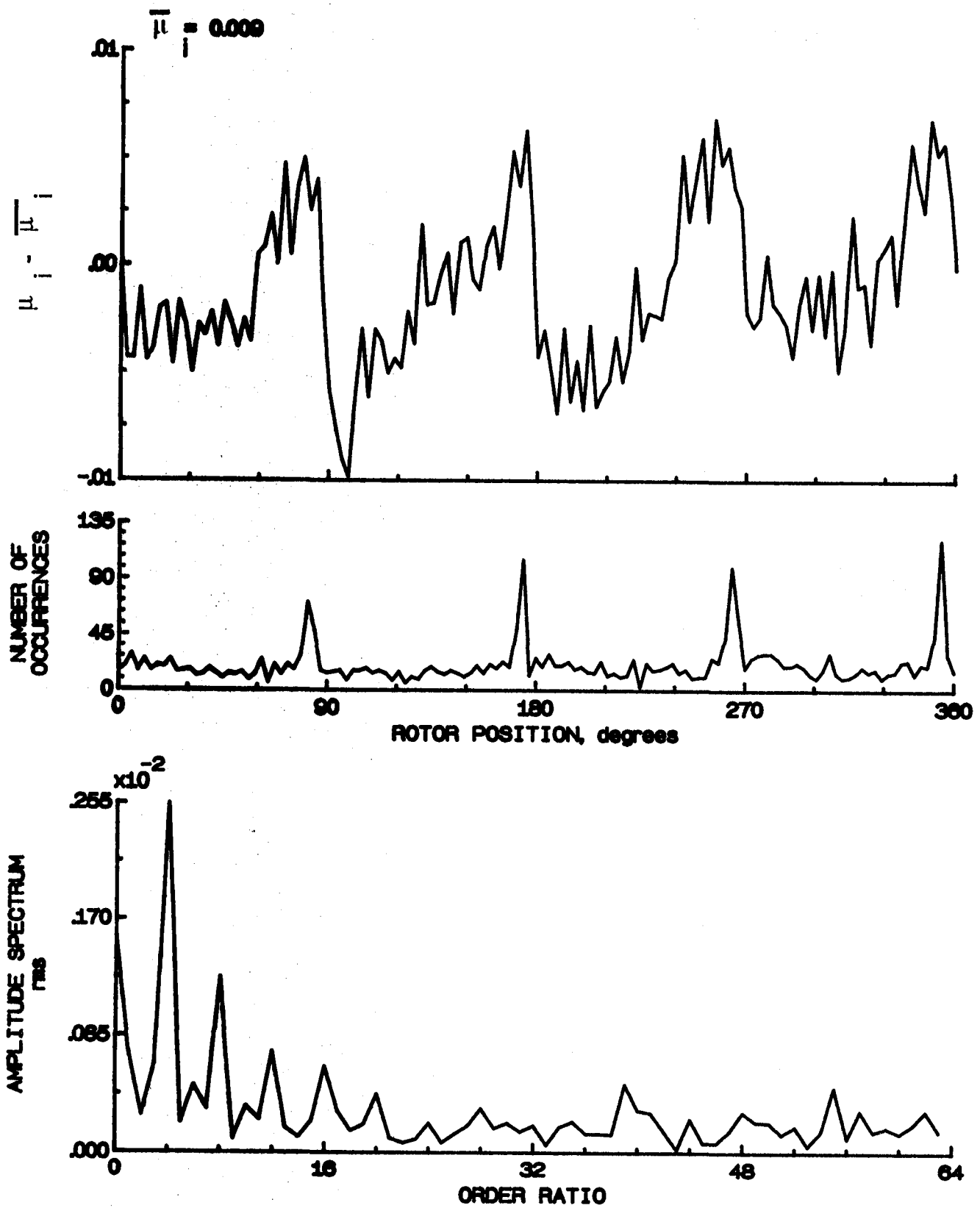


Figure 155.- Induced inflow velocity measured at 270 degrees and  $r/R$  of 0.82.

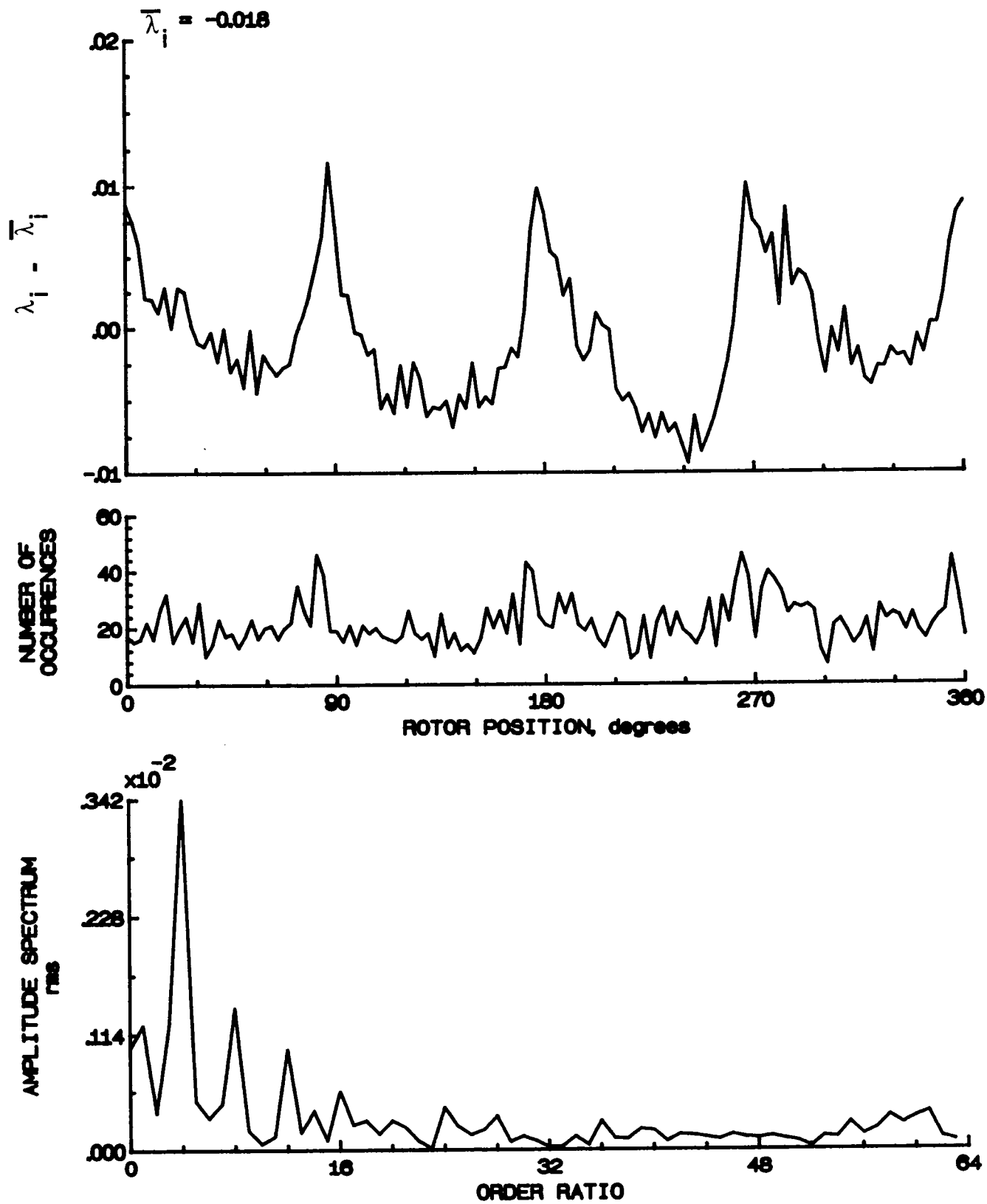


Figure 155.- Concluded.

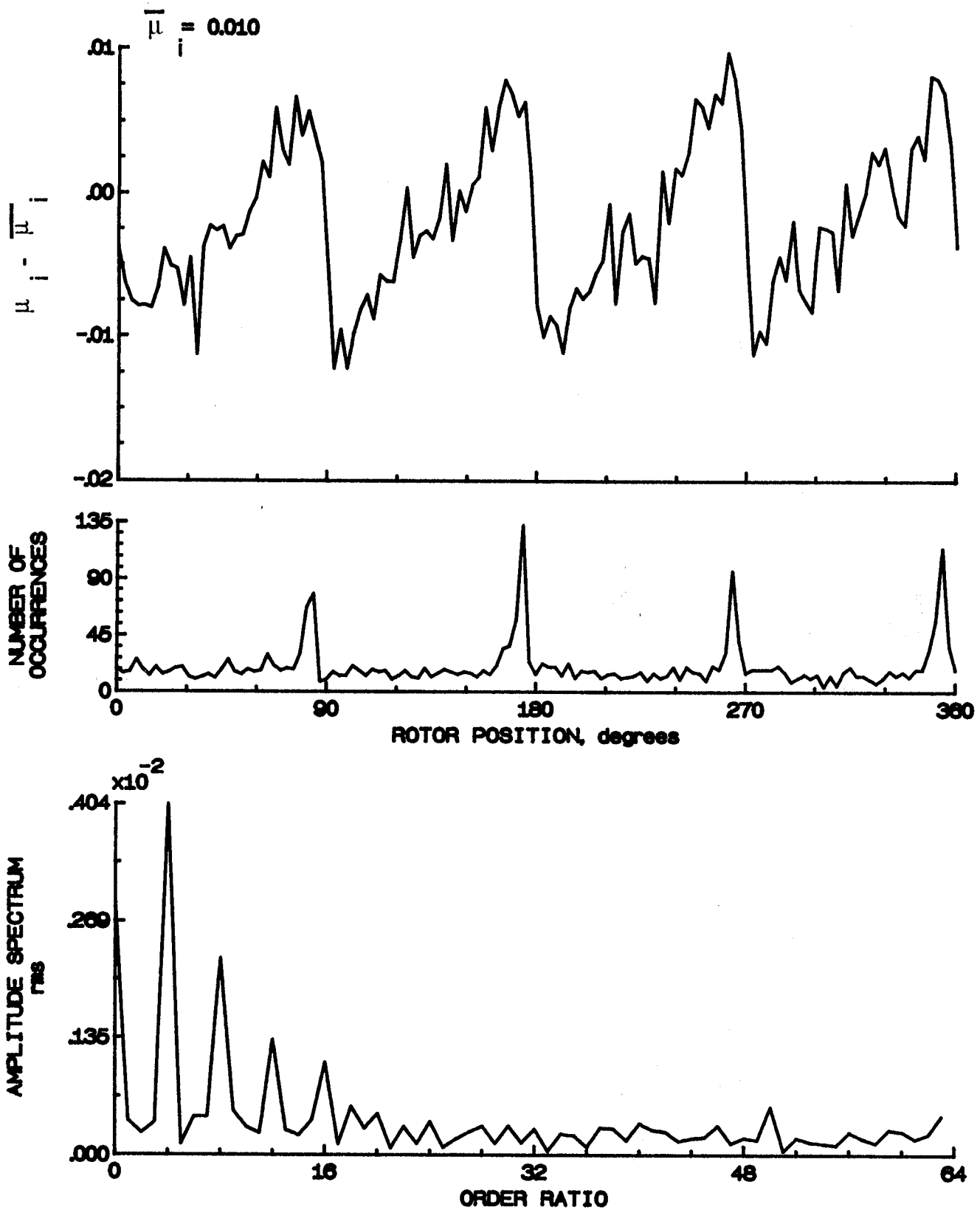


Figure 158.- Induced inflow velocity measured at 270 degrees and r/R of 0.86.



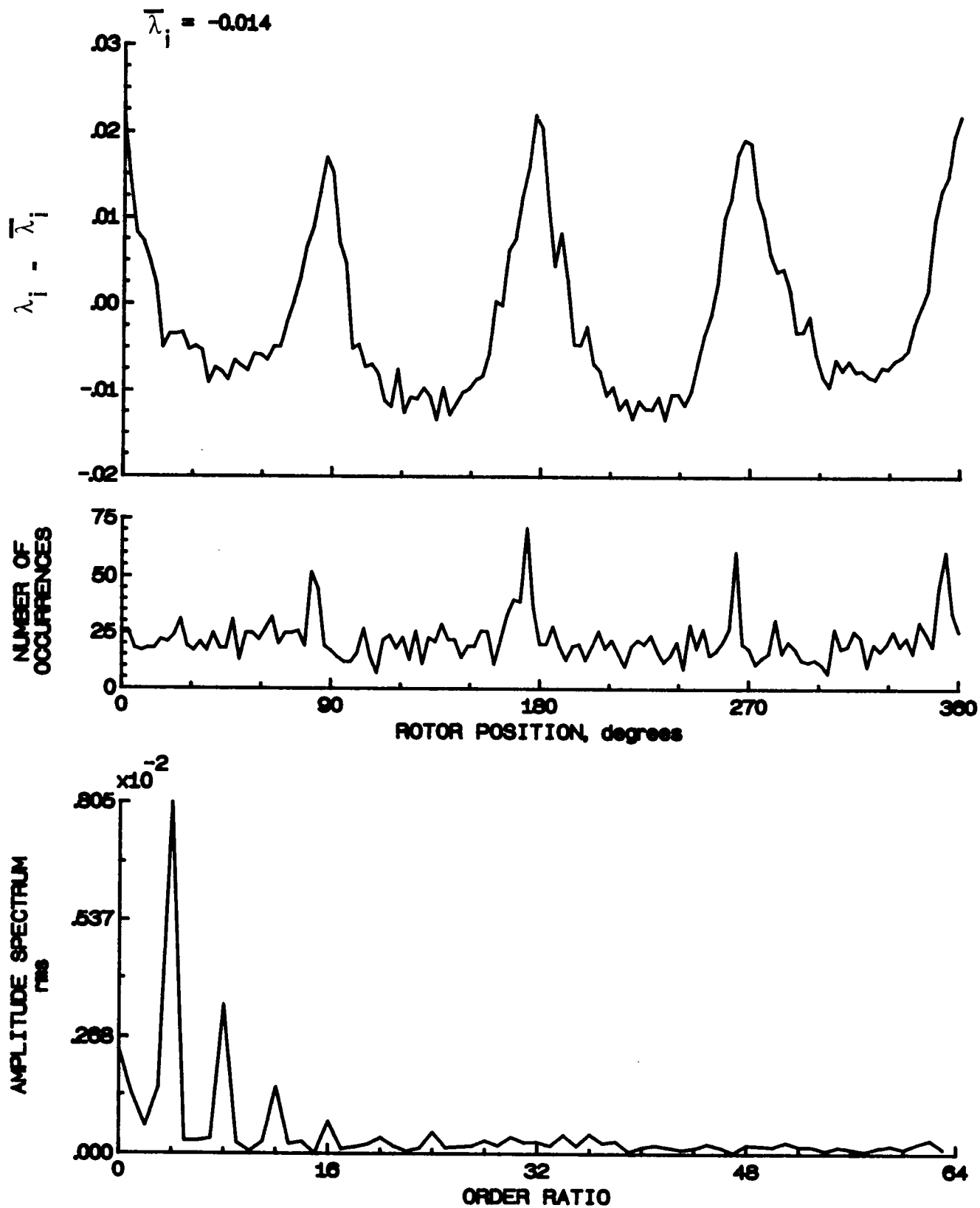


Figure 156.- Concluded.

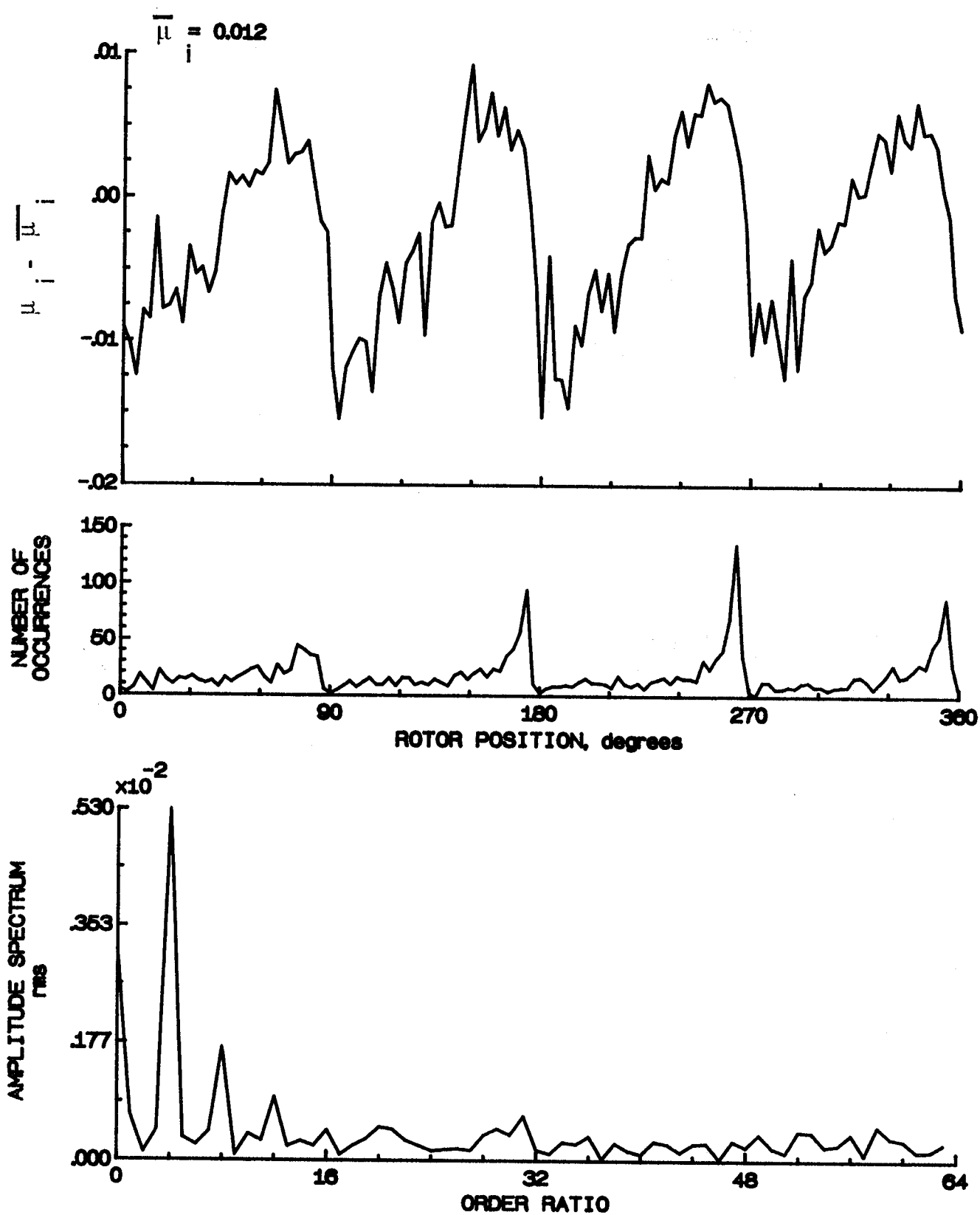


Figure 157.- Induced inflow velocity measured at 270 degrees and  $r/R$  of 0.90.

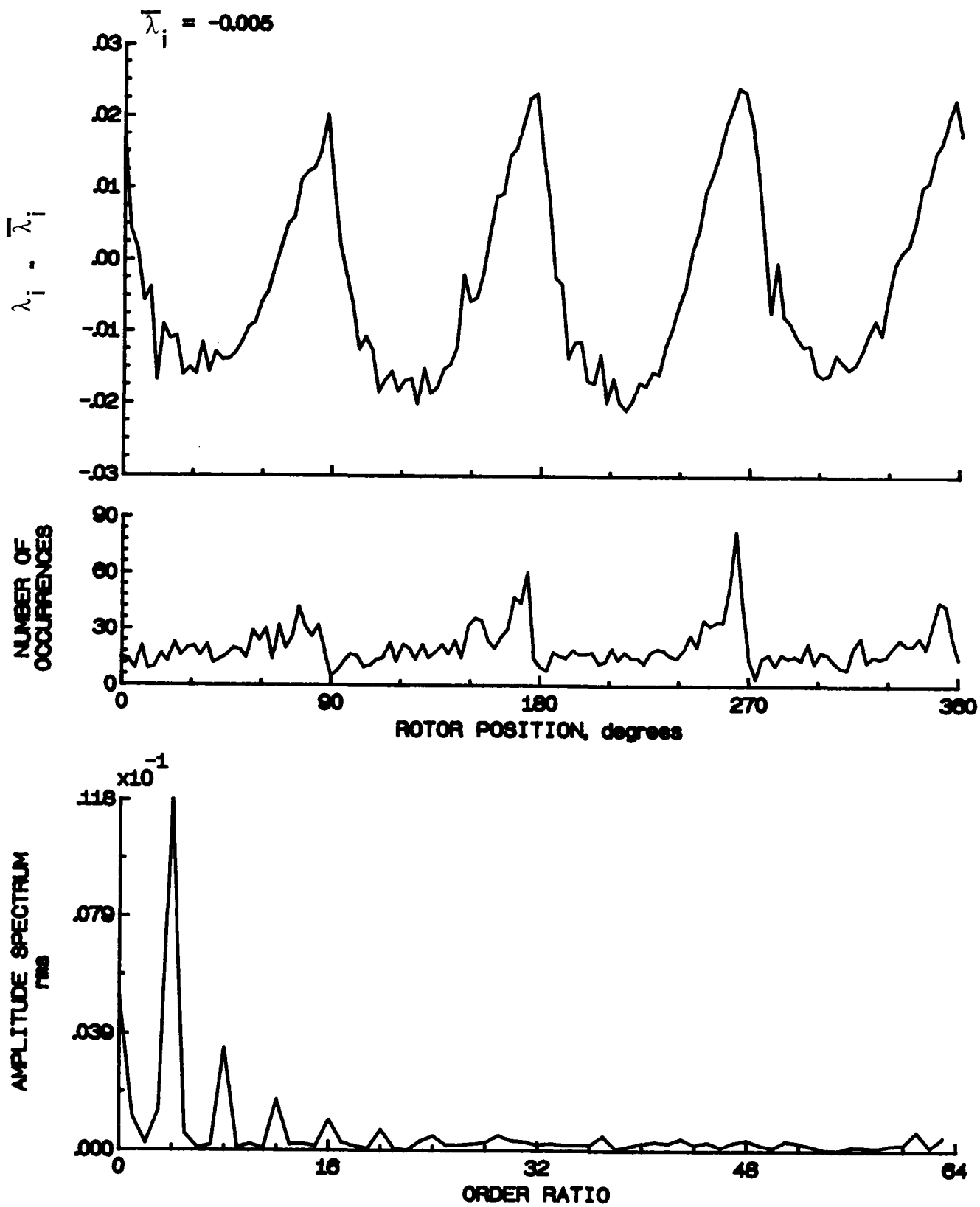


Figure 157.- Concluded.

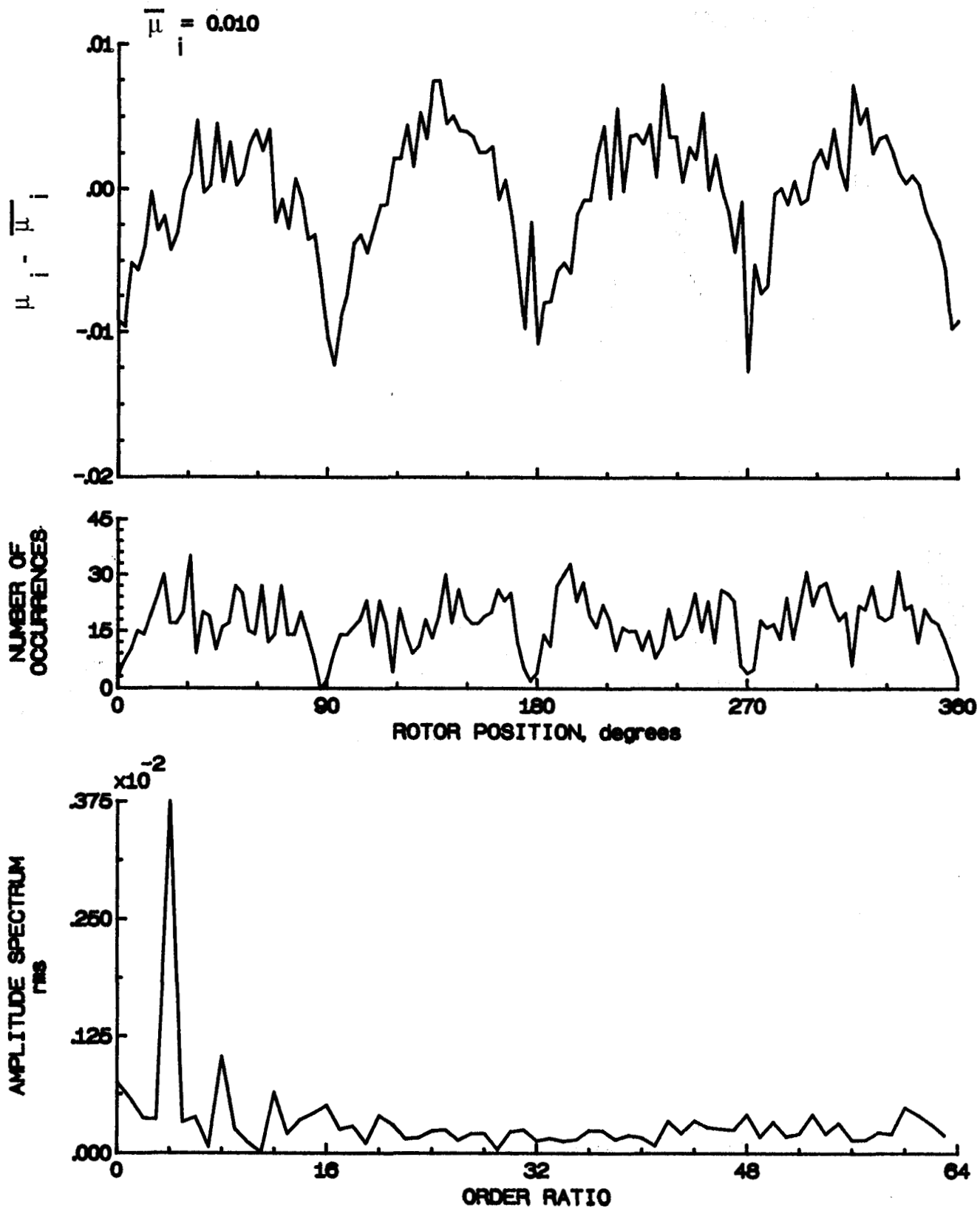


Figure 158.- Induced inflow velocity measured at 270 degrees and  $r/R$  of 0.94.

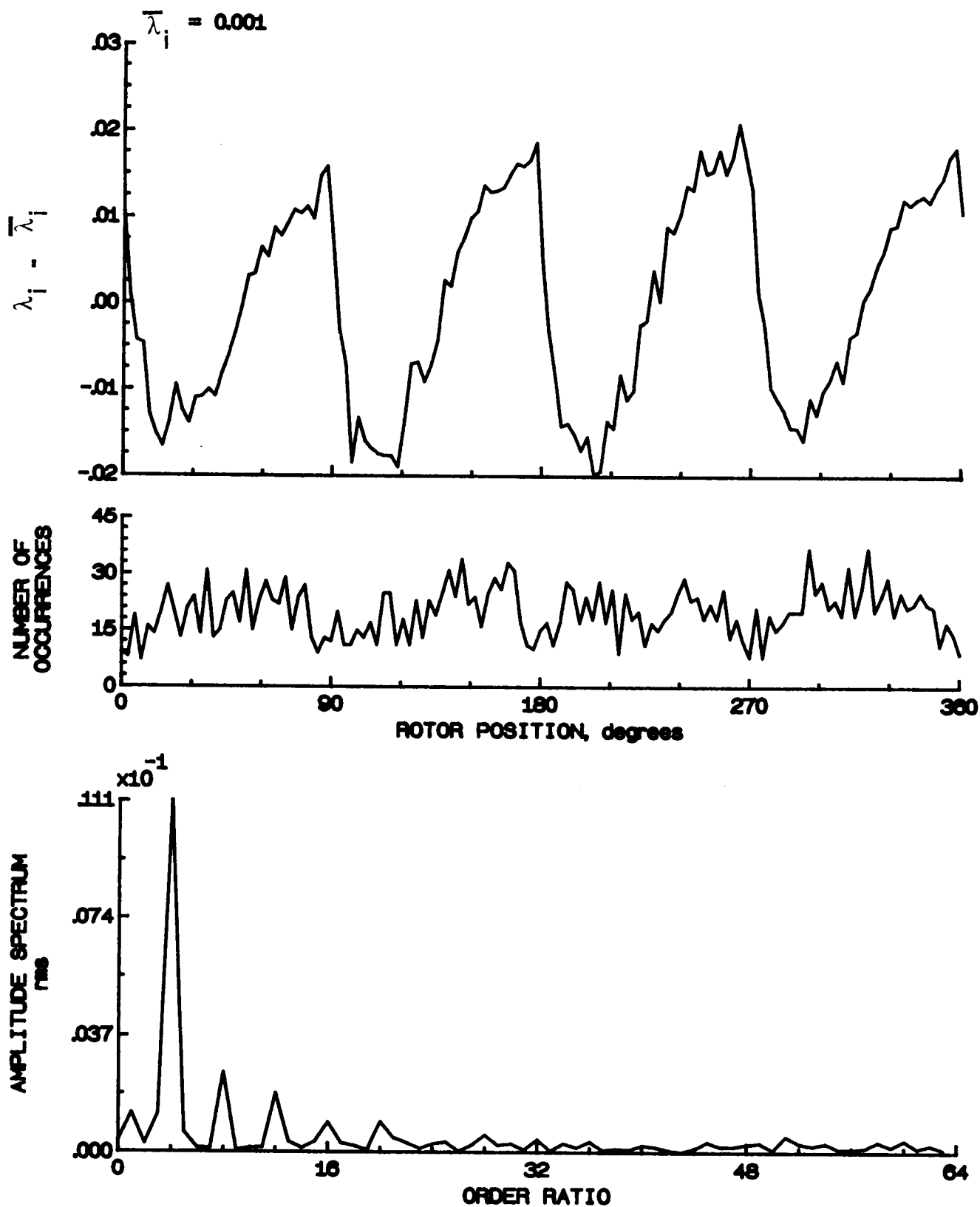


Figure 158.- Concluded.

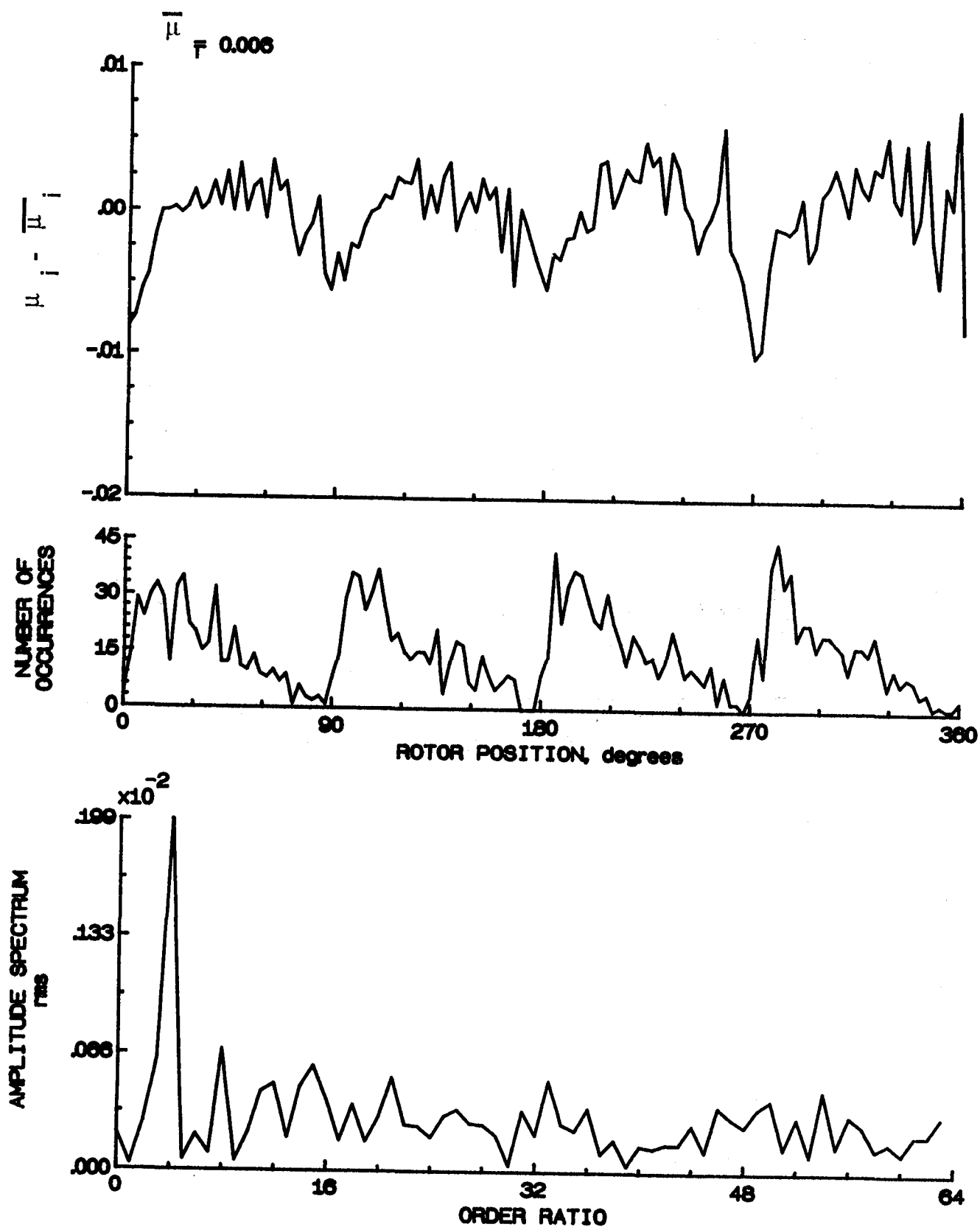


Figure 159.- Induced inflow velocity measured at 270 degrees and  $r/R$  of 0.98.

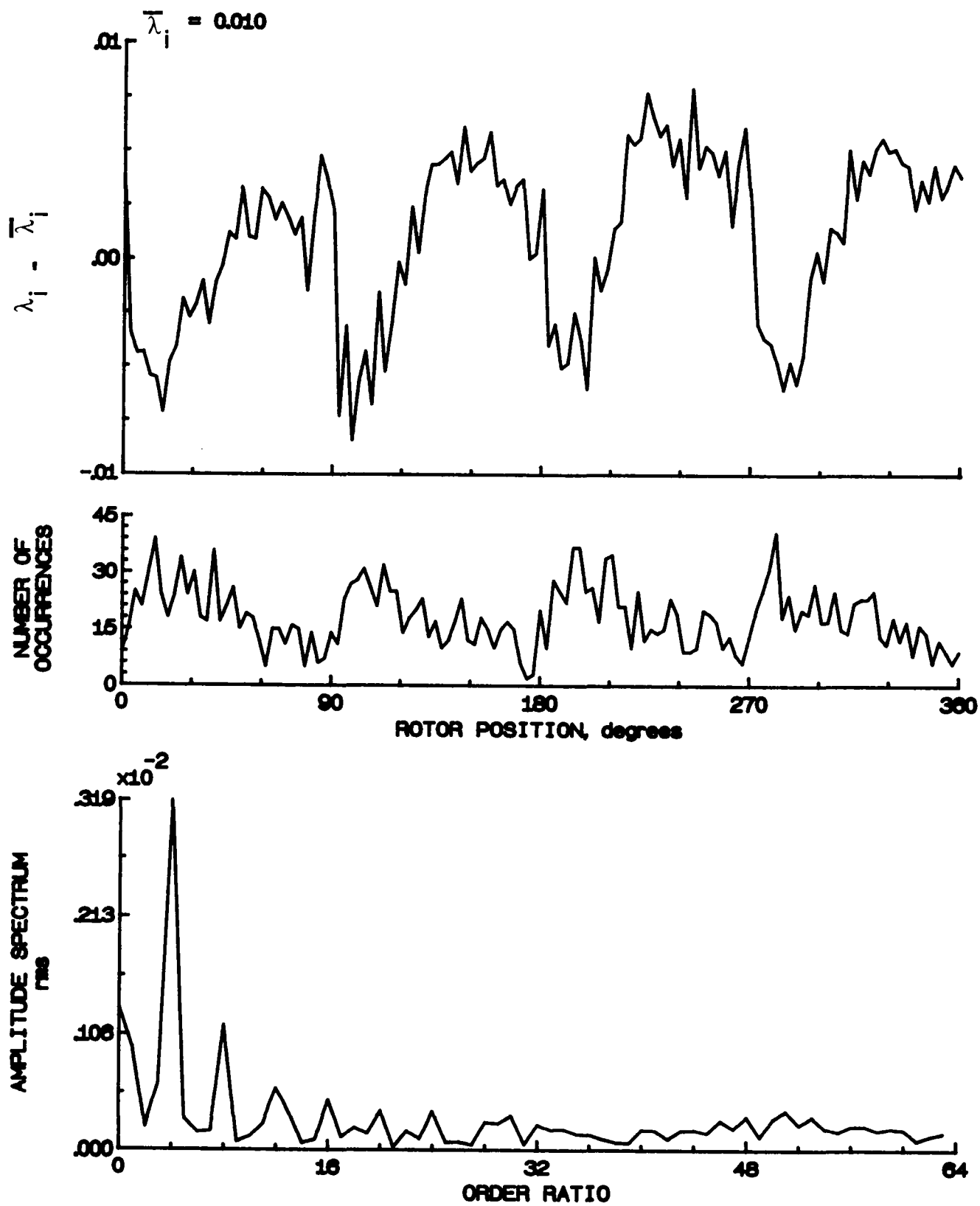


Figure 159.- Concluded.

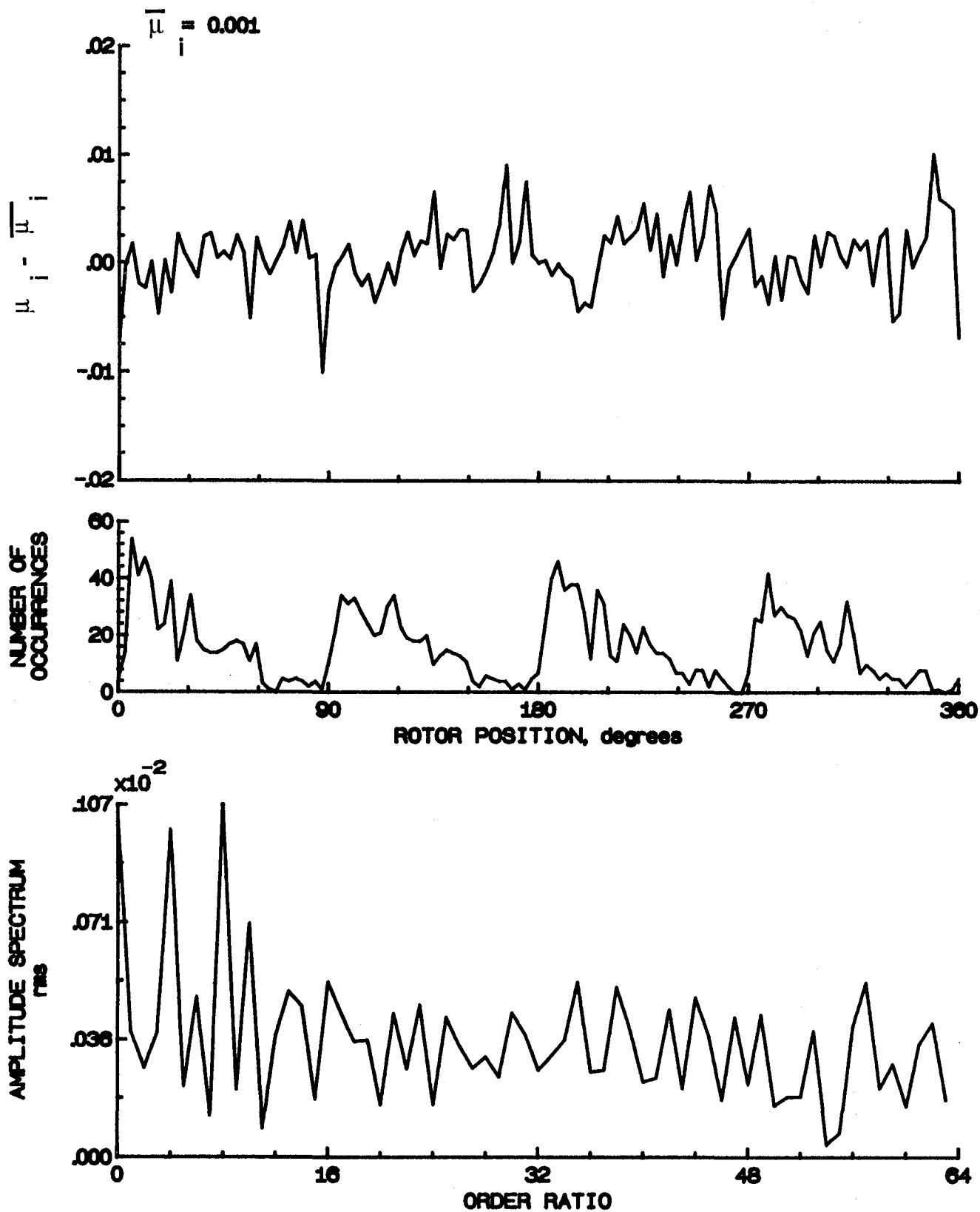


Figure 160.- Induced inflow velocity measured at 270 degrees and r/R of 1.02.



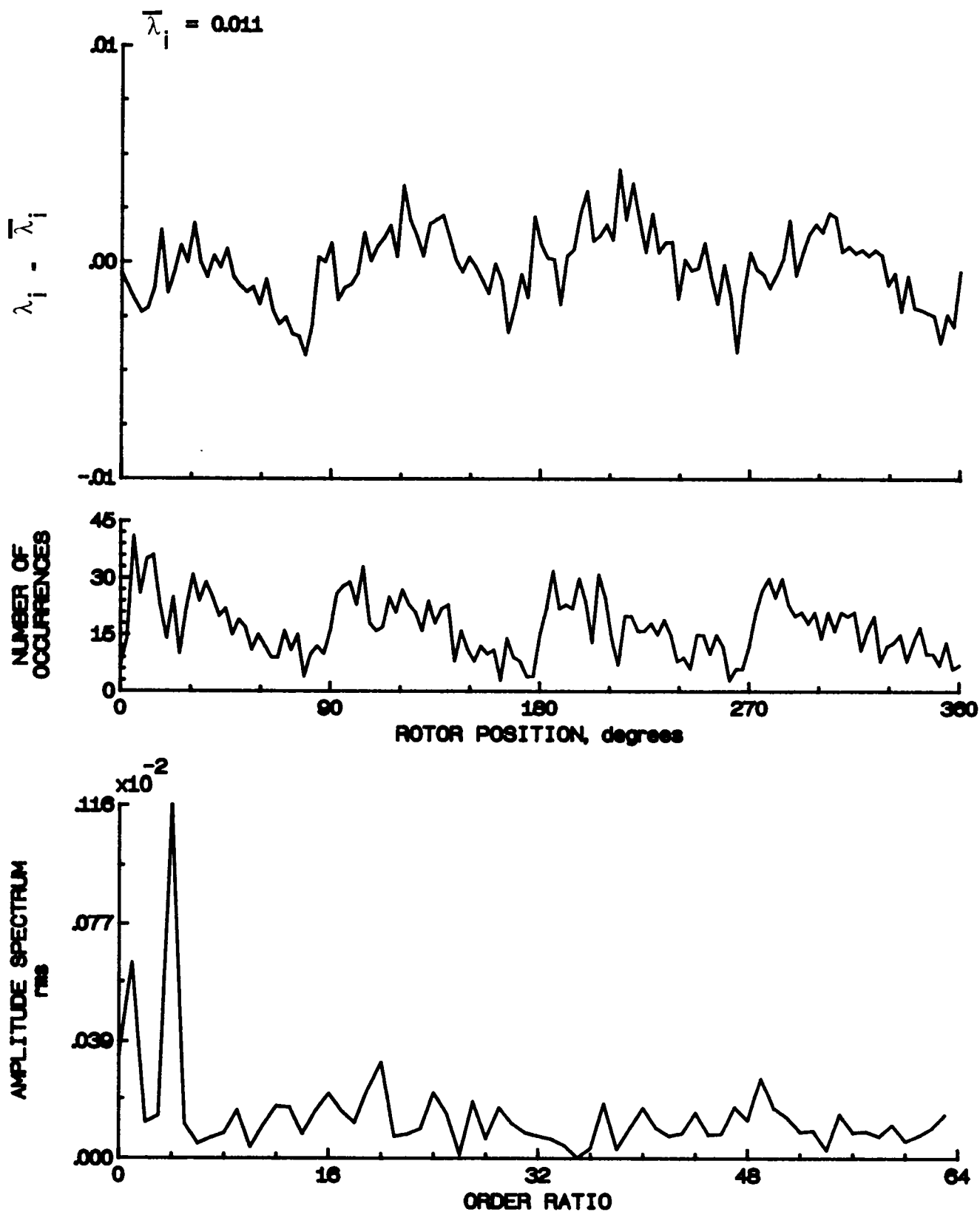


Figure 160.- Concluded.

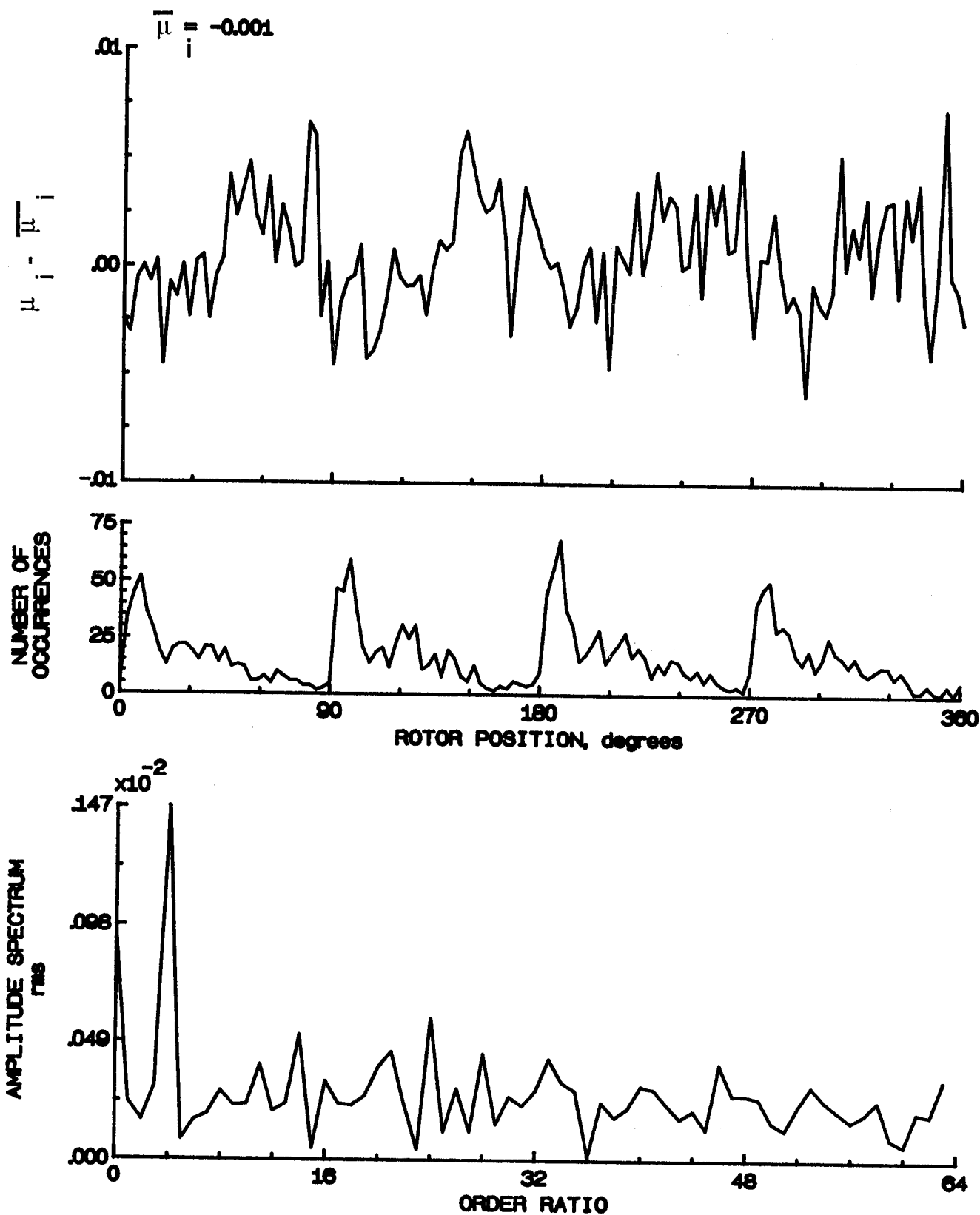


Figure 161.- Induced inflow velocity measured at 270 degrees and r/R of 1.04.

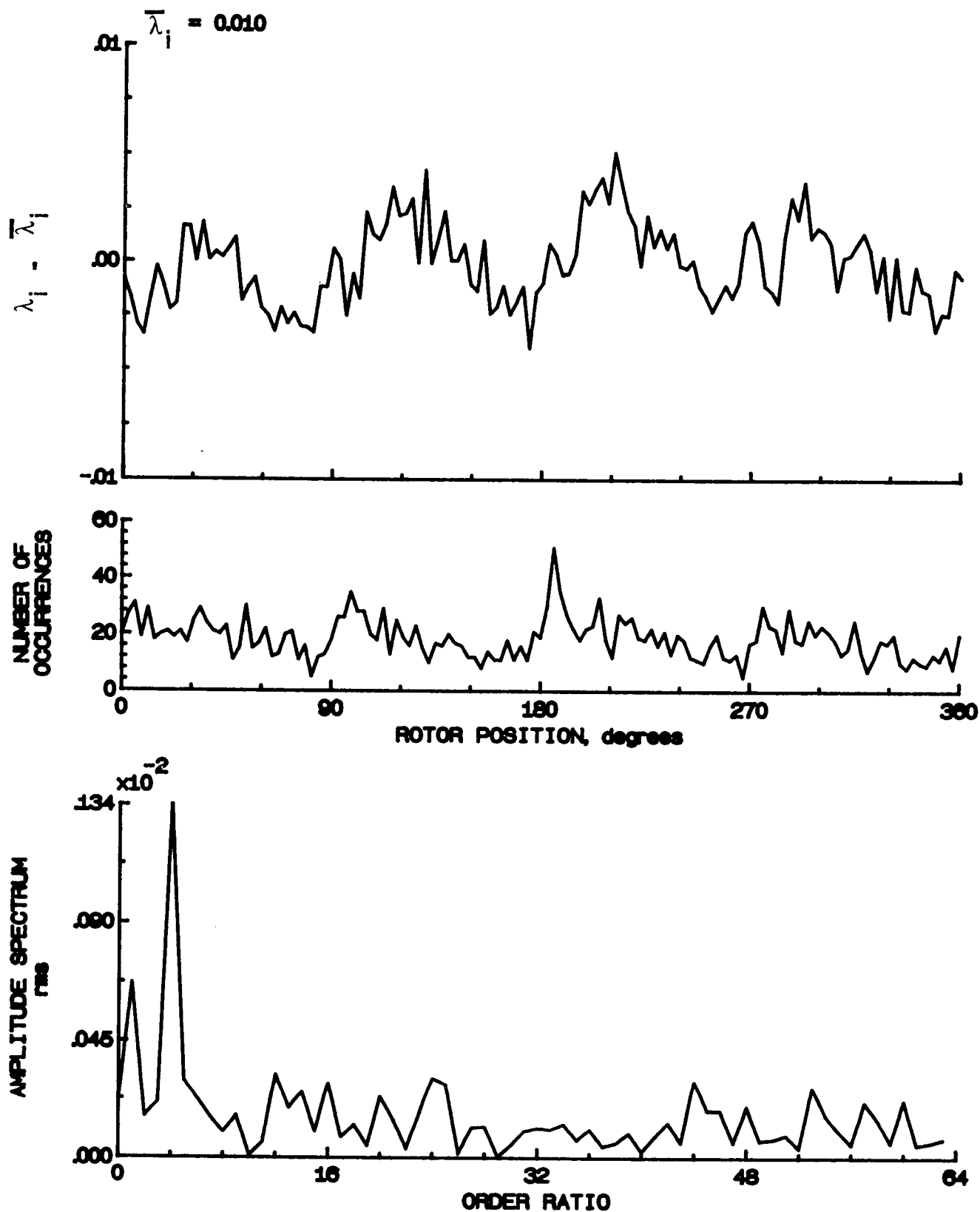


Figure 161.- Concluded.

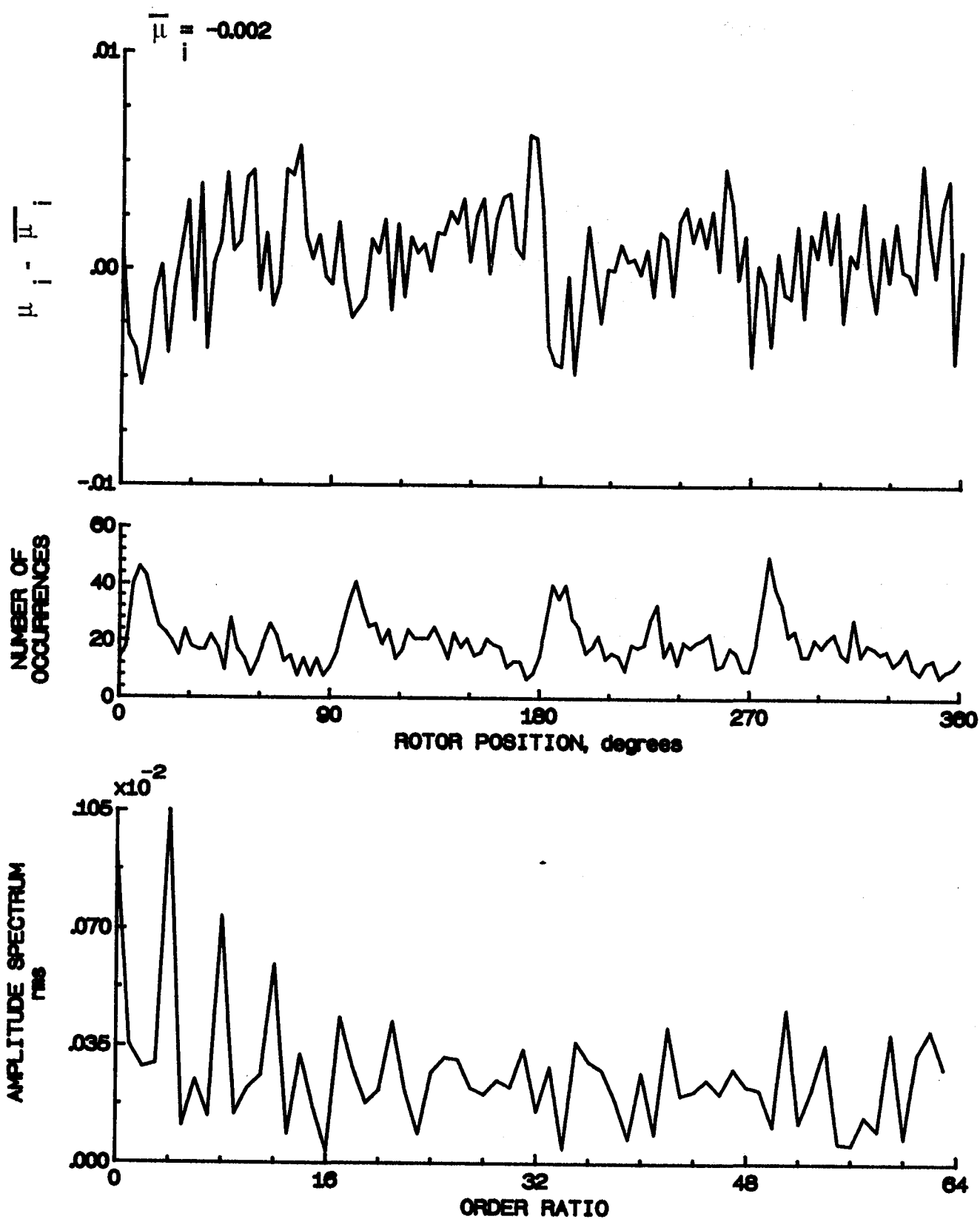


Figure 162.- Induced inflow velocity measured at 270 degrees and r/R of 1.10.

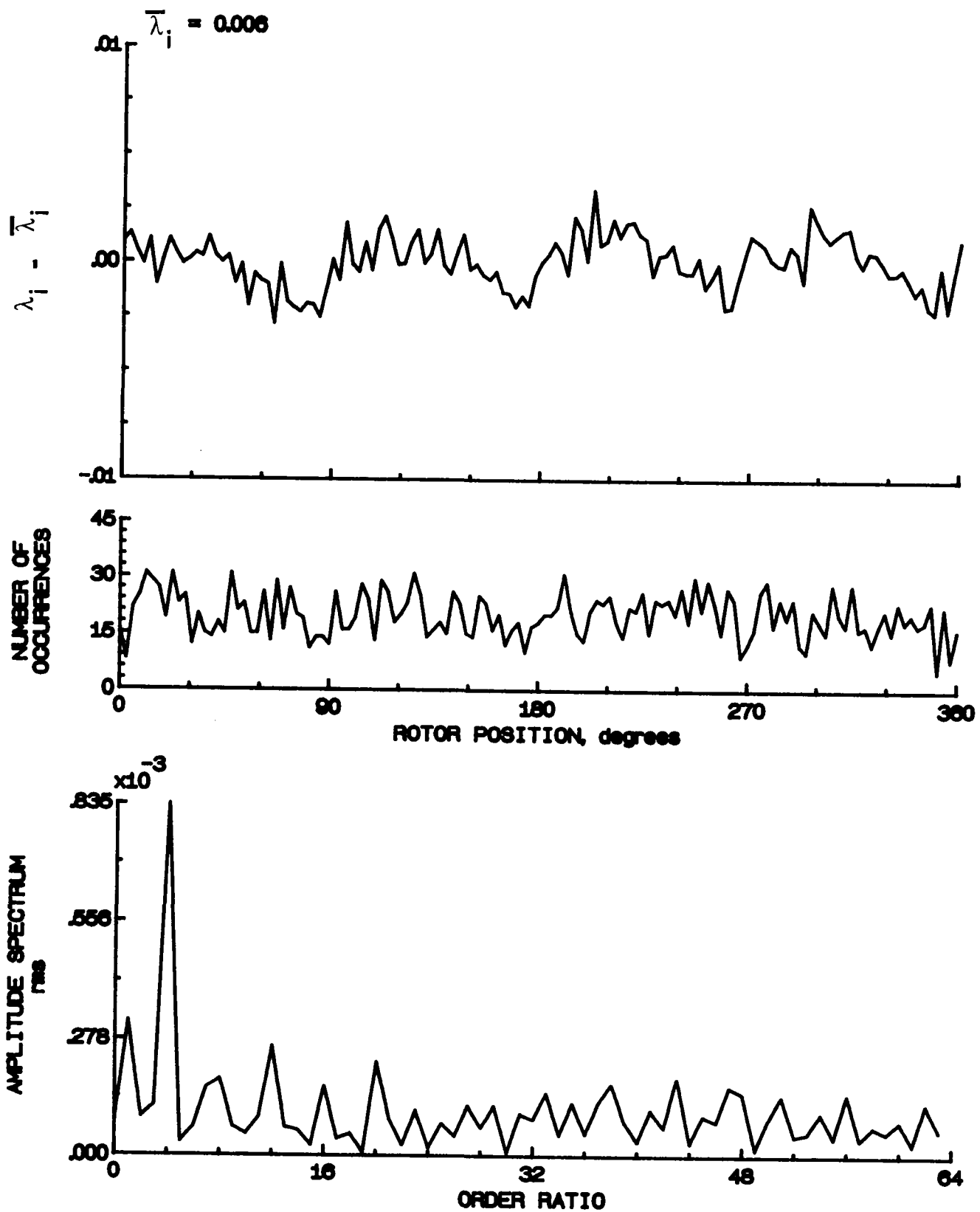


Figure 162- Concluded.

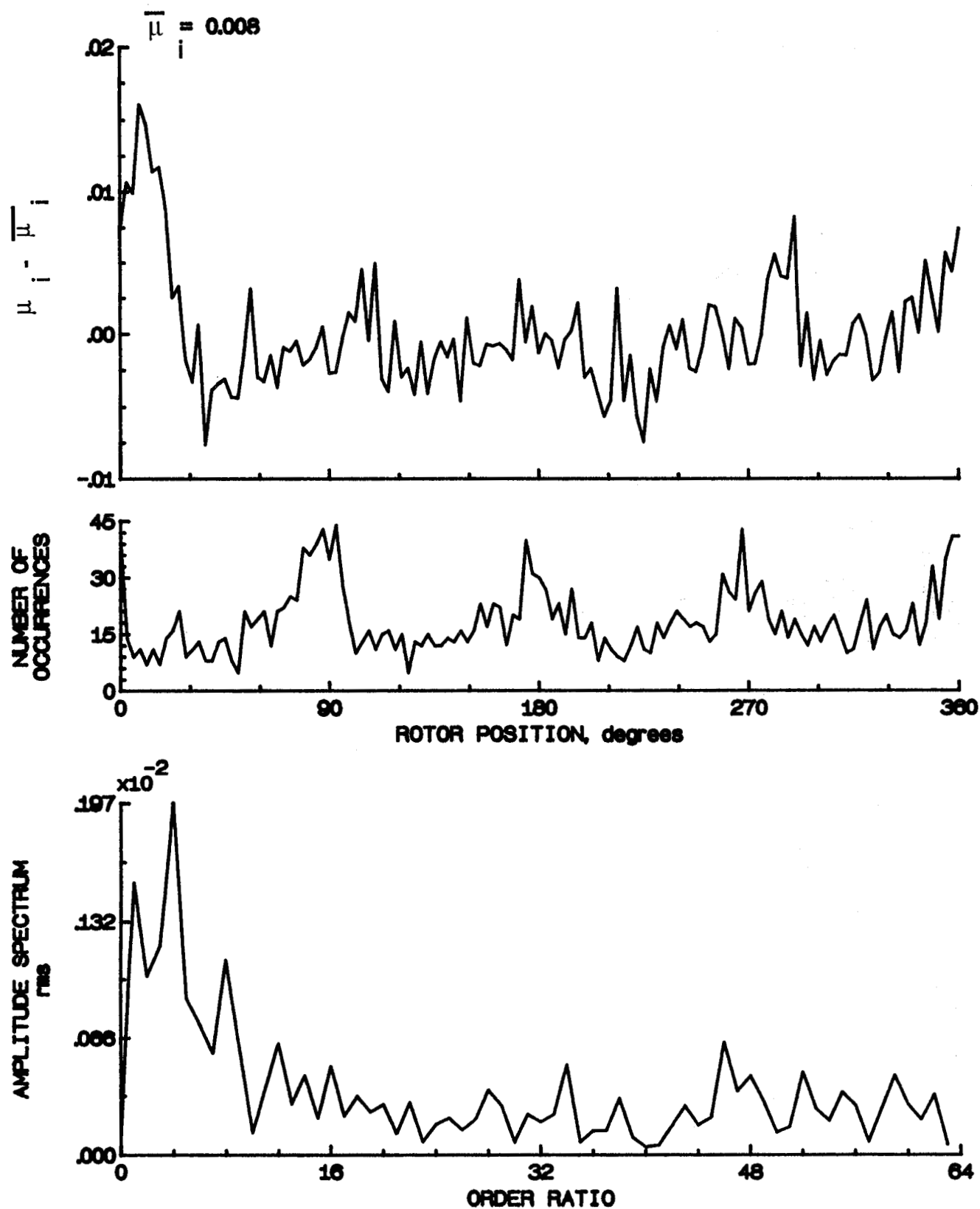


Figure 163.- Induced inflow velocity measured at 300 degrees and  $r/R$  of 0.20.

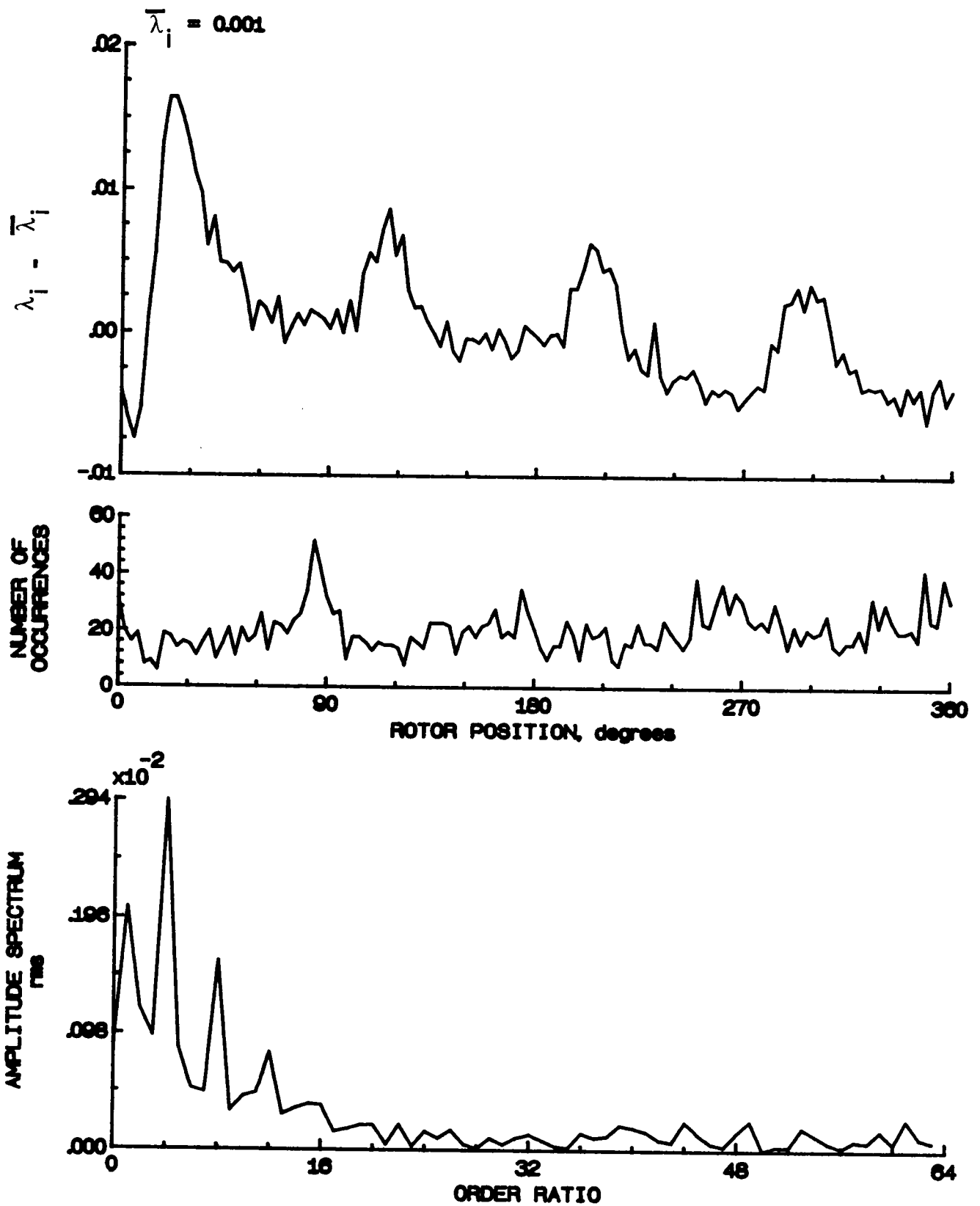


Figure 163.- Concluded.

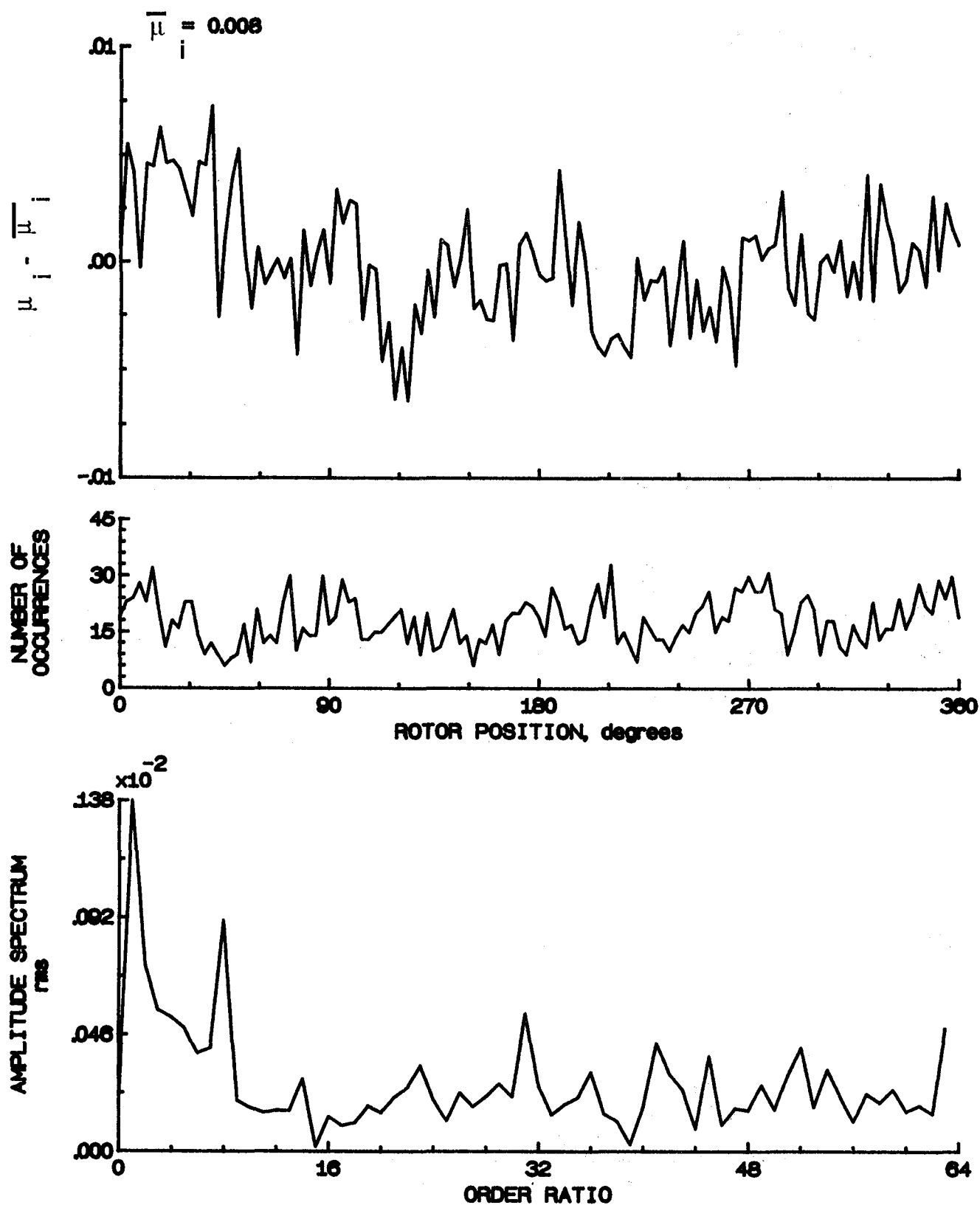


Figure 184.- Induced inflow velocity measured at 300 degrees and r/R of 0.40.



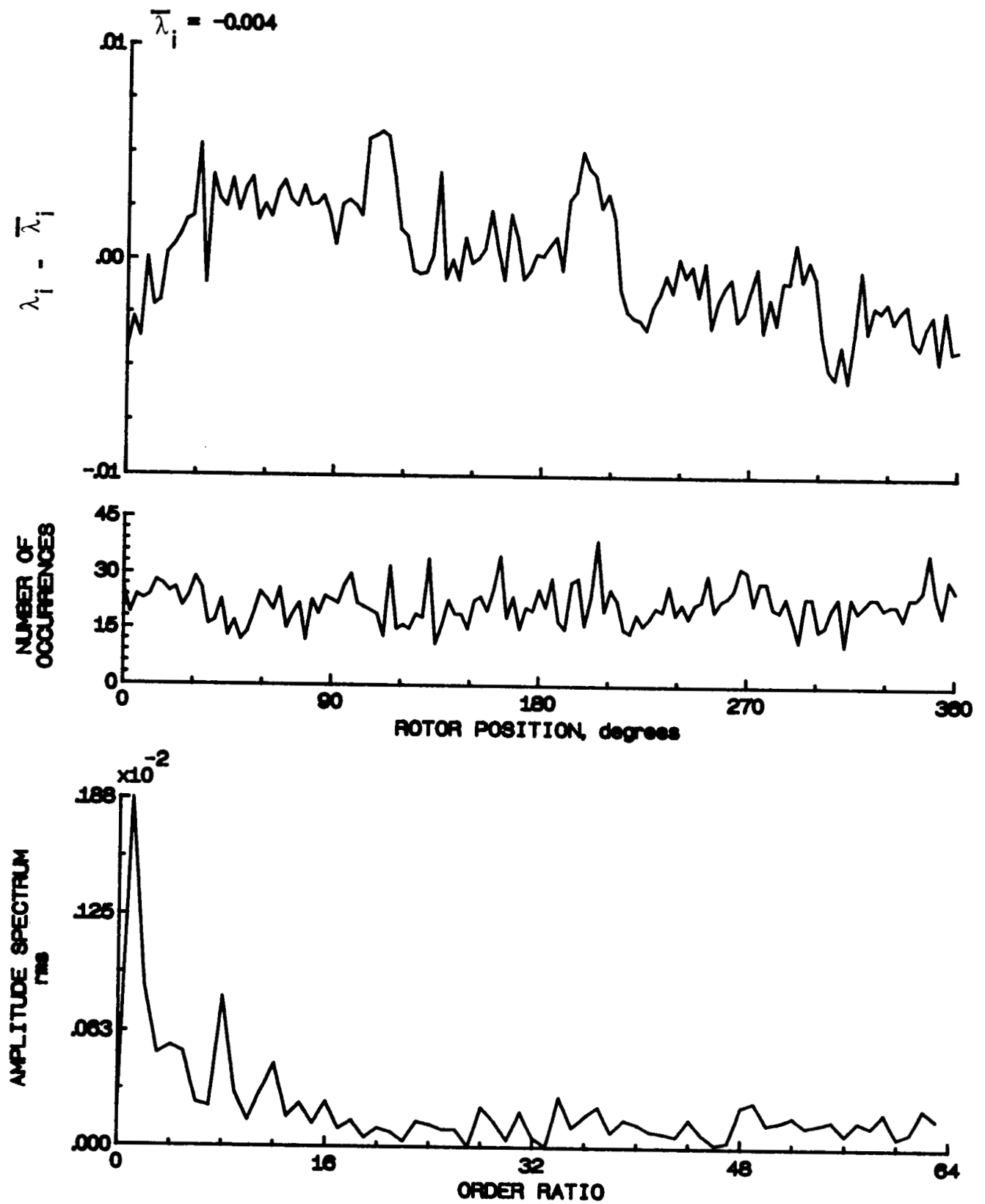


Figure 164.- Concluded.

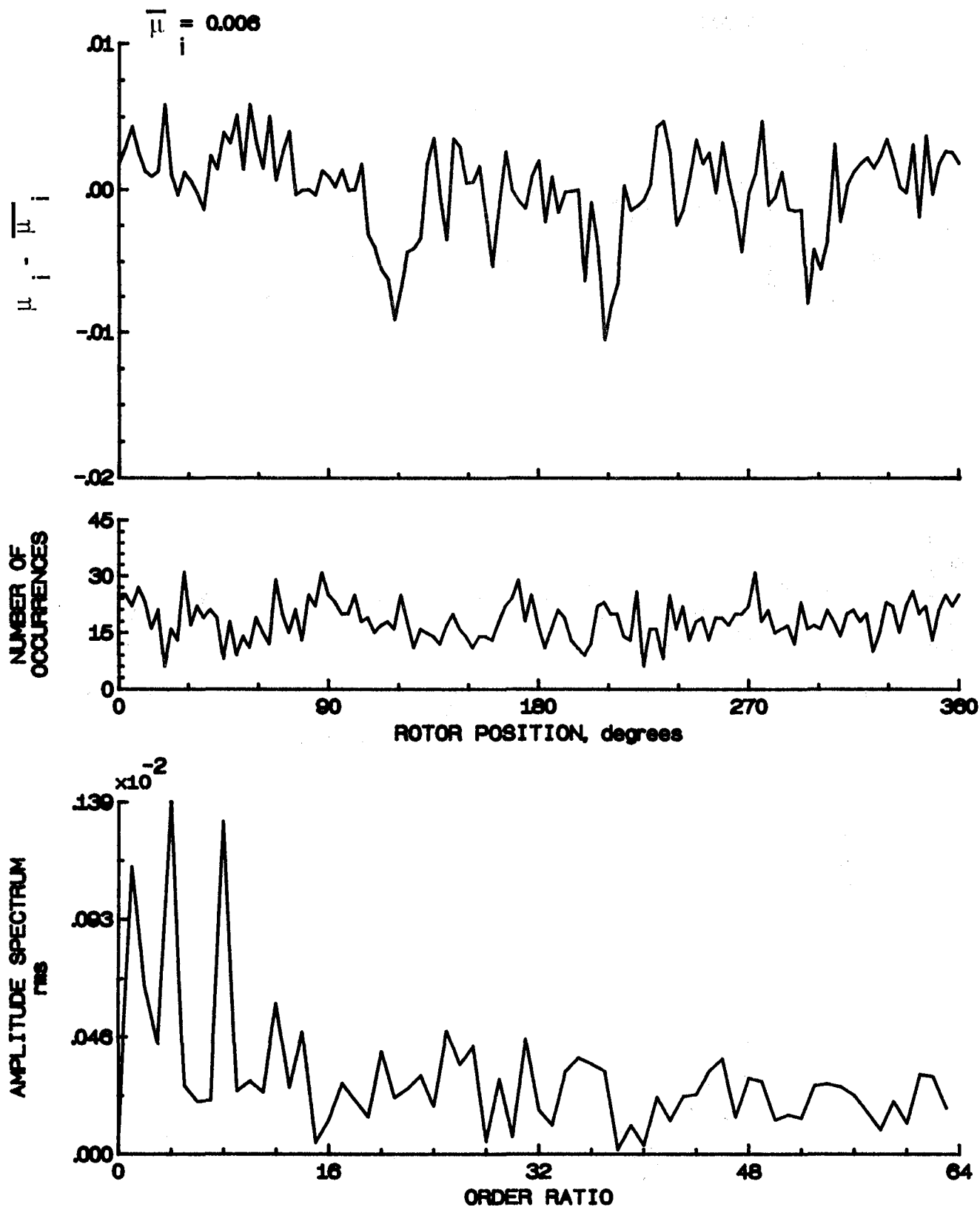


Figure 165.- Induced inflow velocity measured at 300 degrees and  $r/R$  of 0.50.

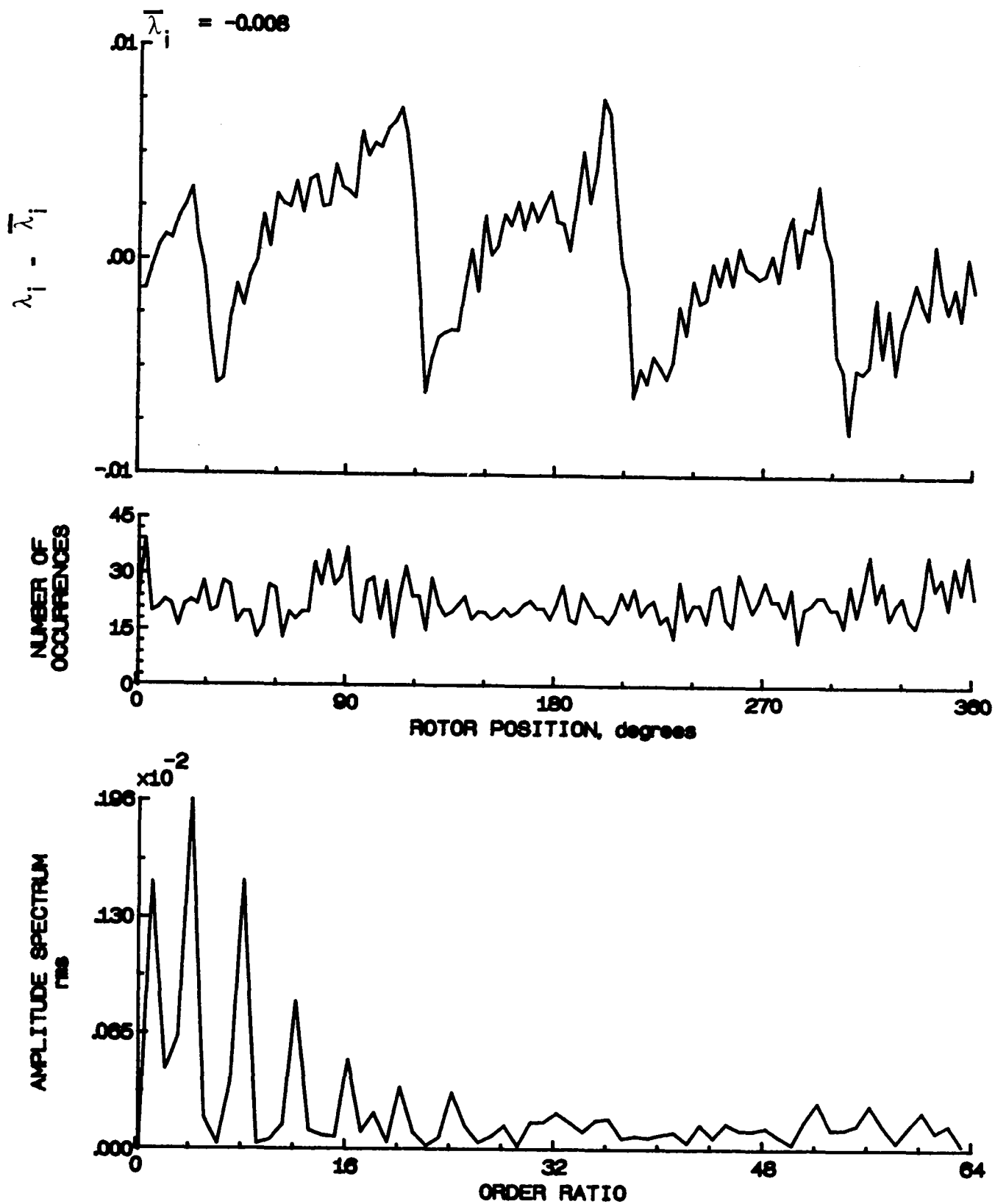


Figure 165.- Concluded.

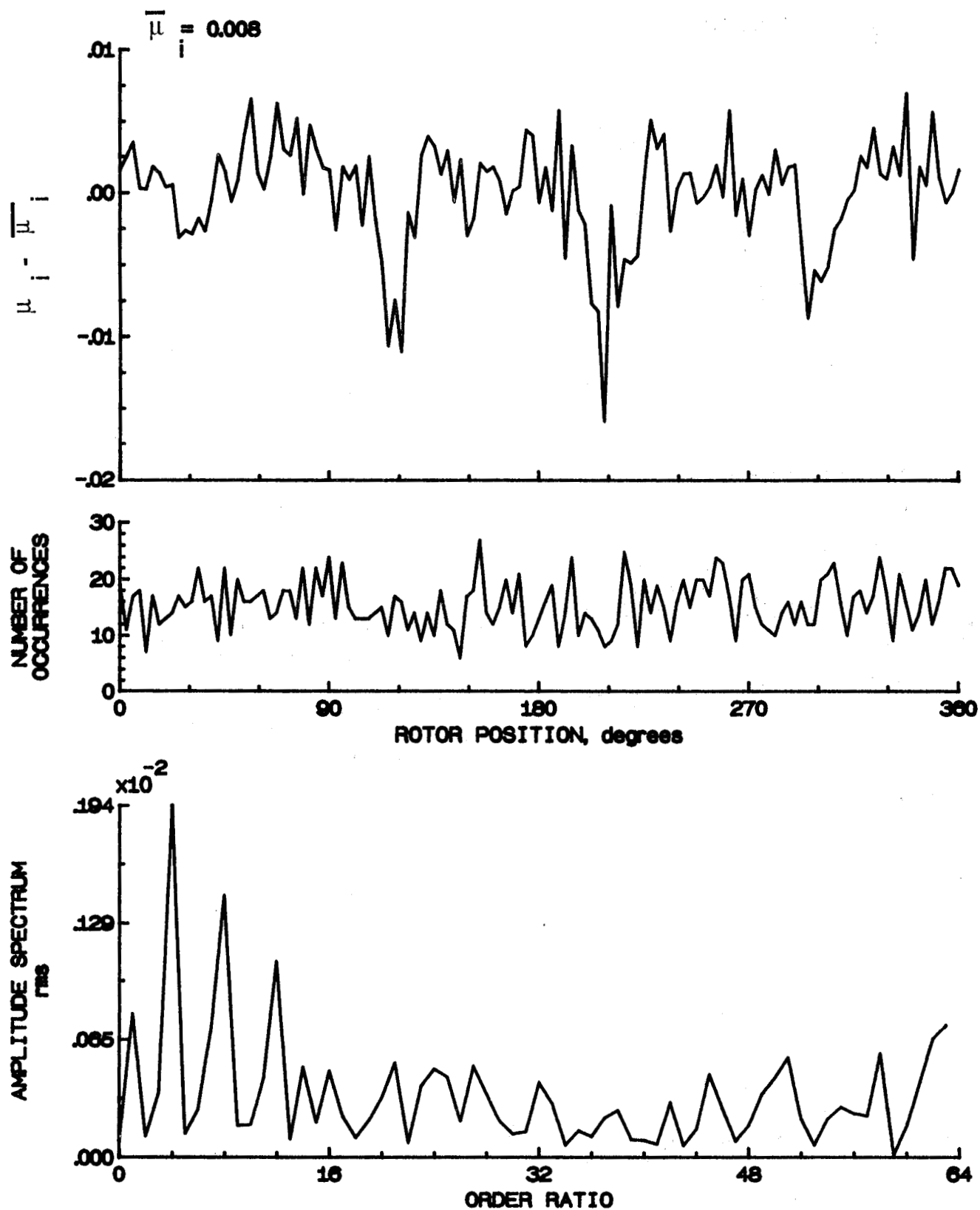


Figure 166.- Induced inflow velocity measured at 300 degrees and  $r/R$  of 0.60.

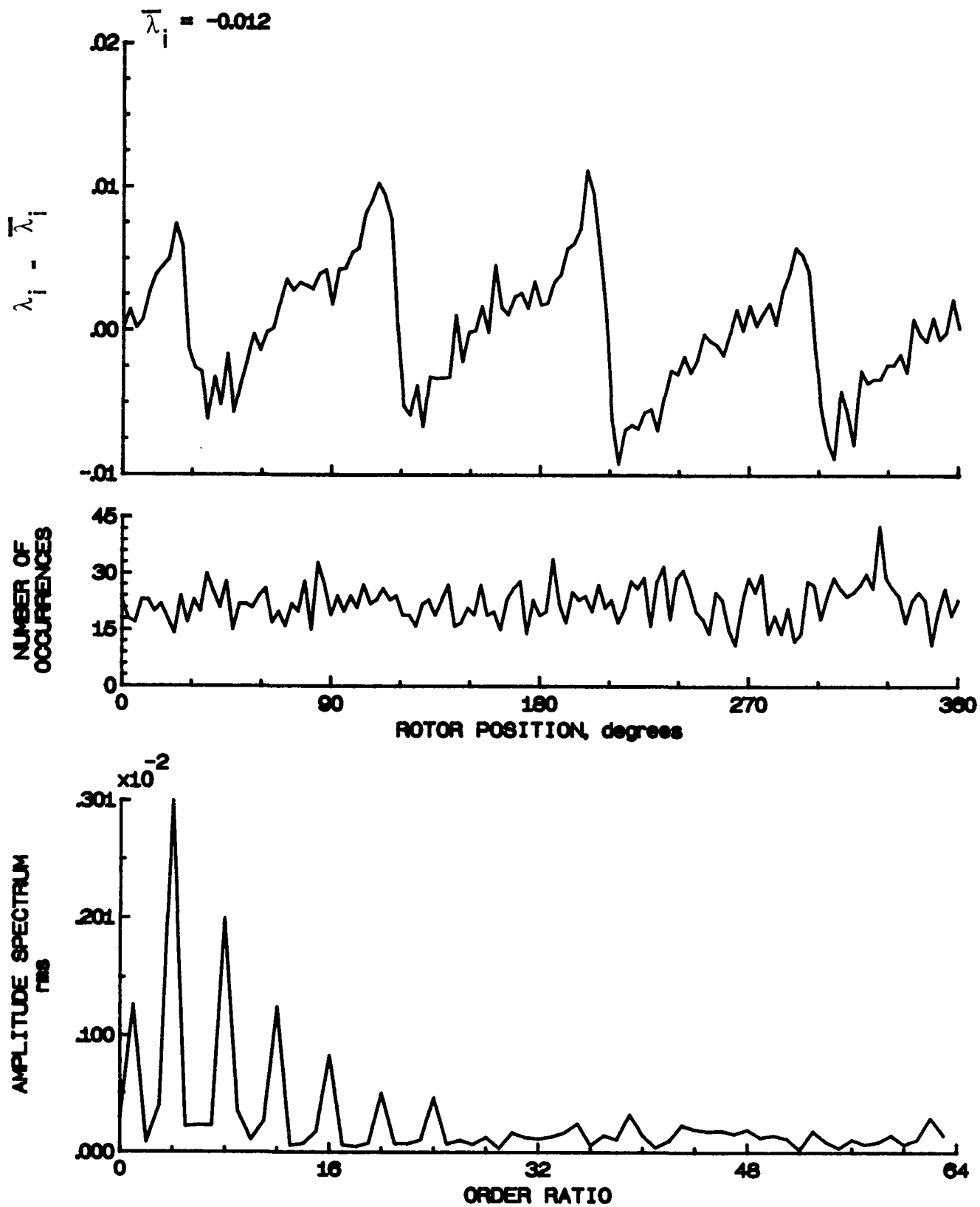


Figure 166.- Concluded.

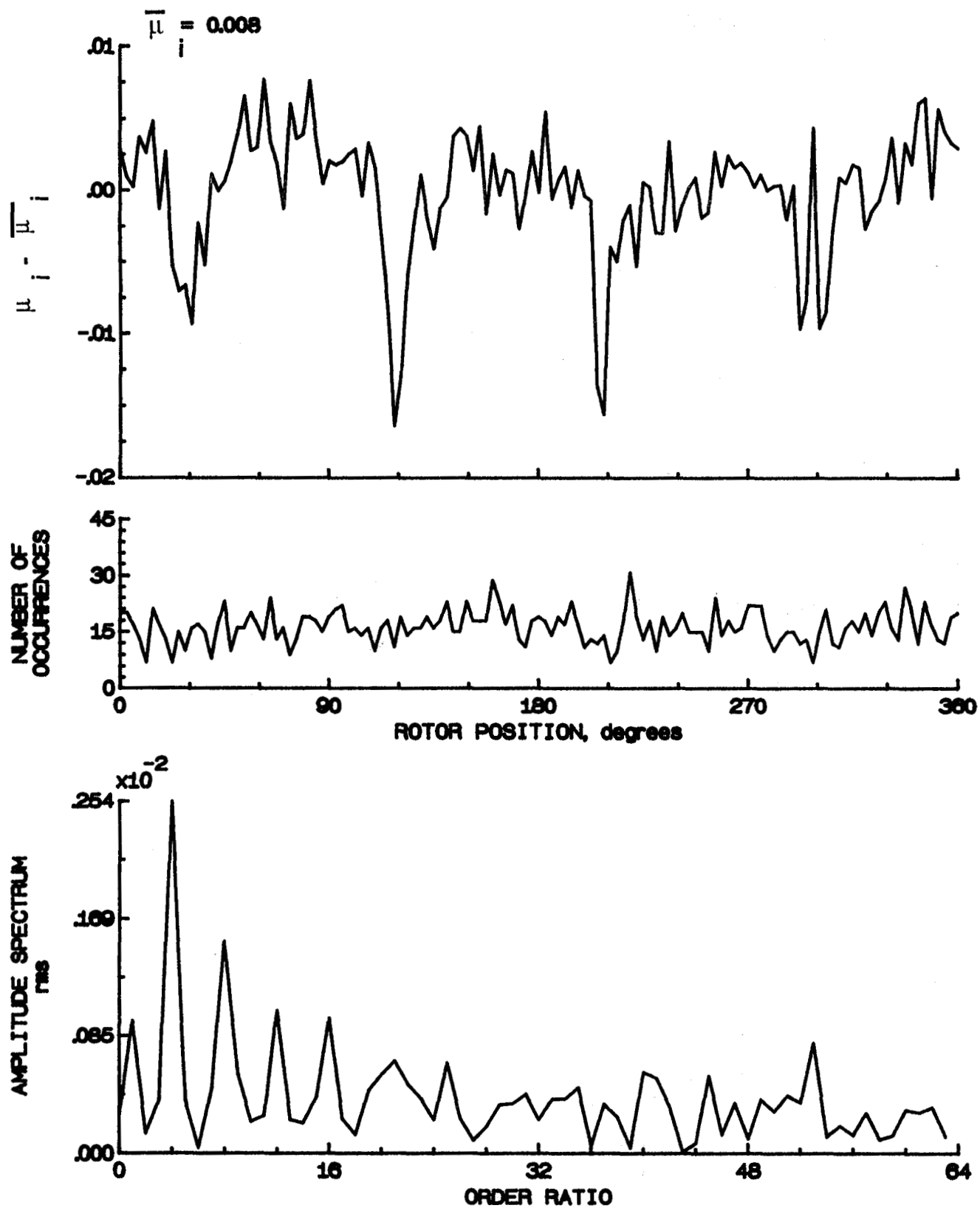


Figure 167.- Induced inflow velocity measured at 300 degrees and r/R of 0.70.

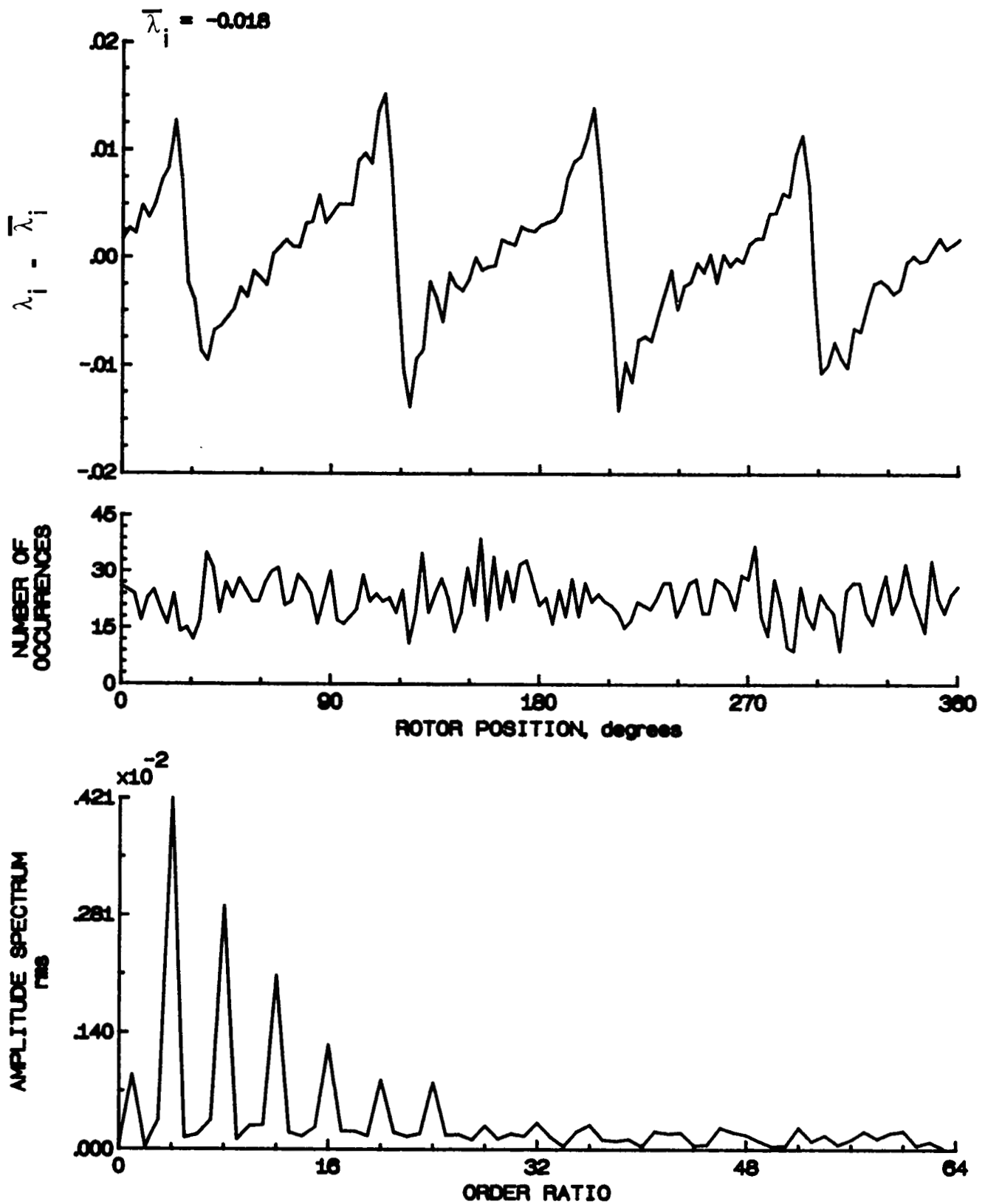


Figure 167.- Concluded.

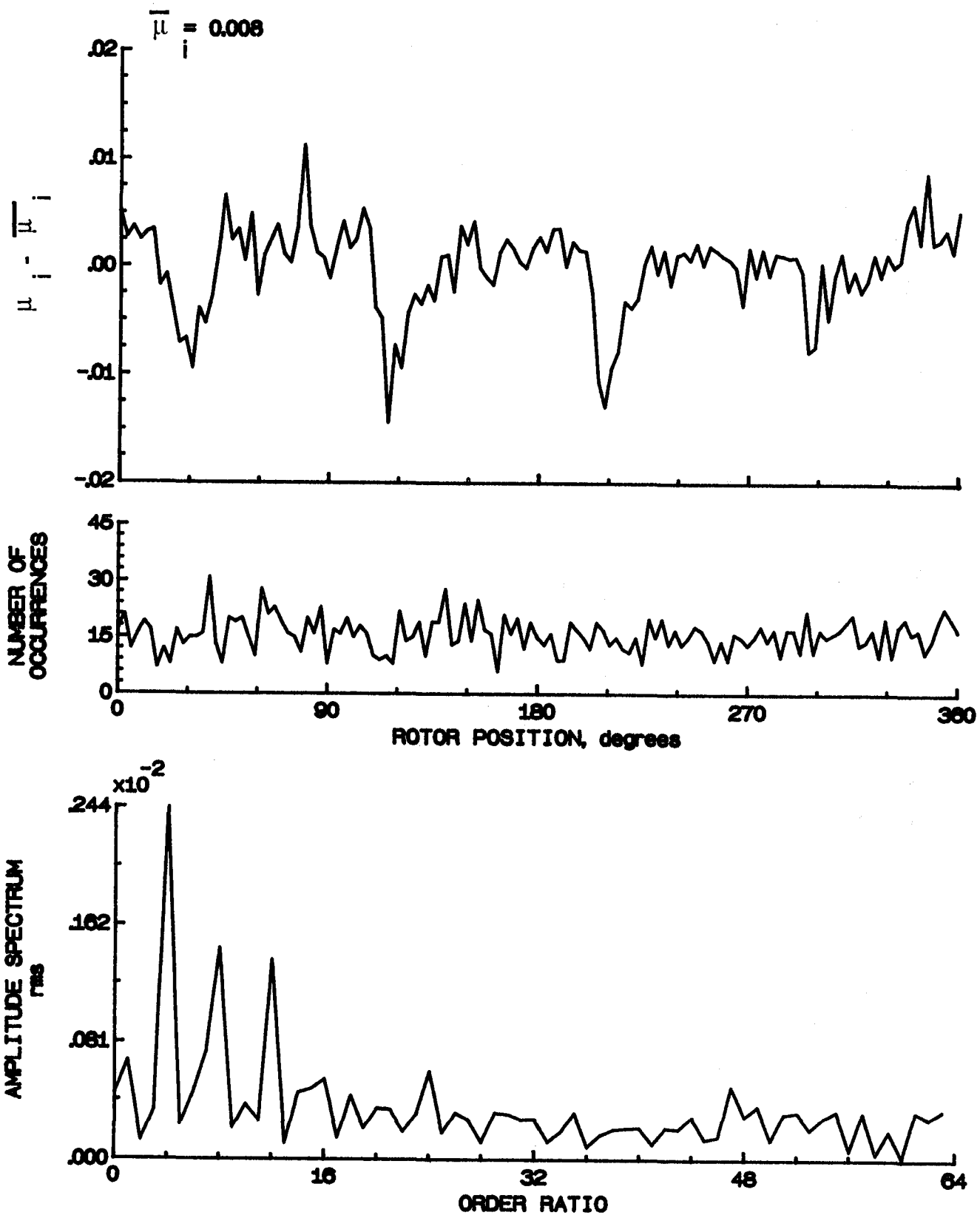


Figure 168.- Induced inflow velocity measured at 300 degrees and r/R of 0.74.



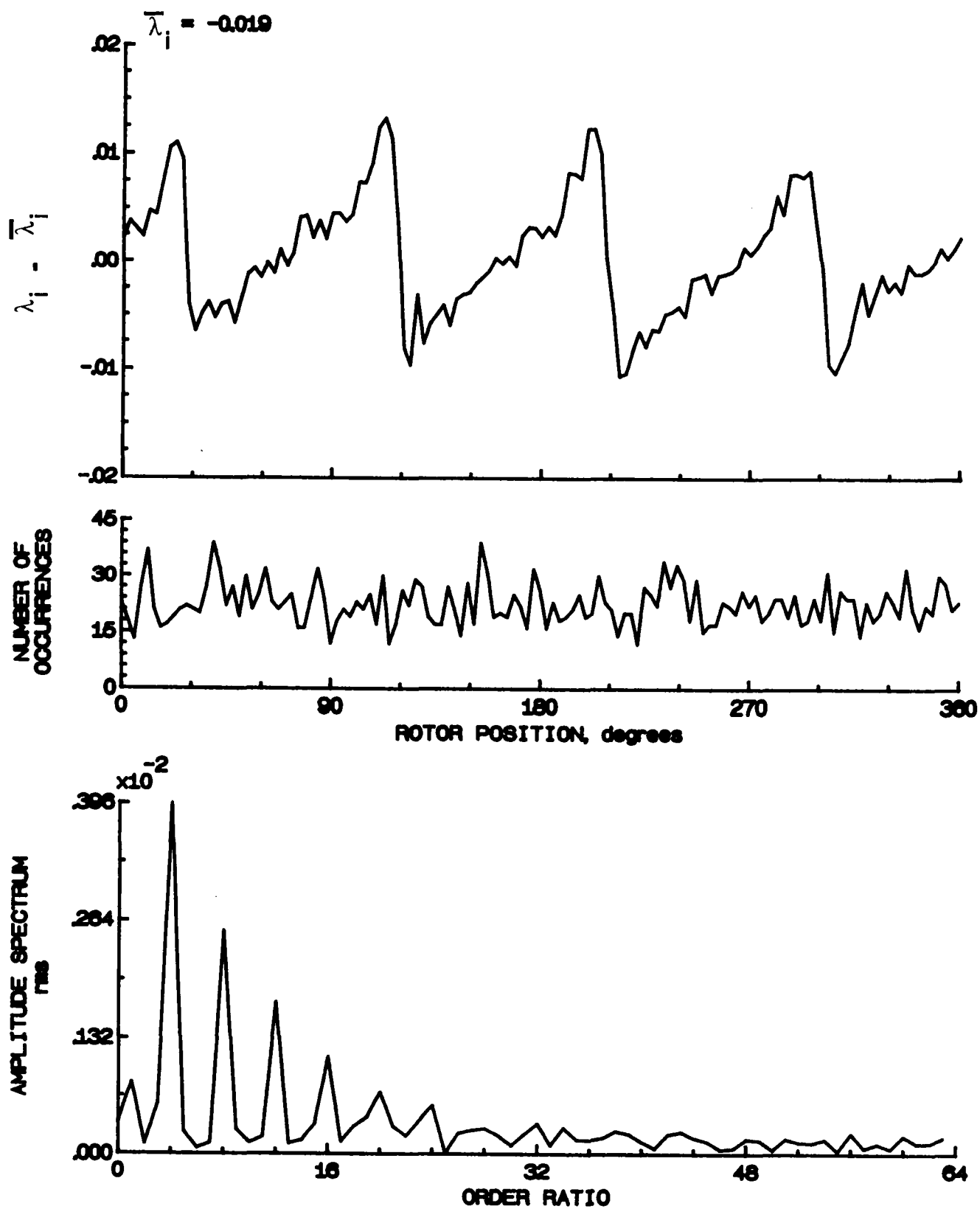


Figure 168.- Concluded.

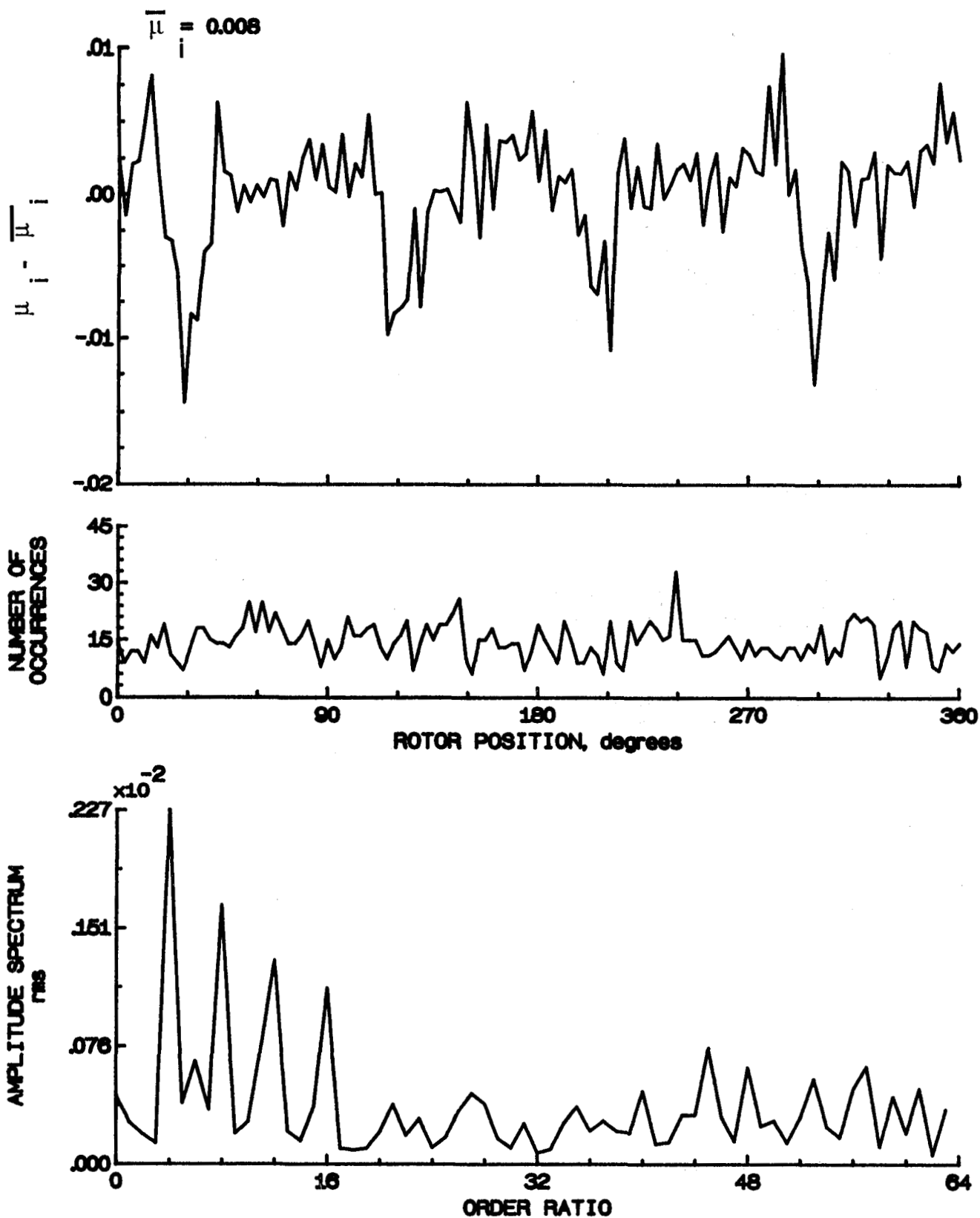


Figure 169.- Induced inflow velocity measured at 300 degrees and r/R of 0.78.

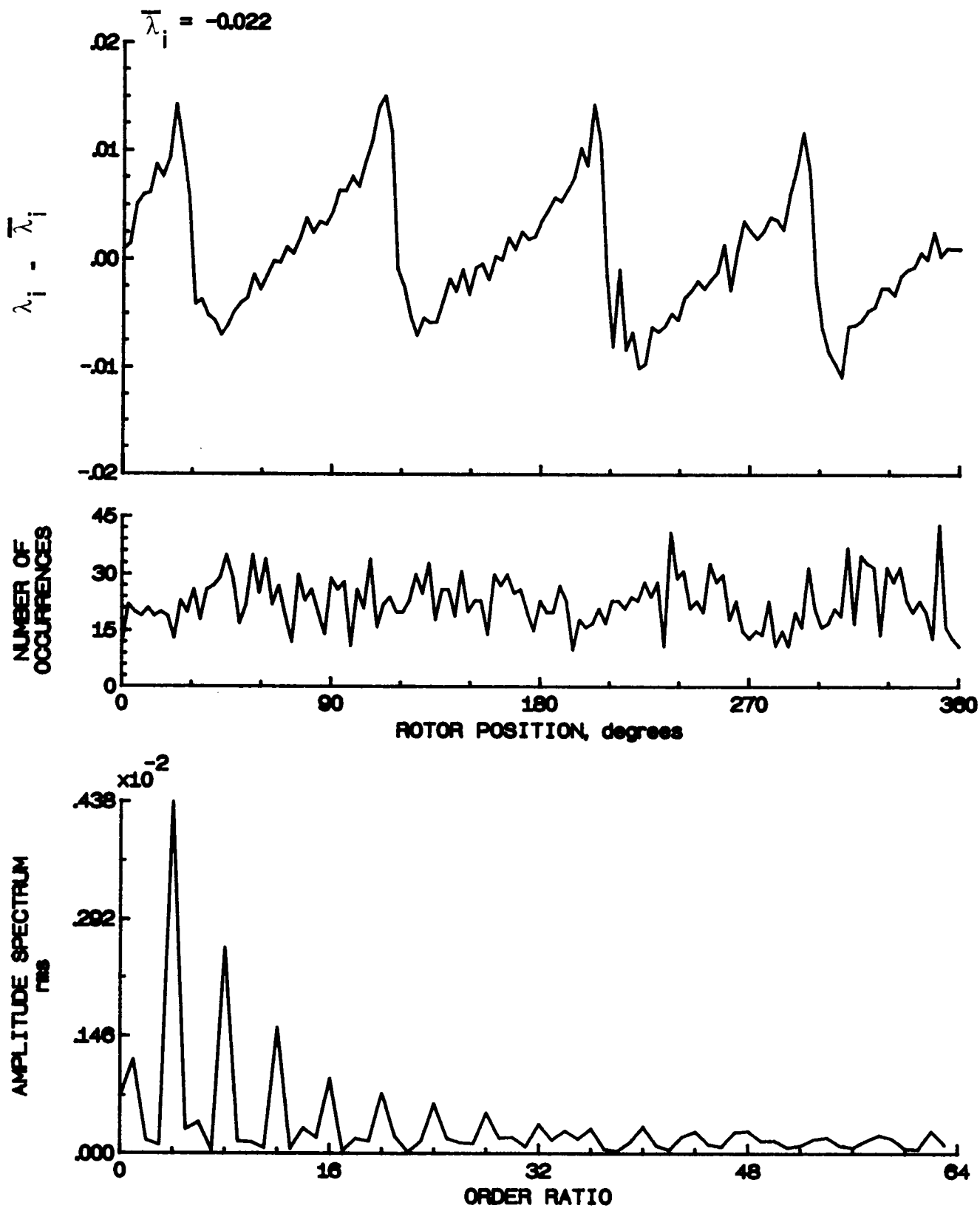


Figure 169.- Concluded.

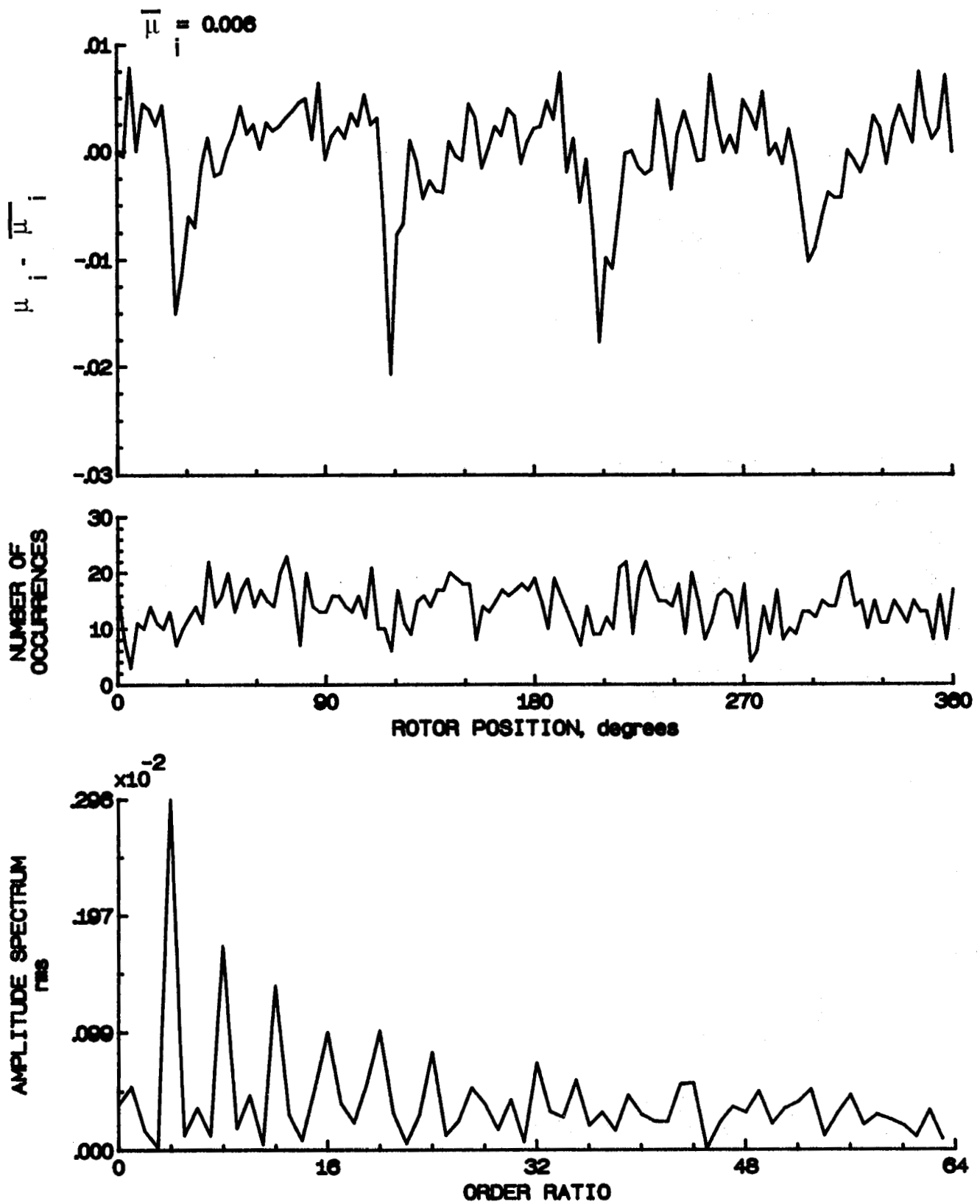


Figure 170.- Induced inflow velocity measured at 300 degrees and  $r/R$  of 0.82.

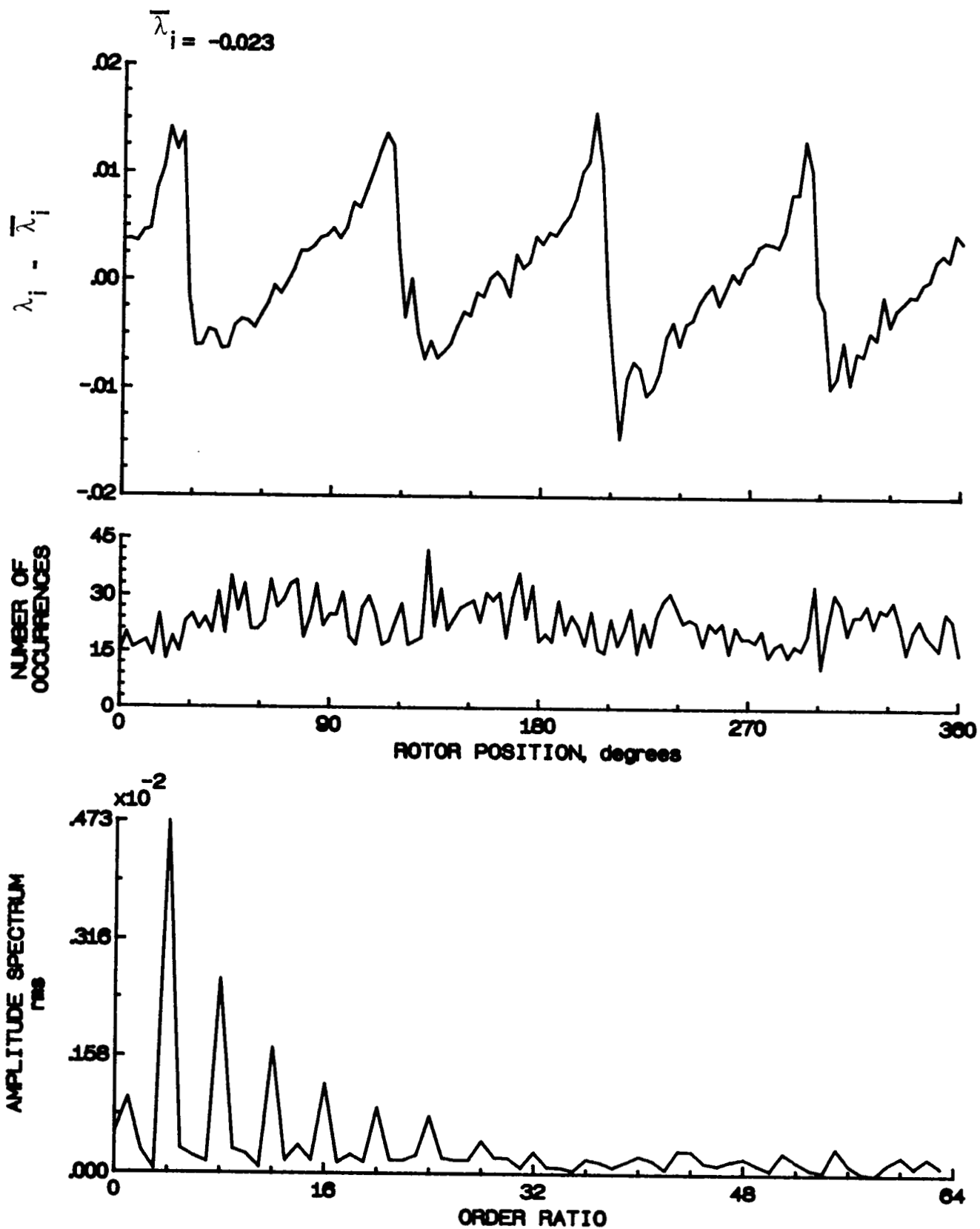


Figure 170.- Concluded.

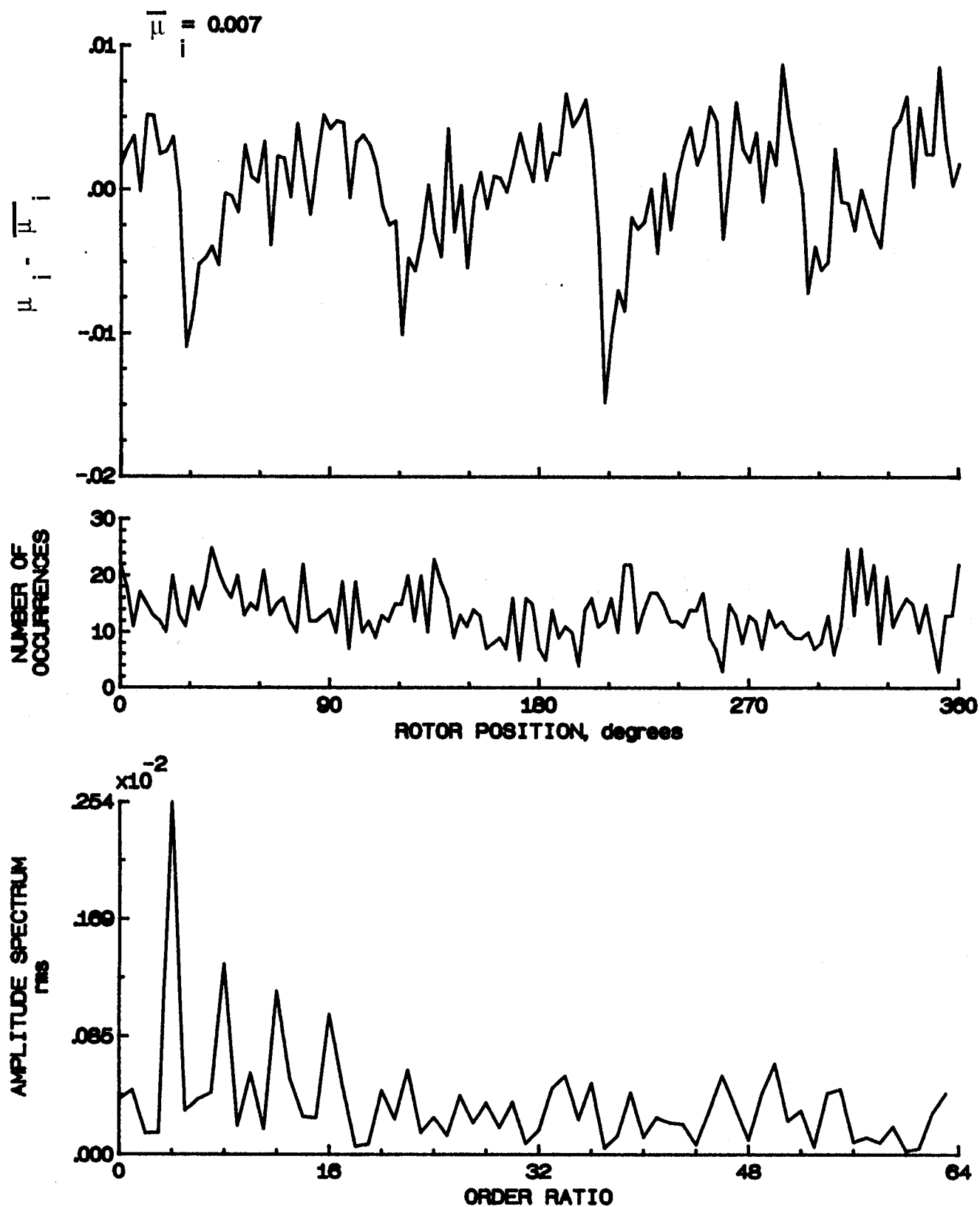


Figure 171.- Induced inflow velocity measured at 300 degrees and r/R of 0.86.

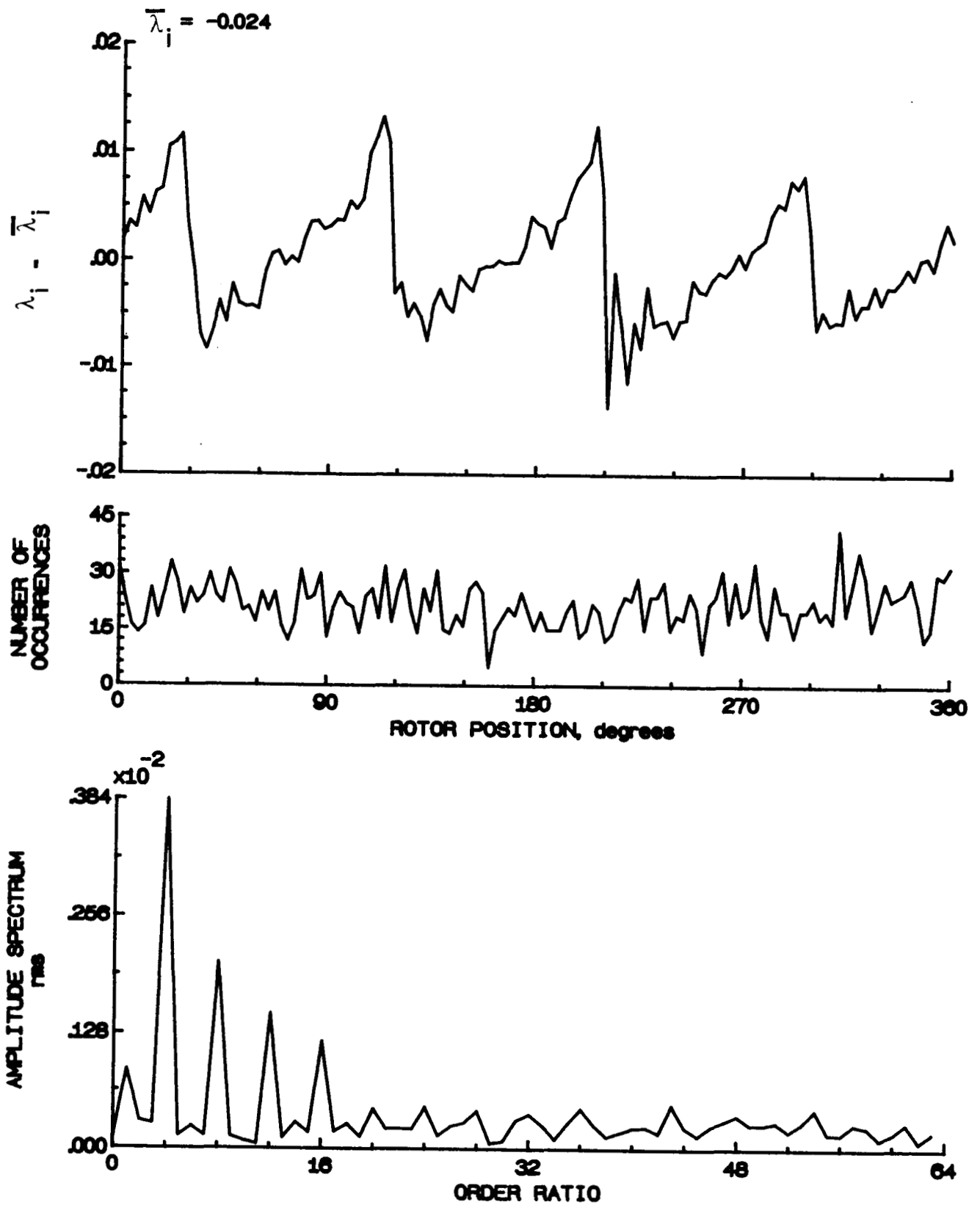


Figure 171- Concluded.

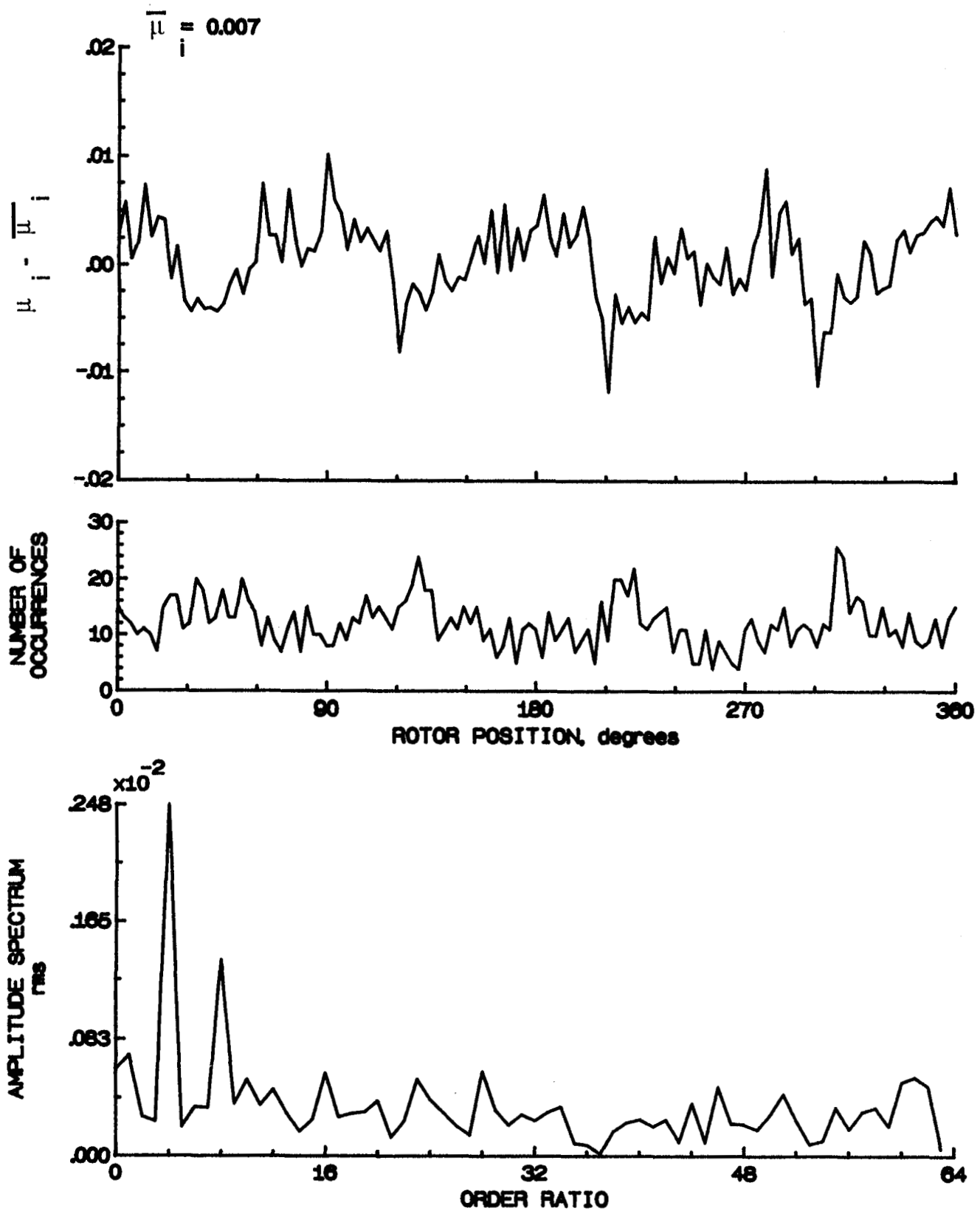


Figure 172.- Induced inflow velocity measured at 300 degrees and r/R of 0.90.



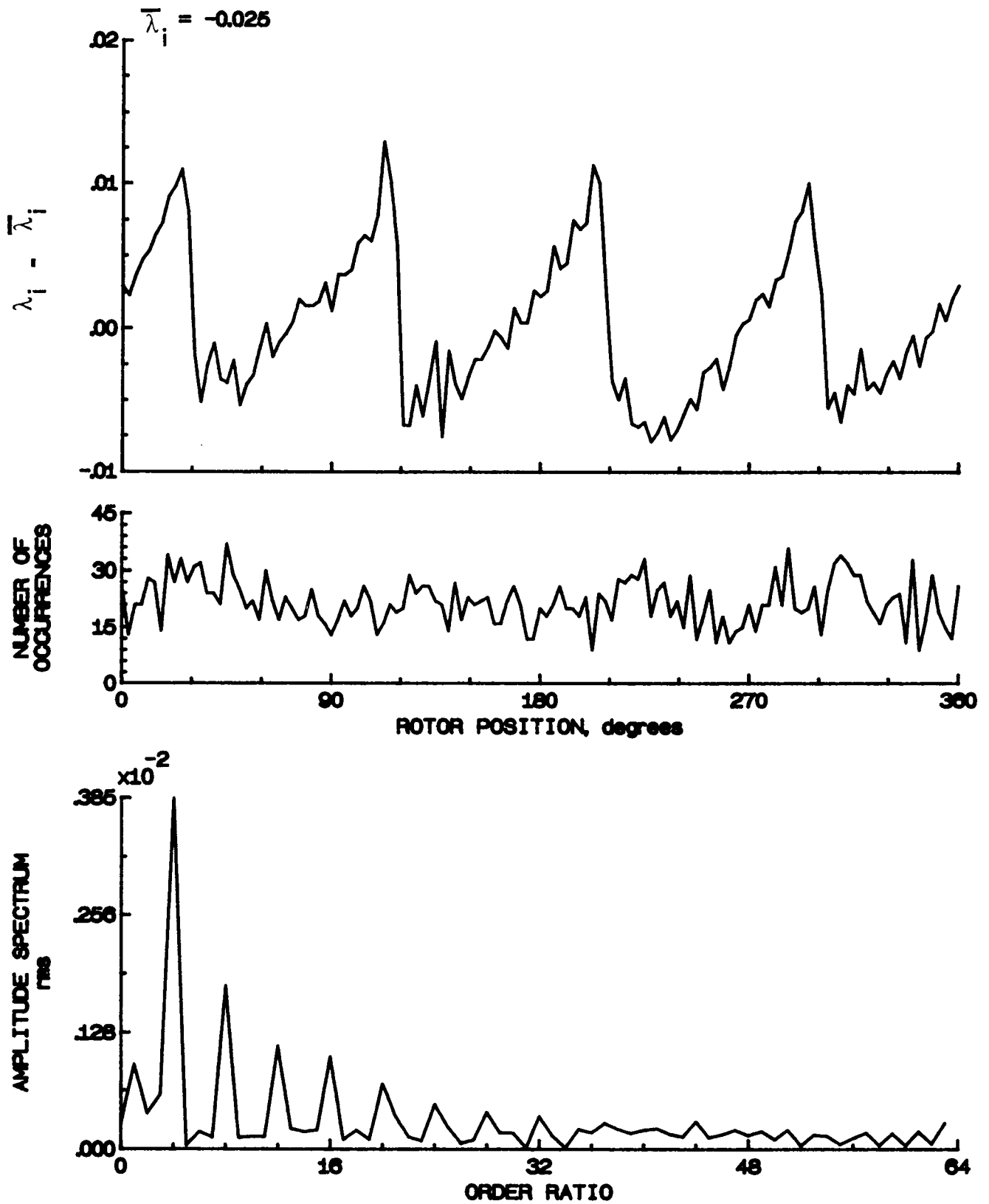


Figure 172.- Concluded.

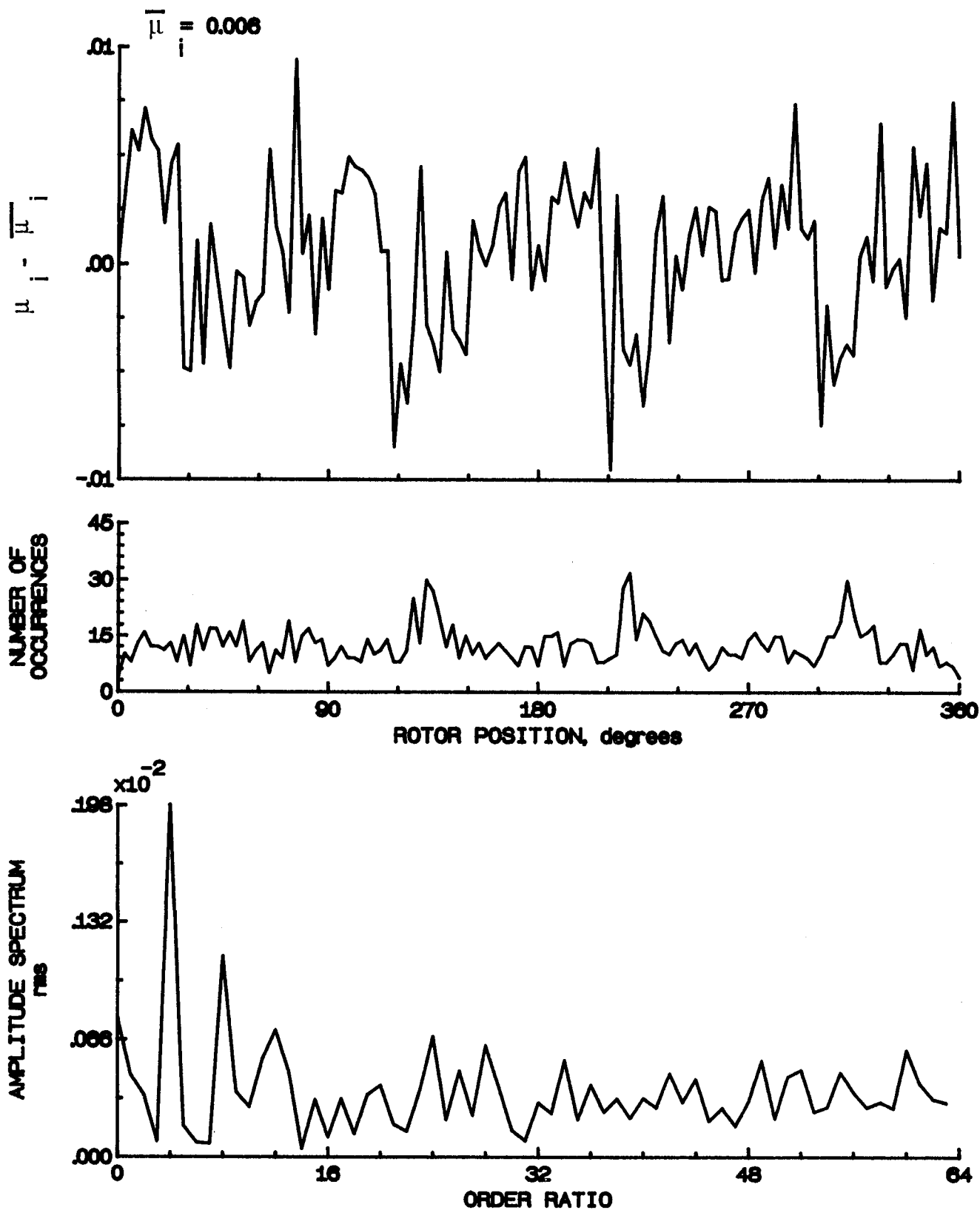


Figure 173.- Induced inflow velocity measured at 300 degrees and r/R of 0.94.

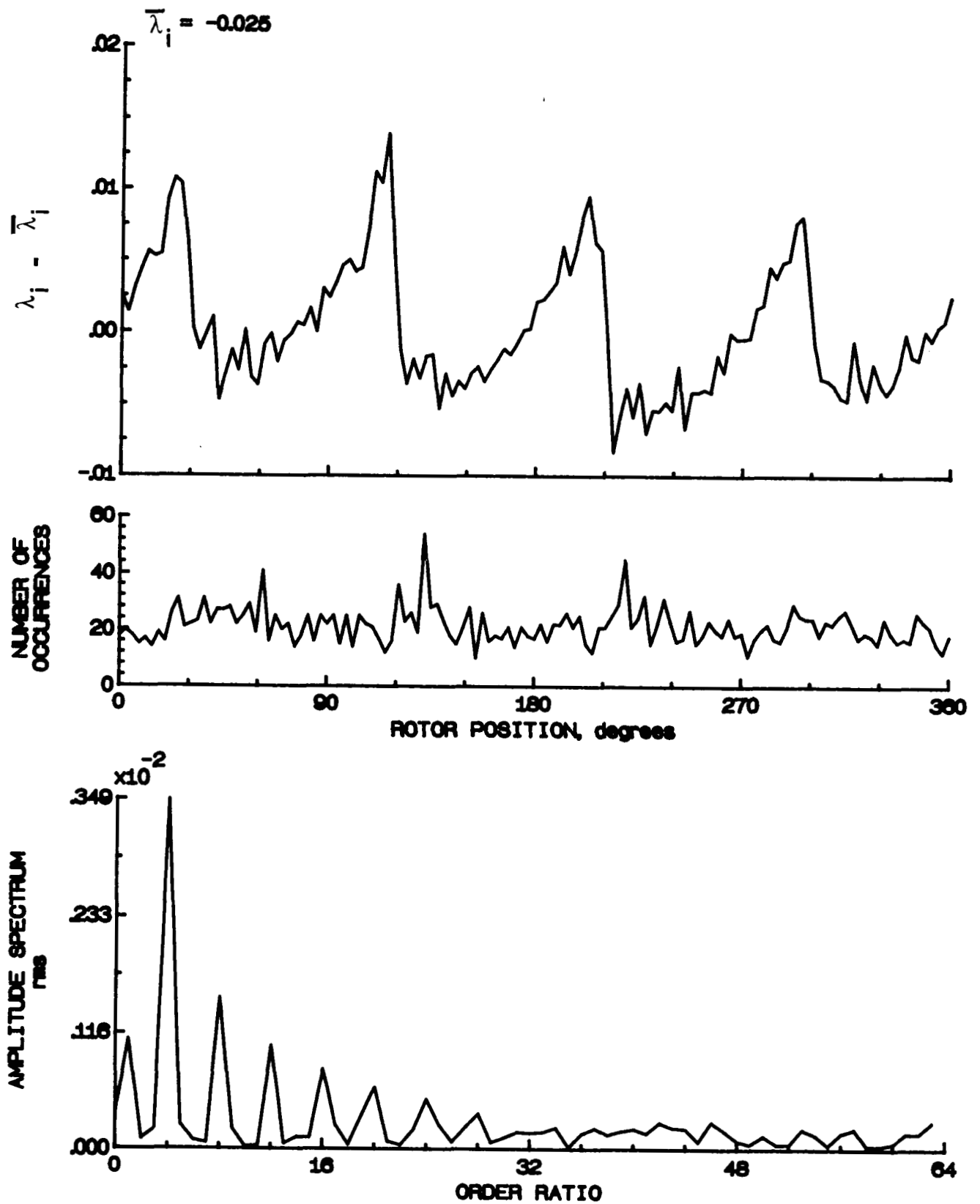


Figure 173.- Concluded.

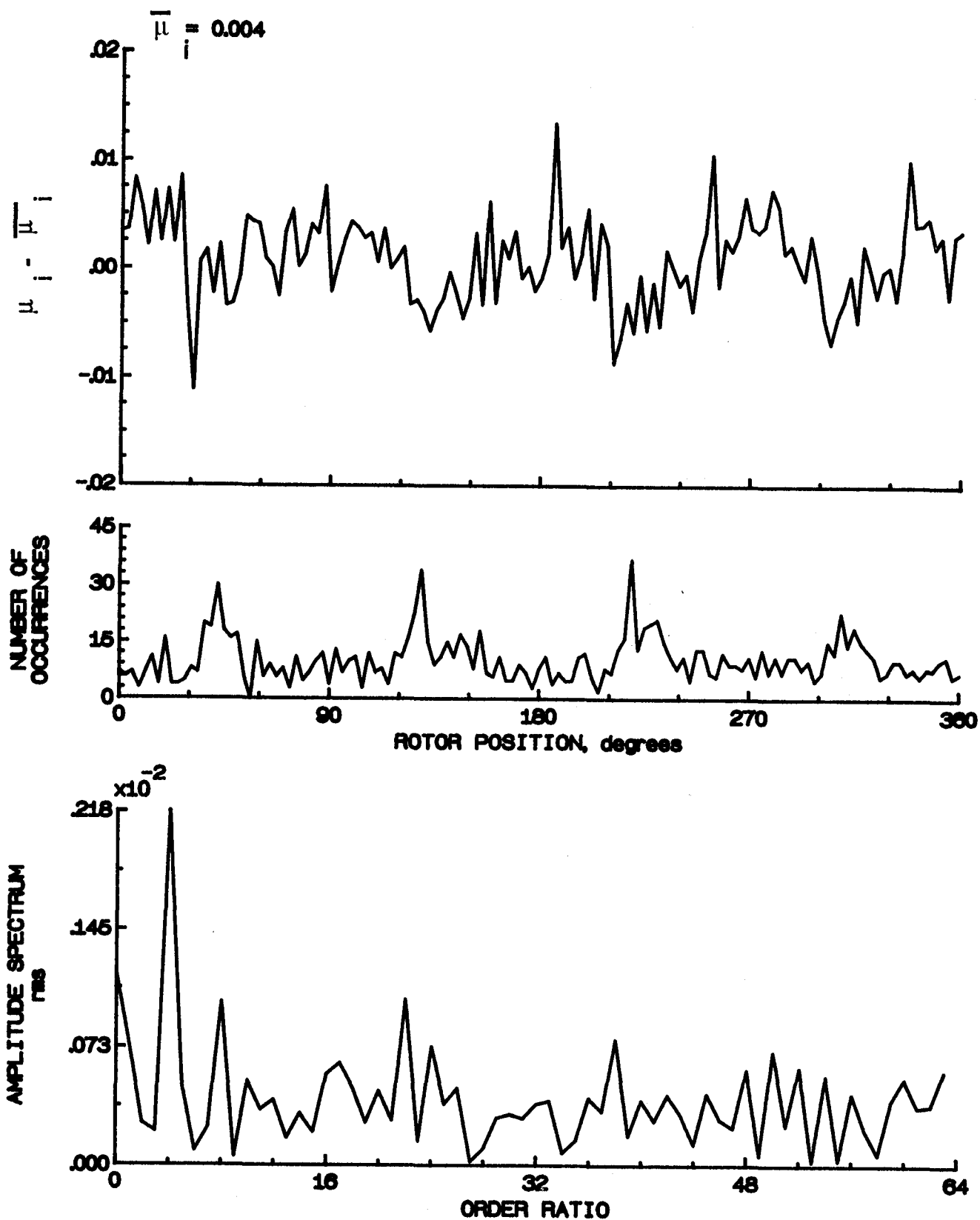


Figure 174.- Induced inflow velocity measured at 300 degrees and  $r/R$  of 0.98.

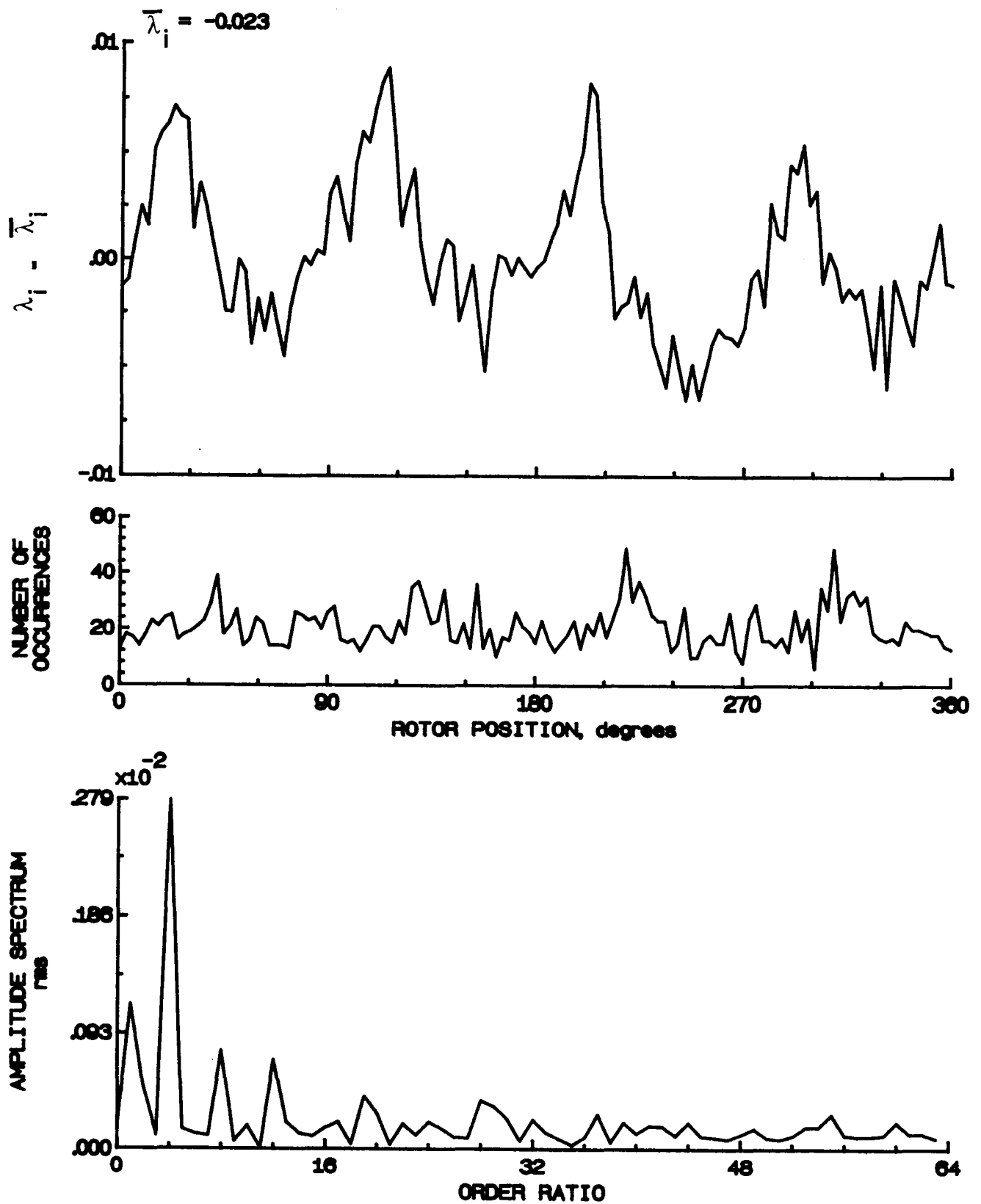


Figure 174.- Concluded.

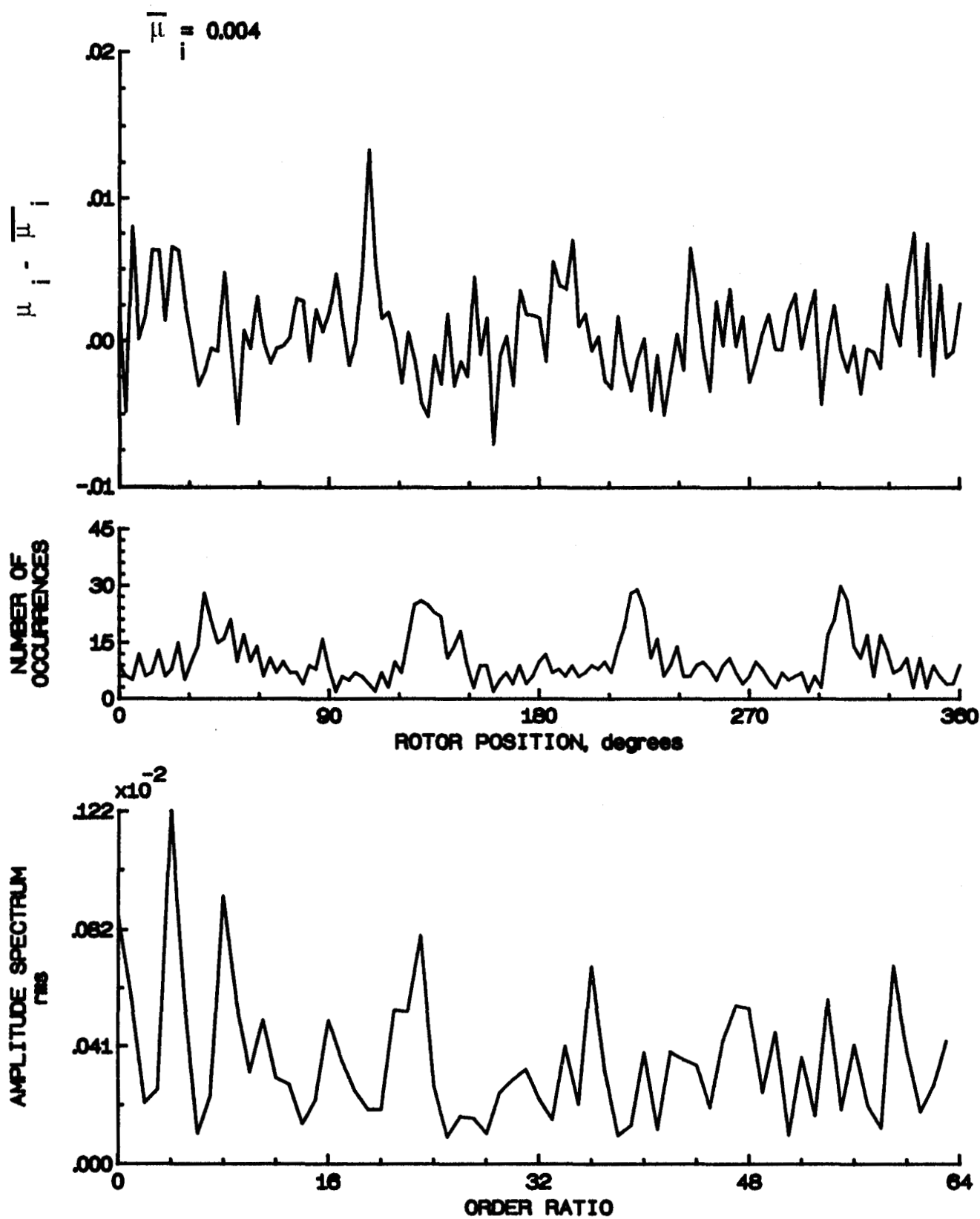


Figure 175.- Induced inflow velocity measured at 300 degrees and r/R of 1.02.

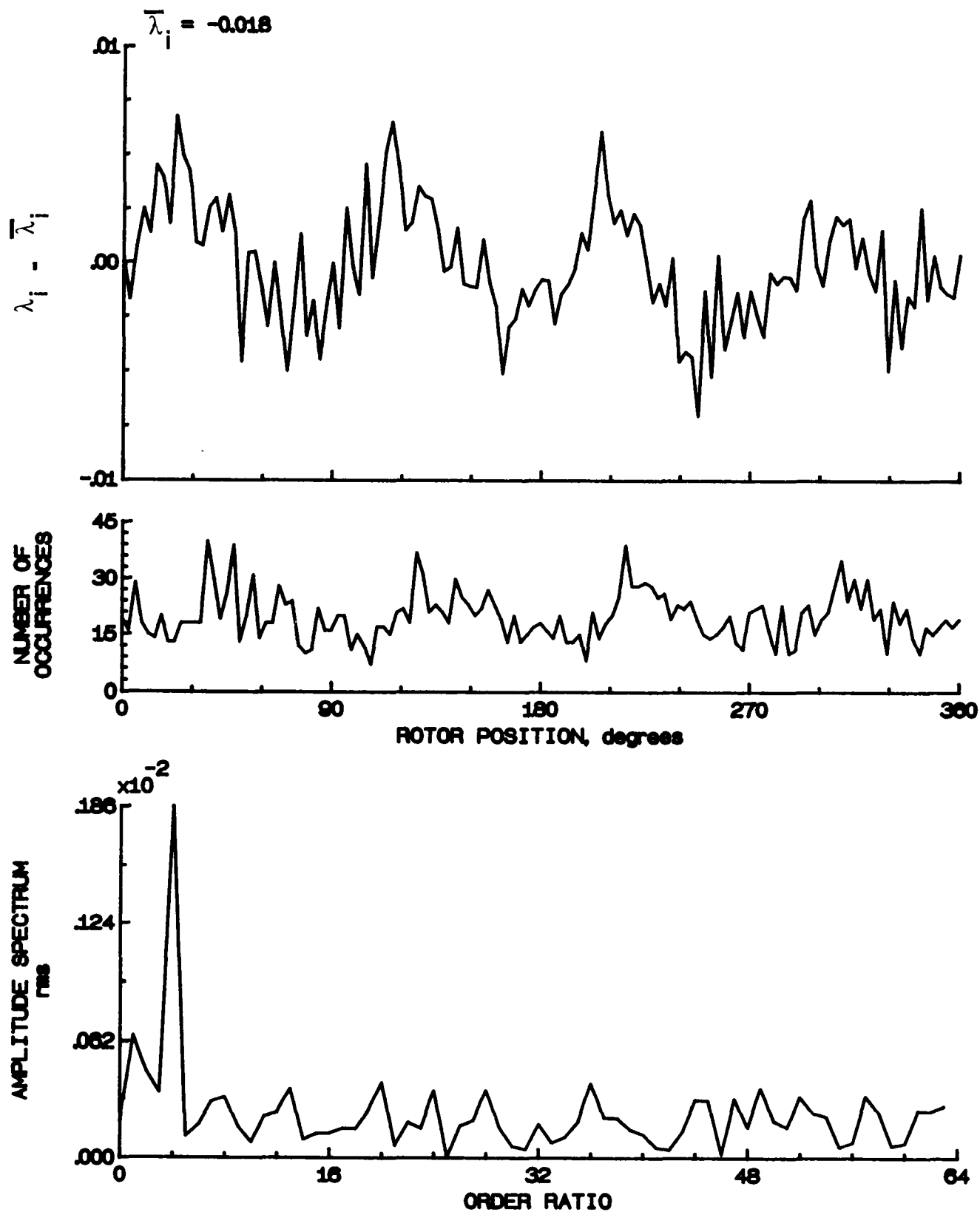


Figure 175.- Concluded.

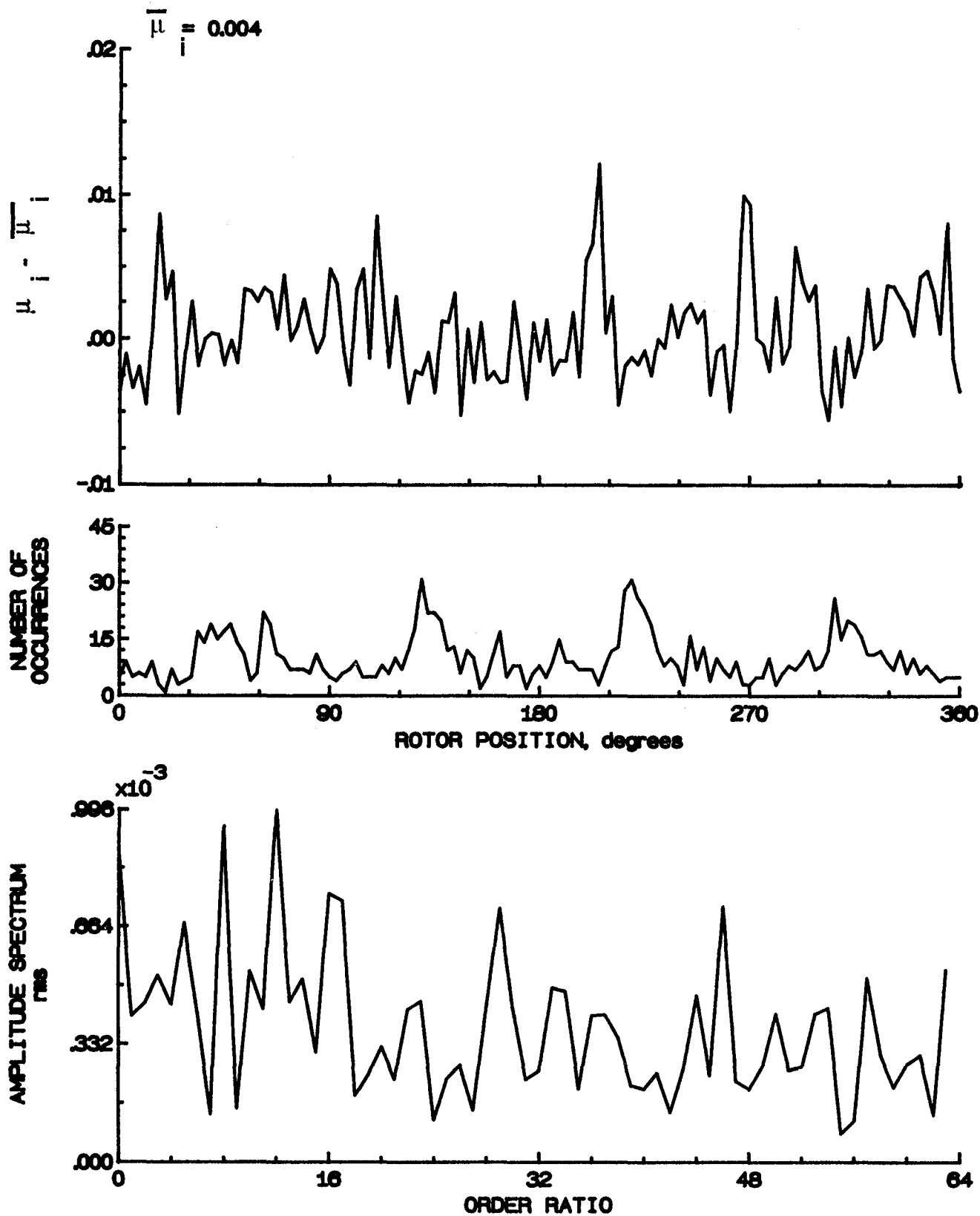


Figure 176.- Induced inflow velocity measured at 300 degrees and r/R of 1.04.



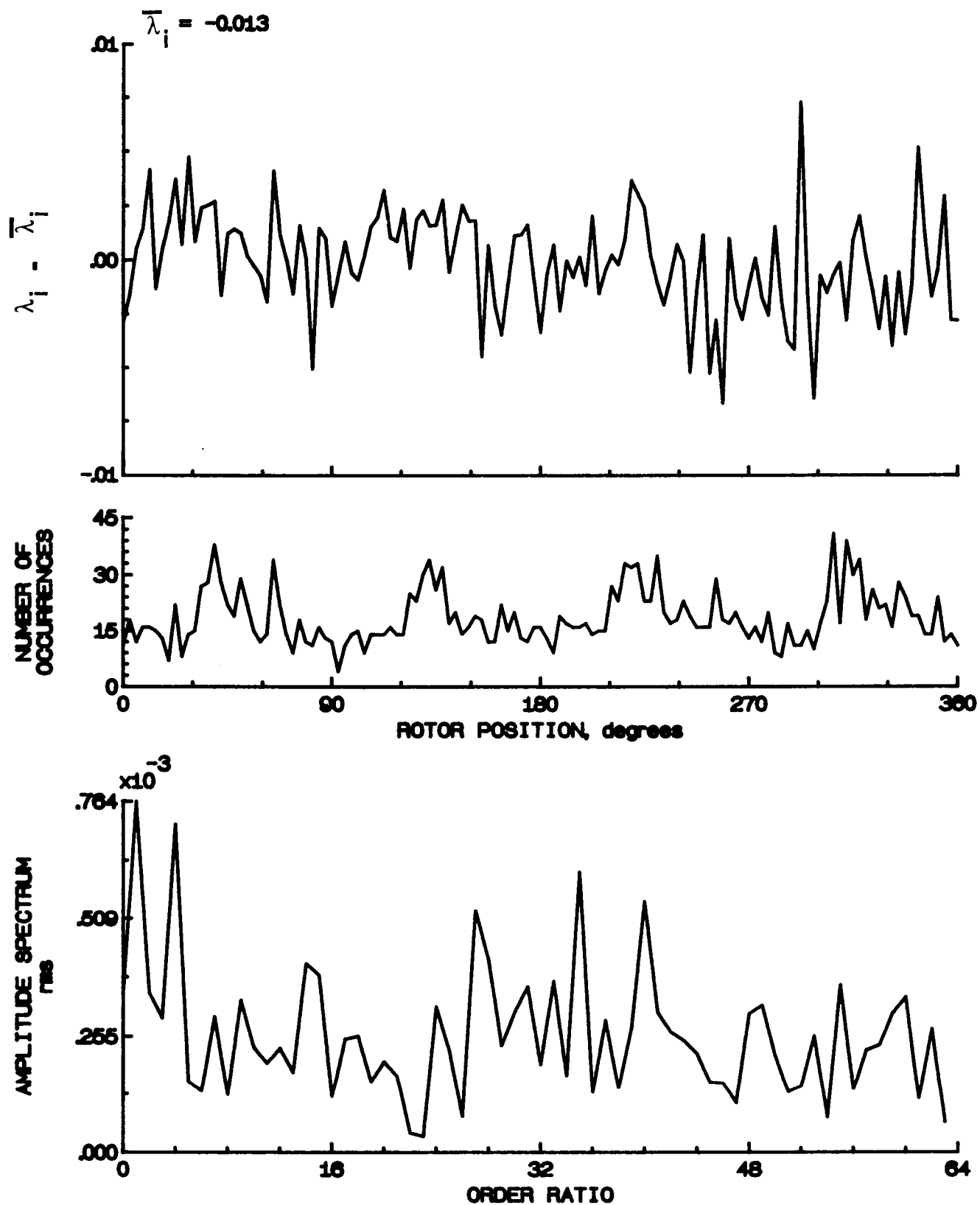


Figure 176.- Concluded.

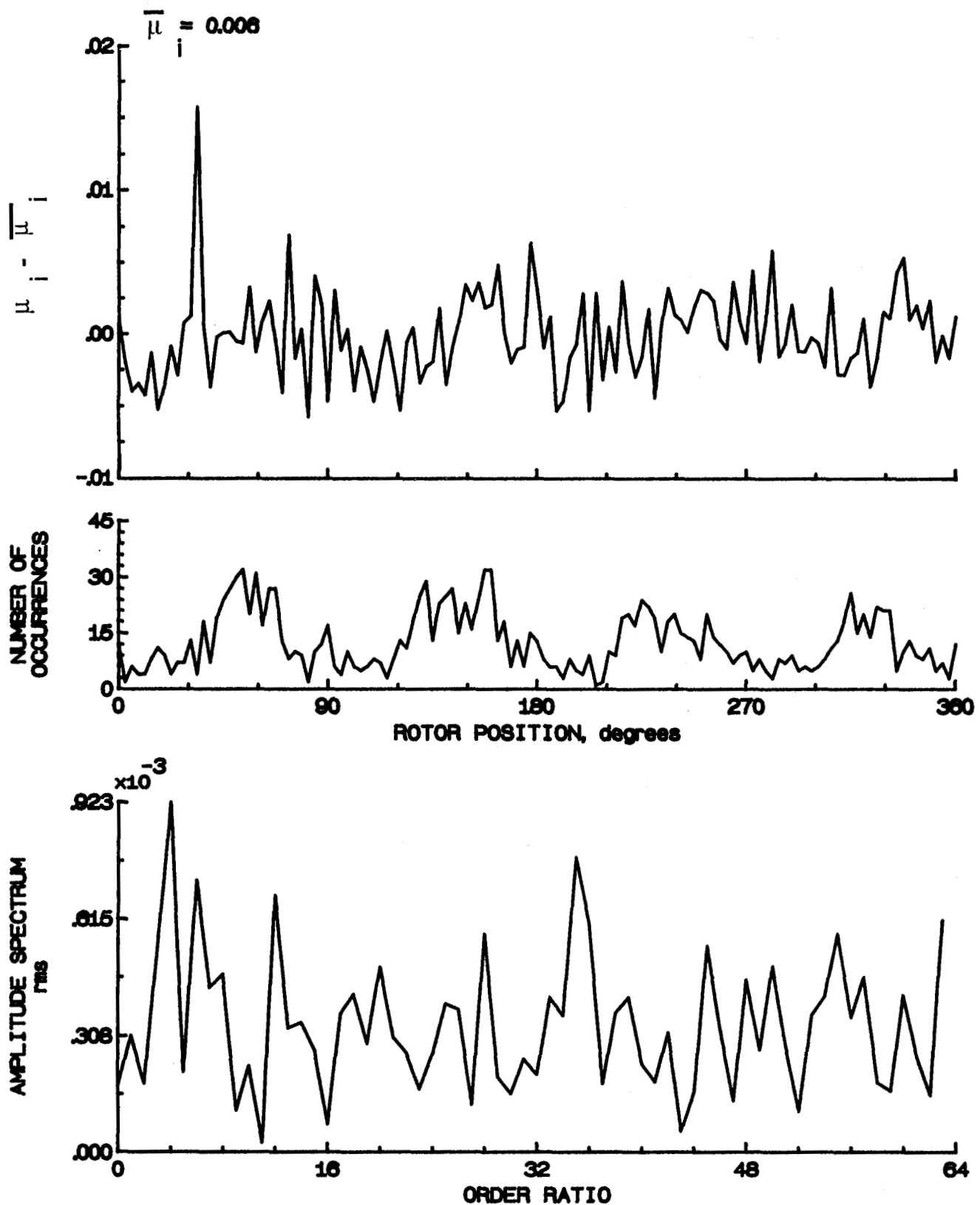


Figure 177.- Induced inflow velocity measured at 300 degrees and r/R of 1.10.

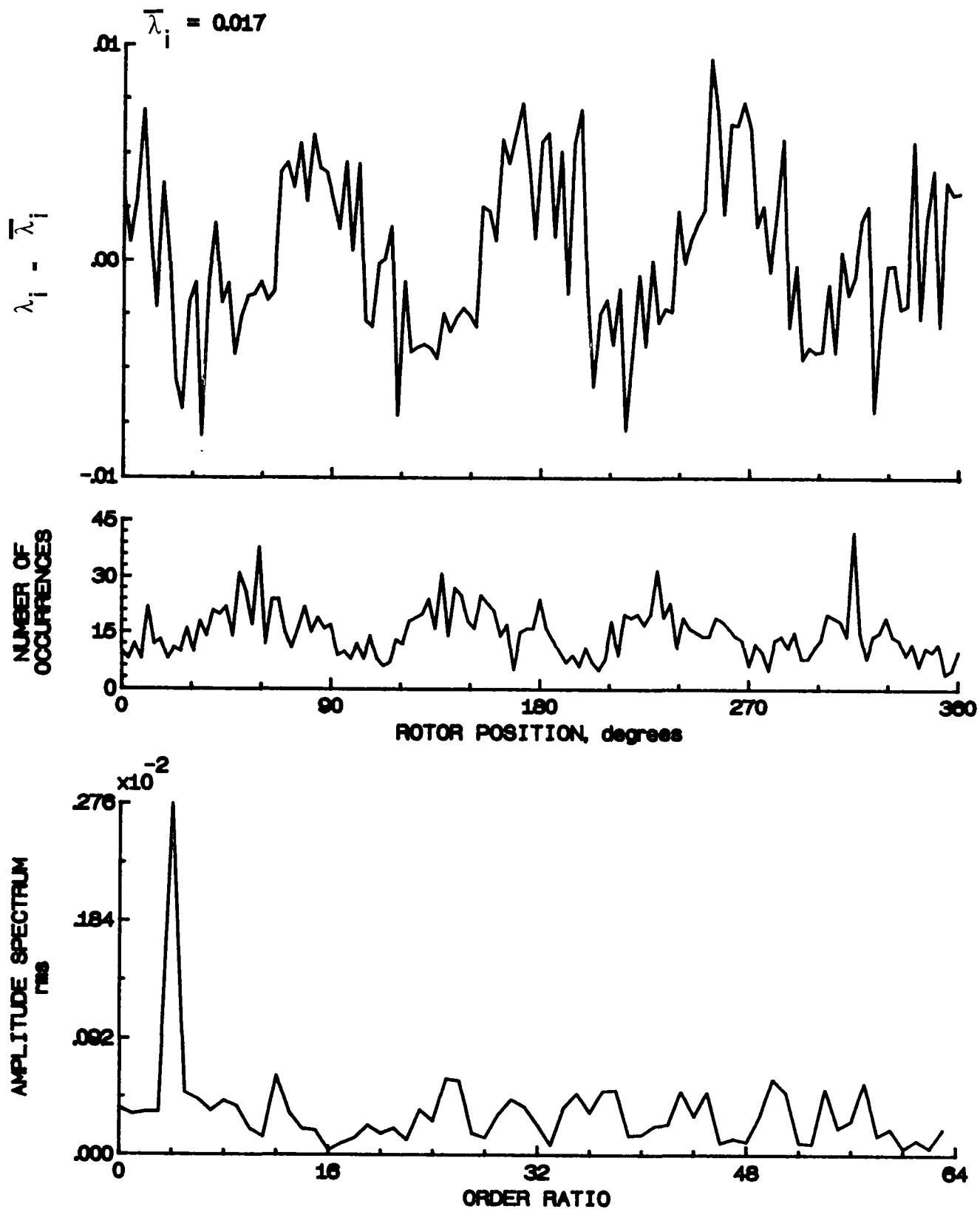


Figure 177.- Concluded.

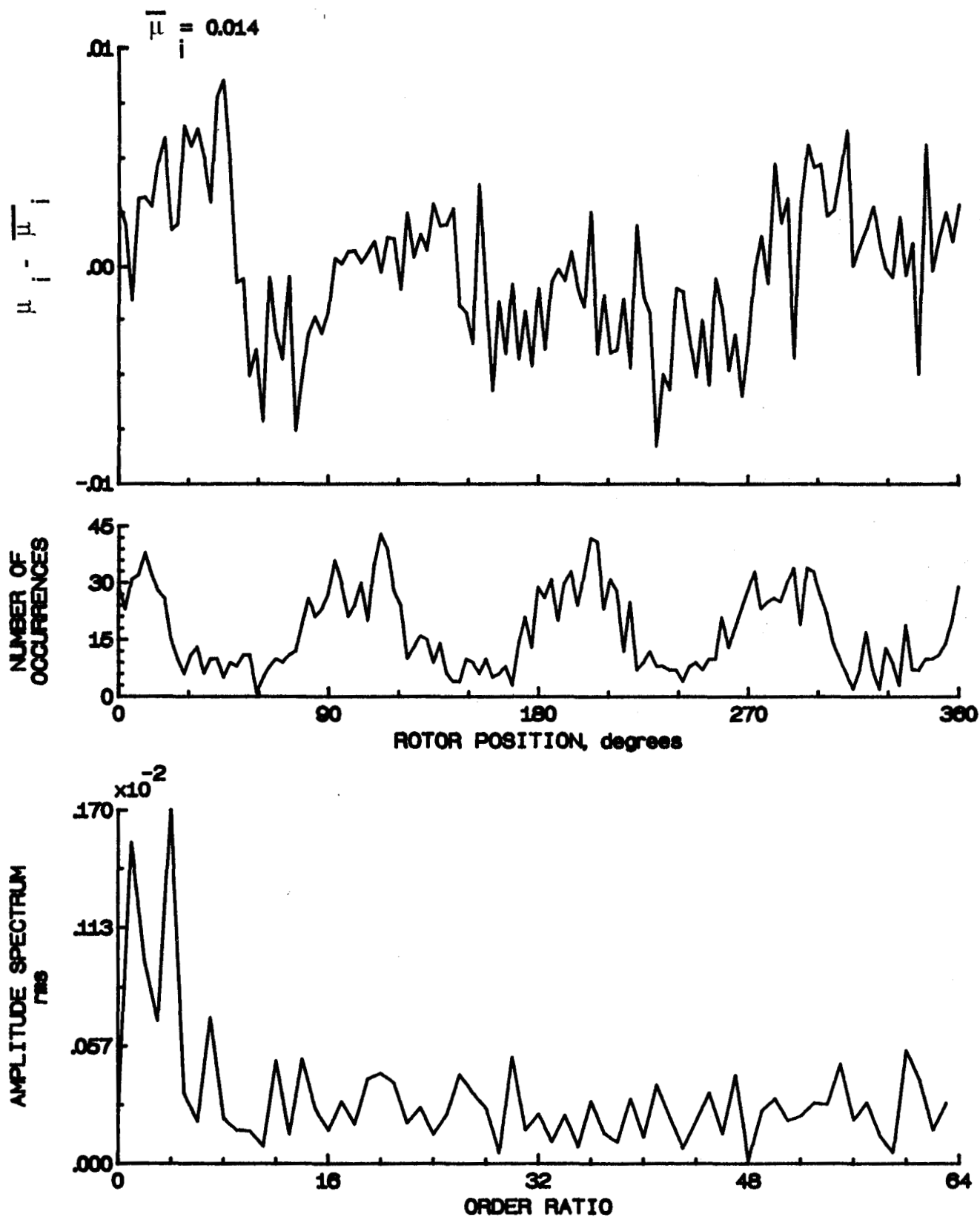


Figure 178.- Induced inflow velocity measured at 330 degrees and r/R of 0.20.

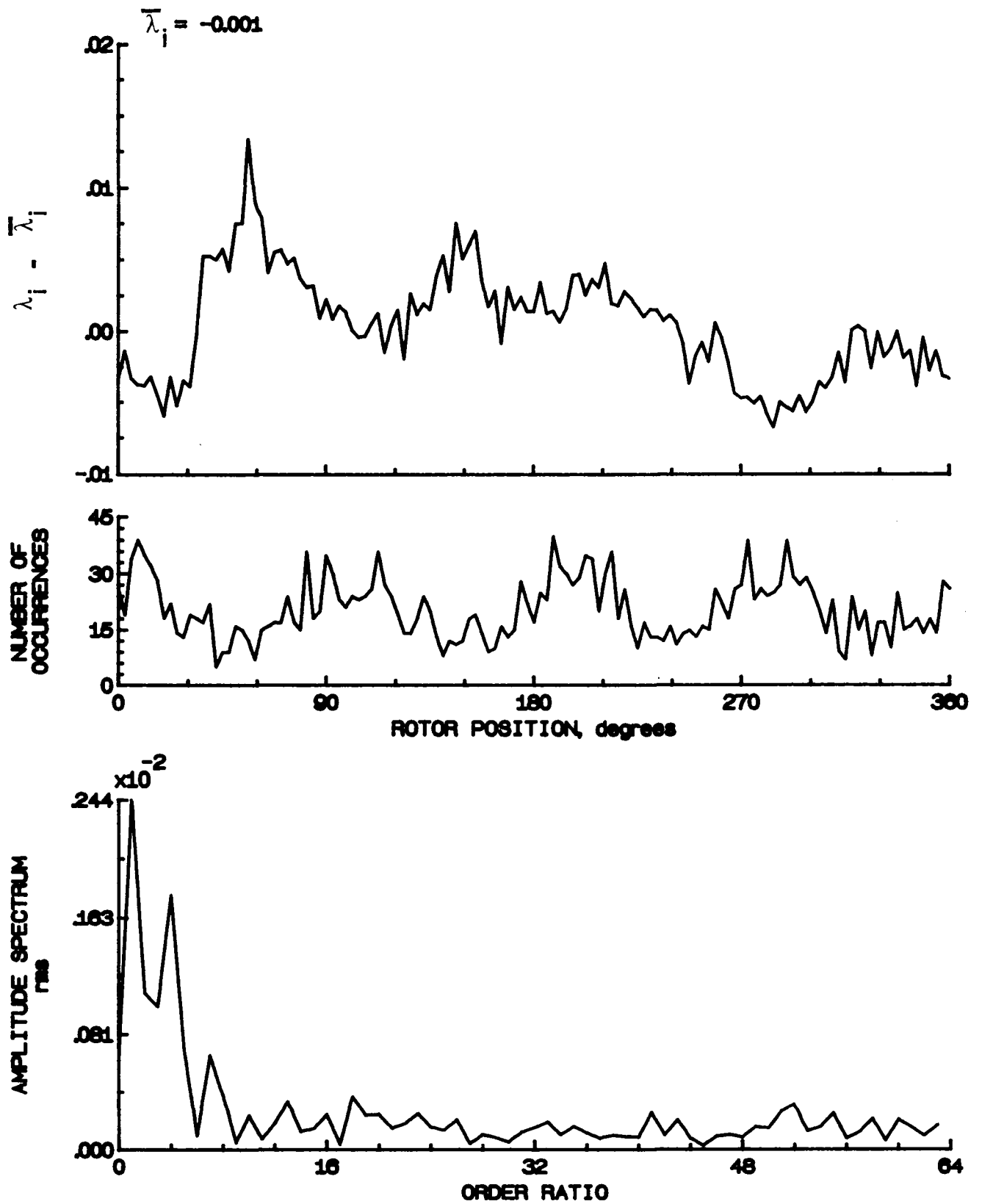


Figure 17A.- Concluded.

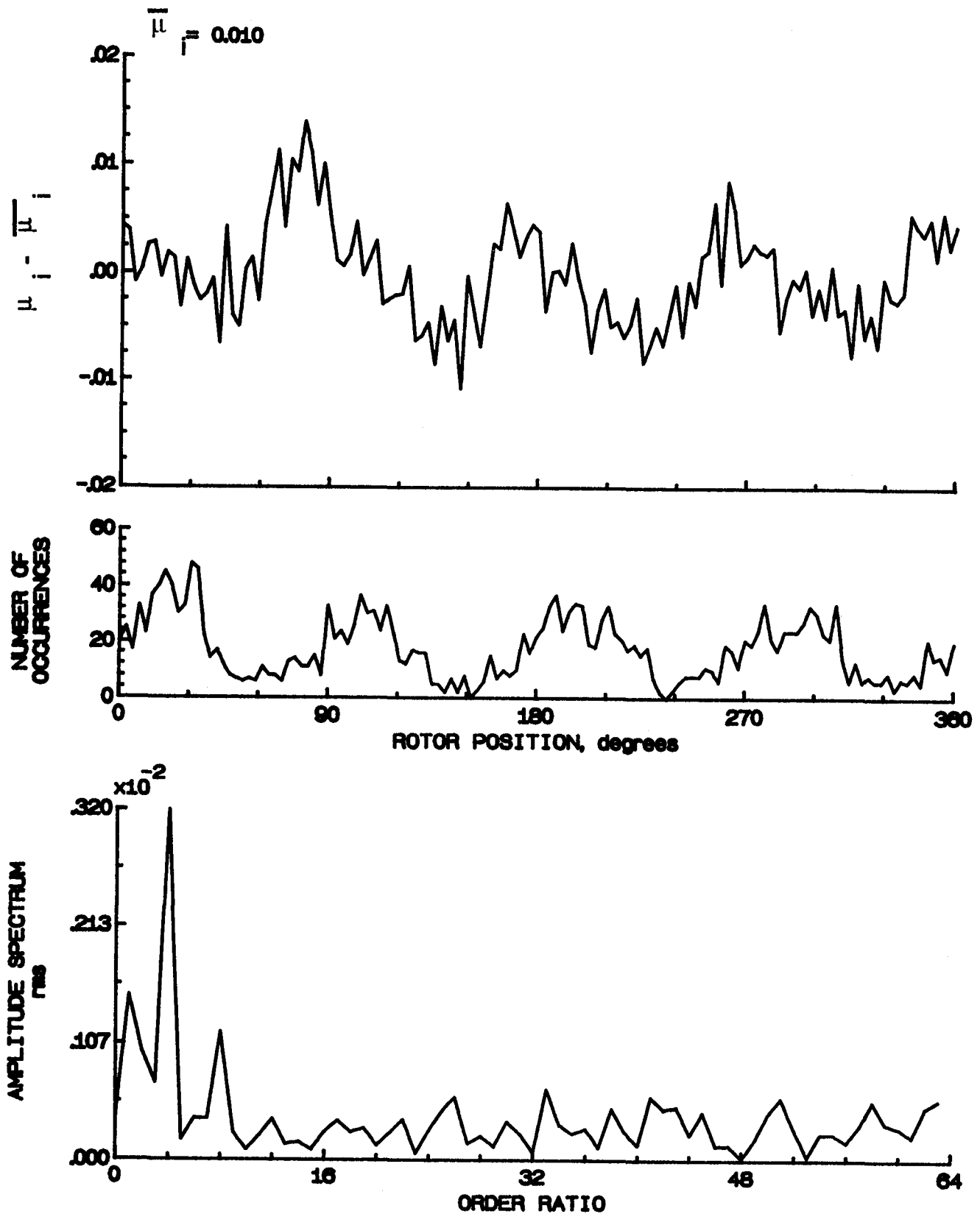


Figure 179.- Induced inflow velocity measured at 330 degrees and r/R of 0.40.

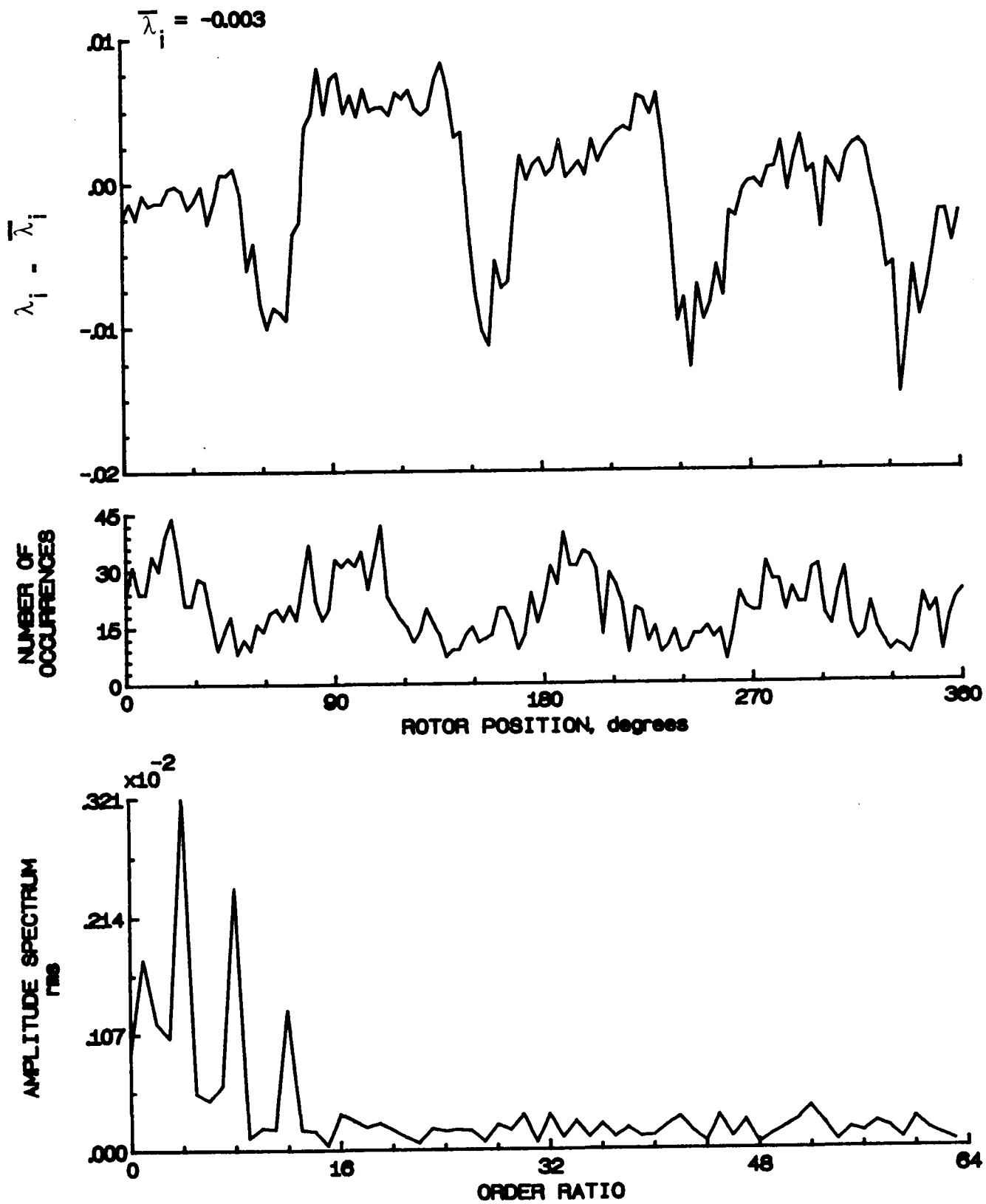


Figure 179.- Concluded.

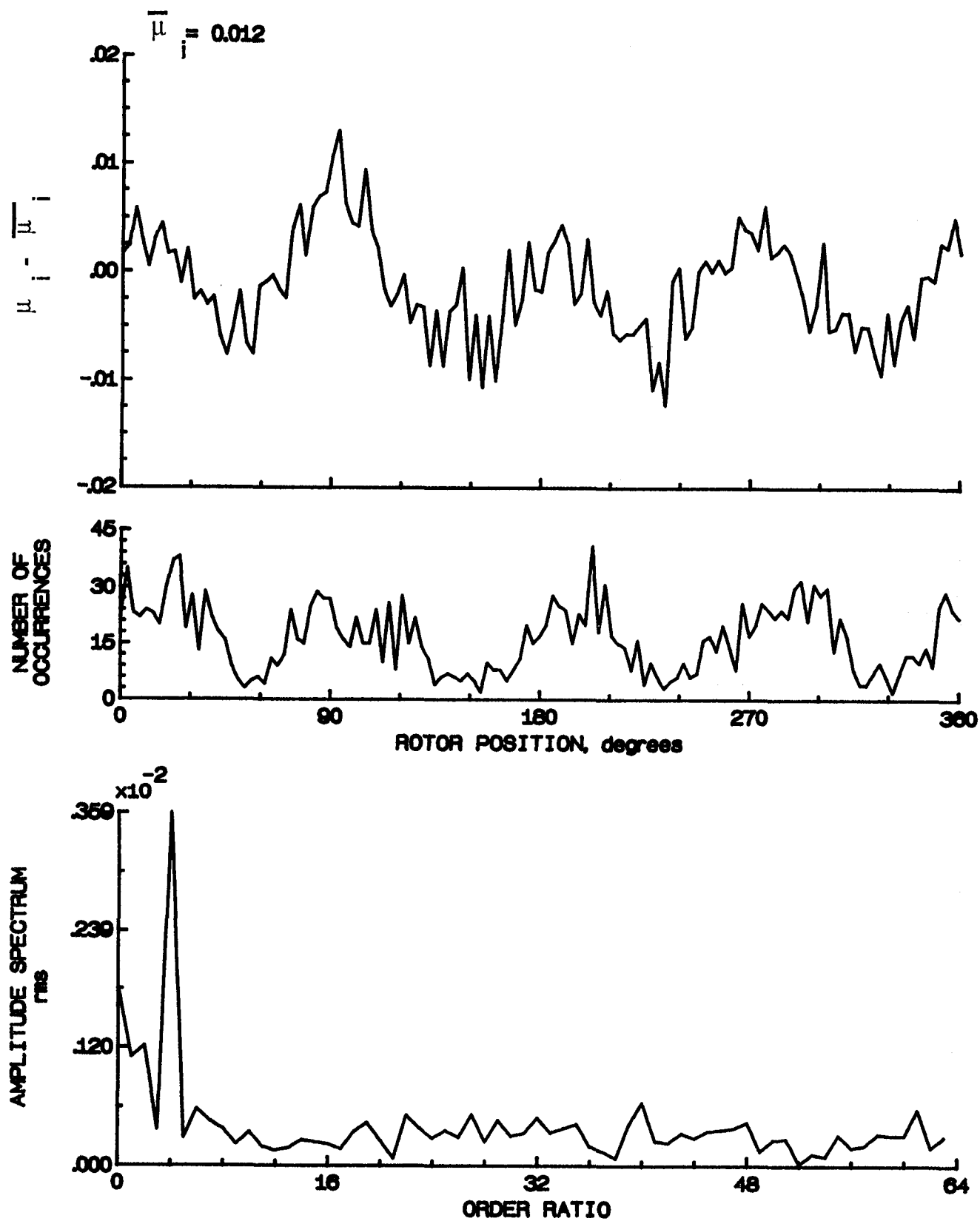


Figure 180.- Induced inflow velocity measured at 330 degrees and  $r/R$  of 0.50.



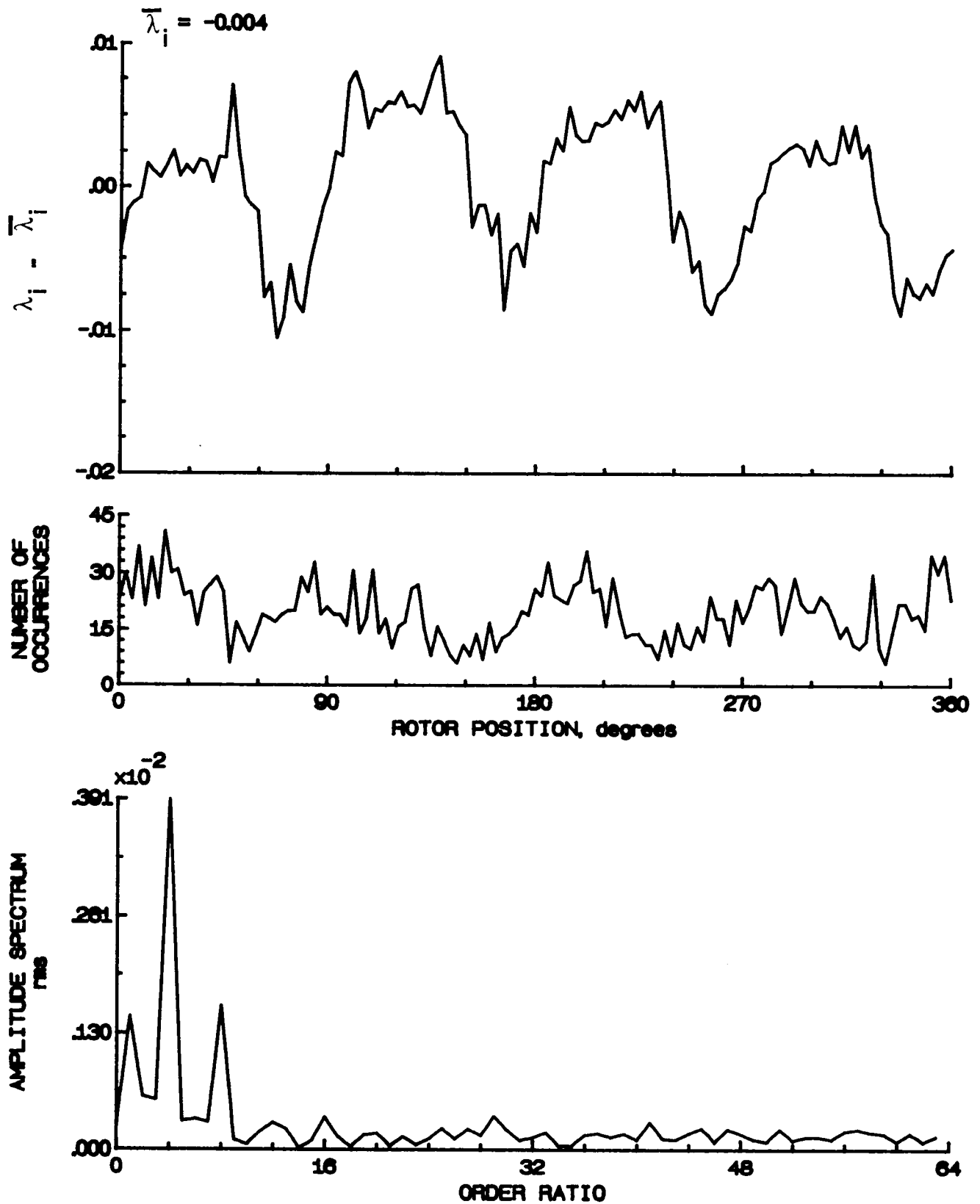


Figure 180.- Concluded.

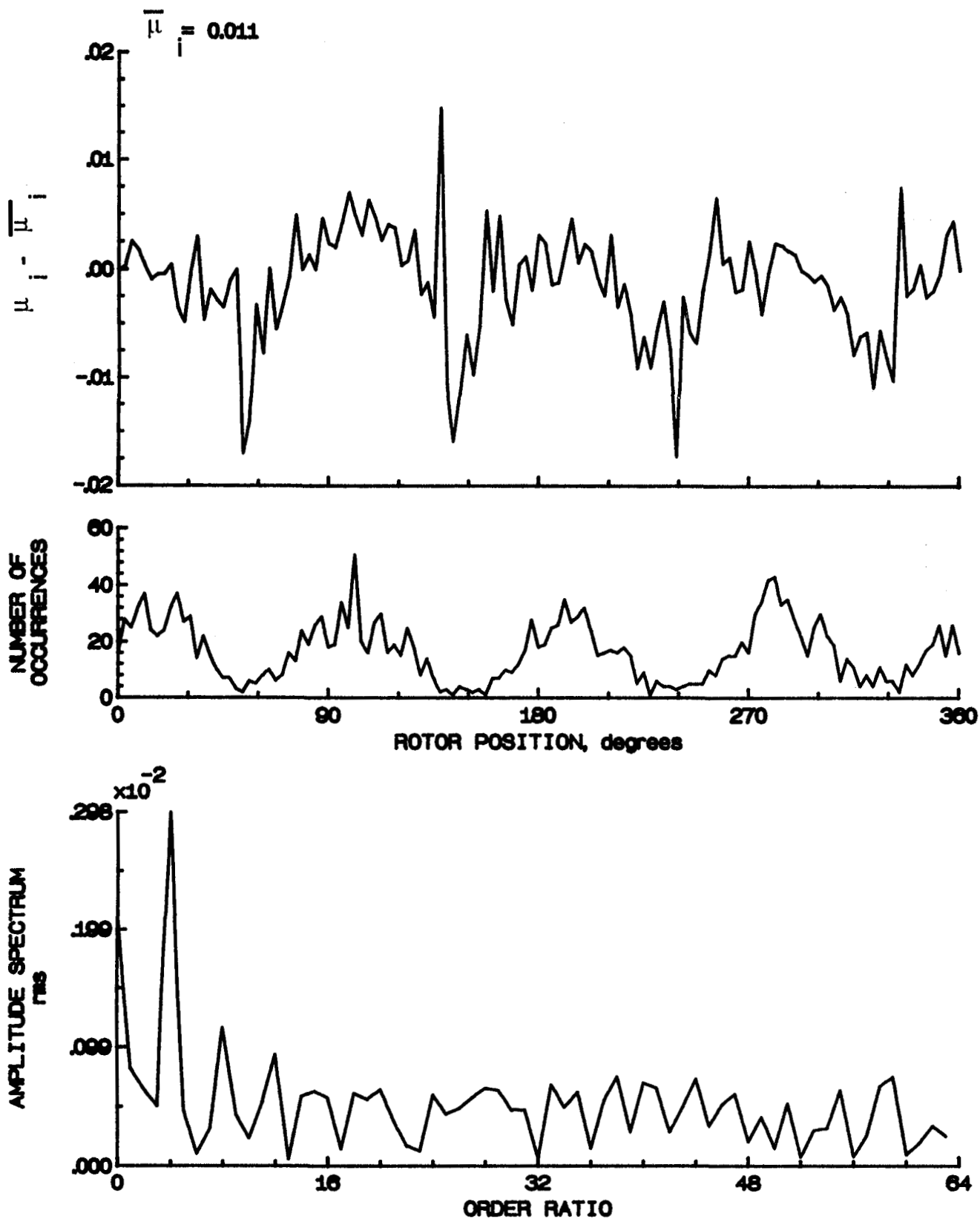


Figure 181.- Induced inflow velocity measured at 330 degrees and  $r/R$  of 0.60.

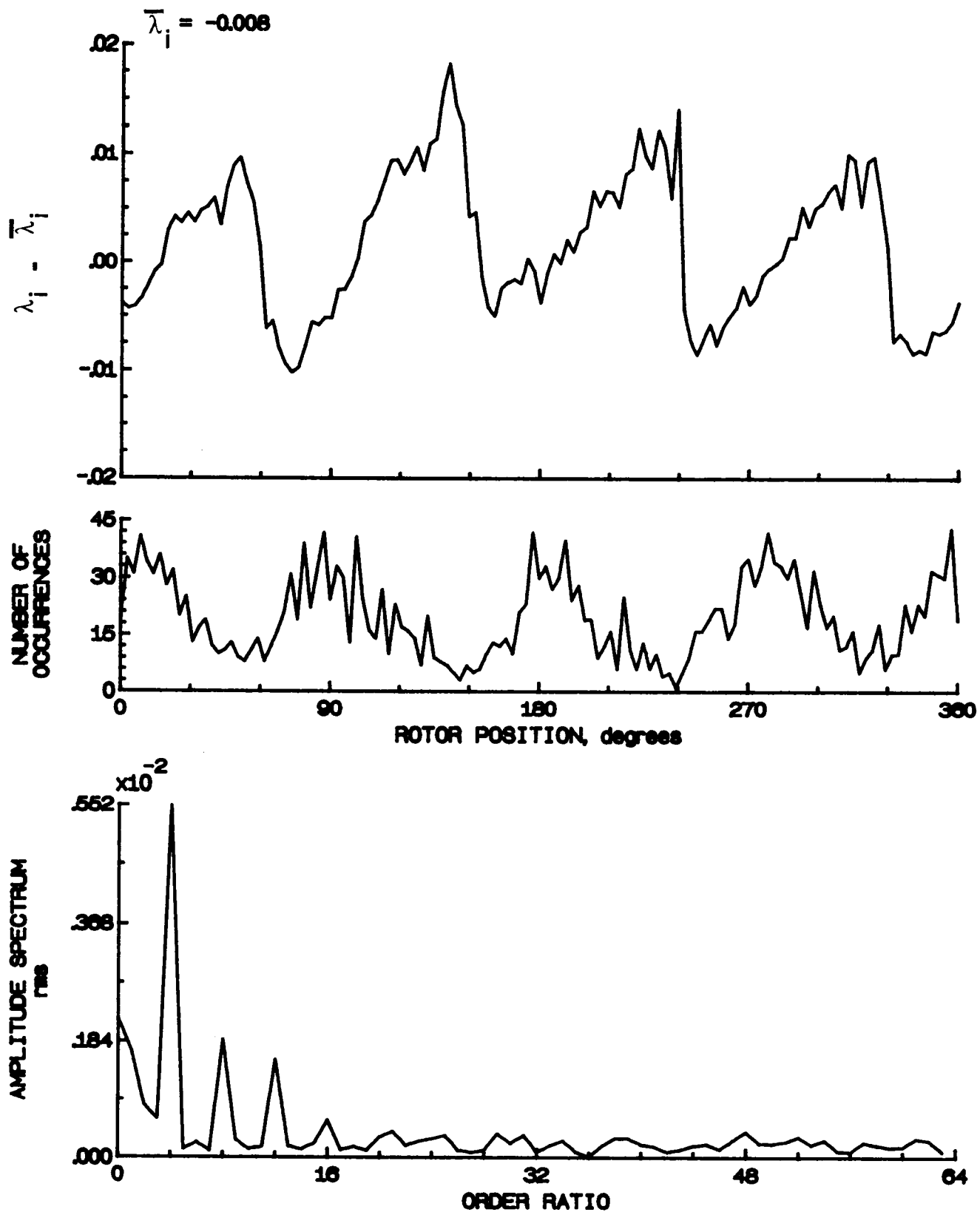


Figure 181- Concluded.

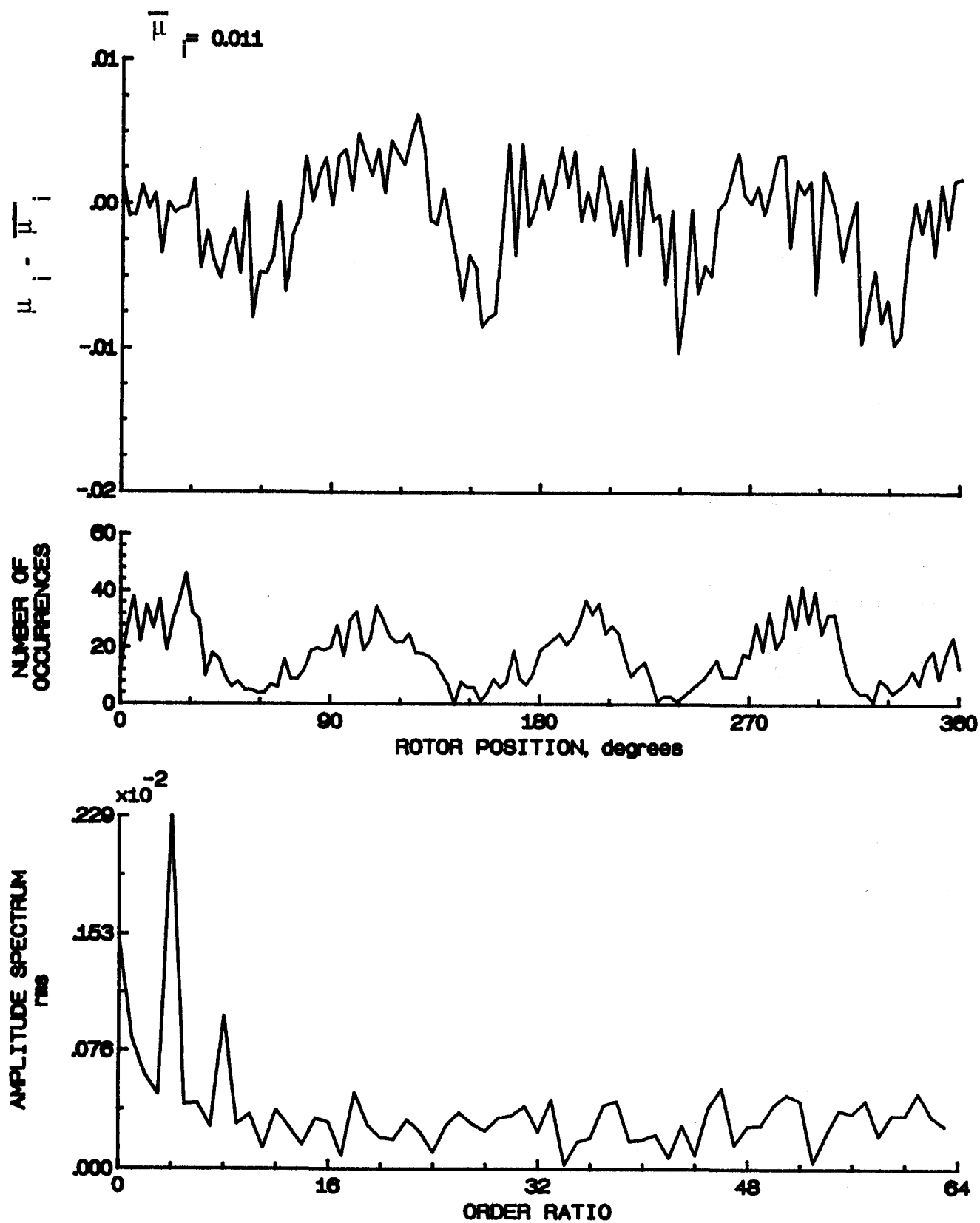


Figure 182.- Induced inflow velocity measured at 330 degrees and  $r/R$  of 0.70.

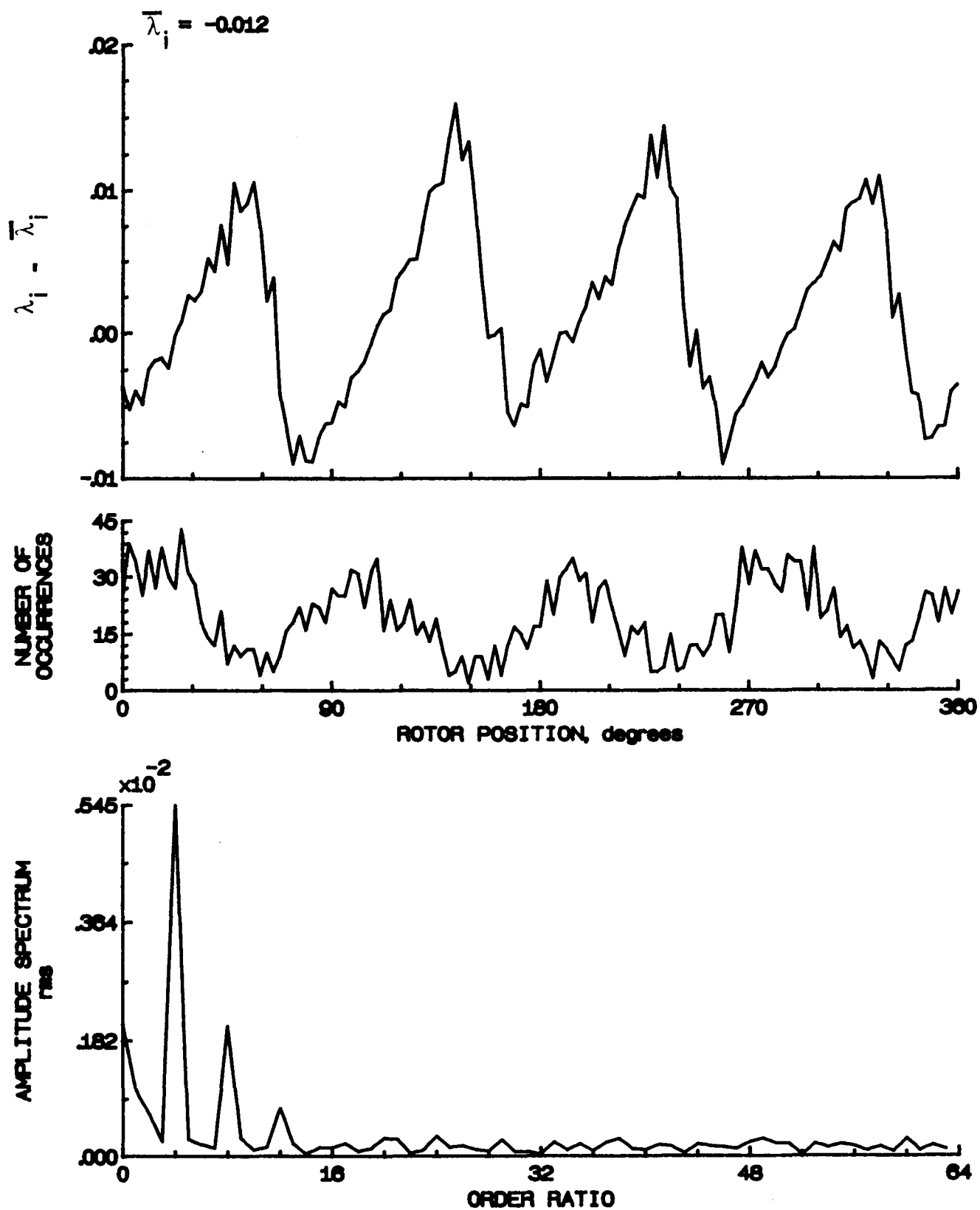


Figure 182.- Concluded.

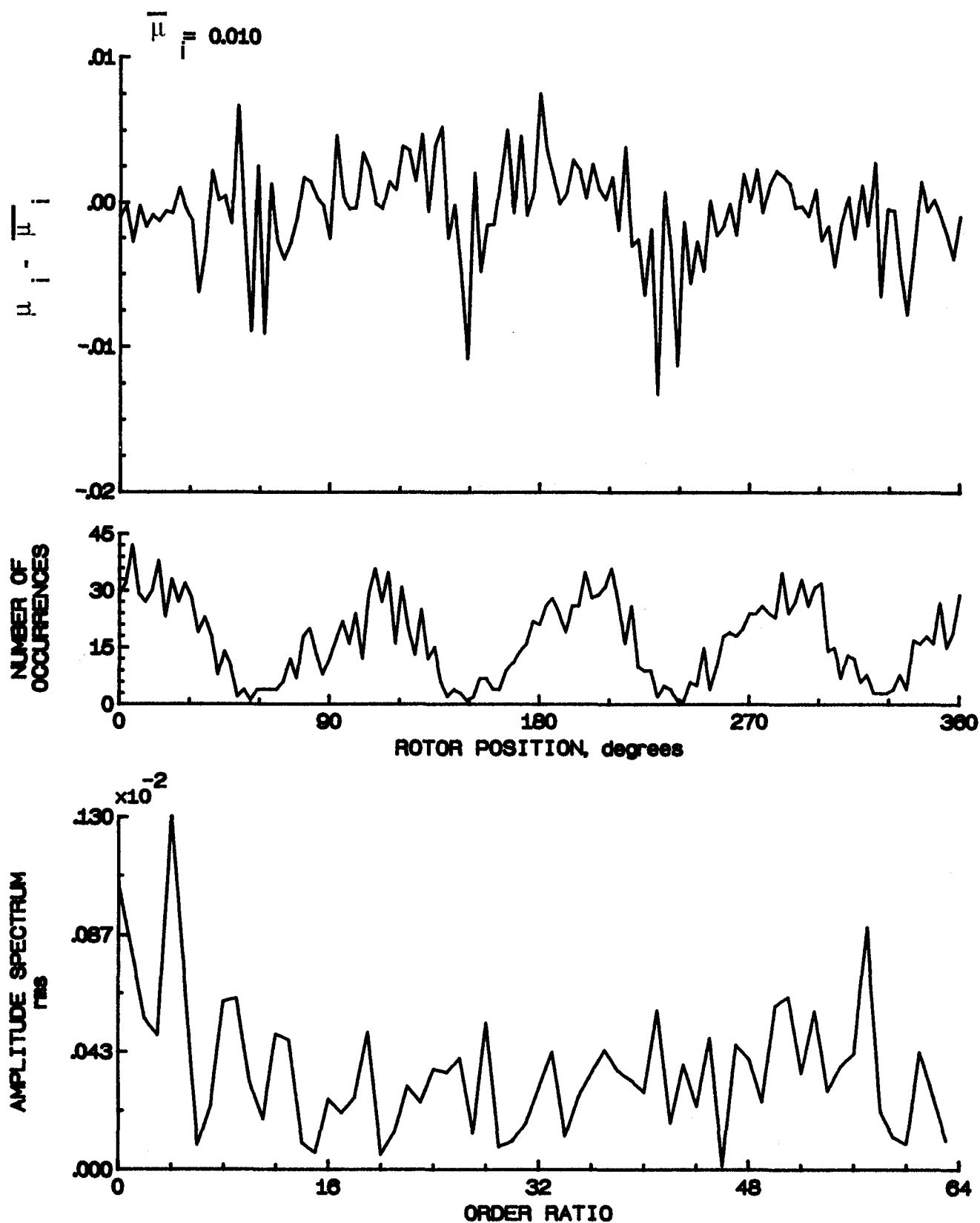


Figure 183.- Induced inflow velocity measured at 330 degrees and  $r/R$  of 0.74.

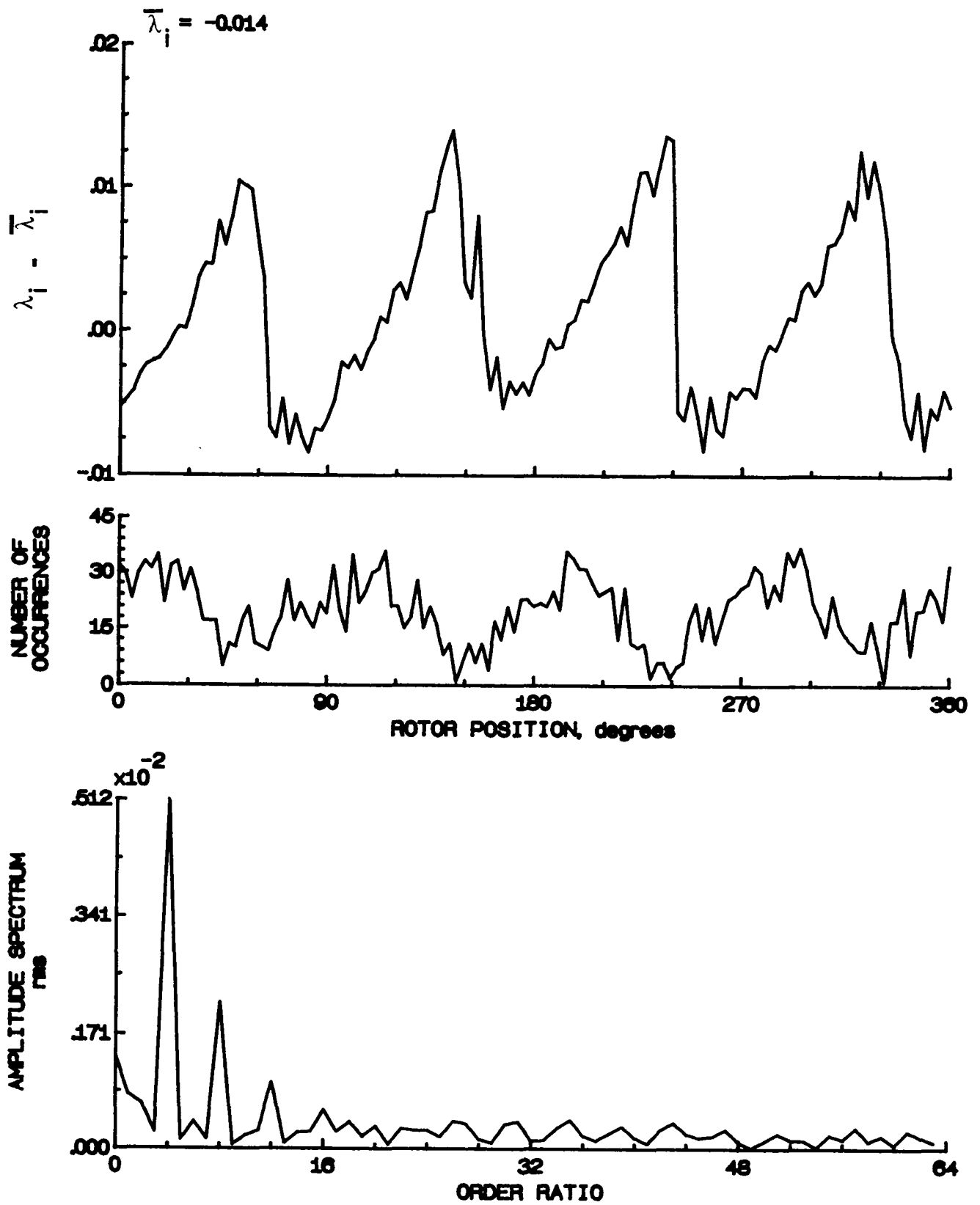


Figure 183.- Concluded.

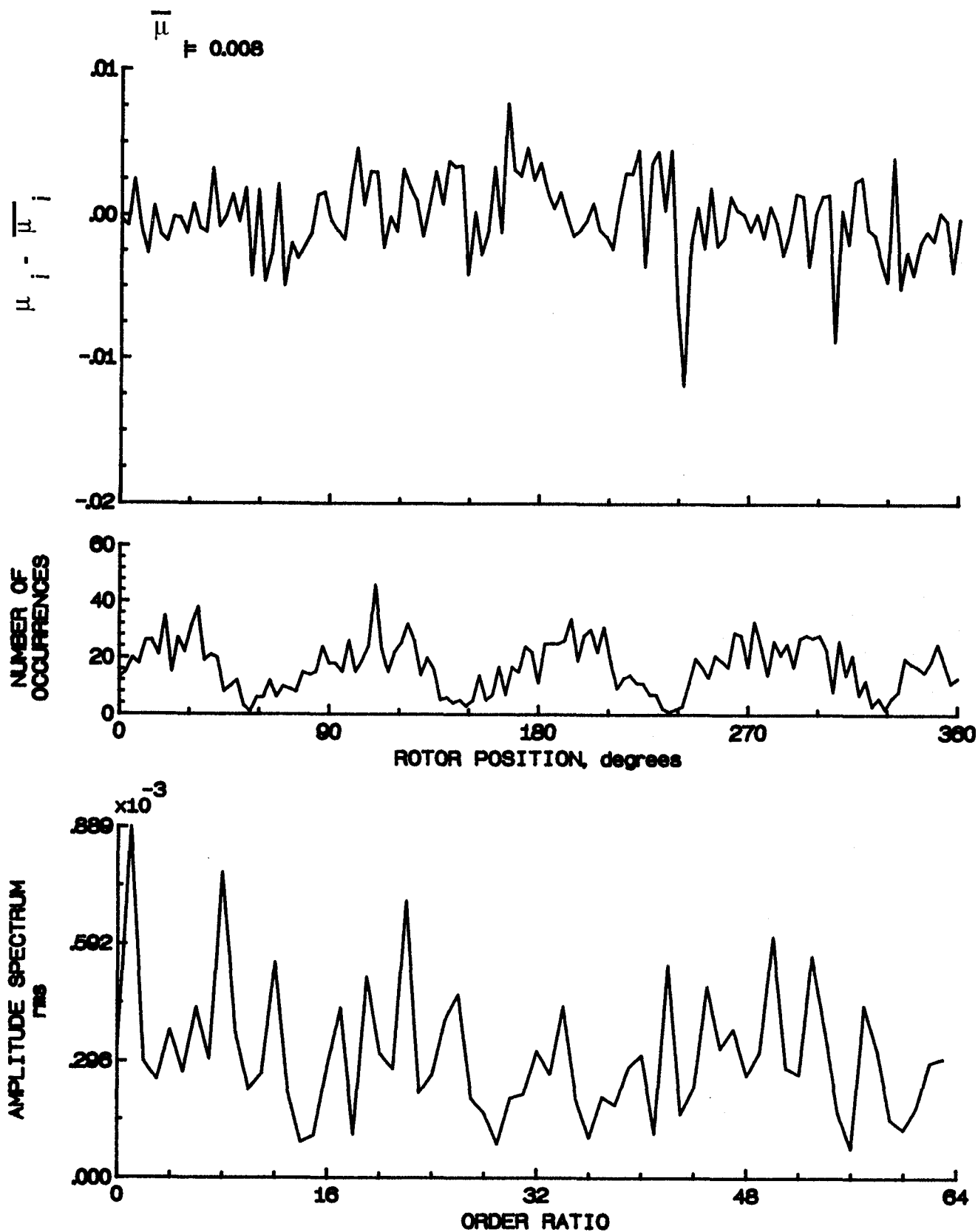


Figure 184.- Induced inflow velocity measured at 330 degrees and r/R of 0.78.



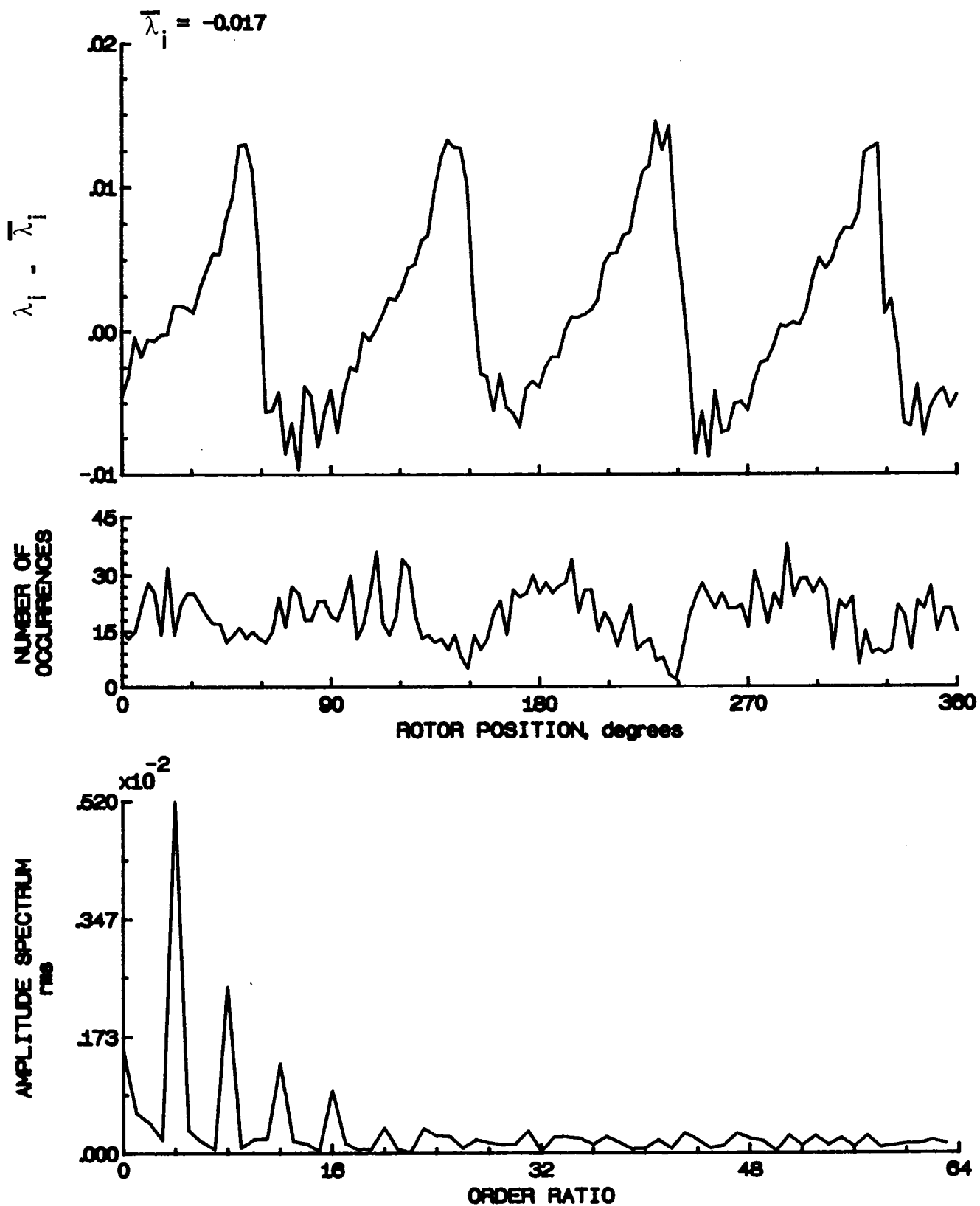


Figure 184.- Concluded.

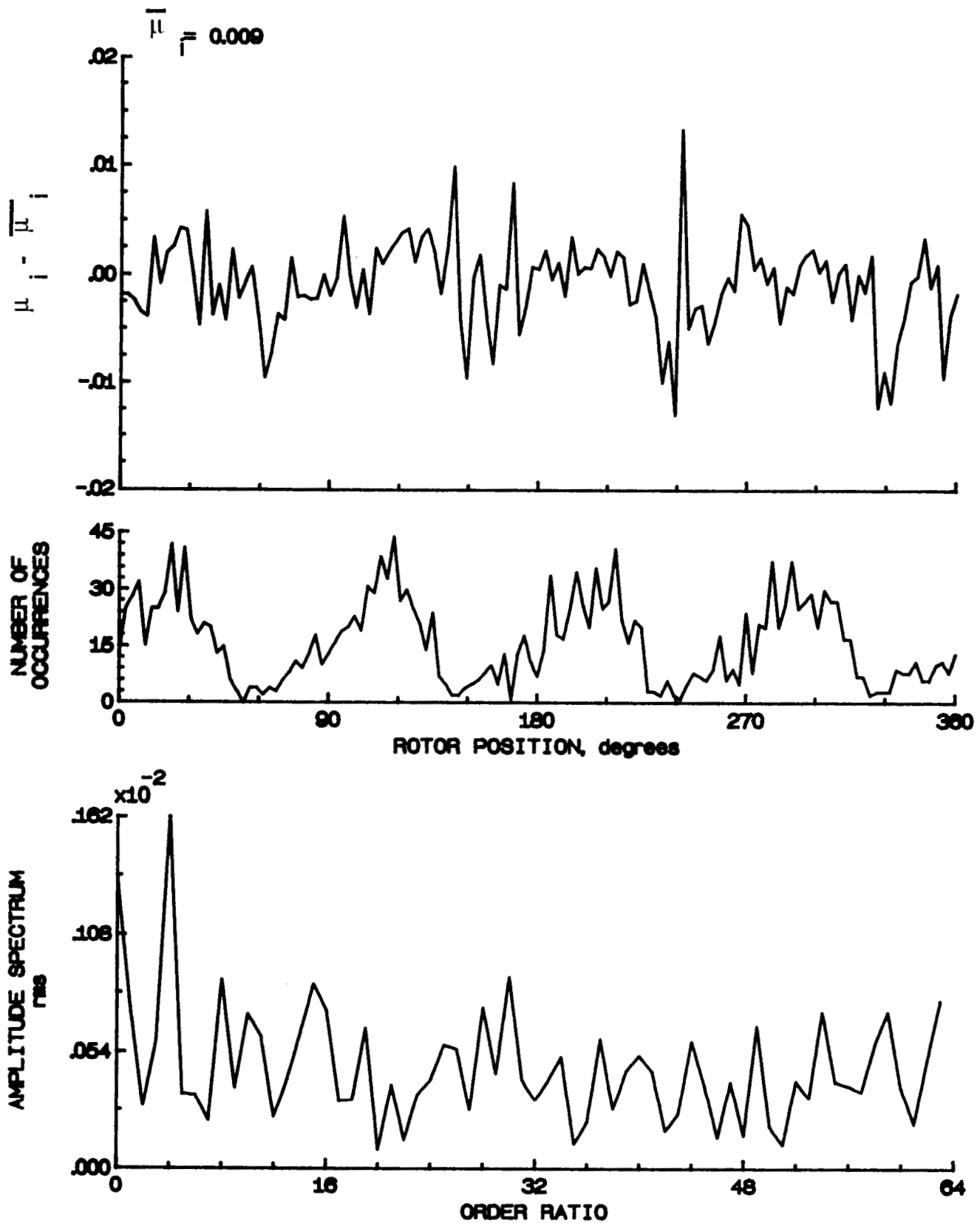


Figure 185.- Induced inflow velocity measured at 330 degrees and  $r/R$  of 0.82.

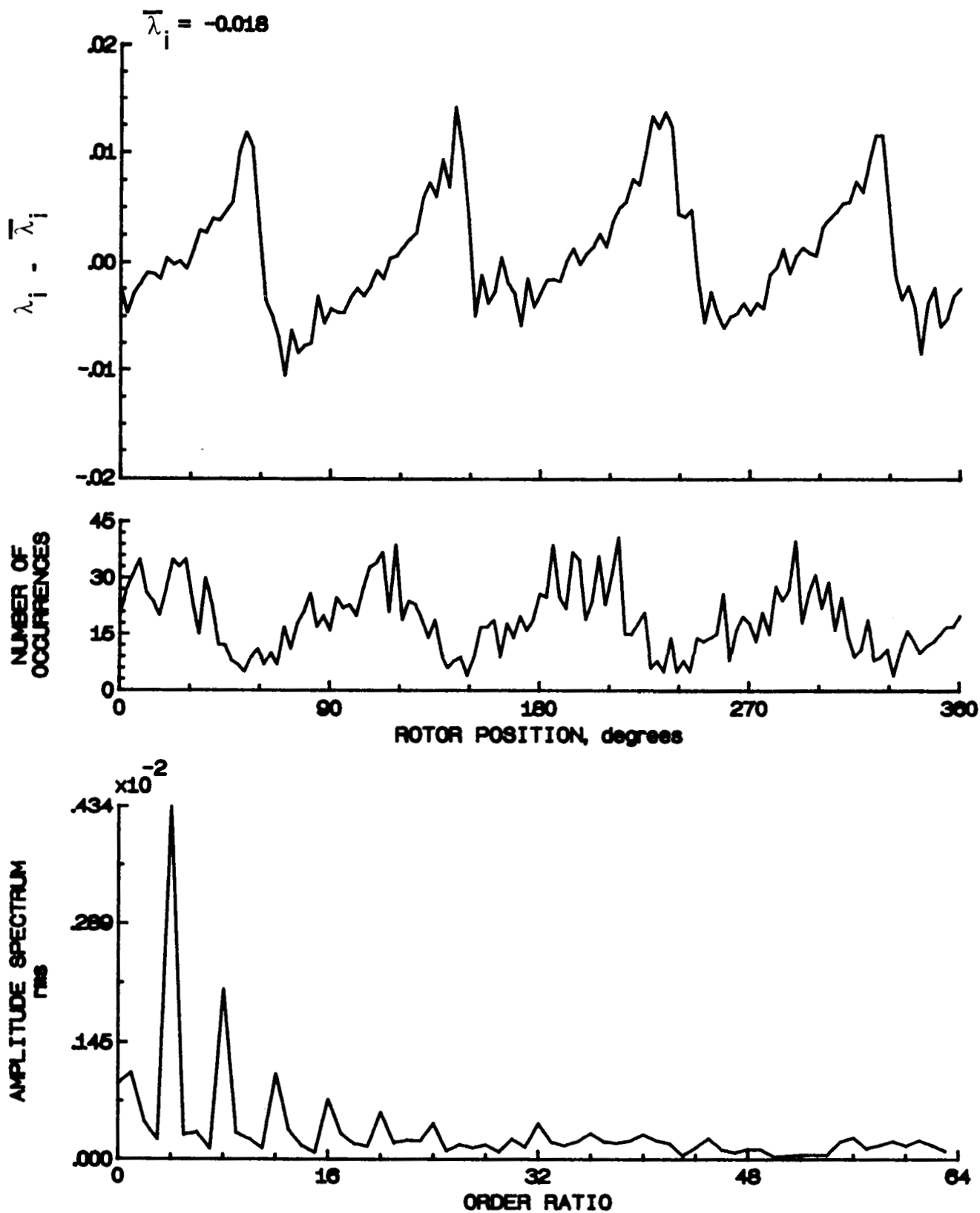


Figure 185.- Concluded.

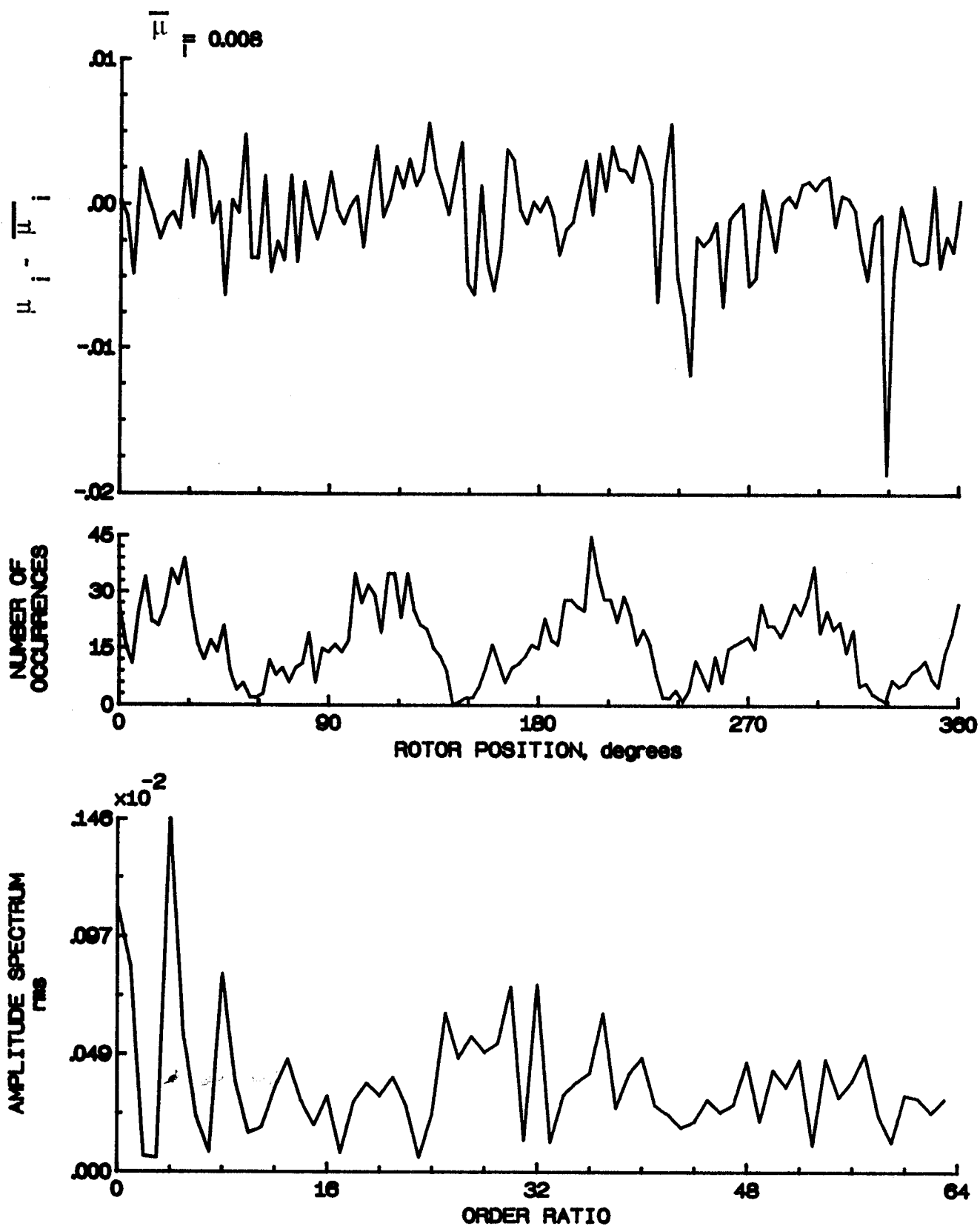


Figure 188.- Induced inflow velocity measured at 330 degrees and  $r/R$  of 0.88.

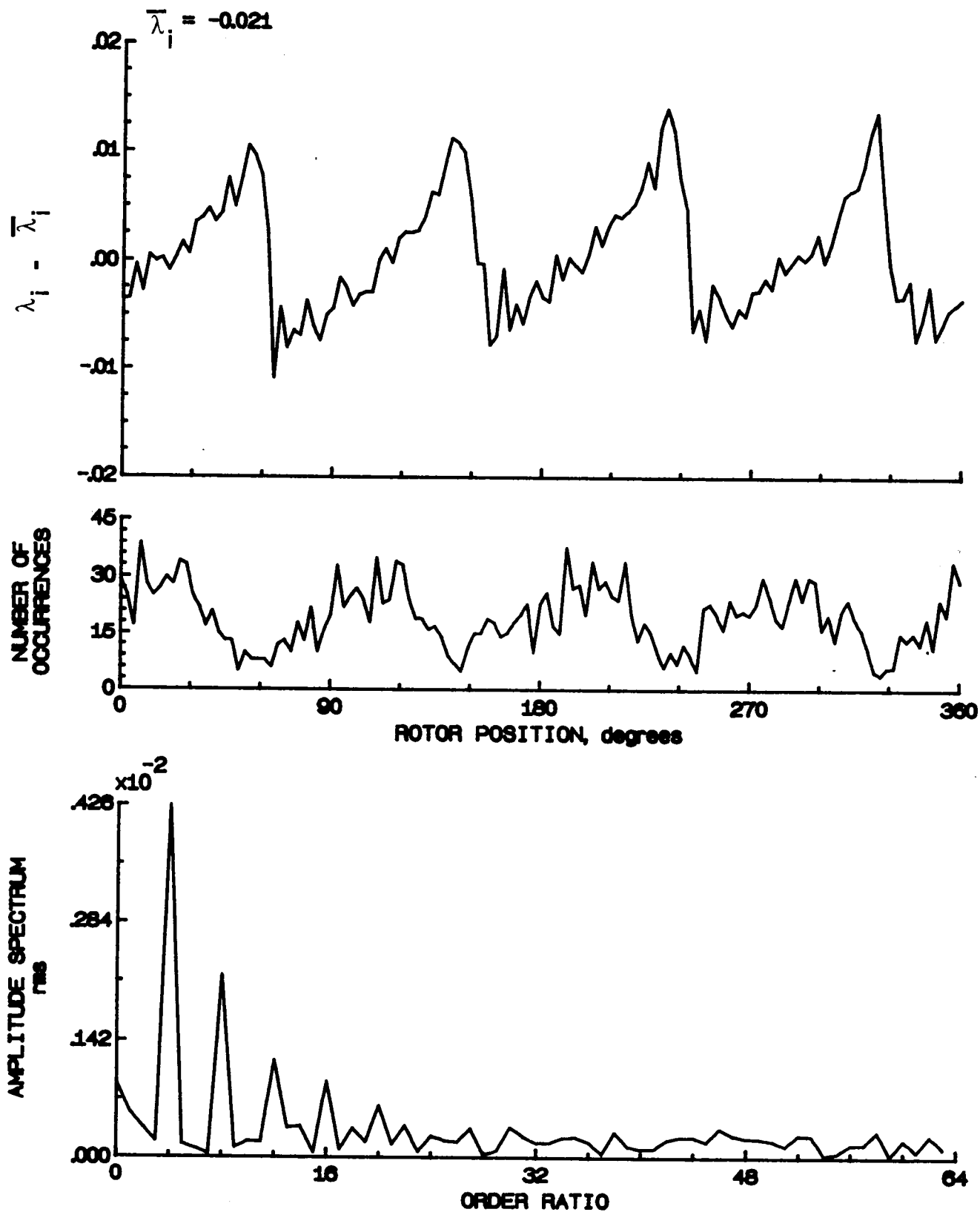


Figure 186.- Concluded.

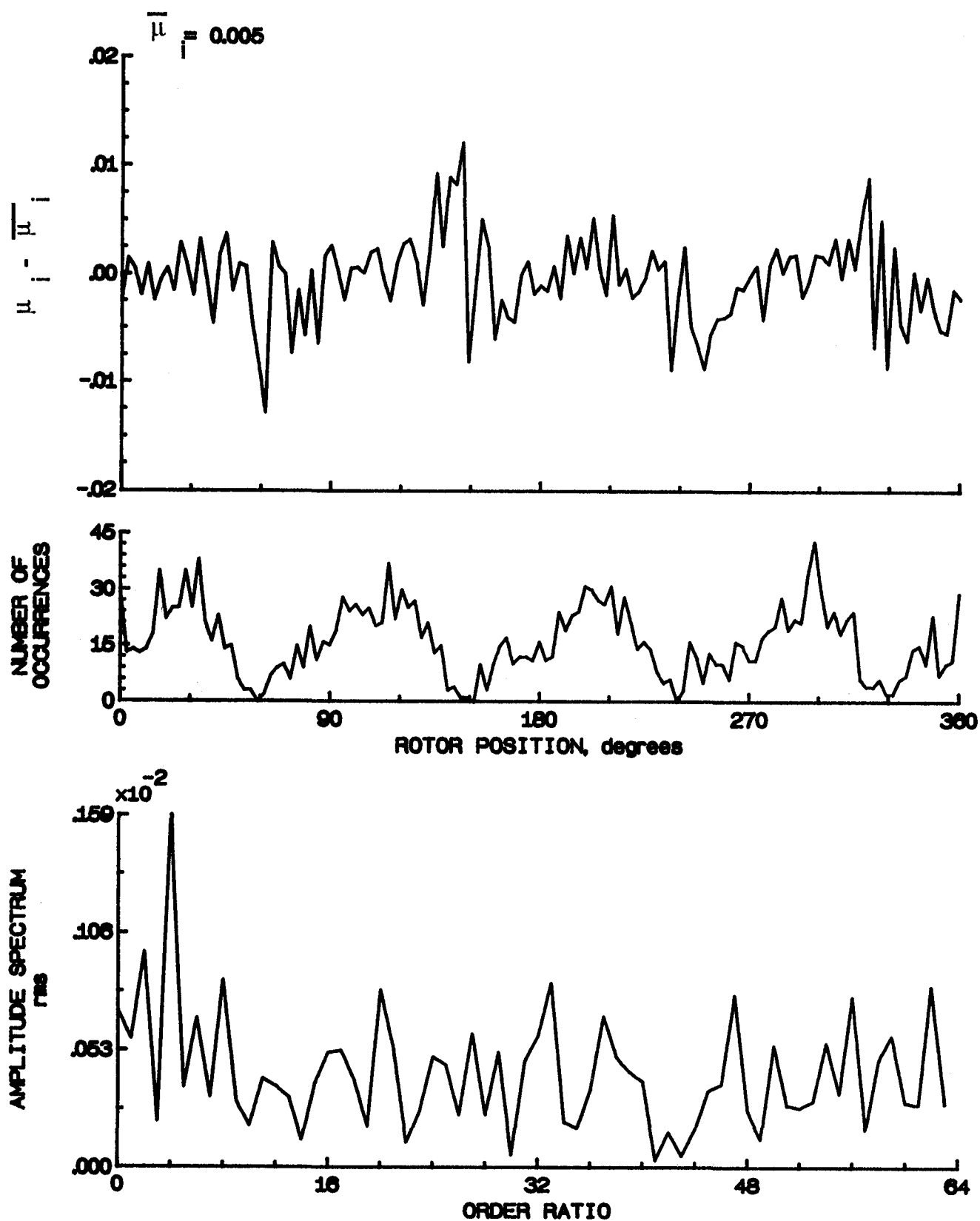


Figure 187.- Induced inflow velocity measured at 330 degrees and  $r/R$  of 0.90.

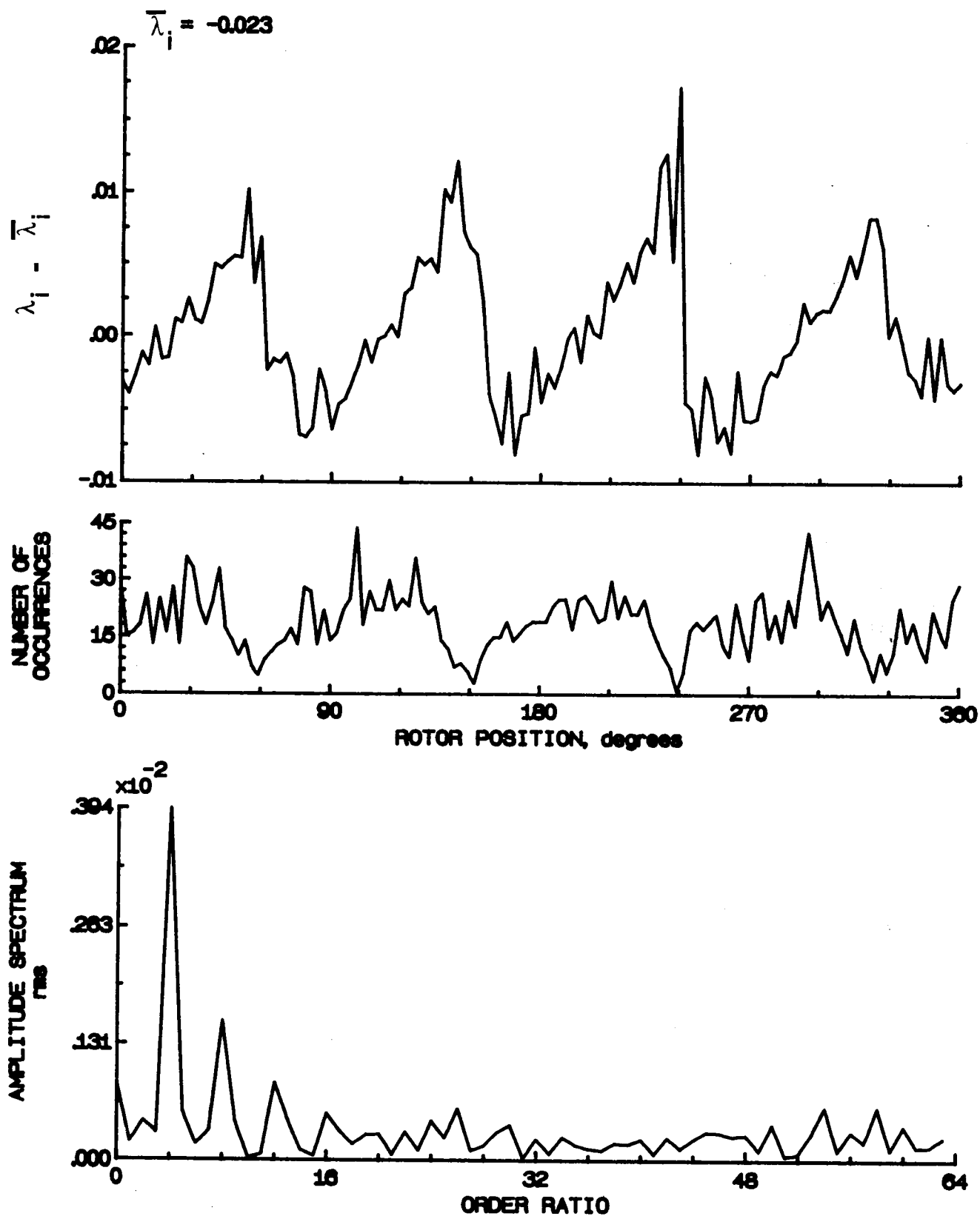


Figure 187.- Concluded.

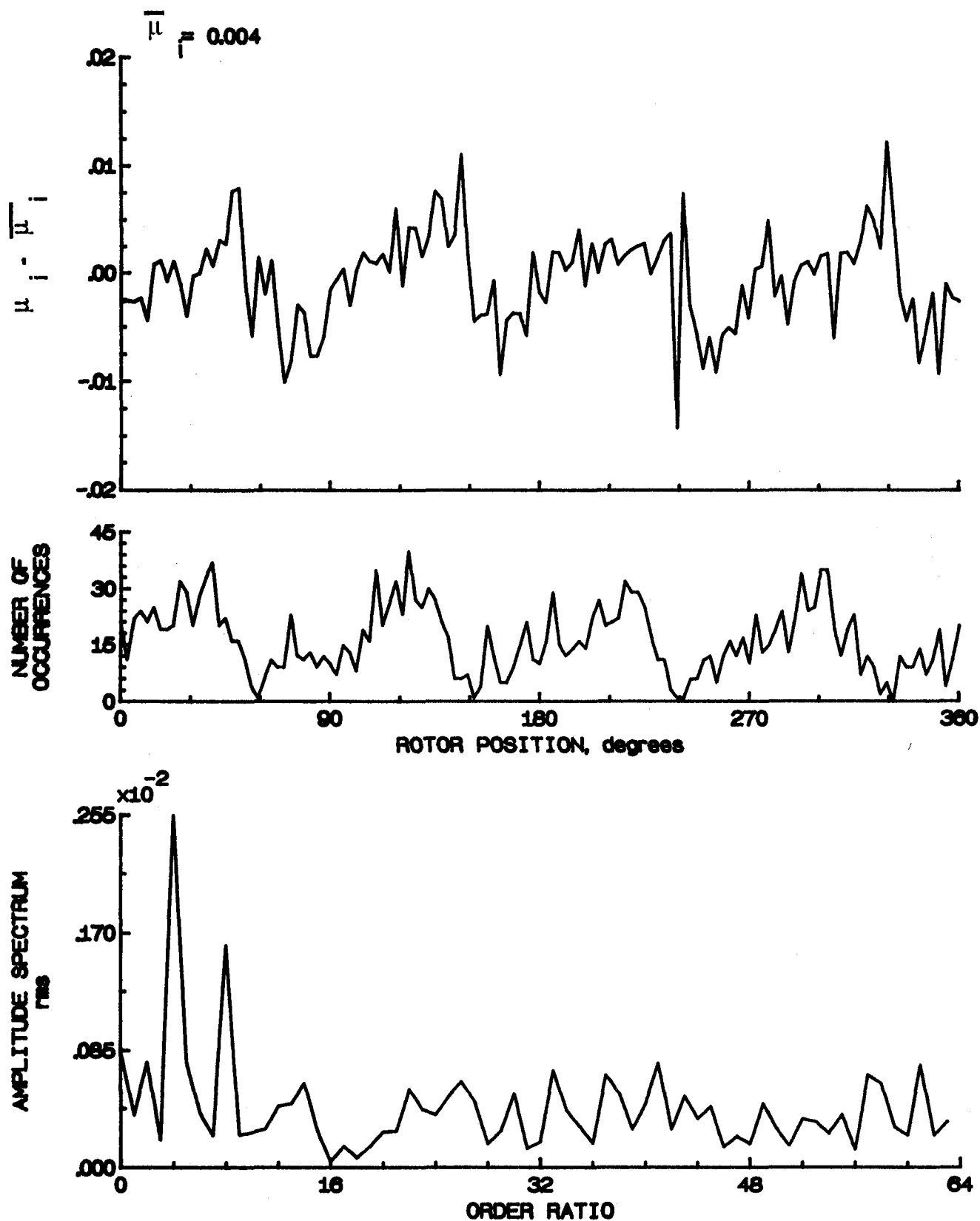


Figure 188.- Induced inflow velocity measured at 330 degrees and  $r/R$  of 0.94.



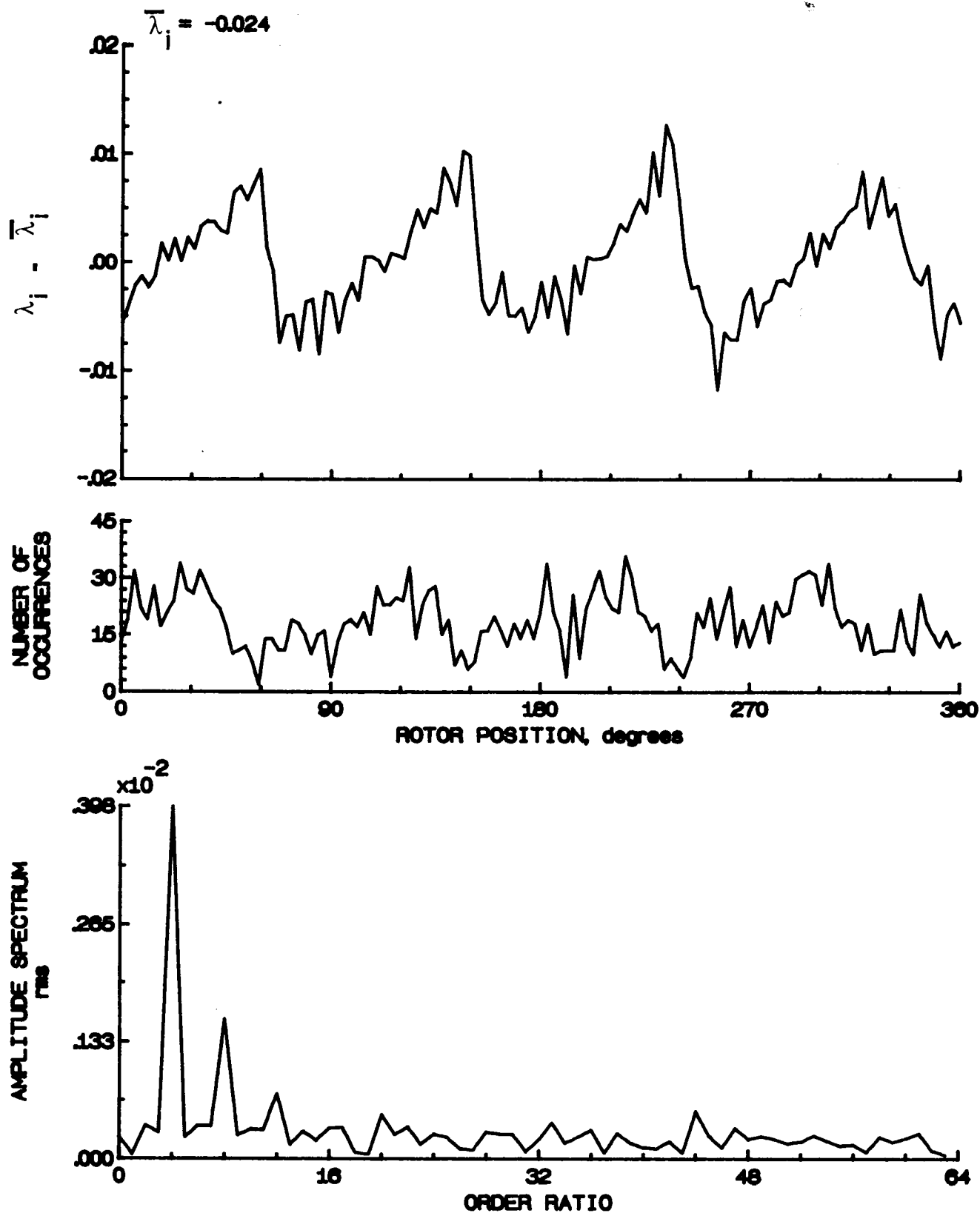


Figure 188.- Concluded.

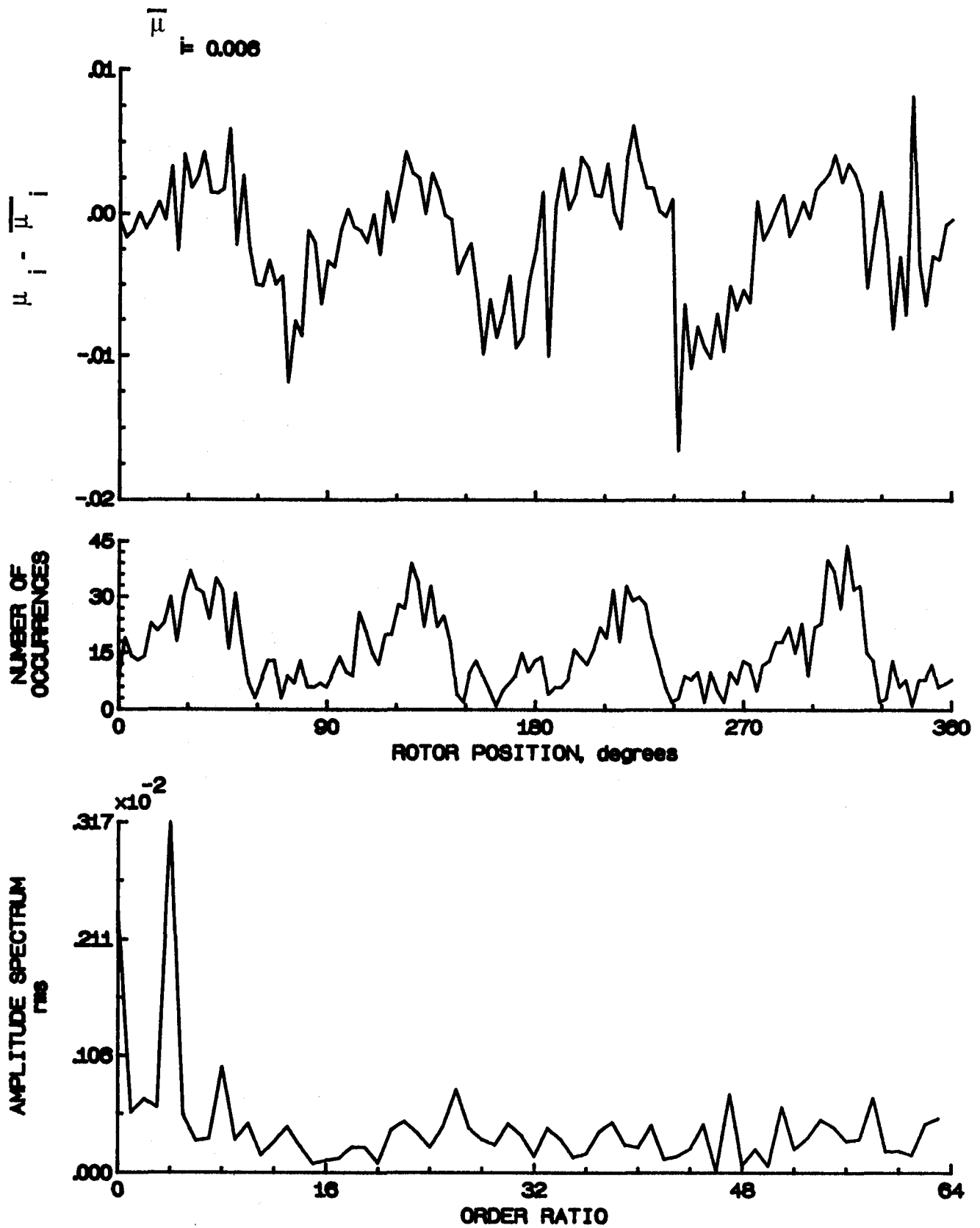


Figure 189.- Induced inflow velocity measured at 330 degrees and  $r/R$  of 0.98.

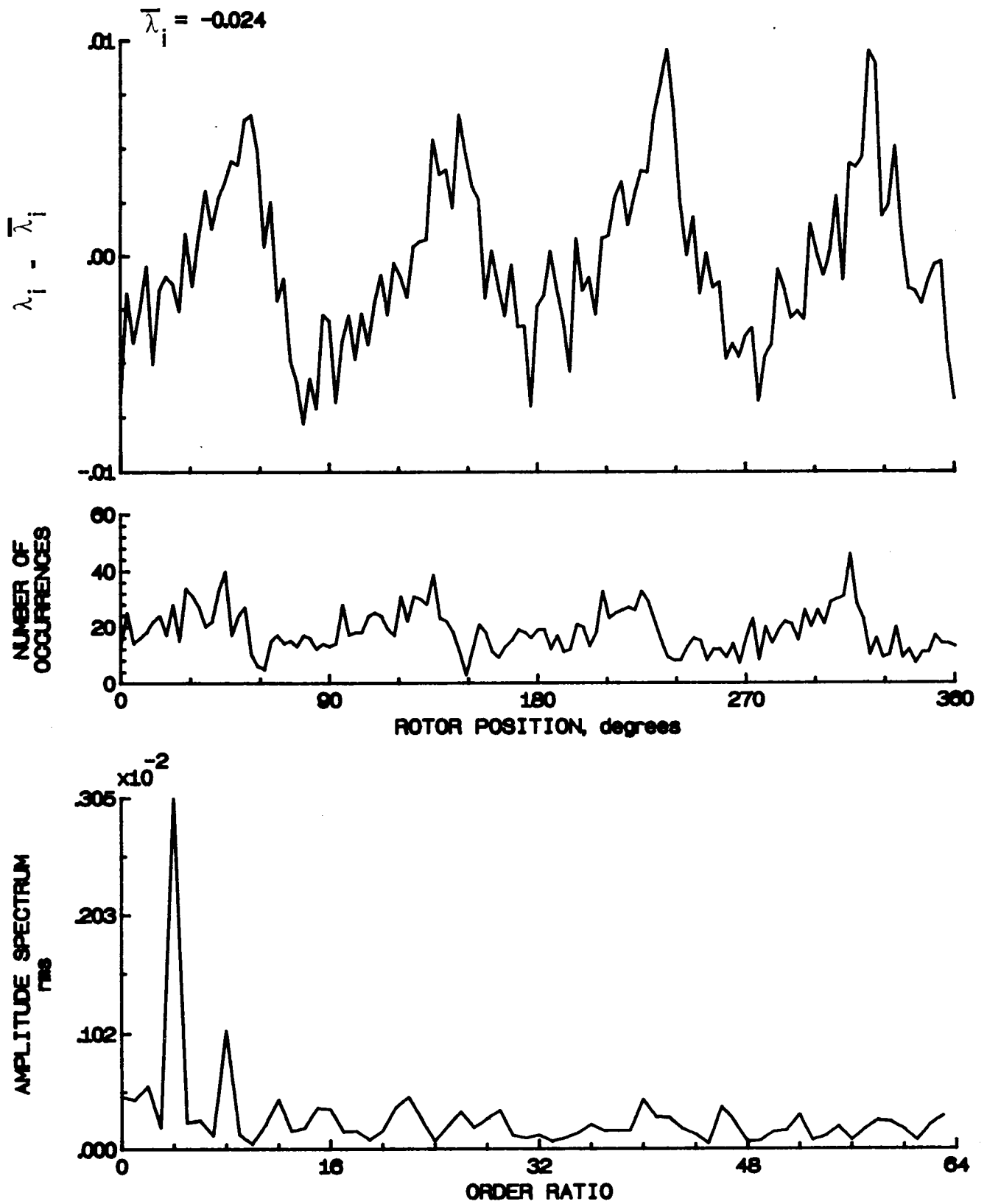


Figure 189.- Concluded.

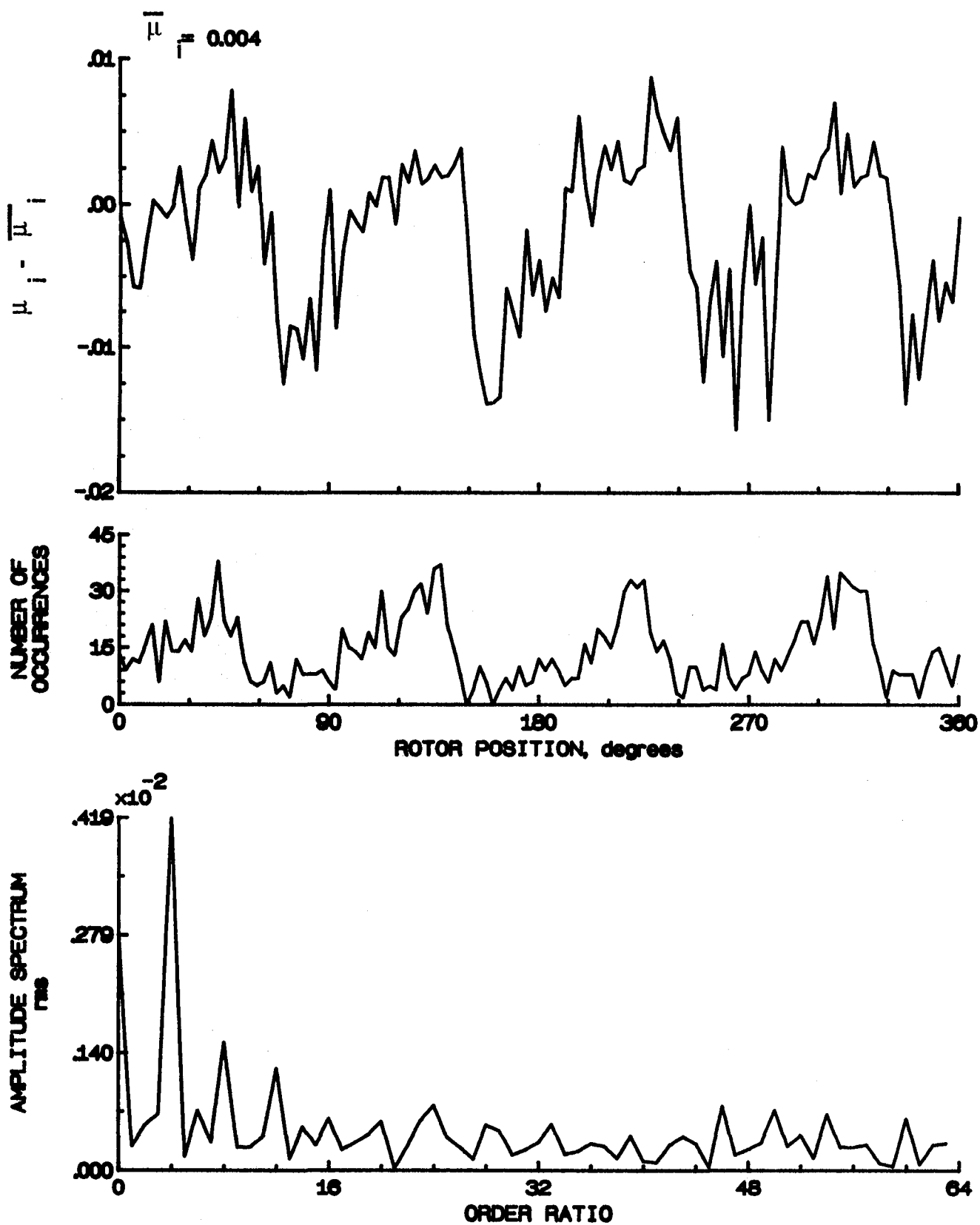


Figure 190.- Induced inflow velocity measured at 330 degrees and  $r/R$  of 1.02.

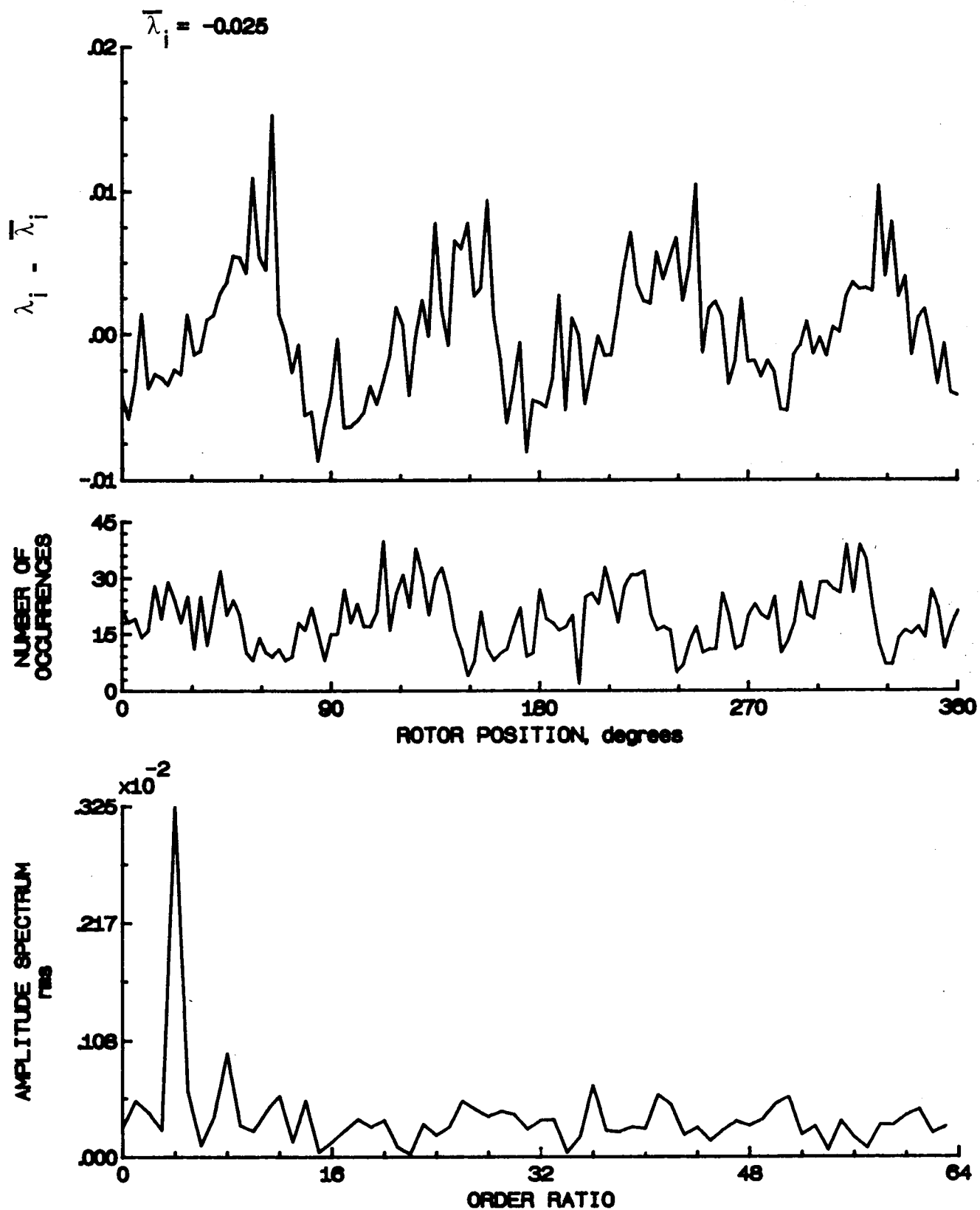


Figure 190.- Concluded.

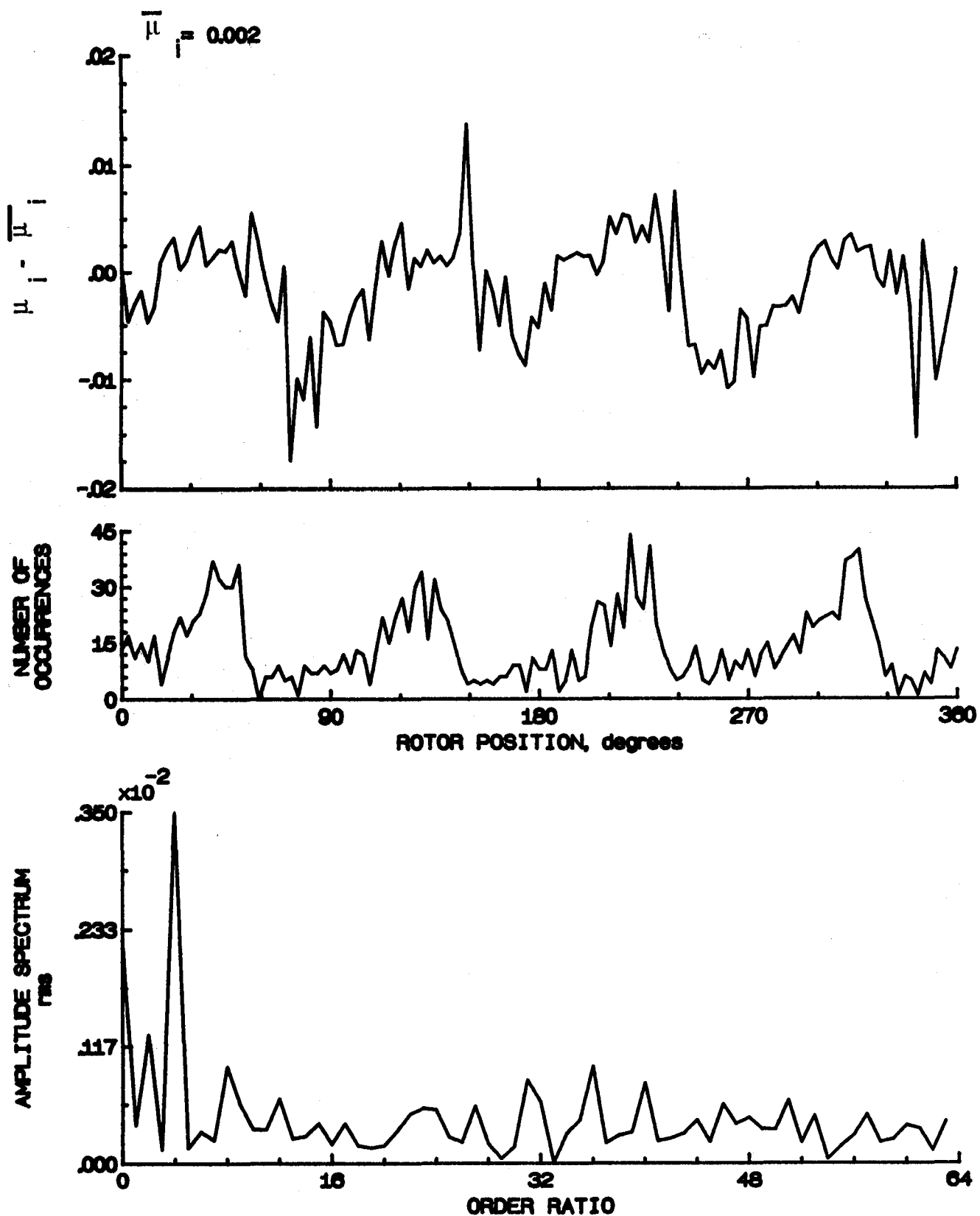


Figure 101.- Induced inflow velocity measured at 330 degrees and r/R of 1.04.

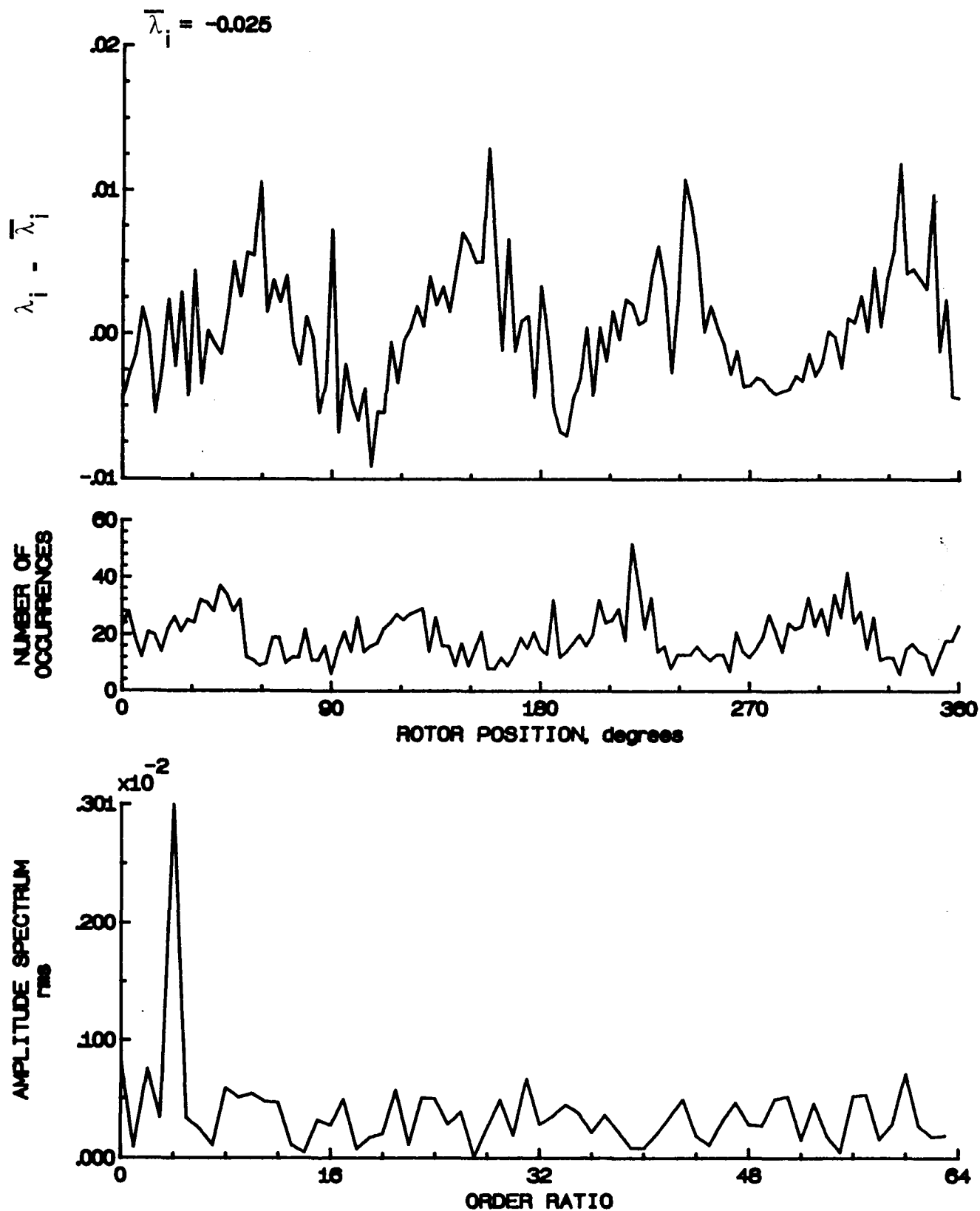


Figure 191.- Concluded.

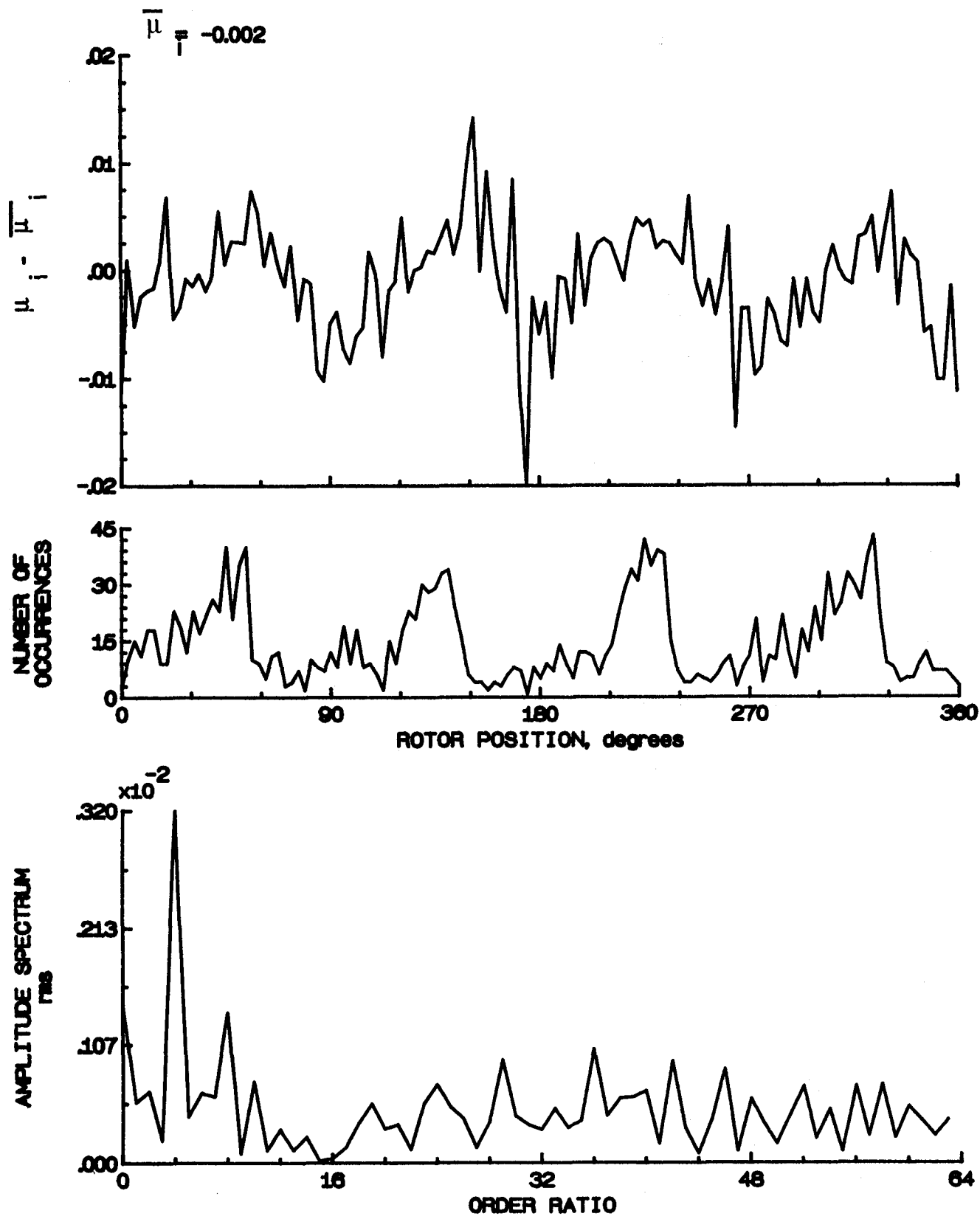


Figure 192- Induced inflow velocity measured at 330 degrees and r/R of 1.10.



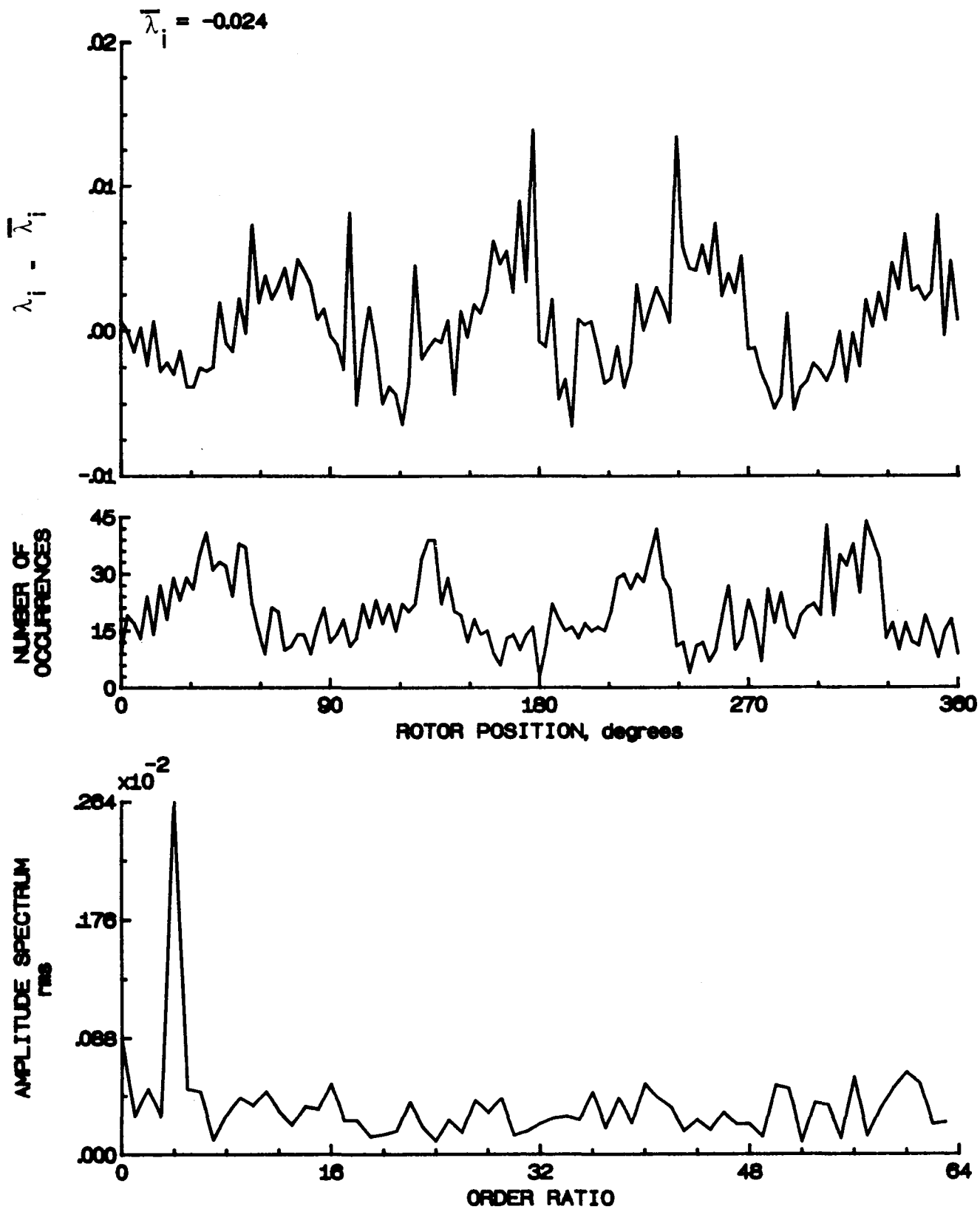


Figure 192.- Concluded.

# Report Documentation Page

1. Report No. NASA TM-102643 AVSCOM TM-90-B-008		2. Government Accession No.		3. Recipient's Catalog No.	
4. Title and Subtitle Inflow Measurements Made With a Laser Velocimeter on a Helicopter Model in Forward Flight--Volume IX: Rectangular Planform Blades at an Advance Ratio of 0.23, 0.75 Chord Above the Tip Path Plane				5. Report Date May 1990	
				6. Performing Organization Code	
7. Author(s) Susan L. Althoff Joe W. Elliott Danny R. Hoad Richard H. Sailey				8. Performing Organization Report No.	
				10. Work Unit No. 505-61-51-10	
9. Performing Organization Name and Address Aerostructures Directorate USAARTA-AVSCOM NASA Langley Research Center Hampton, VA 23665-5225				11. Contract or Grant No.	
				13. Type of Report and Period Covered Technical Memorandum	
12. Sponsoring Agency Name and Address National Aeronautics and Space Administration, Washington, DC 20546-0001 and U.S. Army Aviation Systems Command, St. Louis, MO 63120-1798				14. Sponsoring Agency Code	
15. Supplementary Notes Susan L. Althoff, Joe W. Elliott, and Danny R. Hoad: Aerostructures Directorate, USAARTA-AVSCOM, Hampton, Virginia. Richard H. Sailey: Lockheed Engineering & Sciences Company, Hampton, Virginia.					
16. Abstract An experimental investigation was conducted in the 14- by 22-Foot Subsonic Tunnel at the NASA Langley Research Center to measure the inflow into a scale model helicopter rotor in forward flight ( $\mu = 0.23$ ). The measurements were made with a two-component Laser Velocimeter (LV) 0.75 chord above the plane formed by the path of the rotor tips (tip-path-plane). A conditional sampling technique was employed to determine the position of the rotor at the time that each velocity measurement was made so that the azimuthal fluctuations in velocity could be determined. Measurements were made at a total of 180 separate locations in order to clearly define the inflow character. The mean and standard deviation of the induced inflow ratios and the azimuthally dependent induced inflow ratios are included on 5.25 flexible disk in the pocket on the inside of the rear cover of this report. These data are presented herein without analysis.					
17. Key Words (Suggested by Author(s))  Rotor Inflow Laser Velocimeter			18. Distribution Statement  Unclassified-Unlimited Subject Category 02		
19. Security Classif. (of this report)  Unclassified		20. Security Classif. (of this page)  Unclassified		21. No. of pages 392	
				22. Price A17	